Jitendra K. Pandey
Hitoshi Takagi
Antonio Norio Nakagaito
Hyun-Joong Kim *Editors*

Handbook of Polymer Nanocomposites. Processing, Performance and Application

Volume C: Polymer Nanocomposites of Cellulose Nanoparticles

Springer

Handbook of Polymer Nanocomposites. Processing, Performance and Application

Volume C: Polymer Nanocomposites of Cellulose Nanoparticles

Jitendra K. Pandey • Hitoshi Takagi
Antonio Norio Nakagaito • Hyun-Joong Kim
Editors

Handbook of Polymer Nanocomposites. Processing, Performance and Application

Volume C: Polymer Nanocomposites of Cellulose Nanoparticles

With 251 Figures and 55 Tables

Springer

Editors
Jitendra K. Pandey
University of Petroleum and Energy Studies (UPES)
Bidholi Campus Office Energy Acres
Dehradun, India

Antonio Norio Nakagaito
Department of Mechanical Engineering
Graduate School of Engineering
The University of Tokushima
Tokushima, Japan

Hitoshi Takagi
Advanced Materials Division
Institute of Technology and Science
The University of Tokushima
Tokushima, Japan

Hyun-Joong Kim
College of Agriculture and Life Sciences
Seoul National University
Seoul, Republic of Korea

ISBN 978-3-642-45231-4 ISBN 978-3-642-45232-1 (eBook)
DOI 10.1007/978-3-642-45232-1
Springer Heidelberg New York Dordrecht London

Library of Congress Control Number: 2013955726

Printed on acid-free paper

Springer is part of Springer Science+Business Media (www.springer.com)

Contents

Contributors

H. P. S. Abdul Khalil School of Industrial Technology, Universiti Sains Malaysia, Penang, Malaysia

E. Abraham Department of Chemistry, Bishop Moore College, Mavelikara, Kerala, India

Department of Chemistry, C.M.S. College, Kottayam, Kerala, India

Robert H. Smith Faculty of Agriculture, Food and Environment Hebrew University, Jerusalem, Israel

A. Abu Bakar Materials and Mineral Resources Engineering, Universiti Sains Malaysia, Penang, Malaysia

S. H. Ahn School of Mechanical & Aerospace Engineering, Seoul National University, Seoul, Korea

Ramesh Atmakuru Department of Analytical Chemistry, International Institute of Biotechnology and Toxicology (IIBAT), Padappai, Kancheepuram, Tamilnadu, India

Henriette Monteiro C. Azeredo Embrapa Agroindústria Tropical, Fortaleza, CE, Brazil

A. H. Bhat Department of Fundamental and Applied Sciences, Universiti Teknologi Petronas, Perak, Malaysia

Qingzheng Cheng Forest Products Development Center, Auburn University, Auburn, AL, USA

Agricultural & Biological Engineering, University of Florida, Gainesville, FL, USA

Craig M. Clemons USDA Forest Products Laboratory, Madison, WI, USA

Viviana P. Cyras Facultad de Ingeniería, Instituto de Investigación en Ciencia y Tecnología de Materiales (INTEMA), Universidad de Mar del Plata, Mar del Plata, Argentina

Y. Davoudpour School of Industrial Technology, Universiti Sains Malaysia, Penang, Malaysia

B. Deepa Department of Chemistry, Bishop Moore College, Mavelikara, Kerala, India

Department of Chemistry, C.M.S. College, Kottayam, Kerala, India

Hong Dong Macromolecular Science and Technology Branch, U.S. Army Research Laboratory, Aberdeen, MD, USA

Rani F. Elhajjar College of Engineering & Applied Science, University of Wisconsin, Milwaukee, WI, USA

Waleed K. El-Zawawy Cellulose and Paper Department, National Research Center, Giza, Egypt

Clea Brito de Maria Figueirêdo Embrapa Agroindústria Tropical, Fortaleza, CE, Brazil

M. Laura Foresti Instituto de Tecnología en Polímeros y Nanotecnología (ITPN), Engineering Faculty, University of Buenos Aires, National Research Council (CONICET), Las Heras, Buenos Aires, Argentina

Toru Fujii Department of Mechanical Engineering and Systems, Doshisha University, Kyotonabe, Kyoto, Japan

Mohamed H. Gabr Department of Mechanical Engineering and Systems, Research and Development Center, Kanazawa Institute of Technology, Ishikawa, Kyoto, Japan

Faculty of Industrial Education, Sohag University, Sohag, Egypt

Raed Hashaikeh Materials Science and Engineering Program, Masdar Institute of Science and Technology, Abu Dhabi, United Arab Emirates

Mohammad L. Hassan Cellulose and Paper Department & Advanced Materials and Nanotechnology Group, Centre of Excellence for Advanced Sciences, National Research Centre, Cairo, Egypt

Noriko Hayashi Forestry and Forest Products Research Institute (FFPRI), Tsukuba, Ibaraki, Japan

Maha M. Ibrahim Cellulose and Paper Department, National Research Center, Giza, Egypt

Shinsuke Ifuku Department of Chemistry and Biotechnology, Graduate School of Engineering, Tottori University, Tottori, Japan

Syed H. Imam Bioproduct Chemistry & Engineering Research, WRRC, ARS-USDA, Albany, CA, USA

Yukiko Ishikura Local Independent Administrative Agency, Hokkaido Research Organization, Forest Research Department, Forest Products Research Institute, Asahikawa, Japan

P. Jain Central Institute for Research on Cotton Technology, Matunga, Mumbai, India

M. Jawaid Department of Biocomposite Technology, Institute of Tropical Forestry and Forest Products, Universiti Putra Malaysia, Serdang, Selangor, Malaysia

Sera Jeon Laboratory of Adhesion & Bio-Composites, Program in Environmental Materials Science, Seoul National University, Seoul, Republic of Korea

Mehdi Jonoobi Department of Engineering Sciences and Mathematics, Lulea University of Technology, Lulea, Sweden

Hyun-Joong Kim College of Agriculture and Life Sciences, Seoul National University, Seoul, Republic of Korea

Tetsuo Kondo Biomaterial Design Laboratory, Graduate School of Bioresource and Bioenvironmental Sciences, Kyushu University, Fukuoka, Japan

Rekha Rose Koshy Department of Chemistry, Bishop Moore College, Mavelikara, Kerala, India

Parakalan Krishnamachari Materials Science and Engineering Program, Masdar Institute of Science and Technology, Abu Dhabi, United Arab Emirates

Hyeok-Jin Kwon Laboratory of Adhesion & Bio-Composites, Program in Environmental Materials Science, Seoul National University, Seoul, Republic of Korea

Hyun Taek Lee School of Mechanical & Aerospace Engineering, Seoul National University, Seoul, Korea

Haiqing Liu Fujian Provincial Key Laboratory of Polymer Materials, College of Materials Science and Technology, Fujian Normal University, Fuzhou, China

Ruilai Liu Fujian Provincial Key Laboratory of Polymer Materials, College of Materials Science and Technology, Fujian Normal University, Fuzhou, China

Thiripura Sundari Marimuthu Department of Analytical Chemistry, International Institute of Biotechnology and Toxicology (IIBAT), Padappai, Kancheepuram, Tamilnadu, India

M. Misra Department of Plant Agriculture, or, School of Engineering, University of Guelph, Guelph, ON, Canada

Juan I. Moran Facultad de Ingeniería, Instituto de Investigación en Ciencia y Tecnología de Materiales (INTEMA), Universidad de Mar del Plata, Mar del Plata, Argentina

Antonio Norio Nakagaito Department of Mechanical Engineering, Graduate School of Engineering, The University of Tokushima, Tokushima, Japan

Diego M. do Nascimento Embrapa Agroindústria Tropical, Fortaleza, CE, Brazil

Kazuya Okubo Department of Mechanical Engineering and Systems, Doshisha University, Kyotonabe, Kyoto, Japan

Jitendra K. Pandey University of Petroleum and Energy Studies (UPES), Bidholi Campus Office Energy Acres, Dehradun, India

Ji-Won Park Laboratory of Adhesion & Bio-Composites, Program in Environmental Materials Science, Seoul National University, Seoul, Republic of Korea

Krishna M. Pillai College of Engineering & Applied Science, University of Wisconsin, Milwaukee, WI, USA

L. A. Pothan Department of Chemistry, Bishop Moore College, Mavelikara, Kerala, India

Morsyleide F. Rosa Embrapa Agroindústria Tropical, Fortaleza, CE, Brazil

Enih Rosamah Faculty of Forestry, Mulawarman University, Kelua Samarinda, East Kalimantan, Indonesia

Ronald C. Sabo USDA Forest Products Laboratory, Madison, WI, USA

D. R. Saini Department of Polymer Science and Engineering, National Chemical Laboratory, Pune, India

Yarjan Abdul Samad Materials Science and Engineering Program, Masdar Institute of Science and Technology, Abu Dhabi, United Arab Emirates

P. Satyamurthy Central Institute for Research on Cotton Technology, Matunga, Mumbai, India

Klanarong Sriroth Kasetsart Agricultural and Agro-Industrial Product Improvement Institute, Department of Biotechnology, Kasetsart University, Bangkok, Thailand

Jackapon Sunthornvarabhas Laboratory of Adhesion & Bio–Composites, Program in Environmental Materials Science, Seoul National University, Seoul, Republic of Korea

Cassava and Starch Technology Research Unit, National Center for Genetic Engineering and Biotechnology, Bangkok, Thailand

Pitt Supaphol The Petroleum and Petrochemical College (PPC) and The Center of Excellence on Petrochemical and Materials Technology (PetroMAT), Chulalongkorn University, Pathumwan, Bangkok, Thailand

Orawan Suwantong School of Science, Mae Fah Luang University, Muang, Chiang Rai, Thailand

Paridah Md. Tahir Biocomposite Technology Laboratory, Institute of Tropical Forestry and Forest Products, Universiti Putra Malaysia (UPM), Serdang, Selangor, Malaysia

Hitoshi Takagi Advanced Materials Division, Institute of Technology and Science, The University of Tokushima, Tokushima, Japan

Chunyi Tang College of Biological and Chemical Engineering, Guangxi University of Science and Technology, Liuzhou, China

Kalsang Tharpa Department of Chemistry, University of Mysore, Manasagangothri, Mysore, Karnataka, India

Sabu Thomas School of Chemical Sciences, Mahatma Gandhi University, Kottayam, Kerala, India

International and InterUniversity Centre for Nanoscience and Nanotechnology, Mahatma Gandhi University, Kottayam, Kerala, India

Zhaohui Tong Agricultural & Biological Engineering, University of Florida, Gainesville, FL, USA

A. Vazquez Instituto de Tecnología en Polímeros y Nanotecnología (ITPN), Engineering Faculty, University of Buenos Aires, National Research Council (CONICET), Las Heras, Buenos Aires, Argentina

N. Vigneshwaran Central Institute for Research on Cotton Technology, Matunga, Mumbai, India

Siqun Wang Center for Renewable Carbon, University of Tennessee, Knoxville, TN, USA

Masakazu Yoshikawa Department of Biomolecular Engineering, Kyoto Institute of Technology, Matsugasaki, Kyoto, Japan

I. S. M. Zaidul Faculty of Pharmacy, International Islamic University Malaysia, Kuala Lumpur, Malaysia

Lukmanul Hakim Zaini Biocomposite Technology Laboratory, Institute of Tropical Forestry and Forest Products, Universiti Putra Malaysia (UPM), Serdang, Selangor, Malaysia

Enzymatically Produced Nano-ordered Elements Containing Cellulose I_β Crystalline Domains of *Cladophora* Cellulose

1

Noriko Hayashi and Tetsuo Kondo

Contents

Abstract

This chapter describes a novel top-down type extraction method of nanocellulose using enzymatic hydrolysis of microcrystalline cellulose fibers comprising two crystalline allomorphs of cellulose, Iα and Iβ. In this method, the key issue was the selective removal of cellulose Iα phases by preferential hydrolysis of *Trichoderma* cellulase [1]. This selective hydrolysis process provided short

N. Hayashi (✉)
Forestry and Forest Products Research Institute (FFPRI), Tsukuba, Ibaraki, Japan
e-mail: hayashin@ffpri.affrc.go.jp

T. Kondo
Biomaterial Design Laboratory, Graduate School of Bioresource and Bioenvironmental Sciences, Kyushu University, Fukuoka, Japan
e-mail: tekondo@agr.kyushu-u.ac.jp

J.K. Pandey et al. (eds.), *Handbook of Polymer Nanocomposites. Processing, Performance and Application – Volume C: Polymer Nanocomposites of Cellulose Nanoparticles*,
DOI 10.1007/978-3-642-45232-1_58,

elements having nanoscaled width. X-ray diffraction, electron diffraction, and FT-IR analyses revealed that the "nano-element" was highly crystalline, similar to the untreated microcrystalline cellulose, and mostly consisted of the Iβ phase. The average length of the elements was ca. 350 nm, which corresponded to the value due to the degree of polymerization of 690 for *β*-glucan molecular chains obtained by size-exclusion chromatographic analysis. The close agreement indicates that individual molecular chains may be extended in the longitudinal direction of the obtained element. These characteristic nano-elements have the potential to play a role of nano-ordered particles and may be useful as fillers to enhance the mechanical properties of various materials.

Keywords
Microcrystalline cellulose • Cellulase • Cellulose Iα • Selective degradation • Nano-elements

1 Introduction

Cellulose is a *β*-1,4-glucan polymer that self-aggregates to form minimal-sized crystalline fibers, designated as cellulose microfibrils (CMFs), in the cell wall of plants and algae and tunica of animals. The length of the CMF is about 1 μm, while the diameter is on the nanoscale ranging from 3 to 20 nm, depending on the cellulose source. Therefore, the nano-cellulose attracts much attention as an eco-friendly green nano-composite material.

The filamentous green alga, *Cladophora*, which was employed in this chapter, grows in both marine and freshwater and also in brackish water. Genus *Cladophora* distributes worldwidely and is one of the most species-rich genera among green macroalgae [2–4]. *Cladophora* consists of typically branched filaments. It provides habitat and food for numerous organisms. "Marimo" inhabiting Lake Akan-ko in Japan, being famous as a tourist attraction because of its ball-like shape, is also *Cladophora* sp. From the 1950s, it has been reported that *Cladophora* seasonal blooms in early summer formed thick floating mats and effect on freshwater ecosystems, proving serious nuisance [5, 6]. The eutrophication by the drainage of daily life causes excessive growth of the seaweed, and it often becomes troublesome. Simultaneously, they are also available resources from a different view point. Therefore, the detailed examination is required in *Cladophora* sp.

It was reported that the wall of marine species has a multilayered structure, an amorphous layer, and a microfibrillar layer and is composed lamellarly to be so compacted outwardly [7]. Furthermore, it is most important that *Cladophora* CMF contains highly cellulose crystallite. Generally, each CMF is composed of two crystalline allomorphs with parallel arrangements of the molecular chains that are generally accepted as cellulose Iα and cellulose Iβ [8–11]. Cellulose Iα and cellulose Iβ have one-chain triclinic and two-chain monoclinic lattices, respectively [12, 13]. The ultrastructural localizations of the cellulose Iα and Iβ allomorphs in

a single microfibril have been investigated, and two models have been proposed. In the first, the two crystalline domains are localized laterally [11, 14], while in the second, the two domains coexist alternately longitudinally or laterally [15].

Recently, we investigated enzymatic hydrolyzates of Trichoderma. sp of CMFs secreted from a bacterium, *Gluconacetobacter xylinus* (formerly *Acetobacter xylinum*), and two algae, *Cladophora* sp. and *Valonia* sp., that included both cellulose Iα and Iβ [1, 16]. The results indicated that cellulose Iα was more susceptible to enzymatic degradation by *Trichoderma* cellulase than cellulose Iβ. Furthermore, the nano-elements rich in cellulose Iβ were frequently observed in the residues. Trichoderma cellulase contains three kinds of cellulase, those are cellobiohidrolase, endoglucanase, and β-glucosidase. Enzymatic hydrolysis by *Trichoderma* cellulase is believed to degrade cellulose crystals in a processive manner of cellobiohydrolase from their reducing or nonreducing end of cellulose molecules [17–19]. However, we hypothesized that the nano-elements could not be produced from CMFs as a result of the endo-processive action of cellobiohydrolase alone. Assuming the preferable hydrolysis of cellulose Iα by cellulase as described above, the supramolecular structure of the crystalline cellulose should also contribute to the production of the nano-elements in addition to the manner of the enzymatic action.

In this chapter, the authors will describe the characterization of the larger residues after enzymatic hydrolysis of CMFs and the nano-elements (designated as shortened microcrystalline cellulose: SMCC) obtained from algal cellulose of *Cladophora* sp. using transmission electron microscopy (TEM), atomic force microscopy (AFM), and Fourier transformation infrared (FT-IR) spectroscopy. Finally, we will propose a mechanism for SMCC formation on the basis of the supramolecular structure of *Cladophora* CMFs, which are constructed from cellulose Iα and Iβ allomorphs.

2 Experimental Section

2.1 Enzyme Preparation

The crude enzyme used was the commercially available "Meicelase" (Meiji Seika Co. Ltd., Japan) prepared from *Trichoderma viride*. Exo-1,4-*β*-glucanase I (Cel 7A), one of the cellobiohydrolases which *T. viride* secretes, was isolated and purified by multiple column chromatographies using anion and cation exchangers according to a previously described method [20]. However, a trace amount of contamination was identified in the purified Cel 7A preparation after SDS-PAGE, and hence, it is referred as the Cel 7A-rich fraction.

2.2 Preparation of Cellulose Substrates

Cell wall cellulose was collected from *Cladophora* sp. in the sea at Chiba, Japan. To purify the substrate, it was sequentially treated with 0.1 N aqueous NaOH at 100 °C for 2 h and then 0.05 N aqueous HCl at room temperature overnight,

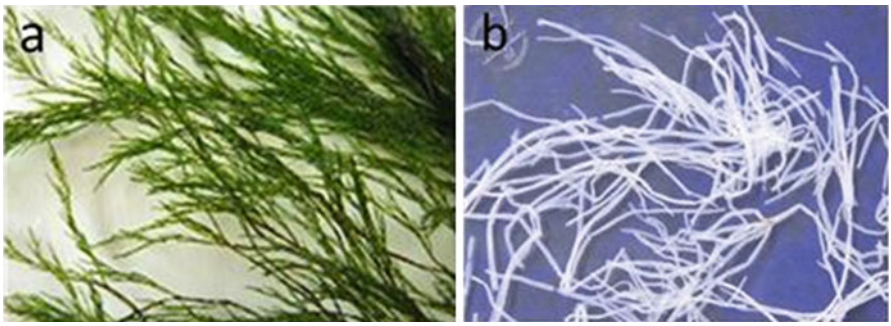

Fig. 1.1 A botanical specimen of green alga *Cladophora* sp. (**a**) and after purification (**b**)

before final rinsing with distilled water (Fig. 1.1). Following homogenization and freeze-drying, the residues were collected as CMFs. The CMFs were further treated with a 66 % (w/w) aqueous H_2SO_4 solution at room temperature for 3 h with strong stirring and then washed by centrifugation to obtain a non-flocculating aqueous suspension of microcrystalline cellulose (designated MCC) at pH 5.0. The MCC was freeze-dried for further study.

2.3 Enzymatic Hydrolysis

The obtained MCC was separately hydrolyzed with the crude cellulase and Cel 7A-rich fraction as follows. Equal quantities of the substrate suspension (1–5 mg of MCC) and the enzyme in 5 ml of 0.1 M of sodium acetate buffer at pH 4.8 were incubated with shaking for 2–3 day at 48 °C for crude cellulase and 38 °C for the Cel 7A-rich fraction. In addition, MCC samples hydrolyzed with shaking were compared with samples hydrolyzed without shaking. After the incubation, the precipitated residues (designated the larger residues) were isolated by centrifugation, thoroughly washed with 1 % NaOH solution and then distilled water, and finally freeze-dried. Following the addition of an excess of 99.5 % ethanol to the supernatants in each washing process mentioned above, short elements (designated as SMCCs) were obtained by centrifugation at 10,000–18,000 rpm and then freeze-dried. The larger residues were repeatedly treated with the enzyme until the total weight loss of the sample reached 80 %.

2.4 Acid Hydrolysis

To compare the enzymatic hydrolyzates with acid hydrolyzates, the purified *Cladophora* CMFs were treated with 2.5 N HCl at 100 °C for 3 or 5 h. The acid-hydrolyzed MCC samples were also subjected to TEM, FT-IR, and size-exclusion chromatographic (SEC) analyses.

2.5 Transmission Electron Microscopy

The samples were observed with a JEM-2000EX electron microscope (JEOL Co. Ltd.) operated at an accelerating voltage of 200 kV. Samples of untreated MCC, acid-hydrolyzed MCC, precipitated larger residues, and SMCCs were individually suspended in 50 % ethanol. A drop of each suspension was deposited on a carbon-coated Cu grid and negatively stained with 1.5 % uranyl acetate solution. Selected area diffractograms were also obtained without staining. The images and diffractograms were recorded on Mitsubishi electron microscope (MEM) films. The electron diffractograms were traced with a microdensitometer (3CS; Joyce-Loebl Co. Ltd.) to estimate the *d* spacings of the crystalline structure.

2.6 Infrared Spectroscopy

Each sample was mounted on a KBr thin plate of about 1 mm in thickness. FT-IR spectra were obtained from a circular area of 100 μm in diameter using a Nicolet-Magna 550 FT-IR spectrometer equipped with a Nic Plan microscopic accessory. The wave number range scanned was 4,000–650 cm^{-1}, and 64 scans of 4 cm^{-1} resolution were signal-averaged and stored. The internal standard band at 2,900 cm^{-1} that is assigned to the C-H stretching in methyl and methylene groups in the crystalline region was commonly employed. The relative ratios between the cellulose Iα and Iβ in the samples were determined by the intensity ratios of their typical FT-IR bands, namely, 750 cm^{-1} for cellulose Iα and over 710 cm^{-1} for cellulose Iβ, using a calibration curve based on previous results [14].

2.7 Determination of Molecular Weight

Some of the SMCCs were isolated and freeze-dried after 2 or 8 day of enzymatic treatments. The residues were then treated with an ice-cooled mixture of nitric acid and phosphorus pentoxide for 30 min for conversion into cellulose trinitrate for the SEC analysis. The products were filtered and washed thoroughly with water. The SEC was performed with tetrahydrofuran as the eluent to determine the average molar weight (Mw) of the cellulose trinitrate obtained from the enzymatic hydrolyzates [21]. The Mw of the acid hydrolyzates of *Cladophora* CMFs was measured in the same manner.

2.8 Atomic Force Microscopy

A drop of the SMCC suspension or the larger residues was deposited onto a mica plate (8 × 8 mm) and then air-dried. The samples were observed using a multimode AFM (NanoScope IIIa; Digital Instruments) equipped with a scanner with a 10 μm

range (E-scanner). All images (400 × 400 pixels) were obtained using a tapping mode in air. The cantilever used was 130 μm in length and had an unmodified silicon nitride tip with a spring constant of 40 Nm^{-1}. The scan rate was 1.5 Hz and the scan angle was varied to obtain the optimum contrast.

3 Characterization of the Residues After Enzymatic Hydrolysis

Short elements (SMCCs) as designated for the nano-element described above were produced during the enzymatic degradation processes of both the crude cellulase and the Cel 7A-rich fraction (Fig. 1.2a, b). During the 2 day enzymatic hydrolysis, the yield of nano-elements reached 15–24 % of the initial sample, as shown in Table 1.1. The SMCCs were produced constantly at almost the same rate for the individual enzymes in the residues after the repeated enzymatic degradation processes. Distinct fibrillation was scarcely observed in the samples after 4 days of enzymatic hydrolysis (Fig. 1.2a). However, the larger residues and SMCCs became thinner and/or fibrillated after 8 days of treatment (Fig. 1.2b, arrowhead), similar to the case for hydrolysis of Iβ-rich cotton-ramie type cellulose [22]. On the other hand, the 5 h acid hydrolysis of *Cladophora* CMFs did not produce such SMCCs (Fig. 1.2c).

The lengths of the obtained SMCCs did not differ significantly between the crude cellulose and the Cel 7A-rich fraction. The distribution in length of the SMCCs produced by the degradation with the crude cellulase was evaluated statistically, as shown in the histogram in Fig. 1.3. The most frequently observed lengths were between 300 and 400 nm.

The SEC results revealed the distributions of the degree of polymerization (DP) based on the Mw for the cellulose molecules in the untreated CMFs, acid-treated CMFs, and SMCCs. The results for the SMCCs after treatment with the crude cellulase for 2 and 8 day are shown in Table 1.2. The DP of the SMCCs was about 690, whereas the acid-hydrolyzed CMFs did not show a significant change in the DP after the treatment was prolonged. More interestingly, the Mw/Mn value of the SMCCs, indicating the distribution of the molecular weight, was much lower than that of the acid-hydrolyzed samples and even smaller than that of the untreated CMFs. These results indicate that only the enzymatically produced SMCCs had a narrower distribution of DP around 690. The value of 690 for the DP of β glucan molecules coincides with the average length of 300–400 nm of the SMCC rod samples, which were obtained experimentally by the TEM observation as described above. This indicates that the length of the SMCC rods may coincide with the extended chain length of the contained β glucan molecules, when it is calculated based on the anhydroglucose unit length of 0.5 nm.

The X-ray diffractograms of the untreated CMFs and the SMCCs are shown in Fig. 1.4. The SMCCs exhibited a high crystallinity after the enzymatic treatments, similar to the untreated CMFs, indicating that noncrystalline regions may not be present in newly produced SMCCs after enzymatic hydrolysis. The field limiting

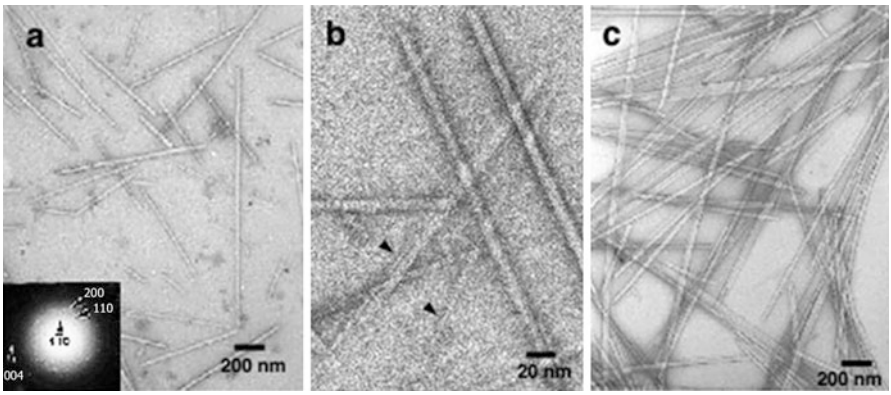

Fig. 1.2 Electron micrographs of the negatively stained short elements (SMCCs) obtained after 4 and 8 day of treatment with the Cel 7A-rich fraction (**a**, **b**) and MCC after acid hydrolysis (**c**). The *arrowhead* shows fibrillated SMCCs (**b**)

Table 1.1 Differences in the yields and Iα contents between the enzymatic treatments with and without shaking

		Yield (%)	Iα content (%)
Control		100	55 ± 17
Meicelase shaked	Larger residue	29.3	43 ± 12
	SMCC	21.2	29 ± 7
Meicelase not shaked	Larger residue	44.3	47 ± 9
	SMCC	15.3	38 ± 2
Cel 7A-rich fraction shaked	Larger residue	47.3	45 ± 6
	SMCC	24.0	39 ± 5
Cel 7A-rich fraction not shaked	Larger residue	56.4	44 ± 15
	SMCC	21.8	37 ± 7

diffraction pattern of the SMCCs inserted in Fig. 1.2a exhibited clear reflected spots that also indicate high crystallinity. The *d* spacings for the SMCCs corresponded to the values for the (110) plane (0.60 nm) and the (110) plane (0.54 nm), which are typically identified as cellulose Iβ. These results indicate that the major crystalline parts of the SMCCs consist of a highly ordered cellulose Iβ phase.

The cellulose Iα and Iβ contents in the obtained samples calculated on the basis of the IR analyses are listed in Table 1.1. The initial sample contained 55 ± 17 % cellulose Iα. After enzymatic hydrolysis with shaking at 50 wt% of the weight loss, 52 % of the initial cellulose Iα content was enzymatically degraded. This result also indicated that the enzyme did not uniformly attack every MCC during the reaction time course since the Iα content differed between the larger residues and SMCCs. The FT-IR results suggested that the SMCCs were predominantly composed of cellulose Iβ, although a trace of cellulose Iα was still remained (Fig. 1.5), when the bands in the region of 3,450–3,150 cm^{-1} were compared before and after the

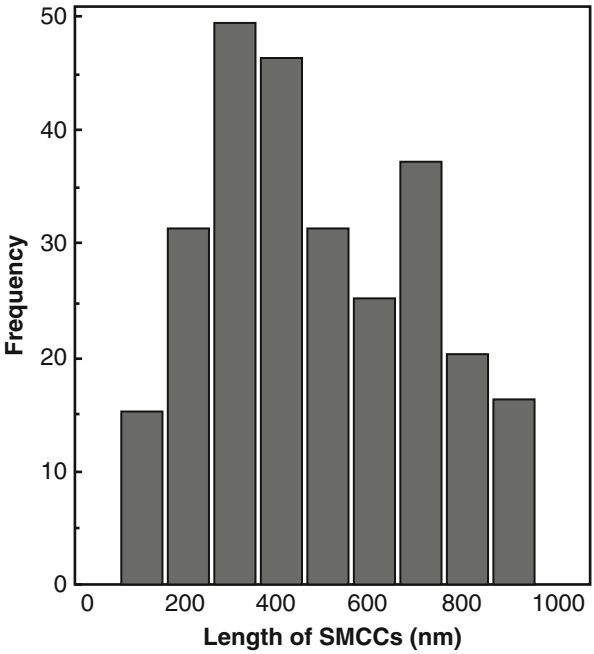

Fig. 1.3 Statistic frequencies of the lengths of SMCCs treated with the crude cellulase for 4 and 8 day or the Cel 7A-rich fraction for 2, 4, and 6 day

Table 1.2 Changes in the average degree of polymerization (DP) based on SEC chromatograms for the nano-elements (SMCCs), together with untreated and acid-treated CMFs of *Cladophora* sp.

			Acid-treated CMF		
	Untreated CMF	Nano-elements (SMCC)	30 min	60 min	180 min
DP	2,870	690	3,010	3,150	3,130
Mw/Mn	9.6	4.7	25.3	21.8	10.0

enzymatic hydrolysis. However, the absorption bands at 3,240 cm^{-1} due to cellulose Iα were drastically decreased after the enzymatic hydrolysis. A trace amount of unhydrolyzed cellulose Iα may still remain at the ends of the SMCCs, after taking into account the preferable enzymatic attack on cellulose Iα. It is generally accepted that certain treatments are able to convert cellulose Iα to cellulose Iβ, but they require a high pressure and high temperature [10, 23]. In this study, the enzymatic degradation could not convert the crystalline cellulose to the microcrystalline form, since the hydrolysis was performed at 38 °C and 48 °C under atmospheric pressure.

Previously, it was reported that short elements were present in Iβ-dominant cotton-ramie type cellulose [24–28]. However, we consider that the SMCC formation from algal-bacterial type cellulose in our case does not represent the same phenomenon. As described above, the two allomorphs cellulose Iα and Iβ are distributed in a complex manner in the algal-bacterial cellulose, whereas cotton-ramie type cellulose mainly contains cellulose Iβ. The results in the present study

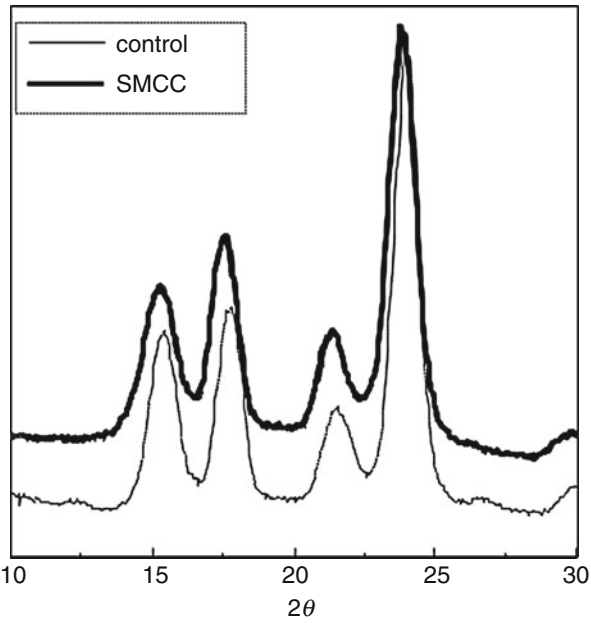

Fig. 1.4 X-ray diffractograms of untreated CMFs (*broken line*) and SMCCs (*solid line*)

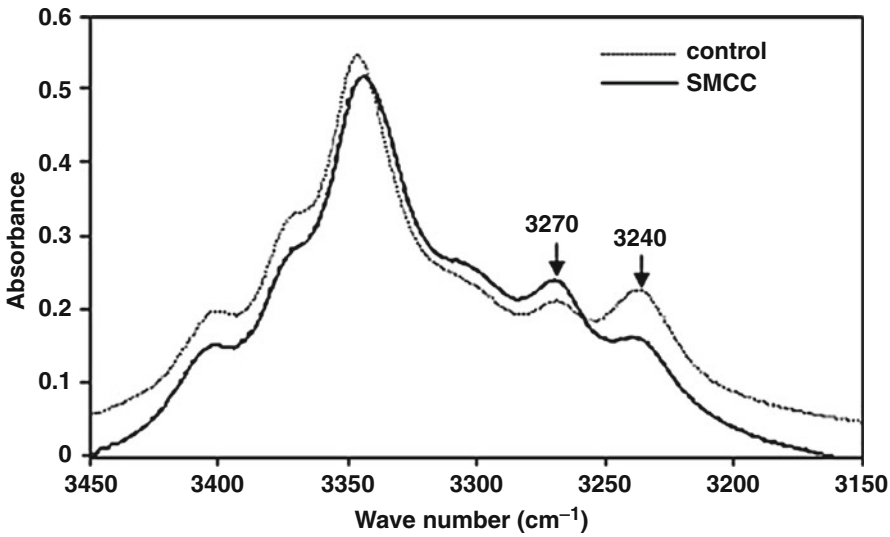

Fig. 1.5 FT-IR spectra for untreated CMFs (*broken line*) and SMCCs (*solid line*; the enzymatic hydrolyzate) in the characteristic regions for the cellulose Iα and Iβ absorption bands. The absorption bands near 3,240 and 3,270 cm^{-1} are assigned to cellulose Iα and Iβ, respectively

appear to confirm that preferential degradation of cellulose Iα accompanied by the SMCC formation occurs in *Cladophora* CMFs, an algal-bacterial type cellulose.

In addition, we investigated the effects of shaking during the enzymatic treatment. It has been considered that shaking samples during the process of degradation may accelerate the action of the enzyme [29]. The yields and cellulose Iα contents of SMCCs after treatment with the crude cellulase and Cel 7A-rich fraction with and without shaking are shown in Table 1.1. The results indicated that shaking during the treatment had an effect on both acceleration of the enzymatic hydrolysis and the preferable degradation of Iα. In particular, the production of SMCCs seemed to be dependent on shaking in the case of the crude cellulase. It is well known that *Trichoderma* crude cellulase contains three kinds of enzymes, each of which reacts synergistically with CMFs, which contain complicated distributions of cellulose Iα and Iβ, leading to efficient acceleration of the preferable degradation of cellulose Iα to yield SMCCs. It is also considered that shaking may provide the enzymes with more opportunity to interact with new reaction sites. In the case of treatment with the Cel 7A-rich fraction, however, the production of SMCCs and decrease in cellulose Iα in the residues were independent of shaking during the incubation. This may be caused by the different manners of degradation between the crude cellulase and an isolated enzyme as described above. These results imply that mechanical force may play an important role not only in the enzymatic movement of Cel 7A to new sites on the substrate but also in cutting the CMFs after Cel 7A attack. Furthermore, the fact that the SMCCs obtained from the series of enzymatic hydrolyses in Table 1.1 showed almost the same values for their cellulose Iα contents indicates that the supramolecular structure of CMFs, such as the distribution of Iα/Iβ composites, may contribute to the production of SMCCs during the enzymatic degradation.

4 Supramolecular Structure of the Iα/Iβ Composite Crystalline Phases in Microcrystalline Cellulose Fibers

An atomic force microscope (AFM) was employed in a tapping mode in air to observe the surface morphology of the samples. Figure 1.6 shows the AFM height images of untreated CMF (a), longer residues after the enzymatic degradation (b), and short elements (SMCCs) (c). The enzymatic hydrolysis produced drastic changes to the surface of the MCC. From the AFM observations, the color of the untreated CMFs was uniform, which means that the thickness of the untreated CMF is about 10 nm, and furthermore, their surface was considered to be smooth (Fig. 1.6a, d). After the enzymatic treatment, however, the surface of the longer residues and SMCCs became relatively rough (Fig. 1.6b, c, and e). AFM observations also revealed that the longer residues had areas cut off as blocks from the original surface not only at the ends but also at the middle (circle in Fig. 1.6e). The lengths of the cutoff areas were within several hundred nanometers, whereas their widths were almost the same as that of the untreated CMFs. Characteristically, the thickness at the cutoff area was 1–4 nm (see the inserted profile of (e); indicating that two or three molecular cellulose chains may be included).

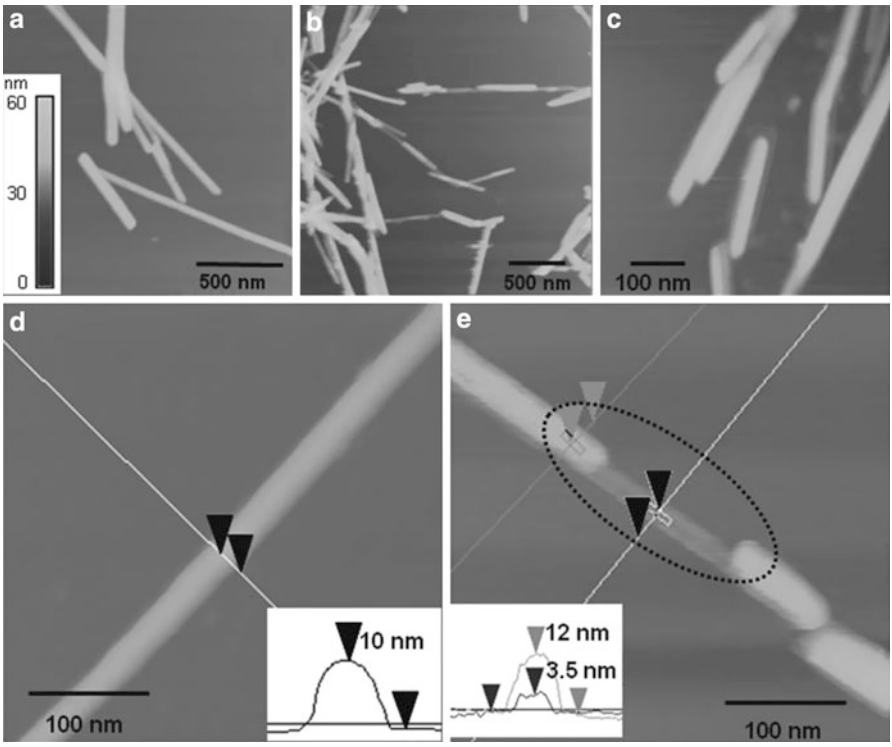

Fig. 1.6 AFM height images (**a**, **c**, and **d**) and section analyses of an untreated CMF (**b**) and a longer residue (**e**). The *circled area* shows a cutoff area observed in the longer residues

The thicknesses of untreated CMFs, SMCCs, and longer residues with and without shaking were 11.7 ± 4.7 nm, 8.06 ± 5.67 nm, 9.65 ± 4.12 nm, and 8.48 ± 5.66 nm, respectively. The thicknesses of the residues after enzymatic hydrolysis were thinner than those of the initial samples. In connection with the length of the SMCCs shown in Fig. 1.2, it is interesting that the width of the cutoff areas with the enzymatic treatments appeared to be almost identical to the size of the SMCCs.

From these results, the cutoff areas are supposed to be removed by preferential degradation of cellulose Iα-rich blocks or correspond to cellulose Iβ-rich domains surrounding Iα-rich parts. The former assumption may agree with the hypothesis for the cellulose Iα/Iβ distributions proposed by Imai and Sugiyama [15] and the latter with that proposed by sugiyama et al. [11, 13] and Yamamoto et al. [14]. In other words, our observations indicate that the domains of cellulose Iα may be partly buried as a block or sheet along the longitudinal axis in the CMFs of *Cladophora* sp., in which cellulose Iα/Iβ are considered to be distributed in a complex manner as interpreted by Imai and Sugiyama [15]. Thus, we can postulate that when the enzyme attacked CMFs, cellulose Iα domains were preferentially hydrolyzed, and the remaining cellulose Iβ-rich domains were consequently extracted as intact crystalline blocks under our reaction conditions.

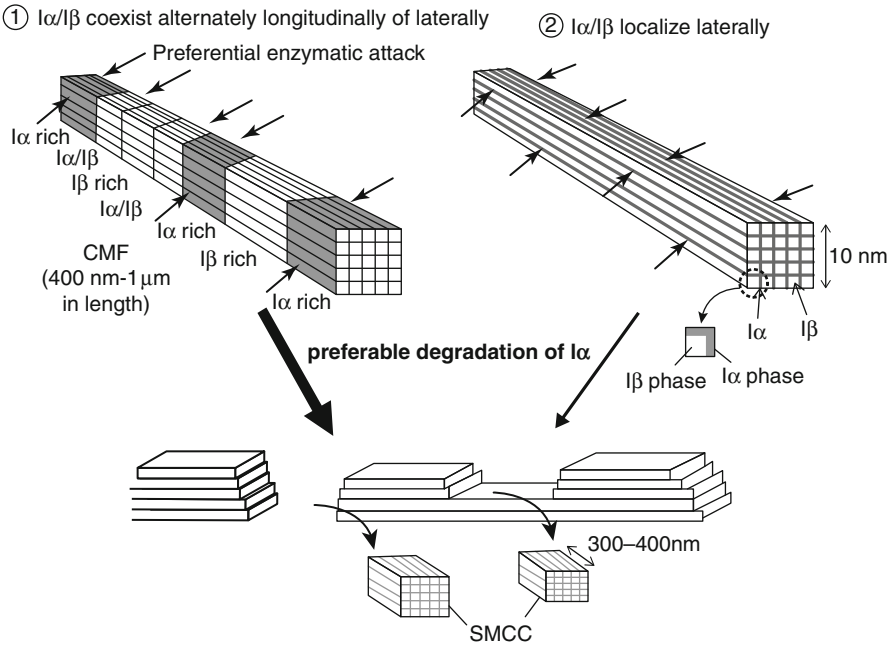

Fig. 1.7 A hypothesis for the formation of nano-elements by enzymatic hydrolysis of *Cladophora* CMFs, in relation to the possible supramolecular structure of CMFs

This phenomenon can be attributed to the low susceptibility to the enzymes of the highly ordered and relatively stable Iβ arrangement of β glucan chains for the SMCCs, as illustrated schematically in Fig. 1.7. The kinks or defects caused by the enzymatic attack may be the initial stage of the cutting of CMFs or peeling off the blocks.

5 Summary

Enzymatic hydrolysis of *Cladophora* CMFs yielded nano-elements, designated as SMCCs, with high crystallinity. The SMCCs were mainly composed of a cellulose Iβ crystalline phase with a width of 10 nm and a length ca. 350 nm, corresponding to the average DP of 690 for the β glucan molecules. However, a trace of cellulose Iα still remained in the SMCCs. This may be induced by the preferential degradation of Iα crystalline domains by the *Trichoderma* crude cellulase and Cel 7A-rich fraction.

AFM observation revealed the appearance of some missing blocks in the residual MCC within a few hundred nanometers at either the ends or the middle. These findings indicate the possibility that crystalline Iα domains of a certain size were buried along the longitudinal axis of the *Cladophora* CMFs. The synergism of the enzymes contained in the crude cellulase and the mechanical force applied by shaking the samples during the enzymatic treatment also assisted the production

of SMCCs. The SMCCs have the potential to act as nano-ordered bio-particles. Currently, there are many researches about cellulose nanofibers, and their application is trying to spread in various fields. Therefore, the dimensions of the cellulose nanofiber should become the important factor of the application. In other words, the SMCCs containing ordered fiber elements on a nanoscale of this size are expected to be useful as fillers for the reinforcement of various impact materials as well as addition to the food and cosmetic industries.

Acknowledgments The authors thank Dr. M. Wada (University of Tokyo) for providing the *Cladophora* cellulose and Dr. J. Sugiyama (Kyoto University) for his valuable suggestions. The assistance of Dr. H. Shibazaki in the SEC measurements is greatly appreciated. We also acknowledge Dr. Y. Kataoka (FFPRI) for his help with the AFM and valuable suggestions.

References

1. Hayashi N, Ishihara M, Sugiyama J, Okano T (1998) The enzymatic susceptibility of cellulose microfibrils of the algal-bacterial type and the cotton-ramie type. Carbohydr Res 305:261
2. Whitton BA (1970) Biology of cladophora in freshwaters. Waters Res 4:457, Pergamon Press
3. Dodds WK, Gudder DA (1992) The ecology of cladophora. J Phycol 28:415
4. Hayakawa YI, Ogawa T, Yoshikawa S, Ohki K, Kamiya M (2012) Genetic and ecophysiological diversity of Cladophora (Cladophorales, Ulvophyceae) in various salinity regimes. Phycolog Res 60:86
5. Morand P, Briand X (1996) Excessive growth of macroalgae: A symptom of environmental disturbance. Botanica Marina 39:491
6. Higgins SN, Malkin SY, Howell ET, Guildford SJ, Campbell L, Hiriart-Baer V, Hecky RE (2008) An ecological review of Cladophora glomerata (Chlorophyta) in the Laurentian Great Lakes. J Phycol 44:839
7. Hanic LA, Craigie JS (1969) Studies on algal cuticle. J Phycol 5:80
8. Atalla RH, VanderHart DL (1984) Native cellulose - a composite of 2 distinct crystalline forms. Science 223:283
9. VanderHart DL, Atalla RH (1984) Studies of microstructure in native celluloses using solid-state carbon-13 NMR. Macromolecules 17:1465
10. Horii F, Hirai A, Kitamaru R (1987) CP/MAS carbon-13 NMR spectra of the crystalline components of native celluloses. Macromolecules 20:2117
11. Sugiyama J, Vuong R, Chanzy H (1991) Electron diffraction study on the two crystalline phases occurring in native cellulose from an algal cell wall. Macromolecules 24:4168
12. Sugiyama J, Okano T, Yamamoto H, Horii F (1990) Transformation of Valonia cellulose crystals by an alkaline hydrothermal treatment. Macromolecules 23:3196
13. Sugiyama J, Persson J, Chanzy H (1991) Combined infrared and electron diffraction study of the polymorphism of native celluloses. Macromolecules 24:2461
14. Yamamoto H, Horii F, Hirai A (1996) In situ crystallization of bacterial cellulose .2. Influences of different polymeric additives on the formation of celluloses I-alpha and I-beta at the early stage of incubation. Cellulose 3:229
15. Imai T, Sugiyama J (1998) Nanodomains of Iα and Iβ Cellulose in Algal Microfibrils Macromolecules 31:6275
16. Hayashi N, Ishihara M, Sugiyama J, Okano T (1998) Selective degradation of the cellulose I-alpha component in Cladophora cellulose with Trichoderma viride cellulase. Carbohydr Res 305:109
17. Imai T, Boisset C, Samejima M, Igarashi K, Sugiyama J (1998) Unidirectional processive action of cellobiohydrolase Cel7A on Valonia cellulose microcrystals. FEBS Lett 432:113

18. Henrissat H (1998) Enzymatic cellulose degradation. Cellulose Commun 5:84
19. Boisset C, Fraschini C, Schulein M, Henrissat B, Chanzy H (2000) Imaging the enzymatic digestion of bacterial cellulose ribbons reveals the endo character of the cellobiohydrolase Cel6A from Humicola insolens and its mode of synergy with cellobiohydrolase Cel7A. Appl Environ Microbiol 66:1444
20. Honda S, Takahashi M, Nishimura Y, Kahei K, Ganno S (1981) Sensitive ultraviolet monitoring of aldoses in automated borate complex anion-exchange chromatography with 2-cyanoacetamide. Anal Biochem 118:162
21. Shibazaki H, Kuga S, Onabe F, Brown RM Jr (1995) Acid hydrolysis behaviour of microbial cellulose II. Polymer 36:4971
22. Hayashi N, Ishihara M, Shimizu K (1995) The features in enzymatic hydrolysis residues of highly crystalline native cellulose. Mokuzai Gakkaishi 41:1132
23. Debzi EM, Chanzy H, Sugiyama J, Tekely P, Excoffier G (1991) The Iα →Iβ transformation of highly crystalline cellulose by annealing in various mediums. Macromolecules 24:6816
24. Marsh PB (1957) Microscopic observations on cotton fibers subjected to enzymatic degradation. Text Res J 27:913
25. Halliwell G (1966) Solubilization of native and derived forms of cellulose by cell-free microbial enzymes. Biochem J 100:315
26. King KW (1966) Enzymic degradation of crystalline hydrocellulose. Biochem Biophys Res Commun 24:295
27. Halliwell G, Riaz M (1970) Formation of short fibres from native cellulose by components of trichoderma-koningii cellulase. Biochem J 116:35
28. Sprey B, Bochem H-P (1993) Formation of cross-fractures in cellulose microfibril structure by an endoglucanase cellobiohydrolase complex from trichoderma-reesei. FEMS Microbiol Let 106:239
29. Lee I, Evans BR, Lane LM, Woodward J (1996) Substrate-enzyme interactions in cellulase systems. Biores Technol 58:163

Nanocrystalline Cellulose from Coir Fiber: Preparation, Properties, and Applications

2

Henriette Monteiro C. Azeredo, Syed H. Imam, Clea Brito de Maria Figueirêdo, Diego M. do Nascimento, and Morsyleide F. Rosa

Contents

Abstract

Nanocrystalline cellulose derived from various botanical sources offers unique and potentially useful characteristics. In principle, any cellulosic material can be considered as a potential source of a nanocrystalline material, including crops, crop residues, and agroindustrial wastes. Because of the variability in cellulose source and methods of preparation, nanocellulosic materials of variable structure, property, and application could be obtained. This chapter provides current knowledge on the acid hydrolysis extraction of nanocrystalline cellulose from coir fiber and its application in composite films. The use of ultrathin cellulose nanocrystals extracted from bleached coir fibers, in composites, has shown improved filler-matrix interaction and enhanced performance in the resulting nanocomposites, identifying a novel application for this feedstock. When incorporated into a hydrophilic polysaccharide-based matrix, nanostructures from coir fiber exhibited

H.M.C. Azeredo • C.B. de Maria Figueirêdo • D.M. do Nascimento • M.F. Rosa (✉)
Embrapa Agroindústria Tropical, Fortaleza, CE, Brazil
e-mail: henriette.azeredo@embrapa.br; clea.figueiredo@embrapa.br; die_quimico@yahoo.com.br; morsyleide.rosa@embrapa.br

S.H. Imam
Bioproduct Chemistry & Engineering Research, WRRC, ARS-USDA, Albany, CA, USA
e-mail: Syed.Imam@ars.usda.gov

J.K. Pandey et al. (eds.), *Handbook of Polymer Nanocomposites. Processing, Performance and Application – Volume C: Polymer Nanocomposites of Cellulose Nanoparticles*,
DOI 10.1007/978-3-642-45232-1_59, © Springer-Verlag Berlin Heidelberg 2015

barrier and mechanical properties comparable to that from cotton fiber, despite the expected low compatibility between the matrix and the residual lignin leftover in the coir fiber. This is attributed to the counterbalancing effect of the higher aspect ratios present in nanocellulose obtained from coir fibers.

Keywords
Cellulose Whiskers • Nanocomposites • Environmental Impact • Unripe Coconut Fiber

1 Introduction

Nanocrystalline cellulose is commonly referred either as cellulose whiskers (CW), cellulose nanocrystals, or nanowhiskers. Such material is of much interest to several industrial sectors due to its availability in abundance, renewability, and light weight. Particularly, CW being elongated structures have two nanometric dimensions. A uniform dispersion of nanoparticles results in a very large matrix/filler interfacial area, which reduces the molecular mobility, changes the relaxation behavior, and improves the overall thermal and mechanical properties of the material. Fillers with a high aspect ratio are particularly interesting because of their high specific surface area which provides better reinforcing effects stimulating a new generation of novel applications [1, 2]. Moreover, well-dispersed nanoparticles induce the formation of an interphase region of altered mobility, resulting in a percolating interphase network which improves the nanocomposite properties [3]. For a constant filler content, a reduction in particle dimensions increases the number of particles bringing them closer to one another and causing the interface layers to overlap, thus altering the bulk properties significantly [4].

Such improved properties are especially important for biopolymers, which usually suffer from poor mechanical, thermal, and barrier properties compared to conventional synthetic counterparts. Due to the worldwide efforts to reduce the waste generated by nonbiodegradable consumer products, biopolymers have been exploited for developing naturally biodegradable materials. In this context, the incorporation of plant-derived nanostructures in biopolymer matrices is considered as one of the most plausible approaches to develop high-quality commercial products replacing petroleum-derived synthetic polymers. For this, coir fiber has been considered as an additional renewable feedstock source for obtaining such nanostructures.

Coir is a renewable and biodegradable lignocellulosic fiber, extracted from the outer shell, or husk, of either mature or immature fruits of the coconut palm (*Cocos nucifera* L.). This is achieved in few simple steps which involve grinding, sieving, and drying. Coir fiber is a waste produced in large quantities every year by the agroindustrial sector in tropical countries. Several researchers have investigated its structure and properties, and several processes and products have been reported that utilize coir fiber as a raw material in industrial products [5–7]. In this chapter, we describe the acid hydrolysis extraction of CW from coir fiber and its impact on the reinforcement and barrier properties in composite films produced from alginate-acerola puree. In addition, an environmental assessment of the production of CW obtained from coir fiber is also presented.

2 Preparation of CW Suspension from Coir Fibers

In a first step, unripe coconut fibers from Northeast Brazil were finely grinded in a Wiley mill (40-mesh sieve) and subjected to a multistep treatment process. Sequential chemical steps were used including pretreatments (alkaline treatment and bleaching) and acid hydrolysis as described elsewhere [8]. Briefly, coir fibers were subjected to a washing in water to remove impurities and soluble extractives (covering of the external surface of fiber cell walls). After washing, coir fibers were subjected to alkali treatment (2 % NaOH solution at 80 °C for 2 h). As lignin still remained within the fibers, two kinds of bleaching were carried out according to a previously published method [9]. One-stage bleaching involved heating (60–70 °C) of 5 g of dried fibers in 150 mL of water containing 1.5 g of sodium chlorite ($NaClO_2$) to which about 8–10 drops of glacial acetic acid were added while reaction mixture was stirred. Upon cooling, the solution was filtered, and the suspension was washed with cold water. For multistage bleaching, the same procedure was used but repeated three more times. The bleached pulps were then treated with 0.05 mol equi/L nitric acid solution for 1 h at 70 °C, sieved (120 μm mesh size), and exhaustively washed in cold water.

The main objective of these chemical pretreatments was to remove the impurities, hemicellulose, and the lignin surrounding cellulose which allowed the defibrillation and opening of fiber bundles, as shown in Fig. 2.1.

The FTIR characterization (Perkin Elmer FTIR spectrometer, Model System 2000, Perkin Elmer, USA) revealed that lignin content decreased with bleaching and that most of it was removed in the first step (one-stage). This partial removal of cementing components and defibrillations are important steps towards more efficient subsequent hydrolysis step.

CW from coir fibers (CrW) were prepared by sulfuric acid hydrolysis, the most well-known and widely used method for extracting CW from botanical sources. CrW were extracted by a 120-min hydrolysis preceded either by one-stage (CrW1)

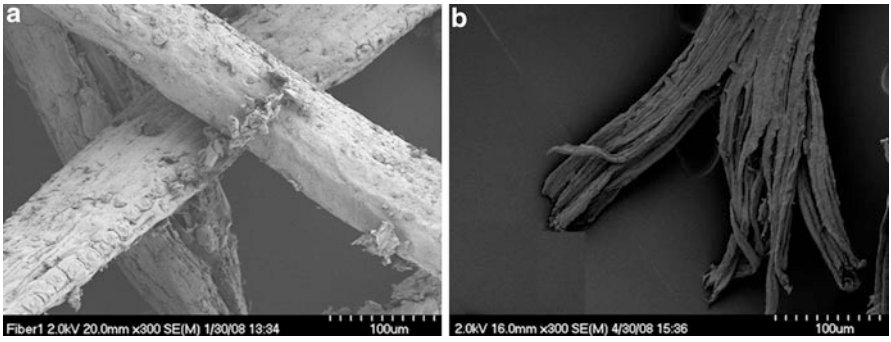

Fig. 2.1 Scanning electron micrographs of (**a**) untreated coir fiber and (**b**) coir fiber subjected to the bleaching process

or multistage bleaching (CrW4) described previously [8]. In brief, bleached fibers were treated in a concentrated sulfuric acid solution (64 wt% sulfuric acid in water) at 45 °C and stirred vigorously for 120 min. The ratio of fibers to acid solution was 1–10 g/ml. After the hydrolysis step, the excess sulfuric acid was removed by washing in water via centrifugation (10,000 rpm, 10 min) followed by the dialysis until constant pH was reached.

3 Properties of Cellulose Whiskers from Coir Fiber

Viscous aqueous suspensions of cellulose whiskers were obtained from coir fibers that appear somewhat brownish in color, indicating that some lignin was still present despite of bleaching treatments. This was confirmed as more aggressive and repeated bleaching process yields more colorless CrW suspensions (CrW1 = dark brown; CrW4 = light brown to yellowish). Remaining residual lignin actually improved the hydrophobicity of CrW making them more compatible with nonpolar polymers such as polyethylene and polypropylene.

A possible correlation between preparation conditions and particle size was not observed. Typically, CrW consisted of ultrathin structures with an average length (L) of 194 ± 70 nm, diameters (D) as low as 4 nm, and high aspect ratio (L/D) of up to 53, which lies in the range of long nano (Fig. 2.2). This high aspect ratio of CrW gives a good reinforcing effect, resulting in improvements in mechanical properties at low loads.

The less vigorous treatment, such as one-stage bleaching, was found to induce a higher thermal stability which was due to remaining lignin. However, there were

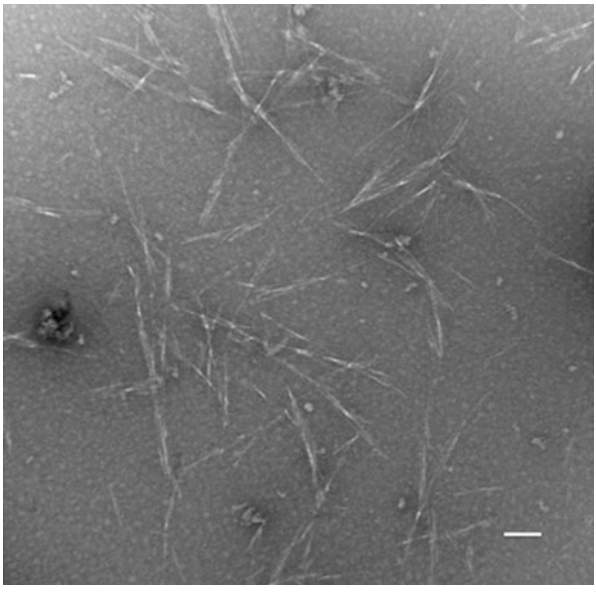

Fig. 2.2 Transmission electron micrographs of CrW. *Scale bars*: 100 nm

no major differences between X-ray diffraction patterns of CrW obtained from the fibers subjected to different bleaching levels, and the crystallinity degree was about 66 % for both samples (Crw1 and CrW4).

4 Applications of Cellulose Nanocrystals from Coir Fiber to Polymer Materials

The composite films were developed from acerola puree and alginate in conjunction with added CW from coir or cotton at various concentrations [10]. In brief, acerola puree was mixed with sodium alginate (Grinsted® FD175, provided by Danisco Brasil Ltda.), CW, distilled water, and corn syrup (Karo, Unilever, São Paulo, SP, Brazil) as plasticizer. Cellulose whiskers from cotton fibers (CtW) were extracted by a 90-min acid hydrolysis, whereas CW from coir fibers (CrW) were extracted by a 120-min hydrolysis, either by one-stage or multistage bleaching process.

The tensile properties and water vapor permeability (WVP) were not significantly affected by the CW type (Table 2.1). With respect to tensile and barrier properties, composite films whether containing CW from coir fiber (either CrW1 or CrW4) or CW from cotton fiber (CtW) were not significantly different. Since lignin is relatively hydrophobic, CtW (without lignin) was expected to show better compatibility with the hydrophilic matrix [11], whereas the CW from coir fiber with remaining residual lignin impaired both tensile and barrier properties. However, CW from coir fiber presented similar performance as those from cotton, which is attributed to the much higher aspect ratios of the former.

Irrespective of the source of CW, the concentration of CW present in films significantly impacted the film's properties (Table 2.1). Increasing the concentration of either CW in formulations yielded films with significantly increased tensile strength and elastic modulus but lower elongation at break (Fig. 2.3). Modulus was the most drastically altered tensile property, having increased by 200 % or more due to the incorporation of CW at 10–15 g/100 g concentration. Such behavior indicates that the whiskers incorporated into the matrix strongly interacted with the biopolymer matrix, restricting its chain motion [12]. Water vapor permeability of the films

Table 2.1 F values resulting from Anova for physical properties of the films

	Source of variation			
Properties	CW type		CW concentration	
Tensile strength	F	1.15	F	50.64
	p	0.33	p	<0.01
Elongation at break	F	0.06	F	54.10
	p	0.94	p	<0.01
Elastic modulus	F	0.13	F	151.11
	p	0.88	p	<0.01
Water vapor permeability	F	2.61	F	65.49
	p	0.08	p	<0.01

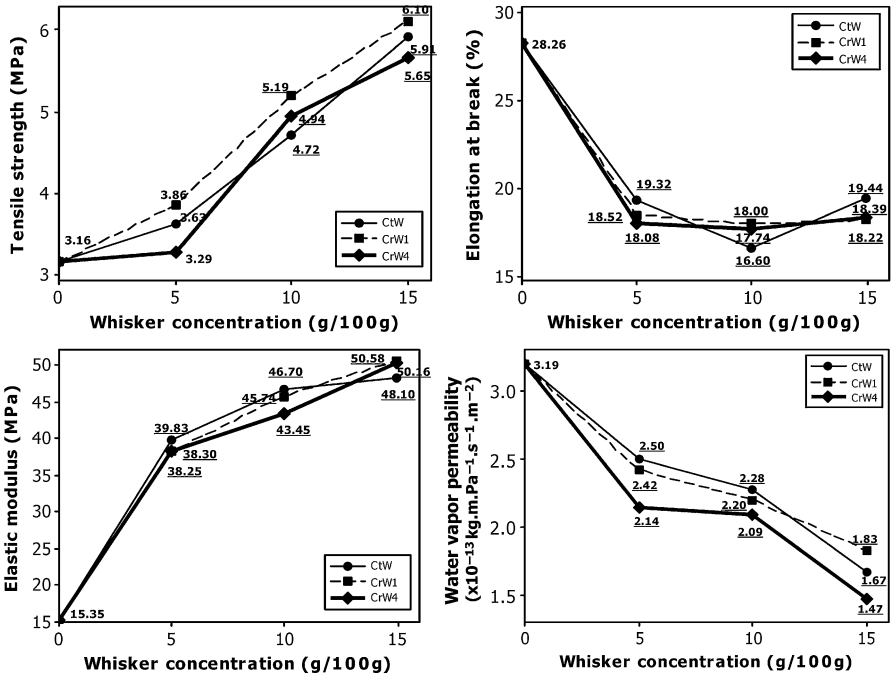

Fig. 2.3 Tensile properties and water vapor permeability of the films containing various concentrations of cellulose whiskers. *CtW* cellulose whiskers from cotton fiber, *CrW1*: cellulose whiskers from coir fiber submitted to one-stage bleaching, *CrW4* cellulose whiskers from coir fiber submitted to multistage bleaching. *Underlined values* were significantly different from those of the control treatment (whisker concentration = 0)

also decreased significantly with increased CW concentration (Fig. 2.3), indicating that the barrier properties were improved by addition of the nanowhiskers.

5 Environmental Evaluation of CrW Extraction Process

The development of nanoparticles extracting processes implies the use of resources and generation of emissions that shall be identified and reduced. It has been recognized that increased research efforts are needed worldwide [13–15] to assess the environmental impacts of nanotechnologies [16].

We also carried out the overall life cycle assessment (LCA) and impact of the process used [8] for the extraction of CW from unripe coir fiber. The intention was to identify environmental hot spots and define improvement options.

The ISO 14040 and 14044 [17, 18] methods were used for evaluating the environmental impacts of the laboratory-scale extraction process used. Environmental evaluations according to this method may consider the whole production chain related to a process or product. In case of evaluating new processes, LCA

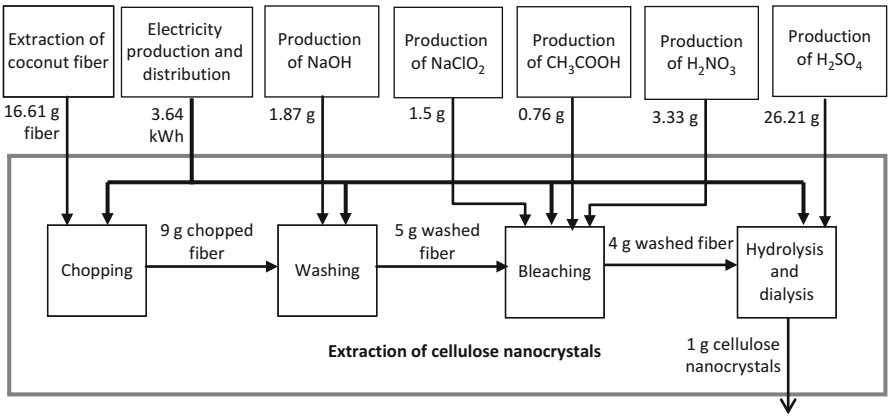

Fig. 2.4 System boundary (cellulose nanocrystals from unripe coconut fiber)

required accounting of all inputs and outputs starting from the production of resource, transportation, preprocessing, materials used, the process itself, and the final disposal of wastes.

The LCA of the process used in this study is presented in Fig. 2.4.

This set of interconnected processes results in the production of CW. The use of resources and generated emissions from the production and distribution of electricity and production of reagents was obtained from the Ecoinvent v2 database [19]. Data regarding resources and emissions from the CW extraction process were measured on site.

From the total amount of coir fiber used for the extraction of 1 g of CW, the yields were quite low (Fig. 2.4). Only 6 % of the unripe coir fibers are converted to CW while this fiber has 28 % of cellulose [20]. This low yield is primarily due to losses occurred during the pretreatment steps. A significant part of the initial mass of coir fibers (77 %) is lost during the grinding, washing, and bleaching steps. Grinding of coir fibers, when only physical modification of this fiber occurs, accounts for 57 % of total fiber loss in the pretreatment steps. As 26 % of the mass of coir fiber used in the hydrolysis step is converted to nanocrystals, there is an opportunity to improve this step further because this mass content is primarily cellulose.

The life cycle inventory analysis of main resources and emissions is presented in Table 2.2, which is based on the extraction of 1 g of nanoparticles. The CW extraction process is responsible for most of the water consumed and polluting load released in water bodies when all processes related to the life cycle of CW are considered. The production and distribution of electricity required by the CW extraction process demand most of the energy and emit a great part of the main greenhouse gases (carbon dioxide, methane, and nitrous oxide).

Energy demand is mostly related to the electricity required to warm up chemical solutions in the washing and hydrolysis stages of the extraction process.

Table 2.2 Life cycle inventory of selected resources and emissions, considering the extraction of 1 g of cellulose nanocrystals

Substance	Unit	Total	Cellulose nanocrystals	Coconut fiber	Sulfuric acid	Nitric acid	Acetic acid	Sodium hydroxide	Sodium chlorite	Electricity
Energy	kJ	15,943.25	0.00	5.78	2.64	0.66	0.87	2.70	8.08	15,922.52
Water	L	135.92	131.65	0.001	1.30	0.01	0.01	0.03	0.38	2.54
BOD	g	3.12	2.48	0.26	0.01	0.01	0.00	0.00	0.01	0.36
COD	g	6.35	5.44	0.45	0.01	0.01	0.00	0.00	0.02	0.41
Furfural	g	0.15	0.15	0.00	0.00	0.00	0.00	0.00	0.00	0.00
HMF	g	77.72	77.72	0.00	0.00	0.00	0.00	0.00	0.00	0.00
Nitrate	g	0.11	0.01	0.00	0.00	0.00	0.00	0.00	0.01	0.09
Total nitrogen	g	0.01	0.01	0.00	0.00	0.00	0.00	0.00	0.00	0.00
Total phosphorus	g	0.005	0.004	0.000	0.000	0.000	0.000	0.000	0.000	0.001
Carbon dioxide	g	941.13	0.00	0.34	3.19	2.15	1.01	2.00	6.48	925.95
Methane	g	8.75	0.00	0.00	0.00	0.00	0.01	0.00	0.02	8.71
Nitrous oxide	g	0.07	0.00	0.00	0.00	0.03	0.00	0.00	0.00	0.04

BOD Biological oxygen demand, *COD* Chemical oxygen demand, *HMF* Hydroxymethylfurfural

Comparing the total energy demanded to make 1 g of CrW (15,943 kJ) to the energy required to make the same quantity of carbon nanotubes (9,635 kJ), carbon nanofibers (10,925–20,000 kJ), or nanoclays (40 kJ), the extraction of CrW appears to be an energy-intensive process [21–23].

Water is mainly consumed to correct pH of CW suspensions during the dialysis stage of the extraction process, with little consumption occurring during the production of chemicals and electricity. Previous study [24] measured the volume of water required during the production of carbon nanotubes using the processes CNT-PFR (0.108 L/g) and CNT-FBR (0.121 L/g). These values are much lower than the volume consumed to extract CrW (131 L/g).

The contamination of water resulting from the nanocrystals extraction process is mainly due to the washing and bleaching of fibers that remove extractives and lignin, releasing organic matter and nutrients that are primarily responsible for the COD, BOD, phenol, and total nitrogen loads. Furfural and HMF loads occur when fiber hydrolysis is performed. The production of furfural and HMF is related primarily to the dehydration of hemicellulose and cellulose at high temperature, especially when subjected to acidic conditions [25].

Life cycle impact assessment shows that the production and distribution of electricity is the main process responsible for impacts on climate change, human toxicity, and eutrophication (Table 2.3). Because 87 % of Brazilian electricity comes from hydroelectric power plants, according to the Ecoinvent database [26], land transformation and the flooding of vegetation during reservoir construction and operation were responsible for the liberation of the higher amounts of carbon dioxide and methane that contribute to climate change.

On the other hand, the production of copper used in the cables that distribute electricity was the main process responsible for the emission of toxic substances and nutrients that lead to human toxicity as well as marine and freshwater eutrophication. The extraction of CrW also generated effluents containing toxic substances and nutrients, as described in the inventory analysis, but the effect of these substances had much lower impact on human toxicity and eutrophication compared to those substances released during the production and distribution of electricity.

The life cycle impact results obtained for CrW can also be compared to the results obtained for carbon nanofibers, considering the categories of climate change and human toxicity were measured in the same units. According to previous study [22], the production of 1 g of carbon nanofibers (using methane as feedstock) impacted climate change in the range of 0.7–1.3 kg of CO_2 equivalent and human toxicity in the range of 0.5–0.53 kg of 1.4-DB equivalent. The values of these impacts obtained for CrW were quite similar to these values.

This environmental assessment shows three main areas of concern that shall be worked to improve the environmental performance of CrW extraction process: yield, water, and electricity demand. Yield may be improved extracting and recovering other substances from coconut fiber such as lignin and hemicellulose. The chopping process must also be reevaluated since most of the fiber is lost in this mechanical procedure. Water is mostly consumed during dialysis but may be

Table 2.3 Life cycle impact assessment, considering the extraction of 1 g of cellulose nanocrystals

	Unit	Total	Extraction of cellulose nanocrystals	Extraction of coconut fiber	Sulfuric acid	Nitric acid	Acetic acid	Sodium hydroxide	Sodium chlorite	Electricity
Climate change	kg CO_2 eq	1.09	0.00	0.00	0.00	0.01	0.00	0.00	0.01	1.06
Freshwater eutrophication	kg P eq	0.0002	0.0000	0.0000	0.0000	0.0000	0.0000	0.0000	0.0000	0.0002
Marine eutrophication	kg N eq	0.0003	0.0000	0.0000	0.0000	0.0000	0.0000	0.0000	0.0000	0.0003
Human toxicity	kg 1,4-DB eq	0.33	0.00	0.00	0.00	0.00	0.00	0.00	0.00	0.32

significantly reduced if a recirculation system is used. Electricity is mainly demanded to warm up chemical solutions during washing and hydrolysis, requiring reevaluation of the adopted time and temperatures used in this process.

We are currently developing a new CrW extraction process. So far, this new process recovers 18 % of the lignin from the coconut fiber, reduces the water usage, and converts 20 % of the coconut fiber into cellulose whiskers. This process also uses hydrogen peroxide (H_2O_2) as an alternative to $NaClO_2$ for bleaching, avoiding possible formation of organochloride compounds. The environmental impact assessment of this improved process is currently being conducted at the Embrapa Tropical Agroindustry located in Fortaleza, Brazil.

6 Conclusions

This chapter highlights our recent research efforts on the production of cellulose whiskers from coir fibers in Brazil and provides information related to their isolation, characterization, and possible application in composites. It has been shown that cellulose whiskers can be successfully extracted from coir fibers via acid hydrolysis and used as an additive in composite films to improve their physical and moisture barrier properties. The LCA evaluation of the extraction process indicated some challenges that need to be overcome to improve environmental compatibility of the process.

References

1. Azizi Samir MAS, Alloin F, Dufresne A (2005) Review of recent research into cellulosic whiskers, their properties and their application in nanocomposite field. Biomacromolecules 6:612
2. Dalmas F, Cavaillé JY, Gauthier C, Chazeau L, Dendievel R (2007) Viscoelastic behavior and electrical properties of flexible nanofiber filled polymer nanocom-posites. Influence of processing conditions. Compos Sci Technol 67:829
3. Qiao R, Brinson C (2009) Simulation of interphase percolation and gradients in polymer nanocomposites. Compos Sci Technol 69:491
4. Jordan J, Jacob KI, Tannenbaum R, Sharaf MA, Jasiuk I (2005) Experimental trends in polymer nanocomposites- A review. Mater Sci Eng A 393:1
5. Satyanarayana KG, Pillai CKS, Sukumaran K, Pillai SGK, Rohatgi PK, Vijayan K (1982) Structure and properties of fibres from various parts of coconut palm. J Mater Sci 17:2453
6. Geethamma VG, Kalaprasad G, Groeninckx G, Thomas S (2005) Dynamic mechanical behavior of short coir fiber reinforced natural rubber composites. ComposPart A Appl Sci Manuf 36(11):1499
7. Corradini E, Morais LC, Rosa MF, Mazzetto SE, Mattoso LH, Agnelli JAM (2006) A Preliminary Study for the Use of Natural Fibers as Reinforcement in Starch-Gluten-Glycerol Matrix. Macromol Symp 245:558
8. Rosa MF, Medeiros ES, Malmonge JA, Gregorski KS, Wood DF, Mattoso LHC, Glenn G, Orts WJ, Imam SH (2010) Cellulose nanowhiskers from coconut husk fibers: effect of preparation conditions on their thermal and morphological behavior. Carbohydr Polym 81:83
9. Wise LE, Murphy M, D'Addieco AA (1946) Chlorite holocellulose, its fractionation and bearing on summative wood analysis and on studies on the hemicelluloses. Paper Trade J 122:35

10. Azeredo HMC, Miranda KWE, Rosa MF, Nascimento DM, De Moura MR (2012) Edible films from alginate-acerola puree reinforced with cellulose whiskers. LWT Food Sci Technol 46:294
11. Kim HJ, Triplett BA (2001) Cotton fiber growth in planta and in vitro. Models for plant cell elongation and cell wall biogenesis. Plant Physiol 127:1361
12. Lu Y, Weng L, Zhang L (2004) Morphology and properties of soy protein isolate thermoplastics reinforced with chitin whiskers. Biomacromolecules 5:1046
13. Karn B, Aguar P (Org.) (2006) Nanotechnology and life cycle assessment: synthesis of results obtained at a workshop. Available at http://www.nanotechproject.org/file_download/168. Accessed 01 May 2011
14. Bauer C, Buchgeister J, Hischier R, Poganietz WR, Schebeck L, Warsen J (2008) Towards a framework for life cycle thinking in the assessment of technology. J Clean Prod 16(8–9):910
15. von Gleich A, Steinfeldt M, Petschow U (2008) A suggested three-tiered approach to assessing the implications of nanotechnology and influencing its development. J Clean Prod 16(8–9):899
16. Helland A, Kastennholz H (2008) Development of nanotechnology in light of sustainability. J Clean Prod 16(8–9):885
17. International Organization for Standardization (ISO) (2006) ISO 14040:2006- Environmental management, life cycle assessment, principles and framework. ISO, Geneva
18. International Organization for Standardization (ISO) (2006) ISO 14044:2006- Environmental management – life cycle assessment – requirements and guidelines. ISO, Geneva
19. Frischknecht R, Jungbluth N (2007) Ecoinvent – overview and methodology. Swiss Centre for Life Cycle Inventories, Dubendorf
20. Corradini E, Rosa MF, Macedo BP, Paladini PD, Mattoso LHC (2009) Chemical composition, thermal and mechanical properties for cultivars of immature coconut fibers. Revista Brasileira de Fruticultura 31(3):837
21. Joshi S (2008) Can nanotechnology improve the sustainability of biobased products? The case of layered silicate biopolymer nanocomposites. J Ind Ecol 12(3):474
22. Khanna V, Bakshi BR, Lee LJ (2008) Carbon nanofiber production: life cycle energy consumption and environmental impact. J Ind Ecol 12(3):394
23. Kushnir D, Sandén BA (2008) Energy requirements of carbon nanoparticle production. J Ind Ecol 12(3):360
24. Singh A, Lou HH, Pike RW, Agboola A, Li X, Hopper JR, Yaws CL (2008) Environmental impact assessment for potential continuous processes for the production of carbon nanotubes. Am J Environ Sci 4(5):522
25. Fengel D, Wegener G (2003) Wood chemistry, ultrastructure, reactions. Ed Verlag Kessel, Remangen
26. Dones R, Bauer C, Bolliger R, Burger B, Faist Emmernergger M, Frichknecht R, Heck T, Jungbluth N, Roder A, Tuchschmid M (2007) Life cycle inventory of energy systems: results for current systems in Switzerland and other UCTE countries: Ecoinvent report no. 5. Paul Scherrer Institut Villigen and Swiss Centre for Life Cycle Inventories, Dubendorf

Biological Synthesis of Nanocrystalline Cellulose by Controlled Hydrolysis of Cotton Fibers and Linters

3

N. Vigneshwaran, P. Satyamurthy, and P. Jain

Contents

Abstract

Particles of cellulose in its nanoform also referred to as nanocrystalline cellulose (NCC) have received increased attention due to their extraordinary mechanical properties such as high Young's modulus and tensile strength. The conventional method of preparation of NCC by concentrated sulfuric acid (65 % w/v) hydrolysis of cellulose is limited due to the environmental hazards posed by the release of toxic effluents. Commercially, NCC is prepared from wood pulp through chemo-mechanical process in which the chemical pretreatment helps in reduction of energy consumption in subsequent mechanical process. Our research group is exploring the possibility for biological synthesis of NCC that provides an eco-friendly alternative to the existing processes. The biological synthesis of NCC refers to the use of cellulose-degrading microbes or their hydrolytic enzymes as agents in the controlled hydrolysis of cellulose to produce NCC. In tropical countries like India, cotton is the major and purest source of cellulose. The non-spinnable cotton fibers and cotton linters are available as raw materials for the production of nanocellulose. Initially, the cotton fibers/linters

N. Vigneshwaran (✉) • P. Satyamurthy • P. Jain
Central Institute for Research on Cotton Technology, Matunga, Mumbai, India
e-mail: nvw75@yahoo.com; sprasad1986@gmail.com; pjainbom07@yahoo.com

J.K. Pandey et al. (eds.), *Handbook of Polymer Nanocomposites. Processing, Performance and Application – Volume C: Polymer Nanocomposites of Cellulose Nanoparticles*,
DOI 10.1007/978-3-642-45232-1_62,

are converted into microcrystalline cellulose (MCC) having the average size of 50 um. Then, they are subjected to controlled hydrolysis by *Trichoderma reesei* (anamorph of *Hypocrea jecorina*) or its purified enzyme (cellulases) resulting in the formation of NCC. Cellulases are a group of multicomponent enzyme system comprised usually of three components that act synergistically in the hydrolysis of cellulose: endoglucanases (EC 3.2.1.4), cellobiohydrolase (EC 3.2.1.91), and cellobiase (β-glucosidase, EC 3.2.1.91). Unlike the conventional acid hydrolysis process which results in the surface modification of NCC with sulfate groups, the surface of NCC produced by using the biological method is not modified and retains the original chemical structure of cellulose. Thus, nanocellulose/NCC is an interesting group of sustainable biopolymeric nanomaterials having potential application in various fields, and the biological method offers a novel eco-friendly method for their synthesis.

Keywords
Biological Synthesis • Cellulase Enzyme • Cotton Fibers • Linters • Nanocrystalline Cellulose

1 Introduction

Cellulose is an organic compound found abundantly in nature. It is chemically a homopolymer of 1, 4-D-glucose molecules linked together to form a linear chain polymer. Among various sources of cellulose such as plants, algae, marine creatures, and bacteria, plants form a major source of cellulose with cellulose forming the primary cell wall component in green plants. Cotton has the highest cellulose content, and the cellulosic content of cotton is 90 %, and the cellulose content of wood is about 40–50 % [1]. From the industrial point of view, the major source of cellulose is from wood pulp and cotton. It is mainly used in the production of paperboard and paper and is also converted into wide variety of derivative products such as cellophane and rayon. Cotton linters are fine, silky fibers which adhere to the seeds of the cotton plant after ginning. These curly fibers typically are less than 1/8 in. (3 mm) long. These cotton linters are traditionally used in the manufacture of paper and as a raw material for cellulose production.

Cellulose can be hydrolyzed chemically by using strong acids, and biologically cellulose is broken down by hydrolytic enzymes produced by a variety of microorganisms collectively referred to as cellulases. The complete hydrolysis of cellulose results in the production of its constitutive monomer glucose, which can be used for the production of ethanol [2], organic acids [3], and other chemicals [4]. In the presence of strong acids or mechanical forces, native cellulose can be broken down into micro- and further into nanocrystalline cellulose whose morphology is generally in the form of whiskers. Acid hydrolysis of cellulose is a well-known process where in the acid hydrolysis results in the breakdown of amorphous regions of cellulose and enables the isolation of crystallites [5]. These crystallites of cellulose known as nanocrystalline cellulose (NCC) have attracted a lot of

interest over the past decade due to their excellent mechanical properties such as high Young's modulus and mechanical strength. The Young's modulus of NCC is as high as 134 GPa while the tensile strength of the crystal structure was estimated in the range of 0.8–10 GPa [6]. Thus, NCC is a novel class of cellulosic material that combines both the properties of biodegradability, nontoxicity, and renewable nature of cellulose along with enhanced mechanical properties at the nano-level. Even though the most widely used method for the production of NCC is the acid hydrolysis method where in an acid is used for the hydrolysis of cellulose into its nanoform, it is limited from the environmental point of view due to the release of toxic waste products into the environment after hydrolysis. Also the acid hydrolysis of cellulose by using sulfuric acid results in the surface modification of cellulose by introduction of the sulfate groups on the surface of cellulose [7]. The other methods of production of NCC such as the mechanical and chemical processes are highly energy intensive and require a huge energy input for the production of NCC. Hence, a biological process for the production of NCC provides an eco-friendly cost-effective alternative for the production of NCC. NCC can be produced by a biological process where in an agent of biological origin such as microbe itself or an enzyme produced by the microbe hydrolyses cellulose reducing its size from the micro size to the nanometer level resulting in production NCC.

2 Biological Production of Nanocrystalline Cellulose (NCC)

Microorganisms have been widely used for carrying out various chemical reactions having their application in a variety of industrial processes. Thus, a biological process for the production of NCC involves the use of a biological agent for the controlled hydrolysis of cellulose ultimately resulting in the production of NCC. NCC can be produced by a biological process wherein an agent of biological origin such as microbe itself or a product produced by the biological agent such as enzyme hydrolyses cellulose from its original size down to nanometer level.

2.1 Cellulases: Production and Mode of Action

Cellulases are a group of multicomponent enzyme system generally secreted by cellulolytic microorganism. These cellulases help the organisms to use cellulose as a source of carbon for their growth and metabolism by converting the water-insoluble cellulose into its water-soluble monomer glucose. The secretion of cellulase by these microorganisms is affected by various physical factors such as pH, temperature, time of incubation, and nature of substrate which in turn affect the hydrolysis of cellulose by these microorganisms. These physical factors can be varied to control the hydrolysis of cellulose so that the end product of hydrolysis is more of NCC.

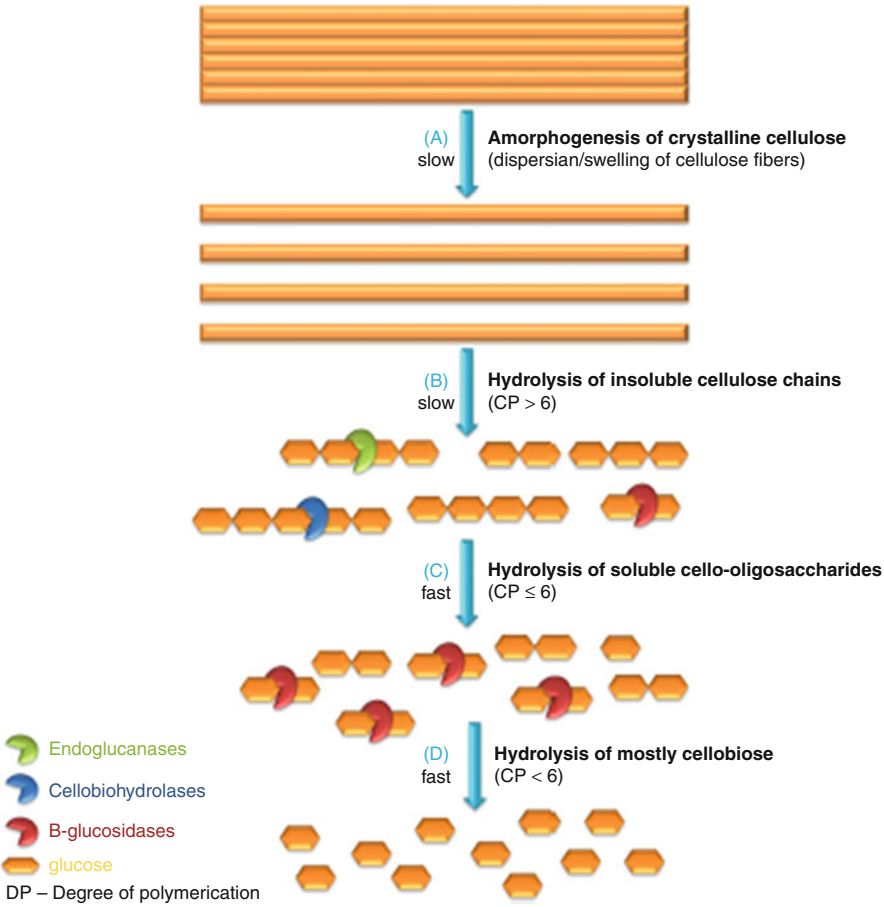

Fig. 3.1 Sequential hydrolysis of cellulose by three components of cellulase enzyme resulting in the production of glucose molecules [9]

Cellulases consist of at least three classes of enzymes, working together to degrade cellulosic material. Endo-1,4-β-D-glucanases (EG, EC 3.2.1.4) hydrolyze internal β-1,4-glucosidic bonds in the cellulose chain, presumably acting mainly on the amorphous or disordered regions of cellulose. Exo-1,4-β-D-glucanases, also called cellobiohydrolases (CBH, EC 3.2.1.91), cleave off cellobiose units from the ends of cellulose chains. Hydrolysis to the final product is accomplished by 1, 4-β-D-glucosidases (BG, EC 3.2.1.21), [8] which hydrolyze cellobiose to glucose and also cleave off glucose units from the various soluble cello-oligosaccharides. BG activity has often been found to be rate limiting in enzyme cocktails during enzymatic hydrolysis of cellulose. Each of these components consists of a catalytic or active site that acts on the substrate and carries out the hydrolytic reaction (Fig. 3.1).

There are two sites in the enzymes which mediate binding: the active site of the catalytic domain and the separately folded and functionally independent carbohydrate-binding module (CBM) which usually is attached through a PTS box. This linker may act as a flexible arm, connecting the two functional parts of the protein but leaving (limited) freedom for the catalytic domain to move around the binding module fixed to the substrate surface. The essential function of the CBM was shown for cellobiohydrolase CBH I from *T. reesei*, for which a detailed three-dimensional model was constructed. The catalytic domain without the CBM (the core enzyme) has a very limited overall action on cellulose. The deletion of CBMs has no effect for activity on soluble substrates (like CMC or barley ß-glucan) where the possible sites of activity on the substrate are not limited. This behavior was confirmed by the characterization of genetically engineered deletion mutants [10].

2.2 Production of NCC by Controlled Microbial Hydrolysis of Cellulose

A microbial process for the synthesis of nanocellulose was described previously wherein NCC was synthesized from microcrystalline cellulose by controlled hydrolysis using the filamentous fungi *Trichoderma reesei* [6]. In this process, the raw material (cotton fiber) was initially converted into microcrystalline cellulose (MCC). This MCC was further hydrolyzed microbially to produce NCC. For the production of NCC, the 24-h inoculum of the fungus *Trichoderma reesei* (ATCC 13631) was prepared in potato dextrose broth by inoculation of spore suspension ($\sim 3 \times 106$ spores/ml). The optimized concentration of inoculum was added in Mandel's medium containing MCC as the sole carbon source and was incubated at 25 °C under shaking condition at 150 rpm.

Unlike other fungus that also can degrade cellulosic biomass like the brown rot fungi which constitutively produce peroxidases in combination with cellulase, *Trichoderma reesei* does not produce peroxidases but only produces cellulases resulting in the degradation of cellulose [11]. This makes *T. reesei* a better candidate for the production of NCC; also it uses the free enzyme mechanism for the degradation of cellulose wherein the cellulase enzyme is secreted extracellularly into the medium, and these cellulases posses the carbohydrate-binding module (CBM) joined by a flexible linker to one end of the catalytic domain, and the cellulases that are present as mixture of multicomponent enzyme systems act synergistically to degrade highly crystalline cellulose [12]. This extracellular production of cellulases is affected by many external factors such as pH, temperature, and substrate concentration that can be manipulated for the controlled hydrolysis of cellulose.

2.2.1 Continuous Batch Process for the Production of Nanocellulose

The major objective of the cellulose-degrading microbes is the formation of the end product glucose that has to be utilized for its growth. Thus, under optimal

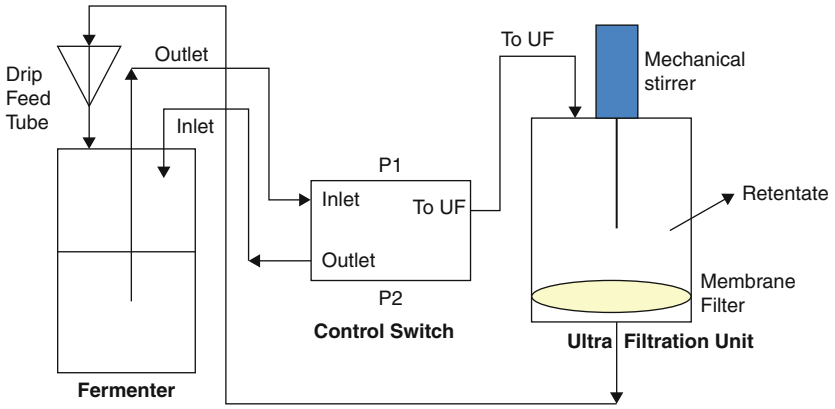

Fig. 3.2 A schematic representation of continuous batch process for nanocellulose production. While cellulose hydrolysis is being carried out in the fermentor, ultrafiltration helps in simultaneous removal of the NCC

conditions, the yield of nanocellulose by microbial hydrolysis is very low. So one of the strategies for increasing the yield of nanocellulose is the continuous removal of nanocellulose as and when it is formed, thus increasing the yield of nanocellulose. A batch fermentation system (Fig. 3.2) for the continuous removal of nanocellulose and its purification is developed, which is a combination of a fermenter coupled with a filtration system with a flow control valve that works on the principle of positive pressure for movement of liquid in the system. In this system, the supernatant from the fermenter containing the cellulose nanocrystals is transferred to the filtration system wherein the cellulose nanocrystals get trapped in the membrane retentate and the filtrate containing the other soluble media components is fed back into the fermenter, thus enabling the continuous separation of cellulose nanocrystals as they are formed preventing their further hydrolysis into the end product of glucose.

2.3 Purification and Characterization of NCC Produced by Microbial Hydrolysis

The nanocellulose formed during the biological process is mixed along with many other impurities such as the biological agents like microbes, enzymes, and many soluble media components. Thus, purification of NCC produced by biological process is an essential step in the production of NCC by biological processes. In the production of NCC by microbial hydrolysis of MCC by the fungus *Trichoderma Reesei*, after fermentation, the broth was subjected to differential centrifugation for

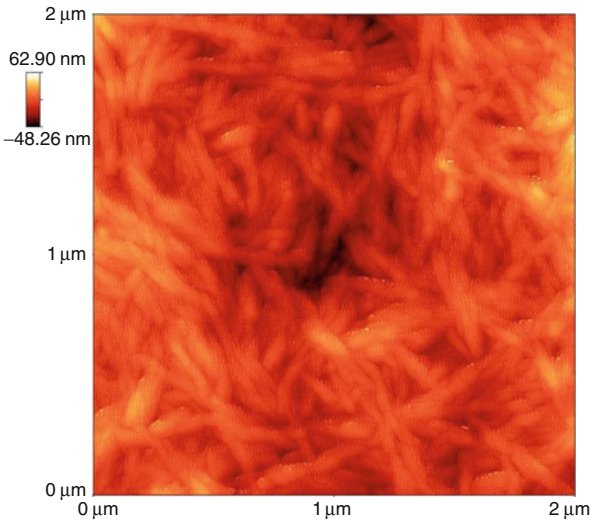

Fig. 3.3 AFM image of NCC produced by controlled microbial hydrolysis

the sedimentation of all particles of size greater than 1 µm. The resultant supernatant was filtered through 100 kDa ultrafiltration membrane by vacuum suction wherein water and lower-molecular-weight solutes pass through the membrane and the NCC which was retained on the surface of membrane was removed with a jet of ultrapure water [6]. Thus, differential centrifugation combined with ultrafiltration was reported to be a good method for the purification of NCC which may also be adopted for the purification of any other nanoparticle synthesized by the biological route. The size and morphology of the purified NCC as analyzed by atomic force microscopy are given in Fig. 3.3.

The particle size distribution as analyzed by dynamic light scattering particle size analyzer is given in Fig. 3.4.

2.4 Production of NCC by Enzymatic Hydrolysis of Cellulose

There are various ways of producing cellulose in nanoform which can be broadly classified as mechanical, chemical, and biological. Among them mechanical methods which are necessarily top-down approaches, although afford better yields, are very expensive and energy intensive. Biological methods [13] involving using cultures of bacteria and fungi are very time consuming. A more feasible route is chemical hydrolysis of cellulose by acids, bases, and oxidation reagents to produce cellulose nanoparticles. However, the use of these routes has a number of critical drawbacks such as corrosivity, surface modification of cellulose, and environmental incompatibility. Enzyme-based hydrolysis of cellulose is potentially an efficient way to produce nanocellulose. Such process will generate negligible effluents and is suitable for producing nanocellulose at low-energy cost.

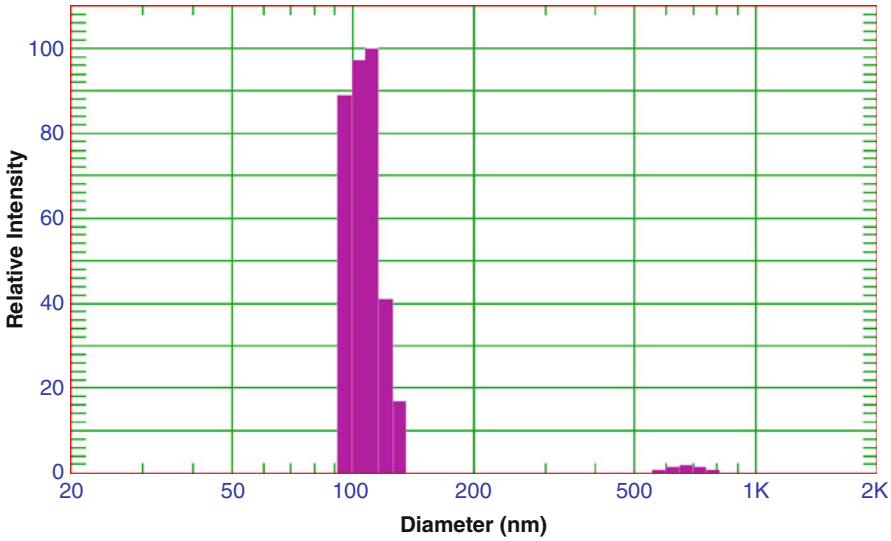

Fig. 3.4 Particle size distribution of NCC produced by controlled microbial hydrolysis

Several enzymes act as natural catalysts for modification of cellulosic materials. Today several commercial preparations are available for biostoning and biofinishing of cotton fabrics that utilize enzymes. Cellulase is a typical example of one such enzyme that can specifically hydrolyze the glycosidic bonds in cellulose. They can act on macromolecular cellulose chains and under controlled conditions shred it down to nano-dimensional size.

The long cellulose polymer chains are depolymerized, by the combined action of three enzyme components. The hydrolysis rate is dependent on a lot of factors such as temperature, pH of medium, enzyme concentration, and substrate concentration. Available literature studies indicate that the cellulase activity (acid cellulases) is highest in the temperature range of 45–50 °C and pH maintained at 4.8. Generally, the substrate concentration is in large excess so as to reduce nonproductive binding [14] of enzymes on the substrate surface. Also the initial rate of reaction is the fastest [15] and accounts for the maximum reactant utilization. During this period, rapid hydrolysis of cellulose molecules takes place. The extent of hydrolysis depends on the reaction time for which the substrate and the enzyme are allowed to interact. The objective of harvesting nanocellulose can be achieved by disrupting the hydrolysis process. This can be achieved by disengaging the enzyme (by denaturation) from the partially hydrolyzed substrate or segregating the partially hydrolyzed cellulose (by ultrafiltration). In this way cellulose nanoparticles may be obtained by separation and the process may be repeated on the unhydrolyzed cellulosic material to increase the yield.

The enzymatic hydrolysis of cellulosic substrate to generate nanocellulose is a very unique approach. There is a vast amount of literature that focuses on production of biofuel from cellulosic material by enzymatic hydrolysis, and

a handful of reports also mention using enzyme cocktails as pretreatments prior to treatment with other reagents. One of the first reports for the preparation of nanocellulose [16] of ~50 nm diameter was by hydrolysis of microcrystalline cellulose using cellulase enzyme. The enzymatic hydrolysis route for generating nanocellulose is not routinely followed since the difficulty lies in maintaining proper conditions for the hydrolysis and periodically harvesting the nanocellulose produced before it gets hydrolyzed further to soluble sugars. Other hurdles, besides high cost of enzyme and low yields, such as loss of enzyme activity due to denaturation and inhibition lead to nonuniform hydrolysis. This results in a broad size distribution of nanocellulose and limits its applications in specialized areas. In spite of these drawbacks, this method is attracting attention mainly due to lesser energy and financial input and most significantly its eco-friendly nature.

Thus, enzymes can be conveniently adapted for biological synthesis of nanocellulose. And with further optimization of operating conditions, this process can be scaled up for industrial-scale production of nanocellulose. The process can further be made more efficient by recycling the spent enzyme. With increased production, low operating costs, and its eco-friendly nature, this process may become the process of choice for the production of nanocellulose.

3 Conclusion

The biological method for the synthesis of nanocellulose opens up a novel eco-friendly method for the synthesis, yet the major bottleneck is the comparatively low yield of NCC than that of commercially established chemo-mechanical process. With the scope of producing nanocellulose with low-energy consumption and using NCC in high-value products, the low yield of NCC by biological route can be compensated for. Also, the yield of NCC can be improved considerably by using a continuous system of production. Overall, the biological route for NCC production shows a lot of promise for commercial exploitation for application in diversified fields.

References

1. Ververis C, Georghiou K, Christodoulakis N, Santas P, Santas R (2004) Fiber dimensions, lignin and cellulose content of various plant materials and their suitability for paper production. Ind Crops Prod 19:245
2. Olsson L, Hahn-Hagerdahl B (1996) Fermentation of lignocellulosic hydrolysates for ethanol production. Enzyme Microb Technol 18:312
3. Luo J, Xia LM, Lin JP, Cen PL (1997) Kinetics of simultaneous saccharification and lactic acid fermentation processes. Biotechnol Prog 13:762
4. Cao NJ, Xia YK, Gong CS, Tsao GT (1997) Production of 2,3- butanediol from pretreated corn cob by Klebsiella oxytoca in the presence of fungal cellulase. Appl Biochem Biotechnol 63:129
5. Krishnamachari P, Hashaikeh R, Chiesa M, Gad ER (2012) Effects of acid hydrolysis time on cellulose nanocrystals properties: nanoindentation and thermogravimetric studies. Cellul Chem Technol 46(1–2):13

6. Prasad S, Prateek J, Balasubramanya RH, Vigneshwaran N (2011) Preparation and characterization of cellulose nanowhiskers from cotton fibres by controlled microbial hydrolysis. Carbohydr Polym 83:122
7. Araki J, Wada M, Kuga S, Okana T (1998) Flow properties of microcrystalline cellulose suspension prepared by acid treatment of native cellulose. Colloids Surf A 42(1):75
8. Andersen N, Johansen KS, Michelsen M, Stenby EH, Krogh KBRM, Olsson L (2008) Hydrolysis of cellulose using mono-component enzymes shows synergy during hydrolysis of phosphoric acid swollen cellulose (PASC), but competition on avicel. Enzyme Microb Technol 42:362
9. Coughlan MP (1985) The properties of fungal and bacterial cellulases with comment on their production and application. In: Russell GE (ed) Biotechnology and genetic engineering reviews, vol 3. Interscience, Newcastle-upon-Tyne, p 37
10. Schwarz WH (2001) The cellulosome and cellulose degradation by anaerobic bacteria. Appl Microbiol Biotechnol 56:634
11. Martınez AT, Speranza M, Ruiz-Duen FJ, Ferreira P, Camarero S, Guille F, Martı´nez MJ, Gutierrez A, del Rıo JC (2005) Biodegradation of lignocellulosics: microbial, chemical, and enzymatic aspects of the fungal attack of lignin. Int J Microbiol 8:195
12. Wilson DB (2011) Microbial diversity of cellulose hydrolysis. Curr Opin Microbiol 14:1
13. Bismarck A, Juntaro J, Mantalaris A, Pommet M, Shaffer MSP (2011) Material comprising microbially synthesized cellulose associated with a support like a polymer and/or fiber. US 2011/0021701 A1
14. Qing Q, Yang B, Wyman CE (2010) Impact of surfactants on pretreatment of corn stover. Bioresour Technol 101:5941
15. Lu Y, Yang B, Gregg D, Saddler JN, Mansfield SD (2002) Cellulase adsorption and an evaluation of enzyme recycle during hydrolysis of steam-exploded softwood residues. Appl Biochem Biotechnol 98–100:641
16. Parlikar KM, Bhatawdekar SP (1984) Hydrolysis of cotton fibers by cellulase enzyme. J Appl Polym Sci 29:2573

Isolation and Characterization of Cellulose Nanofibers from the Aquatic Weed Water Hyacinth: *Eichhornia crassipes*

4

Thiripura Sundari Marimuthu and Ramesh Atmakuru

Contents

Abstract

The water hyacinth is one of the fast growing perennial aquatic weeds with a height of 1 m and doubles their population in 2 weeks and is rich in fiber content. The cellulose nanofibers from the water blocking aquatic weed – water hyacinth – were successfully prepared. The crude and pure cellulose microfibers were initially obtained from the weed plant using the chemical treatments such as bleaching and alkaline and sodium chlorite reactions. The micron-sized fibers obtained from the stems were cryocrushed with liquid nitrogen to release the bundles of nanofibers and followed the sonication for individualization of fibers. The treated fibers were screened through Fourier transform infrared spectroscopy (FTIR) to confirm the removal of impurities from the fibers. The surface morphology of the aqueous suspension before cryocrushing and

T.S. Marimuthu (✉) • R. Atmakuru
Department of Analytical Chemistry, International Institute of Biotechnology and Toxicology (IIBAT), Padappai, Kancheepuram, Tamilnadu, India
e-mail: thiripu@gmail.com; raamesh_a@yahoo.co.in

J.K. Pandey et al. (eds.), *Handbook of Polymer Nanocomposites. Processing, Performance and Application – Volume C: Polymer Nanocomposites of Cellulose Nanoparticles*,
DOI 10.1007/978-3-642-45232-1_55,

after the sonication process was investigated using scanning electron microscopy (SEM) and transmission electron microscopy (TEM) techniques. Thermal stability of the fiber was increased after chemical treatment; this was confirmed by thermogravimetric analysis (TGA). The synthesized nanofibers were in a diameter range of 20–100 nm from the SEM and 25 nm from the TEM analysis. The extracted cellulose nanofibers from the noxious weeds were used for processing of biodegradable nanocomposites in drug delivery, ligament substitute, filtration, and water purification and also used as flexible optical display in electronics.

Keywords
Aquatic weed • *Eichhornia crassipes* • Water hyacinth • Nanofibers

1 Introduction

Nanofibers obtained from fiber-based natural sources have major potential applications in preparation of reinforced composites, biodegradable thin films, adsorbents, filters, etc. Nanofibers are synthesized from these natural plant-based fiber resources following different methods like a combination of chemical and mechanical treatment, enzymatic treatment, oxidative reaction, and electrospinning.

Extraction of cellulose nanofibers was reported from sources like hemp fiber [1], soya bean [2], sugar beet pulp [3], wheat straw and soy hulls [4], sugarcane bagasse [5], sisal [6], banana rachis [7], cassava bagasse [8], wood flour [9], raw kenaf fibers [10], flax fibers [11], softwood, rice straw and potato tuber [12], cotton [13], oil palm empty fruit bunch [14], and refined, bleached beech pulp [15]. The combination of enzymatic treatment and mechanical shearing resulted in preparation of microfibrillated cellulose (MFC) nanofibers from commercial bleached wood sulfite pulps [16]. Electrospinning setup is the latest and the easiest technology for the nanofiber production; it can be used to directly spin from the polymer solutions [17, 18]. The TEMPO (2,2,6,6-tetramethylpiperidine-1-oxy radical)-mediated catalytic oxidation method was used to produce nanofibers from native celluloses in aqueous conditions under alkaline pH. This is the selective oxidization process of converting C6 primary hydroxyl groups of fiber into carboxylate groups via aldehyde mechanism under appropriate conditions [19]. A viscous and transparent gel was obtained by agitating the oxidized cellulose fiber in a blender-type homogenizer or ultrasonic homogenizer [20, 21]. The gel has individual nanofibers of 4–6 nm [22] in width. The water insoluble fractions of oxidized celluloses were used for the determination of carboxyl and aldehyde content [23], and transparent films were prepared by filtration of TEMPO-oxidized cellulose nanofiber through polytetrafluoroethylene (PTFE) membrane [20].

The literature indicates the extensive preparation of nanofibers from various sources of plants, fruits, vegetables, etc.; however, there are no data indicating the utilization of deadly aquatic weeds. The abundant aquatic weed species *Eichhornia crassipes* (water hyacinth) in tropical weather conditions is a major problem in open water bodies like

power generation, irrigation, and boating. Huge amounts are being spent worldwide to selectively remove the weed. The weed is rich in fiber content and has no major differences in the percentage of cellulose content in the shoot and root [24].

In this chapter, *E. crassipes* used as fiber sources for the extraction of cellulose nanofibers is described. The cellulose nanofibers are isolated using the chemical and mechanical treatments. The characterization of these nanofibers was done by SEM, TEM, FTIR, and TGA. The synthesized nanofibers from the above method have a diameter range of 20–100 nm and are of several micrometers in length. The isolated nanofibers have future use for the preparation of bionanocomposites films.

2 Isolation of Water Hyacinth Nanofibers (WHNFs)

Water hyacinth weeds were used as a source of cellulose fibers collected from the local ponds of Tamil Nadu, India. The stems were washed with water, dried, chopped, and stored at room temperature.

2.1 Chemical Treatment

The chopped water hyacinth weeds were dewaxed in a Soxhlet apparatus with 2:1 (v/v) mixture of toluene/ethanol for 6 h. The dewaxed fibers were bleached and boiled with 3 wt% sodium chlorite solutions under acidic condition at pH 4. The suspension was maintained for 3 h at 80 °C and allowed to settle overnight. The bleaching process was repeated twice, washed with distilled water until free from acid, and the white tissues were obtained. The hemicelluloses were removed from the tissues by treating them with 1 wt% of sodium hydroxide solution at 60 °C for 24 h. The samples were centrifuged and washed with distilled water. The lignin was removed by further treatment with 1 wt% sodium chlorite solution under acidic condition and stirred well at 75 °C for 48 h; the samples were centrifuged and washed with distilled water. The remaining hemicelluloses were removed and resulted in pure cellulose fibers by treating with 5 % of NaOH solution at 55 °C for 24 h with continuous stirring. Finally, the obtained residues were centrifuged and washed with distilled water till free from alkali.

2.2 Mechanical Treatment

The chemically treated samples were further broken down into fragments by the mechanical treatment using high shear, high energy transfer, and high impact [25].

The purified cellulose fibers were obtained from the chemical process, dried at 100 °C for 24 h, followed by micronization of water hyacinth fibers using a centrifugal ball mill (Retsch PM100, Germany). In a 50 ml cap, 5 g of sample with 10 pieces of 10 mm of Agate balls was used and centrifuged for 20 min at 550 rpm/min.

The ball milled fibers were dispersed in water, and then nanofibers were released by cryocrushing in a mortar with a pestle by applying high impact then ultrasonicated for 15 min to obtain the uniform dispersion of nanofibers in water. The sonicated suspensions were lyophilized to obtain the cellulose nanofiber.

3 WHNF Morphology Evaluated by Scanning Electron Microscopy (SEM) and Optical Microscopy

The morphology of the cellulose fibers and nanofibers was investigated using Shimadzu scanning electron microscopy. The obtained samples after the chemical and mechanical treatments were mounted in aluminum stub, coated with platinum/gold by an ion sputter coater to prevent charging and scanned using SEM. From the SEM images, the diameters were calculated using the image tool analyzer.

The cellulose fibers were obtained by successive treatments of raw water hyacinth fibers for the removal of hemicelluloses, lignin, pectin, and other soluble components using acidified sodium chlorite and sodium hydroxide solutions. A bleached water hyacinth fiber is in the size 25–50 μm (Fig. 4.1).

The fiber morphology was observed using the optical microscopy (Zeiss, Germany). Optical micrographs (at different magnifications; Fig. 4.2a, b) reveal that the chemical treatment resulted in the bundles of fibers and in which the hemicelluloses, lignin, and the other solubilized impurities were removed.

After the chemical treatment, the fibers in the SEM image (Fig. 4.3a) at 4 K magnification represent the individual cellulose fibers at a diameter of 7 μm and (Fig. 4.3b) at 3 K magnifications show the clusters of fibers with a diameter range of one to two micrometers and lengths in several microns.

During the mechanical treatment, cellulose fibers were ball milled in which the fibers were reduced in size up to submicron level, followed by cryocrushing process that has resulted the agglomeration of fibers and moderately reduced the fiber sizes. The cryocrushed fibers were sonicated for 15 min to obtain the uniformly dispersed and individualized nanofibers. The SEM image shows that the size of the nanofiber from the suspension was measured to be 20–100 nm in diameter at 40 K magnification (Fig. 4.4a). The structure of these resulting nanofibers was obtained as network-like structure.

4 WHNF Morphology Evaluated by Transmission Electron Microscopy (TEM)

The morphology of the cellulose nanofibers was also investigated using transmission electron microscopy. A single drop of diluted nanofiber suspension was mounted in a carbon-coated grid and placed in transmission electron microscopy (TEM), operating at 20–200 kV with a resolution of 2.4 Å, and the TEM images were captured, and the fiber diameters were calculated using the image tool analyzer.

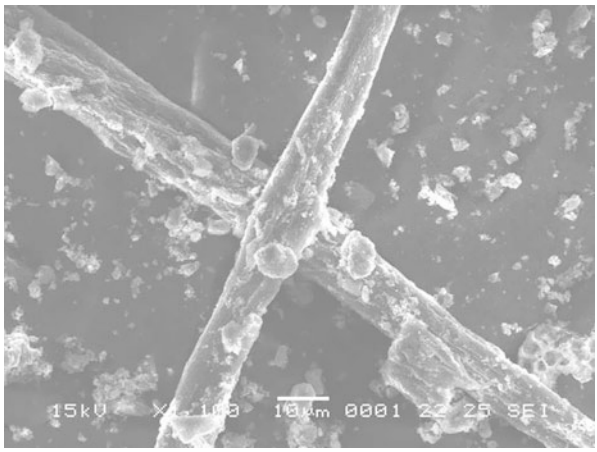

Fig. 4.1 SEM image of bleached raw water hyacinth fibers

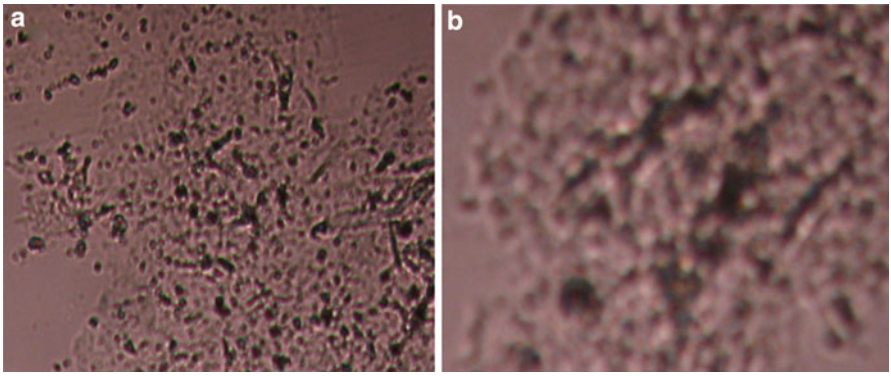

Fig. 4.2 Obtain the purified cellulose fibers from the successive chemical treatment of crude fibers evidenced by an optical micrographic image (**a**) at 10×, (**b**) at 100× magnifications

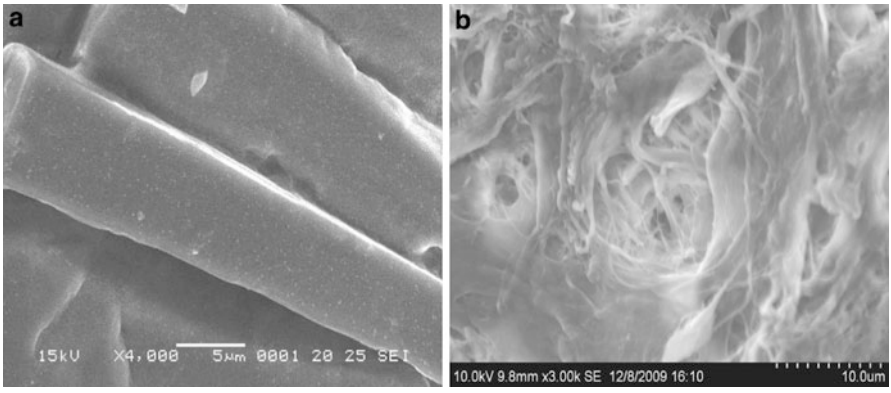

Fig. 4.3 SEM images (**a**) at 4K and (**b**) at 3K magnifications

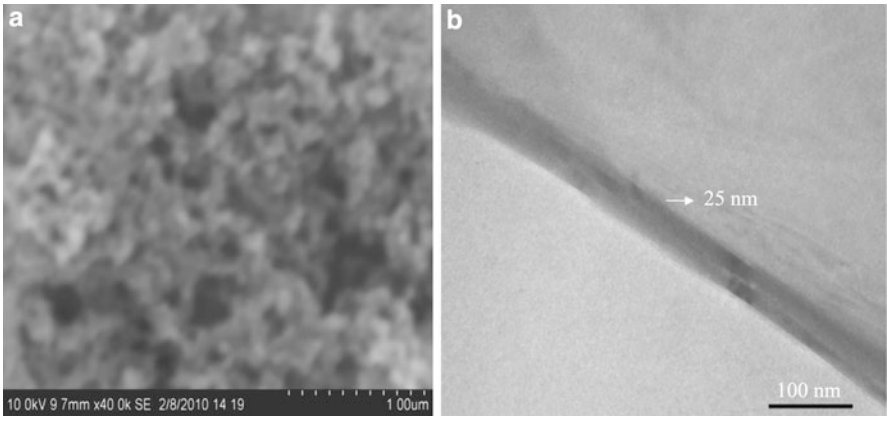

Fig. 4.4 (**a**) SEM image of bundles of cellulose nanofibers before sonication showing <100 nm; (**b**) TEM image showing a single cellulose nanofiber after sonication with a diameter of 25 nm

The TEM image of water hyacinth cellulose nanofibers after the mechanical process was shown in Fig. 4.4b. The sonication process has resulted in the individualization of fibers with a diameter of 25 nm and its length in few microns.

5 WHNF Chemical Composition Assessed by Fourier Transform Infrared Spectroscopy (FTIR)

The FTIR spectroscopy was used to examine the changes in the chemical composition of the chemically treated fibers obtained from water hyacinth. The dried samples of the original crude and treated fibers were crushed into powder, and a thin pellet was made by mixing with potassium bromide (KBr) and scanned in Shimadzu Fourier transform infrared spectroscopy (FTIR 8400S) to obtain the FTIR spectra. The spectrum was obtained in the transmission mode and the range of 4000–400 cm^{-1} at a resolution of 4 cm^{-1} with 40 scans per sample.

The FTIR spectrum of crude fibers and nanofibers from water hyacinth was shown in the Fig. 4.5. The peaks at around 3,400 and 2,900 cm^{-1} are due to –OH and –CH stretching vibration. In the crude fiber, the peak at 1,735 cm^{-1} was observed due to the acetyl and uronic ester linkage of carboxylic group of the ferulic and p-coumaric acids of lignin and/or hemicelluloses. This peak was disappeared in the nanofibers after the chemical and mechanical treatment. The peak at 1,512 cm^{-1} was observed in the original crude fiber; it indicates the C = C stretching of aromatic rings of lignin, but in the treated one, it was disappeared due to the partial removal of lignin [26–28].

In the original fiber, the peak at 1,637 cm^{-1} represents the adsorbed water, and this peak was decreased in the nanofibers due to the removal of hemicelluloses. In the FTIR spectrum of nanofiber, the peaks observed at 1,060 and 896 cm^{-1} were attributed to C–O stretching and C–H rocking vibration of cellulose structure [4].

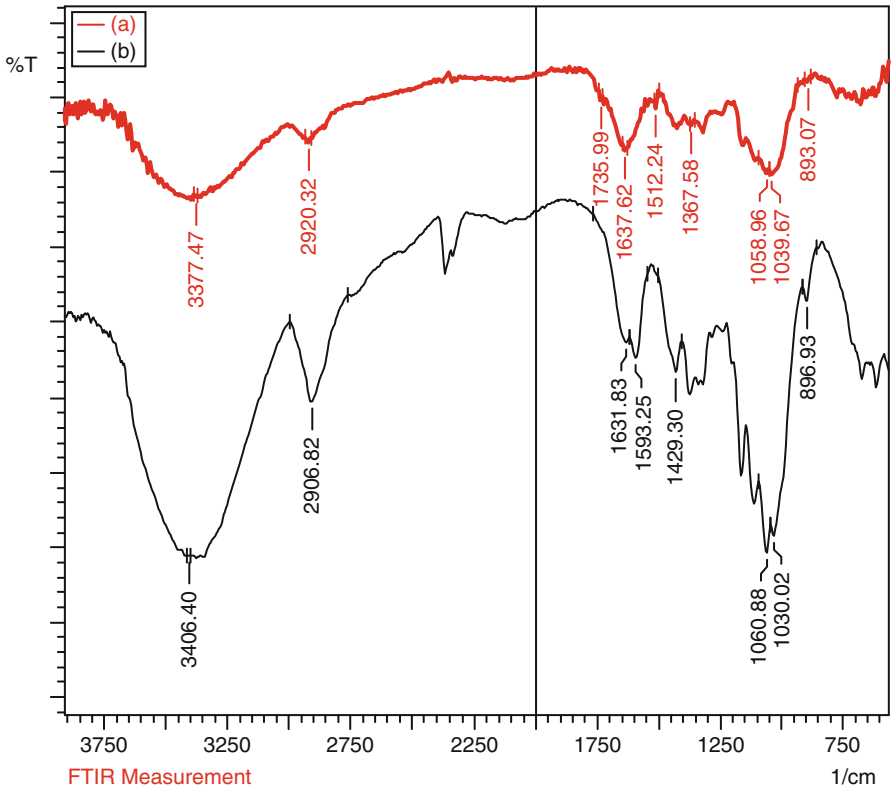

Fig. 4.5 FTIR spectra of (*a*) original crude fibers and (*b*) cellulose nanofibers of water hyacinth

6 WHNF Thermal Stability Assessed by Thermogravimetric Analysis (TGA)

Using a thermogravimetric analyzer (TGA), the thermal characteristics of the original crude and treated cellulose fibers were studied at a temperature range of 50–700 °C in a nitrogen atmosphere at a heating rate of 20 °C/min.

The results obtained from thermogravimetric analysis for original untreated water hyacinth fibers and chemically treated fibers are shown in the Fig. 4.6. The TG curves show that the initial drop occurs between 50 °C and 150 °C attributed to weight loss of absorbed moisture. Due to low decomposition temperature of hemicelluloses, lignin, and pectin, the untreated plant fibers began to degrade around 206 °C [29]. The decomposition temperature of original crude fibers and purified cellulose fibers was found to be at 202 °C and 253 °C, respectively.

The residues remaining in the untreated and treated fibers after heating to 500 °C constitute the presence of carbonaceous materials. The TGA analysis showed minimum residual mass in the purified cellulose fibers probably due to the removal

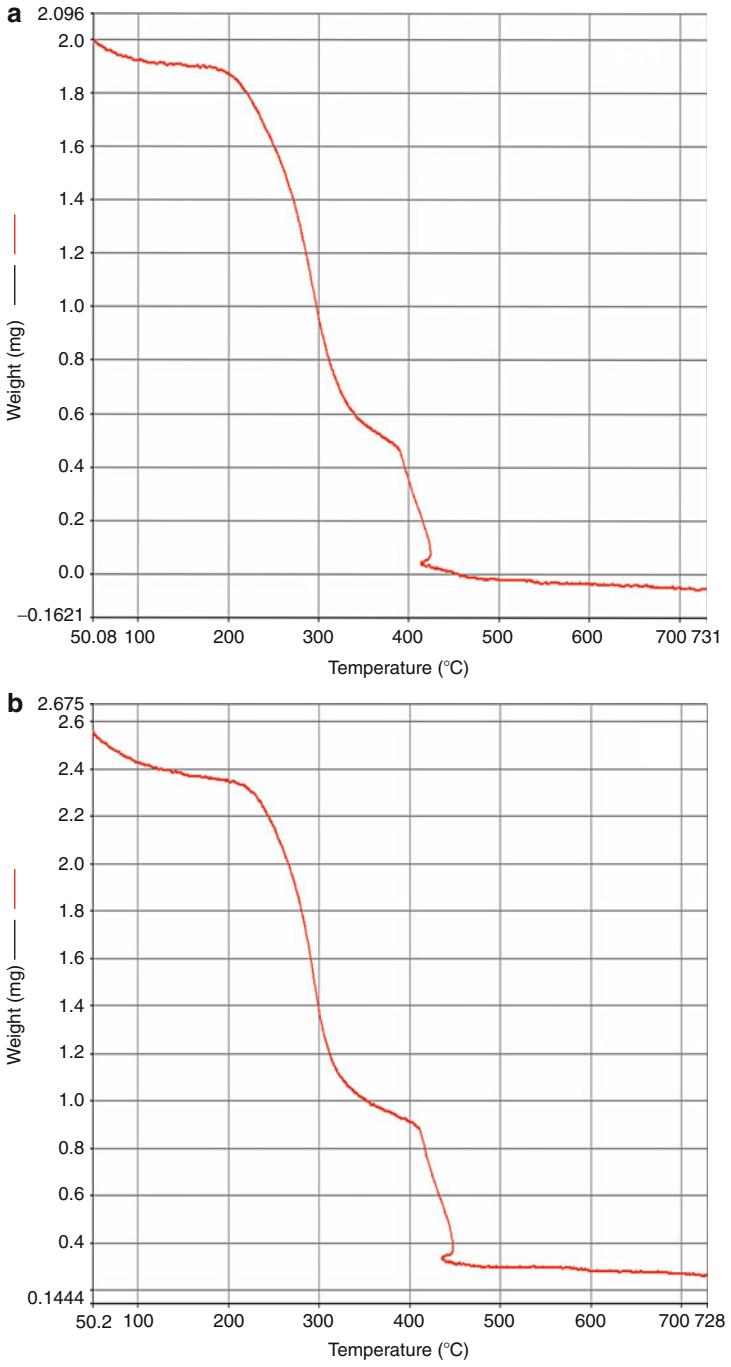

Fig. 4.6 TGA study of (**a**) original crude fibers and (**b**) cellulose fibers of water hyacinth

of hemicelluloses and lignin. The results revealed that the thermal stability of the cellulose fibers increased after the chemical treatment when compared with the original crude fibers [4, 26].

7 Conclusions

Cellulose nanofibers were isolated from the aquatic weed water hyacinth by a combination of chemical and mechanical treatments. The SEM investigation revealed that the pure cellulose fibers have been obtained after the chemical treatment. The TEM analysis evaluated the isolated nanofibers are having diameter of 25 nm and its length in micrometer. The FTIR spectra confirmed the removal of lignin and hemicelluloses when treated with acidified sodium chlorite and sodium hydroxide solutions under various time intervals at appropriate temperatures. The TGA analysis revealed that the decomposition temperature of the fibers increased after the successive chemical treatments. The present investigation has highlighted the utility of the aquatic weed, which is considered as a major cause of polluting in many areas. It has also demonstrated the feasibility of producing cellulose nanofibers, which can have potential applications in the near future.

The cellulose nanofibers extracted from water hyacinth weeds have potential to prepare biodegradable nanocomposite films with improved tensile strength and modulus, high optical transmittance, and increased thermal stability.

Acknowledgment The authors are grateful to the Department of Biotechnology for the financial support of this research study and Management, International Institute of Biotechnology and Toxicology (IIBAT) for providing facility for this study.

References

1. Wang B, Sain M, Oksman K (2007) Appl Compos Mater 14:89–103
2. Wang B, Sain M (2007) Compos Sci Technol 67:2521–2527
3. Leitner J, Hinterstoisser B, Wastyn M, Keckes J, Gindl W (2007) Cellulose 14:419–425
4. Alemdar A, Sain M (2008) Bioresource Technol 99:1664–1671
5. Bhattacharya D, Germinario LT, Winter WT (2008) Carbohyd Polym 73:371–377
6. Moran JI, Alvarez VA, Cyras VP, Vazquez A (2008) Cellulose 15:149–159
7. Zuluaga R, Putaux JL, Cruz J, Velez J, Mondragon I, Ganan P (2009) Carbohyd Polym 76:51–59
8. Teixera EM, Pasquini D, Curvelo AAS, Corradini E, Belgacem MN, Dufresne A (2009) Carbohyd Polym 78:422–431
9. Nogi M, Iwamoto S, Nakagaito AN, Yano H (2009) Adv Mater 21:1595–1598
10. Jonoobi M, Harun J, Mathew AP, Hussein MZB, Oksman K (2010) Cellulose 17:299–307
11. Qua EH, Hornsby PR, Sharma HSS, Lyons G, McCall RD (2009) J Appl Polym Sci 113:2238–2247
12. Abe K, Yano H (2009) Cellulose 16:1017–1023
13. Teixeira EM, Correa AC, Manzoli A, de Leite FL, De Oliveira CR, Mattoso LHC (2010) Cellulose 17:595–606
14. Fahma F, Iwamoto S, Hori N, Iwata T, Takemura A (2010) Cellulose 17:977–985

15. Eyholzer C, Bordeanu N, Suevos FL, Rentsch D, Zimmermann T, Oksman K (2010) Cellulose 17:19–30
16. Henriksson M, Henriksson G, Berglund LA, Lindstrom T (2007) Eur Polym J 43:3434–3441
17. Ohkawa K, Hayashi S, Nishida A, Yamamoto H, Ducreux J (2009) Text Res J 79:1396–1401
18. Kulpinski PJ (2005) Appl Polym Sci 98:1855–1859
19. Saito T, Nishiyama Y, Putaux JL, Vignon M, Isogai A (2006) Biomacromolecules 7:1687–1691
20. Fukuzumi H, Saito T, Iwata T, Kumamoto Y, Isogai A (2009) Biomacromolecules 10:162–165
21. Saito T, Okita Y, Nge TT, Sugiyama J, Isogai A (2006) Carbohyd Polym 65:435–440
22. Okita Y, Saito T, Isogai A (2009) Holzforchung 63:529–535
23. Praskalo J, Kostic M, Potthast A, Popov G, Pejic B, Skundric P (2009) Carbohyd Polym 77:791–798
24. Zhou W, Zhu D, Langdon A, Li L, Liao S, Tan L (2009) Bioresource Technol 100:5366–5369
25. Bhatnagar A, Sain M (2005) J Reinf Plast Compos 24:1259–1268
26. Sain M, Panthapulakkal S (2006) Ind Crop Prod 23:1–8
27. Sun XF, Xu F, Sun RC, Fowler P, Baird MS (2005) Carbohyd Res 340:97–106
28. Xiao B, Sun XF, Sun RC (2001) Polym Degrad Stabil 74:307–319
29. Chen W, Yu H, Liu Y, Hai Y, Zhang M, Chen P (2011) Cellulose 10:433–442

Bagasse and Rice Straw Nanocellulosic Materials and Their Applications

5

Mohammad L. Hassan

Contents

Abstract

Agricultural crop residues are important source for isolation of cellulosic fibers in many countries, especially those that do not have forest. Among these residues, rice straw and bagasse are worldwide agricultural residues that exist in large amounts. Nanocellulosic materials, namely, microfibrillated cellulose and cellulose nanocrystals, from these residues have been isolated, characterized, and used in different nanocomposites for different applications. Microfibrillated cellulose has been isolated from bagasse and rice straw using high-shear ultrafine grinder (or the so-called supermasscolloider) and high-intensity ultrasonication. The uses of biological and chemical pretreatments have been also studied for reducing energy and improving the properties of the isolated microfibrillated cellulose. Microfibrillated cellulose from bagasse and rice straw has been used in preparation of nanocomposites using different natural and synthetic polymer matrices such as chitosan, gelatin, and polypropylene. In addition, microfibrillated cellulose from bagasse has been used to improve the properties of paper sheets prepared from bagasse fibers. Cellulose nanocrystals have been isolated from bagasse and rice straw using sulfuric acid hydrolysis. The isolated nanocrystals have been used with alginate and natural rubber as

M.L. Hassan
Cellulose and Paper Department & Advanced Materials and Nanotechnology Group, Centre of Excellence for Advanced Sciences, National Research Centre, Cairo, Egypt
e-mail: mlhassan2012@yahoo.com

J.K. Pandey et al. (eds.), *Handbook of Polymer Nanocomposites. Processing, Performance and Application – Volume C: Polymer Nanocomposites of Cellulose Nanoparticles*,
DOI 10.1007/978-3-642-45232-1_53,

reinforcing elements. Surface-modified cellulose nanocrystals have been used in polycaprolactone nanocomposites to improve tensile and moisture barrier properties of polycaprolactone.

Keywords
Bagasse • Rice Straw • Microfibrillated Cellulose • Cellulose Nanocrystals • Nanocomposites • Supramolecular

1 Introduction

Bagasse, the residual fibrous material left after extraction of sugar from sugar cane, has been used in many countries for papermaking and board making. Before its use in papermaking or board making, removing the fine nonfibrous fraction, which is known as pith, is necessary to obtain high-quality products. On the other hand, rice straw is among the largest agricultural residues all over the world. Its use in papermaking is not widely practiced at the industrial level due to the problems associated with the presence of silica in significant amount (up to ~15 %) in the straw. Silica is supplied by soil in the form of hydrated silica, transferred and accumulated as amorphous silica (opal) on the polysaccharide matrix in shoots. In the shoot epidermal system, silica becomes localized in stomata, silica cells, trichomes, and long cells [1, 2]. Accumulated silica in the shoots functions to provide support to the shoot system, to deter predators, and to conserve water during moisture stress. It also protects plant from fungal diseases and insects [3]. After pulping and bleaching of rice straw, silica remains in the pulp in significant amounts causing deterioration of strength properties of paper products. In addition, silica in the black liquor left from the alkaline pulping process causes problems during concentration of the liquor to be used as fuel.

Bagasse and rice straw fibers have similar properties to hardwood fibers such as short fiber length, hemicelluloses that consist mainly of pentoses (mainly xylose and arabinose sugars), and lignin nature which consists mainly of syringyl–guaiacyl units [4, 5].

Due to differences in composition and fiber properties (length, diameter, and crystallinity) of the agricultural residues, the properties of cellulosic nanomaterials isolated from cellulosic fibers are different. The differences in the properties of the isolated nanomaterials are reflected in the products where these nanomaterials are used.

Recently, nanocellulosic materials, namely, microfibrillated cellulose (MFC) and cellulose nanocrystals, have been isolated from bagasse and rice straw, characterized, and used in different nanocomposites for different applications.

2 Microfibrillated Cellulose (MFC) from Bagasse and Rice Straw and Their Applications

In plants, the morphological hierarchy of cellulose is defined by elementary fibril, microfibril, and macrofibril bands. The lateral dimensions of these structural units are between 1.5 and 3.5 nm for elementary fibrils, between 10 and 30 nm for

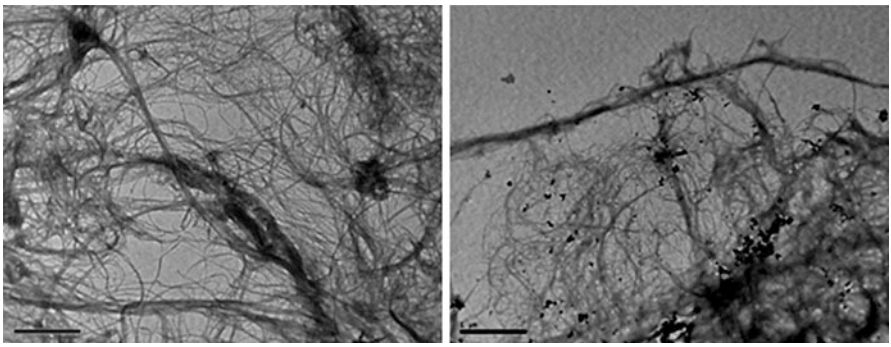

Fig. 5.1 TEM of bagasse (*left*) and rice straw (*right*) microfibrillated cellulose

microfibrils, and in the order of 100 nm for macrofibril bands. The length of the microfibrils is in the order of several hundred nanometers; the microfibrils are embedded in a matrix of hemicelluloses and lignin [6].

For isolation of cellulose microfibrils, so-called microfibrillated cellulose (MFC) from fibers, very high mechanical shearing is required in order to disintegrate the cell wall to liberate the microfibrils. Different technologies for isolation of microfibrillated cellulose of plant fibers have employed mechanical treatments using high-pressure homogenizers, grinders, cryo-crushing, ultrasonic and chemi-mechanical method, and high-shear ultrafine friction grinding [7].

Micro- and nanocellulose fibrils were isolated from rice straw fibers using high-intensity ultrasonication [8]. Rice straw fibers were soaked in water for 24 h followed by high-intensity ultrasonication. About 90 % of the isolated fibrils had diameter in the range from 7 to 80 μm, whereas about 6 % had a diameter less than 500 nm.

MFC was isolated from bagasse and rice straw pulps using high-shear ultrafine grinder (or the so-called supermasscolloider) and high-pressure homogenization (Fig. 5.1) [38]. The pulps were refined using high-shear ultrafine grinder and then homogenized using high-pressure homogenizer. The pulps were sent through the grinder from 10 to 30 times and then through the high-pressure homogenizer from 1 to 10 times. Optimization of the isolation processes was investigated using optical microscopy (OM), transmission electron microscopy (TEM), and atomic force microscopy (AFM). Main isolation of the microfibrils took place during refining using the ultrafine grinding process, while high-pressure homogenization resulted in slightly smaller-diameter and more homogeneous size of microfibrils. Cellulose microfibrils with diameters ranging from 3.5 to 50 nm were obtained. In addition, microfibrillar bands of diameter up to 150 nm were also observed. No significant differences in the dimensions of the bagasse and rice straw MFC were found. But in the case of rice straw MFC, the silica particles, which had nano-size dimensions, were noticed in the TEM and AFM images with the isolated MFC. The presence of silica was also proofed using energy-dispersive X-ray (EDX) microanalysis. Refining using supermasscolloider and high-pressure homogenizer had no detrimental effect on the DP of the fibers. Paper sheets, which were called nanopaper sheets,

were prepared from the isolated microfibrillated cellulose from bagasse and rice straw pulps after the grinding and homogenization steps. The sheets were prepared by drying a filtered mat of the isolated MFC under heat and pressure. The tensile strength, especially wet tensile strength, of nanopaper sheets was remarkably higher than that known for the regular paper sheets prepared from the bagasse and rice straw fibers using the standard paper sheet making methods. The presence of silica with the rice straw MFC significantly affected tensile strength and transparency of the nanopaper sheets. Nanopaper sheets prepared from rice straw MFC had lower tensile strength and transparency than those prepared from bagasse MFC. The highest values of tensile strength and modulus of nanopaper sheets were about 110 MPa and 6.1 GPa for bagasse and 78 MPa and 4.9 GPa for rice straw, respectively. The higher opacity and lower tensile properties of rice straw nanopaper sheets was attributed to the presence of significant amounts of silica particles, i.e., lower fiber content in the case of rice straw pulp. These particles can also reduce the hydrogen bonding between the nanofibers and thus the strength of the paper sheets. Further passing the obtained microfibrils through the high-pressure homogenizer increased the tensile strength up to 130.5 and 96.7 MPa and the tensile modulus up to 8.5 and 5.1 GPa in the case of bagasse and rice straw, respectively. The wet tensile strength of nanopaper sheets obtained from bagasse and rice straw MFC was up to 19.5 and 16.5 MPa, respectively, compared to 1.5 and 1.2 MPa for paper sheets prepared from the original pulps. The porosity of nanopaper sheets was lower than that of paper sheets made from the original pulps by about 24 % and 50 % in the case of bagasse and rice straw MFC, respectively. The very smooth and tight texture of nanopaper sheets made from MFC was clear compared to that made from the original pulps.

The use of chemical or enzymatic pretreatment of cellulose fibers before the mechanical action for isolation of MFC using the different technologies mentioned before has been used to facilitate the isolation of MFC from the cell wall, to reduce the possible damage of the microfibril structure, and to reduce the energy consumption [7].

Bagasse pulp was pretreated with dilute hydrochloric acid, dilute sodium hydroxide, cellulase, or xylanase enzymes with the aim to reduce energy consumed in MFC isolation using the supermasscolloider and improve nanopaper sheet properties made from the isolated MFC [9]. The pretreated pulps were passed through the grinder from 10 to 30 times and then through the high-pressure homogenizer from 1 to 10 times. The dimensions and properties of the isolated nanofibers were followed at the different processing stages using OM, TEM, and AFM and by testing tensile strength properties (wet and dry). The diameter of the microfibrils obtained from the different pulps was in the range of 7–30 nm. But larger microfibrillar bands (width up to 150 nm) were observed in the case of MFC isolated from untreated bagasse pulp than that isolated from the pretreated pulps (width up to 90 nm). Broken nanofibers were seen in TEM and AFM images of MFC obtained from acid-treated bagasse pulp. The tensile strength properties of the nanopaper sheets made from the isolated MFC were correlated to the chemical composition, crystallinity, and degree of polymerization (DP) of the pretreated pulps.

Dilute hydrochloric acid pretreatment (5 % at 50 °C for 45 min) resulted in removal of most of hemicelluloses and a slight degradation of cellulose chains as it was clear from the DP value. Dilute alkali treatment (5 % at 50 °C for 45 min) resulted in partial removal of hemicelluloses and short-chain cellulose (beta- and gamma-cellulose). Therefore, an increase in DP was found. Xylanase treatment resulted in an increase in α-cellulose content and DP due to partial removal of xylan fraction (the majority of hemicelluloses in bagasse) by xylanase enzymes. In addition, crude xylanase enzymes may contain small amounts of cellulase enzymes, which have the ability to degrade cellulose. Treatment of bagasse pulp with cellulases resulted in a decrease in DP as a result of hydrolysis of cellulose; a slight decrease in hemicelluloses was also noticed. The crystallinity index values were 74.2, 76.1, 76, 76.4, and 73.9 for untreated, alkali-, acid-, cellulase-, and xylanase-treated pulps, respectively.

After 30 passes through the supermasscolloider, tensile strength of nanopaper sheets made from MFC isolated from untreated, alkali-treated, xylanase-treated, cellulose-treated, and acid-treated bagasse was 110.2, 138.2, 138.3, 107.1, and 100.7 MPa, respectively, and tensile modulus was 6.1, 6.18, 6.17, 5.86, and 5.08 GPa, respectively. Further passing the obtained microfibrils through the high-pressure homogenizer increased the tensile strength up to 130.5, 143.7, 142.4, 128.6, and 112.9 MPa and tensile modulus up to 8.45, 8.13, 6.81, 7.7, and 7.06 GPa in the case of MFC isolated from untreated, alkali-treated, xylanase-treated, cellulose-treated, and acid-treated bagasse, respectively. The wet tensile strength of nanopaper sheets prepared from untreated, alkali-treated, xylanase-treated, cellulose-treated, and acid-treated bagasse was 18.8, 26.9, 26.2, 20.9, and 20 MPa, respectively.

Microfibrillated cellulose from bagasse and rice straw has been used in preparation of nanocomposites using different natural and synthetic polymer matrices. Rice straw micro-/nanofibrils isolated by high-intensity ultrasonication were investigated as reinforcement in polypropylene polymer in the presence of maleated polypropylene as a coupling agent [8]. Twin-screw extruder was used for mixing the micro-/nanofibrils with polypropylene; loading up to 10 % was used. A slight increase in tensile strength of polypropylene (∼3 %) occurred as a result of adding the micro-/nanofibrils, while tensile modulus of polypropylene increased about 12 %. Due to the higher stiffness of cellulose fibers than polypropylene, the strain at break of polypropylene decreased as a result of adding the micro-/nanofibers.

MFC isolated from bagasse pulp pretreated with dilute alkali and xylanase enzymes using ultrahigh friction grinding and high-pressure homogenization was used for preparation of chitosan/MFC nanocomposites [34]. The MFC loading ranged from 2.5 % to 20 %. The effect of MFC loading on moisture sorption, dry and wet tensile strength, crystallinity, thermal stability, and dynamic mechanical thermal properties was studied using tensile testing, X-ray diffraction (XRD), thermogravimetric analysis (TGA), and dynamic mechanical thermal analysis (DMTA). Nanocomposites with good transparency were obtained at the different MFC loadings. Chitosan nanocomposites made using MFC isolated from bagasse fibers treated with xylanase or alkali showed higher dry and wet tensile strength than those made using MFC isolated from untreated bagasse pulp.

The improvement in dry tensile strength was significant even at 2.5 % MFC loading and was attributed to the formation of percolated/interconnected network of the MFC within the chitosan matrix [10]. The increase in tensile strength values at 20 % MFC loading was about 192 %, 220 %, and 211 % for chitosan nanocomposites containing MFC isolated from untreated bagasse, xylanase-treated bagasse, and alkali-treated bagasse, respectively. Regarding wet tensile strength, films made from neat chitosan suffered from large increase in width due to swelling in the buffer solution used before the tensile test. In the case of chitosan nanocomposites, the increase in width was very small even at 2.5 % loading. This is an important requirement for materials used in tissue engineering where dimensional stability is important in wet conditions. The wet tensile strength of the chitosan nanocomposites was significantly improved even at the low MFC loading. At the highest MFC loading (20 %), the wet tensile strength of chitosan/MFC nanocomposites prepared using the different MFC was up to 15 times that of chitosan. The significant improvement of wet tensile strength and the decrease of swelling of chitosan due to addition of cellulose microfibrils was reported before and was attributed to the formation of percolated/interconnected network of the nanofibers and cross-linking between chitosan and the trace amount of carbonyl groups that exist in cellulose [10, 11]. Nanocomposites made using the nanofibers isolated from xylanase and alkali-treated pulps had higher wet tensile strength than that made using nanofibers isolated from the untreated pulp. DMTA results showed higher storage modulus and indicated higher glass transition temperature for the chitosan nanocomposites than that of neat chitosan. XRD patterns showed that, at low nanofibers loading, addition of bagasse nanofibers to chitosan matrix increased ordering of chitosan chains upon drying the nanocomposite films.

Rice straw MFC isolated using ultrahigh friction grinding and high-pressure homogenization was also used with chitosan polymer to prepare chitosan/MFC nanocomposites [012Has]. Up to 20 % of rice straw MFC was used. The effect of MFC loading on dry and wet tensile strength, dynamic mechanical thermal properties, and crystallinity of chitosan were studied using tensile testing, dynamic mechanical thermal analysis, and X-ray diffraction. Addition of rice straw MFC to chitosan resulted in significant improvement in wet and dry tensile strength and shift of glass transition temperature (T_g) of chitosan matrix to higher values. Chitosan nanocomposites prepared using rice straw MFC had remarkable wet and dry tensile strength, which could be attributed to the presence of both nanofibers and nanosilica particles originally present in rice straw fibers. Tensile strength (wet and dry) of chitosan/rice straw MFC was higher than those of chitosan/bagasse MFC nanocomposites [37]. The maximum increase in tensile strength of chitosan was about 192 % in the case of using bagasse MFC, while it was 355 % in the case of rice straw MFC. The authors pointed to a possible role of the silica nanoparticles that exist with rice straw MFC. The same trend was found for wet tensile strength where the improvement in wet tensile strength of chitosan was increased about 9 and 16 times in the case of using bagasse and rice straw MFC, respectively. In addition, DMTA results showed higher shift of the tan delta peak at T_g of chitosan in the case of using rice straw MFC than in the case of using bagasse nanofibers.

Microfibrillated cellulose (MFC) isolated from bagasse using ultrahigh friction grinding and high-pressure homogenization was used to prepare nanocomposites using cross-linked gelatin polymer matrix [12]. MFC loadings up to 25 % were used. The prepared nanocomposites were characterized regarding their transparency, wet and dry tensile strength, water sorption, and water vapor permeability. Nanocomposite surfaces were examined by scanning electron microscopy (SEM); the SEM images indicated homogeneous distribution of MFC in the gelatin matrix. Gelatin/MFC nanocomposites showed high transparency even at the highest MFC loading. Neat gelatin film showed transparency of about 89 %, while the transparency of gelatin/MFC nanocomposites at the different MFC loadings ranged from 84 % to 78 %. Microfibrillated cellulose improved wet and dry maximum tensile stress and modulus of cross-linked gelatin but resulted in a decrease of its strain at break. The increase in tensile strength was about 20 % at the maximum MFC loading. The increase in tensile modulus of gelatin at 25 % of MFC loading was about 279 %. Regarding the wet tensile strength, the improvement in wet tensile strength and tensile modulus was about 173 % and 750 %, respectively, at the maximum MFC loading. MFC did not affect the water absorption of cross-linked gelatin but significantly improved its moisture barrier property. The maximum decrease in water vapor permeability of gelatin was about 35 % on adding 5 % of bagasse MFC.

In the area of papermaking, microfibrillated cellulose isolated from xylanase-treated bagasse pulp using ultrahigh friction grinding and high-pressure homogenization was used to improve the properties of paper sheets made from bagasse fibers [35]. The standard handsheet papermaking method was used. The effect of adding different amounts of MFC on tensile strength (wet and dry), tear resistance, burst strength, opacity, and porosity of paper sheets was studied. Tensile strength increased 7 % and 27 % as a result of adding MFC 10 % and 50 %, respectively. At MFC content higher than 50 % and up to 80 %, there was no substantive change in tensile strength. A slight increase in tensile strength occurred at greater than 80 % MFC. Adding MFC to bagasse pulp at ratios more than 30 % resulted in a decrease in extension at break. The decrease in extension was remarkable at high MFC ratios (>60 %), which was attributed to the low extension at break of the MFC caused by their nano-size. MFC remarkably improved the wet tensile strength of paper sheets. With addition of 40 % MFC, improvement in wet tensile strength was about 188 %. No further improvement of wet tensile strength occurred with increasing MFC. Adding up to 30 % MFC to bagasse pulp did not deteriorate tear resistance of paper sheets. Further increase in MFC resulted in a decrease in tear resistance of the paper sheets. Adding MFC to bagasse pulp did not substantively affect the burst strength of paper sheets up to about 50 % MFC. At higher MFC content, the burst strength decreased, and the decrease was remarkable at MFC content greater than 70 %. Under the conditions used in paper sheets making, no significant change in opacity of paper sheets was found with addition of MFC. Substituting MFC for bagasse resulted in a slight decrease in porosity, and at the different MFC ratios, the time recorded for passing 100 cm^3 of air ranged from 25 to 28 s. The effect of adding 30 % of bagasse MFC to bagasse fibers was compared that occurred on

adding 30 % of softwood long fibers. Paper sheet containing bagasse MFC had higher tensile strength (wet and dry) than softwood paper sheets, but those containing softwood paper sheets had higher tear resistance and burst strength.

3 Cellulose Nanocrystals from Bagasse and Rice Straw and Their Applications

Cellulose is a natural high-molecular-weight linear homopolymer constituted of repeating β-D-glucopyranosyl units joined by 1–4 glycosidic linkages in a variety of arrangements [13]. The length of cellulose chains, described in terms of the average value of the number of monomeric units, or the degree of polymerization (DP), depends on its origin. Cellulose chains are biosynthesized and self-assembled into microfibrils. These microfibrils are constituted by amorphous and crystalline domains. The degree of crystallinity (ratio between the mass of crystalline domains and the total mass of the cellulose) and dimensions of these microfibrils are dependent on their origin. Cellulose chains present in the amorphous regions are randomly oriented and susceptible to acid attack due to the hydrolytic cleavage of the glycosidic bonds leading to the formation of microcrystalline cellulose and finally releasing rodlike crystallites of nano-size, the so-called cellulose whiskers or cellulose nanocrystals [14]. Subjecting the hydrolyzed cellulose to strong ultrasonic treatment for a short time is important to liberate the cellulose nanocrystals. The dimensions of cellulose nanocrystals obtained after hydrolysis depend on the percentage of amorphous regions, which varies from a source to the other. Cellulose nanocrystals are characterized by very high elastic modulus of about 138 GPa and specific surface area of several hundred m^2/g [15]. In addition, they have relatively low density, renewable character, high specific strength, and biodegradability associated with the highly specific properties of nanoparticles. The nanoscale dimensions of these nanocrystals enable them to be transparent in well dispersed composites [16]. By virtue of their strength and shape, cellulose nanocrystals have qualifications for polymer reinforcement. Another interesting property of cellulose nanocrystals is their ability to form liquid crystalline phase at a critical concentration in water. Due to their rigid rodlike shape, they have a strong tendency to align along a vector director [17]. When the suspension reaches the critical concentration, the nanocrystals can form a chiral nematic ordered phase displaying optical characteristics of a typical cholesteric liquid crystal. The chiral nematic orders can be retained after evaporation of water, leaving iridescent films of cellulose I crystal structure [17, 18].

Cellulose nanocrystals were prepared from different cellulosic materials, agro-based fibers, and agricultural residues such as cotton, cotton linter, ramie, hemp, flax, sisal, wheat straw, palm, bleached softwood and hardwood pulps, microcrystalline cellulose, sugar beet pulp, bacterial cellulose, and tunicates [19]. Acid hydrolysis usually carried out using sulfuric acid or hydrochloric acid. The use of hydrobromic acid and phosphoric acid was also reported. The use of sulfuric acid in

hydrolysis leads to nanocrystals with negatively charged surfaces due to esterification of the hydroxyl groups and formation of sulfate groups. Therefore, the properties of sulfuric acid-hydrolyzed cellulose nanocrystal water suspension will be different from the others prepared using the other mineral acids [19].

Because of their high aspect ratio and rodlike morphology, biodegradability, availability of raw materials, high surface area, amenability for chemical modification, liquid crystalline properties, transparency of the prepared nanocomposites, good mechanical response to stress, and their high reinforcing effect at relatively low concentrations, cellulose nanocrystals have been widely studied with many natural and synthetic polymer matrices mainly to improve their mechanical properties [20].

Use of bagasse and rice straw for isolation of cellulose nanocrystals and their use for cellulosic nanocomposites preparation have been reported.

Cellulose nanocrystals were prepared from cellulose microfibers isolated from bagasse [21]. The microfibers were first isolated from bleached bagasse pulp by a two-stage high-pressure homogenization process and then acid hydrolyzed by refluxing with 60 % (w/v) sulfuric acid for 2.5 h at 60 °C. The produced particles had size ranged from a few 100 nm to a couple of microns. The optimum hydrolysis conditions were 2 h at 60 °C using 60 % sulfuric acid. However, under the optimum conditions mentioned, it was not possible to totally isolate the nanocrystals.

Cellulose nanocrystals were directly extracted from cassava bagasse, a by-product of the cassava starch industry [22]. The morphological structure of the ensuing nanoparticles was investigated using SEM, TEM, and AFM. The nanocrystals were extracted from cellulose fibers using 6.5 M sulfuric acid (∼50 wt% concentration) at 60 °C under vigorous stirring for 40 min. The resulting nanofibrils display a relatively low crystallinity and were found to be around 2–11 nm thick and 360–1,700 nm long. The isolated nanofibrils were used as reinforcing elements in a thermoplastic cassava starch matrix plasticized using either glycerol or a mixture of glycerol/sorbitol (1:1) as plasticizer. Nanocomposite films were prepared by a melting process. DMTA and tensile test proved the reinforcing effect of the nanofibrils. The reinforcing effect was dependent of plasticizer used. The incorporation of cassava bagasse cellulose nanofibrils in the thermoplastic starch matrices has resulted in a decrease of its hydrophilic character especially for glycerol-plasticized sample. The reinforcing capability of cellulose nanocrystals extracted from cassava bagasse was also investigated using natural rubber as matrix [23]. Nanocrystal loadings from 2 % to 10 % were used. High mechanical properties were observed from DMTA results for the nanocomposites at different loadings. The storage modulus increased with increasing the nanocrystal loading. The nanocrystals had no effect on the temperature that corresponds to the relaxation process at the glass–rubber transition.

Cellulose nanocrystals were isolated from bagasse and rice straw pulps using 65 % sulfuric acid; different reaction conditions (time, temperature, pulp-to-acid ratio) were tested to reach the optimum condition regarding yield and aspect ratio of the isolated nanocrystals (Fig. 5.2) [33]. The nanocrystals were characterized regarding yield, sulfur content (as a measure for sulfate groups), thermal stability, and dimensions.

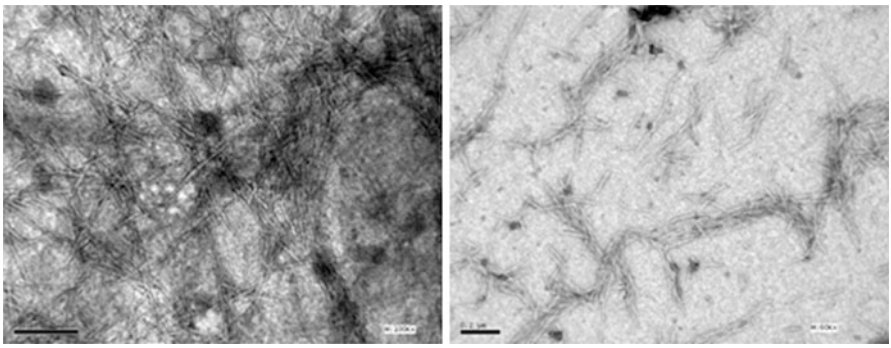

Fig. 5.2 TEM of bagasse (*left*) and rice straw (*right*) cellulose nanocrystals

At the optimum conditions (20 min at 45 °C using 1:20 cellulose to acid liquor ratio), the length of the cellulose nanocrystals was in the range of 76–101 and 75–104 for bagasse and rice straw, respectively, while the width was in the order of 5–8 nm for both of them. The sulfur content of bagasse nanocrystals was higher than that of rice straw ones, while the yield of rice straw nanocrystals was lower than bagasse ones. At the different conditions studied, sulfur content of bagasse and rice straw nanocrystals was in the range from 0.56 % to 0.83 % and 0.54 % to 0.7 %, respectively, while the yield was in the range from about 13 % to 30 % and 26 % to 44 %, respectively. These results were attributed to the presence of silica nanoparticles with rice straw nanocrystals. The presence of silica with rice straw cellulose nanocrystals was confirmed using EDX analysis. No significant difference in thermal stability between bagasse and rice straw nanocrystals was found except for the higher residual ash remained in the case of rice straw nanocrystals due to the presence of silica. The presence of silica with the nanocrystals in the case of rice straw affected the rheological properties of nanocrystal suspension in water. Viscosity of rice straw nanocrystal suspensions was lower than that of bagasse nanocrystal suspensions.

Polysaccharide nanocomposite films were prepared from sodium alginate and cellulose nanocrystals isolated from bagasse and rice straw by solution casting; loading ratios from 2.5 % up to 10 % were used. The effect of cellulose nanocrystal loading on the viscosity of alginate solution was studied at different shear rates. The presence of cellulose nanocrystals resulted in decreasing the viscosity of alginate solution. The decrease was significant even on the addition of small quantities of nanocrystals. The casted nanocomposite films were soaked in calcium chloride solution for cross-linking of alginate. Thermal properties, thermal stability, crystallinity, and tensile strength of alginate/cellulose nanocrystal nanocomposites were characterized using dynamic mechanical thermal analysis (DMTA), thermogravimetric analysis (TGA), X-ray diffraction (XRD), and tensile testing, respectively. The different alginate nanocomposite films had slightly lower onset degradation temperature than neat alginate. The presence of cellulose nanocrystals did not affect the crystallinity of alginate in the prepared nanocomposite films. Cellulose nanocrystals significantly increased tensile strength of the alginate films even at

2.5 % of nanocrystals. Gradual increase in tensile strength occurred with increasing nanocrystal concentration above 2.5 % in the case of bagasse, while a slight decrease in tensile strength was observed with increased contents of rice straw nanocrystals. Tensile strength of alginate/rice straw nanocomposites was lower than that of bagasse at nanocrystal concentration of more than 2.5 %. The percent increase in tensile strength reached 237 % and 131 % in the case of bagasse and rice straw nanocrystals, respectively. Previous studies explained the reinforcing effect of cellulose nanocrystals in amorphous polymers in terms of mechanical percolation phenomenon yielded by cellulose nanocrystal interaction (nanocrystal/nanocrystal) through hydrogen bonding and the formation of nanocrystal network within the host matrix [41]. DMTA also showed the reinforcing effect of cellulose nanocrystals using bagasse and rice straw cellulose nanocrystals as seen from the storage modulus values of neat alginate and nanocomposite films. Addition of cellulose nanocrystals to alginate resulted in a decrease of moisture sorption of the prepared nanocomposites when left at 60 % relative humidity for 48 h.

Bagasse cellulose isolated using 65 % sulfuric acid at 45 °C for 45 min was also used as reinforcing element in natural rubber matrix [24]. Nanocrystal loadings from 2.5 % to 10 % were used. The effect of nanocrystal loading on tensile properties, thermal properties, moisture sorption, water vapor permeation, and soil biodegradation was studied. Significant improvement of Young's modulus and tensile strength was observed as a result of addition of nanocrystals to the rubber matrix especially at high nanocrystal loading. The maximum increase of tensile stress and modulus of rubber matrix was 374 % and 530 %, respectively, and was achieved for 10 wt% of nanocrystals. This high reinforcing effect was assigned as already reported to a mechanical percolation phenomenon of cellulose nanocrystals which form a stiff continuous network of cellulosic nanoparticles linked through hydrogen bonding [25]. The formation of this continuous network is supposed to form above the percolation threshold of the rodlike nanoparticles. It strongly depends on the aspect ratio of the rodlike reinforcing particles and therefore on the origin of cellulose. For rodlike nanoparticles with an aspect ratio of 13 like bagasse nanocrystals, the percolation threshold is around 5.15 vol%, equivalent to 7.7 wt%, assuming a density of 1 and 1.5 g/cm^3 for the NR matrix and crystalline cellulose, respectively. This might explain the significant increase in tensile strength at high nanocrystal loading (10 wt%).

Dynamic mechanical thermal analysis (DMA) and differential scanning calorimetry (DSC) results showed no change in the glass transition temperature (T_g) of the rubber matrix upon addition of cellulose nanocrystals, but at softening of rubber, cellulose nanocrystals have reinforcing effect on the rubber. The presence of bagasse nanocrystals resulted in an increase in moisture sorption of rubber films up to 5 % nanocrystal loading, while at higher nanocrystal loading, the moisture sorption tended to decrease.

The use of cellulose nanocrystals as fillers that can reduce water vapor permeation was claimed by some authors [26, 27]. The suggested mechanism was related to the high crystallinity, the rod shape of the cellulose nanocrystals, and the induced tortuosity. However, the high moisture sorption of cellulose nanocrystals could

result in increasing moisture penetration. This could be explained by the fact that cellulose nanocrystals can act as absorbent or trap for moisture because of their high sensitivity to humidity compared to natural rubber. Moisture barrier properties of natural rubber/cellulose nanocrystal nanocomposites decreased on increasing cellulose nanocrystals up to 7.5 % nanocrystal loadings and then increased with further increase in nanocrystal loading. The results mean that cellulose nanocrystals acted mainly as trap for moisture and not as a barrier for moisture penetration. Interesting results were reported regarding the increase biodisintegration of rubber in soil when cellulose nanocrystals are used in the nanocomposite films. Neat natural rubber film lost about 19 % of its weight after being buried in soil for 4 weeks, while natural rubber containing 7.5 and 12.5 wt% of cellulose nanocrystals lost about 62 % and 71 %, respectively, after the same period buried in soil.

Despite the unique properties of cellulose nanocrystals in nanocomposites, their applications are restricted to hydrophilic polymers because of their non-dispersibility in nonpolar organic solvents or hydrophobic polymers melt. To overcome this problem, several investigations have been made to stabilize the nanocrystals in organic solvents, such as use of *N*,*N*-dimethylformamide [28] and use of surfactant [29], or chemically modify the surface of cellulose nanocrystals [30].

Bagasse nanocrystals isolated from bleached bagasse pulp were chemically modified using *n*-octadecyl isocyanate in the presence of dibutyltin dilaurate as a catalyst [36]. Due to the heterogeneous conditions used, the degree of substitution (DS) of modified cellulose nanocrystals was low (N content 0.76 %, DS $\sim$ 0.025). However, the modified cellulose nanocrystals were easily dispersed in toluene, which was used as a solvent for polycaprolactone. Chemical modification of bagasse nanocrystal surfaces with octadecyl side chains greatly influenced the water contact angle and surface energy. The modified cellulose nanocrystals were used in ratios from 2.5 % to 15 % with polycaprolactone (PCL) polymer to prepare nanocomposite films by solution/casting technique. The prepared nanocomposites were characterized regarding their moisture barrier, moisture sorption, biodegradability in soil, mechanical, thermal, and thermomechanical properties. The nanocomposites containing the different modified nanocrystal loadings had very low moisture absorption (from 1.88 % to 2.49 %) after 4 weeks of exposure to 75 % relative humidity, but it was higher than that of neat PCL (1.79 %). Water vapor permeability (WVP) of PCL films decreased by about 50 % as a result of the addition of only 2.5 % of modified cellulose nanocrystals. The maximum decrease in WVP was obtained at 5 % of modified cellulose nanocrystal loading and was about 55 %; this was consistent with the expected percolation threshold value for bagasse cellulose nanocrystals, which have an aspect ratio of 12.8 [29]. No further decrease in WVP of PCL films was observed at higher modified nanocrystal loadings (7.5–15 %), and WVP of the prepared PCL nanocomposites was lower than that of neat PCL by about 41–45 %. The lower WVP of PCL nanocomposites containing the modified cellulose nanocrystals than neat PCL was attributed to the presence of long alkyl chains on the surface of the nanocrystals, homogeneous distribution of the nanocrystals in PCL matrix as well as their rodlike shape and high crystallinity. The presence of the modified cellulose nanocrystals resulted in an

increase in the biodisintegration of polycaprolactone in soil. OM pictures showed that biodegradation and/or biodisintegration of PCL in soil occurred in a laminar manner, i.e., erosion of the surface of the PCL. In the case of the presence of cellulose nanocrystals, in addition to the erosion of the PCL surface, much more of tiny pits were formed and thus increased the rate of biodisintegration of PCL soil. In addition, the weight loss as a result of biodisintegration of PCL nanocomposites in soil was much higher than that of neat polycaprolactone film. The effect was significant up to addition of 7.5 % of modified nanocrystals; at higher loading the weight loss tended to decrease, but it was still higher than neat PCL. The results indicated that the presence of cellulose nanocrystals, even after modification, did not noticeably inhibit the attack of microorganisms on cellulose or PCL. It should be mentioned that by using burring in soil test and measuring weight loss, it could be confirmed that the modified cellulose nanocrystals favor the disintegration of the nanocomposites in soil and thus may facilitate its biodegradation. However, measuring the CO_2 production rate is necessary to determine the effect of the modified cellulose nanocrystals on rate of biodegradability. Addition of the modified cellulose nanocrystals to PCL resulted in significant increase in its modulus, especially at nanocrystal loading of 5 % or higher, i.e., at and above the percolation threshold, where bagasse cellulose nanocrystals form a stiff percolating network [30]. The maximum increase in modulus was about 77 % and was achieved at 12.5 % nanocrystal loading. The increase in the modulus of the prepared PCL nanocomposites indicated good dispersion of the modified cellulose nanocrystals in the hydrophobic PCL matrix and good interfacial adhesion between the modified cellulose nanocrystals and PCL as well as the nanocrystal–nanocrystal interaction. The increase in modulus of PCL as a result of addition of modified cellulose nanocrystals was also attributed to increase in crystallinity of PCL in the presence of modified nanocrystals [31]. The tensile strength of nanocomposite films slightly increased on addition of modified cellulose nanocrystals to PCL up to 5 % of nanocrystal loading and then slightly decreased on addition of higher amounts of nanocrystals. The decrease in tensile strength of PCL on addition of 12.5 % modified cellulose nanocrystals, e.g., at the highest modulus obtained, was only about 9 %. Due to the high stiffness of the nanocrystals, the strain at break of the nanocomposites containing the different ratios of nanocrystals was greatly reduced, especially at 2.5–7.5 % of modified nanocrystals. No significant further decrease in the strain at break took place at higher levels of modified nanocrystal loading. Modified nanocrystals in PCL matrix did not noticeably affect its glass transition and melting temperatures.

Functionalization of cellulose nanocrystals to obtain new derivatives that can lead to new utilitarian applications has been recently investigated [30]. Recently, bagasse nanocrystals were used in preparation of terpyridine-modified nanocellulose derivatives and their corresponding transition metal complexes with unique physicochemical properties and the possibility of formation of supramolecular derivatives with wide range of functionalities and applications [39]. Terpyridines are *N*-heterocycles that have very high binding affinity toward many transition metal ions due to their potential for dπ-pπ* back bonding to the

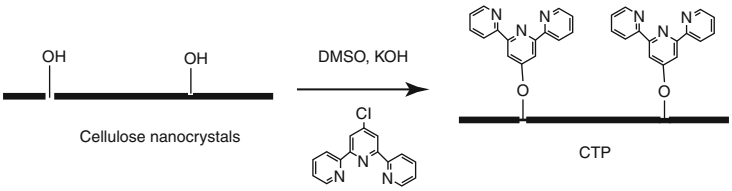

Scheme 5.1 Preparation of terpyridine-modified cellulose (*CTP*) nanocrystals

coordinated metals and a chelate effect. Transition metal terpyridine complexes have been investigated for the design of new functional smart materials because of their distinct photophysical, electrochemical, and magnetic properties, as well as reversibility of the metal bonding by varying pH, temperature, or exposure to more competitive ligands [32].

The surface hydroxyl groups of bagasse nanocrystals were reacted with 4′-chloro-2,2′:6′,2″-terpyridine in the presence of KOH to produce the terpyridine-modified cellulose derivative, as shown in Scheme 5.1. The nanocrystals were suspended in dimethyl sulfoxide (DMSO) and the reaction was carried out under heterogeneous conditions. The terpyridine-modified cellulose nanocrystals (CTP) were characterized using TEM, wide-angle X-ray diffraction (XRD), magic-angle spinning ^{13}C nuclear magnetic resonance (MAS-^{13}C NMR), elemental analysis, as well as Fourier transform infrared (FTIR) and UV-visible spectroscopy. The TEM and XRD confirmed preservation of the nanocrystals to their shape and cellulose I crystal structure, i.e., successful surface modification of the nanocrystals. Elemental analysis for nitrogen of terpyridine-modified cellulose nanocrystals was ~0.8 %. This value corresponds to a degree of substitution (DS) for the cellulose hydroxyl groups of ~0.032. The low DS was expected due to a high degree of crystallinity and the heterogeneous reaction conditions used. MAS-^{13}C NMR, FTIR, and UV spectroscopy confirmed occurrence of the modification. Metallo-CTP with different optical properties, and expected magnetic and catalytic properties, were easily obtained upon reaction of the prepared CTP with different di- and trivalent transition metal ions (Fe^{+2}, Mn^{+2}, Co^{+2}, and Ru^{+3}). Complexation of transition metal ions with the terpyridine-modified cellulose nanocrystals occurred immediately and led to the formation metallo-nanocellulosic materials with different optical properties (Scheme 5.2).

Using the well-known Ru^{III} to Ru^{II} reduction by *N*-ethylmorpholine in the presence of other terpyridine ligands led to preparation of asymmetric *bis*-terpyridine complexes with octahedral coordination geometry and having a wide variety of properties depending on the substitution patterns (Scheme 5.3). For example, the prepared Ru^{III}-terpyridine-modified cellulose nanocrystals were used in preparation of metallo-supramolecular derivatives with other terpyridine units bearing terminal amine or adamantane functional groups.

Highly fluorescent nanocellulosic material was prepared via surface modification of cellulose nanocrystals with 2,2′:6′,2″-terpyridine side chains

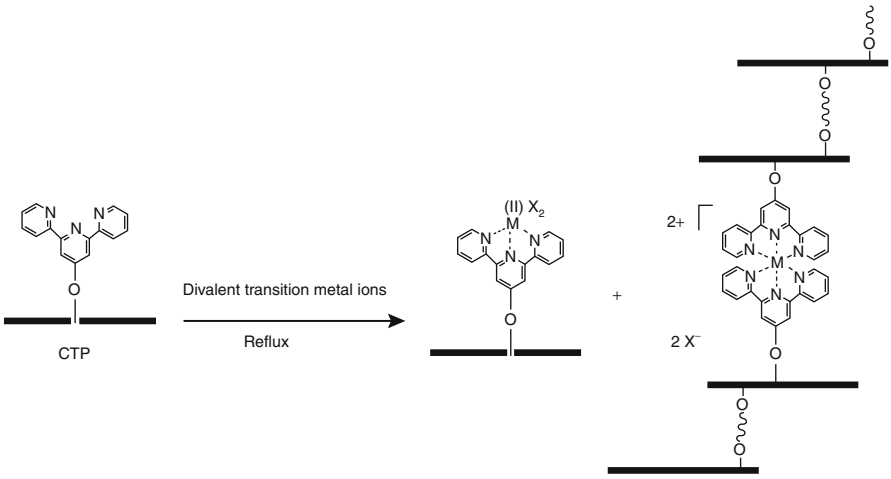

Scheme 5.2 Reaction of terpyridine-modified cellulose nanocrystals (*CTP*) with divalent transition metal ions (the *curved line* depicts *bis*-terpyridine connectivity)

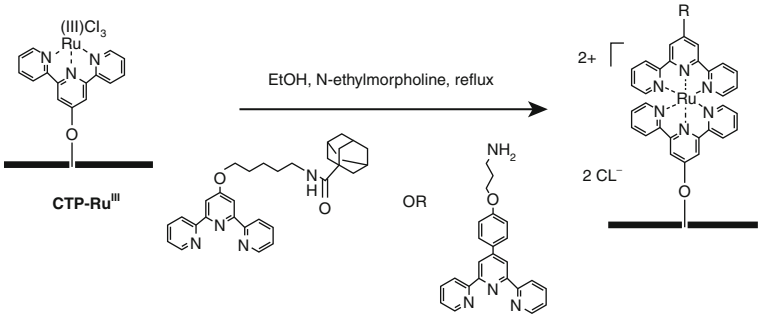

Scheme 5.3 Reaction of Ru^{III}-terpyridine-modified cellulose nanocrystals (*CTP-Ru^{III}*) with different terpyridine ligands

followed by supramolecular assembly of terpyridine-modified perylene dye onto the terpyridine-modified cellulose nanocrystals (CTP) via Ru^{III}/Ru^{II} reduction (Scheme 5.4) [40]. The prepared terpyridine-modified cellulose-Ru^{II}-terpyridine-modified perylene (CTP-Ru^{II}-PeryTP) fluorescent nanocrystals were characterized using CP/MAS ^{13}C NMR, FTIR, UV-visible, and fluorescence spectroscopy. In addition, further self-assembly of terpyridine units with azide functional groups onto CTP-Ru^{II}-PeryTP was possible via repeating the Ru^{+3}/Ru^{+2} reduction protocol to prepare supramolecular fluorescent nanocrystals with azide functionality (CTP-Ru^{II}-PeryTP-Ru^{II}-AZTP). According to elemental analysis results, nitrogen content of the prepared CTP-Ru^{II}-PeryTP-Ru^{II}-AZTP was 3 %, i.e., DS of 0.029 (close to that of CTP 0.032), which further proved successful complex formation between CTP and both of

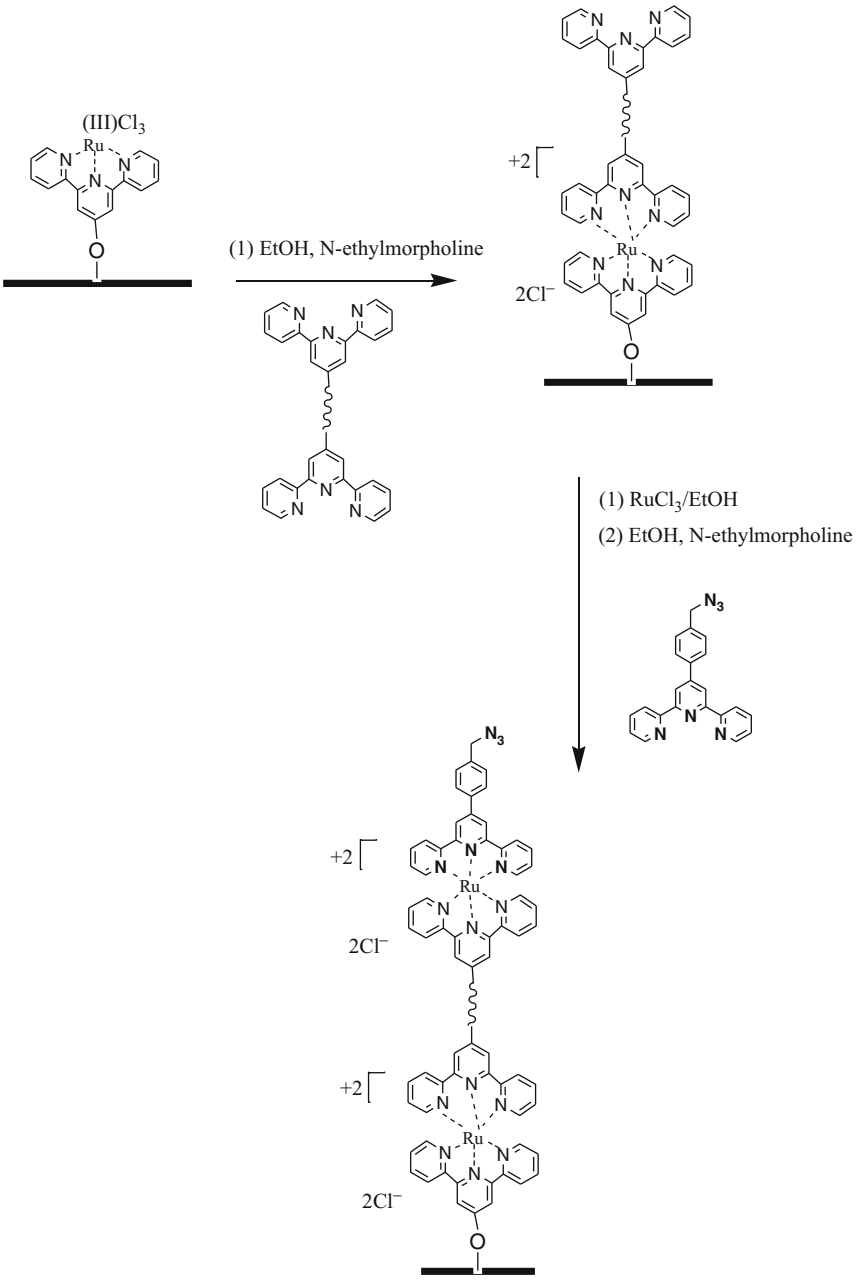

Scheme 5.4 Preparation of supramolecular CTP-Ru^{II}-PeryTP and CTP-Ru^{II}-PeryTP-Ru^{II}-AZTP nanocellulosic derivatives. *Curved line* represents perylene motifs

terpyridine-modified perylene and azide-terminated terpyridine. The prepared fluorescent nanocrystals were recommended for potential application in bio-imaging since the terminal azide groups can be easily reacted with antigens via "click" chemistry reaction.

References

1. Kaufman PB, Takeoka Y, Carlson TJ, Bigelow WC, Jones JD, Moore PH, Ghosheh NS (1979) Studies on silica deposition in sugarcane (Saccharum spp.) using scanning electron microscopy, energy-dispersive X-ray analysis, neutron activation analysis, and light microscopy. Phytomorphology 29:185
2. Maeda H, Nakajima M, Hagiwara T, Sawaguchi T, Yano S (2006) Bacterial cellulose/silica hybrid fabricated by mimicking biocomposites. J Mater Sci 41:5646
3. Yoshida S, Onishhi Y, Kitagishi K (1959) Soil Plant Food 5:127
4. Hans JS, Rowell RM (1997) Chemical composition of fibers. In: Rowell MR, Young RA, Rowell JK (eds) Paper and composites from agro-based resources. CRC Lewis Publishers, New York, p 83
5. Rials TG, Wolcott MP (1997) Physical and mechanical properties of agro-based fibers. In: Rowell MR, Young RA, Rowell JK (eds) Paper and composites from agro-based resources. CRC Lewis Publishers, New York, p 63
6. Klemm D, Heublein B, Fink H-P, Bohn A (2005) Cellulose: fascinating biopolymer and sustainable raw material. Angew Chem Int Ed 44:3358
7. Siró I, Plackett D (2010) Microfibrillated cellulose and new nanocomposite materials: a review. Cellulose 17:459
8. Wu Y, Zhou D-G, Wang S-Q, Zhang Y (2009) Preparation and characterization of PVA composites with cellulose nanofibers obtained by ultrasonication. Bioresources 4:1487
9. Hassan ML, Mathew AP, Hassan EA, Oksman K (2010) Effect of pretreatment of bagasse pulp on properties of isolated nanofibers and nanopaper sheets. Wood Fiber Sci 43:1
10. Nordqvist D, Idermark J, Hedenqvist MS (2007) Enhancement of the wet properties of transparent chitosan-acetic-acid-salt films using microfibrillated cellulose. Biomacromolecules 8:2398
11. Hosokawa J, Nishiyama M, Yoshihara K, Kubo T, Terabe A (1991) Ind Eng Chem Res 30:788
12. Fadel SM, Hassan ML, Oksman K (2013) Improving tensile strength and moisture barrier properties of gelatin using microfibrillated cellulose. J Compos Mater 47:1977
13. Klemm D, Philipp B, Heinze T, Heinze U, Wagenknecht W (2004) Introduction. In: Comprehensive cellulose chemistry: fundamentals and analytical methods, vol 1. Wiley-VCH, Weinheim, Chap. 2.1
14. Azizi Samir MAS, Alloin F, Dufresne A (2005) Review of recent research into cellulosic whiskers, their properties and their application in nanocomposite field. Biomacromolecules 6:612
15. Nishino T, Takano K, Nakamae KJ (1995) Elastic modulus of the crystalline regions of cellulose polymorphs. J Polym Sci Polym Phys 33:1647
16. Hajji P, Cavaille JY, Favier V, Gauthier C, Vigier G (1996) Tensile behavior of nanocomposites from latex and cellulose whiskers. Polym Compos 17:612
17. De Souza LM, Borsali R (2004) Macromol Rapid Commun 25:771
18. Araki J, Wada M, Kuga S, Okano T (1998) Colloids Surf 142:75
19. Habibi Y, Lucia LA, Rojas OJ (2010) Cellulose Nanocrystals: Chemistry, Self-Assembly, and Applications. Chem Rev 110:3479
20. Siqueira G, Bras J, Dufresne A (2010) Cellulosic bionanocomposites: A review of preparation, properties and applications. Polymers 2:728

21. Bhattacharya D, Germinario LT, Winter WT (2008) Isolation, preparation and characterization of cellulose microfibers obtained from bagasse. Carbohydr Polym 73:371
22. Teixeira EM, Pasquini D, Curvelo AAS, Corradini E, Belgacem MN, Dufresne A (2009) Cassava bagasse cellulose nanofibrils reinforced thermoplastic cassava starch. Carbohydr Polym 78:422
23. Pasquini D, Teixeira EM, Curvelo AAS, Mohamed MN, Dufresne A (2010) Extraction of cellulose whiskers from cassava bagasse and their applications as reinforcing agent in natural rubber. Ind Crop Prod 32:486
24. Bras J, Hassan ML, Bruzzese C, Hassan EA, Dufresne A (2010) Mechanical, barrier, and biodegradability properties of bagasse cellulose whiskers reinforced natural rubber nanocomposites. Ind Crop Prod 32:627
25. Dufresne A (2008) Cellulose-based composites and nanocomposites. In: Gandini A, Belgacem MN (eds) Monomers, polymers and composites from renewable resources. Elsevier, Oxford, p 401
26. Garcia de Rodriguez NL, Thielemans W, Dufresne A (2006) Sisal cellulose whiskers reinforced polyvinyl acetate nanocomposites. Cellulose 13:261
27. Paralikar SA, Simonsen J, Lombardi J (2008) Poly(vinyl alcohol)/cellulose nanocrystal barrier membranes. J Membr Sci 320:248
28. Azizi Samir MAS, Alloin F, Sanchez J-Y, Elkessi N, Dufresne A (2004) Preparation of Cellulose Whiskers Reinforced Nanocomposites from an Organic Medium Suspension. Macromolecules 37:1386
29. Heux L, Chauve G, Bonini C (2000) Nonflocculating and chiral-nematic self-ordering of cellulose microcrystals suspensions in nonpolar solvents. Langmuir 16:8210
30. Peng BL, Dhar N, Liu HL, Tam KC (2011) Chemistry and applications of nanocrystalline cellulose and its derivatives: a nanotechnology perspective. Can J Chem Eng 9999:1
31. Siqueira G, Bras J, Dufresne A (2009) Cellulose whiskers versus microfibrils: influence of the nature of nanoparticle and its surface functionalization on the thermal and mechanical properties of nanocomposites. Biomacromolecules 10:425
32. Schubert US, Winter A, Newkome GR (2011) Terpyridine-based materials – for catalytic, optoelectronic and life science applications. Wiley-VCH, Weinheim, p 509
33. Hassan ML, Oksman K, El-Wakil NA, Hassan EA, Fadel SM (2009) Preparation and characterization of cellulose whiskers from bagasse, rice straw, and sugar beet and their use in alginate nanocomposites. 10th international conference on wood & biofiber plastic composites & cellulose nanocomposites symposium, Madison, 11–13 May 2009
34. Hassan ML, Hassan EA, Oksman K (2011) Effect of pretreatment of bagasse fibers on the properties of chitosan/microfibrillated cellulose nanocomposites. J Mater Sci 46:1732
35. Hassan EA, Hassan ML, Oksman K (2011) Improving bagasse pulp paper sheet properties with microfibrillated cellulose isolated from xylanase-treated bagasse. Wood Fiber Sci 43:76
36. Hassan ML, Bras J, Hassan EA, Fadel SM, Dufresne A (2012) Polycaprolactone/modified bagasse whisker nanocomposites with improved moisture-barrier and biodegradability properties. J Appl Polym Sci 125:E10
37. Hassan ML, Fadel SM, El-Wakil NA, Oksman K (2012) Chitosan/rice straw nanofibers nanocomposites: Preparation, mechanical, and dynamic thermomechanical properties. J Appl Polym Sci 125:E216
38. Hassan ML, Mathew AP, Hassan EA, El-Wakil NA, Oksman K (2012) Nanofibers from bagasse and rice straw: Process optimization and properties. Wood Sci Technol 46:193
39. Hassan ML, Moorefield CM, Elbatal HS, Newkome GR (2012) New metallo-supramolecular terpyridine-modified cellulose functional nanomaterials. J Macromol Sci A 49:1
40. Hassan ML, Moorefield CM, Elbatal HS, Newkome GR, Modarelli DA, Romano NC (2012) Fluorescent cellulose nanocrystals via supramolecular assembly of terpyridine-modified cellulose nanocrystals and terpyridine-modified perylene. Mater Sci Eng B-Adv 177:350
41. Favier V, Cavaille JY, Canova GR, Shrivastava SC (1997) Mechanical percolation in cellulose whisker nanocomposites. Polymer Engineering and Science, 37:1732

Extraction and Characterization of Cellulose Nanofibers from Banana Plant

6

B. Deepa, E. Abraham, Rekha Rose Koshy, L. A. Pothan, and Sabu Thomas

Contents

B. Deepa
Department of Chemistry, Bishop Moore College, Mavelikara, Kerala, India

Department of Chemistry, C.M.S. College, Kottayam, Kerala, India
e-mail: deepabkrishnan@gmail.com

E. Abraham
Department of Chemistry, Bishop Moore College, Mavelikara, Kerala, India

Department of Chemistry, C.M.S. College, Kottayam, Kerala, India

Robert H. Smith Faculty of Agriculture, Food and Environment Hebrew University, Jerusalem, Israel
e-mail: eldhoabraham@gmail.com

R.R. Koshy • L.A. Pothan (✉)
Department of Chemistry, Bishop Moore College, Mavelikara, Kerala, India
e-mail: rekhakoshy2@gmail.com; lapothan@gmail.com

S. Thomas (✉)
School of Chemical Sciences, Mahatma Gandhi University, Kottayam, Kerala, India

International and InterUniversity Centre for Nanoscience and Nanotechnology, Mahatma Gandhi University, Kottayam, Kerala, India
e-mail: sabuchathukulam@yahoo.co.uk

J.K. Pandey et al. (eds.), *Handbook of Polymer Nanocomposites. Processing, Performance and Application – Volume C: Polymer Nanocomposites of Cellulose Nanoparticles*,
DOI 10.1007/978-3-642-45232-1_54,

Abstract

Isolation of cellulose nanofibers from renewable resources is becoming an important area of research. The use of these novel nature-based materials has garnered interest from the scientific community because of their high strength and stiffness combined with low weight, biocompatibility, and renewability. The nanodimensions of cellulose fibrils result in a high surface area and hence the powerful interaction of these celluloses with surrounding species, such as water, organic and polymeric compounds, nanoparticles, and living cells. In this context, cellulose nanofibers from banana plant have attracted much interest due to its potential use as a reinforcing agent in novel eco-friendly nanocomposite preparation. This chapter introduces the current knowledge on the extraction of nanocellulose from banana plant and the different characterization techniques employed to understand the reinforcing potential of these nanofibers.

Keywords

Banana plant • Extraction • Nanocellulose • Nanocomposites

1 Introduction

Nowadays, ecological concern and economic situation has resulted in a renewed interest in the introduction of new materials and products based on renewable resources. In this context, the application of cellulose nanofibers as reinforcement in polymer matrixes has attracted considerable attention since it offers a unique combination of high physical properties and environmental benefits [1–5]. Cellulose-based nanocomposites generally exhibit significant improvements in thermal, mechanical, and barrier properties compared to the neat polymer or conventional composites [6–8].

Cellulose is the most eminent representative of nanomaterial that consists of aggregates of cellulose fibrils with diameters in the nanometer range and lengths in the micrometer scale. Nanometer-sized single-crystal cellulose, which is commonly referred to as nanocrystalline cellulose (NCC), cellulose microcrystallites, microcrystals, microfibrils, nanowhiskers, nanofibers, or nanofibrils, can be obtained from various sources such as woods, annual plants, microbes, and animals. A lot of research work has been performed all over the world on the use of natural fibers as a reinforcing material for the preparation of various types of biocomposites [9–11]. The main features that stimulate the use of cellulose nanofibers as polymer reinforcement agents are their large specific surface area (estimated to be several hundreds of m^2g^{-1}), their very high modulus of elasticity (approximately 150 GPa), their great aspect ratio, and their ability to act as a significant reinforcement at low filler loading levels. Other attractive advantages of cellulose nanofibers are their low density (about 1.566 g/cm^3), nonabrasive nature, nontoxic character, biocompatibility, and biodegradability [12–14]. Additionally, the cellulose nanofibers come from renewable natural sources which are very abundant and therefore low-costing;

it is not necessary to synthesize them, and they allow the production of composite films with excellent visible light transmittance which are easily modified chemically (their structure has a reactive surface of –OH side groups) that facilitate grafting chemical species to achieve different surface properties [15–17]. These novel nanocrystalline materials have great potential application in various fields, such as regenerative medicine, optically transparent functional materials, tissue engineering scaffolds, catalysts, textiles, surface coatings, drug delivery, food packaging, and green nanocomposite preparation [18–21].

Several methods have been applied to extract highly purified nanofibrils from the plant cell wall. These methods include treatments, such as pulp beating [22], high-pressure homogenizing [23], ultrasonic technique [24], and cryocrushing [25]. All of them lead to different types of nanomaterial, depending on the composition of cellulose raw material its pretreatment conditions and the disintegration process. The most well known and widely used method for the isolation of cellulose nanofibers is based on acid hydrolysis [26–28]. This process breaks the disordered and amorphous parts of the cellulose, releasing single and well-defined crystals. The nature of the acid, the acid concentration, the acid-to-cellulosic fibers ratio, the temperature, and the time of reaction are also important parameters that affect the morphology and properties of cellulose nanofibers [1, 4, 28].

It is known that the morphology and properties of cellulose nanofibers show variations according to the raw material source and the extraction process [4, 17]. The incoming fibers naturally vary with respect to length, microfibril angle, amount of non-cellulosic residues (e.g., lignin, hemicelluloses), and quality according to source and to whether the biomass is a primary stream or a waste stream. Therefore, the isolation of cellulose nanofibers from different sources is relevant since it dictates the overall performance of the cellulose nanofibers as a reinforcing agent. Several sources of cellulose have been used to obtain cellulose nanostructures with different morphologies and crystallinities via the acid hydrolysis method. Examples include wheat straw [29], cotton [30], bacterial cellulose [31], bamboo [32], sisal [33], coconut [34], soy hulls [14], banana residues [35–37], hemp [38], mengkuang leaves [39], jute [40], and mulberry [41]. This chapter provides an overview of the recent research efforts on the extraction and characterization of nanocellulose from banana plant in order to evaluate the reinforcing potential of these nanofibers for the development of green nanocomposites.

2 Nanocellulose from Banana Plant

The banana plant fibers are one of the main agricultural waste products of pseudostems and leaves left over after banana cultivation. India is one of the largest producers of banana plants. Banana cultivation generates a considerable amount of cellulosic-based waste. The comestible part, the fruit, constitutes only 12 % by weight of the plant. The remaining parts become agricultural waste, causing environmental problems in banana farming regions. This residual material

Table 6.1 Physical properties of banana fiber

Cellulose content	63–64 %
Hemicellulose	19 %
Lignin	5 %
Moisture content	10–11 %
Density	1.35 g/cm^3
Tensile strength	650–750 MPa

represents an abundant, inexpensive, and readily available source of nanocellulose. Table 6.1 shows the physical properties of banana fiber. The use of biomass residues in the production of high performance materials is a prospective commercial application that would unlock the potential for a generation of value-added products from agro-industrial commodities [42, 43].

2.1 Preparation of Nanocellulose

Recently, steam explosion treatment has been extensively studied as a promising pretreatment method for the extraction of nanocellulose from the pseudo-stem of banana plant [27, 35, 37]. Lignocellulosic biomass materials can be fractionated into biopolymer constituents by steam explosion technology. The treatment of lignocellulosic resources with high-pressure steam, for short periods of time, followed by sudden decompression (explosion) represents a simple treatment for biomass that achieves defibrillization by a combination of chemical and mechanical action. The advantages of steam explosion include a significantly lower environmental impact, low energy consumption, lower capital investment, and less hazardous process chemicals. Both the aspect ratio and percentage yield of nanocellulose obtained by this technique have been found to be very high as compared to other conventional methods.

The extraction process includes alkaline steam treatment, bleaching, and acidic steam treatment phases. The immersion of lignocellulosic fibers in dilute alkaline medium facilitates the adhesive nature of the fiber surface by removing natural and artificial impurities and causes the separation of structural linkages between lignin and carbohydrate and the disruption of lignin structure. The aim behind the bleaching process is the removal of lignin left after the alkaline steam treatment. The bleaching treatment done in the presence of sodium chlorite solution popularly used in laboratories to remove lignin from the vegetable fiber. The mechanism of bleaching involves oxidation of lignin, which leads to lignin dissolution and its degradation. Further treatment (acid steam treatment), which helps in the production of cellulose nanofibrils, is the main phase of the extraction method. Acid treatment hydrolyzes the traces of hemicelluloses and lignin remaining after the bleaching phase by breaking down the polysaccharides to simple sugars and

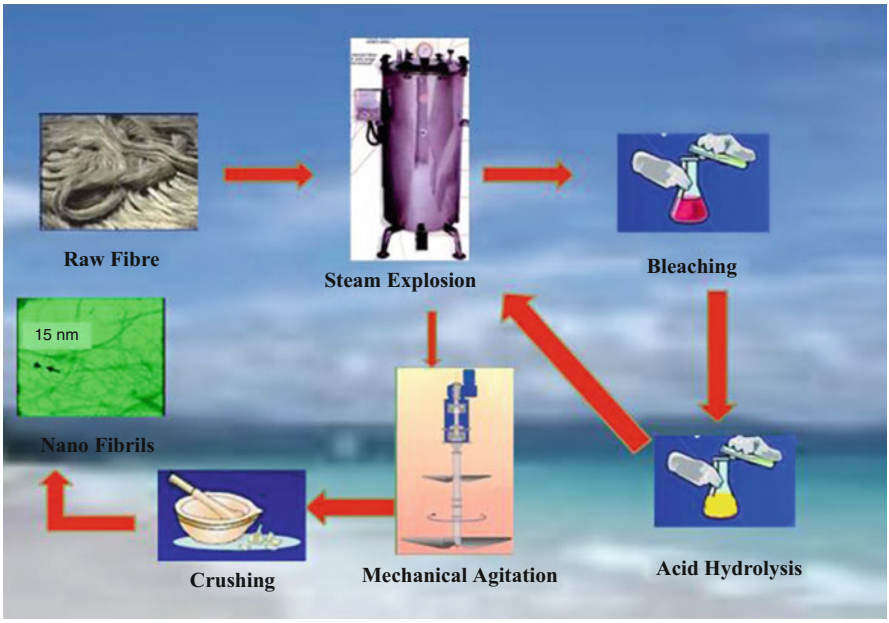

Fig. 6.1 Method for the preparation of nanofibrils

hence release the cellulose fibers. The combined acid steam treatments effectively reduce the long microfibril chains to nanodimensions by the maximum explosion of pressurized steam into the interfibrillar region. The details of the steam explosion process are given in Fig. 6.1.

Elanthikkal et al. [36] applied sulfuric acid hydrolysis method for the preparation of cellulose microfibers from banana fibers and to characterize the resultant microfibers. The effect of preparation conditions such as time, temperature, acid concentration, and initial dimension of the banana fibers on the cellulose microfiber structure and characteristics have also been investigated.

In another report, Zuluaga et al. [44] have isolated cellulose microfibrils from banana rachis, using a combination of chemical and mechanical treatments. The chemical treatment involved treatment of bleached banana rachis residues with a mixture of 80 % acetic acid solution and 70 % nitric acid solution at 120 °C for 15 min. The washed and purified cellulose was sonicated for 15 min. In the mechanical process, a bleached residue was suspended in water and homogenized. It was noted that an acidic treatment resulted in shorter aggregates of parallel cellulose microcrystallites. Individualized or bundled microfibrils were obtained by homogenization.

Table 6.2 FTIR analysis of the banana fibers in different stages [27]

FTIR (cm^{-1}) spectra (%T)							
Sample	–OH stretching	C–H vibration	C–O stretching	Absorbed water	C–H stretching	Aromatic ring vibration of lignin	C–C stretching
Raw banana fiber	3,400	2,923	1,736	1,638	1,369	1,247	1,029
Steam-exploded banana fiber	3,397	2,924	1,735	1,625	1,369	–	1,020
Bleached banana fiber	3,390	2,922	–	1,607	1,370	–	1,019

3 Characterization of Nanofibrillated Cellulose

Different characterization techniques were employed to characterize the fibers and cellulose nanofibers of banana in order to investigate the chemical composition, crystallinity index, thermal stability, and surface morphology. Chemical and structural analysis of the fibers can be studied by FTIR and XRD analysis. The precise morphological and surface topographical features are studied by scanning electron microscopy (SEM), transmission electron microscopy (TEM), and atomic force microscopy (AFM). A detailed understanding of the thermal degradation behavior of nanocellulose has been analyzed by thermogravimetric analysis (TGA) and differential scanning calorimetric (DSC) techniques.

3.1 Chemical Analysis

Chemical characterization of the banana fibers was estimated according to the ASTM standards and confirmed that the cellulose content was increased from 64 % to 95 % due to the application of alkali and acid treatments. The lignin and hemicellulose components were found to decrease from raw to bleached fibers. This fact is again confirmed by the Fourier transform infrared spectroscopy (FTIR) studies of banana fiber. Table 6.2 shows the FTIR analysis of banana fiber in various stages. FTIR analysis revealed that there is a reduction in the quantum of binding components present in the fibers due to the process of steam and chemical treatment. The raw fibers have a characteristic peak in between 1,730–1,740 cm^{-1} and 1,200–1,300 cm^{-1}. These peaks are chiefly responsible for the hemicellulose and lignin components. These characteristic peaks are completely absent in the final bleached cellulose fiber.

3.2 Morphological Analysis

Detailed comparison of the surface morphology of the nanocellulose of banana was carried out by techniques like SEM, TEM, and AFM. The shape, particle length and diameter distribution, aspect ratio, and aggregated or isolated state of the nanocrystals have been studied by TEM and AFM. Figure 6.2 shows the SEM pictures of banana fiber at different processing stages. SEM micrographs show the clear demonstration of the removal of the surface impurities along with defibrillation. Studies revealed that there is a reduction in the fiber diameter during the steam explosion followed by acid treatments. Figure 6.3 shows the AFM picture of banana nanofiber. Aspect ratios of the cellulose nanofibers of banana were estimated from atomic force micrographs. The aspect ratios of the nanofibers is shown in Fig. 6.4. The aspect ratio is found to be 57 for maximum number of fractions.

Cherian et al. [35] applied the scanning force microscopy (SFM) and TEM method to measure the dimensions of cellulose nanofibers extracted from the pseudo-stem of the banana plant. Figures 6.5 and 6.6 show the SFM and TEM pictures of banana nanofibers, respectively. Characterization of the fibers by SFM and TEM shows that there is reduction in the size of banana fibers to the nanometer

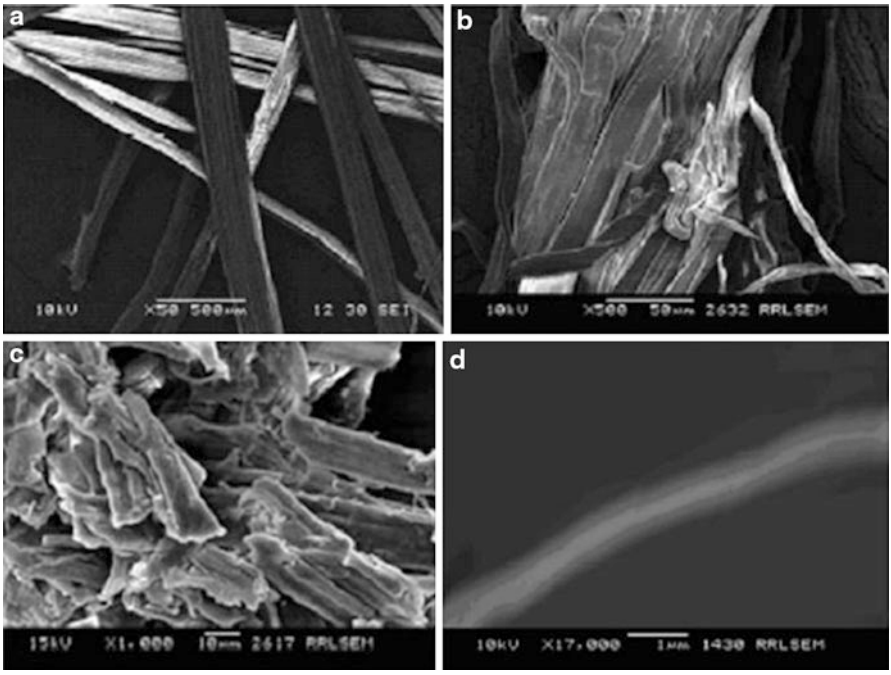

Fig. 6.2 SEM of banana fibre in various stages [37] (**a**) Raw banana fibre (**b**) Steam exploded banana fibre (**c**) Bleached banana fibre (**d**) Acid treated banana fibre

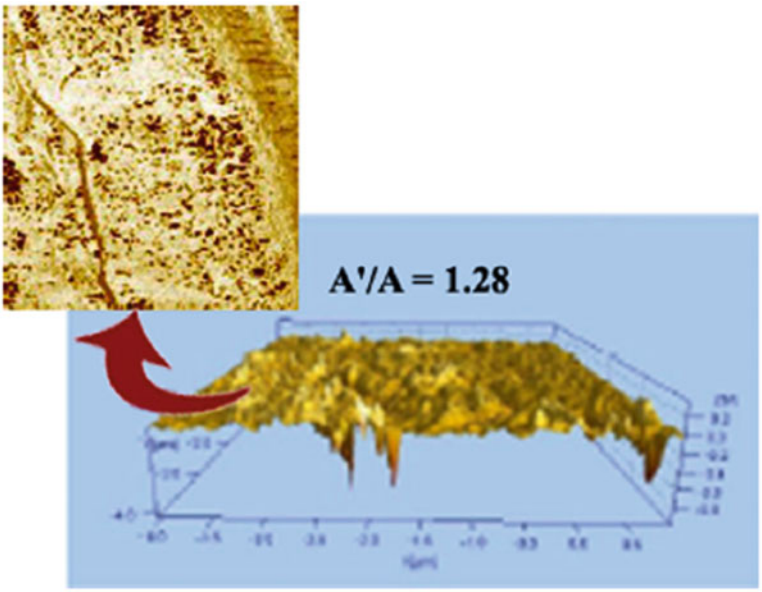

Fig. 6.3 AFM topography of banana nanofibre [37]

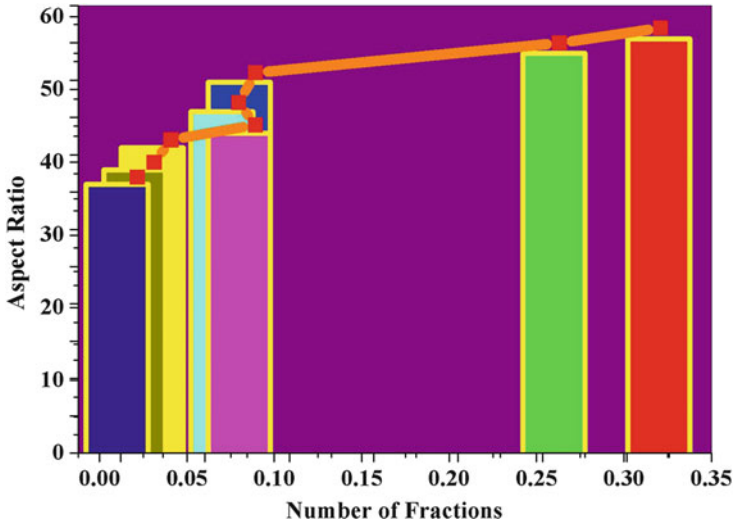

Fig. 6.4 Aspect ratios of the banana nanofibres [37]

range (below 40 nm). The average length and diameter of the developed nanofibrils were found to be between 200–250 nm and 4–5 nm, respectively.

Morphological analysis substantiates the dissolution of the non-cellulosic components present in the fiber cell wall by the acid correlated steam treatment process,

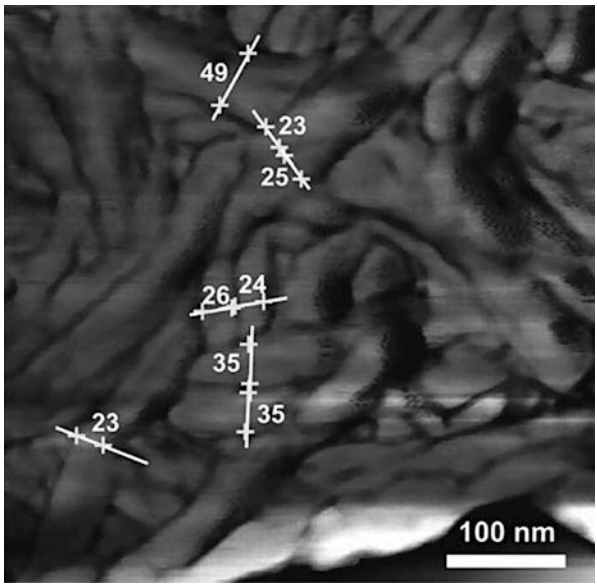

Fig. 6.5 SFM image of banana nanofibre [35]

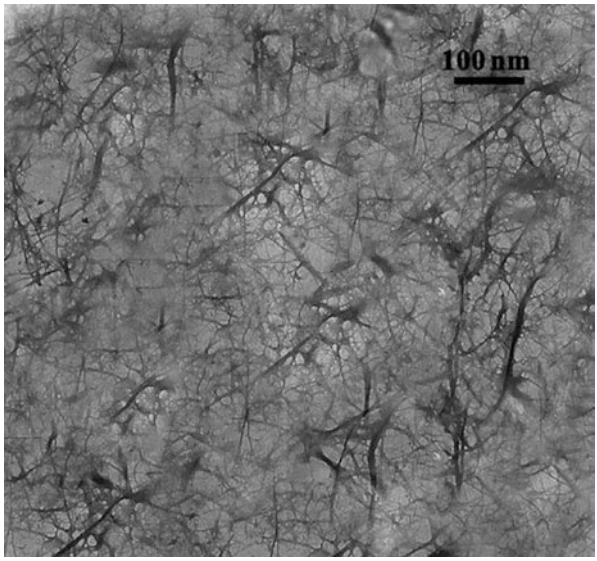

Fig. 6.6 TEM image of banana nanofibre [35]

which enhances the extraction of crystalline cellulose components from the fiber. The aspect ratio and percentage yield of nanocellulose fibers obtained by this technique have been found to be very high as compared to conventional methods. Therefore, these nanofibers can exhibit a high reinforcing capability in polymeric matrices.

3.3 X-Ray Diffraction (XRD) Analysis

The fiber diameter and percentage crystallinity of the banana fibers were investigated using X-ray diffraction studies. Figure 6.7 shows the XRD pattern of variously treated banana fibers. The XRD graphs of banana fiber show that they are in a crystalline nature. In raw fiber, crystalline cellulose components are oriented in the matrix of lignin, hemicellulose, pectin, etc. During chemical treatment the cementing materials (matrix) will be dissolved, and the remaining pure crystalline particles isolated. These particles show increasing orientation along a particular axis, due to their similarity in shape. The effect of various treatments on the crystallinity of the fibers was also calculated. Table 6.3 shows the crystallinity index values of banana fibers. The crystallinity index of the fiber can be calculated using the formula:

$$\text{Crystallinity Index} = \frac{I_{\text{crystalline}} - I_{\text{amorphous}}}{I_{\text{crystalline}}} \times 100$$

The crystallinity was found to vary depending on the conditions applied. The maximum crystallinity was obtained for the acid-treated fiber. In natural cellulose

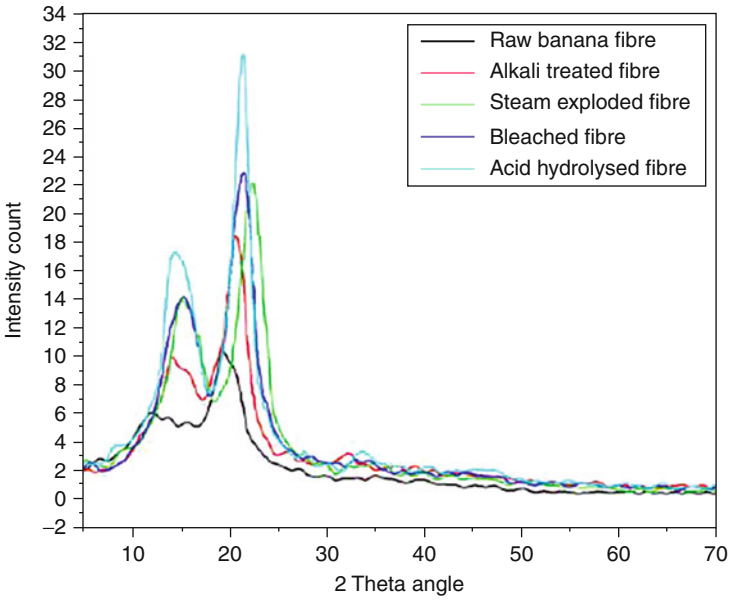

Fig. 6.7 XRD pattern of banana fibre [27]

Table 6.3 The crystallinity index of the banana fibers [27]

Material	Crystallinity index (Ic)
Raw banana fiber	10.5
Steam-exploded banana fiber	54.1
Bleached banana fiber	83.8

Table 6.4 Zeta potential values of aqueous suspensions of cellulose [36]

Sample	Zeta potential (mV)
4A45[a]	−41.32
4B45[b]	−22.35
4C45[c]	−20.72
4C65	−28.53
6C65	−29.67
8C65	−32.01

[a]4, treatment time in hours; A, acid conc. 76 wt%; 45, reaction temp. in °C
[b]4, treatment time in hours; B, acid conc. 70 wt%; 45, reaction temp. in °C
[c]4,6,8 treatment time in hours; C, acid conc. 64 wt%; 45, 65, reaction temp. in °C

fibers, the regions of intermediate order in the structure play an important role in the determination of the degree of crystallinity. From the peak intensity of the variously treated fibers, it has been found that acid hydrolysis changes the fiber diameter as well as the crystallinity.

3.4 Zeta Potential Analysis

The zeta potential is an important parameter for examining dispersion stability. Elanthikkal et al. [36] investigated the zeta potential measurements of an aqueous dispersions of banana microfibrous cellulose samples, prepared under the specified hydrolysis conditions (Table 6.4). All of the cellulose suspensions, in neutral water, showed a negative zeta potential value. Among the cellulose samples generated, using the 76 wt% sulfuric acid solution gave the highest negative value. In the C series (cellulose samples prepared by using the 64 wt% sulfuric acid solution), the zeta potential increases with increase in the temperature of the hydrolysis reaction. From these results, it is clear that the influence of temperature is dominant, being more significant than the reaction time at a given temperature.

3.5 Thermal Analysis

A detailed understanding of the degradation characteristics of polymers on heating is essential for selecting materials with improved properties for specific applications. Fundamental information regarding the thermal stability of the fibers used in the production of composites can be obtained from thermogravimetric analysis (TGA) and differential scanning calorimetry (DSC).

3.5.1 Thermogravimetric Analysis (TGA)

Thermogravimetric analysis of banana fiber specimens was analyzed to compare the degradation characteristics of the chemically treated fibers with the untreated fiber. The natural fibers present three main weight loss regions. The initial weight loss in the region 50–100 °C is mainly due to moisture evaporation.

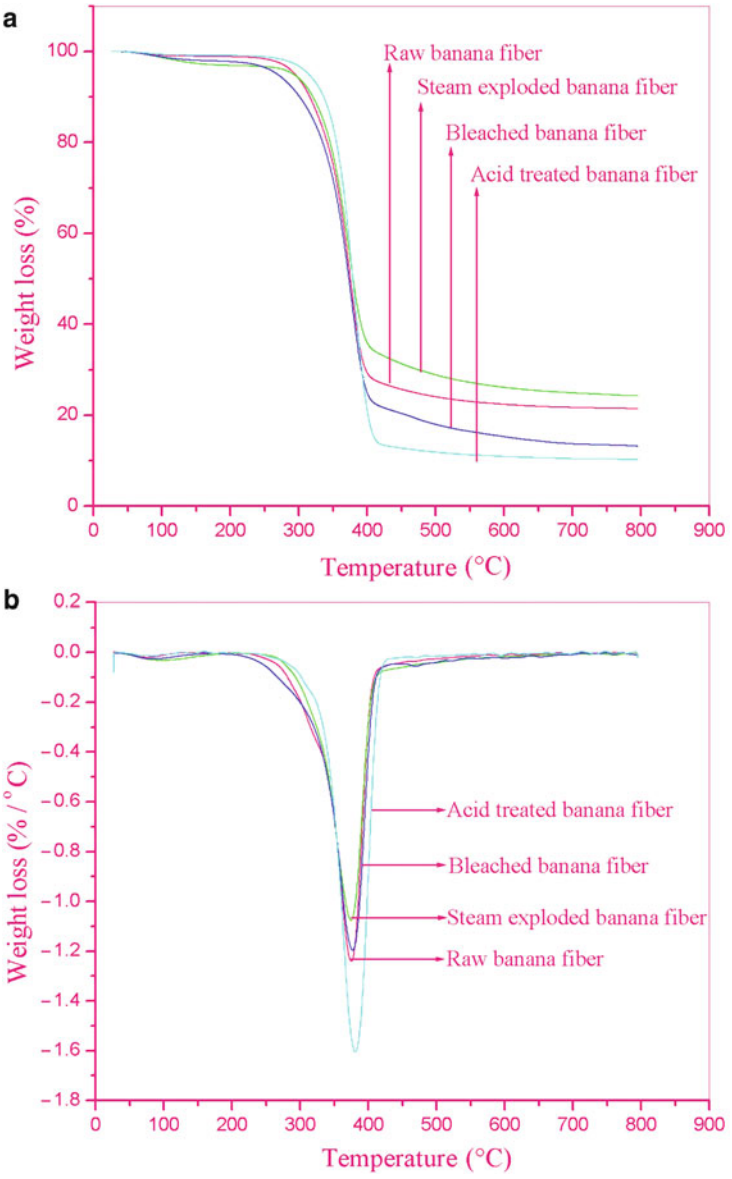

Fig. 6.8 (**a**) TG curves of the raw and treated banana fibres (**b**) DTG curves of raw and treated banana fibres [37]

The temperature region ranging from 220–300 °C is mainly attributed to thermal depolymerization of hemicellulose and the cleavage of glycosidic linkages of cellulose [45]. The broad peak in the region from 200–500 °C is contributed by lignin components, and the degradation of cellulose takes place between 275 °C and 400 °C [46, 47]. Figure 6.8a, b represents the thermogravimetric (TG) and

Table 6.5 Thermal behavior of raw and variously treated banana fibers [37]

Fiber characteristics	Peak temperature (°C)	% of degradation	Ash content at 800 °C
Raw banana fiber	374.6 (0.32)[a]	51.3 (0.003)	24.3 (0.12)
Steam-exploded fiber	80 (0.82)[b]	0.6 (0.002)	21.4 (0.07)
	373.3 (0.53)[a]	43.6 (0.04)	
Bleached banana fiber	93.9 (0.61)[b]	1.2 (0.01)	13.2 (0.24)
	376 (0.46)[a]	51.3 (0.03)	
Acid-treated fiber	380.1 (0.06)[*]	52.2 (0.02)	10.2 (0.06)

[*]Standard deviation
[a]Peak temperature corresponds to the thermal decomposition of the α-cellulose
[b]Peak temperature corresponds to the evaporation of moisture

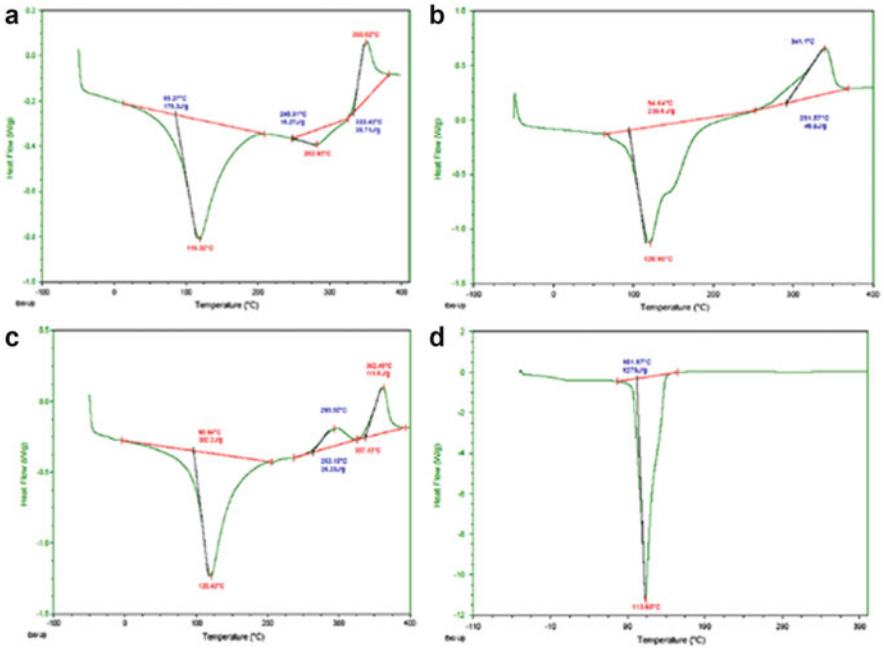

Fig. 6.9 DSC curves of banana fibre in various stages [37] (**a**) Raw banana fibre (**b**) Steam exploded banana fibre (**c**) Bleached banana fibre (**d**) Acid treated banana fibre

derivative thermogravimetric (DTG) curves of the raw and treated banana fibers, respectively. From Fig. 6.8 a, b, it is clear that there is a shift in the major decomposition temperature from 374–380 °C as we go from raw fiber to acid-treated banana fiber. Table 6.5 shows the thermal behavior of raw and variously treated banana fibers. TGA results confirmed that the thermal stability of the fibers increases during each processing step, having a higher value for acid-treated fiber.

3.5.2 Differential Scanning Calorimetry (DSC)

DSC measurements of banana fiber were conducted in a temperature range from 50 °C to 400 °C, at a constant heating rate of 10 °C/min. The heating DSC curves for raw and acid-treated banana fibers were expressed in terms of heat flow (Fig. 6.9). The DSC curves of all samples reveal evaporation of water around 110–120 °C, the degradation of the hemicellulose around 280–290 °C, followed by decomposition of α-cellulose around 340–360 °C. DSC studies substantiate that the treated fibers exhibit higher enthalpy values than the untreated fiber. The enthalpy value is minimum for the raw fiber and maximum for the acid-treated fiber. The increased percentage crystallinity of the fibers and the increased H-bonding between the closely packed cellulose chains during each treatment tend to stabilize the structure and increase the enthalpy values. The DSC and TGA results proved that the cellulose nanofibers of banana exhibit enhanced thermal properties, making them less prone to degradation and therefore can be processed at elevated temperatures over their untreated counterparts.

4 Conclusion

Nanocellulose based on agro-industrial waste products has become a fascinating building block for the design of new biomaterials. In this context, cellulose nanofibers from banana plant appear as a promising reinforcing component in the production of high performance polymer nanocomposites. This chapter has provided an overview of the current research efforts directed towards the extraction and characterization of nanocellulose from banana plant wastes. Several methods have been applied to extract highly purified nanofibrils from the plant cell wall. All of them lead to different types of nanomaterials, depending on the composition of cellulose raw material, its pretreatment conditions and the disintegration process. Steam explosion method has been found to be successful in obtaining fibers in the nanodimension from raw banana fiber. The comparisons of structural, morphological, and thermal properties of nanocellulose were characterized by various techniques like FTIR, XRD, SEM, TEM, AFM, and TGA. Studies revealed that banana nanofibers can be effectively utilized as a potential reinforcing candidate for the development of biocomposites.

References

1. Habibi Y, Lucia LA, Rojas OJ (2010) Cellulose Nanocrystals: Chemistry, Self-Assembly, and Applications. Chem Rev 110:3479
2. Eichhorn SJ (2011) Cellulose nanowhiskers: promising materials for advanced applications. Soft Matter 7:303
3. Klemm D, Kramer F, Moritz S, Lindstrom T, Ankerfors M, Gray D, Dorris A (2011) Nanocelluloses: A New Family of Nature-Based Materials. Angew Chem Int Ed 50:5438
4. Peng BL, Dhar N, Liu HL, Tam KC (2011) Chemistry and Applications of Nanocrystalline Cellulose and its Derivatives: A Nanotechnology Perspective. Can J Chem Eng 89:1191

5. Khalil HPSA, Bhat AH, Yusra AFI (2012) Green composites from sustainable cellulose nanofibrils: A review. Carbo Hyd Polym 87:963
6. Azeredo HMC, Mattoso LHC, Wood D, Williams TG, Avena-Bustillos RJ, Mchugh TH (2009) Nanocomposite edible films from mango puree reinforced with cellulose nanofibers. J Food Sci 74:31
7. Fukuzumi H, Saito T, Wata T, Kumamoto Y, Isogai A (2009) Transparent and high gas barrier films of cellulose nanofibers prepared by TEMPO-mediated oxidation. Biomacromolecules 10:162
8. Cho MJ, Park BD (2011) Tensile and thermal properties of nanocellulose-reinforced poly (vinyl alcohol) Nanocomposites. J Ind Eng Chem 17:36
9. Tonoli GHD, Teixeira EM, Corrêa AC, Marconcini JM, Caixeta LA, Pereira-da-Silva MA, Mattoso LHC (2012) Cellulose micro/nanofibres from Eucalyptus kraft pulp: Preparation and properties. Carbo Hyd Polym 89:80
10. Wei L, Yue J, Liu S (2012) Preparation of nanocrystalline cellulose via ultrasound and its reinforcement bcapability for poly(vinyl alcohol) composites. Ultrason Chem 19:479
11. Morais JPS, Rosa MF, Filho MMS, Nascimento LD, Nascimento DM, Cassales AR (2013) Extraction and characterization of nanocellulose structures from raw cotton linter. Carbo Hyd Polym 91:229
12. Cao X, Ding Yu J, Al-Deyab SS (2012) Cellulose nanowhiskers extracted from TEMPO-oxidized jute fibers. Carbo Hyd Polym 90:1075
13. Lin N, Bruzzese C, Dufresne A (2012) TEMPO-Oxidized Nanocellulose Participating as Crosslinking Aid for Alginate-Based Sponges. ACS Appl Mater Interfaces 4:4948
14. Neto WPF, Silverio HA, Dantas NO, Pasquini D (2013) Extraction and characterization of cellulose nanocrystals from agro-industrial residue – Soy hulls. Ind Crop Prod 42:480
15. Ioelowich M (2008) Cellulose as a nanostructured polymer: a short review. Bioresources 3:1403
16. Siqueira G, Bras J, Dufresne A (2010) Cellulosic Bionanocomposites: A Review of Preparation, Properties and Applications. Polymer 2:728
17. Moon RJ, Martini A, Nairn J, Simonsen J, Youngblood J (2011) Cellulose nanomaterials review: structure, properties and nanocomposites. Chem Soc Rev 08:3941
18. Nogi M, Iwamoto S, Nakagaito AN, Yano H (2009) Optically transparent nanofibre paper. Adv Mater 21:1595
19. Ping L, Hsieh YL (2009) Cellulose nanocrystal-filled poly(acrylic acid) nanocomposite fibrous membranes. Nanotechnology 20:415604
20. Deng H, Zhou X, Wang X, Zhang C, Ding B, Zhang QH, Du Y (2010) Layer-by layer structured polysaccharides film-coated cellulose nanofibrous mats for cell culture. Carbo Hyd Polym 80:475
21. Das K, Ray D, Bandyopadhyay NR, Sahoo S, Mohanty KA, Misra M (2011) Physicomechanical properties of the jute micro/nanofibril reinforced starch/polyvinyl alcohol biocomposite films. Compos B 42:376
22. Nakagaito AN, Yano H (2004) The effect of morphological changes from pulp fiber towards nano-scale fibrillated cellulose on the mechanical properties of high strength plant fiber based composites. Appl Phys A Mater Sci Proc 78:547
23. Stenstad P, Andresen M, Tanem BS, Stenius P (2008) Chemical surface modification of microfibrillated cellulose. Cellulose 15:35
24. Cheng Q, Wang S, Rials TG (2009) Poly(vinyl alcohol) nanocomposites reinforced with cellulose fibrils isolated by high intensity ultrasonication. Compos A Appl Sci Manuf 40:218
25. Chakraborty A, Sain M, Kortschot M (2005) Cellulose microfibrils: A novel method of preparation using high shear refining and cryocrushing. Holzforschung 59:102
26. Cherian BM, Leao AL, Souza SF, Thomas S, Pothan LA, Kottaisamy M (2010) Isolation of nanocellulose from pineapple leaf fibres by steam explosion. Carbo Polym 81:720
27. Abraham E, Deepa B, Pothan LA, Jacob M, Thomas S, Cvelbar U, Anandjiwala R (2011) Extraction of nanocellulose fibrils from lignocellulosic fibres: A novel approach. Carbo Polym 86:1468

28. Teixeira EM, Bondancia TJ, Teodoro KBR, Correa AC, Marconcini JM, Mattoso LHC (2011) Sugarcane bagasse whiskers: extraction and characterizations. Ind Crop Prod 33:63
29. Kaushik A, Singh M (2011) Isolation and characterization of cellulose nanofibrils from wheat straw using steam explosion coupled with high shear homogenization. Carbohyd Res 346:76
30. Teixeira EM, Corrêa AC, Manzoli A, Leite FL, Oliveira CR, Mattoso LHC (2010) Cellulose nanofibers from white and naturally colored cotton fibers. Cellulose 17:595
31. Woehl MA, Canestraro CD, Mikowski A, Sierakowski MR, Ramos LP, Wypych F (2010) Bionanocomposites of thermoplastic starch reinforced with bacterial cellulose nanofibres: Effect of enzymatic treatment on mechanical properties. Carbo Polym 80:866
32. Chen W, Yu H, Liu Y, Hai Y, Zhang M, Chen P (2011) Isolation and characterization of cellulose nanofibers from four plant cellulose fibers using a chemical-ultrasonic process. Cellulose 18:433
33. Moran JI, Alvarez VA, Cyras VP, Vazquez A (2008) Extraction of cellulose and preparation of nanocellulose from sisal fibers. Cellulose 15:149
34. Rosa MF, Medeiros ES, Malmonge JA, Gregorski KS, Wood DF, Mattoso LHC (2010) Cellulose nanowhiskers from coconut husk fibers: Effect of preparation conditions on their thermal and morphological behavior. Carbo Polym 81:82
35. Cherian BM, Pothan LA, Nguyen-Chung T, Mennig G, Kottaisamy M, Thomas S (2008) A novel method for the synthesis of cellulose nanofibril whiskers from banana fibers and characterization. J Agr Food Chem 56:5617
36. Elanthikkal S, Gopalakrishnapanicker U, Varghese S, Guthrie J (2010) Cellulose microfibres produced from banana plant wastes: Isolation and characterization. Carbo Hyd Polym 80:852
37. Deepa B, Abraham E, Cherian BM, Bismarck A, Blaker JJ, Pothan LA, Leao AL, de Souza SF, Kottaisamy M (2011) Structure, morphology and thermal characteristics of banana nano fibres obtained by steam explosion. Bioresource Technol 102:1988
38. Bhatnagar A, Sain M (2005) Processing of cellulose nanofibers-reinforced composites. J Reinf Plast Comp 24:1259
39. Sheltamia RM, Abdullaha I, Ahmada I, Dufresne A, Kargarzadeh H (2012) Extraction of cellulose nanocrystals from mengkuang leaves (Pandanus tectorius). Carbo Polym 88:772
40. Das K, Ray D, Banerjee C, Bandyopadhyay NR, Sahoo S, Mohanty AK (2010) Physicomechanical and thermal properties of jute nanofiber reinforced biocopolyester composites. Ind Eng Chem Res 49:2775
41. Rongji LR, Fei J, Cai Y, Li Y, Feng J, Yao J (2009) Cellulose whiskers extracted from mulberry: A novel biomass production. Carbo Hyd Polym 76:94
42. Alemdar A, Sain M (2008) Isolation and characterization of nanofibers from agricultural residues – wheat straw and soy hulls. Bioresource Technol 99:1664
43. Purkait BS, Ray D, Sengupta S, Kar T, Mohanty A, Misra M (2011) Isolation of cellulose nanoparticles from sesame husk. Ind Eng Chem Res 50:871
44. Zuluaga R, Putaux JL, Restrepo A, Mondragon I, Ganan P (2007) Cellulose microfibrils from banana farming residues: Isolation and characterization. Cellulose 14:585
45. Manfredi BL, Rodriguez ES, Wladyka-Przybylak M, Vazquez A (2006) Thermal degradation and fire resistance of unsaturated polyester modified acrylic resins and their composites with natural fibers. Polym Degrad Stab 91:255
46. Alvarez VA, Vázquez A (2004) Thermal degradation of cellulose derivatives/starch blends and sisal fiber biocomposites. Polym Degrad Stab 84:13
47. Ouajai S, Shanks RA (2005) Composition, structure and thermal degradation of hemp cellulose after chemical treatments. Polym Degrad Stab 89:327

Extraction and Production of Cellulose Nanofibers

7

A. Vazquez, M. Laura Foresti, Juan I. Moran, and Viviana P. Cyras

Contents

Abstract

The chapter will content the review of different methodologies used for obtaining nanofibers of cellulose from lignocellulosic materials and bacterial cellulose. The first part of the chapter will deal with the extraction of cellulose. The classic methodology implies alkaline and acid treatment, but new ones include milder chemical conditions as well as chemo-enzymatic protocols. The second part deals with production of nanofibers from cellulose. Extraction of cellulose nanoparticles from lignocellulose materials has different routes: acid hydrolysis, mechanical, and enzymatic treatments. Strong acid hydrolysis promotes transversal cleavage of non-crystalline fractions of cellulose microfibrils,

A. Vazquez (✉) • M.L. Foresti
Instituto de Tecnología en Polímeros y Nanotecnología (ITPN), Engineering Faculty, University of Buenos Aires, National Research Council (CONICET), Las Heras, Buenos Aires, Argentina
e-mail: avazquez@fi.uba.ar; mforesti@fi.uba.ar

J.I. Moran • V.P. Cyras
Facultad de Ingeniería, Instituto de Investigación en Ciencia y Tecnología de Materiales (INTEMA), Universidad de Mar del Plata, Mar del Plata, Argentina
e-mail: jmoran@fi.mdp.edu.ar; vpcyras@fi.mdp.edu.ar

J.K. Pandey et al. (eds.), *Handbook of Polymer Nanocomposites. Processing, Performance and Application – Volume C: Polymer Nanocomposites of Cellulose Nanoparticles*,
DOI 10.1007/978-3-642-45232-1_57,

leading to the so-called cellulose nanocrystals or whiskers. Nanocrystals are characterized by high crystallinity and their aqueous suspensions display a colloidal behavior. On the other hand, strong mechanical treatment that imposes high shear forces to cellulose fibers allows the extraction of microfibrils and microfibril aggregates with high aspect ratio which form highly entangled networks. This kind of nanocellulose is called microfibrillated cellulose (MFC). Although widely used the mechanical process developed for the production of MFC has an important drawback which is the high energy input involved (several passes through high-pressure homogenizers which get blocked frequently). In the last years, enzymatic and chemical pretreatments have been proposed to reduce the energy input of the process. Moreover, microbially produced cellulose pellicles appear also as an attractive route of cellulose nanofibers, which will also be described in the chapter.

Keywords
Cellulose • Nanofibers • Isolation methods

1 Introduction

During the last decades, the use of agro-based fibers as an alternative to synthetic inorganic fibers has drawn much attention of researchers and markets all over the world. Attention has been initially driven to the use of natural fibers and has lately been directed towards the use of pure cellulose and nanocellulose fibers as reinforcement for both synthetic polymers and biopolymers.

The production of nanoscale cellulose fibers and their application in composite materials have gained increasing attention, as it is evidenced by the increasing number of scientific articles and reviews published in the last 5 years [1–9]. This is due to a number of desirable characteristics of nanocellulose which include renewability, abundance and low cost of the raw material, large surface-to-volume ratio, high strength and stiffness, very low coefficient of thermal expansion, low weight, low density, high aspect ratio, and biodegradability [10]. Applications of nanocellulose particles are vast, including reinforcement of composite materials, moistening masks for cosmetic applications, filtration media, thickening agents, rheology modifiers, adsorbents, paper reinforcement, synthesis of polymers with liquid crystalline behavior for electronic applications, delivery of drugs, flavor carriers, suspension stabilizer, and optically transparent films, among others [11–14]. Moreover, in the last years an outstanding number of uses of nanocellulose in biomedical applications have been reported including not only tissue engineering scaffolds but also wound coverage, regeneration of damaged organs, blood vessel replacement, and more [7, 10, 15, 16].

Two are the main sources of nanocellulose: lignocellulose material and bacterial cellulose. Isolation of cellulose nanoparticles from lignocellulose sources normally needs a first stage devoted to the purification of the source material or pulping methods. In the case of lignocellulosic sources such as wood and natural fibers,

pretreatment implies complete or partial removal of matrix materials (hemicellulose, lignin, impurities) and the isolation of individual cellulose fibers (micron sized). Kraft pulp and dissolving pulp are cellulose sources widely used for nanocellulose extraction. In reference to tunicates, which are the only animals known to produce cellulose microfibrils, pretreatment involves the isolation of the mantel and extraction of individual cellulose fibrils by removal of the protein matrix in which they are embedded. For algae-derived cellulose, removal of algae wall matrix material is needed. The following part of the chapter will review both methods.

2 Cellulose from Lignocellulose Sources and Isolation Methods

2.1 Cellulose Sources

Cellulose is the most abundant renewable organic material produced in the biosphere, having an annual production that is estimated to be over 7.5×10^{10} t [17]. It is the major component of wood and most natural fibers such as cotton, flax, hemp, jute, ramie, and sisal, and it is also produced by a family of sea animals called tunicates, several species of algae and bacteria, and also by some fungi and amoeba. Regardless of its source, cellulose consists of a linear homopolysaccharide composed of β-D-glucopyranose units linked by β-1-4-linkages [18]. The repeat unit of cellulose is called cellobiose, and it comprises two anhydroglucose rings $(C_6H_{10}O_5)_n$ linked together through an oxygen covalently bonded to C1 of one glucose ring and C4 of the adjoining ring, the so-called $\beta - 1\text{–}4$ glucosidic bond [1]. Although as raw material cellulose fibers and many of their derivatives have been known and used for more than a hundred and fifty years, in the last decade cellulose has received a revived interest based on the understanding that macrofibers are built up by smaller and mechanically stronger entities which can be extracted under proper conditions. Since then extraction of cellulose nanoparticles (i.e., cellulose elements having at least one dimension in the 1–100 nm range), generally referred as nanocellulose, has received increasing attention. Figure 7.1 illustrates the hierarchical structure of wood, in which nanoscale dimensions of its constituents are shown.

During biosynthesis of cellulose chains, van der Waals forces and hydrogen bonding between hydroxyl groups and oxygens of adjacent molecules promote parallel stacking of multiple cellulose chains forming elementary fibrils that further aggregate into larger microfibrils [8]. Depending on their origin, the microfibrils diameters may vary, but in general they are within 5–50 nm and several microns in length. Microfibrils contain crystalline and amorphous zones. In fact, each microfibril can be considered as a string of cellulose nanocrystals linked along the microfibril axis by disordered amorphous domains, e.g., twists and kinks [1, 20]. The length of crystallites of cellulose from various origins has been reported to be in the range 50–150 nm, while disordered domain lengths are 25–50 nm [2].

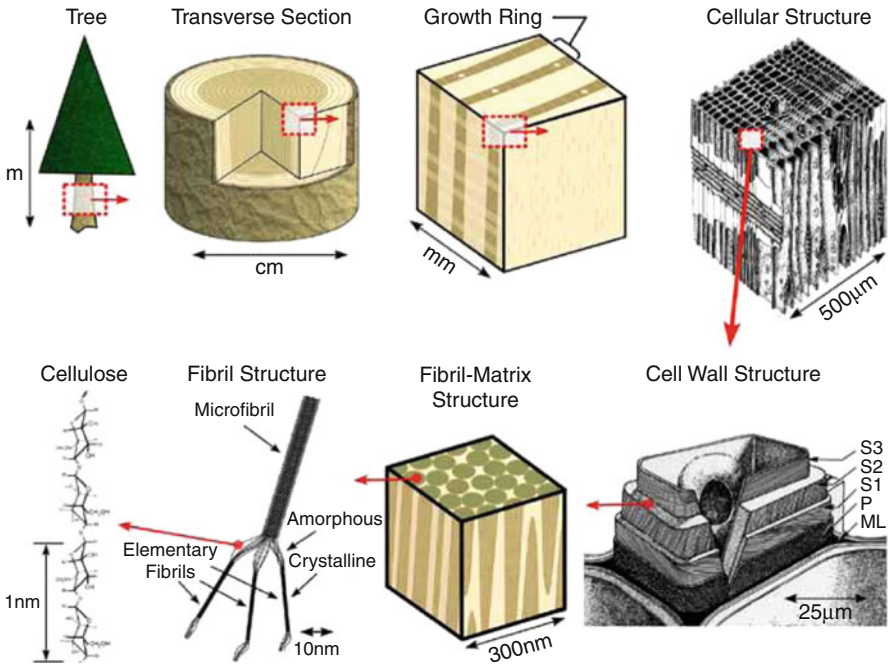

Fig. 7.1 Schematic of the wood hierarchical structure [19]

Cellulose, which awards for the mechanical properties of the complete natural fibers, appears as parallel microfibrils embedded in a continuous matrix of lignin and hemicellulose [21, 22]. Cellulose microfibrils can be found as intertwined microfibrils in the cell wall (2–20 lm diameter and 100–40,000 nm long depending on it source) [23, 24]. The first references to the existence of definite crystalline zones interposed in the amorphous structure of cellulose materials were made by Nageli and Schwendener, who in 1877 already confirmed the optical anisotropy of vegetable products both in cell walls and in fibers [1]. Hemicellulose is composed of different types of cycled saccharides such as xylose, mannose, and glucose, among others. It forms a highly branched random structure. Lignins are amorphous polymers formed by phenylpropane units. They mainly consist of aromatic units such as guaiacyl, syringyl, and phenylpropane. Table 7.1 illustrates the composition of some lignocellulosic fibers.

Physical treatments of lignocellulosic biomass, such as crushing, grinding, steam explosion, and irradiation, have been proven to be effective in creating accessibility to chemicals and enzymes. These methods for isolating cellulose and making it readily available for its use as reinforcement will be reviewed later in this chapter.

2.2 Isolation Methods or Pulping Processes

Pulp consists of cellulose fibers, usually acquired from wood. The liberation of these fibers from the wood matrix can be done in three ways: mechanically,

Table 7.1 Composition of some lignocellulosic fibers [25]

Type of biofibre	Composition (%)				
	Source	Cellulose	Hemicellulose	Lignin	Extract
Wood	Hardwood	43–47	25–35	16–24	2–8
	Softwood	40–44	25–29	25–31	1–5
Non-wood	Bagasse	40	30	20	10
	Coir	32–43	10–20	43–49	4
	Corn cobs	45	35	15	5
	Corn stalks	35	25	35	5
	Cotton	95	2	1	0.4
	EFB	50	30	17	3
	Flax (retted)	71	21	2	6
	Flax (unretted)	63	12	3	13
	Hemp	70	22	6	2
	Henequen	78	4–8	13	4
	Istle	73	4–8	17	2
	Jute	71	14	13	2
	Kenaf	36	21	18	2
	Ramie	76	17	1	6
	Sisal	73	14	11	2
	Sunn	80	10	6	3
	Wheat straw	30	50	15	5

chemically, or enzymatically. Mechanical methods are energy consuming, usually demanding high levels of pressure or kinetic energy. The product obtained by mechanical pulping has the same composition than the original feeding. Different intensive mechanical processes have been used to extract cellulose fibrils from a diversity of cellulose sources. Main mechanical methods include grinders/refiners [26–29], cryocrushing [30–34], and high-intensity ultrasonic treatments [35].

Chemical pulping involves several agents aimed to dissolve the lignin-hemicellulose matrix that surrounds the cellulose fibers. Therefore, lower yields are achieved (depending on the cellulose source), and usually a great extent of carbohydrate degradation takes place simultaneously. One of the most important problems regarding chemical pulping is related to the environmental impact of the by-products and residues of the process. The most common processes for dissolving lignin and hemicellulose are based on the Kraft process, which dates from 1884 [36] and utilizes sodium hydroxide (NaOH) and sodium sulfide (Na_2S), followed by a bleaching stage usually involving hydrogen peroxide (H_2O_2), chlorine dioxide (ClO_2), ozone (O_3), or peracetic acid. Several chlorine- and/or sulfide-free treatments have been proposed in order to reduce the ecological impact of the pulping process [37].

Besides the traditional pulping processes, biological or enzymatic pulping is receiving a lot of attention. This method relies on the ability of certain microorganisms and their secreted enzymes (i.e., xylanase) to directly depolymerize

hemicellulose and attack the lignin/cellulose interface. This pulping method facilitates the separation of purified cellulose with minimal degradation and superior quality pulps [38, 39].

2.2.1 Chemical Pulping

Obtaining pure cellulose from different type of plants and bioresources by chemical methods has been extensively studied. In general, the first stage is elimination of lignin and then the hemicellulose, because the delignification can significantly facilitate the extraction of the hemicelluloses before it is possible to obtain cellulose with high purity. There are various chemical methods; some of them are alkali extraction, alkaline and sodium chlorite treatment, alkaline and peroxide extraction, organic solvent extraction, acidic method, liquid-phase oxidation, or a combination of these treatments [40–43].

As mentioned earlier, the most common chemical pulping method and still used by more than 75 % of the commercial papermaking industries is the Kraft method [42]. However, researchers are constantly developing improved pulping processes in order to maximize cellulose yields and purity, obtain a specific type of cellulose, or reduce the environmental impact (reduce energy consumption and generation of toxic by-products). Johar et al. [41], extracted cellulose fibers from rice husk with alkali (4 wt% NaOH) and bleaching treatments: by acetic acid, aqueous chlorite (1.7 wt%) at reflux (100–130 °C) for 4 h. The material obtained was characterized by scanning electron microscopy (SEM), transmission electron microscopy (TEM), Fourier transform infrared (FTIR) spectroscopy, X-ray diffraction (XRD) analysis, and thermogravimetric analysis (TGA). The color of the rice husk is brown; it changes to brownish-orange after alkaline treatment and to white after bleached treatment. The color changes are due to the removal of non-cellulosic materials, i.e., lignin, hemicelluloses, pectin, and wax, upon chemical treatment of the rice husks (Fig. 7.2) [41].

The effects of different stages of treatment in chemical structure of rice husk were analyzed by spectroscopic analysis (FTIR) (Fig. 7.3). The peaks corresponding to cellulose structure appear in all the samples indicating that the cellulose is present in all of them (3,440–3,400 cm^{-1}, C-H and O-H groups). Instead, the peak at 1,700 cm^{-1} (acetyl and ester groups in hemicellulose or carboxylic acid groups in the lignin) present in the spectrum of rice husk disappears after treatment indicating the removal of non-cellulosic materials.

Sun and Sun [43] performed the extraction of hemicellulose with alkali, peroxide, and alkali with sodium borate treatment from barley straw. This successive extraction resulted in dissolution of 91.1 % of hemicellulose and 84.8 % of lignin. Also, the hemicellulose isolated with alkaline peroxide had much higher molecular weights than those isolated with alkali alone. Figure 7.4 shows a scheme of the methodology used.

Sun et al. [44] used a chlorine-free procedure in order to isolate cellulose from wheat straw. The first treatment was performed with NaOH/methanol at 60 °C under ultrasonic irradiation. Then the sample was treated with H_2O_2-TAED at 48 °C, to solubilized hemicelluloses and lignin. The cellulose obtained contained

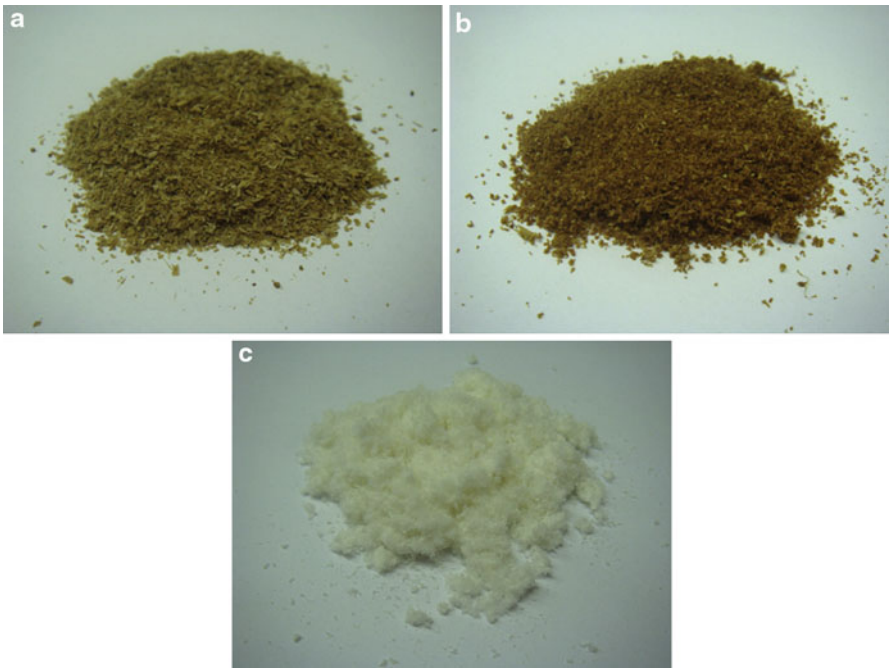

Fig. 7.2 Photographs of rice husk: (**a**) Untreated, (**b**) alkali-treated, and (**c**) bleached rice husk [41]

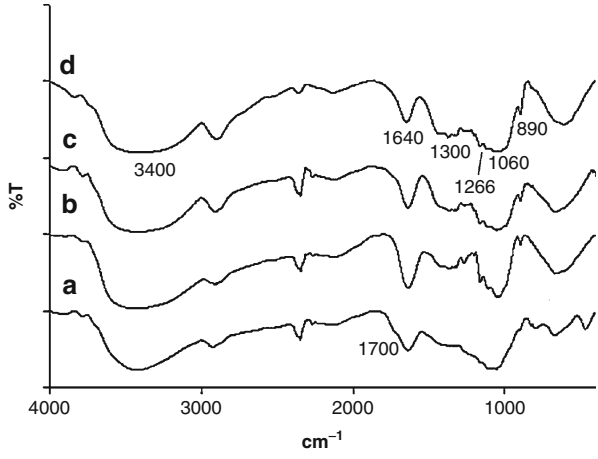

Fig. 7.3 FTIR spectra recorded for (**a**) Raw, (**b**) alkali-treated, (**c**) bleached, and (**d**) acid-hydrolyzed rice husk [41]

11.2–12.2 % of hemicelluloses and 2.5–2.9 % of lignin. To purify the cellulose the sample finally was treated with 80 % acetic acid/70 % nitric acid. The cellulose was studied by FTIR and CP/MAS ^{13}C NMR spectroscopy. The scheme of this method is showed in Fig. 7.5 [40].

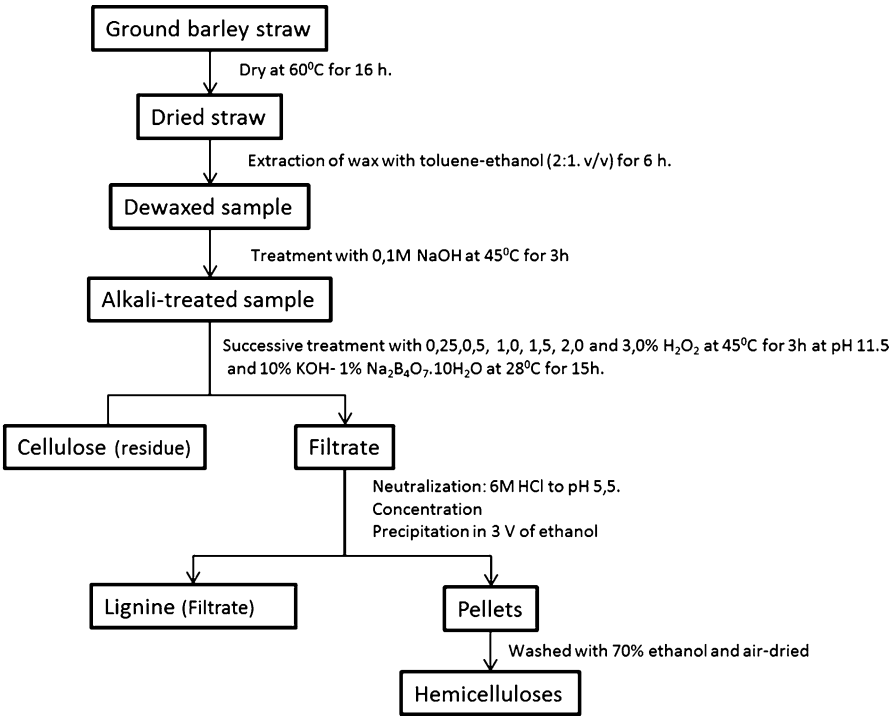

Fig. 7.4 Scheme of the methodology used by Sun and Sun [43]

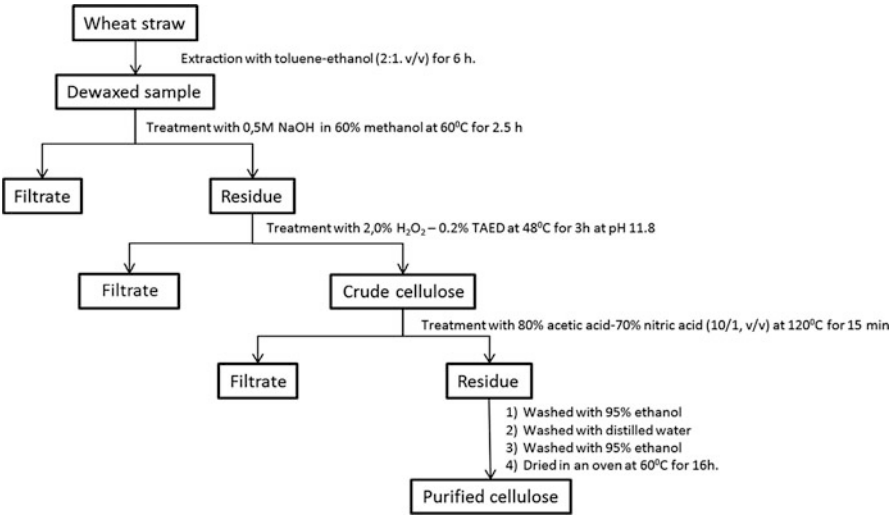

Fig. 7.5 Scheme of the methodology used by Sun and Sun [44]

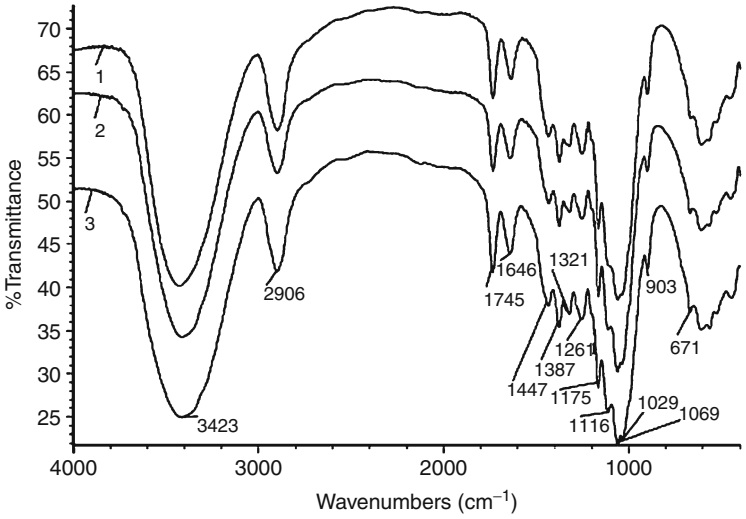

Fig. 7.6 FTIR spectra of purified cellulose obtained by treatment with 80 % acetic acid/70 % nitric acid at 120°C without ultrasonic assistance (spectrum 1) and with ultrasonic assistance for 15 (spectrum 2) and 30 min (spectrum 3) and treated with H_2O_2-0.2 % TAED [44]

Figure 7.6 shows the effect of the different stages in the chemical structure of sample. The treatment with 80 % acetic acid/-70 % nitric acid removed the residual lignin (which is inferred by the disappearance of the absorbance at 1,512 cm^{-1}), and acetylation occurred (appearance of acetyl ester bands at 1,745 cm^{-1}, 1,387 cm^{-1}, and 1,261 cm^{-1} [40, 44]).

Sun et al. [45] obtained cellulose from wheat straw by delignification with acetic and formic acid and methanol and ethanol treatment, followed by a bleaching with cyanamide-activated hydrogen peroxide in order to degrade the residual hemicelluloses and lignin. Organic acids were more effective than alcohols on the degradation of lignin and hemicelluloses. Figure 7.7 shows a scheme of the procedure. The cellulose was characterized by FTIR and CP/MAS 13C NMR spectroscopy and thermogravimetric analysis (TGA).

The FTIR spectrum of the sample obtained after the bleaching treatment did not show the band at 1,513 cm^{-1}, which indicates that lignin was removed (Fig. 7.8). Nevertheless, the lignin associated to the hemicelluloses or cellulose is strongly bound, and it resists the attack.

Sun et al. [46, 47] extracted the lignin and hemicelluloses from wheat straw with acidic dioxane/water solution and dimethyl sulfoxide. The scheme of extraction is showed in Fig. 7.9. The products of extraction were studied by sugar analysis, nitrobenzene oxidation, Fourier transform infrared (FTIR), one- and two-dimensional NMR spectroscopy, and gel permeation chromatography (GPC).

Morán et al. [37], compared two procedures for cellulose extraction from sisal fibers. One of these treated sisal fibers with NaOH at 45 °C, with H_2O_2 at 45 °C, and finally with 80 % acetic acid/70 % nitric acid. The other procedure is a chlorine

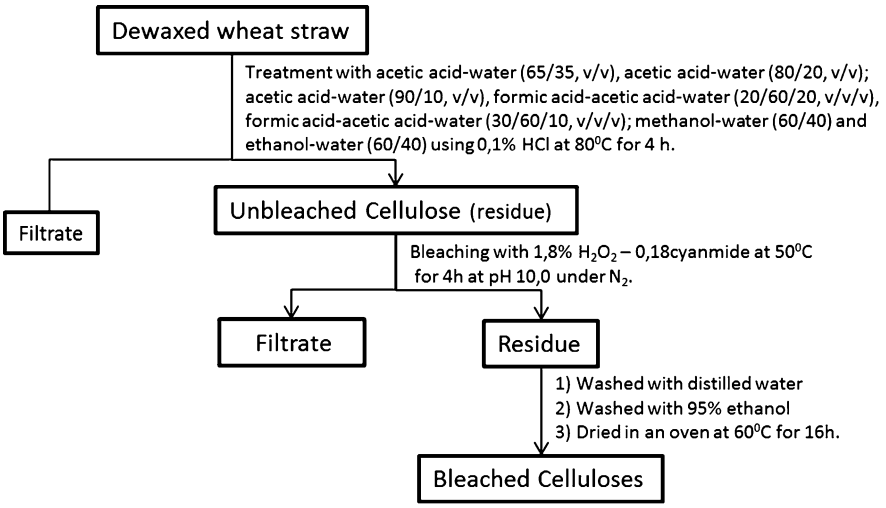

Fig. 7.7 Scheme of the methodology used by Sun et al. [45]

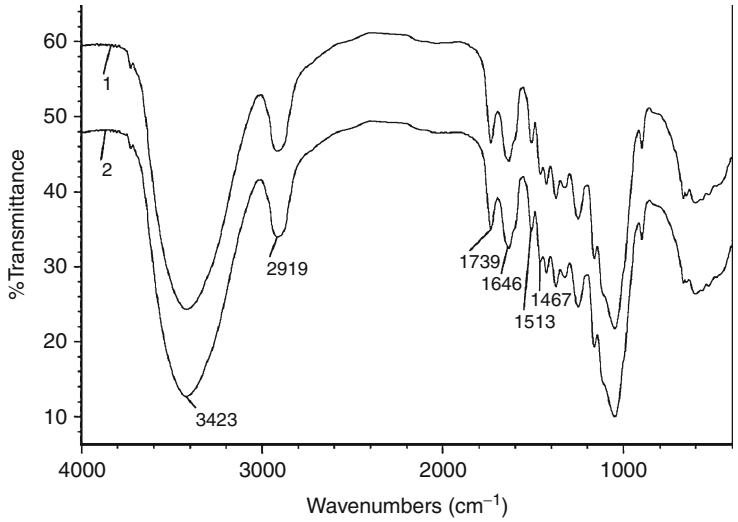

Fig. 7.8 FTIR spectra of unbleached cellulose samples obtained in the presence of alcohol [45]

method. The first method assayed was less environmentally aggressive. On the other hand, the second one involved less stages, and the obtained fibers showed a more homogeneous diameter distribution (Fig. 7.10). In order to characterize the obtained cellulose, TGA, FTIR, DSC, and XRD were done. Figure 7.11 shows a scheme of the two procedures performed.

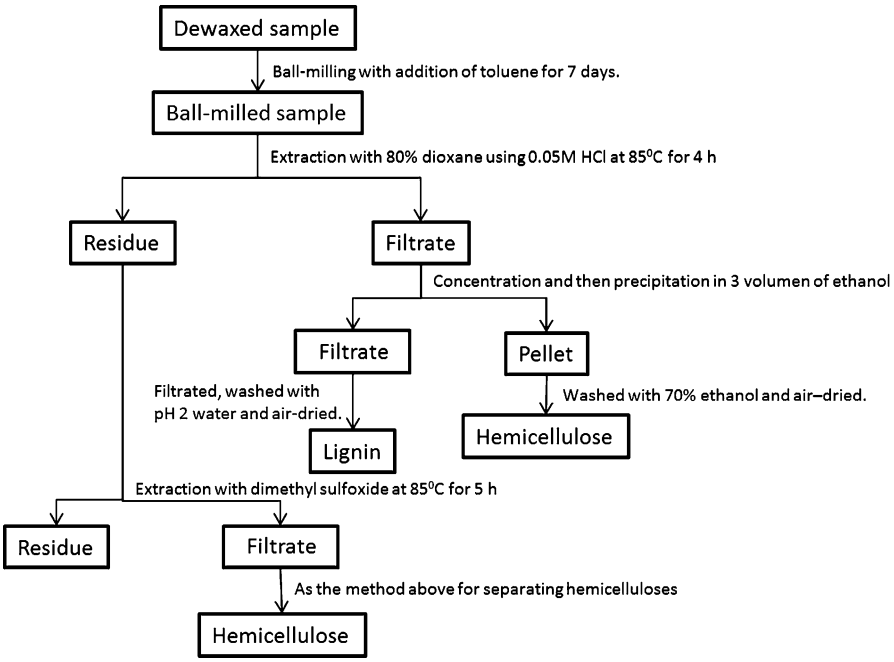

Fig. 7.9 Scheme of the methodology used by Sun et al. [46]

Yan et al. [48] used liquid-phase oxidation to extract cellulose from palm kernel. Palm kernel was treated in water at 180 °C and with 30 % H_2O_2 at 60 °C. In this step the lignin was converted to water-soluble compounds, and the hemicellulose was converted to saccharides by the hot water treatment. Pure cellulose was obtained and characterized by Fourier transform infrared spectroscopy (FTIR). The scheme for extraction is shown in Fig. 7.12.

Wang et al. [49] obtained cellulose from different wood sources by an environmentally friendly method, which consists of the utilization of 1-allyl-3-methylimidazolium chloride and molten salts with glass transition or melting temperatures below 100 °C. The method is able to destroy inter- and intramolecular hydrogen bonds between lignocelluloses. The reaction time can be significantly reduced by microwave irradiation. In order to analyze the cellulose obtained, authors used ^{13}C CP/MAS NMR, FTIR, XRD, and SEM [31, 49, 50].

Brendel et al. [51], extracted cellulose from pine wood samples with high purity by the method shown in Fig. 7.13. The method is fast and needs standard laboratory equipment and chemicals. In order to analyze the cellulose-obtained anion exchange chromatography with pulsed amperometric detection, DRIFT spectroscopy and elemental analysis were used [51].

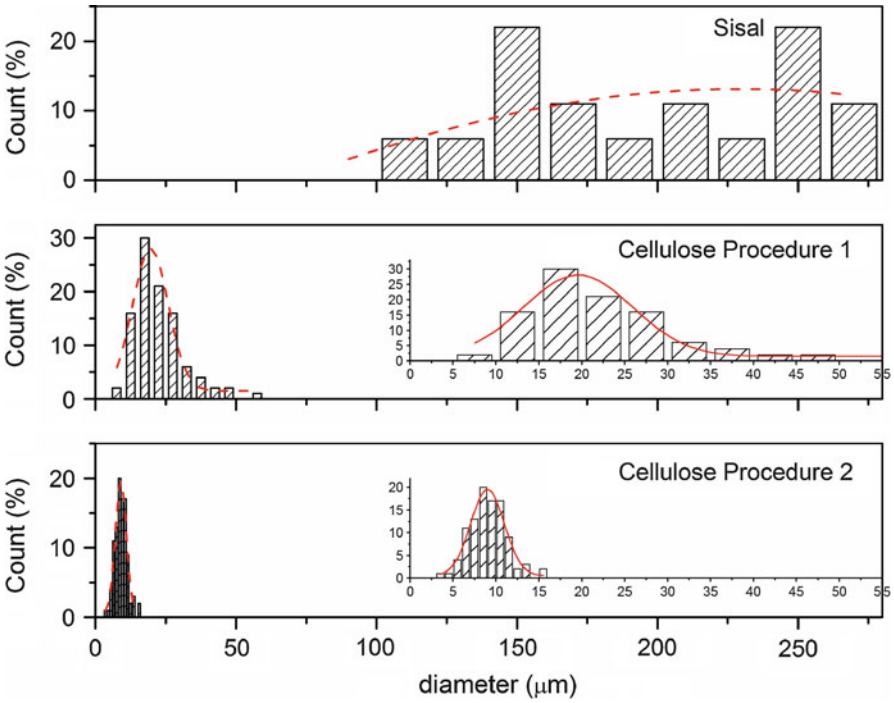

Fig. 7.10 Diameter distribution of extracted cellulose microfibrils [37]

2.2.2 Grinding, Refining and Cryocrushing

Groundwood pulp is produced by pressing roundwood logs against a rotating cylinder made of sandstone, scraping the fibers off. Dry grinding potentially pretreats biomass increasing its reactivity without any effluent production. However, energy consumption is held to be the limiting factor of applying biomass fine grinding industrially [52].

Another type of mechanical pulp is refiner pulp, obtained by feeding wood chips into the center of the rotating, refining discs in the presence of water spray. The disks are grooved; the closer the wood material gets to the edge of the disk, the finer the pulp [53]. The refining process used is common in the paper industry and is accomplished via a piece of equipment called a refiner. In a disk refiner, the dilute fiber suspension to be treated is forced through a gap between the rotor and stator disks, which have surfaces fitted with bars and grooves, against which the fibers are subjected to repeated cyclic stresses. This mechanical treatment brings about irreversible changes in the fibers, increasing their bonding potential by modification of their morphology and size.

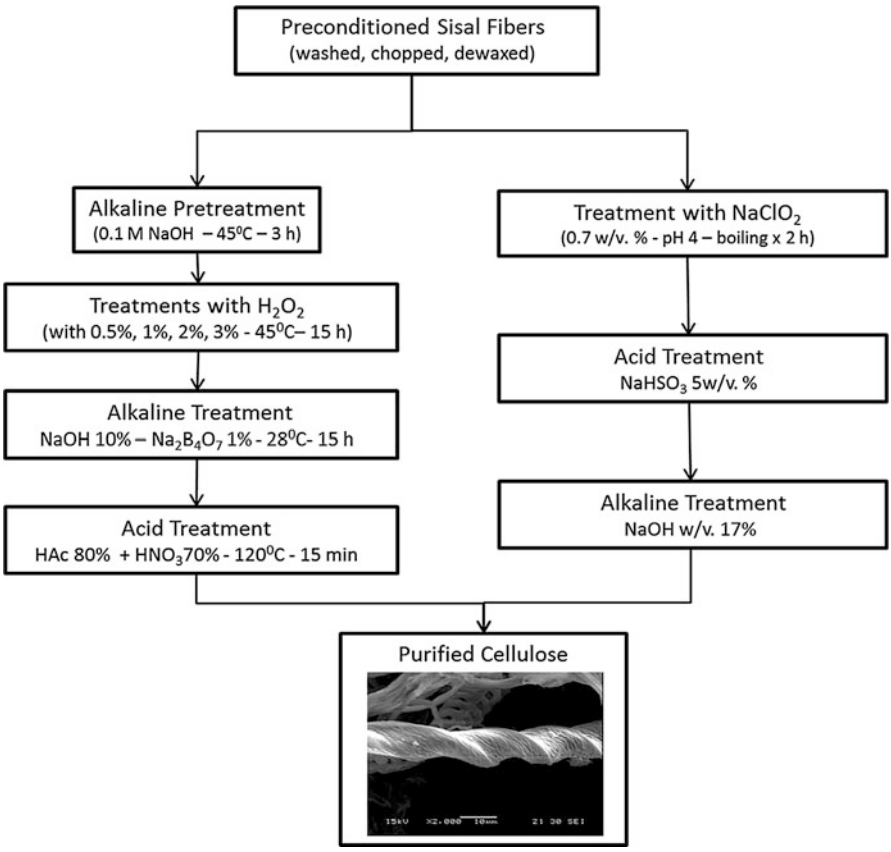

Fig. 7.11 Scheme of the methodology used by Moran et al. [37]

2.2.3 Steam Explosion

The steam explosion treatment has been and is still being extensively studied as a promising mechanical pulping method [54–56]. Lignocellulosic biomass materials can be fractionated into biopolymer constituents by steam explosion technology. The steam explosion process was invented by Mason in 1927 as a process to produce fibers for board production. The steam explosion treatment of lignocellulosic resources involves filling a cylinder with wood chips, sealing and pressurizing with saturated steam at pressures up to 1,000 psi. The chips are permeated by the saturated steam and develop high internal pressures. When the pressure is suddenly released, the chips are defibrated by the sudden decompression [7]. During the steam explosion significant amounts of sugars and phenolic compounds are obtained due to partial hemicellulose hydrolysis and lignin depolymerization. These degradation reactions (autohydrolysis) are catalyzed by acetic acid formed when the acetyl groups present in hemicelluloses are exposed to high temperatures [58].

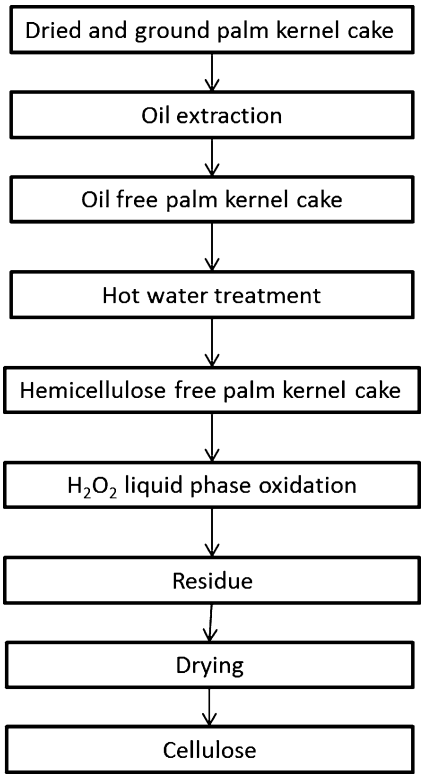

Fig. 7.12 Scheme for extraction of cellulose used by Yan et al. [48]

Researchers have attempted to avoid fiber degradation by the application of different chemicals. Steam was first replaced with ammonia and later with liquid sulfur dioxide, but the commercial application was precluded by some technical and economic problems. Finally, steam explosion of aqueous systems at moderate temperatures and higher pressures led to non-degraded cellulosic pulps, overcoming the problem of oxidation and hydrolytic degradation [59]. Figure 7.14 shows the fractionation scheme of hemp fibers by steam explosion treatment.

2.2.4 Biological Pulping

Traditional chemical bleaching processes produce hazardous toxic by-products that are released into the environment together with waste waters. In the last years, a new tendency is the replacement of the classical process with biobleaching processes. Biobleaching involves using microorganisms and enzymes to bleach pulp. Xylanases are xylan-degrading enzymes which attack hemicellulose and alter the interface between the cellulose and lignin, thereby facilitating the removal of the lignin-associated hemicellulose fraction. The isolation of purified cellulose with minimal damage (depolymerization) requires to obtain cellulose-free xylanases capable of attacking the non-cellulose components of the lignocellulosic materials exclusively as shown in Fig. 7.15 [38, 39].

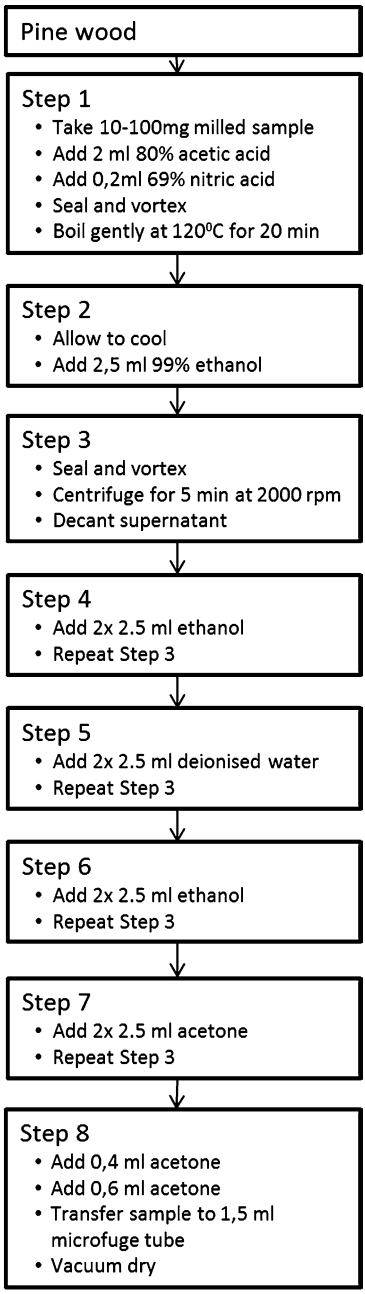

Fig. 7.13 Scheme for extraction of cellulose used by Brendel et al. [51]

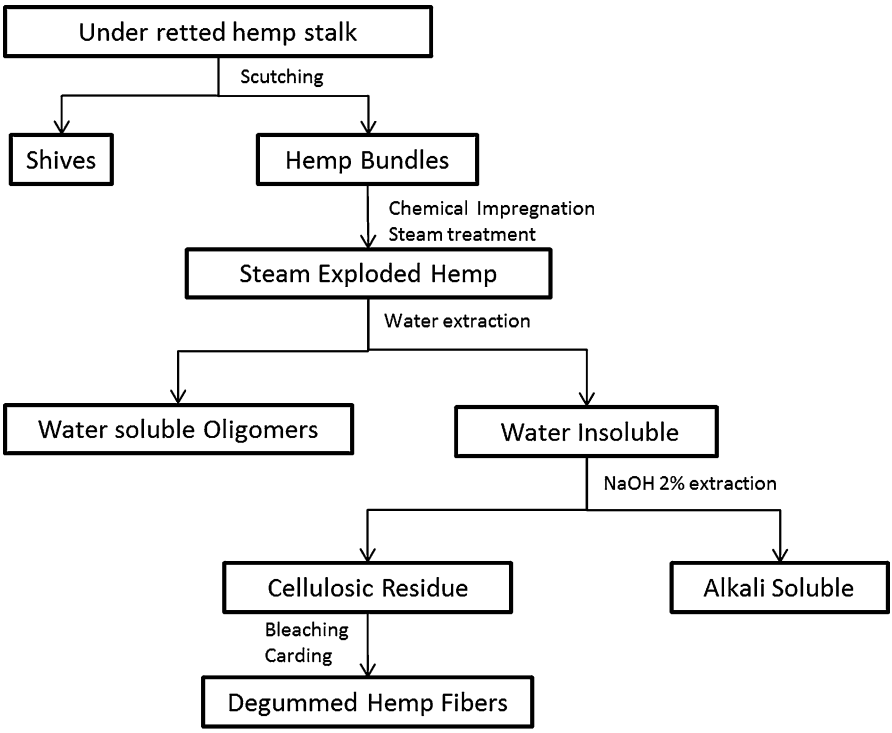

Fig. 7.14 Fractionation scheme of the hemp stalk [60]

2.2.5 Combined Pulping Methods

Each of the presented methods has its own advantages and disadvantages. For that reason, it is not uncommon to find reports of studies combining mechanical and chemical pulping processes in order to achieve higher yields of cellulose with lower energy consumption and a reduced use of chemical agents. The most common physicochemical process is the combination of a mechanical method for reducing the reaction times by improving chemical accessibility. The tight intertwined fiber architecture is loosened by mechanical forces, and the area exposed to the chemical action is increased. Sun et al. proposed a steam explosion pretreatment followed by an alkaline peroxide bleaching step [61]. Other authors have proposed chemo-mechanical pulping processes, where the surrounding matrix is dissolved by chemical action and the cellulosic fibers are dissolved by mechanical forces such as ultrasonication. As the matrix has been previously attacked, the energy consumption results much lower than that of ŧ direct steam explosion [62, 63].

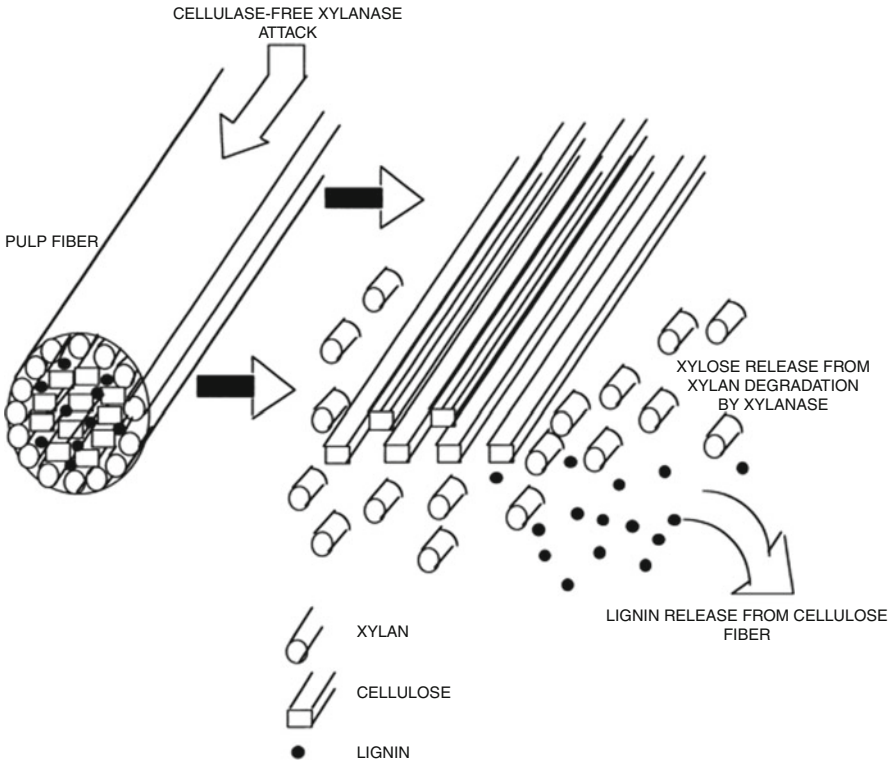

Fig. 7.15 Lignin-associated hemicellulose fraction removal from pulp structure by the action of cellulose-free xylene [39]

3 Cellulose Nanoparticles

3.1 Nomenclature of Cellulose Nanoparticles

Nomenclature of nanocellulose particles has not yet been standardized. Actually, TAPPI has recently established a Nanotechnology Division devoted to the standardization of cellulose nanomaterial definitions. A preliminary draft has been prepared for the first cellulose nanomaterial standard (TAPPI WI 3021: Standard Terms and Their Definition for Cellulose Nanomaterials), and comments on this standard are currently under review. Literature revision clearly demonstrates that different terminologies have been and are still used to describe nanocellulose particles, which frequently leads to misunderstanding and ambiguities. The terminology problem has been pointed out in a number of recent nanocellulosic reviews [5, 6, 8, 10]. General terms that have been applied to refer to nanoscaled cellulose

elements include cellulose nanoparticles, cellulose nanofibers, cellulose nanofibrils, cellulose microfibrils, cellulose fibrils, nanocellulose, nanoscale cellulose, and nanocellulosic and nano-sized cellulose fibrils [3, 5–7]. Moreover, nanoparticles resulting from the use of different isolation methods (acid hydrolysis, mechanical processes, microbial routes; see details on these methods in the following Section) have also received a wide variety of ensuing nomenclatures. A recent review made by some of us evidenced the wide dispersity of names that rodlike nanocellulose particles extracted by acid hydrolysis have received throughout the years, including cellulose monocrystals, cellulose microcrystals, cellulose crystallites, cellulose microcrystallites, microcrystalline cellulose, and more recently cellulose nanowhiskers, cellulose nanocrystals, nanocrystalline cellulose, nanorods, rodlike cellulose microcrystals, rodlike cellulose crystals, and nanowires [10]. In reference to microfibrils extracted from cellulose sources by mechanical means, the variety of terminologies that have been used is somewhat lower, including mainly microfibrillated cellulose (see details later on), but also microfibrillar cellulose, microfibrilized cellulose, nanofibrillated cellulose, nanofibrillar cellulose, nanoscale-fibrillated cellulose, cellulosic fibrillar fines, microfibril, microfibril aggregates, nanofiber, nanofibril, and fibril aggregates [2–8, 64, 65]. Nanocellulose derived from bacterial routes has been called mainly bacterial cellulose (BC), although bacterial cellulose, bacterial nanocellulose, bacterium cellulose, bacterial nanocellulose, bacteria-produced cellulose, biocellulose, and microbial cellulose have all been used [2–8, 10, 66, 67].

3.2 Isolation of Cellulose Nanoparticles

Isolation of cellulose nanoparticles has traditionally been performed mainly by two routes: acid hydrolysis and mechanical treatment. Strong mechanical treatment that imposes high shear forces to cellulose fibers allows the extraction of microfibrils and microfibril aggregates with high aspect ratio which form highly entangled networks. The product obtained is generally called *microfibrillated cellulose*. On the other hand, strong acid hydrolysis promotes transversal cleavage of non-crystalline fractions of cellulose microfibrils, leading to the so-called cellulose nanocrystals or (nano)whiskers which are rodlike particles with diameters in the range of 2–20 nm and 100–600 nm in length [6]. A promising approach for a relatively simple and eco-friendly obtention of cellulose microfibrils that has received great attention in the last decade is the microbial route, in which specific aerobic bacteria synthesize cellulose microfibrils as a primary metabolite. In the following paragraphs the methods mentioned for nanocellulose particles isolation are described in detail.

3.2.1 Mechanical Methods

Mechanical processes used to isolate cellulose nanofibers produce high shear that causes transverse cleavage along the longitudinal axis of the cellulose microfibrillar structure, resulting in the extraction of long cellulose microfibrils. Microfibrillated

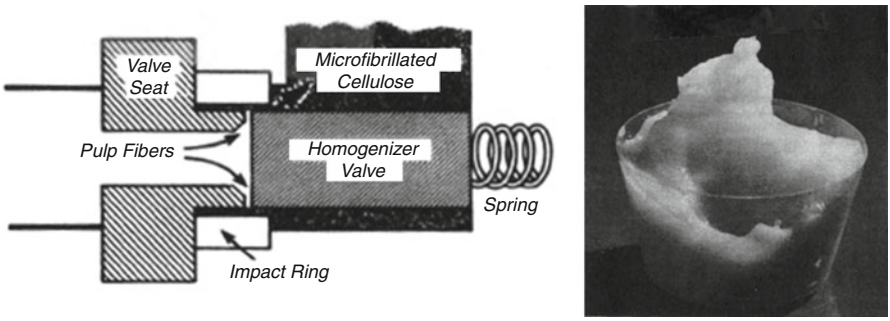

Fig. 7.16 Obtention of MFC by use of a Manton–Gaulin high-pressure homogenizer [65]

cellulose was first produced from a 3 % slurry of chopped pulp fibers at the ITT Rayonier Eastern Research Division (ERD) Lab in Whippany, N.J., USA in 1977 [68]. Authors used a high-pressure homogenizer called Manton Gaulin-type milk homogenizer and observed that when the slurry reached 80 °C and 8,000 psi, the fibers underwent a total phase change and turned into a translucent firm gel that they called microfibrillated cellulose. Pressure, cavitation, shear, and impact forces of the homogenizer had broken down the cell walls of the microfibers and liberated the desired nanofibrils [64, 65, 68]. The product obtained was a gel consisting of strongly entangled and disordered networks of cellulose nanofibers. Figure 7.16 shows a scheme of the Manton-Gaulin high-pressure milk homogenizer and the gel obtained by Turbak et al. [65].

MFC is now a commercial product available from various companies such as Daicel (Japan), Rettenmaier (Germany), Innventia AB (Sweden), UPM-Kymmene and VTT (Finland), and Borregaard (Norway) [6, 68]. A recent review of patents involving MFC technology showed a notorious increase in number of patents published every year since 2006–2007. The observed behavior was explained in terms of the current worldwide interest in nanotechnology and the end of protection set by most patents of the 1980s (those of Turbak et al.) [65]. Companies which throughout the years have shown highest presence on MFC technology field (owning most patents) are Daicel (Japan), Stora Enso Oyj (Finland), Akzo Nobel (Netherlands), and UPM-Kymmene Corporation (Finland) [10].

The manufacture of MFC is now generally performed by a mechanical treatment consisting of refining and high-pressure homogenizing steps [69–71]. The refining step implies the use of a disk refiner, in which dilute fiber suspensions are forced through a gap and subjected to several cyclic stress against disk surfaces fitted with bars and grooves [6]. Refining induces the peeling off the external cell wall layers and exposition of the S2 layer. Refined cellulose fibers are then subjected to high-pressure homogenization in which pumping at high pressure through an opening-closing valve induces a large pressure drop in shearing and impact forces that result in microfibrillated cellulose [72]. The cellulose slurry normally needs to be passed several times through the homogenizer (i.e., 10–15 cycles), and the process has been described as prohibitively unstable since the constrictions chambers of the

homogenizer quickly become blocked [70]. After each pass through the homogenizer, the particles get generally smaller and more uniform in diameter, while mechanical damage to the crystalline cellulose and the energy required for the process increases.

Mechanical treatment by cryocrushing is another method used for isolation of microfibrils. The process implies freezing cellulose fibers using liquid nitrogen and subject them to high shear forces [30]. Cryocrushing combined with high-pressure fibrillation has been used for the isolation of nanofibers from natural fibers and soybean stock [6, 31, 32]. High impact forces applied to the frozen fibers induce ice crystals to exert pressure on the cell walls causing them to rupture and liberate microfibrils [32]. Grinding processes in which the fibers slurry is passed between a static grindstone and a rotating stone (∼1,500 rpm) induce shearing forces that can also result in fiber fibrillation and nanofiber isolation [26–29].

Independently of the mechanical method used to obtain MFC, it is often reported that MFC suspensions are not homogeneous and that they consist of microfibrils and microfibrils aggregates. Suspensions may also contain a certain amount of larger fiber fragments and unfibrillated fibers [73, 74]. The previous is due to the high density of hydroxyl groups on the surface of the microfibrils, which strongly interact forming extensive hydrogen bonding and leading to agglomeration [75]. A filtration step is then often included in MFC production in order to remove the larger unfibrillated and partially fibrillated fractions [8]. Figure 7.17 shows microfibrillated cellulose obtained by the mechanical methods described.

As described before, fibrillation of cellulose fibers into nanoscale elements by mechanical methods is a high energy-demanding process. Production of MFC solely by shear forces normally requires multiple passes through the disintegration devices which, besides, get frequently blocked. Energy consumption values of 20,000–70,000 kWh/t have been reported for the production of MFC by mechanical means [6]. In this context, in the last years an important challenge in MFC production research has been the development of pretreatments capable of reducing the energy demand of the later mechanical fibrillation process. As an answer, enzymatic and oxidation pretreatments have been proposed to reduce the energy input of the process [70, 77, 78].

In 2006 Saito et al. [77] reported a novel way of introducing charged carboxylate groups into cellulosic materials which facilitated disintegration into microfibrils with smaller widths, by using a much lower energy input than traditional pure mechanical treatment [77]. The approach involved oxidation of never-dried native celluloses mediated by the 2,2,6,6-tetramethylpiperidine-1-oxyl (TEMPO) radical, followed by a homogenizing mechanical treatment. Bleached sulfite wood pulp, cotton, tunicin, and bacterial cellulose were assayed. The resulting product consisted of long individual microfibrils which yielded transparent and highly viscous suspensions [77]. Upon TEMPO oxidation the accessible primary hydroxyls on the surface of the microfibrils become modified with anionic carboxylate groups, which results in repulsion between nanofibers that eases fibrillation.

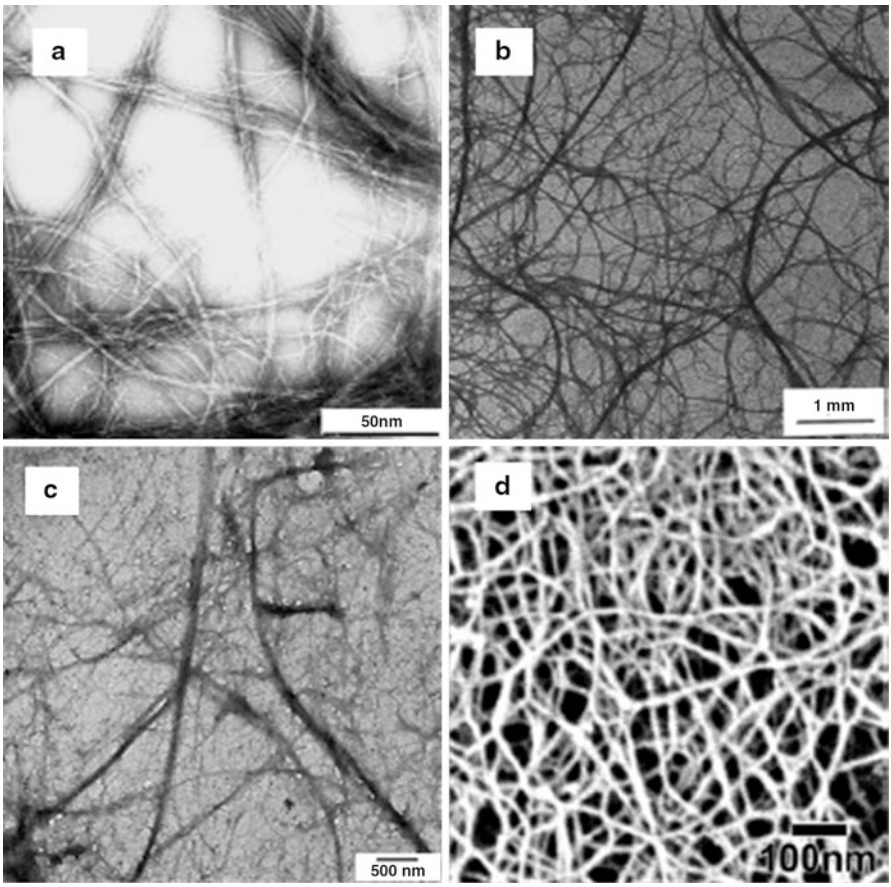

Fig. 7.17 Cellulose microfibrils obtained by different mechanical methods. (**a**) TEM micrograph of microfibrillated cellulose obtained by Habibi et al. [76] from prickly pear skin after negative staining. Purified and bleached cellulose was disrupted in a Waring blender operated at full speed for 5 min and later treated with a laboratory scale Manton–Gaulin homogenizer (15 passes at a pressure of 500 bars); (**b**) TEM micrograph of sugar beet cellulose microfibrils obtained by Dufresne et al. [34] by chemical treatment followed by homogenization in Manton–Gaulin apparatus during 2 h (pressure gradient of 500 bars); (**c**) TEM micrograph of wheat straw nanofibers obtained by Alemdar and Sain [33] by cryocrushing of chemically treated fibers followed by disintegration at 2,000 rpm and high-pressure homogenization (20 passes) [33]; (**d**) FE-SEM micrograph of freeze-dried nanofibers obtained by Abe et al. [27] by grinding treatment (one pass) of water-swollen cellulose fibers after matrix removal (lignin, hemicellulose, extractives) [27]

The mechanism of the TEMPO-mediated oxidation of cellulose is schematized in Fig. 7.18.

The oxidation begins by the addition of NaClO to aqueous cellulose suspensions in the presence of catalytic amounts of TEMPO and NaBr at pH 10–11 and room temperature. The C6 primary hydroxyl groups of cellulose are converted to

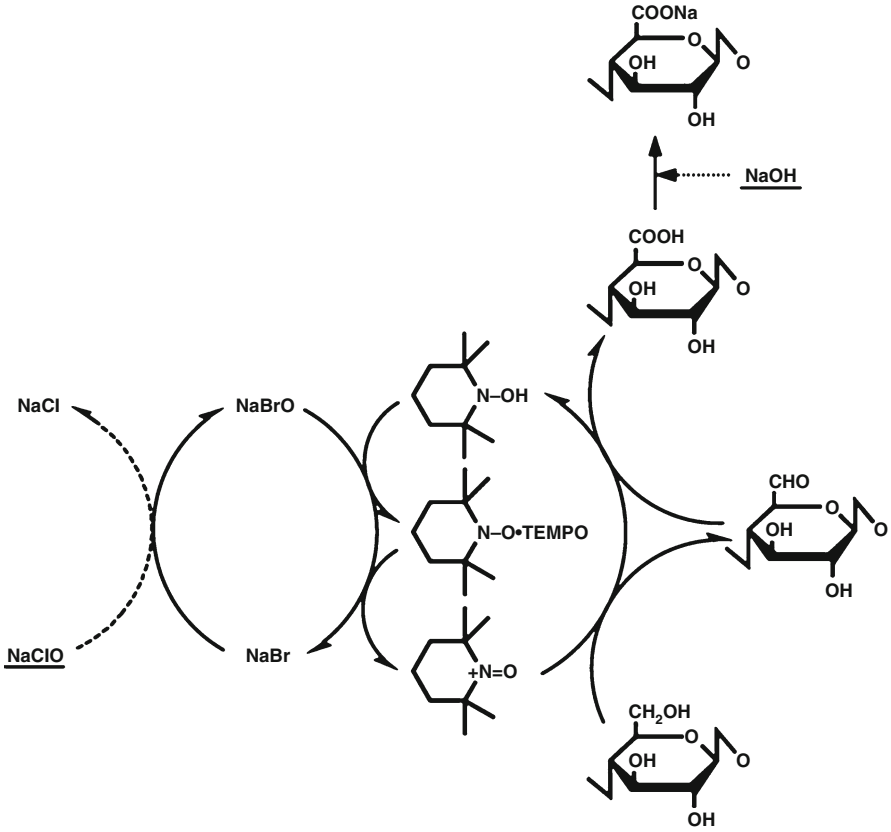

Fig. 7.18 Scheme of TEMPO-mediated oxidation of cellulose to form C6-carboxylate groups via C6-aldehyde groups [79]

carboxylate groups via C6-aldehyde groups, and NaClO and NaOH are consumed as the oxidation proceeds [79]. Figure 7.19 shows images of microfibrils obtained by TEMPO-mediated oxidation of never-dried samples of different cellulose sources.

In 2007, Pääkkö et al. [70] and Henriksson et al. [78] proposed a novel method for easing fibrillation and production of MFC which combines enzymatic hydrolysis and mechanical shearing [70, 78]. The enzymes used are monocomponent endoglucanases, which are a class of cellulases which preferentially hydrolyze unordered regions of cellulose. Authors demonstrated that a combination of high-pressure shear forces and mild enzymatic hydrolysis is an efficient method to prepare MFC with well-controlled nano-sized diameters. Enzyme-treatment was found to facilitate disintegration and prevent homogenizer blocking, and the MFC nanofibers produced showed higher average molar mass and larger aspect ratio than nanofibers mildly pretreated with HCl [78]. The process is considered environmentally friendly since no solvent or harsh chemical reactants are used.

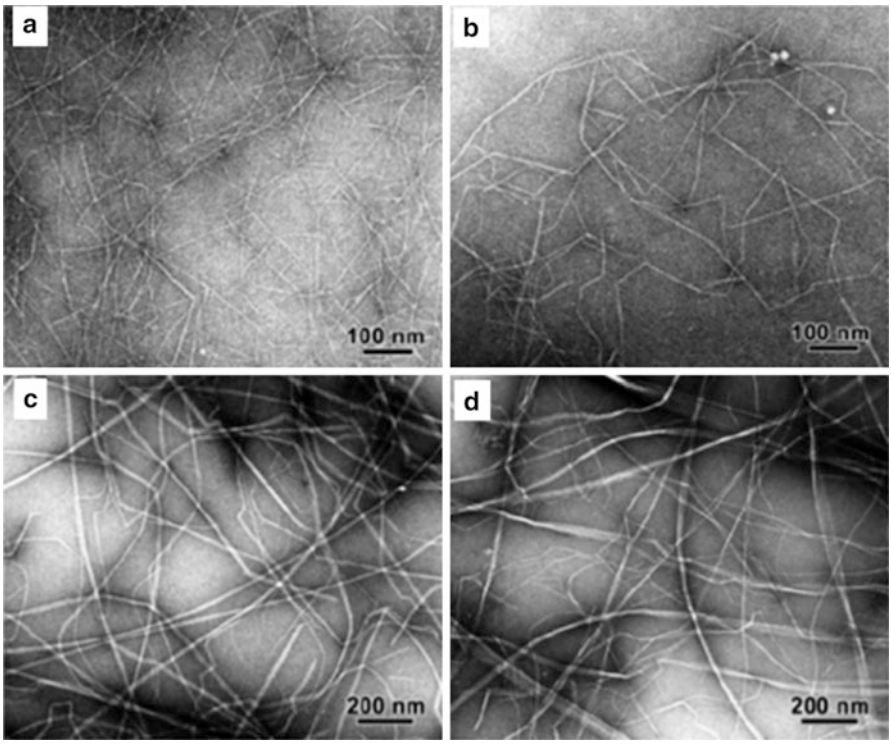

Fig. 7.19 Transmission electron micrographs of cellulose microfibrils disintegrated after TEMPO-mediated oxidation of never-dried samples: (**a**) Bleached sulfite wood pulp, (**b**) cotton, (**c**) tunicin, and (**d**) bacterial cellulose. The preparations were negatively stained with uranyl acetate. Sulfite wood pulp and cotton were disintegrated by homogenization with a Waring Blendor, whereas tunicin and bacterial cellulose were disintegrated by sonication for a few seconds [77]

Moreover, reductions and important energy input reductions are achieved as demonstrated by Pääkkö et al. 2007 [70]. The technology is being developed by the Finnish pulp and paper manufacturer Stora Enso Oyj, the Swedish INNVENTIA, the Japanese Nippon Paper Industries Co. Ltd., and the forest biotechnology company SweTree Technologies [10]. Figure 7.20 proposes a hypothetical mechanism of the action of endoglucanases on cellulose substrates.

Figure 7.21 shows micrographs of microfibrils obtained using the enzymatic pretreatment [70].

3.2.2 Acid Hydrolysis

Cellulose microfibrils are composed of crystalline cellulosic domains and less ordered amorphous domains located at the surface and along their main axis. Upon contact with strong acid solutions, amorphous domains are preferentially cleaved, whereas crystalline regions that have a higher resistance to acid attack

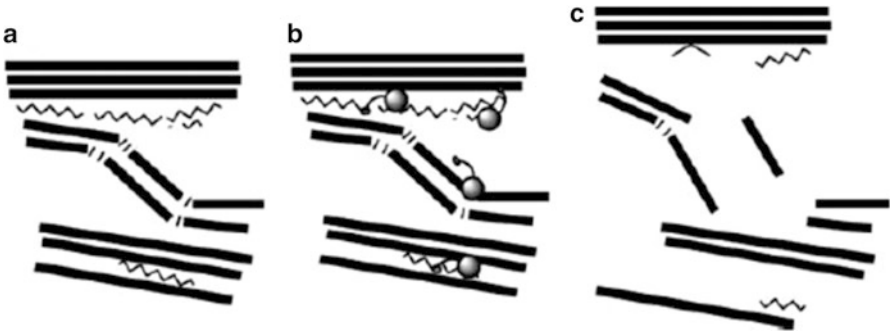

Fig. 7.20 Hypothetical mechanism of the action of monocomponent endoglucanase. (**a**) The cellulose in the pulp fibers consists mainly of crystalline fibrils (▬), but more amorphous cellulose is located on the surface and between fibrils (〰), or in shorter segments within the fibrils (▮▮▮▮▮); (**b**) the monocomponent C-type endoglucanase (●) preferentially attacks the more amorphous cellulose; (**c**) partial degradation and nicking of the amorphous regions in the cellulose leads to separation of the fibrils [80]

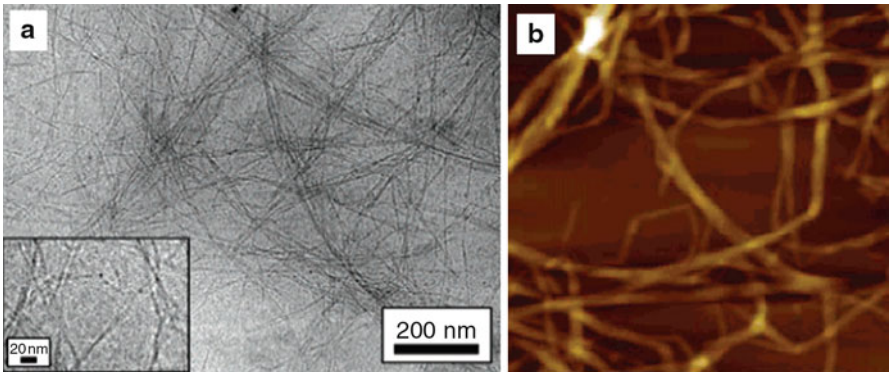

Fig. 7.21 (**a**) Cryo-TEM of frozen 2 % w/w MFC gel obtained by refining, enzymatic hydrolysis, and homogenization processes; (**b**) topographical AFM image of microfibrillated cellulose (*ca.* 0.05 % w/w) on mica after drying. The scan size was 1 × 1 μm [70]

(cellulose nanocrystals) remain essentially intact. Figure 7.22 illustrates the preferential action of acid on amorphous zones of cellulose microfibrils, resulting in rodlike cellulose nanocrystals.

The pioneers in the cellulose hydrolysis process were Ranby and Ribi who in the early 1950s produced stable suspensions of colloidal-sized cellulose crystals by sulfuric acid hydrolysis of wood and cotton cellulose [81–83]. After treating wood pulp with boiling 2.5 N sulfuric acid for 12 h, authors obtained colloidal suspensions of rodlike particles with lengths between 50 and 60 nm and widths between 5 and 10 nm [84]. In the 1990s, the ability of cellulose nanocrystal suspensions to form stable chiral nematic liquid-crystalline phases with unusual optical properties

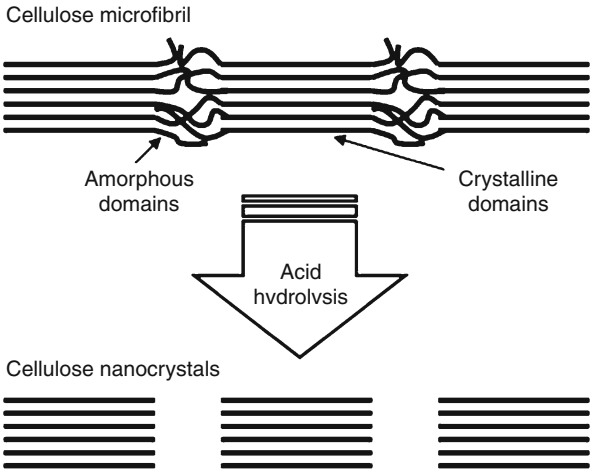

Fig. 7.22 Scheme of preferential action of acid on amorphous domains of cellulose microfibrils leading to nanocrystals

discovered by Revol et al. [85], as well as the works of Favier and co-workers demonstrating the reinforcing properties of cellulose nanocrystals [86, 87], brought a renaissance of interest to the nano-sized rodlike cellulose particles. Following this advance, the incorporation of cellulose nanocrystals from different sources into composite materials for mechanical properties enhancement was largely investigated and reviewed [1, 4, 7].

Current production of cellulose nanocrystals implies contacting a purified cellulose source with a concentrated solution of acid under strictly controlled conditions of temperature, agitation, and time. Sulfuric acid is the most frequently used one, although other acids such as hydrochloric acid [20, 31, 78, 86], phosphoric acid [88, 89], hydrobromic acid [90, 91], and maleic acid [92] have also been assayed. A well-known advantage of using sulfuric acid as a hydrolyzing agent is that it reacts with the surface hydroxyl groups of cellulose to yield negatively charged surface sulfate ester groups. Surface sulfate groups ease the dispersion of nanocrystals in water via electrostatic repulsions and allow more stable suspensions [2, 4], although heat may cause de-esterification [93]. On the other hand, if cellulose whiskers are prepared by hydrolysis with hydrochloric acid, their ability to disperse is limited and their aqueous suspensions tend to flocculate [94]. Posttreatment with sulfuric acid has been studied as a means to introduce sulfate moieties on uncharged nanocrystal surfaces [94–96]. The concentration of sulfuric acid used for cellulose hydrolysis is typically between 60 % and 65 % (wt), whereas reaction temperatures between room values and 70 °C have been used. Depending on the temperature used, reaction time varies (i.e., 30 min to overnight) [4]. After acid hydrolysis of the cellulosic substrate, recovery operations imply dilution with water to quench the reaction, centrifugation/filtration, and successive washing and dialysis steps in order to remove the remaining acid. Ultrasonic treatments are frequently used to redisperse the nanocrystals.

Acid hydrolysis has been used to extract the crystalline particles from different cellulose sources including wood pulp, natural fibers, microcrystalline cellulose, tunicates, algae, and bacterial cellulose. Dimensions of cellulose whiskers vary widely with the source of the cellulosic material and the hydrolysis conditions. The variability in width (w) and length (L) of the obtained nanowhiskers is notorious with typical values of w = 3–5 nm and L = 100–200 nm for wood-derived whiskers, w = 5–10 nm and L = 70–300 for nanocrystals obtained from cotton and other natural fibers sources such as ramie and sisal, w = 5–50 nm and L = 100–1,000 nm for bacterial cellulose whiskers, and w = 10–30 nm and L = 500–3,000 nm for tunicate sources [4]. Thus, the aspect ratio of cellulose whiskers (L/w) spans a broad range. Larger dimensions of tunicate and bacterial cellulose whiskers have been explained in terms of the high crystallinity of these cellulose sources, which thus have lower fractions of amorphous regions that need to be cleaved during hydrolysis [97]. Besides dimensions, depending on the cellulose source, cellulose whiskers show different crystal structure and mechanical properties. Figure 7.23 shows images of cellulose nanocrystals obtained from different cellulose sources.

Besides their high mechanical properties which make cellulose nanocrystals a very attractive and widely studied reinforcing material, another interesting characteristic of cellulose nanowhisker aqueous suspensions is their capability of self-organizing into stable chiral nematic phases with unusual optical properties [1]. When a critical concentration is exceeded in the nanocrystal suspension, whiskers align in the same direction and form a colloidal chiral_nematic phase [84]. The chiral ordering has been attributed to the geometrical twists in the nanocrystals and/or helical distribution of their surface charge [85, 102, 103]. When ordered colloidal phases of cellulose nanocrystals are dried down slowly, the chiral nematic structure of the suspension can be preserved in solid films [84], which have important potential applications such as those for security papers [1].

Revision of patents dealing with cellulose nanocrystals shows an increasing interest for the technology during the last decade. Since 2009 nanocrystal published patents show nearly a 100 % annual increase [10]. In terms of companies interested in the technology, most nanocrystal patents are owned by FPInnovations (Canada) and the French Centre National de la Recherche. It is interesting to note that these cellulose nanoparticles still show a low level of transfer of the technology to the private sector, with nearly 50 % of the patents in the area owned by public institutions [10].

4 Bacterial Cellulose

It is now well known that under proper conditions, a number of acetic acid bacteria secrete cellulose microfibrils with nanometric widths as an extracellular primary metabolite. Bacteria able to do so are those belonging to the genera *Acetobacter, Agrobacterium, Alcaligenes, Pseudomonas, Rhizobium, Aerobacter, Achromobacter,*

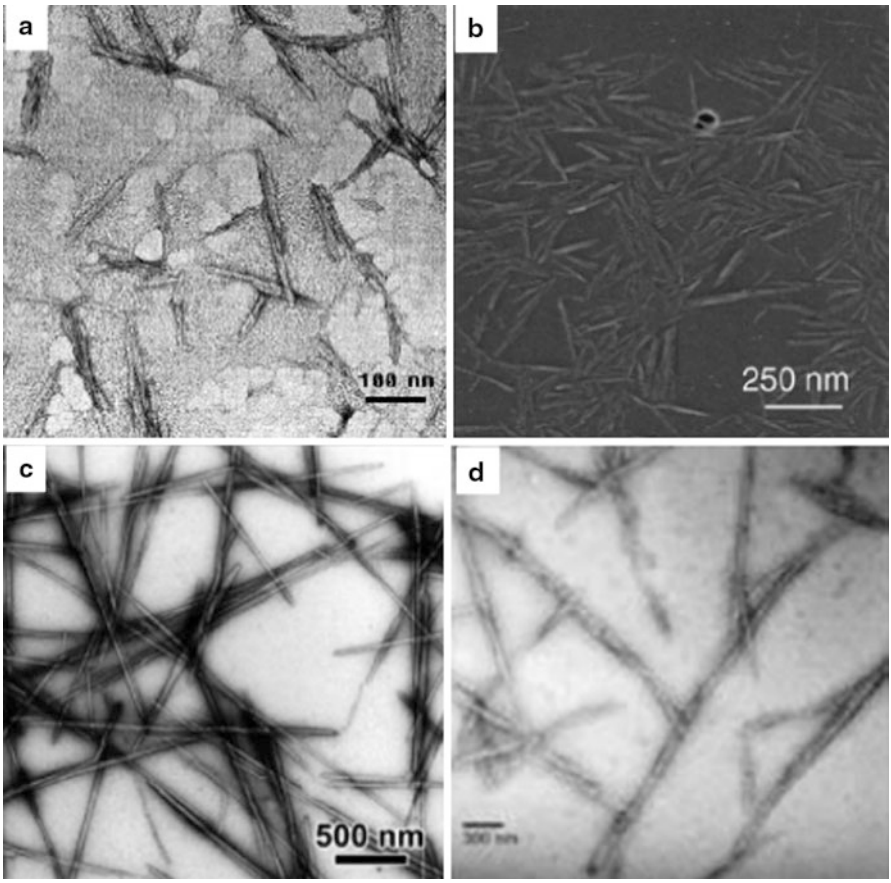

Fig. 7.23 Cellulose nanocrystals obtained by acid hydrolysis of different cellulose sources. (**a**) TEM micrograph of cellulose nanocrystals obtained by Bai et al. [98] by sulfuric acid hydrolysis (64 % w/v, 5 h, 45 °C) of MCC [98]; (**b**) SEM micrograph of whiskers obtained by Roohani et al. [98] by sulfuric acid hydrolysis (65 wt.%, 45 min, 45 °C) of cotton fibers [99]; (**c**) TEM micrograph of nanocrystals obtained by Elazzouzi-Hafraoui et al. [100] by sulfuric acid hydrolysis (48 % w/v, 13 h, 55 °C) of tunicate cellulose [100]; (**d**) TEM micrograph of cellulose whiskers obtained by Grunert and Winter [101] by acid hydrolysis of bacterial cellulose [101]

Azotobacter, Salmonella, or *Sarcina* [104, 105]. Among those, the most efficient producer, and the one that has been studied most, is *Acetobacter xylinum*, now reclassified and included within the novel genus *Gluconacetobacter*, as *G. xylinus* [106, 107]. The *Acetobacteraceae* are gram-negative, aerobic, rodlike microorganisms of unusual acid tolerance which grow well below pH 5.0. They are found wherever the fermentation of sugars and plant carbohydrates takes place, e.g., on damaged fruits and flowers and in unpasteurized or unsterilized juice, beer, and wine [7]. The effectiveness of microbial cellulose depends mainly on the strain used, the composition of the culture medium, the fermentation temperature, oxygen

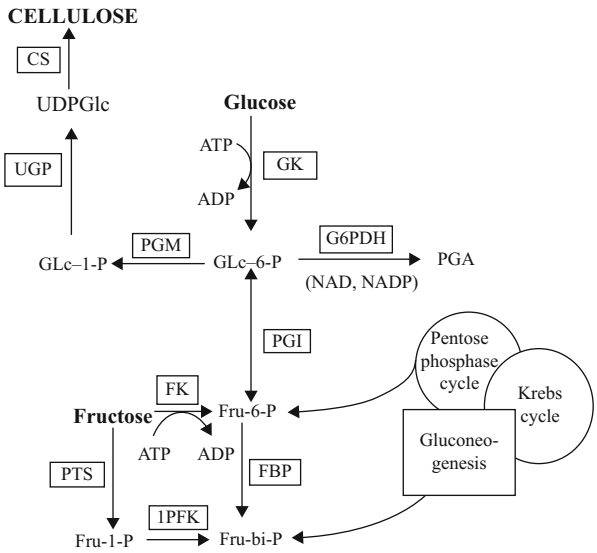

Fig. 7.24 Pathways of carbon metabolism in *A. xylinum*. *CS* cellulose synthase (EC 2.4.2.12); *FBP* fructose-1,6-biphosphate phosphatase (EC 3.1.3.11); *FK* glucokinase (EC 2.7.1.2); *G6PDH* glucose−6-phosphate dehydrogenase (EC 1.1.1.49); *1PFK* fructose-1-phosphate kinase (EC 2.7.1.56); *PGI* phosphoglucoisomerase; PGM phosphoglucomutase (EC 5.3.1.9); *PTS* system of phosphotransferases; *UGP* pyrophosphorylase UDPGlc (EC 2.7.7.9); *Fru-bi-P* fructose−1,6-biphosphate; *Fru-6-P* fructose-6-phosphate; *Glc-6(1)-P* glucose-6(1)-phosphate; *PGA* phosphogluconic acid; *UDPGlc* uridine diphosphoglucose [67]

supply, and carbon source used (e.g., glucose). Synthesis of BC is a precisely and specifically regulated multistep process, involving a large number of both individual enzymes and complexes of catalytic and regulatory proteins. The process includes the synthesis of uridine diphosphoglucose (UDPGlc), which is the cellulose precursor, followed by glucose polymerization into the β-1,4-glucan chain, and nascent chain association into characteristic ribbon-like structure, formed by hundreds or even thousands of individual cellulose chains [67]. Figure 7.24 schematizes bacterial cellulose biosynthesis from glucose via uridine diphosphate glucose (UDPGlc) in *Acetobacter xylinum*.

The first report of the synthesis of bacterial cellulose was done by A.J. Brown who in 1886 obtained an extracellular gelatinous mat whose chemical composition and reactivity were the same as cell wall cellulose [108, 109]. Besides, bacterial cellulose pellicles obtained from coconut water had long been used in the preparation of an indigenous dessert food of Southeast Asia called *nata de coco*. In the mid-1980s reports of the remarkable mechanical properties of bacterial cellulose pellicles brought a resurgence in the area [110, 111], and its use as composite materials reinforcement grew rapidly after [112, 113]. Nowadays, the microbial route appears as a very promising eco-friendly source of cellulose microfibrils.

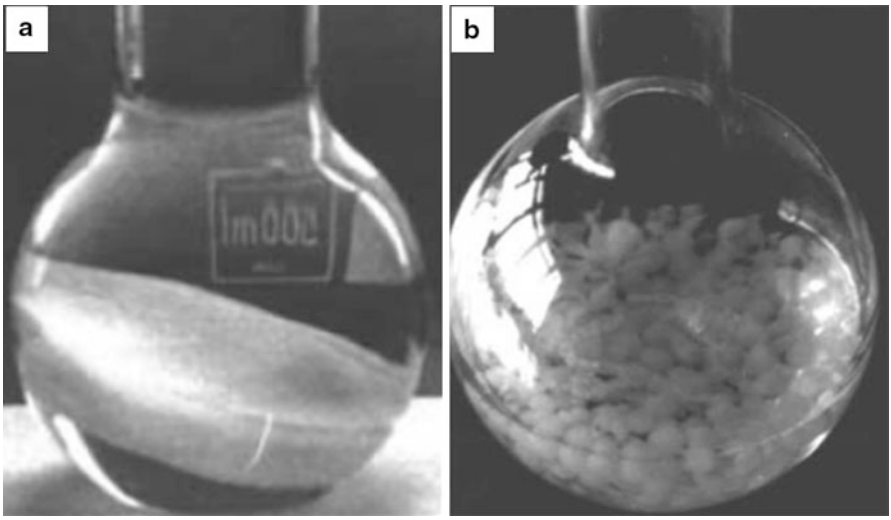

Fig. 7.25 BC pellicle formed in (**a**) Static culture [67] and (**b**) agitated culture

Microbial cellulose biosynthesis from low-molecular-weight sugars or other carbon sources is carried out in static or agitated conditions at temperatures around 28–30 °C. The most used carbon source has been D-glucose, although the costs associated for large-scale production have triggered in the last years the search of alternative substrates, mainly agroforestry industrial residues [114–117]. During fermentation the system initially becomes turbid, and after a few days, a gelatinous pellicle appears on the air–liquid surface of the fermentation vessel. Since bacteria used are aerobic, cellulose pellicle is formed only in the vicinity of the air–liquid interface, and it conforms to its shape. The reason why the bacteria generate cellulose is unclear, but it has been suggested that it is a mean of maintaining their position close to the surface of culture solution, a mechanism to guard bacteria from ultraviolet radiation, and/or a barrier to bacteria enemies such as yeast, fungi, and heavy metal ions, whereas nutrients diffuse easily along the pellicle [7, 66]. During fermentation, it is believed that cellulose molecules are synthesized in the interior of the cell and spun out to form protofibrils of *ca*. 2–4 nm diameter, which are crystallized into microfibrils, these into bundles and the latter into ribbons [66, 67]. The overlapping and intertwisted bacterial cellulose ribbons form a 3D dense reticulated structure stabilized by extensive hydrogen bonding containing up to 99 % of water (pellicle). In agitated fermentations, bacterial cellulose nanofibers interconnect less frequently forming, instead of a pellicle, granules, stellate and fibrous strands well dispersed in culture broth. Figure 7.25 shows bacterial cellulose pellicle and bacterial cellulose pellets obtained in static and agitated culture, respectively.

The recovery of BC (generally after 12–14 days of fermentation) implies the need of removing bacteria and culture medium. The pellicles (or pellets) are then

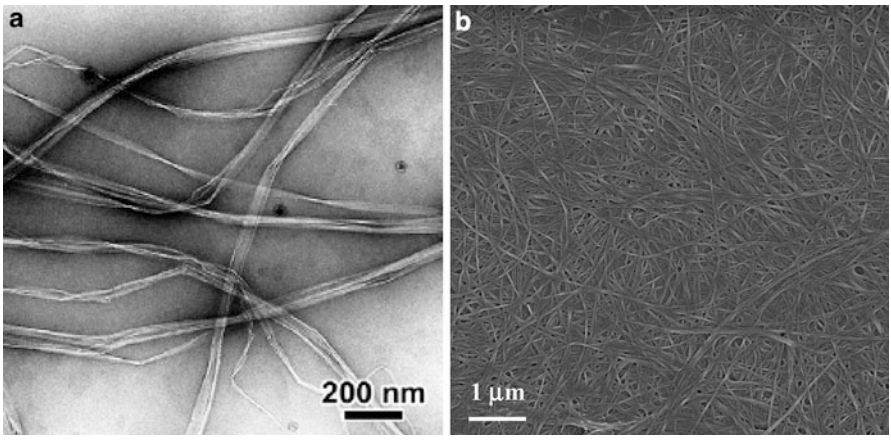

Fig. 7.26 Bacterial cellulose microfibrils obtained from different carbon sources and strains. (**a**) TEM micrograph of negatively stained BC obtained by Castro et al. [117] from pineapple peel juice using *Gluconacetobacter swingsii sp.* in static conditions [117]; (**b**) SEM micrograph of BC obtained by Vazquez et al. [10] from grape bagasse using *Gluconacetobacter xylinum* (Unpublished results)

isolated from the culture vessel, typically boiled in alkali solution at a low concentration (~2 % NaOH or KOH), and thoroughly washed till neutrality. Occasionally, NaOH and NaClO treatments have been used for further purification of the BC microfibrils [66, 111, 118]. Mechanical treatment can be applied to bacterial cellulose in order to break the entangled networks. Bacteria-produced ribbons typically show rectangular cross sections with thicknesses around 3–10 nm, 30–100 nm in width, and 1–9 m in length [8, 119, 120]. An interesting feature of bacterial cellulose is that by adjusting culturing conditions, it is possible to alter the microfibril formation and crystallization. Moreover, the presence of additives may interfere with the aggregation of the elementary fibrils into the normal ribbon assembly leading to squared cross-section microfibrils [121]. In relation to D-glucose, BC is formed in yields up to 40 % which is a high efficiency for a biotechnological process [122]. Figure 7.26 shows electron images of bacterial cellulose microfibrils.

Although chemically identical to plant cellulose, microbial cellulose is characterized by a unique fibrillar nanostructure which determines its extraordinary physical and mechanical properties. Well-separated nano- and microfibrils of microbial cellulose create an extensive surface area which allows it to hold a large amount of water while maintaining a high degree of conformability. The hydrogen bonds between these fibrillar units stabilize the whole structure and confer its high mechanical strength [123, 124]. The nanofibers of BC are immobilized in a stable network, which is an important aspect with respect to health risks considerations of distributed and mobile nanoparticles [7]. Microbial cellulose is characterized by high polymerization degree and crystallinity and high stability of the single cellulose fibers. Moreover, and different to wood and plant

cellulose sources, the high chemical purity of bacterial cellulose avoids the need of chemical treatments devoted to the removal of hemicellulose and lignin, which imply extra isolation costs.

Microbial cellulose has proven to be a remarkably versatile biomaterial with plenty applications such as in paper products, electronics, acoustic membranes, reinforcement of composite materials, membrane filters, hydraulic fracturing fluids, edible food packaging films, etc. [10]. However, in the last decade the main application of bacterial cellulose has been in the biomedical materials field [7, 16]. Due to its unique nanostructure and properties, microbial cellulose is a natural candidate for numerous medical and tissue-engineered applications. The nonwoven ribbons of microbial cellulose microfibrils closely resemble the structure of native extracellular matrices, positioning it as an attractive scaffold for the production of tissue-engineered constructs, wound healing devices, and regenerative medicine uses [16]. Recent clinical performance tests on bacterial cellulose showed its application in high-quality wound dressings based on the capability of microbial cellulose for maintaining a moist environment at the wound surface and not allowing external bacteria to penetrate into the wound bed (nanoporous structure), as well as the easiness to sterilize it, its high elasticity and conformability that allows painless removal, and its high mechanical stability and nontoxicity [16]. Very important, in terms of biocompatibility (ability of a material to remain in contact with living tissue without causing any toxic or allergic side effects), in vivo tests on animal models have shown no macroscopic signs of inflammation [7, 122, 125]. The fact that the shape of BC pellicles can be designed by choosing the appropriate reactor form and function (static or agitated cultivation) allows production of fleeces of several centimeters height, films/patches, spheres, and hollow tubes [7], the latter with potential use as replacement of blood vessels or other tubular structures such as the ureter, the trachea, or the digestive tract [16].

In terms of patents dealing with microbial cellulose, it is by large the nanocellulose particle field which holds more published patents [10]. Similarly to cellulose nanocrystals and microfibrillated cellulose, the number of patents involving bacterial cellulose published every year shows notorious rising profile, with percentual annual increments between 15 % and 30 % since 2005 [10]. In reference to companies involved in the sector microbial cellulose, most technology seems to be concentrated in three main competitors, i.e., the Japanese Biopolymer Res: KK, the Chinese public University of Donghua, and Mitsubishi Paper Mills Ltd. (Japan). Other public institutions with important presence in the sector as patent owners are the University of Kyoto (Japan) and the University of Hainan (China) [10].

5 Summary

Based on their renewability, biodegradability, low density, high mechanical properties, high surface area, biocompatibility, etc., nanocellulose particles are currently the focus of much scientific research. The need of purified cellulose sources and methods available to obtain it were described in the first part of the chapter.

Several routes were identified for obtaining purified cellulose from diverse sources. Chemical pulping is the most traditional process for isolating purified cellulose from wood and agro-based resources, including alkali extraction, alkaline and peroxide extraction, organic solvent extraction, acidic method, liquid-phase oxidation, and a combination of these treatments. Other routes for cellulose isolation have been investigated, including mechanical, chemo-mechanical, physicochemical, and biological pulping. In addition, microbial cellulose has been recognized as a promising cellulose source for many applications. The type, intensity, and conditions of the selected pulping/synthesis route were found to have a deep impact on the final properties of the obtained cellulose. In the second part of the chapter, most important methods for the isolation of nanocellulose particles have been reviewed. Mechanical methods for the production of microfibrillated cellulose, acid hydrolysis leading to cellulose whiskers, and fermentation routes used for the obtention of bacterial cellulose have all been described. Pretreatments of cellulose sources prior to mechanical fibrillation have also been described since oxidation and enzymatic pretreatments appear as promising tools for making the mechanical fibrillation a less energy-demanding process. In terms of obtaining cellulose microfibrils, microbial-produced cellulose appears as a promising eco-friendly route, although large-scale production requires the use of low-cost carbon, optimization of strains, and bioreactor aeration configuration to be economically feasible. For the production of cellulose nanocrystals, acid hydrolysis is a feasible route at laboratory scale; although for large-scale obtention of cellulose whiskers, reducing the amount of harsh acids and easier recovery methods need to be studied.

References

1. Azizi Samir MAS, Alloin F, Dufresne A (2005) Review of recent research into cellulosic whiskers, their properties and their application in nanocomposite field. Biomacromolecules 6:612–626
2. Hubbe MA, Rojas OJ, Lucia LA, Sain M (2008) Cellulosic nanocomposites: A review. Bioresources 3:929–980
3. Eichhorn S, Dufresne A, Aranguren M, Marcovich N, Capadona J, Rowan S, Weder C, Thielemans W, Roman M, Renneckar S, Gindl W, Veigel S, Keckes J, Yano H, Abe K, Nogi M, Nakagaito A, Mangalam A, Simonsen J, Benight A, Bismarck A, Berglund L, Peijs T (2010) Review: current international research into cellulose nanofibres and nanocomposites. J Mater Sci 45:1–33
4. Habibi Y, Lucia LA, Rojas OJ (2010) Cellulose nanocrystals: chemistry, self-assembly, and applications. Chem Rev 110:3479–3500
5. Siqueira G, Bras J, Dufresne A (2010) Cellulosic Bionanocomposites: A Review of Preparation, Properties and Applications. Polymers 2:728–765
6. Siró I, Plackett D (2010) Microfibrillated cellulose and new nanocomposite materials: a review. Cellulose 17:459–494
7. Klemm D, Kramer F, Moritz S, Lindström T, Ankerfors M, Gray D, Dorris A (2011) Nanocelluloses: A New Family of Nature-Based Materials. Angew Chem Int Ed 50:5438–5466
8. Moon RJ, Martini A, Nairn J, Simonsen J, Youngblood J (2011) Cellulose Nanomaterials Review: Structure, Properties and Nanocomposites. Chem Soc Rev 40:3941–3994

9. Peng BL, Dhar N, Liu HL, Tam KC (2011) Chemistry and applications of nanocrystalline cellulose and its derivatives: A nanotechnology perspective. Can J Chem Eng 89:1191–1206
10. Charreau H, Foresti ML, Vazquez A (2012) Nanocellulose Patents Trends: A Comprehensive Review on Patents on Cellulose Nanocrystals, Microfibrillated and Bacterial Cellulose. Recent Pat Nanotechnol 26:26
11. Ljungberg N, Bonini C, Bortolussi F, Boisson C, Heux L, Cavaille JY (2005) New nanocomposite materials reinforced with cellulose whiskers in atactic polypropylene: effect of surface and dispersion characteristics. Biomacromolecules 6:2732–2739
12. Noorani S, Simonsen J, Atre S (2007) Nano-enabled microtechnology: polysulfone nanocomposites incorporating cellulose nanocrystals. Cellulose 14:577–584
13. Xu Q, Yi J, Zhang X, Zhang H (2008) A novel amphotropic polymer based on cellulose nanocrystals grafted with azo polymers. Eur Polym J 44:2830–2837
14. Jalal Uddin A, Araki J, Gotoh Y (2011) Toward "Strong" Green Nanocomposites: Polyvinyl Alcohol Reinforced with Extremely Oriented Cellulose Whiskers. Biomacromolecules 12:617–624
15. Svensson A, Nicklasson E, Harrah T, Panilaitis B, Kaplan DL, Brittberg M, Gatenholm P (2005) Bacterial cellulose as a potential scaffold for tissue engineering of cartilage. Biomaterials 26:419–431
16. Czaja WK, Young DJ, Kawecki M, Brown RM (2006) The Future Prospects of Microbial Cellulose in Biomedical Applications. Biomacromolecules 8:1–12
17. French AD, Bertoniere NR, Brown RM, Chanzy H, Gray D, Hattori K, Glasser W (2004) Cellulose, in Kirk-Othmer encyclopedia of chemical technology. In: Seidel R (ed). John Wiley & Sons, Inc. Hoboken NJ
18. Sjostrom E (1993) Wood chemistry, fundamentals and applications. Academic, California
19. Postek MT, Vladár A, Dagata J, Farkas N, Ming B, Wagner R, Raman A, Moon RJ, Sabo R, Wegner TH, Beecher J (2011) Development of the metrology and imaging of cellulose nanocrystals. Meas Sci Technol 22:024005
20. Montanari S, Roumani M, Heux L, Vignon MR (2005) Topochemistry of Carboxylated Cellulose Nanocrystals Resulting from TEMPO-Mediated Oxidation. Macromolecules 38:1665–1671
21. Rong MZ, Zhang MQ, Liu Y, Yang GC, Zeng HM (2001) The effect of fiber treatment on the mechanical properties of unidirectional sisal-reinforced epoxy composites. Compos Sci Technol 61:1437–1447
22. Vignon MR, Heux L, Malainine ME, Mahrouz M (2004) Arabinan-cellulose composite in Opuntia ficus-indica prickly pear spines. Carbohydr Res 339:123–131
23. Benziman M, Haigler CH, Brown RM Jr (1980) Cellulose biogenesis: Polymerization and crystallization are coupled processes in Acetobacter xylinum. Proc Natl Acad Sci USA 77:6678–6682
24. Itoh T, Brown M (1984) Assembly of cellulose microfibrils in Valonia macrophysa Kutz. Planta 160:372–381
25. Abdul Khalil HPS, Bhat AH, Ireana Yusra AF (2012) Green composites from sustainable cellulose nanofibrils: A review. Carbohydr Polym 87:963–979
26. Iwamoto S, Nakagaito AN, Yano H, Nogi M (2005) Optically transparent composites reinforced with plant fiber-based nanofibers. Appl Phys A-Mater Sci Process 81: 1109–1112
27. Abe K, Iwamoto S, Yano H (2007) Obtaining cellulose nanofibers with a uniform width of 15 nm from wood. Biomacromolecules 8:3276–3278
28. Iwamoto S, Nakagaito AN, Yano H (2007) Nano-fibrillation of pulp fibers for the processing of transparent nanocomposites. Appl Phys A-Mater Sci Process 89:461–466
29. Taniguchi T, Okamura K (1998) New films produced from microfibrillated natural fibres. Polym Int 47:291–294
30. Chakraborty A, Sain M, Kortschot M (2005) Cellulose microfibrils: A novel method of preparation using high shear refining and cryocrushing. Holzforschung 59:102–107

31. Wang B, Sain M (2007) Isolation of nanofibers from soybean source and their reinforcing capability on synthetic polymers. Compos Sci Technol 67:2521–2527
32. Wang B, Sain M (2007) Dispersion of soybean stock-based nanofiber in a plastic matrix. Polym Int 56:538–546
33. Alemdar A, Sain M (2008) Isolation and characterization of nanofibers from agricultural residues - Wheat straw and soy hulls. Bioresour Technol 99:1664–1671
34. Dufresne A, Cavaillé J-Y, Vignon MR (1997) Mechanical behavior of sheets prepared from sugar beet cellulose microfibrils. J Appl Polym Sci 64:1185–1194
35. Johnson R, Zink-Sharp A, Renneckar S, Glasser W (2009) A new bio-based nanocomposite: fibrillated TEMPO-oxidized celluloses in hydroxypropylcellulose matrix. Cellulose 16:227–238
36. Dahl GF (1884) Process of manufacturing cellulose from wood. USP Office, Editor, United States of America. US296935
37. Morán JI, Alvarez VA, Cyras VP, Vázquez A (2008) Extraction of cellulose and preparation of nanocellulose from sisal fibers. Cellulose 15:149–159
38. Beg QQK, Bhushan B, Kapoor M, Hoondal GSG (2000) Enhanced production of a thermostable xylanase from Streptomyces sp. QG-11-3 and its application in biobleaching of eucalyptus kraft pulp. Enzyme Microb Technol 27:459–466
39. Techapun C, Poosaran N, Watanabe M, Sasaki K (2003) Thermostable and alkaline-tolerant microbial cellulase-free xylanases produced from agricultural wastes and the properties required for use in pulp bleaching bioprocesses: a review. Process Biochem 38:1327–1340
40. Xiao B, Sun XF, Sun R (2001) Chemical, structural, and thermal characterizations of alkali-soluble lignins and hemicelluloses, and cellulose from maize stems, rye straw, and rice straw. Polym Degrad Stab 74:307–319
41. Johar N, Ahmad I, Dufresne A (2012) Extraction, preparation and characterization of cellulose fibres and nanocrystals from rice husk. Ind Crops Prod 37:93–99
42. Toland J, Galasso L, Lees D, Rodden G (2002) Annual Review. Pulp paper international, vol 5. Paperloop
43. Sun RC, Sun XF (2002) Fractional and structural characterization of hemicelluloses isolated by alkali and alkaline peroxide from barley straw. Carbohydr Polym 49:415–423
44. Sun XF, Sun RC, Su Y, Sun JX (2004) Comparative Study of Crude and Purified Cellulose from Wheat Straw. J Agric Food Chem 52:839–847
45. Sun XF, Sun RC, Fowler P, Baird MS (2004) Isolation and characterisation of cellulose obtained by a two-stage treatment with organosolv and cyanamide activated hydrogen peroxide from wheat straw. Carbohydr Polym 55:379–391
46. Sun X-F, Sun R, Fowler P, Baird MS (2005) Structural characterization and isolation of lignin and hemicelluloses from barley straw. J Agric Food Chem 53:860–870
47. Sun X-F, Jing Z, Fowler P, Wu Y, Rajaratnam M (2011) Extraction and characterization of original lignin and hemicelluloses from wheat straw. Ind Crops Prod 33:588–598
48. Yan FYAN, Krishniah D, Rajin M, Bono A (2009) Cellulose extraction from palm kernel cake using liquid phase oxidation. J Eng Sci Technol 4:57–68
49. Wang X, Li H, Cao Y, Tang Q (2011) Cellulose extraction from wood chip in an ionic liquid 1-allyl-3-methylimidazolium chloride (AmimCl). Bioresour Technol 102: 7959–7965
50. Ighwela KA, Ahmad AB (2012) Production of Cellulose from Barley Husks as a Partial Ingredient of Formulated Diet for Tilapia Fingerlings. J Biol Agric Healthc 2:19–25
51. Brendel O, Iannetta PPM, Stewart D (2000) A rapid and simple method to isolate pure alpha-cellulose. Phytochem Anal 11:7–10
52. Silva GGD, Couturier M, Berrin J-G, Buléon A, Rouau X (2012) Effects of grinding processes on enzymatic degradation of wheat straw. Bioresour Technol 103:192–200
53. Ek M, Gellerstedt G, Henriksson G (eds) (2009) Pulp and paper chemistry and technology: pulping chemistry and technology. Walter de Gruyter, Berlin

54. Deepa B, Abraham E, Cherian BM, Bismarck A, Blaker JJ, Pothan LA, Leao AL, de Souza SF, Kottaisamy M (2011) Structure, morphology and thermal characteristics of banana nano fibers obtained by steam explosion. Bioresour Technol 102:1988–1997
55. Donaldson LA, Wong KKY, Mackie KL (1988) Ultrastructure of steam-exploded wood. Wood Sci Technol 22:103–114
56. Chornet E, Overend PR (1989) A unified treatment for liquefaction, in Research on thermo-chemical biomass conversion. Elsevier Appl. Sci. Inc, Amsterdam, The Netherlands
57. Schultz TP, Biermann CJ, McGinnis GD (1983) Steam explosion of mixed hardwood chips as a biomass pretreatment. Ind Eng Chem Prod Res Dev 22:344–348
58. Liu CF, Sun RC (2010) Cellulose. In: Sun RC (ed) Cereal straw as a resource for sustainable biomaterials and biofuels: chemistry, extractives, lignins, hemicelluloses and cellulose. Elsevier, Amsterdam, pp 131–167
59. Kokta BV, Ahmed A (1998) Steam explosion pulping. In: Young RA, Ahktar M (eds) Environmentally friendly technologies for the pulp and paper industry. Wiley, New york
60. Garcia C, Dupeyre D, Vignon MR (1998) Fibres from semi-retted hemp bundles by steam explosion treatment. Biomass Bioenerg 14:251–260
61. Sun XF, Xu F, Sun RC, Fowler P, Baird MS (2005) Characteristics of degraded cellulose obtained from steam-exploded wheat straw. Carbohydr Res 340:97–106
62. Cheng Q, Wang S, Rials TG (2009) Poly(vinyl alcohol) nanocomposites reinforced with cellulose fibrils isolated by high intensity ultrasonication. Compos Appl Sci Manuf 40:218–224
63. Cheng Q, Wang S, Han Q (2010) Novel process for isolating fibrils from cellulose fibers by high-intensity ultrasonication. II. Fibril characterization. J Appl Polym Sci 115:2756–2762
64. Herrick FW, Casebier RL, Hamilton JK, Sandberg KR (1983) Microfibrillated Cellulose: Morphology and Accessibility. Proceedings of the Ninth Cellulose Conference (Applied Polymer Symposia, 37:797–813). New York, USA
65. Turbak AF, Snyder FW, Sandberg KR (1983) Microfibrillated cellulose, a new cellulose product: properties, uses, and commercial potential. J Appl Polym Sci, Appl Polym Symp 37:815–823
66. Iguchi M, Yamanaka S, Budhiono A (2000) Bacterial cellulose–a masterpiece of nature's arts. J Mater Sci 35:261–270
67. Bielecki S, Krystynowicz A, Turkiewicz M, Kalinowska H (2005) Bacterial cellulose. In: Vandamme EJ, De Baets S, Steinbüchel A (eds) Biopolymers online. Wiley-VCH Verlag GmbH & Co. KGaA, New york
68. Turbak AF Birth of nanocellulose. http://www.naylornetwork.com/PPI-OTW/articles/?aid=150993&issueID=22333. Retrieved 23 Feb 2012
69. Nakagaito AN, Yano H (2005) Novel high-strength biocomposites based on microfibrillated cellulose having nano-order-unit web-like network structure. Appl Phys A Mater Sci Process 80:155–159
70. Pääkkö M, Ankerfors M, Kosonen H, Nykänen A, Ahola S, Österberg M, Ruokolainen J, Laine J, Larsson PT, Ikkala O, Lindström T (2007) Enzymatic Hydrolysis Combined with Mechanical Shearing and High-Pressure Homogenization for Nanoscale Cellulose Fibrils and Strong Gels. Biomacromolecules 8:1934–1941
71. Stenstad P, Andresen M, Tanem B, Stenius P (2008) Chemical surface modifications of microfibrillated cellulose. Cellulose 15:35–45
72. Nakagaito AN, Yano H (2004) The effect of morphological changes from pulp fiber towards nano-scale fibrillated cellulose on the mechanical properties of high-strength plant fiber based composites. Appl Phys A Mater Sci Process 78:547–552
73. Andresen M, Johansson L-S, Tanem BS, Stenius P (2006) Properties and characterization of hydrophobized microfibrillated cellulose. Cellulose 13:665–677
74. Andresen M, Stenius P (2007) Water-in-oil Emulsions Stabilized by Hydrophobized Microfibrillated Cellulose. J Dispers Sci Technol 28:837–844

75. Zimmermann T, Pöhler E, Geiger T (2004) Cellulose Fibrils for Polymer Reinforcement. Adv Eng Mater 6:754–761
76. Habibi Y, Mahrouz M, Vignon MR (2009) Microfibrillated cellulose from the peel of prickly pear fruits. Food Chem 115:423–429
77. Saito T, Nishiyama Y, Putaux J-L, Vignon M, Isogai A (2006) Homogeneous Suspensions of Individualized Microfibrils from TEMPO-Catalyzed Oxidation of Native Cellulose. Biomacromolecules 7:1687–1691
78. Henriksson M, Henriksson G, Berglund LA, Lindström T (2007) An environmentally friendly method for enzyme-assisted preparation of microfibrillated cellulose (MFC) nanofibers. Eur Polym J 43:3434–3441
79. Saito T, Isogai A (2006) Introduction of aldehyde groups on surfaces of native cellulose fibers by TEMPO-mediated oxidation. Colloids Surf A Physicochem Eng Asp 289:219–225
80. Henriksson G, Christiernin M, Agnemo R (2005) Monocomponent endoglucanase treatment increases the reactivity of softwood sulphite dissolving pulp. J Ind Microbiol Biotechnol 32:211–214
81. Rånby B (1949) Fibrous macromolecular systems. Cellulose and muscle. The colloidal properties of cellulose micelles. Acta Chem Scand 3:649–650
82. Rånby B, Ribi E (1950) Über den Feinbau der Zellulose. Cell Mol Life Sci 6:12–14
83. Rånby BG (1951) Aqueous colloidal solutions of cellulose micelles. Discuss Faraday Soc 11:158–164
84. Roman M, Winter WT Cellulose nanocrystals: from discovery to application. TAPPI International Conference on Nanotechnology for the Forest Products Industry, Atlanta, GA
85. Revol JF, Bradford H, Giasson J, Marchessault RH, Gray DG (1992) Helicoidal self-ordering of cellulose microfibrils in aqueous suspension. Int J Biol Macromol 14:170–172
86. Favier V, Chanzy H, Cavaille JY (1995) Polymer Nanocomposites Reinforced by Cellulose Whiskers. Macromolecules 28:6365–6367
87. Favier V, Canova GR, Cavaillé JY, Chanzy H, Dufresne A, Gauthier C (1995) Nanocomposite materials from latex and cellulose whiskers. Polym Advan Technol 6:351–355
88. Okano T, Kuga S, Wada M, Araki J, Ikuina J (1999) Japan, Nisshin Oil Mills Ltd. JP 98/151052
89. Ono H, Matsui T, Miyamato I (1999) Japan, Asahi Kasei Kogyo Kabushiki Kaisha. WO 98/JP5462
90. Lee S-Y, Mohan D, Kang I-A, Doh G–H, Lee S, Han S (2009) Nanocellulose reinforced PVA composite films: Effects of acid treatment and filler loading. Fiber Polym 10:77–82
91. Sadeghifar H, Filpponen I, Clarke S, Brougham D, Argyropoulos D (2011) Production of cellulose nanocrystals using hydrobromic acid and click reactions on their surface. J Mater Sci 46:7344–7355
92. Filson PB, Dawson-Andoh BE (2009) Sono-chemical preparation of cellulose nanocrystals from lignocellulose derived materials. Bioresour Technol 100:2259–2264
93. Beck-Candanedo S, Roman M, Gray DG (2005) Effect of Reaction Conditions on the Properties and Behavior of Wood Cellulose Nanocrystal Suspensions. Biomacromolecules 6:1048–1054
94. Araki J, Wada M, Kuga S, Okano T (1998) Flow properties of microcrystalline cellulose suspension prepared by acid treatment of native cellulose. Colloids Surf A 142:75–82
95. Araki J, Wada M, Kuga S, Okano T (2000) Birefringent Glassy Phase of a Cellulose Microcrystal Suspension. Langmuir 16:2413–2415
96. Araki J, Wada M, Kuga S, Okano T (1999) Influence of surface charge on viscosity behavior of cellulose microcrystal suspension. J Wood Sci 45:258–261
97. Heux L, Chauve G, Bonini C (2000) Nonflocculating and Chiral-Nematic Self-ordering of Cellulose Microcrystals Suspensions in Nonpolar Solvents. Langmuir 16:8210–8212

98. Bai W, Holbery J, Li K (2009) A technique for production of nanocrystalline cellulose with a narrow size distribution. Cellulose 16:455–465
99. Roohani M, Habibi Y, Belgacem NM, Ebrahim G, Karimi AN, Dufresne A (2008) Cellulose whiskers reinforced polyvinyl alcohol copolymers nanocomposites. Eur Polym J 44:2489–2498
100. Elazzouzi-Hafraoui S, Nishiyama Y, Putaux J-L, Heux L, Dubreuil F, Rochas C (2007) The Shape and Size Distribution of Crystalline Nanoparticles Prepared by Acid Hydrolysis of Native Cellulose. Biomacromolecules 9:57–65
101. Grunert M, Winter WT (2002) Nanocomposites of Cellulose Acetate Butyrate Reinforced with Cellulose Nanocrystals. J Polym Environ 10:27–30
102. Revol JF, Marchessault RH (1993) In vitro chiral nematic ordering of chitin crystallites. Int J Biol Macromol 15:329–335
103. Orts WJ, Godbout L, Marchessault RH, Revol JF (1998) Enhanced Ordering of Liquid Crystalline Suspensions of Cellulose Microfibrils: A Small Angle Neutron Scattering Study. Macromolecules 31:5717–5725
104. El-Saied H, Basta AH, Gobran RH (2004) Research Progress in Friendly Environmental Technology for the Production of Cellulose Products (Bacterial Cellulose and Its Application). Polym Plast Technol Eng 43:797–820
105. Chawla PR, Bajaj IB (2009) Microbial cellulose: fermentative production and applications. Food Technol Biotech 47:107–124
106. Yamada Y, Hoshino K, Ishikawa T (1997) The phylogeny of acetic acid bacteria based on the partial sequences of 16S ribosomal RNA: the elevation of the subgenus Gluconoacetobacter to the generic level. Biosci Biotechnol Biochem 61:1244–1251
107. Yamada Y (2000) Transfer of Acetobacter oboediens Sokollek et al 1998 and Acetobacter intermedius Boesch et al. 1998 to the genus Gluconacetobacter as Gluconacetobacter oboediens comb. nov. and Gluconacetobacter intermedius comb. nov. Int J Syst Evol Microbiol 6:2225–2227
108. Brown AJ (1886) On an acetic ferment which forms cellulose. J Chem Soc 49:172–186
109. Brown AJ (1886) An acetic ferment which forms cellulose. J Chem Soc 49:432–439
110. Yamanaka S, Watanabe K, Kitamura N, Iguchi M, Mitsuhashi S, Nishi Y, Uryu M (1989) The structure and mechanical properties of sheets prepared from bacterial cellulose. J Mater Sci 24:3141–3145
111. Nishi Y, Uryu M, Yamanaka S, Watanabe K, Kitamura N, Iguchi M, Mitsuhashi S (1990) The structure and mechanical properties of sheets prepared from bacterial cellulose. J Mater Sci 25:2997–3001
112. Bicerano J, Brewbaker JL (1995) Reinforcement of polyurethane elastomers with microfibres having varying aspect ratios. J Chem Soc Faraday Trans 91:2507–2513
113. Tajima K, Fujiwara M, Takai M, Hayashi J (1995) Synthesis of bacterial cellulose composite by Acetobacter xylinum. I. Its mechanical strength and biodegradability. Mokuzai Gakkaishi 41:749–757
114. Carreira P, Mendes JAS, Trovatti E, Serafim LS, Freire CSR, Silvestre AJD, Neto CP (2011) Utilization of residues from agro-forest industries in the production of high value bacterial cellulose. Bioresour Technol 102:7354–7360
115. Moosavi-Nasab M, Yousefi A (2011) Biotechnological production of cellulose by Gluconacetobacter xylinus from agricultural waste. Iran J Biotech 9:94–101
116. Rani MU, Rastogi NK, Appaiah KAA (2011) Statistical Optimization of Medium Composition for Bacterial Cellulose Production by Gluconacetobacter hansenii UAC09 Using Coffee Cherry Husk Extract – an Agro-Industry Waste. J Microbiol Biotechnol 21:739–745
117. Castro C, Zuluaga R, Álvarez C, Putaux J-L, Caro G, Rojas OJ, Mondragon I, Gañán P (2012) Bacterial cellulose produced by a new acid-resistant strain of Gluconacetobacter genus. Carbohydr Polym 89:1033–1037

118. Gea S, Torres FG, Troncoso OP, Reynolds CT, Vilasecca F, Iguchi M, Peijs T (2007) Biocomposites Based on Bacterial Cellulose and Apple and Radish Pulp. Int Polym Process 5:497–501
119. de Souza Lima MM, Borsali R (2004) Rodlike Cellulose Microcrystals: Structure, Properties, and Applications. Macromol Rapid Commun 25:771–787
120. Horikawa Y, Sugiyama J (2009) Localization of Crystalline Allomorphs in Cellulose Microfibril. Biomacromolecules 10:2235–2239
121. Haigler CH, White AR, Brown RM, Cooper KM (1982) Alteration of in vivo cellulose ribbon assembly by carboxymethylcellulose and other cellulose derivatives. J Cell Biol 94:64–69
122. Klemm D, Schumann D, Udhardt U, Marsch S (2001) Bacterial synthesized cellulose – artificial blood vessels for microsurgery. Prog Polym Sci 26:1561–1603
123. Woodcock C, Sarko A (1980) Packing Analysis of Carbohydrates and Polysaccharides. 11. Molecular and Crystal Structure of Native Ramie Cellulose. Macromolecules 13:1183–1187
124. O'Sullivan A (1997) Cellulose: the structure slowly unravels. Cellulose 4:173–207
125. Helenius G, Bäckdahl H, Bodin A, Nannmark U, Gatenholm P, Risberg B (2006) In vivo biocompatibility of bacterial cellulose. J Biomed Mater Res A 76A:431–438

Preparation of Nanocellulose from Kenaf (*Hibiscus cannabinus L.*) via Chemical and Chemo-mechanical Processes

8

Paridah Md. Tahir, Lukmanul Hakim Zaini, Mehdi Jonoobi, and H. P. S. Abdul Khalil

Contents

Keywords

Kenaf • Kenaf cellulose whiskers • Nanocellulose • Chemo-mechanical

P.M. Tahir (✉) • L.H. Zaini
Biocomposite Technology Laboratory, Institute of Tropical Forestry and Forest Products, Universiti Putra Malaysia (UPM), Serdang, Selangor, Malaysia
e-mail: parida.introp@gmail.com; lukmanulhakimzaini@yahoo.com

M. Jonoobi
Department of Engineering Sciences and Mathematics, Lulea University of Technology, Lulea, Sweden
e-mail: mehdij1978@gmail.com

H.P.S. Abdul Khalil
School of Industrial Technology, Universiti Sains Malaysia, Penang, Malaysia
e-mail: akhalilhps@gmail.com

J.K. Pandey et al. (eds.), *Handbook of Polymer Nanocomposites. Processing, Performance and Application – Volume C: Polymer Nanocomposites of Cellulose Nanoparticles*,
DOI 10.1007/978-3-642-45232-1_52,

1 Introduction

A fundamental understanding of the relationships between basic fiber properties, methods of processing, and composite end use performance properties has been well developed due to recent advances within the biocomposites research community. Simultaneously, advanced engineered biocomposites are currently being developed to meet the diverse needs of users for high-performance materials as well as economical commodity products. Advancements in nanotechnology have led to industrial isolation of nanocrystalline cellulose [1, 2]. While nanocrystalline cellulose may be only 1/10 as strong as carbon nanotubes – currently the strongest known structural material [3, 4] – it may cost 50–1,000 times less to produce [5, 6]. Engineered biocomposites employing nanocrystalline cellulose reinforcement could soon provide advanced performance, durability, value, service life, and utility, while at the same time being a fully sustainable technology.

A critical tool to achieve the goal of developing advanced biocomposites requires using the new science of nanotechnology to manipulate and control materials and processes at the nanoscale. Once many of its apparent promises are achieved, nanotechnology may well present a major tool to improve structural performance and extend serviceability by orders of magnitude. The next generation of engineered biocomposites needs to provide materials and products that far exceed current expectations. Whether it is for construction, building, automotive, marine, or aerospace, such products need to be of lower cost, higher performance, and lower maintenance and more adaptable and reliable and possess smart material properties.

Some characteristics of these products are [7]:

1. Able to develop synergistic performance through combination of wood, inorganic materials, and natural biofiber
2. Provide enhanced performance and superior serviceability
3. Be more durable, dimensionally stable, moisture proof, and fire resistant
4. Possess advanced sensory capabilities for warning users when problems are imminent
5. Possess advanced biomimetic capabilities for fixing itself when problems are encountered
6. Be renewable, recyclable, and sustainable
7. Decrease environmental impacts from processing and use
8. Have both materials and processes engineered to customize and optimize performance

According to Winandy et al. [7], nanotechnology offers three potential opportunities for the development of advanced lignocellulosic-based biocomposites:

1. Development of new analytical technologies that will provide a fundamental understanding of material behavior at the nanoscale.
2. Application of nanoparticles (inorganic and organic) in advanced biocomposites to enhance its performance.
3. Modifications of the wood and lignocellulosic raw material surfaces at the nanoscale.

This knowledge will then provide tools with which we can begin to fundamentally understand and then possibly control and manipulate critical materials–process–performance relationships.

1.1 Nanocellulose

Even though nanocellulose was introduced in the 1970s by Turbak, Snyder, and Sandberg in New Jersey, USA, it is not until the mid-1990s that it was taken up by the Japanese group, first by Taniguchi and co-workers and later by Yano and co-workers [8]. In the USA, a host of major companies such as P&G©, J&J, 3 M©, McNeil, etc. have used this technology in their products. Today, there are still extensive research and development efforts around the world in this field.

Nanocellulose or sometimes known as microfibrillated cellulose (MFC) can be prepared from any cellulose source material, but wood pulp is normally used. The nanocellulose fibrils are isolated from the wood-based fibers using high-pressure homogenizers which are controlled by speed, temperature, and pressure. The homogenizers are used to delaminate the cell walls of the fibers and liberating the nano-sized fibrils. This production route is normally connected to high energy consumptions (usually over 30 MWh/ton) being associated with the fiber delamination. Pretreatments such as enzymatic/mechanical and introduction of charged groups, e.g., through carboxymethylation or TEMPO-mediated oxidation [9], are sometimes used to address this problem. Another type of nanocellulose is cellulose nanowhiskers, a more crystalline form of nanocellulose which is formed by acid hydrolysis of native cellulose fibers using a concentrated inorganic salt, commonly sulfuric or hydrochloric acid. The amorphous sections of native cellulose are hydrolyzed, and after careful timing, the crystalline sections can be retrieved from the acid solution by centrifugation and washing. Cellulose nanowhiskers are rod-like highly crystalline particles (relative crystallinity index above 75 %) with a rectangular cross section. Its dimensions depend on the native cellulose source material, and hydrolysis time and temperature. Nanowhiskers are shorter (100–1,000 nm) than the nanofibrils obtained through the homogenization route (10 nm to several microns).

Nanocellulose/MFC is composed of nano-sized cellulose fibrils with a high aspect ratio (length to width ratio). Typical lateral dimensions are 5–20 nm, and the longitudinal dimension is in a wide range from 10s of nanometers to several microns. Nanocellulose is a pseudoplastic and exhibits the property of certain gels or fluids that are thick (viscous) under normal conditions, but flow (become thin, less viscous) over time when shaken, agitated, or otherwise stressed. This property is known as thixotropy. When the shearing forces are removed, the gel regains much of its original state.

The unique rheology of nanocellulose dispersions was recognized by the early investigators [10]. The high viscosity at low nanocellulose concentrations makes

nanocellulose very interesting as a non-calorie stabilizer and gellant in food applications, the major field explored by the early investigators. The dynamic rheological properties have been investigated in great detail [11], and it has been found that the storage and loss modulus were independent of the angular frequency at all nanocellulose concentrations between 0.125 % and 5.9 %. The storage modulus values are particularly high (104 Pa at 3 % concentration) compared to results for cellulose nanowhiskers (102 Pa at 3 % concentration). There is also a particular strong concentration dependence as the storage modulus increases 5 orders of magnitude if the concentration is increased from 0.125 % to 5.9 %.

It has long been known that crystalline cellulose has interesting mechanical properties for use in material applications. The stiffness of crystalline cellulose has been shown to be in the order of 140–220 GPa, which is comparable to Kevlar and is better than glass fibers that are currently used as reinforcement for plastics. Films made from nanocellulose have been shown to have high strength (over 200 MPa), high stiffness (around 20 GPa), and high strain (12 %).

1.2 Kenaf

Agro-based lignocellulosics intended for use in composite products can be categorized into two types: agricultural residues and lignocellulosics grown specifically for their fiber. The residue types include sugarcane bagasse, cereal straws, coconut coir, corn stover, oil palm stems and empty fruit bunch, and cotton stalks, whereas planted crops are annual crops that originate from various sources such as hemp, flax, sisal, abaca, jute, ramie, kenaf, etc.

> The overall limitations for using agricultural lignocellulosic materials include: lack of established delivery systems, processing complications caused by fiber density and morphology, process-temperature limitations, risk of decay, and or emission during processing and use [62].

Low thermal-degrade temperatures, high volatile emissions, and high moisture absorption of agro-fibers may also limit their processing options [68]. Compared to wood fiber, agro-fibers have lower density, higher stiffness-to weight ratio, and enhanced recyclability and biodegradability [62]. Although inorganic fibers such as fiberglass are stronger, bio-fibers have a more desirable balance of strength to weight.

Kenaf is categorized as hard fiber plant that comprises woody inner core and fibrous outer bast which provide excellent source of cellulose fibers. The proportion of these two sections is different based on stem height that normally contains about 35 % bast and 65 % core. Separation of long fibers from the bast generates higher monetary returns over whole stalk kenaf. The quality of the resulting fibers, however, depends on several factors among others which include methods of separation, machinery involved, chemical used, and state of the stem prior to separation [12].

1.2.1 History of Kenaf

There are many factors that make kenaf more attractive than the other bast fibers such as hemp, flax, and jute. Kenaf is a warm-season annual fiber crop growing in temperate and tropical areas. The height of this plant can reach 2.7–3.6 m, and the fiber, the most valuable part, can be extracted from its bark or bast. The characteristics of kenaf fibers are similar to those of wood, and the yields of kenaf are greater than those of hemp, flax, and jute, thus providing more cost-effective raw materials [13–15]. The fiber from kenaf is usually used to manufacture products such as grade pulps for the pulp and paper industry, protective packaging for fruits and vegetables, filters, composite boards, and textile.

The interest in kenaf started way back in the 1960s where the United State Department of Agriculture (USDA) has embarked on a large screening of potential plant crops for fiber production [16]. Kenaf has been listed together with other fiber crops such as jute, hemp, flax, and ramie. Japan has been the world major consumer of wood-fiber papers is keen on increasing its usage of non-wood fiber and is reported to have indicated its preference for kenaf as the preferred feedstock. India, China, and Thailand account for 90 % of world plantation with more than 95 % of world production of kenaf. In 2005–2006, total kenaf production was 0.33 million tons of which India, China and Thailand produced 42 %, 25 % and 11 %, respectively, while other countries produced the difference [17].

Compared to wood, kenaf production yields are favorable. Kenaf fiber can achieve an average of 17.8 metric tons (t) per hectare (ha) per annum (a) versus 2.2 ton/ha for tree fiber. Therefore, a significant contribution to the supply of raw material for cellulose pulp and other product from kenaf plants potentially substitutes wood resources. Kenaf fibers have been considered as reinforcing agents in polymer matrix [18]. The cell walls of lignocellulosic fiber are formed from oriented reinforcing semicrystalline cellulose microfibrils embedded in a hemicellulose/lignin matrix of varying composition. These microfibrils are made of cellulose molecules in extended chain conformation which provide the strength to the fibers, with a typical diameter of about 30–100 nm [19]. At this size, the cellulosic microfibrils can actually be considered to be nanofibers.

1.2.2 Anatomical Structures of Kenaf Fibers

Generally, kenaf bast fiber bundles are composed of elongated thick-walled ultimate cells which are joined together, both end to end and side by side, forming aggregates of fiber bundles along the height of the tree stem. During growing period of the stem, a circumferential layer of primary fibers is developed from the protophloem, but as vertical growth ceases in the lower parts, the secondary phloem fibers (where the bast fibers can be obtained) are developed as a result of cambial activity. Figure 8.1 shows a cross section of cell structure of kenaf stem. Unlike cotton which is unicellular, kenaf fibers have multicellular type cells. Depending on the location in the stem, kenaf contains three types of fiber: bast, core, and pith. Bast fiber is long and has thick cell wall, while those of core fiber are thinner with much

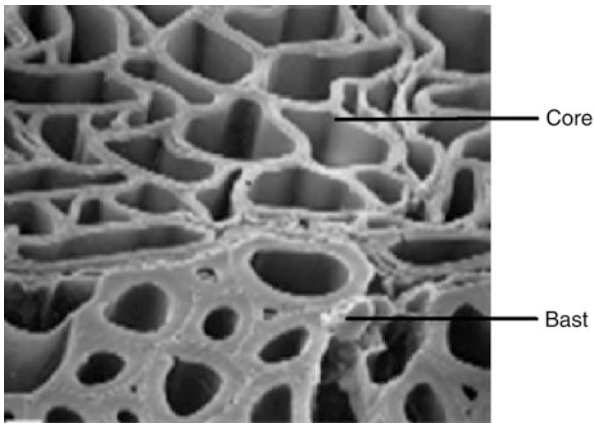

Fig. 8.1 Cross section of kenaf stem: bark (*lower part*) and core (*upper part*) in transverse section

shorter fiber length [20]. The core fibers appear as wedge-shaped bundles of cells and intermingle with parenchyma cells and other soft tissue. The pith consists exclusively of parenchymatous cells which are not typically prismatic but polygonal in shape. During fiber processing, the pith particles dried up and naturally detached from the rest of the fibers. In mature plants, kenaf can reach a height of 2.5–3.5 m [21]. Zhang [22] reported that the lengths of kenaf fibers are shorter at the bottom of the stalk and longer at the top. The increase in fiber length from the bottom to the top was found not to be gradual, but S-shaped [23]. Fiber length grew in the early part of the plant cycle and reduced again as the plants mature [24]. Kenaf single fibers are only about 1–7 mm long and about 10–30 μm wide, thus too short for textile processing [25].

Several studies have reported the anatomical structure of kenaf stem [21, 23, 26, 27]. The core fibers have larger lumen and a thinner cell wall than bast fibers. The width of the bast fibers is lower than that of the core fibers. The average kenaf fiber length from three kenaf cultivars was 2.45 mm and the average fiber width was about 12 μm [28]. Fiber length and width were similar among those cultivars and also similar at different stages of maturity. The core has very similar proportion of chemicals content of wood, while bastfiber was different. Table 8.1 compares basic properties of kenaf fibers with other types of bast fibers [20]. Apparently, kenaf varies greatly in terms of chemical properties, tensile strength, and equilibrium moisture content (EMC). Such differences may be attributed to the retting method employed when extracting the long fibers.

Many studies have been conducted on isolated nanofibers from cellulosic materials such as hemp, wheat straw, and wood pulp using nano reinforcements in polymer matrix [37–39]. These studies have derived a common conclusion to use nanofibers in various polymer matrices as reinforcement to improve the mechanical properties of the resulting nanocomposites. Nanofibers derived from cellulose fibrils contain nano-sized microfibrils that have high structural strength and stiffness [38]. Because of this reason, cellulose nanofibers have gained the world attention since the last decade, mainly on extracting cellulose microfibrils from

Table 8.1 Characteristics of long bast fibers produced from hemp, jute, flax, and kenaf

	Fiber chemical content									
Type	Fiber length (mm)	Fiber diameter (microns)	Lignin (%)	Cellulose (%)	Pectin (%)	Hemicellulose (%)	Tensile strength (mm)	EMC (%)	Retting methods	References
Hemp	15–55	17–22.8	5–3	70–92	0.9	18–22	310–750	<15	Chemical retting	5,7, 14,15,16,17,18
Jute	2–5	15.9–20.7	5–13	51–84	0.2	12–20	200–450	23	Dew retting	5,7,8,9
Flax	9–70	5–38	14–19	60–81	0.9	2.3	345–1,100	10–12	Enzymatic retting	2,5,7,9, 11,12
Kenaf	2.6–4	17–21.9	15–19	44–57	2	21	295–1,191	10–20	Water retting	1,2,3,4,5,6

Source: 1-Misra [29]; 2-Mohanty et al. [30]; 3-Rowell and Han [23]; 4-Anon [31]; 5-Calamari et al. [25]; 6-Chen et al. [24]; 7-Sikorski [32]; 8-Gassan et al. [66]; 9-Rowell and Stout [21]; 11-Alann [67]; 12-Biogiotti et al. [48]; 14-Kozlowski [15]; 15-Mwaikambo and Ansell [33]; 16-Preston [34]; 17-Ranalli [35]; 18-Mwaikambo [36]

various natural sources and using them as reinforcement in composite manufacturing [40, 41]. Nevertheless, since this is a relatively new field, the most challenging element would be in the extraction technique, i.e., fiber isolation and separation processes, which involve cleavage of the strong hydrogen bonding [42]. Thus, limitations on low yield, entanglement of fibers, and dispersion of fiber are anticipated that makes it uneconomical for pilot-scale production.

There are essentially many ways to extract cellulose nanofibers. This chapter discusses preparation of cellulose whiskers from kenaf via sulfuric acid reaction and extraction of nanofibril using chemo-mechanical processes.

2 Materials and Methods

2.1 Preparation of Cellulose Whiskers from Kenaf Bast Fibers

Four-month-old kenaf (*Hibiscus cannabinus* L.) from variety V36 was used to prepare the nanocellulose. Kenaf stems were peeled to separate the outer (bast) from the inner (core) part. Kenaf basts and core were dried to <10 % moisture content in an industrial oven. The dried bast fibers were kept in plastic bags and stored in dry condition until further use.

The process of whiskers production from kenaf bast was adopted from [63] with some modification in speed and time of centrifugation. The sequence of work is briefly illustrated in Fig. 8.2. Firstly, the kenaf bast was ground using a FRITSCH universal cutting mill pulverizer. The powdered bast was then treated with 4 % (w/w) NaOH solution at 80 °C for 2 h. At the end of reaction, the fibers were washed with distilled water and filtered. These steps (from alkali treatment to washing) were repeated three times until the alkali was completely removed. Subsequently, a bleaching treatment was applied by soaking the fiber in a solution containing equal parts of acetate buffer, aqueous chlorite 1.7 % (w/w), and distilled water. Then the fibers were washed with distilled water and filtered. The bleaching sequence was repeated four times under mechanical stirring.

Acid hydrolysis was performed by subjecting 4–6 % (w/w) kenaf bast bleached fibers in preheated sulfuric acid (65 %) at 50 °C for 60 min. The suspension was constantly mixed using magnetic stirrers. Separation was carried out in a centrifuge maintained at 4,000 rpm for 30 min and dialyzed with distilled water. Subsequently, whiskers suspension was homogenized by using an Ultra Tura T25 homogenizer for 5 min. Several drops of chloroform were added to the whiskers suspension to protect against bacteria growth. The whiskers suspension was stored at 4 °C.

2.2 Preparation of Kenaf Nanofibers Using Chemo-mechanical Process

The whole kenaf stem, bast, and core were used in this study. Kenaf bast was stripped from the core manually and immersed in water at 1:20 (bast to water) until

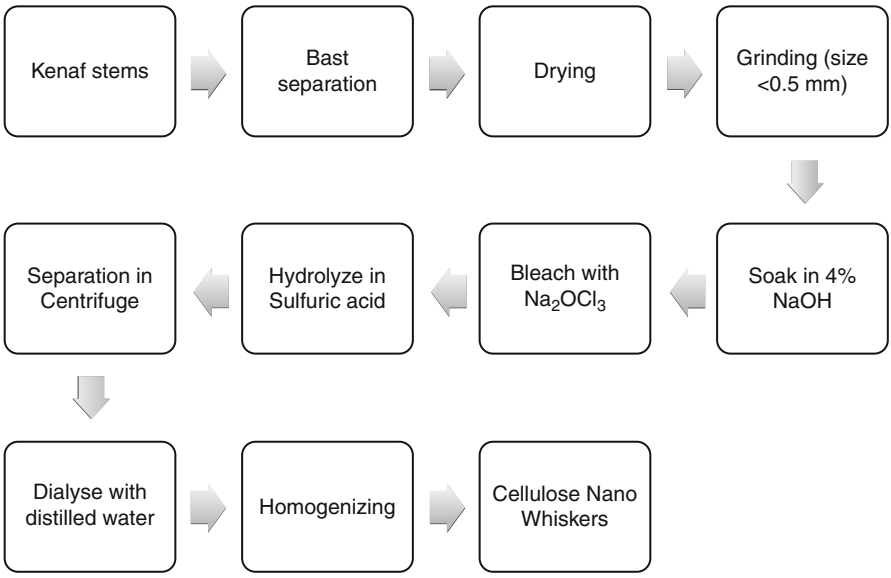

Fig. 8.2 Flow chart for preparing cellulose whiskers from kenaf bast

the fibers were loosened and separated out from the bast. The water-retted bast fibers were then air-dried prior to pulping.

2.2.1 Pulping and Bleaching

Kenaf bast fibers were cut to lengths of 2–3 cm, whereas kenaf whole stem and core were chipped into 2–3 cm dimension. Subsequently, 300 g of oven-dried, short kenaf fibers were cooked in a digester (MK model, USA) with NaOH 15 % and 0.1 % of anthraquinone (AQ). The ratio of cooking liquid to kenaf fibers was 7:1. The maximum cooking temperature was set to 160 °C, and this temperature was reached after 60 min. Another 45 min of cooking were carried out at the maximum temperature. Table 8.2 lists the conditions of the NaOH-AQ pulping process applied in this study. A three-stage bleaching was performed to ensure complete removal of hemicellulose and lignin. Table 8.3 shows the conditions of the bleaching processes.

2.2.2 Mechanical Treatments

Bleached and unbleached kenaf pulps (with dry weights of 24 g) were immersed in distilled water for 8 h. The fibers were distributed in the water using a laboratory disintegrator (Ihon-Rigoku-SP ¼ Japan model) at 3,000 rpm for 20 min. A pulp mat, which has a total weight of 240 g, was prepared with 10 % fiber concentration. With the purpose of defibrillating the fibers, the mat was then placed in a laboratory-type PFI mill (PTI Australian model) with a treatment level of 100,000 revolutions. Subsequently, the refined pulp was immersed in liquid nitrogen, where it was subjected to a cryo-crushing process, as developed by Bhatnagar and Sain [43]. According to this

Table 8.2 Condition of NAOH-AQ pulping process

Cooking process	NaOH-AQ
NaoH (%)	15
Anthraquinone (AQ) (%)	0.1
Liquor to fiber ratio	7:1
Maximum temperature (°C)	160
Time to maximum temperature (min)	60
Time at maximum temperature (min)	45–75

Table 8.3 Conditions of bleaching process

Stage	D1	Ep	D2
Chemical charged	Sodium chlorite (2 %)	NaOH (1.5 %)	Sodium chlorite (1.25 %)
	Acetic acid (3 %)	H_2O_2 (1 %)	Acetic acid (3 %)
Pulp consistency	10 %	10 %	10 %
Temperature	70 °C	70 °C	70 °C
Time	180 min	90 min	90 min

method, the pulp was placed in liquid nitrogen and crushed using a mortar and pestle. Crushed pulp was then washed with distilled water and filtered.

Diluted suspensions (0.2 %) of bleached and unbleached pulp were prepared, and the nanofibers were individualized with a high-pressure homogenizer (APV-1000). Prior to the homogenization process, all suspensions were ground in a mechanical blender apparatus for 15 min. The suspensions were passed through the homogenizer 40 times, and the pressure was held constant at 500 bar.

2.3 Fiber Analysis and Characterization

2.3.1 Fiber Yield

A small amount of the sample from each treatment was oven-dried at 105 °C for 24 h. The dried specimen was kept in a desiccators prior to weighing. The yields after each stage of chemical treatment were calculated as percentage of dried fiber over initial weight of kenaf sample.

2.3.2 Morphology of Fibers

A Philips XL30 ESEM was used to study the effect of the treatments on the fiber morphology. The acceleration voltage was set to 20 kV; all samples had been sputter coated with gold to avoid charging. The structure and size of the nanofibers were studied by transmission electron microscopy on a Hitachi model H-7100. A drop of diluted kenaf nanofiber suspension was deposited on the

carbon-coated grid and allowed to dry at room temperature. Measurements of the fiber diameters were carried out using an image analyzer program, XL Docu. Totally, 150 fibers of each material were measured.

2.3.3 Chemical Analysis

The chemical compositions of kenaf fibers before and after chemical treatment were determined according to TAPPI standard, 203 om-93. The percentages of holocellulose and lignin were determined following Wise and Murphy [44] and TAPPI standards, 222 om-88, respectively.

2.3.4 Field Emission Scanning Electron Microscopy (FE-SEM)

Glimmer plates were fixed with conducting carbon on a specimen holder. A drop of diluted fibril/water suspension (1:20) was put onto it. The samples were air-dried and the remaining fibrils were sputtered with a platinum layer of about 5 nm. The images were taken with 2 kV accelerating voltage.

2.3.5 Transmission Electron Microscope (TEM) Characterization

The size and shape of whiskers were studied under a transmission electron microscope (TEM) Hitachi model H-7100. A drop of diluted kenaf whiskers/chemo-mechanical nanocellulose suspension that was prior stained with 0.5 % solution of uranyl acetate was deposited onto a carbon-coated grids plate and allowed to dry at room temperature.

The nanocomposite film sample was evaluated for nanostructure and whiskers/chemo-mechanical nanocellulose distribution by TEM at an acceleration voltage of 100 kV. A small rectangular sample was cut to 2×7 mm^2in size from the film. The cut specimens were then embedded in a mix of Benzyldimethylamine (BDMA), methyl nadic anhydride (MNA), and dodecenyl succinic anhydride (DDSA) resins and cured for 2 days. The final ultra microtoming was performed with a diamond knife at room temperature generating electron transparent foils, being approximately 50 nm in thickness. The foils were gathered on 300 mesh Cu grid. The fiber's diameter measurements were carried out using an image analyzer program, XL Docu.

2.3.6 Fourier Transform Infrared Spectroscopy (FTIR)

The Fourier transform infrared spectroscopy (FTIR) study was done using Perkin-Elmer spectrometer 100, USA. Prior to this analysis, crude fibers, alkali-treated fibers, bleached fiber kenaf whiskers, and chemo-mechanical nanocellulose were prepared by grinding into 100 μm sized powder, mixed with KBr, and pressed into transparent pellets. In the case of thin nanocomposite film (containing cellulose acetate butyrate (CAB) and kenaf whiskers), the analysis was done within the range of 4,000–500 cm^{-1} transmittance mode.

2.3.7 X-Ray Diffraction

The structural and phase analysis of the samples was performed using the X-ray diffractometer (Philips P W 3040/60 X' pert Pro) with CuKα radiation (wavelength

of 1.5405 Å) and step-scan mode (2θ range: 5–50°). The phase identification of the samples was performed using the X' Pert Highscore software with the support of ICDD PDF-2 database, and the lattice parameter was calculated using the X' pert plus. The crystalline index of cellulose, C_{Ir}, was calculated using the following equation (Segal empirical method 1959):

$$C_{Ir}(\%) = [(I_{002} - I_{am})/I_{002}] \times 100$$

where I_{002} is the intensity of lattice peak diffraction and I_{am} is the peak intensity of the amorphous fraction. A diffraction angle of around $2\theta = 22.5°$ was peak for plane (002), and the lowest intensity at a diffraction angle of around $2\theta = 18.0°$ was measured as the amorphous part.

2.3.8 Thermogravimetric Analysis (TGA)

Thermal stability data was obtained using thermogravimetric analyzer (TGA Q500 – TA instruments) under linear temperature conditions. The samples (10.0 ± 1.0 mg) were heated in a platinum pan at 25–600 °C, with a heating rate of 10 °C/min in a nitrogen atmosphere.

3 Results and Discussion

3.1 Properties of Kenaf Cellulose Whiskers

Cellulose comprises between 35 % and 50 % of the total dry mass and consists of long chains of β-anhydroglucose units linked by β1,4-glucoside bonds. About 50–90 % of the cellulose in lignocellulosic materials is bound laterally by hydrogen bonds and forms crystalline structure. The remaining portion is less ordered and is often called amorphous cellulose [45]. It is the crystallinity of cellulose that poses the first of the major challenges in effective hydrolysis. Accessible surface area is another challenge for effective hydrolysis and this can be overcome by pretreating the fiber in NAOH prior to acid hydrolysis [33]. Another significant challenge in cellulose hydrolysis is the physical protection of cellulose provided by hemicellulose and lignin. Hence, in all the production of whiskers from woody materials, bleaching via oxidation of both hemicellulose and lignin is essential to ensure pure cellulose is produced for the next hydrolysis sequence. Reaction conditions vary from fiber types and origins.

3.1.1 Whiskers Yield

The yield of kenaf whiskers after each chemical treatment was calculated based on initial weight of kenaf fiber before treatment. The results show that 50 % of fibers can be collected upon NaOH treatment. Alkali treatment has apparently degraded almost all lignin and hemicellulose that normally present, respectively, between 15–19 % and 21 % (see Table 8.1). Subsequent bleaching further removed the remaining lignin, thus reducing the fiber yield to only 38 %. It was obvious that almost pure cellulose has been obtained as the color of the fibers was almost white

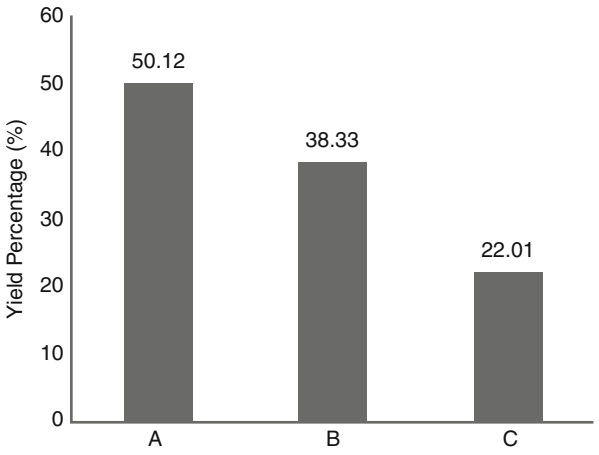

Fig. 8.3 Yields of kenaf fiber after alkali treatment (*A*), after alkali treatment and bleaching (*B*), and after alkali treatment, bleaching, and acid hydrolysis – cellulose whiskers (*C*)

indicating all lignin has been extracted. Upon acid hydrolysis, this "cellulose" yielded about 22 % cellulose whiskers (Fig. 8.3).

3.1.2 Fiber Morphology

The isolation of whiskers from kenaf bast is a multistep processes which involve chemical treatments. Hence, optimum chemical treatments are needed to avoid damage on the cellulose. Figure 8.4a–c exhibits field emission scanning electron micrograph images of kenaf bast fiber after it has undergone three steps of fiber treatment: alkali, bleaching, and acid hydrolysis. There was noticeable reduction in size after more treatments were applied to the fibers. Figure 8.4a shows untreated (crude) kenaf bast single fiber having almost similar diameter size which is around 100 μm. After being treated with NaOH, the diameter of the fiber reduced to a wider range, 20–90 μm, due to unequal reaction with alkali Fig. 8.4b. On further reaction with aqueous chlorite (bleaching stage), sufficient energy appears to be formed that breaks the lignin in the middle lamella that bonds the fibers together. Consequently smoother surface individual fibers revealed as can be seen in Fig. 8.4c. At this point, diameter of the fibers reduced to an average 11 ± 3 μm.

Figure 8.4d shows whiskers with a needle-like structure. The tendency to agglomerate could also be observed from this image which is to be expected as the cellulose crystals loss its H-bonding when the water evaporates during drying. Figure 8.5 shows the diameter distribution of whiskers extracted by sulfuric acid hydrolysis. Based on measurements of 150 individual whiskers, the diameter of cellulose whiskers was between 2 and 5 nm; most of the samples had diameter within 2–4 nm. The average diameter of cellulose kenaf whiskers was 3.03 nm. Compared to whiskers extracted from sugarcane bagasse which was 4 ± 2 nm [46], the diameters were quite similar. Kenaf whiskers length was around 150–450 nm, with an average of 332 ± 68 nm. Based on average length and diameter measurements, the aspect ratio was 110, suggesting that cellulose kenaf whiskers have a high reinforcing capability.

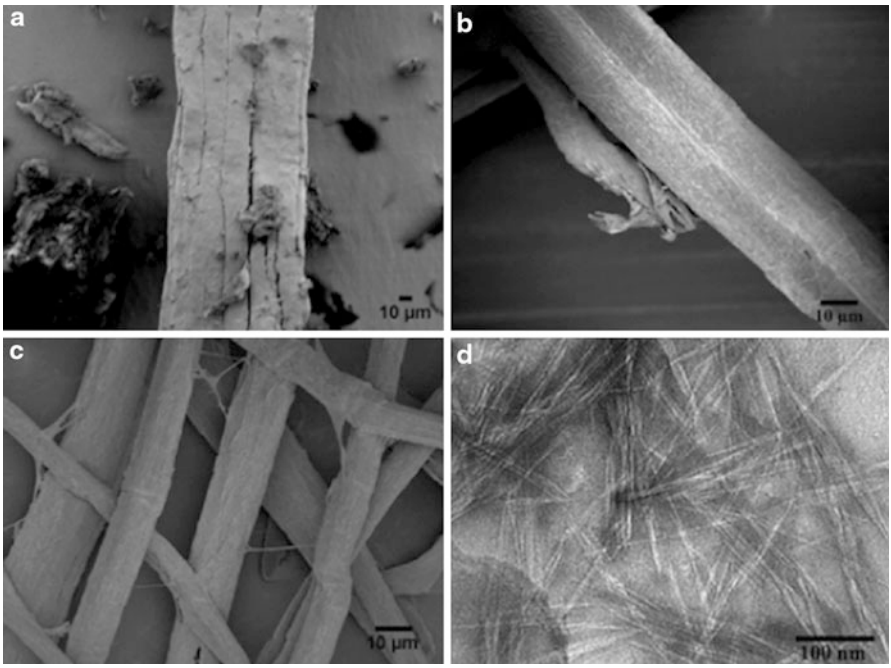

Fig. 8.4 Field emission scanning electron micrographs of (**a**) raw bast kenaf fiber and (**b**) after alkali treatment, (**c**) after alkali and bleaching, and (**d**) after alkali, bleaching, and acid hydrolysis – kenaf bast whiskers

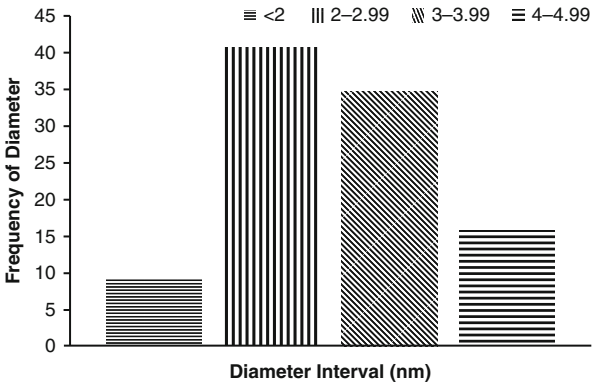

Fig. 8.5 Size distribution of kenaf bast whiskers isolated by sulfuric acid hydrolysis

3.1.3 Structural Analysis

FTIR Analysis

Infrared spectra of raw bast kenaf, alkali-treated fibers, bleached fibers, and kenaf whiskers are shown in Fig. 8.6 and summarized in Table 8.4. All spectra revealed a broad and intense peak at 3,300 cm^{-1} region which can be attributed to the

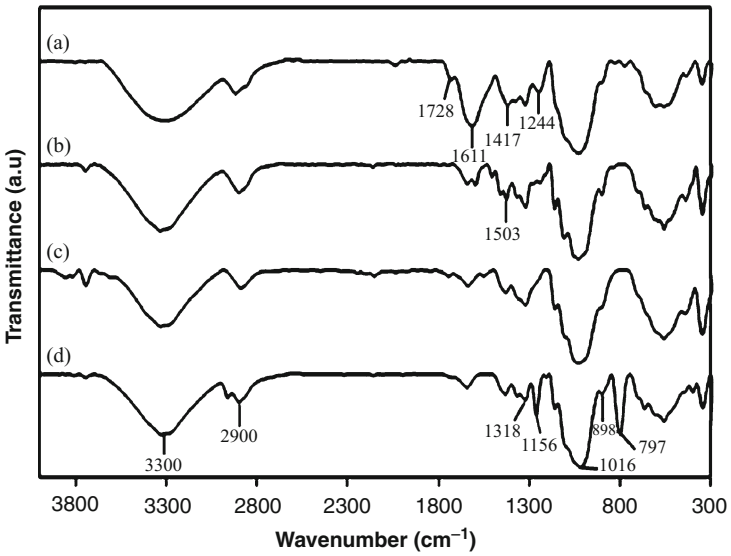

Fig. 8.6 FTIR spectra of different chemically treatment of bast kenaf fiber: (*a*) raw kenaf bast fiber, (*b*) alkali-treated fiber, (*c*) alkali-treated bleached fiber, and (*d*) kenaf whiskers

Table 8.4 FTIR characteristic peaks of kenaf bast fibers, alkali-treated fibers, bleached fibers, and kenaf whiskers samples

Kenaf bast fibers peak (cm^{-1})	Alkali-treated fibers peak (cm^{-1})	Alkali-treated bleached fibers peak (cm^{-1})	Kenaf whiskers peak (cm^{-1})	Assignment
3,324	3,335	3,332	3,329	O–H stretching
2,918	2,900	2,889	2,962	C–H symmetrical stretching and CH_2 symmetrical stretching
1,728	–	–	–	C = O stretching
1,612	1,642	1,637	1,641	C = C groups
1,418	1,425	1,428	1,430	C–H bonds
1,321	1,318	1,319	1,319	C–O aromatic ring
1,245	–	–	1,259	C–O stretching
–	1,158	1,156	1,157	C–O–C bond

characteristic of polysaccharides hydroxyl bonds [47]. C–H symmetrical stretching and CH_2 symmetrical stretching at 2,900–2,800 cm^{-1} indicated polysaccharide, wax, and oil present [47].

The peak located at 1,728 in the raw kenaf fiber was assigned to the C = O stretching of the acetyl groups of hemicelluloses and p-coumaric acids of lignin [48–50]. This peak was only seen in crude kenaf fiber suggesting the removal

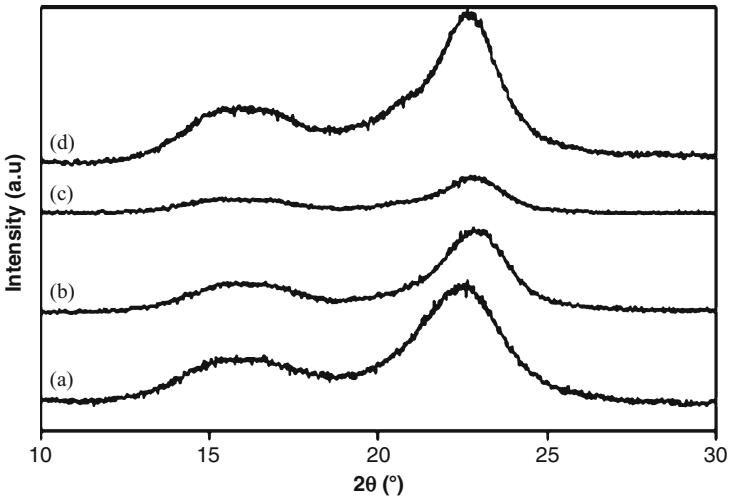

Fig. 8.7 X-ray diffraction patterns of the (*a*) raw bast kenaf, (*b*) alkali-treated fiber, (*c*) alkali-treated bleached fiber, and (*d*) kenaf whiskers

of lignin and most of the hemicellulose during the chemical treatments. The observation peak at 1,503 cm^{-1}in (b) implies that lignin was not completely removed after NaOH treatment. This peak, however, disappeared in the bleached sample (c) as well as in whiskers (d). The intensity of the peak at 1,610–1,640 corresponds to water absorbed in cellulose [47, 51]. The peak 1,430 cm^{-1} representing crystalline region in both whiskers and peak 1,417–1,427 cm^{-1} are characteristic of the C–H bonds in all organic molecules for the other samples [47, 8]. The intensity peak at 1,317–1,320 cm^{-1} region corresponds to cellulose with the C–O aromatic ring characteristic [47].

The peaks observed at 1,244 cm^{-1} in raw kenaf fiber was associated to the C–O stretching of the aryl group in lignin [47] which disappeared once the fiber was treated either with NaOH alone or bleached with aqueous chlorite. The intensity peak at 1,155–1,158 cm^{-1} region was due to the antisymmetrical deformation of the C–O–C bond [53]. The vibration peak at 898 cm^{-1} in the alkali-treated fiber and whiskers was assigned to C–H out of plane ring stretching in cellulose due to β-linkage or the glycoside bonds, which are symmetric in polysaccharides [47, 54].

X-Ray Diffraction

The X-ray diffraction of raw kenaf bast, alkali-treated fiber, alkali-treated bleached fiber, and kenaf whiskers are shown in Fig. 8.7. The crystallinity index (C_{Ir}) can be seen in Table 8.5. The crystallinity of the fibers increased after more treatments were applied to the fibers. Raw kenaf bast fiber had 67 % crystallinity which increased to 77 % after NaOH treatment and to 79 % after subsequent bleaching. It is believed that the removal of lignin and hemicelluloses caused the increase of its crystallinity. Kenaf whiskers generated from sulfuric acid hydrolysis only have 72 % crystallinity.

Table 8.5 Crystallinity index (C_{Ir}%) and initial degradation temperature (T_{id}) of raw, alkali-treated, alkali-treated bleached, and whiskers from kenaf bast

Material	$C_{I\%}$ (%)	T_{id} (°C)
Raw bast kenaf	67	177
Alkali-treated fibers	77	256
Alkali-treated bleached fibers	79	220
Kenaf whiskers	72	171

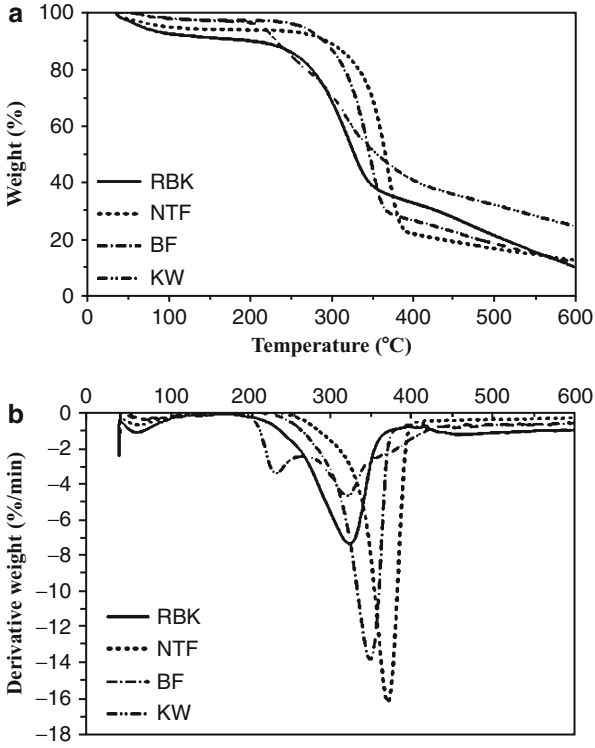

Fig. 8.8 TG and DTG curves of raw bast kenaf (*RBK*), alkali-treated fibers (*NTF*), alkali-treated bleached fibers (*BF*), and kenaf whiskers (*KW*)

Since there are many parameters that influence whiskers properties such as acid concentration, time, and temperature, the relatively lower crystallinity found in kenaf whiskers may be attributed to sulfuric acid hydrolysis reaction, attacking the crystalline region of the whiskers. Despite a lower crystallinity, kenaf whiskers formed a stable suspension which is in agreement with the study done by Araki et al. [55]. Stable suspension is an important property in order to achieve good dispersion of whiskers as matrix filler in reinforcement application.

Thermal Analysis

As reinforcement material, thermal stabilities of kenaf whiskers are important particularly in meeting minimal thermal acceptance in processing. Depending on the type of matrix/binder used, generally biocomposites are manufactured at a temperature between 150 °C and 300 °C. Figure 8.8 shows TG and DTG curves

of raw bast kenaf, alkali-treated fibers, alkali-treated bleached fibers, and kenaf whiskers. We could see from TG curves that weight loss of these samples started at 35 °C. Raw bast kenaf was observed to start degrading at 177 °C inferring degradations of both hemicellulose and lignin. Hemicellulose is very easy to remove at low temperature, while lignin degrades in a wider temperature ranging from 100 °C to 900 °C [56]. A peak at 320 °C on the DTG curve may be attributed to cellulose decomposition. The alkali-treated fibers show the greatest peak at 367 °C, while the alkali-treated bleached fibers show peak at 345 °C. Kenaf whiskers show multiple peaks at 228 °C and 316 °C that implies thermal instability, suspected to be instigated by the presence of sulfate groups on the cellulose surface. According to Wang et al. [19], thermal stability could be improved if there is less access of sulfate group onto cellulose surface. This claim may be true in the case of kenaf whiskers. The fact that kenaf whiskers recorded the lowest initial degradation temperature, i.e., 171 °C (Table 8.5), confirms its thermal instability which may be caused by the introduction of sulfate groups. The alkali-treated fibers and alkali-treated bleached fibers showed initial degradation at 256 °C and 220 °C, respectively, due to cellulose depolymerization.

3.2 Properties of Chemo-mechanical Kenaf Nanofibers

3.2.1 Chemical Composition

The chemical compositions of the kenaf fibers after various stages of chemo-mechanical treatment are presented in Table 8.6. NaOH was found to be efficient in removing the lignin from kenaf fibers. Based on the chemical composition analysis, almost all lignin was removed after bleaching process. The three-stage D1, Ep, and D2 bleaching sequence was found to increase the yield of nanofiber.

3.2.2 Fiber Morphology

The morphological structure of kenaf fibers as affected by various treatments is shown in Fig. 8.9. It was obvious that the crude kenaf fiber bundles are composed of individual fibers linked together by lignin (Fig. 8.9a). The diameter of the crude kenaf fibers ranged from 10 to 80 μm; more than 61 % of the fibers were found to have diameters between 20 and 40 μm. Figure 8.9b ,cshows structure of the fibers after pulping and bleaching processes, respectively. Clearly, both processes were able to separate the fiber bundles into individual fibers causing a significant decrease in its diameter. More than 79 % of the unbleached pulp fibers had diameters between 5 and 15 μm, and more than 88 % of the bleached pulp fibers displayed diameters between 1 and 8 μm. Figure 8.9d, e depicts the morphology of the unbleached and bleached pulp fibers after the refining process and cryo-crushing, respectively. The image analysis study showed that 49 % of the unbleached pulp fibers as well as 58 % of the bleached pulp fibers have diameters 0.1–1 μm. These results proved that the diameter of kenaf fiber can be reduced to nanosize by applying PFI refining followed by cryo-crushing.

Table 8.6 Chemical compositions of kenaf stem, bast, and core fibers after being subjected to different treatments

Materials		Cellulose (%)	Hemicellulose (%)	Lignin (%)	Extractive free (%)	Ash (%)
NaOH-treated fibers	Stem	58.00 ± 1.0	22.0 ± 1.0	17.50 ± 1.3	1.70 ± 0.2	2.40 ± 0.4
	Bast	81.5 ± 1.0	12.7 ± 1.9	2.5 ± 0.3	0.9 ± 0.4	2.2 ± 0.8
	Core	46.0 ± 0.5	33.0 ± 2.0	20.0 ± 1.0	2.20 ± 0.5	3.0 ± 0.4
Bleached pulp	Stem	91.00 ± 1.0	6.00 ± 1.8	1.00 ± 00	1.00 ± 0.5	0.25 ± 00
	Bast	92.0 ± 1.4	5.2 ± 0.6	0.5 ± 0.4	0.5 ± 0.3	–
	Core	92.0 ± 1.0	4.00 ± 1.0	0.70 ± 0.6	1.50 ± 0.2	0.5 ± 0.5
Bleached nanofibers	Stem	92.00 ± 0.5	5.00 ± 0.7	0.50 ± 0.5	0.60 ± 0.3	0.20 ± 00
	Bast	92.8 ± 0.5	46.0 ± 0.5	0.5 ± 0.3	0.4 ± 0.1	–
	Core	94.0 ± 0.5	4.7 ± 0.7	0.50 ± 0.5	0.80 ± 0.5	0.5 ± 0.1

The transformation of kenaf fibers from crude to nanosize is depicted in Fig. 8.10a–c. Clearly, the surface of the raw fiber (scale in 50 μm) was covered by a number of impurities suspected to be hemicellulose, lignin, pectin, and waxy substances. Conversely, the surface of bleached pulp fibers (scale in 50 μm) was much cleaner and smoother. Pulping had seemingly extracted out almost all hemicellulose and some lignin, while the subsequent bleaching practically removed all the lignin. Figure 8.10c demonstrates TEM image of kenaf nanofibers (scale in 1 μm) generated in this study which noticeably fall within nanosize (<100 nm).

3.2.3 Structural Analysis

FTIR Analysis

The IR spectra of the kenaf fibers after different treatments are shown in Fig. 8.11 [57]. The absorbance peaks in the 3,400–3,300 cm^{-1} region were attributed to the stretching of O–H groups, whereas those around 2,900–2,800 cm^{-1} were due to the stretching of C–H [58]. The peak located at 1,731 cm^{-1} in the raw kenaf was assigned to the C = O stretching of the acetyl group in hemicellulose [64, 65] or the ester linkage of carboxylic group in the ferulic and p-coumeric acids of lignin and/or hemicellulose [59]. This peak disappeared completely in the spectra of the unbleached and bleached pulps as well as for the bleached and unbleached nanofibers, thus indicating the removal of lignin and hemicellulose after these processes. In the raw kenaf, the peak at 1,242 cm^{-1} was associated to the C–O stretching of the aryl group in lignin [47]. Detailed explanation of absorbance peaks has been reported by Mehdi et al. [57].

X-Ray Diffraction

The X-ray diffractograms and crystallinity indices of the unbleached fibers, bleached pulp fibers, and nanofibers are shown in Fig. 8.12 and Table 8.7.

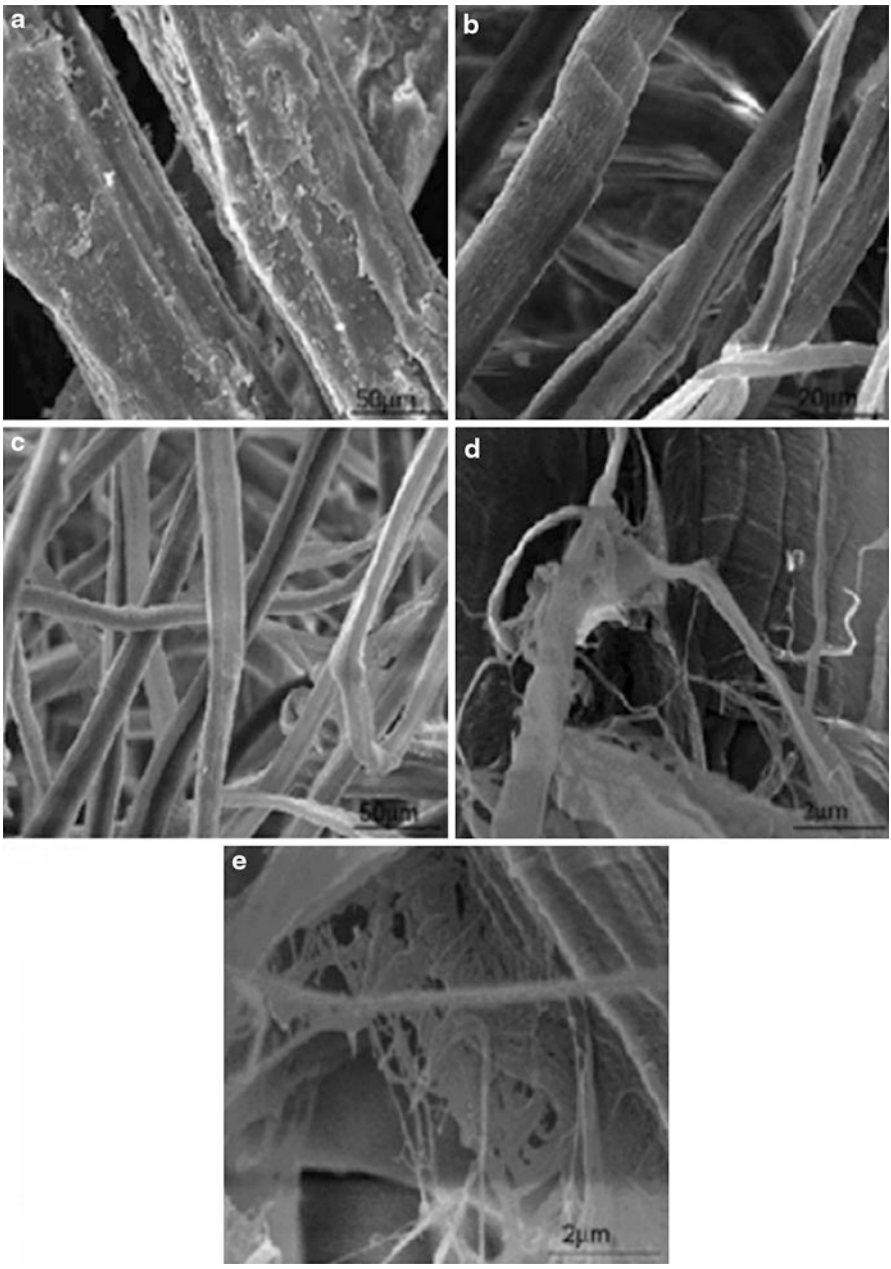

Fig. 8.9 ESEM micrographs of the structure of the kenaf fibers before and after chemical treatment for (**a**) raw kenaf fibers, (**b**) unbleached pulp, (**c**) bleached pulp, (**d**) fibers after cryo-crushing and treatment in a PFI mill, and (**e**) bleached pulp after cryo-crushing and treatment in a PFI mill [57]

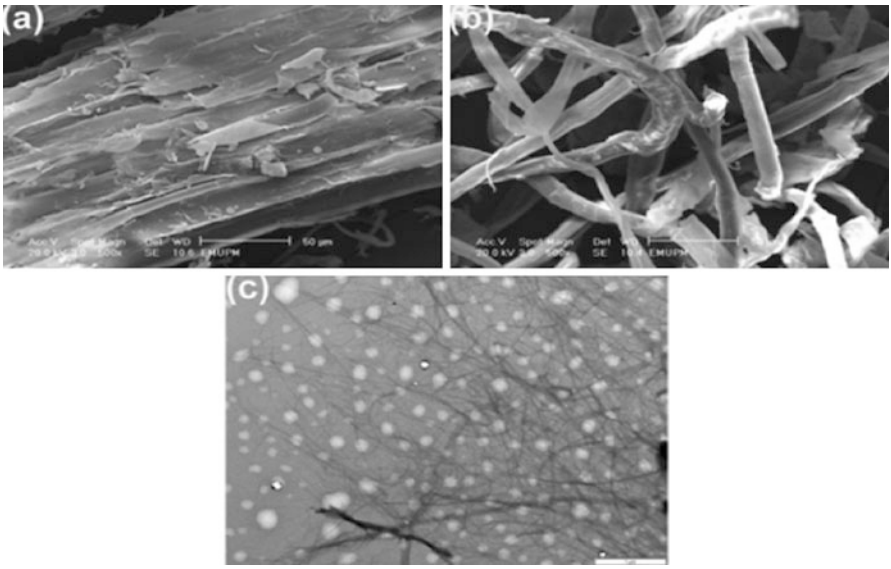

Fig. 8.10 Micrographs of (**a**) raw fibers, (**b**) bleached pulp fibers (chemo-mechanical treatments), and (**c**) TEM image of kenaf nanofibers

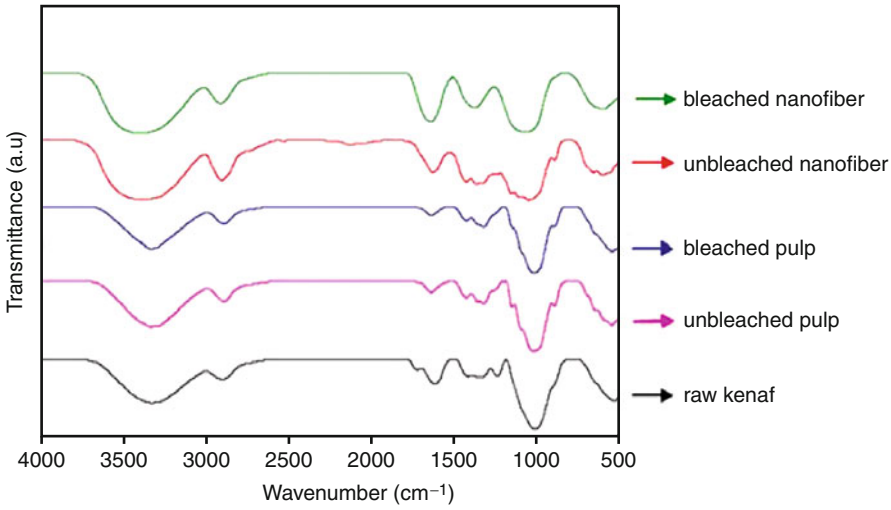

Fig. 8.11 Infrared spectra of kenaf fibers after various treatment

The crystallinity pattern of native cellulose (cellulose I) was exhibited by all of the samples. However, in contrast with the fibers, there were no crystalline transformations in the structures of the treated samples which displayed their major peak intensities at 2θ values close to 22.5°.

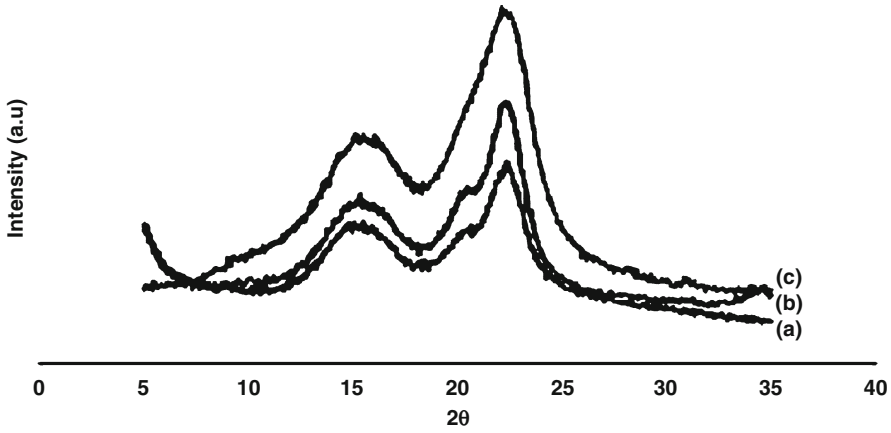

Fig. 8.12 X-ray diffraction patterns of (*a*) raw fibers, (*b*) bleached pulp fibers, and (*c*) nanofibers

Table 8.7 The crystallinity of the kenaf stem, bast, and core fibers before and after chemo-mechanical treatments

Material		Crystallinity (%)
Fibers	Stem	44
	Bast	68
	Core	41
Bleached pulp	Stem	60
	Bast	77
	Core	53
Bleached nanofibers	Stem	67
	Bast	81
	Core	62

These results clearly demonstrate the increase in the degree of crystallinity after chemo-mechanical treatments. The results also pointed towards the large difference in crystallinity between the raw kenaf fiber (41–68 %) and the bleached nanofiber (62–81 %). Among the kenaf types, the bast has the highest crystallinity at all levels of treatment. According to Alemdar and Sain [59], the increase in crystallinity is caused by greater removal of lignin and hemicellulose. The results gathered from the X-ray diffraction measurements also demonstrated that the mechanical treatments had some effects on the degree of crystallinity of the cellulose fiber. In this case, the proportion of crystalline regions was increased significantly after being subjected to high-pressure homogenization. On the other hand, cellulose nanofibers comprise pure cellulose chains, causing the crystallinity index to be higher. It is believed that higher crystallinity leads to higher tensile strength of the fiber and thereby may improve mechanical properties of the corresponding nanocomposites [59].

Thermogravimetric Analysis (TGA)

The thermal behavior of lignocellulosic materials depends on their chemical composition, structure, and degree of crystallinity [60]. In the case of kenaf bast fibers, the raw fiber cellulose decomposition occurred at 306 °C, while the bleached pulp and nanofibers were at 330 °C and 341 °C, respectively. The degradation temperatures for raw kenaf, unbleached pulp, bleached pulp, unbleached nanofibers, and bleached nanofibers were at 313 °C, 321 °C, 342 °C, 348 °C, and 351 °C, respectively.

The higher amount of residue in the raw kenaf fiber as opposed by the fibers after chemo-mechanical treatments was due to the presence of ash as well as lignin, which have a very slow degradation [56, 61].

4 Conclusions

Cellulose nano fibers can be produced from kenaf whole stem, bast, and core. Isolation of kenaf whiskers from raw bast kenaf via sulfuric acid hydrolysis was successfully conducted without apparent degradation of the cellulose. Treating the fiber with NaOH followed by bleaching in aqueous chlorite is effective in removing lignin and hemicellulose in the fiber. The kenaf whiskers produced in this study had crystallinity of 71 % and was able to form a stable suspension.

Cellulose nanofibers can also be isolated from kenaf stem via chemo-mechanical extraction. The nanofibers isolated from kenaf stem fibers had diameters 15–25 nm, whereas kenaf core, 20–25 nm. Chemical analysis of the fiber after each stage of treatment exhibited an increase in cellulose content and a decrease in lignin and hemicellulose content. The results from the FTIR confirmed that the lignin, as well as most of hemicellulose, can be removed during the chemical process. The TGA analysis demonstrated that the thermal stability of fibers improved after chemo-mechanical treatments. The crystallinity results showed that the chemo-mechanical treatments are more effective in increasing the crystalline structure of the kenaf cellulose. Among the kenaf sections, nanofiber produced from bast has the highest crystallinity (81 %). Both kenaf whiskers and nanofibers formed a stable suspension.

Acknowledgments The authors would like to thank the Economic Planning Unit (EPU) and the Ministry of Plantation Industry and Commodity (MPIC), Malaysia, for funding the project under grant KENAF-EPU 5488500.

References

1. Rousseau S, Tolnai B (2010) Method of manufacturing nano-crystalline cellulose film. US 2010/0124651 A1
2. Christiane L (2012) Hemicellulose and cellulose modifications. In: Sundqvist H (ed) Research highlights in industrial biomaterials, vol 2. VTT Research Highlights, Espool, pp 31–46

3. Xanthos M (2005) Chapter 2, Modification of polymer mechanical and rheological properties with functional fillers. In: Xanthos M (ed) Functional fillers for plastics. Wiley-VCH, Weinheim, FRG, p 21
4. Samir MASA, Alloin F, Defresne A (2005) Review of Recent Research into Cellulosic Whiskers, Their Properties and Their Application in Nanocomposite Field. Biomacromolecules 5:612–626
5. Koo JH (2007) What are nanoplastics? The Future of Nanoplastics, 22–23 Feb 2007, San Antonio
6. Simonsen J (2005) Bio-based nanocomposites: challenges and opportunities. In: Society of Wood Science and Technology 48th annual convention, 19 June 2005, Quebec, Canada
7. Winandy JE, Rudie AW, Williams RS, Wegner TH (2008) Integrated biomass technologies: future vision for optimally using wood and biomass. For Prod J 58(6):6–16
8. Berglund L, Mohanty AK, Misra M, Drzal L (2005) Natural Fibers, Biopolymers, and Biocomposites. CRC Press, Boca Raton, pp 807–832
9. Wågberg L, GeroDecher MN, Tom Lindström MA, Karl A (2008) Cellulose-based nanocomposites. Langmuir 24(3):784–795
10. Tatsumi D, Satoshi I, Takayoshi M (2002) Effect of Fiber Concentration and Axial Ratio on the Rheological Properties of Cellulose Fiber Suspensions. J Soc Rheol 30(1):27–32
11. Pääkkö M, Ankerfors M, Kosonen H, Nykänen A, Ahola S, Österberg M, Ruokolainen J, Laine J, Larsson PT, Ikkala O, Lindström T (2007) Enzymatic Hydrolysis Combined with Mechanical Shearing and High-Pressure Homogenization for Nanoscale Cellulose Fibrils and Strong Gels. Biomacromolecules 8(6):1934–1941
12. Tahir PM, Amel BA, Syeed OA, Saiful A, Zakiah A (2011) Retting Process Of Some Bast Plant Fibres And Its Effect On Fibre Quality: A Review. BioResources 10(4):1–8
13. Wood I (2000) Fibre crops-new opportunities for Australian agriculture. CSIRO, Brisbane
14. Rymsza TA (2000) Advancements of kenaf in the USA-kenaf paper and nonpaper developments. In: International kenaf conference, Japan Kenaf Association, p 10
15. Kozlowski R (2000) Potential and diversified uses of green fibers. In: 3rd international wood and natural fibers, composites symposium, pp 1–14
16. Fisher G (1994) Proceeding of the Tappi pulping conference 1994. Tappi Press, Atlanta, pp 91–94
17. FAO (2006) Jute, kenaf, sisal, aabaca, coir and allied fibers statistics. http://www.fao.org/es/esc/en/20953/21005/highlight_51023en
18. Liu W, Drzal LT, Mohanty AK, Misra M (2007) Influence of processing methods and fiber length on physical properties of kenaf fiber reinforced soy based biocomposites. Compos B 38(3):352–359
19. Wang B, Sain M, Oksman K (2007) Study of Structural Morphology of Hemp Fiber from the Micro to the Nanoscale. Appl Compos Mater 14(2):89–103
20. Amel BA, Paridah MT, Sudin R, Anwar U, Hussein AS (2013) Effect of fiber extraction methods on some properties of kenaf bast fiber. Industrial Crops and Products 46:117–123
21. Rowell RM, Stout HP (1998) Jute and kenaf. In: Handbook of fiber chemistry, 2nd edn. Marcel Dekker, New York, pp 465–504
22. Zhang T (2003) Improvement of kenaf yarn for apparel applications. Master thesis of Louisiana State University
23. Rowell RM, Han JS (2000) Characterisation and factors effecting fiber properties. In: Frolini E, Leao AL, Mattosso LHC (eds) Natural polymers and agrofibers composites. Embrapa Instrumentacao Agropecuaria, San Carlos, pp 115–127
24. Chen L, Columbus EP, Pote JW, Fuller MJ, Black JG (1995) Kenaf bast and core separation. Kenaf Association, Irving, pp 15–19
25. Calamari TA, Tao W, Goynes WR (1997) A preliminary study of kenaf fiber bundles and their composite cells. Tappi J 80(8):149–154
26. Abdul Khalil HPS, Ireana Yusra AF, Bhat AH, Jawaid M (2010) Cell wall ultrastructure, anatomy, lignin distribution, and chemical composition of Malaysian cultivated kenaf fiber. Indus Crops Prod 31(1):113–121

27. Voulgaridis E, Passialis C, Grigoriou A (2000) Anatomical characteristics and properties of kenaf stems (Hibiscus cannabinus). IAWA J 21(4):435–442
28. Calamari TA, Tao W, Andrew ED (1999) Kenaf properties, processing and products. Mississippi State University, Mississippi, pp 32–57
29. Misra DK 1987. Cereal Straw: Chapter VI in Pulp and Paper Manufacture; Secondary Fibers and Non-Wood Fibers. In: Hamilton F, Leopold B (eds). TAPPI, Atlanta, GA
30. Mohanty AK, Misra M, Drzal LT (2001) Surface modifications of natural fibers and performance of the resulting biocomposites: an overview. Compos Interfaces 8(5):313–343
31. Anon (2001) Kenaf – an alternative fiber crop. Natural Life Magazine, International Kenaf Association, p 42
32. Sikorski J (1963) The fine structure of animal and man-made fibers. In: Hearle JWS, Peters RH (eds) Fiber structure. Butterworth & Company/The Textile Institute, London, pp 269–310
33. Mwaikambo LY, Ansell MP (2005) Mechanical properties of alkali treated plant fibers and their potential as reinforcement materials. Part I. Hemp fiber, Journal of Materials Science, 41(8): 2483–2496
34. Preston RD (1963) Observed structure in plant fibers. In: Hearle JWS, Peters RH (eds) Fiber structure. Butterworth & Company/The Textile Institute, London, pp 235–268
35. Ranalli P (1999) Advances in hemp research. Haworth Press: Binghamton, NY, p 272
36. Mwaikambo LY (2002) Plant-based resources for sustainable composites. PhD thesis, University of Bath, Department of Engineering and Applied Science, Bath
37. Alemdar A, Sain M (2008) Biocomposites from wheat straw nanofibers: morphology, thermal and mechanical properties. Compos Sci Technol 68(2):557–565
38. Wang B, Sain M (2007) Dispersion of soybean stock-based nanofiber in a plastic matrix. Polym Int 56(4):538–546
39. Taniguchi T, Okamura K (1998) New films produced from microfibrillated natural fibres. Polym Int 47(3):291–294
40. Chakraborty A, Sain M, Kortschot M (2005) Cellulose microfibrils: a novel method of preparation using high shear refining and cryocrushing. Holzforschung 59(1):102–107
41. Nakagaito AN, Yano H (2005) Novel high-strength biocomposites based on microfibrillated cellulose having nano-order-unit web-like network structure. Appl Phys A 80(1):155–159
42. Oksman K, Sain M (2006) Introduction to cellulose nanocomposites. In: Cellulose nanocomposites; processing, characterization and properties, ASC symposium series 938, Oxford Press, pp 2–8
43. Bhatnagar A., Sain M (2003) Manufacturing of nanofibrils. Canadian Patent 02437616
44. Wise LE, Murphy M (1946) Chlorite Holocellulose, its Fractionnation and Bearing on Summative Wood Analysis and on Studies on the Hemicelluloses. Pap Trade J 122:35–43
45. Brigham JS, Adney WS, Himmel ME (1996) Handbook on bioethanol: production and utilization. Taylor and Francis, Washington, DC, pp 119–141
46. Teixeira SR, Agda Eunice de Souza, Angel Fidel Vilche Peña, Regiane Godoy de Lima, Álvaro Gil Miguel (2011) Use of charcoal and partially pirolysed biomaterial in fly ash to produce briquettes: sugarcane bagasse, alternative fuel. Maximino Manzanera (ed)
47. Troedec M, Sedan D, Peyratout C, Bonnet J, Smith A, Guinebretiere R, Gloaguen V, Krausz P (2008) Influence of various chemical treatments on the composition and structure of hemp fibres. Compos A 39(3):514–522
48. Biogiotti J, Puglia D, Kenny JM (2004) A review on natural fibre-based composites-part I: structure, processing and properties of vegetable fibres. J Nat Fib 1(2):37–68
49. Liu W, Mohanty AK, Drazal LT, Askel P, Misra M (2004) Effects of alkali treatment on the structure, morphology and thermal properties of native grass fibers as reinforcements for polymer matrix composites. J Mater Sci 39(3):1051–1054
50. Sun XF, Xu F, Sun RC, Fowler P, Baird MS (2005) Characteristics of degraded cellulose obtained from steam-exploded wheat straw. Carbohydr Res 340(1):97–106

51. Nacos M, Katapodis P, Pappas C, Daferera D, Tarantilis PA, Christakopoulos P, Polissiou M (2006) Kenaf xylan - A source of biologically active acidic oligosaccharides. Carbohydr Polym 66(1):126–134
52. Keshk S, Suwinarti W, Sameshima K (2006) Physicochemical characterization of different treatment sequences on kenaf bast fiber. Carbohydr Polym 65(2):202–206
53. Silva MC, Lopes OR, Colodette JL, Porto AO, Rieumont J, Chaussy D, Belgacem MN, Silva GG (2008) Characterization of three non-product materials from a bleached eucalyptus kraft pulp mill, in view of valorising them as a source of cellulose fibres. Ind Crop Prod 27(3):288–295
54. Adel AM, Abd El-Wahab ZH, Ibrahim AA, Al-Shemy MT (2011) Part II: physicochemical properties. Carbohydr Polym 83(2):676–687
55. Araki J, Wada M, Kuga S, Okano T (2000) Flow properties of microcrystalline cellulose suspension prepared by acid treatment of native cellulose. Colloids Surf A Physicochem Eng Asp 142(1):75–82
56. Yang H, Yan R, Chen H, Lee D, Zheng C (2007) Characteristics of hemicellulose, cellulose and lignin pyrolysis. Fuel 86:1781–1788
57. Mehdi J, Jalaludin H, Alireza S, Manjusri M, Kristiina O (2009) Chemical composition, crystallinity, and thermal degradation of bleached and unbleached kenaf bast (Hibiscus cannabinus) pulp and nanofibers. BioResources 4(2):626–639
58. Khalil HPA, Ismail H, Rozman HD, Ahmad MN (2001) The effect of acetylation on interfacial shear strength between plant fibres and various matrices. Eur Polym J 37(5):1037–1045
59. Alemdar A, Sain M (2007) Isolation and characterization of nanofibers from agricultural residues–Wheat straw and soy hulls. Bioresour Technol 99(6):1664–1671
60. Fisher T, Hajaligol M, Waymack B, Kellogg D (2002) Pyrolysis behavior and kinetics of biomass derived materials. J Anal Appl Pyrol 2(2):331–349
61. Ashori A, Jalaluddin H, Raverty WD, MohdNor MY (2006) Chemical and morphological characteristics of Malaysian cultivated kenaf (Hibiscus cannabinus) fiber. Polym-Plast Technol Eng J 45(1):131–134
62. Clemons CM, Canlfieid DF (2005) Natural fibers, Chapter 11. In: Xanthos M (ed) Functional fillers for plastics. Wiley-VCH, Weinheim
63. Siqueira G, Abdillahi H, Bras J, Dufresne A (2010) High reinforcing capability cellulose nanocrystals extracted from *Syngonanthus* nitens (Capim Dourado). Cellulose 17(2):289–298
64. Sgriccia N, Hawley M, Misra M (2008) Characterization of natural fiber surfaces and natural fibre composites. Compos. Part A-Appl. S. 39(10):1632–1637
65. Tserki V, Zafeiropoulos NE, Simon F, Panayiotou C (2005) A study of the effect of acetylation and propionylation surface treatments on natural fibres. Composites Part A 36:1110–1118
66. Gassan J, Chate A, Bledzki AK (2001) Calculation of elastic properties of natural fibres. J. Mater. Sci. 36(15): 3715–3720
67. Alann A (2006) Fibres for strengthening of timber structures. Research report: 03, http://www.google.com.my/#hl=en&&sa=X&ei=F1bATP6sOZL5cZqslJoM&ved=0CBQQvgUoAA&q, Accessed on 21.10.2010
68. Rowell RM, Sanadi AR, Caulfield DF, Jacobson RE (1997) Utilization of natural fibers in plastic composites: problems and opportunities. Lignocellulosic-plastic composites: 23–51

Extraction of Cellulose Nanofibers from Cotton Linter and Their Composites

9

Maha M. Ibrahim and Waleed K. El-Zawawy

Contents

Abstract

For some time now, nanocellulose has been at the focus of a good deal of industrial and scientific interest as a novel biomaterial due to their wide abundance, their renewability, and their outstanding mechanical properties. Cellulose is the most abundant biopolymer on earth, derived from a variety of living species. Cotton linter is the by-product from cotton textile and has high cellulose content, beside pectins, proteinaceous matter, waxes, ash, and minor soluble polysaccharides. As an essentially regenerative natural resource, it has been applied widely owing to its low cost. This chapter provides an overview of the recent research on the fundamental and composite properties of nanoparticles extracted from cotton linter. It contains a general introduction to cellulose and basic techniques of nanocellulose preparation with its properties. The incorporation of nanocellulose in composite materials including processing methods and properties is also presented.

Keywords

Cotton linter • Nanocellulose • Composite

M.M. Ibrahim • W.K. El-Zawawy (✉)
Cellulose and Paper Department, National Research Center, Giza, Egypt
e-mail: mwakleed@hotmail.com; wkzawawy@yahoo.com

J.K. Pandey et al. (eds.), *Handbook of Polymer Nanocomposites. Processing, Performance and Application – Volume C: Polymer Nanocomposites of Cellulose Nanoparticles*,
DOI 10.1007/978-3-642-45232-1_76,

1 Introduction

In nature, a large number of plants and animals synthesize extracellular high-performance skeletal biocomposites consisting of a matrix reinforced by fibrous biopolymers [30]. Research for development of biodegradable materials from renewable sources is increasing. The availability of biopolymers, relatively cheaper, which occur in abundance in nature, can be cited as an important reason. An example of biopolymers presenting these advantages is cellulose [14]. It is a classical example where the reinforcing elements exist as whisker-like microfibrils that are biosynthesized and deposited in a continuous manner [26]. Cellulose is the world's most abundant natural renewable biodegradable polymer and has been estimated that globally around 1.5×10^{12} tonnes are synthesized and also destroyed each year [27].

The primary occurrence of cellulose is the existing lignocellulosic material in forests, with wood as the most important source. Other cellulose-containing materials include agriculture residues, water plants, grasses, and other plant substances. Besides cellulose, they contain hemicelluloses, lignin, and a comparably small amount of extractives [1].

Linter is an important by-product of the textile industry. Cotton linter is the short fiber that cannot be used in the textile process. When the regular cotton fibers are extracted in the ginning process, the linter remains attached to the seed coat. The fuzzy seed needs to be subjected to an additional process that will mechanically remove the linter [31]. The amount of linter produced worldwide is around 2.5 million metric tons [21, 44]. The cotton linter has an excess of 80 % of holocellulose, and more than 3/4 of it is alpha-cellulose. This cellulose content is within the normal range for cotton linter [44], and it is compared to the cellulose content of naturally colored cotton, which ranges from 74.0 % to 80.3 % [51]. However, it is lower than the 97.7 % of cellulose found in hydrophilic (medicinal) cotton. As an essentially regenerative natural resource, cotton linter has been applied widely owing to its low cost [50]. Traditional products made from linter are absorbent cotton, special papers, cellulose nitrate, and acetate [44]. In some cases, the linter is not extracted, but kept with the seed (when it is used for oil extraction) or chemically dissolved (for planting the seed).

The development of low-cost, sustainable, and renewable resources is critical to meet the growing environmental concerns and energy demands. The recent interest in using stiff nanometric particles as reinforcement materials in polymeric matrixes, composites or nanocomposites, has been increasing. Two good examples of these types of particles are carbon nanotubes and cellulose nanocrystals [14].

Producing cellulose nanocrystals is an interesting use for linter. Nanocrystals of cellulose, with diameters ranging from 2 to 20 nm and length ranging from 100 nm to 2.1 μm are called whiskers, nanowhiskers, or nanofibrils, and they can be obtained from many natural fibers [11, 34, 43]. Cellulose nanocrystals are the crystalline domains of cellulosic fibers, isolated by means of acid hydrolysis, and are called in this way due to their physical characteristics of stiffness, thickness, and length [15]. Natural fibers are used because they are cheap, abundant, renewable,

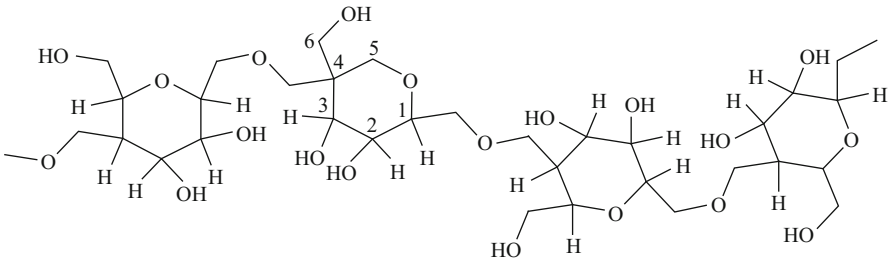

Fig. 9.1 Cellulosic units joined by glycosidic linkages (From [1])

Table 9.1 Lignocellulosical composition of cotton linter (From [31])

Component	Content (%, w/w)[a]
Moisture	6.33 ± 0.06
Ashes	2.32 ± 0.04
Extractives	5.59 ± 1.91
Insoluble lignin	0.68 ± 0.35
Holocellulose	81.51 ± 4.12
Hemicellulose	4.60 ± 0.60
Alpha-cellulose	76.91 ± 7.19

[a]Mean ± standard error

and biodegradable [20, 47, 51]. Nanocrystals can be used as fillers in composites [11, 20, 49, 51] because they have interesting mechanical properties such as low gas permeability [49] and stiffness enhancing capacity [33]. They can also be used as reinforcements for adhesives and components of electronic devices, biomaterials, foams, aerogels, and textiles [20, 33, 34, 52].

2 Structure of Cellulose

Cellulose is defined as a macromolecule, a nonbranched chain of variable length of 1–4-linked β-D-anhydroglucopyranose units (AGU). The length of these β (1,4) glucan chains depends on the source of cellulose [1]. Figure 9.1 shows the molecular-structure of cellulose as a carbohydrate polymer generated from repeating β-D-glucopyranose molecules that are covalently linked through acetal functions between the equatorial OH group of C4 and the C1 carbon atom (β-1,4-glucan), which is, in principle, the manner in which cellulose is biogenetically formed.

Yu et al. [55] reported the morphology and orientation of cellulose in the vessels of vascular bundles of wheat straw. In the vascular bundles, cellulose acts as the framework, and cellulose chains are high in orientation. In the thickening part of the vessels, cellulose exists in the form of cellulose crystalline lamellae but not cellulose microfibrils. For cotton linter, Morais et al. [31] mentioned that the cotton linter has an excess of 80 % of holocellulose (Table 9.1). Under the scanning

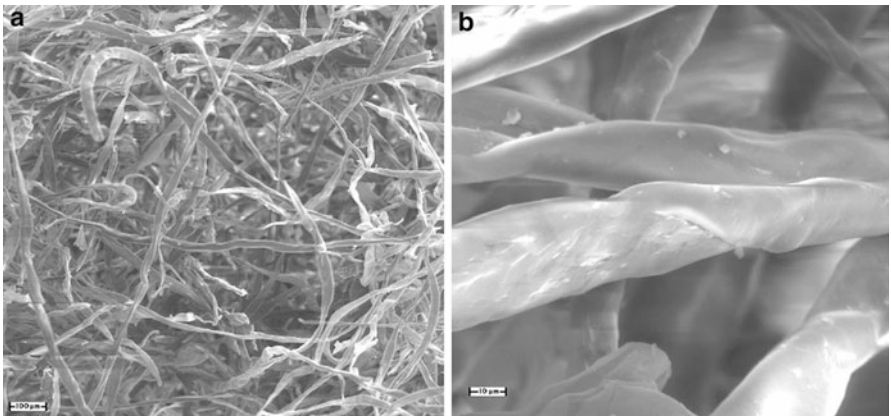

Fig. 9.2 SEM pictures of cotton linter (From [31])

electron microscope (SEM), a curled and soft flat shape can be observed for the linter (Fig. 9.2a). They noticed that the surface was rough with some pits. The average width was 23.04 μm, with a confidence interval of 1.01 μm (Fig. 9.2b). Morais et al. [31] mentioned that this curled shape increases the surface area and makes the fiber more reactive than typical cotton fibers. Also, they mentioned that the flat shape of this fiber increases its specific area and favors chemical reactions such as acidic hydrolysis.

3 Nanocellulose Preparation

Nanocellulose is the crystalline domain obtained from renewable cellulosic sources, used to increase mechanical properties and biodegradability in polymer composites [14].

Crystalline and amorphous regions are found in cellulose fibers in proportions that vary among plant species. For that reason, the characteristics (particularly the dimensions) of nanocellulosic materials depend largely on the raw material. Even though all cellulose nanocrystals are made of the same biopolymer, different raw materials can be used to obtain nanowhiskers tailored to specific needs [9, 20, 34, 43].

Cotton linter is an attractive source of nanowhiskers because it has more cellulose than other natural fibers commonly used. Cotton linter is also available in large amounts because it is a by-product of the textile industry. Cotton fiber is a traditional source of cellulose nanostructures [39], but its chemical composition can be influenced by many factors including the genotype and the environment where it was produced. However, in the literature on cotton nanocrystals, there is scarce information on how and where the cotton was produced [25, 28]. The use of regular cotton fiber can also result in a product different from those made of linter [6, 51, 54]. The knowledge on basic properties of the raw material is important for the reliable use of these nanostructures.

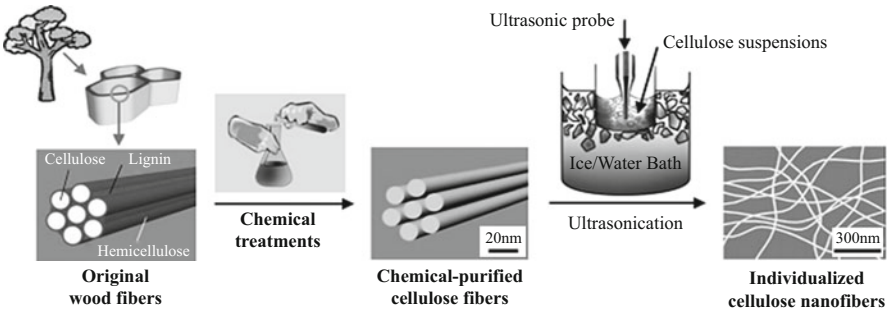

Fig. 9.3 Procedure for individualizing cellulose nanofibers (From [13])

Several processes have been used to extract highly purified nanofibers from cellulosic materials which lead to different types of nanofibrillar materials, depending on the cellulose raw material and its pretreatment and, more importantly, depending on the disintegration process itself. Roohani et al. [42] extracted the cellulose nanocrystals or whiskers from the cotton linter by ultrasonication. This process consists of combination of chemical pretreatment and high-intensity ultrasonication (Fig. 9.3).

Roohani et al. [42] milled the cotton linter with a laboratory milling device to obtain fine particulate substance. The cotton fibers were then extracted in a 2 wt% aqueous NaOH solution for 12 h at room temperature under mechanical stirring, and the filtered was rinsed with distilled water after this treatment step. Acid hydrolysis was done in 65 wt% aqueous sulfuric acid solution (11 wt% cotton fibers) at 45 °C under mechanical stirring for 45 min to allow fiber hydrolysis, and the yield of the resulting cellulose whiskers, with respect to the initial amount of cotton linters, was 64 %. At the end, dialysis against distilled water was performed to remove free acid in the suspension, as detected by the neutrality of the dialysis effluent. The dispersion of whiskers was completed by an ultrasonic treatment. By the electron micrograph, it was noticed that the cotton whiskers occurred as rodlike nanoparticle with average diameter and length of approximately 14.6 ± 3.9 and 171.6 ± 48.2 nm, respectively (Fig. 9.4). The average aspect ratio (l/d, l being the length and d the diameter) of these whiskers was measured to be around 11–12. Those values were close to the values reported for cotton whisker in the literature [16].

In a previous work [25], we treated the cotton linter with a solution of 5.0 M sodium hydroxide (NaOH) at 80 °C for 3 h. After washing till neutrality the cellulosic fibers were further treated with dimethyl sulfoxide (DMSO) at 80 °C for another 3 h. At the end, the fibers were washed and transferred into acidic aqueous solution containing mixed acids from 10.0 N of hydrochloric acid (HCl) and 36.0 N of sulfuric acid (H_2SO_4) for the preparation of nanocellulose at 80 °C with continuous stirring until the fiber slurry turned milky colloid suspension. After centrifugation, the electrophoretic mobilites of the resulting nanocellulose particles were measured and analyzed with a Zeiss EM-10 at 60 kV with a magnification of 40,000.

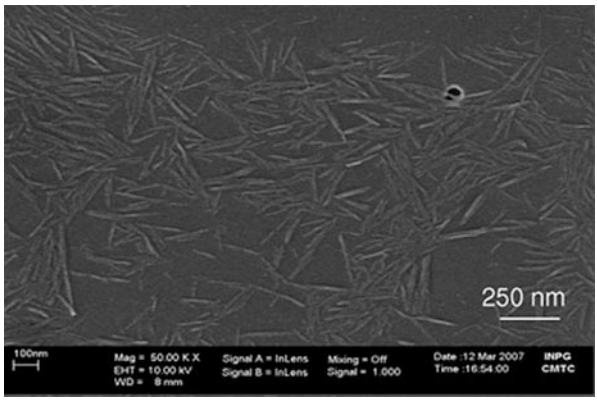

Fig. 9.4 Scanning electron micrograph (SEM–FEG) of a dilute suspension of cotton whiskers (From [42])

Fig. 9.5 TEM image of cellulose nanoparticles with an average size of 5.9 nm for cotton linter (× 40,000) (From [25])

The particle size analysis of the resulting nanocellulose was approximately 5.9 nm. Additional studies on the image morphometry demonstrated that particle area for the resulting nanocellulose was 16.35 μm^2 with a distance of 15.76 μm. Moreover, the transmission electron microscopy (TEM) image showed spherical shape for the nanocellulose resulting from cotton linter (Fig. 9.5).

On the other hand, Morais et al. [31] stirred mechanically the linter at a ratio of 1:20 (w/v) of aqueous concentrated sulfuric acid (60 %, w/w) with a Teflon© bar dispersing element, at 45 °C, for 60 min. The nanowhisker suspension was centrifuged for 15 min at 13,000 rpm, and the precipitate was resuspended in distilled water and dialyzed with tap water until a pH of 6–7 was reached. The obtained nanocellulose suspension was noticed to have a white gel appearance (Fig. 9.6a), and a bundles of crystals were depicted in the TEM pictures (Fig. 9.6b). The resulting whiskers were 177 nm long (ranging from 161 to 193) and 12 nm wide (ranging from 10 to 13) and had an aspect ratio (l/d) of 19 (ranging from 20 to 24).

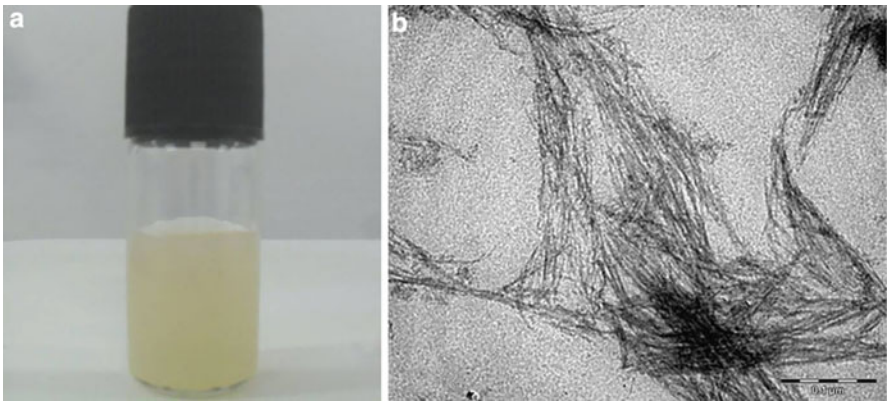

Fig. 9.6 Nanocellulose suspension (**a**) and TEM picture of cotton linter nanowhiskers (**b**) (From [31])

The TEM pictures (Fig. 9.6b) also depict agglomeration of nanocellulose bundles, points with dispersed crystallites, and individual crystals.

The isolation of nanocrystalline cellulose (NCC) from cellulose fibers using a simple, low-cost, and environment-friendly method is a great challenge [53]. The nanocrystals' dimensions are influenced by the hydrolysis conditions or pretreatments. However, it is widely accepted that the raw material is the most important factor [9, 11, 20, 34, 46]. The stability of the aqueous suspensions depends on the dimensions, size polydispersity, and surface charge of the dispersed species. The use of sulfuric acid to prepare nanocrystals leads to more stable aqueous suspensions than those prepared using hydrochloric acid [2, 4]. It was shown that the H_2SO_4-prepared nanoparticles present a negatively charged surface, while the HCl-prepared nanoparticles are not charged. During acid hydrolysis via sulfuric acid, acidic sulfate ester groups are likely formed on the nanoparticle surface. This creates an electric double-layer repulsion between the nanoparticles in suspension, which plays an important role in their interaction with a polymer matrix and with each other [19].

Moreover, the aspect ratio (l/d) of the crystals extracted from linter is noticed to differ from those extracted from other raw materials ([10, 11, 23, 43, 45, 51]). The aspect ratio of linter nanowhiskers does not overlap with any of other whiskers prepared from other raw material, and the cotton linter can be used as a unique raw material if nanocrystals with specific dimensions are required by industry.

Morais et al. [31] compared between the decomposition pattern of the raw linter and the produced nanocellulose (Fig. 9.7). They noticed that there were a small weight losses around 45–50 °C for the raw linter which was related to the moisture. The main T_{onset} of raw linter was at 312.92 °C, and the peak was at 340.29 °C (Fig. 9.6a). In the nanocellulose (Fig. 9.6b), the T_{onset} was reduced to 200.95 °C, and the main peak was reduced to 219.00 °C. There were also two new weight losses

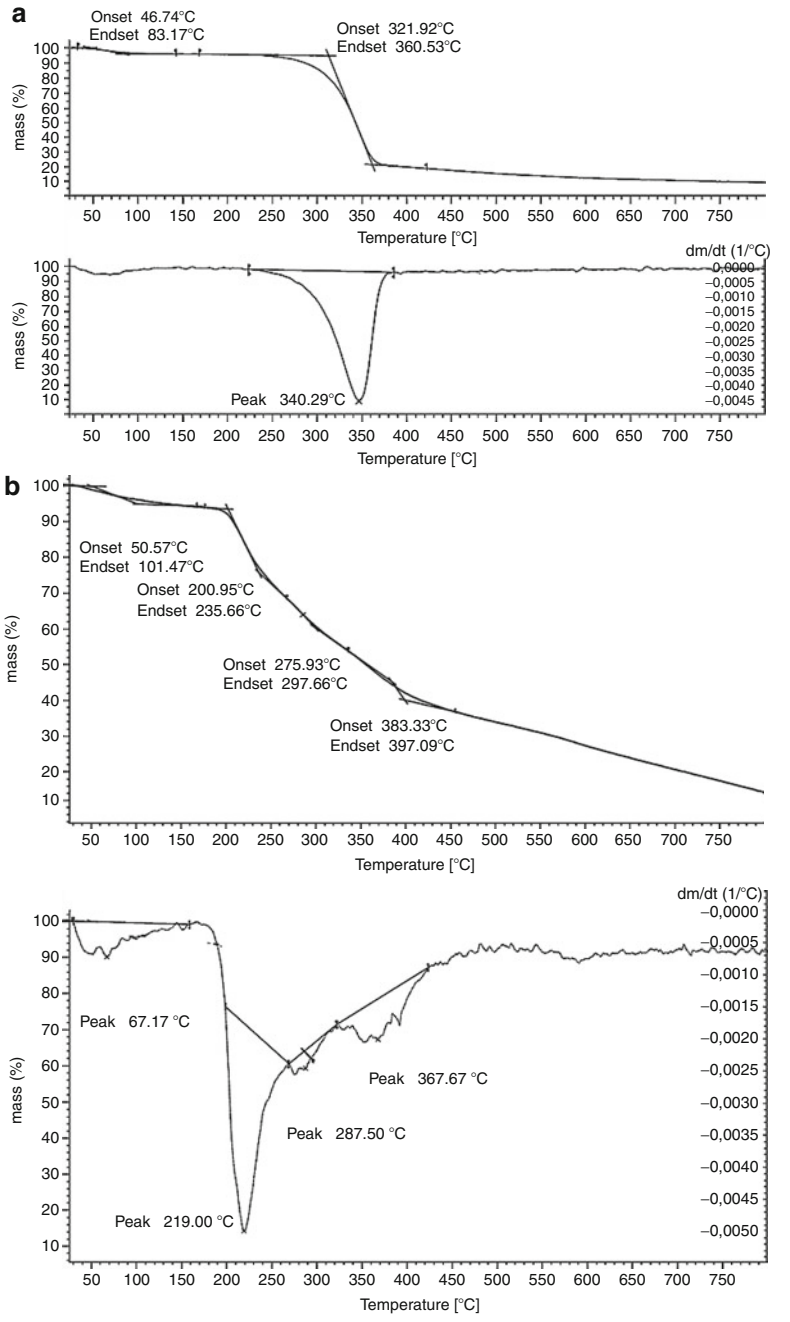

Fig. 9.7 Thermal decomposition profile of raw linter (**a**) and linter nanowhiskers (**b**) (From [31])

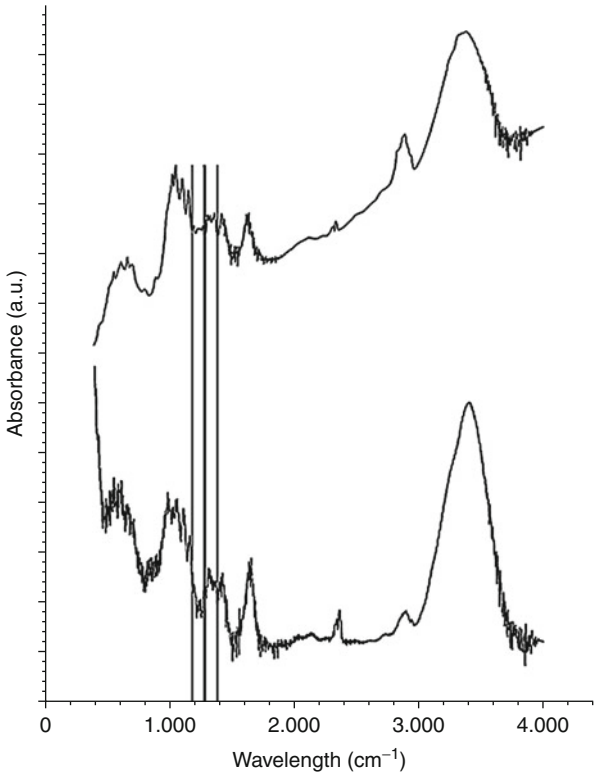

Fig. 9.8 FTIR spectra of raw linter (*bottom*) and linter nanowhiskers (*top*) (From [31])

noticed with peaks at 287.50 °C and 367.67 °C. On the other hand, there was a reduction of the number of peaks and an increase of the spectrum resolution in the nanocellulose FTIR curve in comparison to the linter FTIR spectrum (Fig. 9.8).

Furthermore, Morais et al. [31] noticed that the diffractograms of linter and nanocellulose had peaks related to the crystallographic plans of cellulose as indicated by the International Centre for Diffraction Data – ICDD (Fig. 9.9). The raw linter has a crystallographic pattern very similar to the standard ICDD cellulose, while the nanocellulose diffractogram had a greater (0 0 2) lattice peak that suggests an increased crystallinity. The crystallinity was 64.42 % for linter and 90.45 % for nanocellulose. Thus, the linter nanocellulose has a high crystallinity, and this property can be important for the composites made of these nanofillers.

4 Nanocellulose in Nanocomposite Applications

Nanocomposites in general are two-phase materials in which one of the phases has at least one dimension in the nanometer range (1–100 nm). The advantages of nanocomposite materials when compared with conventional composites are their superior thermal, mechanical and barrier properties at low reinforcement levels

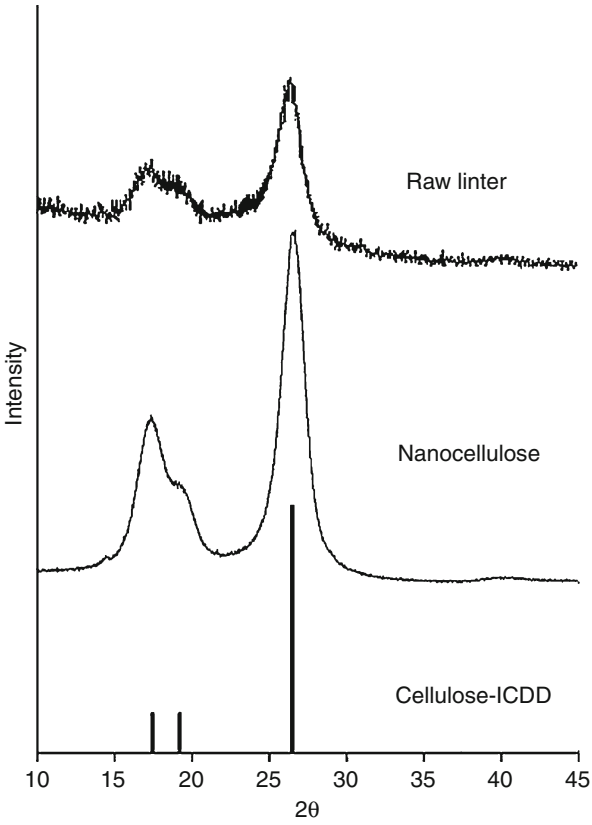

Fig. 9.9 X-ray diffractogram pattern of untreated linter (*top*) and cellulose nanowhiskers (*middle*) in comparison with cellulose X-ray diffraction pattern as ICDD (*bottom*) (From [31])

(e.g., B5 wt%), as well as their better recyclability, transparency, and low weight [32, 48]. Biodegradable polymers, in particular, may require improvement in terms of brittleness, low thermal stability, and poor barrier properties [48]. A number of researchers have therefore explored the concept of fully bio-derived nanocomposites as a route to development of bioplastics or bioresins with better properties [32, 36, 37]. Biopolymer-based nanocomposites have also been the subject of recent reviews [35, 40].

In nature, a large number of animals and plants synthesize extracellular high-performance skeletal biocomposites that consist of a matrix reinforced by fibrous biopolymers. In fact, during the last decade there has been a growing interest in using cellulose nanocrystals or whiskers [7, 18, 29]. Rånby and Ribi (1949 & [38]) were the first to produce stable suspensions of colloidal-sized cellulose crystals by sulfuric acid hydrolysis of wood and cotton cellulose. Using acid hydrolysis, native cellulose suspensions have been prepared from a variety of sources, including bacterial cellulose [3, 41], microcrystalline cellulose [5], sugar beet primary cell wall cellulose [8], cotton [17], tunicate cellulose (or tunicin) [22], and softwood pulp (mostly black spruce) [4]. The investigation for preparing cellulose

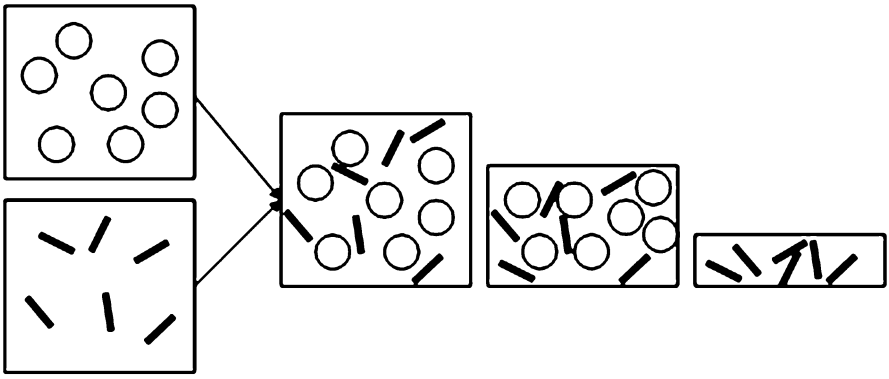

Fig. 9.10 Processing of polysaccharide nanocrystals reinforced polymer nanocomposite films using polymer latex (From [19])

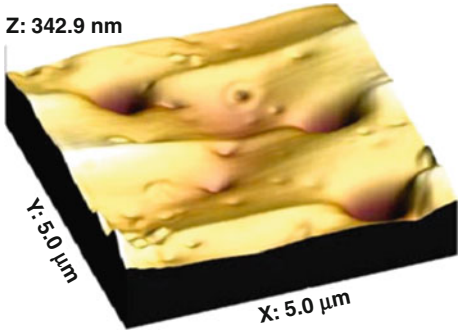

Fig. 9.11 AFM of the plain PLA film (From [12])

nanocomposites started around 1994. Nanocomposites were prepared by solution casting of various matrices and nanoreinforcements in aqueous medium [22, 24]. Solid nanocomposite films can be obtained by mixing and casting the two aqueous suspensions followed by water evaporation performed above the glass transition temperature of the polymer (Fig. 9.10) [19]. During water evaporation, the solid content in the medium increases, and the latex particles get closer. When getting in touch of each other, these soft polymeric particles deform and adopt a polyhedral form. Boundary between the former particles disappears by chain diffusion leading to a continuous polymer film containing the dispersed polysaccharide nanoparticles.

Chang et al. [12] produce NCC from hydrolyzing cotton linter with 60 % H_2SO_4 at 45 °C for 5 min. The resulting NCC had a yield of 54.4 wt% with average diameter of 319.0 nm. Different NCC percents, i.e., 5 %, 10 %, and 15 %, were incorporated in polylactic acid (PLA) for the production of NCC/PLA film composite. From the atomic force microscope (AFM), Chang et al. [12] noticed that the model of PLA film has a roughness of 27.4 nm (Fig. 9.11). For the surface models of NCC/PLA composite films (Figs. 9.12, 9.13, and 9.14), Chang et al. [12] noticed the addition of NCC reduces the surface roughness of the composites by 74.6–90.9 %.

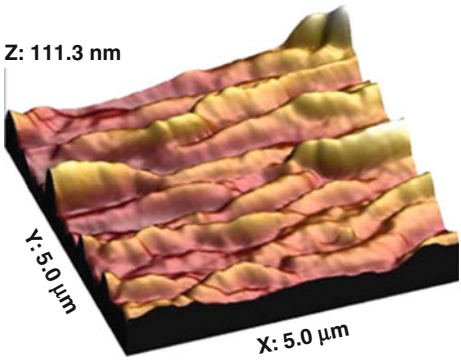

Fig. 9.12 AFM of a 5 % NCC/PLA composite film (From [12])

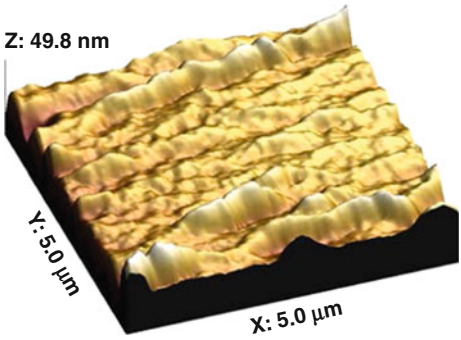

Fig. 9.13 AFM of a 10 % NCC/PLA composite film (From [12])

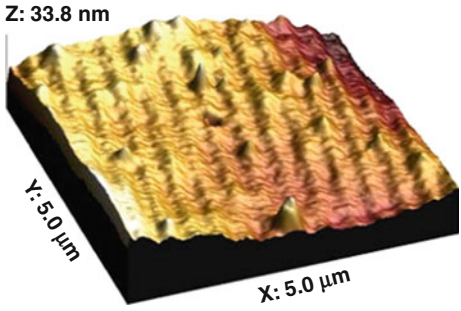

Fig. 9.14 AFM of a 15 % NCC/PLA composite film (From [12])

They mentioned that this can be due to the fact that the producing NCC has short rods which can be suitable for filling the pores and pits of the PLA.

In our work [25], nanocellulose fibers from cotton linter (CL) were dispersed in poly(vinyl alcohol) (PVA) solution to form nanocellulose–PVA composite films. A percent of 5 % starch (wt.%); 75 %, 55 %, and 35 % PVA (wt%); and 20 %, 40 %, and 60 % nanocellulose fiber (wt%); and 2.5 % glycerol and 40 mL of distilled water were used to cast films. From the morphological structure of the nanocellulose–PVA composite films (Fig. 9.15), we noticed that the cross section of the PVA films (Fig. 9.15a) showed a smooth dense surface. On the other hand,

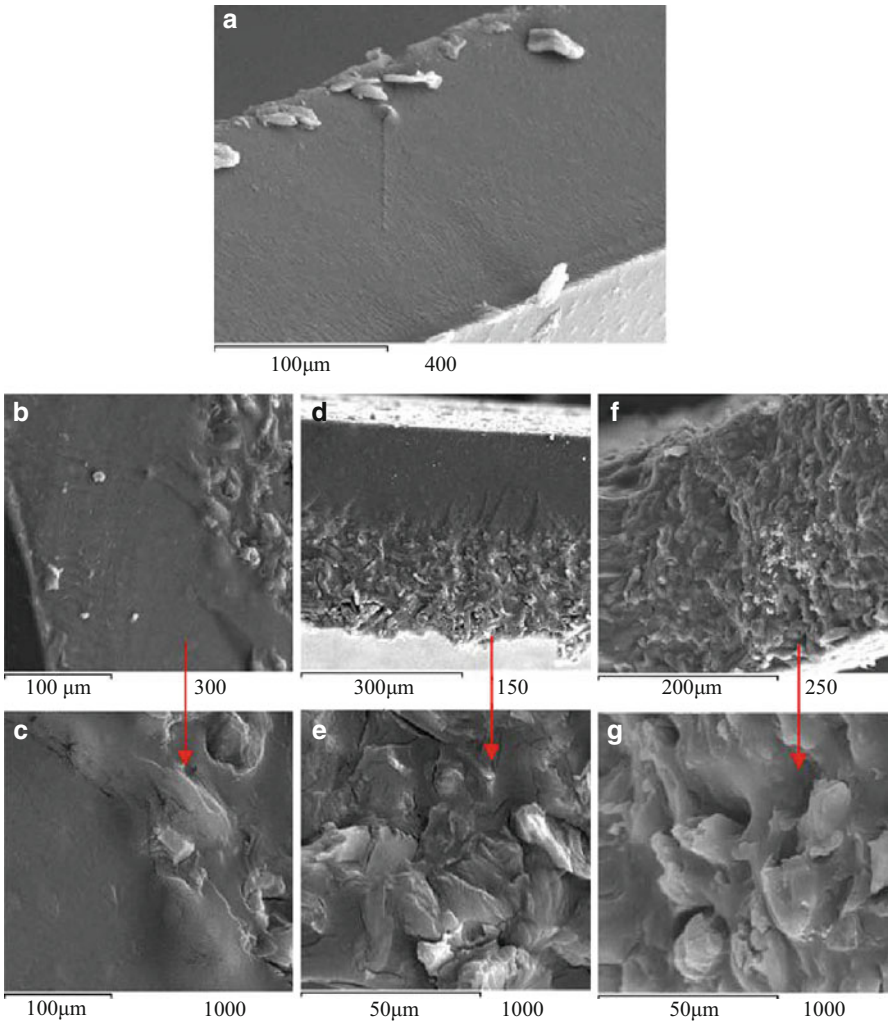

Fig. 9.15 Scanning electron micrographs (SEM) showing a cross section of (**a**) PVA, (**b**) and (**c**) 20 % CL/PVA, (**d**) and (**e**) 40 % CL/PVA, and (**f**) and (**g**) 60 % CL/PVA (from [25])

the cross section for nanocellulose–PVA from cotton linter (Fig. 9.15b, c, and d) indicates a dispersion of the nanoparticles with the PVA forming a hole which can be seen at higher magnification (Fig. 9.15e, f, and g).

The calculated mechanical properties, such as tensile strength and percentage elongation at break, of the PVA and nanocellulose–PVA composite films showed a slight variation in the tensile strength for all the compositions of nanocellulose–PVA compared with the tensile strength of plain PVA film (Figs. 9.16 and 9.17). From Fig. 9.16, a decrease in the tensile strength was noticed in the presence of nanocellulose from cotton linter. Moreover, the percentage elongation at break

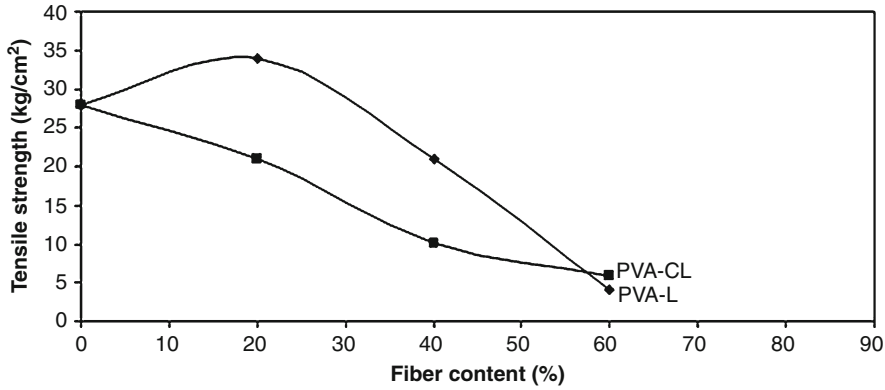

Fig. 9.16 Tensile strength for PVA–nanocellulose from cotton linter and linen (From [25])

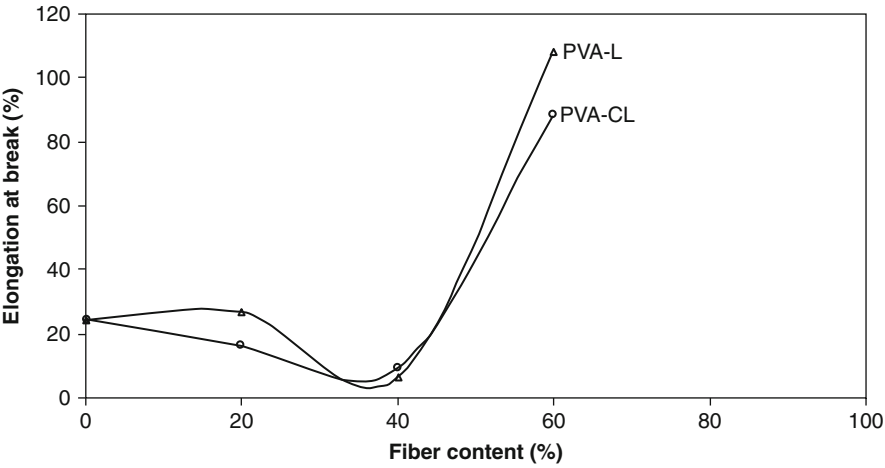

Fig. 9.17 Elongation at break for PVA–nanocellulose from cotton linter and linen (From [25])

of the nanocellulose–PVA composite films was in the range of 16.58–88.74, whereas for plain PVA film, it was 24.44 (Fig. 9.17). The improvement or reduction in the tensile behavior of the nanocellulose–PVA composite films was attributed to the change in the morphological structure of the resulting films. The results were also compared to the composite made by the use of nanocellulose resulting from linen (Figs. 9.16 and 9.17).

On the other hand, Roohani et al. [42] dispersed a specific amounts of cotton whiskers, 0, 3, 6, 9, and 12 wt%, to two different grades of PVA, i.e., PVA 4 (Mowiol 23–88, M_w of 150 × 10^3 g mol^{-1} and degree of hydrolysis of 87.5 %) and PNA 6 (Mowiol 28–99, M_w of 145 × 10^3 g mol^{-1} and degree of hydrolysis of 99.4 %), to obtain films around 200–350 μm thick. They characterize the morphology of the resulting nanocomposite films by the scanning electron microscopy (SEM). It was observed that the freshly fractured surface of the unfilled films either

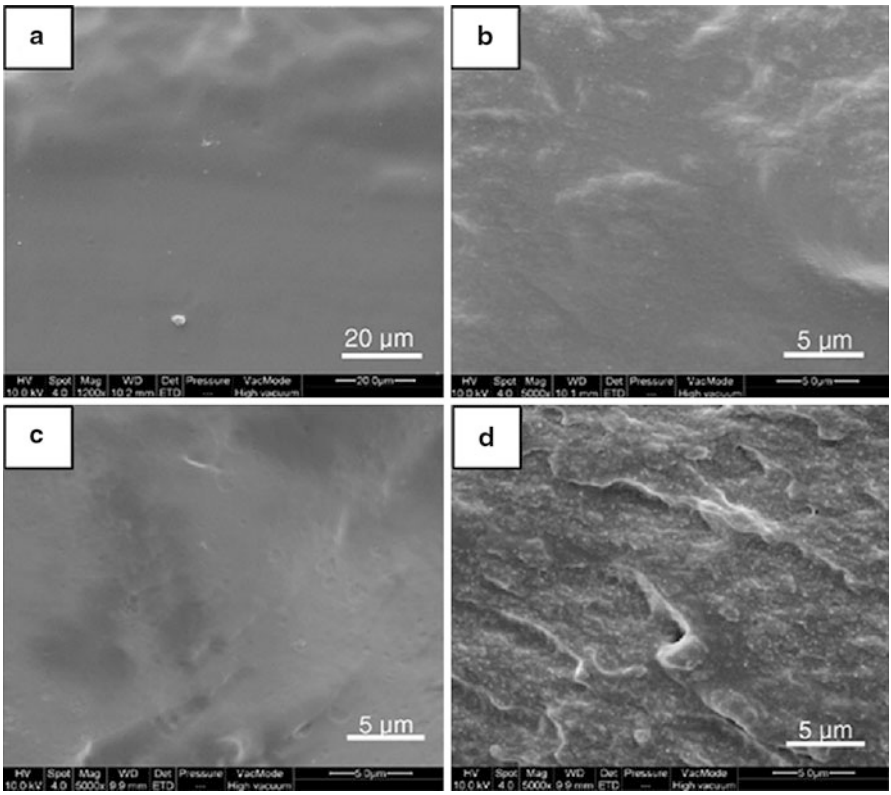

Fig. 9.18 Scanning electron micrographs from the fractured surfaces of PVA 4-based nanocomposite films reinforced with 0 (**a**) and 12 wt% and (**b**) cotton whiskers and PVA 6-based nanocomposite films reinforced with 0 (**c**) and 12 wt% and (**d**) cotton whiskers (From [42])

partially or fully hydrolyzed PVA (Fig. 9.18a and c) is smooth and uniform, while for the nanocomposite films (Fig. 9.18b and d), no clear evidence of the presence of the cellulosic nanoparticles was observed. They concluded that this was due to the scale of the reinforcing phase, but it also indicated that no aggregates were present in the nanocomposite films and that the dispersion of the filler within the polymeric matrix was rather good.

The evolution of the Young's modulus, as a function of whisker content and relative humidity for nanocomposite films prepared from PVA 1 (M_w between 146 and 186 $\times$ 10^3 g mol^{-1} and degree of hydrolysis of 99 %), was studied by Roohani et al. [42]. The tensile modulus of nanocomposite films was noticed to increase when increasing the whisker content for each relative humidity condition (Fig. 9.19). Also, they noticed that for given filler content, increasing the humidity results in a clear and significant decrease of the tensile modulus. They attributed that to the shift of the glass transition temperature toward lower values, below the room temperature.

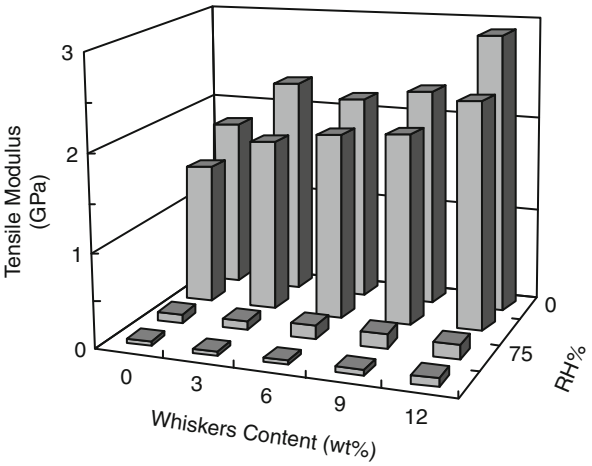

Fig. 9.19 Evolution of the Young's modulus as a function of both the whisker content and relative humidity for nanocomposites PVA 1-based nanocomposite films reinforced with cotton whiskers (From [42])

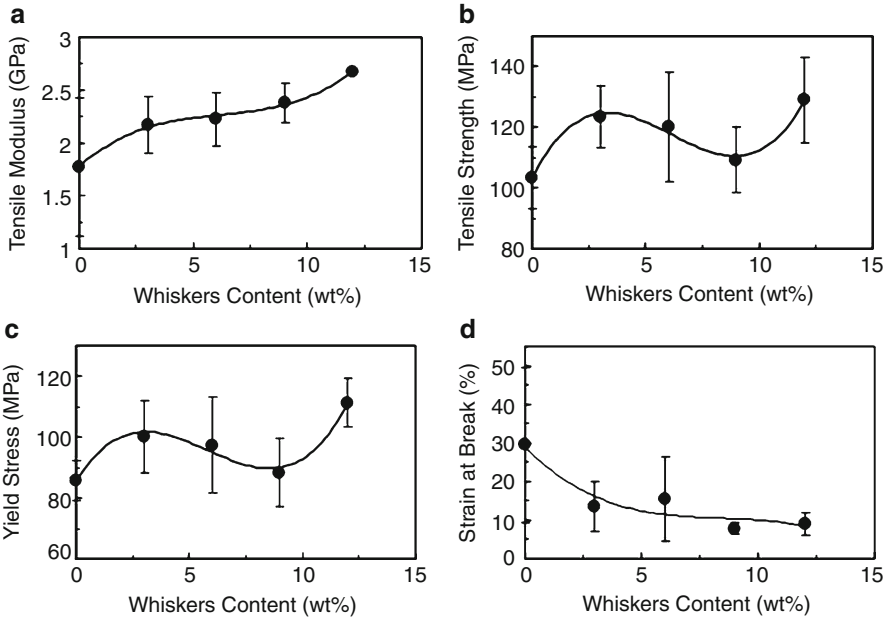

Fig. 9.20 Evolution of the tensile mechanical properties for PVA 2-based nanocomposite films reinforced with cotton whiskers and conditioned at 0 % RH. (**a**) Tensile modulus, (**b**) tensile strength, (**c**) yield stress, and (**d**) strain at break versus cotton whiskers content. The *solid lines* serve to guide the eye (From [42])

Moreover, Roohani et al. [42] represented the evolution of the mechanical properties of PVA 2-based nanocomposite films (M_w between 124 and 186 $\times$ 10^3 g mol^{-1} and degree of hydrolysis of 89 %) conditioned at 0 % relative humidity (RH). They noticed that, when the results were compared to the unfilled

PVA matrix, the addition of cotton whiskers induced an increase of the tensile modulus, tensile strength, and yield stress (Fig. 9.20). At the same time, the strain at break decreases from 29.5 % for the unfilled matrix down to 9.1 % for the nanocomposite film reinforced with 12 wt% of cotton whiskers.

Generally, Roohani et al. [42] noticed that all the results showed that stronger filler/matrix interactions occur for fully hydrolyzed PVA compared to partially hydrolyzed samples. These stronger interactions result in an increase of the glass temperature and a decrease of both the melting point and degree of crystallinity of the polymeric matrix in dry atmosphere. For moist samples, T_g increases significantly upon whisker addition regardless of the degree of hydrolysis of the matrix, because of the formation of a water layer at the interface, the PVA matrix becoming less plasticized by water. They came to a conclusion that the mechanical percolation of cellulose whiskers is affected by cellulose/PVA interactions. The reinforcing effect was found to be all the higher as the degree of hydrolysis of the matrix was high.

5 Conclusions

Nanomaterials derived from renewable biomaterials, especially cellulose and lignocellulose, will undoubtedly play a large role in the nanotechnology research effort. Over the past decade, there has been growing interest in incorporating cellulosic fibers as reinforcements in polymer matrices. The hydrolysis of cellulosic materials with a strong sulfuric acid or hydrochloric acid yields highly crystalline, well-defined, slender rodlike nanoparticles which are termed nanocellulose or cellulose whiskers.

Due to their abundance, high strength and stiffness, low weight, and biodegradability, nanoscale cellulosic materials serve as promising candidates for the preparation of nanocomposites. The potential of nanocomposites in various sectors of research and application is promising and is attracting increasing investments. A broad range of applications of these nanoparticles exists, even if a large number of unknowns remain to date. The homogeneous dispersion of cellulosic nanoparticles in a polymer matrix is challenging. In addition, there are many safety concerns about nanomaterials, as their size allows them to penetrate into cells and eventually remain in the system. Also, increasing latex particle size leads to an increase of the excluded volume, and these geometrical constraints seem to affect the whisker network formation.

References

1. Abdul Khalil HPS, Bhat AH, Ireana Yusra AF (2012) Green composites from sustainable cellulose nanofibrils: A review. Carbohydr Polym 87:963
2. Angellier H, Putaux JL, Molina-Boisseau S, Dupeyre D, Dufresne A (2005) Starch nanocrystals fillers in an acrylic polymer matrix. Macromol Symp 221:95

3. Araki J, Kuga S (2001) Effect of Trace Electrolyte on Liquid Crystal Type of Cellulose Microcrystals. Langmuir 17:4493
4. Araki J, Wada M, Kuga S, Okano T (1998) Flow properties of microcrystalline cellulose suspension prepared by acid treatment of native cellulose. Colloid Surface A 142:75
5. Araki J, Wada M, Kuga S, Okano T (1999) Influence of surface charge on viscosity behavior of cellulose microcrystal suspension. J Wood Sci 45:258
6. Ass BAP, Ciacco GT, Frollini E (2006) Cellulose acetates from linters and sisal: Correlation between synthesis conditions in DMAc/LiCl and product properties. Bioresour Technol 97:1696
7. Azizi Samir MAS, Alloin F, Dufresne A (2005) Review of Recent Research into Cellulosic Whiskers, Their Properties and Their Application in Nanocomposite Field. Biomacromolecules 6:612
8. Azizi Samir MAS, Alloin F, Paillet M, Dufresne A (2004) Preparation of Cellulose Whiskers Reinforced Nanocomposites from an Organic Medium Suspension. Macromolecules 37:4313
9. Beck-Candanedo S, Roman M, Gray DG (2005) Effect of reaction conditions on the properties and behavior of wood cellulose nanocrystal suspensions. Biomacromolecules 6:1048
10. Cao X, Dong H, Li CM (2007) New nanocomposite materials reinforced with flax cellulose nanocrystals in waterborne polyurethane. Biomacromolecules 8:899
11. Capadona JR, Shanmuganathan K, Trittschuh S, Seidel S, Rowan SJ, Weder C (2009) Polymer nanocomposites with nanowhiskers isolated from microcrystallinecellulose. Biomacromolecules 10:712
12. Chang CP, Perng YS, Wang EI (2012) Institute of Paper Science and Technology at Georgia Tech, Biomaterials Posters. www.ipst.gatech.edu/faculty/ragauskas_art/global/. . ./biomaterials_5.pdf
13. Chen W, Yu H, Liu Y, Chen P, Zhang M, Yunfei H (2011) Individualization of cellulose nanofibers from wood using high-intensity ultrasonication combined with chemical pretreatments. Carbohydr Polym 83:804
14. Cherian BM, Leão AL, de Souza SF, Costa LMM, de Olyveira GM, Kottaisamy M, Nagarajan ER, Thomas S (2011) Cellulose nanocomposites with nanofibres isolated from pineapple leaf fibers for medical applications. Carbohydr Polym 86:1790
15. De Souza Lima M, Borsali R (2004) Rodlike Cellulose Microcrystals: Structure, Properties, and Applications. Macromol Rapid Commun 25:771
16. De Souza Lima MM, Wong JT, Paillet M, Borsali R, Pecora R (2003) Translational and Rotational Dynamics of Rodlike Cellulose Whiskers. Langmuir 19:24
17. Dong XM, Revol JF, Gray DG (1998) Effect of microcrystallite preparation conditions on the formation of colloid crystals of cellulose. Cellulose 5:19
18. Dufresne A (2006) Comparing the Mechanical Properties of High Performances Polymer Nanocomposites from Biological Sources. J Nanosci Nanotechnol 6:322
19. Dufresne A (2010) Processing of Polymer Nanocomposites Reinforced with Polysaccharide Nanocrystals. Molecules 15:4111
20. Eichhorn SJ, Dufresne A, Aranguren M, Marcovich NE, Capadona JR, Rowan SJ, Weder C, Thielemans W, Roman M, Renneckar S, Gindl W, Veigel S, Keckes J, Yano H, Abe K, Nogi M, Nakagaito AN, Mangalam A, Simonsen J, Benight AS, Bismarck A, Berglund LA, Peijs T (2010) Review: Current international research into cellulose nanofibres and nanocomposites. J Mater Sci 45:1
21. FAOSTAT (FOOD AND AGRICULTURE ORGANIZATION OF THE UNITED NATIONS) Agricultural data (2012) Production. Crops. Food and Agriculture Organization of the United Nations. http://faostat.fao.org/default.aspx/. Accessed 02 May 2012
22. Favier V, Canova GR, Cavaillé JY, Chanzy H, Dufresne A, Gauthier C (1995) Nanocomposite materials from latex and cellulose whiskers. Polym Adv Technol 6:351
23. de Garcia de Rodriguez NL, Thielemans W, Dufresne A (2006) Sisal cellulose whiskers reinforced polyvinyl acetate nanocomposites. Cellulose 13:261

24. Helbert W, Cavaillé JY, Dufresne A (1996) Thermoplastic nanocomposites filled with wheat straw cellulose whiskers. Part I: Processing and mechanical behavior. Polym Compos 17:604
25. Ibrahim MM, El-Zawawy WK, Nassar MA (2010) Synthesis and characterization of polyvinyl alcohol/nanospherical cellulose particle films. Carbohydr Polym 79:694
26. Itoh T, Brown RM Jr (1984) The assembly of cellulose microfibrils in Valonia macrophysa. Planta 160:372
27. Klemm D, Heublein B, Fink H-P, Bohn A (2005) Cellulose: Fascinating biopolymer and sustainable raw material. Angew Chem Int Edit 44:3358
28. Lin N, Chen G, Huang J, Dufresne A, Chang PR (2009) Effects of polymergrafted natural nanocrystals on the structure and mechanical properties of poly(lactic acid): A case of cellulose whisker-graft-polycaprolactone. J Appl Polym Sci 113:3417
29. Mathew AP, Dufresne A (2002) Morphological Investigation of Nanocomposites from Sorbitol Plasticized Starch and Tunicin Whiskers. Biomacromolecules 3:609
30. Mohanty AK, Misra M, Hinrichsen G (2000) Biofibres, biodegradable polymers and biocomposites: An overview. Macromol Mater Eng 276/277:1
31. Morais JPS, Rosa MF, de Souza Filho MM, do Nascimento LD, Nascimento DM, Cassales A (2013) Extraction and characterization of nanocellulose structures from raw cotton linter. Carbohydr Polym 91:229
32. Oksman K, Mathew AP, Bondeson D, Kvien I (2006) Manufacturing process of cellulose whiskers/polylactic acid nanocomposites. Compos Sci Technol 66:2776
33. Pääkkö M, Vapaavuori J, Silvennoinen R, Kosonen H, Ankerfors M, Lindström T, Berglund LA, Ikkala O (2008) Long and entangled native cellulose I nanofibers allow flexible aerogels and hierarchically porous templates for functionalities. Soft Matter 4:2492
34. Pandey JK, Ahn SH, Lee CS, Mohanty AK, Misra M (2010) Recent advances in the application of natural fiber based composites. Macromol Mater Eng 295:975
35. Pandey JK, Kumar AP, Misra M, Mohanty AK, Drzal LT, Singh RP (2005) Recent advances in biodegradable nanocomposites. J Nanosci Nanotechnol 5:497
36. Petersson L, Kvien I, Oksman K (2007) Structure and thermal properties of poly(lactic acid)/cellulose whiskers nanocomposite materials. Compos Sci Technol 67:2535
37. Plackett D, Andersen TL, Pedersen WB, Nielsen L (2003) Biodegradable composites based on l -polylactide and jute fibres. Compos Sci Technol 63:1287
38. Rånby BG, Ribi E (1950) The microstructure of cellulose. Experientia 6:12
39. Rånby BG (1949) Aqueous Colloidal Solutions of Cellulose Micelles. Acta Chem Scand 3:649
40. Rhim JW (2007) Potential use of biopolymer-based nanocomposite films in food packaging applications. Food Sci Biotechnol 16:691
41. Roman M, Winter WT (2004) Effect of Sulfate Groups from Sulfuric Acid Hydrolysis on the Thermal Degradation Behavior of Bacterial Cellulose. Biomacromolecules 5:1671
42. Roohani M, Habibi Y, Belgacem NM, Ebrahim G, Karimi AN, Dufresne A (2008) Cellulose whiskers reinforced polyvinyl alcohol copolymers nanocomposites. Eur Polym J 44:2489
43. Rosa MF, Medeiros ES, Malmonge JA, Gregorski KS, Wood DF, Mattoso LHC, Glenn G, Orts WJ, Imam SH (2010) Cellulose nanowhiskers from coconut husk fibers: Effect of preparation conditions on their thermal and morphological behavior. Carbohydr Polym 81:83
44. Sczostak A (2009) Cotton linters: An alternative cellulosic raw material. Macromol Symp 280:45
45. Shanmuganathan K, Capadona JR, Rowan SJ, Weder C (2010) Bio-inspired mechanically-adaptive nanocomposites derived from cotton cellulose whiskers. J Mater Chem 20:180
46. Silva R, Haraguchi SK, Muniz EC, Rubira AF (2009) Aplicac, ões de fibras lignocelulósicas na química de polímeros e em compósitos. Quim Nova 32:661
47. Siqueira G, Bras J, Dufresne A (2009) Cellulose whiskers versus microfibrils: Influence of the nature of the nanoparticle and its surface functionalization on the thermal and mechanical properties of nanocomposites. Biomacromolecules 10:425

48. Sorrentino A, Vittoria GGV (2007) Potential perspectives of bio-nanocomposites for food packaging applications. Trends Food Sci Tech 18:84
49. Stelte W, Sanadi AR (2009) Preparation and characterization of cellulose nanofibers from two commercial hardwood and softwood pulps. Ind Eng Chem Res 48:11211
50. Sun Y, Yue Q, Gao B, Li Q, Huang L, Yao F, Xu X (2012) Preparation of activated carbon derived from cotton linter fibers by fused NaOH activation and its application for oxytetracycline (OTC) adsorption. J Colloid Interface Sci 368:521
51. Teixeira EM, Corrêa AC, Manzoli A, Leite FL, Oliveira CR, Mattoso LHC (2010) Cellulose nanofibers from white and naturally colored cotton fibers. Cellulose 17:595
52. Ummartyotin S, Juntaro J, Sain M, Manuspiya H (2012) Development of transparent bacterial cellulose nanocomposite film as substrate for flexible organic light emitting diode (OLED) display. Ind Crop Prod 35:92
53. Wang SQ, Cheng QZ (2009) A novel process to isolate fibrils from cellulose fibers by high-intensity ultrasonication. Part 1: Process optimization. J Appl Polym Sci 113:1270
54. Yang Q, Fukuzumi H, Saito T, Isogai A, Zhang L (2011) Transparent cellulose films with high gas barrier properties fabricated from aqueous alkali/urea solutions. Biomacromolecules 12:2766
55. Yu H, Liu RG, Shen DW, Jiang Y, Huang Y (2005) Study on morphology and orientation of cellulose in the vascular bundle of wheat straw. Polymer 46:5689

Chitin Nanofibers: Preparations, Modifications, and Applications

10

Shinsuke Ifuku

Contents

Abstract

Chitin nanofibers of 10–20 nm width and high aspect ratio were prepared using a series of chemical treatments followed by mechanical grinding treatment from exoskeletons of crabs and prawns and cell wall of mushrooms. The nanofibers obtained are uniform and have both linear and network structures. Mechanical treatment under acidic (pH 3–4) conditions facilitated nano-fibrillation. The cationization of amino groups on the fiber surface of chitin improved fibrillation by electrostatic repulsion. Nanofiber surface was modified by acetylation for increasing applications of nanofibers. The sheet of neat chitin nanofibers was opaque; however, it became transparent by blending nanofibers with different types of acrylic resins due to nano-sized structure of fibers. Young's moduli and the tensile strengths increased significantly, while thermal expansion of acrylic resins decreased as a result of reinforcement of resins with chitin nanofibers. Chitin nanofiber showed chiral separation ability as well. Chitin nanofiber

S. Ifuku
Department of Chemistry and Biotechnology, Graduate School of Engineering, Tottori University, Tottori, Japan
e-mail: sifuku@chem.tottori-u.ac.jp

J.K. Pandey et al. (eds.), *Handbook of Polymer Nanocomposites. Processing, Performance and Application – Volume C: Polymer Nanocomposites of Cellulose Nanoparticles*,
DOI 10.1007/978-3-642-45232-1_73,

membrane transported the D-isomer of glutamic acid, phenylalanine, and lysine from the corresponding racemic amino acid mixtures faster than L-isomer. From the viewpoint of medical applications, chitin nanofibers improved clinical symptoms and suppressed ulcerative colitis in dextran sulfate sodium-induced mouse model of acute ulcerative colitis.

KeyWords
Chitin • Nanofiber • Nanocomposite • Acetylation

1 Introduction

Generally, nanofibers are defined as fibers with a diameter of <100 nm and an aspect ratio of >100. Since nanofibers have extremely high surface to volume ratio, their physicochemical properties are different from those of micro-sized fibers. Thus, decreasing the width and increasing the aspect ratio of nanofibers compared to microfibers add unique dimensions to optical, mechanical, electrical, and other characteristics to the development of new promising advanced materials from the application viewpoint. Electro-spinning process has been applied to prepare nanofibers artificially from polymer solution based on the principle of fluid dynamics involving electrically charged surfaces and electrically charged liquids. Due to the environmentally benign, biodegradable, biocompatible, renewable, and sustainable biomass, the nanofibers from biopolymers are growing in importance. A variety of naturally occurring nanofibers such as collagen triple helix fibers, fibroin fibrils, and keratin fibrils are commonly known. These nanofibers consist of complex hierarchical organization. Thus, the nanofibers could be extracted from biomass based organized structural units. Among the variety of biomass-based products, cellulose is the most abundant biopolymer found mainly in wood cell walls (Fig. 10.1). The cellulose nanofibers so-called microfibrils are highly crystalline structures with 3–4 nm thickness consisting of 30–40 cellulose macromolecules. The bundles of microfibrils are embedded in matrix substances such as hemicellulose and lignin matrix that form the wood cell wall. Cellulose microfibrils have extremely tough physical properties. Young's modulus, tensile strength, and thermal expansion coefficient are 138 GPa [1], 2 GPa [2], and 0.1×10^{-6} 1/K [3], respectively. Cellulose nanofibers have the potential as a high performance material. A number of chemical processes followed by mechanical treatments have been mainly employed for cellulose nanofibers preparation. The mechanical treatments include employing high-pressure homogenizers [4], grinders [5, 6], cryocrushing [7, 8], ultrasonic disintegrators [9], or enzymatic methods [10]. Abe et al. isolated cellulose nanofiber bundles of 15-nm-sized nanofibers from wood by a simple method [11]. Apart from wood the cellulose nanofibers were isolated from rice straw, potato tuber pulp, and parenchymal cells of bamboo and fruits [12–14]. Isogai et al. converted wood cellulose to nanofibers of 3–4 nm width and high aspect ratio by 2,2,6,6-tetramethylpiperidine-1-oxyl radical (TEMPO)-mediated oxidation. TEMPO-oxidation forms carboxylate groups on the cellulose surface.

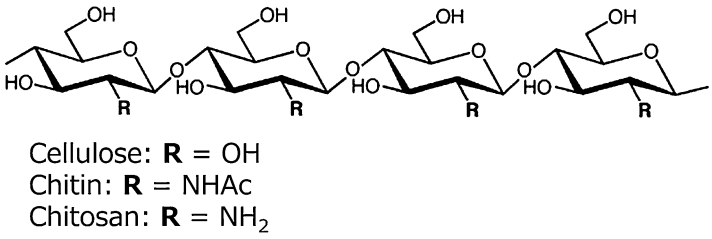

Fig. 10.1 Chemical structures of cellulose, chitin, and chitosan

Electrostatic repulsion arises due to anionic charges of carboxylate at the cellulose surface that caused complete disintegration of cellulose bundles into nanofibers [15–18].

Chitin and chitosan are known to be cellulose analogues with a (1,4)-*β*-*N*-acetyl glycosaminoglycan repeating structure and its deacetylated derivative, respectively (Fig. 10.1). After cellulose, chitin is the second most abundant biopolymer found mainly in the exoskeletons of shellfish and insects and the cell walls of mushroom. The annual production of chitin is 10^{10}–10^{11} t. Chitin is thrown away as waste in fish industry. The sources of chitin are exoskeleton of crabs, shrimps, prawn, and insect and cell wall of mushrooms. The microfibrils found on the above species consist of nanofibers of 2–5 nm diameter and about 300 nm long embedded in a protein matrix [19–22]. In this chapter, we review the development of a simple method for the preparation of chitin nanofibers, its properties, and applications.

2 Preparation of Chitin Nanofibers

The hierarchical organization of exoskeleton structure of crab shells at various structural levels is shown in Fig. 10.2. Chitin nanofibers have been extracted from crab shells having such complicated hierarchical structures [23, 24]. The small flakes of crab shell were treated by a series of chemical treatments followed by mechanical grinding treatment. The matrix components of proteins and minerals were removed from the crab shells by a series of chemical treatments with aqueous NaOH and HCl, respectively [25, 26]. After the chemical treatments, thus, obtained 1 wt% of purified neat chitin in water was passed through a grinder to convert chitin into nanofibers. After grinder treatment, the chitin slurry formed a gel suggesting that disintegration was accomplished. The chitin nanofibers are highly uniform with a width of 10–20 nm, high aspect ratio, and uniform structure (Fig. 10.3). The FT-IR spectrum of prepared chitin nanofibers was in good agreement with that of pure chitin, showing matrix components were well removed by a series of the chemical treatments. The X-ray diffraction profile of chitin nanofibers shows characteristic antiparallel crystal patterns typical of *α*-chitin, indicating that original crystalline structure was maintained.

The preparation method for chitin nanofibers from crab is applicable to prawn shells as well as black tiger prawn, Japanese tiger prawn, and Alaskan pink shrimp, which are important food sources [27]. Figure 10.4 shows the chitin nanofibers

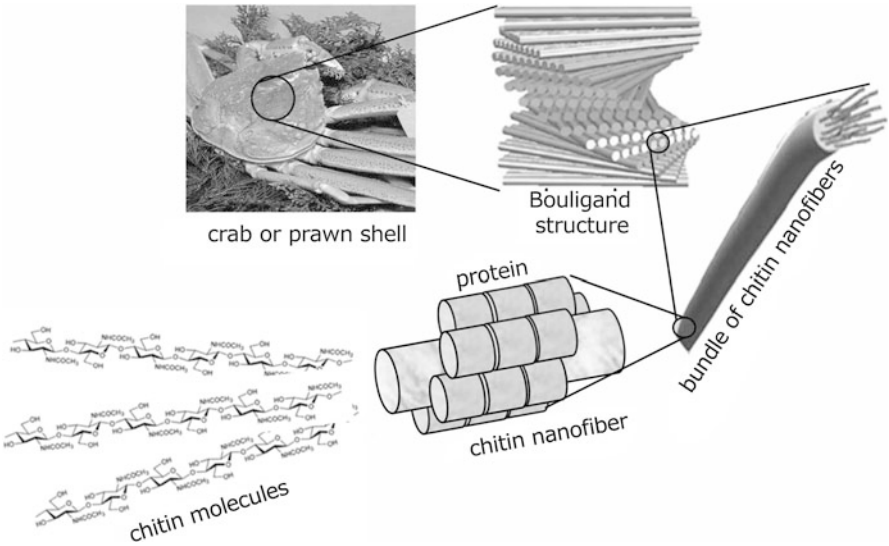

Fig. 10.2 Schematic presentation of the exoskeleton structure of crab shells

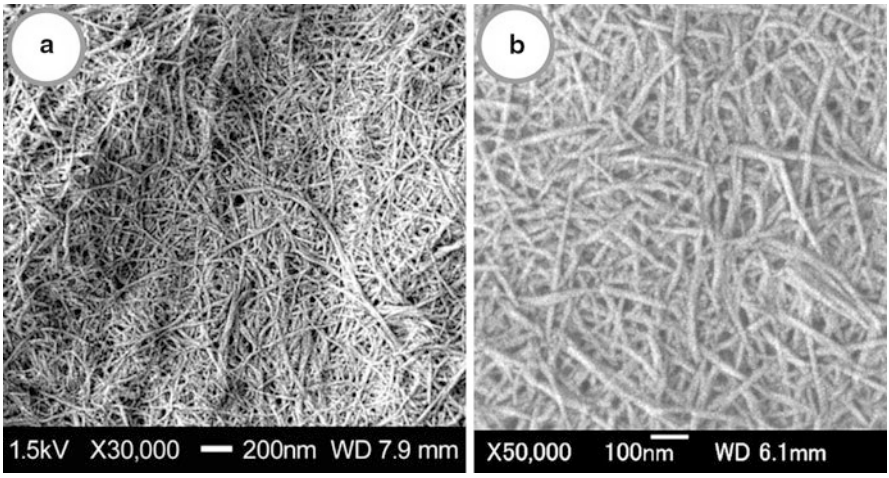

Fig. 10.3 FE-SEM micrographs of chitin nanofibers from crab shells after one passes through the grinder. The lengths of the scale bars are (**a**) 200 nm and (**b**) 100 nm (Reprinted with permission from Ref. [23]. Copyright (2009) American Chemical Society)

prepared from prawn shell. A uniform structure was observed over an extensive area. The thickness of the nanofibers was 10–20 nm, same as that from crab shells. The advantage of chitin nanofibers from prawn shell is that the chitin from prawn shell can be fibrillated into nanofibers with lower mechanical load due to the morphological difference.

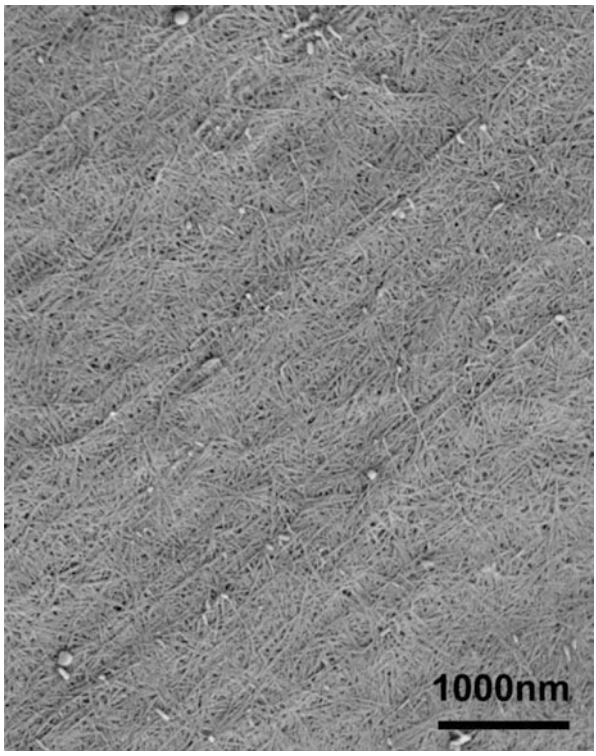

Fig. 10.4 FE-SEM micrograph of chitin nanofibers from black tiger prawn shells. The length of the scale bar is 1,000 nm (Reproduced with permission from Ref. [27]. Copyright 2011, Elsevier)

The cell walls of mushrooms also consist of a chitin nanofibers network. And it is embedded in the matrix substances, mainly consisting of glucans. Thus, the isolating method of chitin nanofibers is applicable for mushrooms [28]. The chitin nanofibers were obtained from five species of mushrooms, *Pleurotus eryngii* (king trumpet mushroom), *Agaricus bisporus* (common mushroom), *Lentinula edodes* (shiitake), *Grifola frondosa* (maitake), and *Hypsizygus marmoreus* (bunashimeji), by a series of chemical treatments with NaOH, HCl, and $NaClO_2$ to remove the associated components, proteins, pigments, glucans, and minerals. Thus, purified chitin was passed through a grinder. The obtained chitin from these mushrooms had uniform and very thin structure. The width of mushroom nanofibers varied from 20 to 28 nm depending on the glucan content in mushroom. The dietary nano-sized fibers obtained from edible mushrooms should have a wide range of applications as functional food ingredients and medical applications.

Figure 10.5a shows SEM images of dried chitin prepared from crab shells by a series of chemical treatments followed by drying [29]. The dried chitin has regularly structured bundles of nanofibers. The dried chitin was passed through a grinder with and without acetic acid. In the case of the grinding without acetic acid, the dried chitin was not fibrillated at all and thick bundles of chitin nanofibers remained (Fig. 10.5b). This was due to the strong hydrogen bonding caused

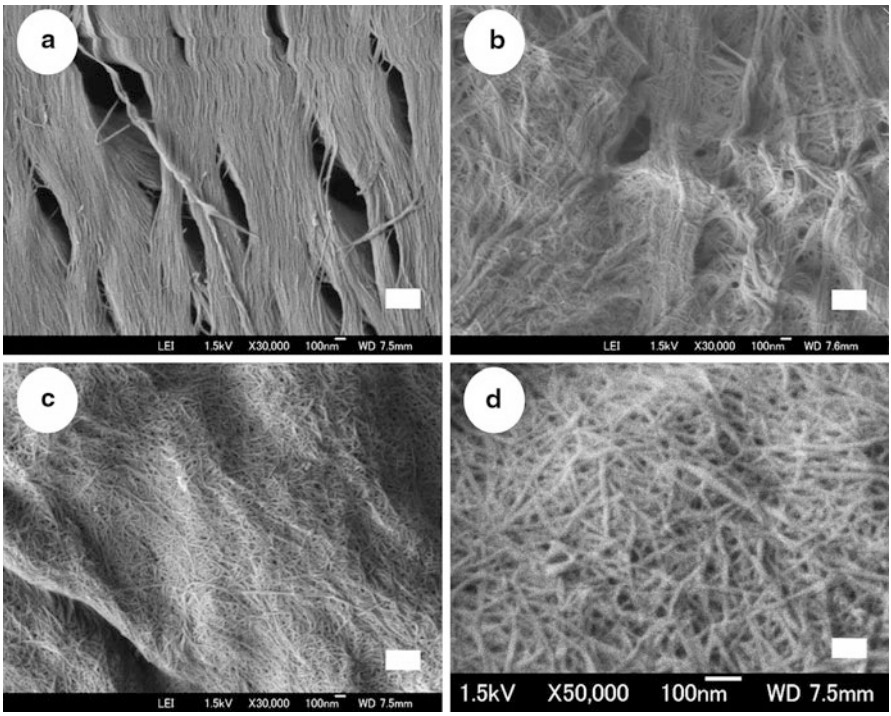

Fig. 10.5 FE-SEM micrographs of (**a**) a crab shell after removing matrix components and chitin fibers after one passes through the grinder treated (**b**) without and (**c**, **d**) with acetic acid. The lengths of the scale bars are (**a**–**c**) 300 nm and (**d**) 100 nm (Reproduced with permission from Ref. [29]. Copyright 2011, Elsevier)

between chitin nanofiber surfaces, which made it difficult to fibrillate bundles of chitin nanofibers. On the other hand, in acetic acid medium, the dry chitin was successfully fibrillated by just one pass grinder treatment (Fig. 10.5c, d) due to repulsive forces caused by the cationization of amino groups. The chitin sample had a very fine nanofiber network with a uniform width of 10–20 nm. It seemed very similar to that of nanofibers prepared with the abovementioned conventional process in which the chitin was never dry. The preparation method is applicable for commercially available dry chitin powder as well. Since commercial chitin is also made up of aggregates of nanofibers, the aggregates can clearly be fibrillated into homogeneous nanofibers by the assistance of repulsive force in pH 3–4 medium. Production of chitin nanofibers from commercial chitin has advantage in nanofibers research and development. Large amount of chitin can be obtained within a few hours by a simple fibrillation in acidic conditions without any time-consuming purification methods which can save at least 5 days. The advantage of the use of ready-made commercial chitin, however, is not applicable for cellulose nanofibers preparation, since cellulose does not have ionic functional groups to cause electrostatic repulsion that chitin has.

3 Modification of Chitin Nanofibers

Nanofibers have uniform width of 10–20 nm, high aspect and surface-to-volume ratios, and scope for conversion into novel green materials. To increase the number of applications of chitin nanofibers, it will be crucial to chemically enhance chitin nanofiber properties by modifying their surfaces. Fan et al. reported partially deacetylated α-chitin nano-whiskers [30]. The method used to prepare nano-whiskers was deacetylation by 33 % NaOH treatment at 90 °C for 2–4 h and subsequent disintegration in water at pH 3–4. The obtained nano-whiskers have an average width and length of approximately 6.2 and 250 nm, respectively, and the degree of substitution (DS) of acetyl group was 0.70–0.74. The crystalline index and crystal size of the original α-chitin did not change, indicating that the deacetylation mainly took place at the nano-whisker surface. Thus, conversion of chitin to surface modification and nano-whisker preparation was achieved by NH_3^+ cationic charges on whisker surfaces with high density.

By capping of hydrophilic hydroxyl groups at C3 and C6 positions of chitin nanofibers with hydrophobic functional groups, the dispersibility of chitin nanofibers in nonpolar solvents increased, and hygroscopicity and affinity for hydrophobic matrices improved for fiber-reinforced composite materials. For these purposes, surface acetylation is considered to be a simple, popular, and cheaper approach to change the surface properties of chitin nanofibers [31]. Thus, chitin nanofibers were acetylated with different DS values and were characterized [32]. Chitin nanofibers were acetylated by treatment with a mixture of acetic anhydride and perchloric acid at room temperature. The acetyl DS increased from 1 to 3 after a 50-min acetylation, indicating complete substitution of acetyl groups in the chitin nanofibers. The inside of nanofibers was acetylated gradually after immediate surface acetylation. Figure 10.6 shows SEM images of the acetylated chitin nanofibers. Although nanofiber network morphology has not been affected after introduction of bulky acetyl groups, the thickness of the nanofibers increased with the increase in the substitution of acetyl groups. After surface acetylation, the moisture absorption of the chitin nanofiber composite significantly decreased.

4 Application of Chitin Nanofibers

4.1 Fabrication of Optically Transparent Chitin Nanofiber/Acrylic Resin Composite

Chitin nanofiber-reinforced composites have been prepared using chitin nanofiber sheets. Yano et al. have reported that cellulose nanofibers are a very promising material for reinforcing materials [33]. Due to the nanofiber size effect, the composites are optically transparent even with a high fiber content. The nano-size effect of chitin nanofibers can be also applied for preparation of transparent composite, since the transparency strongly depends on the fiber width. Thus, chitin nanofiber composites were prepared with eleven different types of acrylic resins (Fig. 10.7) [34]

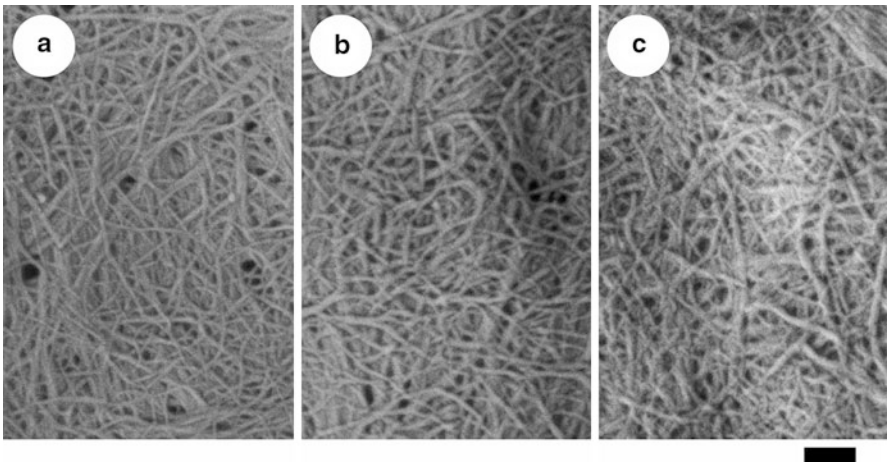

Fig. 10.6 SEM images of acetylated chitin nanofiber samples of (**a**) DS 0.99, (**b**) DS 1.81, and (**c**) DS 2.96.The length of scale bar is 200 nm (Reprinted with permission from Ref. [32]. Copyright (2010) American Chemical Society)

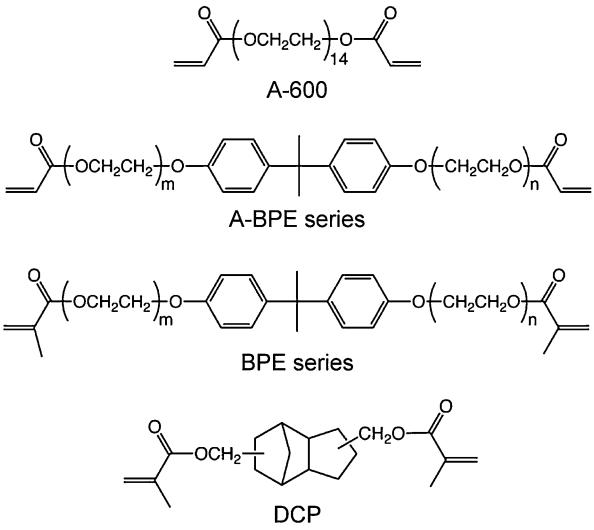

Fig. 10.7 Chemical structures of the acrylic resins used in this study (Reproduced from Ref. [34]. Copyright 2011, the Royal Society of Chemistry)

and characterized in their physical properties. Chitin nanofiber sheets were impregnated with bifunctional acrylic resin monomers. The resin impregnated sheets were polymerized by UV irradiation. All nanocomposites have high transparency (Fig. 10.8) despite the high fiber content of 40 wt%.

Chitin nanofibers have a characteristic extended crystal structure; they have a high mechanical strength and high Young's modulus. Thus, chitin nanofibers are considered to be a better reinforcement filler to improve the mechanical properties of composite materials. Tensile strength tests were carried out to study

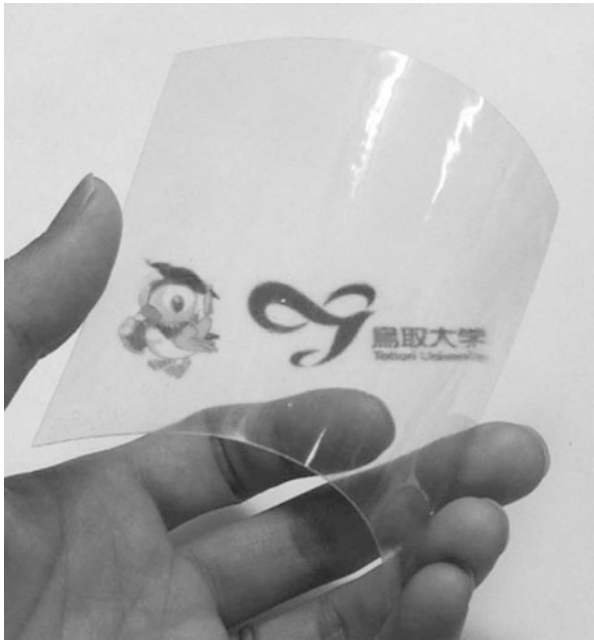

Fig. 10.8 Appearance of DCP films reinforced with chitin nanofibers (Reproduced from Ref. [34]. Copyright 2011, the Royal Society of Chemistry)

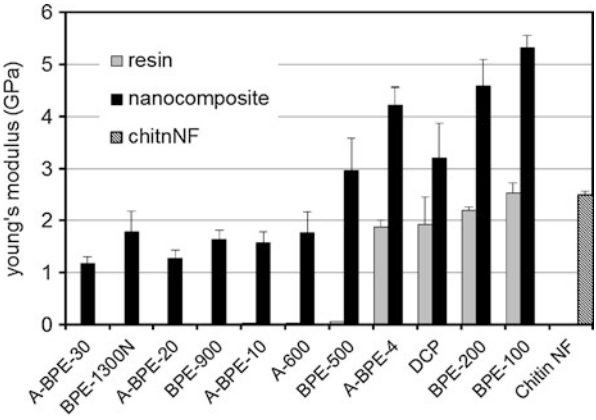

Fig. 10.9 Young's modulus of acrylic resin films and their nanocomposites. *Error bars* show standard deviations (Reproduced from Ref. [34]. Copyright 2011, the Royal Society of Chemistry)

the reinforcement effect of chitin nanofibers. Young's moduli and tensile strengths of several types of acrylic resins and their chitin nanofiber composites are shown in Figs. 10.9 and 10.10, respectively. Both rigid and soft resins were used in the study; Young's moduli of some resins increased significantly by up to 3.0 GPa. The tensile strengths of nanocomposites also increased from 20 to 44 MPa. Tensile strength of some low strength resins increased > 30 MPa. The results of mechanical properties strongly support the application of chitin nanofibers sheet to fabricate effectively reinforced composites.

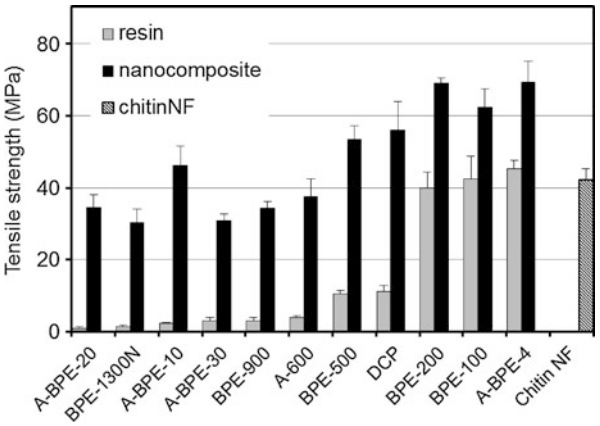

Fig. 10.10 Tensile strength of acrylic resin films and their nanocomposites. *Error bars* show standard deviations (Reproduced from Ref. [34]. Copyright 2011, the Royal Society of Chemistry)

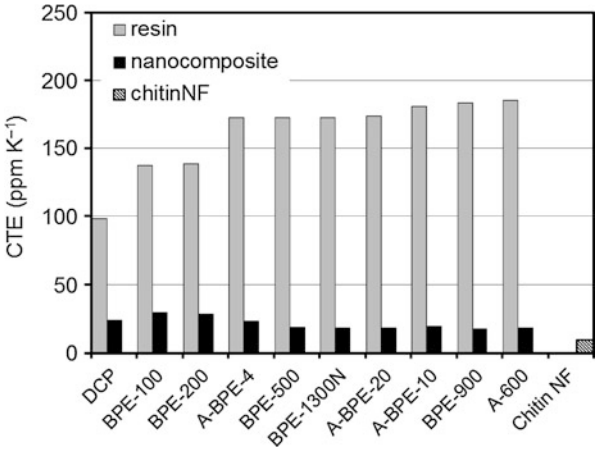

Fig. 10.11 Coefficient of thermal expansion of (meth) acrylic resin films and their nanocomposites (Reproduced from Ref. [34]. Copyright 2011, the Royal Society of Chemistry)

The coefficient of thermal expansion (CTE) of neat chitin nanofibers is very small. Therefore, it is an available candidate as a reinforcement to reduce the thermal expansion of resins. The detailed CTE data of composites are shown in Fig. 10.11. CTE of a chitin nanofiber sheet was only 9.8 ppm K^{-1}. On the other hand, the CTEs of neat acrylic resins were quite high, ranging from 98.3 to 185.4 ppm K^{-1}. The CTEs of resin nanocomposites decreased significantly in the range 17.5–29.5 to ppm K^{-1}. The decrease in CTE of composite corresponds to 70.0–90.6 %. Thus, chitin nanofibers with a low CTE and a high Young's modulus decreased the thermal expansion of acrylic resins by a reinforcing effect.

4.2 Chitin Nanofiber Sheets for Chiral Separation

Since naturally occurring carbohydrate polymers are optically active biopolymers, they show chiral recognition. The authors have found that chitin nanofiber sheets showed

chiral separation ability [35]. Chitin nanofiber sheet was fixed between two chambers of a permeation cell. An aqueous solution of a racemic mixture of amino acids, glutamic acid (Glu), phenylalanine (Phe), and lysine (Lys) was placed on one side of the chamber. The amounts of the D- and L-isomers were determined by LC equipment. Concentration gradient was the natural driving force for transport of amino acids through the sheet. The D-isomers of all amino acids were transported preferentially compared to L-isomer. The permeation selectivity toward D-isomers of Phe, Glu, and Lys, which were defined as the flux divided by the concentration ratio, were 1.16, 1.04, and 1.07, respectively. Due to nano-sized morphology and their better physical properties, chitin nanofiber sheets proved to be excellent candidates as membrane for chiral separation.

4.3 Bioactivities of Chitin Nanofibers

Chitin nanofibers are considered to have great potential for application in tissue engineering scaffolds, drug delivery, and wound dressing as well. However, there has been no report on in vivo effect of chitin nanofibers in oral administration.

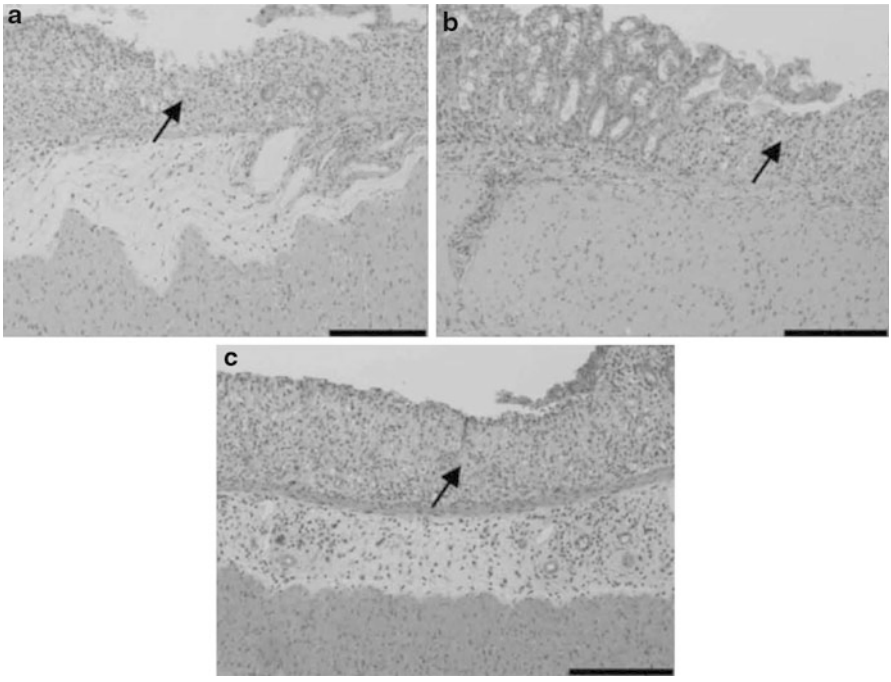

Fig. 10.12 Effect of chitin nanofiber administration on histopathological changes in DSS-induced acute UC mice. The colon was fixed, and tissue sections were stained with hematoxylin and eosin. Data are presented for 1 mouse each from the control (**a**), chitin nanofiber (**b**), and chitin powder (**c**) groups on day 6. Erosion is indicated by an arrow. Bar = 100 mm. Reproduced with permission from ref. 37. Copyright 2012, Elsevier

Inflammation in the intestinal tract is a common condition known as inflammatory bowel disease (IDB). A common model of IBD is dextran sulfate sodium (DSS)-induced colitis [36]. We investigated the preventive effects of chitin nanofibers in a mouse model of DSS-induced acute ulcerative colitis [37, 38]. The therapy of chitin nanofibers on the disease activity index weight loss, loose stools, and bleeding in DSS-induced acute ulcerative colitis mice was studied. The chitin nanofiber-administered group exhibited a significant reduction in disease activity index. The administration of DSS shortened colon length. Colon length incorporated by chitin nanofibers became significantly greater than those in the control group. We monitored damage in the intestinal mucosa microscopically (Fig. 10.12). In the control group on day 6, severe erosions, crypt destruction, edema, and some ulcers were noticed. While in the chitin nanofibers group, treated erosions, crypt destruction, and edema were markedly suppressed compared with those in the control.

5 Conclusion

Chitin nanofibers were prepared from the exoskeletons of crabs and prawns and the cell walls of mushrooms. Prepared chitin nanofibers have a fine network morphology with 10–20 nm uniform width and a high aspect ratio. Chitin nanofibers derivatives were also prepared for wider applications. Hydroxyl groups of chitin were capped by hydrophobic acetyl group to disperse them in nonpolar solvents and make the material compatible to hydrophobic matrices. Optically transparent chitin nanofiber/acrylic resin sheet was also prepared. The sheet had better mechanical and thermal properties without losing its transparency. Application of chitin nanofibers membrane for chiral separation was also demonstrated. Neat chitin nanofibers have application as a drug for inflammatory bowel disease.

Since chitin is obtained from crab and prawn shells, it is more expensive than cellulose. This is a disadvantage for chitin nanofibers. However, chitin nanofibers have several advantages over cellulose nanofibers, that is, (1) chitin and chitosan are known to have a variety of bioactivities, (2) chitin nanofibers can be easily prepared from dry chitin samples assisted by electrostatic repulsion as mentioned above, (3) the filtering speed to remove water from the sample is higher than that of cellulose nanofibers, (4) most of the matrix can be removed from crab and prawn shells by a conventional method, and (5) naturally rare cationic-charged nanofibers are prepared by partial deacetylation of chitin nanofibers. Utilizing these advantages is important to define the separate roles of chitin and cellulose for expanding the application of these nanofibers. This simple and efficient process allowed us to obtain homogeneous chitin nanofibers in their original state. We believe that nanofibers with a characteristic morphology, very high surface area, and excellent mechanical properties have great potential for novel green nanomaterials. In general, chitin precipitates in water. On the other hand, since the chitin nanofibers could be dispersed homogeneously in water, they

were easy to handle and shape into the desired forms. This characteristic led to the above-described applications of chitin nanofibers. We expect that other novel applications of chitin nanofibers will be discovered in the near future.

References

1. Sakurada I, Nukushina Y, Ito T (1962) Experimental determination of the elastic modulus of crystalline regions in oriented polymers. J Polym Sci 57:651
2. Page DH, Elhosseiny F (1983) The mechanical properties of single wood pulp fibers. 6. fibril angle and the shape of the stess-strain curve. J Pulp Pap Can 84:99
3. Nishino T, Matsuda I, Hirao K (2004) All-cellulose composite. Macromolecules 37:7683
4. Turbak AF, Synder FW, Sandberg KR (1983) Microfibrillated cellulose, a new cellulose product: properties, uses, and commercial potential. J Appl Polym Sci Appl Polym Symp 37:815
5. Taniguchi T, Okamura K (1998) New films produced from microfibrillated natural fibres. Polym Int 47:291
6. Iwamoto S, Nakagaito AN, Yano H, Nogi M (2005) Optically transparent composites reinforced with plant fiber-based nanofibers. Appl Phys A 81:1109
7. Chakraborty A, Sain M, Kortschot M (2005) Cellulose microfibrils: a novel method of preparation using high shear refining and cryocryshing. Holzforschung 59:102
8. Bhatnagar A, Sain M (2005) Processing of cellulose nanofiber-reinforced composites. J Reinf Plast Compos 24:1259
9. Zhao HP, Feng XQ, Gao H (2007) Ultrasonic technique for extracting nanofibers from nature materials. Appl Phys Lett 90:073112
10. Pääkkö M, Ankerfors M, Kosonen H, Nykänen A, Ahola S, Österberg M, Rukolainen J, Laine J, Larsson PT, Ikkala O, Lindström T (2007) Enzymatic hydrolysis combined with mechanical shearing and high-pressure homogenization for nanoscale cellulose fibrils and strong gels. Biomacromolecules 8:1934
11. Abe K, Iwamoto S, Yano H (2007) Obtaining cellulose nanofibers with a uniform width of 15 nm from wood. Biomacromolecules 8:3276
12. Abe K, Yano H (2009) Comparison of the characteristics of cellulose microfibril aggregates of wood, rice straw and potato tuber. Cellulose 16:1017
13. Abe K, Yano H (2010) Comparison of the characteristics of cellulose microfibril aggregates of wood, rice straw and potato tuber. Cellulose 17:271
14. Ifuku S, Adachi M, Morimoto M, Saimoto H (2011) Fabrication of cellulose nanofiber from parenchyma cells of pear and apple. Sei-i Gakkaishi 67:86
15. Isogai A, Saito T, Fukuzumi H (2011) TEMPO-oxidized cellulose nanofibers. Nanoscale 3:71
16. Saito T, Nishiyama Y, Putaux J-L, Vignon M, Isogai A (2006) Homogeneous suspensions of individualized microfibrils from TEMPO-catalyzed oxidation of native cellulose. Biomacromolecules 7:1687
17. Saito T, Kimura S, Nishiyama Y, Isogai A (2007) Cellulose nanofibers prepared by TEMPO-mediated oxidation of native cellulose. Biomacromolecules 8:2485
18. Saito T, Hirota M, Tamura N, Kimura S, Fukuzumi H, Heux L, Isogai A (2009) Individualization of nano-sized plant cellulose fibrils by direct surface carboxylation using TEMPO catalyst under neutral conditions. Biomacromolecules 10:1992
19. Raabe D, Romano P, Sachs C, Fabritius H, Al-Sawalmih A, Yi SB, Servos G, Hartwig HG (2006) Microstructure and crystallographic texture of the chitin–protein network in the biological composite material of the exoskeleton of the lobster Homarus americanus. Mater Sci Eng A 421:143
20. Chen P, Lin AY, McKittrick J, Meyers MA (2008) Structure and mechanical properties of crab exoskeletons. Acta Biomater 4:587

21. Giraud-guille MM (1984) Fine structure of the chitin-protein in the crab cuticle. Tissue Cell 16:75
22. Raabe D, Sachs C, Romano P (2005) The crustacean exoskeleton as an example of a structurally and mechanically graded biological nanocomposite material. Acta Mater 53:4281
23. Ifuku S, Nogi M, Abe K, Yoshioka M, Morimoto M, Saimoto H, Yano H (2009) Preparation of chitin nanofibers with a uniform width as alpha-chitin from crab shells. Biomacromolecules 10:1584
24. Ifuku S, Saimoto H (2012) Chitin nanofibers: preparations, modifications, and applications. Nanoscale 4:3308
25. Shimahara K, Takiguchi Y (1998) Preparation of crustacean chitin. In: Wood WA, Kellogg ST (eds) Methods in enzymology, vol 6. Academic, California, p 417
26. BeMiller JN, Whistler RL (1962) Alkaline degradation of amino sugars. J Org Chem 27:1161
27. Ifuku S, Nogi M, Abe K, Yoshioka M, Morimoto M, Saimoto H, Yano H (2011) Preparation of chitin nanofibers with a uniform width as α-chitin from crab shells. Carbohyd Polym 84:762
28. Ifuku S, Nomura R, Morimoto M, Saimoto H (2011) Preparation of chitin nanofibers from mushrooms. Materials 4:1417
29. Ifuku S, Nogi M, Yoshioka M, Moromoto M, Yano H, Saimoto H (2010) Fibrillation of dried chitin into 10–20 nm nanofibers by a simple method under acidic conditions. Carbohyd Polym 81:134
30. Fan Y, Saito T, Isogai A (2010) Individual chitin nano-whiskers prepared from partially deacetylated α-chitin by fibril surface cationization. Carbohyd Polym 79:1046
31. Kim DY, Nishiyama Y, Kuga S (2002) Surface acetylation of bacterial cellulose. Cellulose 9:361
32. Ifuku S, Morooka S, Morimoto M, Saimoto H (2010) Acetylation of chitin nanofibers and their transparent nanocomposite films. Biomacromolecules 11:1326
33. Yano H, Sugiyama J, Nakagaito AN, Nogi M, Matsuura T, Hikita M, Handa K (2005) Optically transparent composites reinforced with networks of bacterial nanofibers. Adv Mater 17:153
34. Ifuku S, Morooka S, Nakagaito AN, Morimoto M, Saimoto H (2011) Preparation and characterization of optically transparent chitin nanofiber/(meth)acrylic resin composites. Green Chem 13:1708
35. Sueyoshi Y, Hashimoto T, Yoshikawa M, Ifuku S (2011) Chitin nanofiber membranes for chiral separation. Sust Agric Res 1:42
36. Melgar S, Karlsson A, Michaelsson E (2005) Acute colitis induced by dextran sulfate sodium progresses to chronicity in C57BL/6 but not in BALB/c mice: correlation between symptoms and inflammation. Am J Physiol-Gastr L 288:G1328
37. Azuma K, Osaki T, Wakuda T, Ifuku S, Saimoto H, Tsuka T, Imagawa T, Okamoto Y, Minami S (2012) Beneficial and preventive effect of chitin nanofibrils in a dextran sulfate sodium-induced acute ulcerative colitis model. Carbohyd Polym 87:1399
38. Azuma K, Osaki T, Wakuda T, Ifuku S, Saimoto H, Tsuka T, Imagawa T, Okamoto Y, Minami S (2012) α–Chitin nanofibrils improve inflammatory and fibrosis responses in inflammatory bowel disease mice model. Carbohyd Polym 90:197

Dispersion of Nanocellulose (NC) in Polypropylene (PP) and Polyethylene (PE) Matrix

11

Jitendra K. Pandey, Hyun Taek Lee, Hitoshi Takagi, S. H. Ahn, D. R. Saini, and M. Misra

Contents

Abstract

PP and PE are considered as environmental polluter mainly because of their greater resistance toward biological degradation in the environment upon disposal. Although this property contributes to their popularity for development of medical devices, still the repercussions of PP and PE litter create a serious threat

J.K. Pandey
University of Petroleum and Energy Studies (UPES), Bidholi Campus Office Energy Acres, Dehradun, India
e-mail: jeetu_ncl@yahoo.com

H.T. Lee • S.H. Ahn
School of Mechanical & Aerospace Engineering, Seoul National University, Seoul, Korea
e-mail: wow21star@gmail.com; ahnsh@snu.ac.kr

H. Takagi
Advanced Materials Division, Institute of Technology and Science, The University of Tokushima, Tokushima, Japan
e-mail: takagi@tokushima-u.ac.jp

D.R. Saini
Department of Polymer Science and Engineering, National Chemical Laboratory, Pune, India
e-mail: dsaini2010@gmail.com

M. Misra (✉)
Department of Plant Agriculture, or, School of Engineering, University of Guelph, Guelph, ON, Canada
e-mail: mmisra@uoguelph.ca

J.K. Pandey et al. (eds.), *Handbook of Polymer Nanocomposites. Processing, Performance and Application – Volume C: Polymer Nanocomposites of Cellulose Nanoparticles*,
DOI 10.1007/978-3-642-45232-1_56,

for chocking of water ways, sewage pipes, etc. Since one of the main objectives to use NC as reinforcer for polymer matrixes is to develop environmentally friendly composites, it is essential to review the potential of NC-based PP and PE composites as environment friendly natural nanofiller. Highly crystalline nature, aspect ratio, well-established extraction processes, renewability, and sustainability of NC make it one of the best nanofillers to improve the material properties of different hydrophilic polymer. The mechanical performance of resulting hybrids is mainly governed by the proper dispersion of NC inside polymer. Because of their highly hydrophilic nature, it is always a challenge to mix NC with hydrophobic polymer matrixes such as PP and PE. The present chapter is aimed to discuss the dispersion of NC in PP and PE matrix and associated challenges with brief description of possible solutions and future direction.

Keywords
Biodegradation • Nano-cellulose • Nano-composite • Polyethylene [PE] • Polypropylene [PP]

1 Introduction

Structure, extraction process, and properties of nanocellulose have already been discussed elaborately in the different chapters of this book. One of the most inspirational factors to fill the polymer matrixes with naturally origin filler is to insert the environment friendly or biodegradable character into the so-called nonbiodegradable petroleum-based polymers such as polypropylene (PP) and polyethylene (PE) [1]. This class of thermoplastics is considered harmful for the environment when disposed after use because of their resistance against environmental degradation agents. Thus, long life and stability of litters significantly contribute to the spread of litter which is difficult to solve by landfill and burning due to soil and air pollution, respectively. It has been shown that hybrid with cellulose fibers may be environment friendly because the preferential microbial consumption of cellulose in natural fiber composites generated fragmented polymers chains with large surface area that can enter into biocycle resulting in ultimate conversion of material into carbon dioxide and water leaving behind some residues [2].

Concentration and dispersion of cellulose fibers in the matrix play a detrimental role on the environment- friendly character and mechanical performance of composites [3]. Biodegradability may be accelerated by increasing the concentration of natural filler in the matrix; however, increase in weight of composite may limit their applicability when weight is seriously concerned, for example, fuel consumption efficiency of automobiles [4]. To balance the weight and environmental concerns, research has been shifted toward nanofillers from nature. High surface area of nanofillers creates the possibility of dramatic improvement in the mechanical performance of resulting hybrid at very low filler load, subject to proper dispersion and interaction at interphase. It is believed that cellulose chains are deposited in

continuous fashion to form microfibrils after aggregation and arrange themselves as threadlike bundles of molecules stabilized laterally through hydrogen bonds [5]. The pattern of chain conformation and morphology provides them significant load carrying capability. Depending on their origin, the nanocellulose diameter ranges vary from 2 to 60 nm and length of several nanometers [6] consisting cellulose crystals joined by amorphous domains. Nanocellulose can be extracted from almost every kind of cellulose-containing entity either by mechanical analysis or by taking the advantage of lower susceptibility of amorphous regions during acids treatments [7]. The hydronium ions can penetrate the cellulose chains in these amorphous domains, promoting the hydrolytic cleavage of the glycosidic bonds and finally releasing individual crystallites.

The term "cellulose crystallites" is normally used for rodlike cellulose crystals of nanometer dimensions (2–20 nm wide) [6, 7]. Mechanical treatment permits the dispersion of the aggregates and finally produces colloidal suspensions. Because of their stiffness, thickness, and length, these rodlike particles are commonly called "whiskers" [7]. The terminology varies most of the time in current literature and has been tabulated in Table 11.1 [3, 7], with description of extraction process and source. "Nanocellulose" has been used in general sense during the discussion in the chapter to increase the clarity toward the objective of the article which is to evaluate reinforcing capacity in hydrophobic thermoplastics. Nanocellulose is winning the race as preferred natural nano-reinforcer to develop nanocomposites because of its abundant availability, renewability, and extraction process. However, their dispersion in matrix of non-water-soluble polymers seems the only limiting factor for their application to develop composites for engineering applications. The high level of dispersion may be attained for water-soluble polymers due to the outstanding affinity of nanocellulose with water by the hydrogen bonding through numerous hydroxyl groups on the surface [8]. The present chapter describes the nanocellulose-based composites with PE, PP, and the pattern of extrusion with other polymers. PE and PP are selected for the discussion because of immediate need to develop the biodegradable plastics from these polymers for commodity applications.

2 Dispersion and Processing of Nanocellulose-Based Composites

The key criteria are to reduce the surface energy of nanocellulose in order to make them compatible with hydrophobic matrixes. Surface properties of NC may be permanently altered through different reactions, viz., isocyanates, anhydrides [9] silane reagents [10, 11, 12], polystyrene chains [13], and poly(ε-caprolactone) [14]. Some of the examples include macro kenaf fibers, modified with acetic anhydride, and nanocellulose were isolated from the acetylated fibers through mechanical isolation methods [15]. Researchers believed that the kenaf fibers tend to swell upon treatment with acetylating reagents resulting in the penetration of reagents into cell walls where acetylation takes place. The limiting factor in the presented reaction seems the use of pyridine catalyst in terms of the development of environment-friendly material.

Table 11.1 Acronyms, source of nano-dimensional cellulose, and their process of extraction (Reproduced from Ref. [7])

Acronyms	Name	Source	Process
CNW	Cellulose nanowhiskers	Ramie	H_2SO_4 hydrolysis
		MCC	H_2SO_4 hydrolysis
		MCC	H_2SO_4 hydrolysis
		Grass fiber	H_2SO_4 hydrolysis
		MCC	LiCl:DMAc
CNXL	Cellulose nanocrystals	Cotton Whatman filter paper	H_2SO_4 hydrolysis
		Bacterial cellulose	H_2SO_4 hydrolysis
		Cotton (cotton wool)	H_2SO_4 hydrolysis
		MCC	H_2SO_4 hydrolysis
		MCC	Sonication
CNW-HCl	Cellulose nanowhiskers	Cotton linters	HCl hydrolysis
Wh	Whiskers	Cellulose fibers	H_2SO_4 hydrolysis
NF	Nanofibers	Wheat straw	HCl + mechanical treatment
NCC	Nanocrystalline cellulose	MCC	H_2SO_4 hydrolysis
MFC	Microfibrillated cellulose	Pulp Gailin	Homogenizer
		Pulp Daicel	–
		Pulp Daicel	–
NFC	Nanofibrillated cellulose/ cellulose nanofibrils	Sulfite pulp	Mechanical
MCC	Microcrystalline cellulose	Alpha cellulose fibers	Hydrolysis
–	Cellulose crystallites	Cotton Whatman filter paper	H_2SO_4 hydrolysis
–	Nanocellulose	Sisal fibers	H_2SO_4 hydrolysis
–	Cellulose microcrystal	Cotton Whatman filter paper	HCl hydrolysis
–	Nanofibers	Soybean pods	Chemical treatment + high-pressure defibrillator

Bacterial cellulose (BC) nanofibers were acetylated by Ifuku et al. [16] to enhance the properties and develop the optically transparent composites of acrylic resin (Fig. 11.1). NC was acetylated from degree-of-substitution (DS) 0–1.76 by using acetic acid and perchloric acid after replacing water with acetone or methyl alcohol. Interaction between modified fiber and resin was found related to the high transparency. Acetylated hydrophobic surface may have better affinity with hydrophobic resins, and composites become transparent within 1 hr under pressure where the degree of trenchancy was found associated with the degree of substitution of hydroxyl groups of cellulose. Pandey et al. [17] obtained NC from grass by acid treatments and modified with maleic anhydride in order to make them compatible with PLA matrix. Modification extent, NC shape and size were monitored through scanning electron

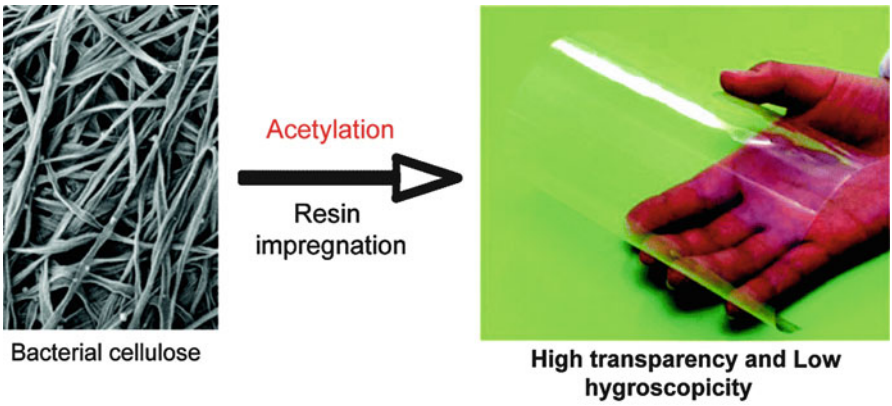

Fig. 11.1 Transparent film of modified nanocellulose of bacterial cellulose (Reprinted [adapted] with permission from Ifuku S., Nogi M., Abe K., Handa K., Nakatsubo F., Yano H., Biomacromolecules 8 (2007) 1973., [16], Copyright (2007) American Chemical Society)

microscopy and FT-IR analysis, respectively (Fig. 11.2). The main objective of this work was to study the effect of modification of filler on the thermal and mechanical characteristics of resulting hybrids where a dramatic increase in mechanical properties could not be observed at 7 % and 10 % filler load. Interestingly, the 5 % filler concentration exhibited little improvement in tensile strength (neat PLA 50.9 MPa, at 5 % 51.7 MPa) with maintained elongation at break (neat PLA 2.3 and 5 % was 2.7 %).

Mixing of nanocellulose, particularly by conventional melt compounding, with polymer matrixes is never easy even after modification. Cellulose nanocomposite processing via a master batch with high content of nanofibers in PLA was attempted. The master batch and the bulk PLA were premixed and compounded during extrusion to obtain nanocomposites with different fiber compositions. The evaluation of the mechanical properties of the PLA and its nanocomposite showed a trend that the tensile strength and modulus were improved with increased nanofiber content. The modulus of the PLA was increased from 2.9 to 3.6 GPa with the addition of 5 wt% nanofibers, and a 21 % increase of tensile strength was observed [18]. Composites of polypropylene (PP) and crystalline cellulose were prepared by Pandey et al. [19] after modification of the host matrix through reactive extrusion grafting of maleic anhydride. Suspension of micro- and nanocrystalline cellulose was obtained by acid, alkali, and mechanical treatment of wood flour (WF), and cellulose modified layered silicates (clay) were used as filler in the PP matrix at various concentrations via a melt-blending process. It was observed that agglomeration increased with increasing filler concentration which was directly attributed to the higher bonding between clay and cellulose that promoted random accumulation of silicate tactoids. Dispersion was found better at lower concentrations, probably due to availability of a greater amount of functional groups from maleic anhydride-grafted polymer chains in these samples. Because the mechanical properties improved at lower filler loadings,

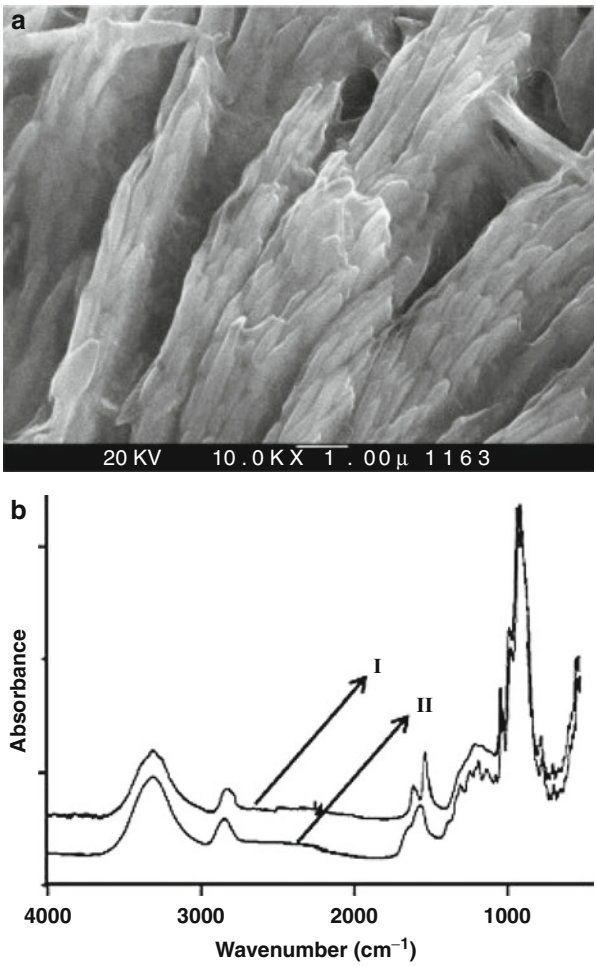

Fig. 11.2 (**a**) SEM of acid-treated sample (**b**) FT-IR spectra of modified (*I*) and unmodified NC (*II*) (Reproduced with permission from Pandey J., Chu W., Kim C., Lee C., Ahn S., Composites Part B: Engineering 40 (2009) 676., [17])

uniform dispersion of fillers was considered more important than the filler concentration in the host matrix. Composites with PP were reported with different types of nano-cellulose without melt mixing. Nanocellulose-reinforced polypropylene was obtained [20] by solvent casting from toluene by using three types of cellulose whiskers as the reinforcing phase: (i) aggregated in toluene (ii) suspension of nanocellulose in water was mixed with a surfactant, phosphoric ester of polyoxyethylene nonylphenyl ether, and (iii) grafted with maleated polypropylene or individualized. Nanocomposites were prepared by solvent casting procedure through mixing of solubilized a-tactic polypropylene in hot toluene (110 °C) with one of the three kinds of NC dispersed in toluene at desired concentration. The NC as cellulose monocrystals, commonly called whiskers,

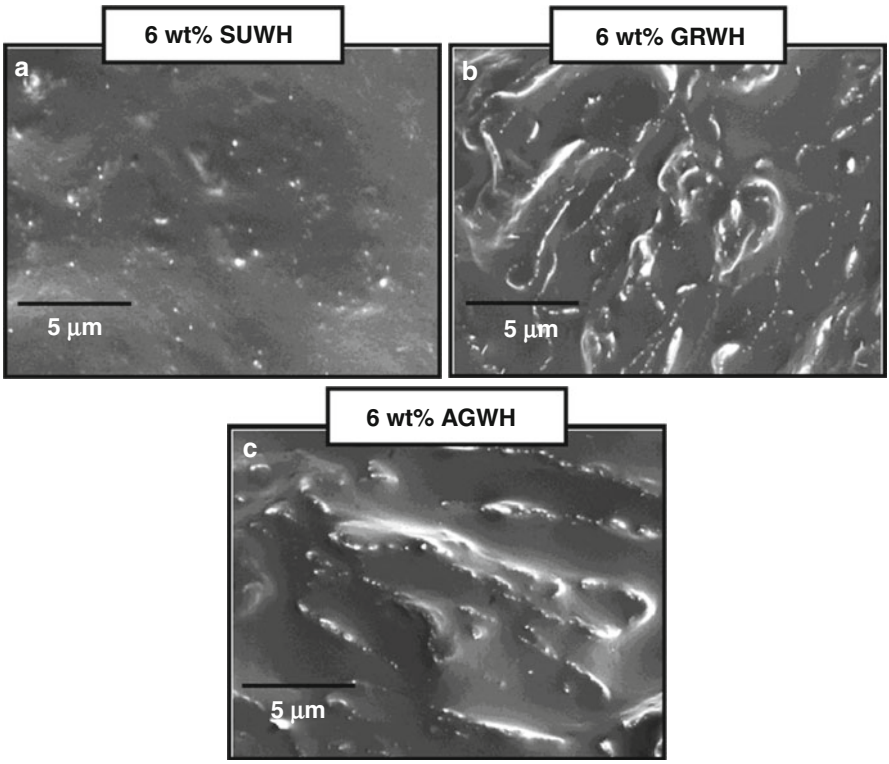

Fig. 11.3 Cryofracture of _PP composite films reinforced with (**a**) 6 wt% SUWH, (**b**) 6 wt% AGWH, and (**c**) 6 wt% GRWH (Reprinted [adapted] with permission from Ljungberg N., Bonini C., Bortolussi F., Boisson C., Heux L., Cavaillé J.Y., Biomacromolecules 6 (2005) 2732., [20], Copyright (2005) American Chemical Society)

was extracted from tunicin, animal cellulose after acid hydrolysis treatment. The nanocomposite films reinforced with toluene aggregated and grafted fillers were found to be opaque, and the film of surfactant-modified filler composites was transparent in nature. SEM images of composites with three different celluloses are presented in Fig. 11.3 where the bright dots were considered as crystals of cellulose. Authors found that mechanical behavior in the nonlinear range exhibited increases in the tensile strengths of the nanocomposite films as compared to the neat matrix. In terms of the ductility and elongation at break of the materials, it was found that the elongation at break could be maintained by surfactant-coated nanofillers. It was observed that the mechanical properties of the composites were determined not only on the filler/filler interactions but also on the extent of the dispersion. Authors proposed that the presented method of obtaining nanocomposites with surfactant-modified whiskers may have potential

to develop nanocomposites with a-polar matrixes. Nanocellulose extracted from soybean source has been incorporated into the polymer matrix of PP and PE, using a Brabender in solid phase melt-mixing methods, and a change in the stress–strain behavior of the prepared composites was observed [21]. Increase in modulus and decrease in elongation was detected. Acrylic monomer, ethylene–acrylic oligomer emulsion, was applied by researchers to reduce the interaction between hydroxyl groups by hydrophobization and promote the dispersion in composites. It was assumed that acrylic oligomer may act as a bridge between the hydrophilic and hydrophobic components. However, the improvement in properties was lower in comparisons of nanocomposites with water-soluble polyvinyl alcohol. NC was not uniformly dispersed in the polyethylene matrix, and a possible degradation occurred during processing. Nanocellulose, extracted by acid hydrolysis of commercial microcrystalline cellulose, have also been used as reinforce for polypropylene (PP) matrix without chemical modification of surface [22]. Maleic anhydride grafter polypropylene (MAPP) was employed as compatibilizing phase between nanocellulose and host matrix. MAPP and PP were dissolved in toluene separately at around 105–110 °C. The NC (0–15 %) was added into the dissolved MAPP followed by sonication for 2 h to improve the dispersion. MAPP solution with filler was then added into the dissolved PP. Samples were prepared by solvent casting. Researchers obtained film with good transparency; however, SEM images could not confirm the uniform dispersion of filler inside the matrix. The tensile strength was surprisingly improved in the reinforced composites which were around 70–80 %. This is a good indication for future possibility to enhance the span of nanocellulose-based composites. An increase in the crystallinity was also improved in the resulting hybrids.

Templating process (Fig. 11.4) has also been applied for the preparation of composites of NC with hydrophobic polymers. For example, polystyrene have been filled in a three-dimensional template of well-individualized nanocellulose [23] which allows for the fabrication of nanocomposites of immiscible components. The first step consists of the formation of a nanocellulose template via a sol/gel process which involves the formation of a homogeneous aqueous dispersion followed by gelation through solvent exchange with a water-miscible solvent. Further as a second step, the gelled NC scaffold was imbibed with a hydrophobic polymer by immersion in a polymer solution, before the nanocomposite is dried. For a successful template approach, the polymer solvent must be miscible with the gel solvent and must not re-disperse the nanofibers. Polystyrene (PS)/cellulose whisker nanocomposites with a content of 2.5–16.7 % v/v were prepared by this approach, and a dramatic reinforcement was observed above Tg. Although these methods appeared as quite successful for nanocellulose-reinforced composite development, feasibility at industrial scale needs to be established as with other processing techniques of polymer compounding such as extrusion method. There is inherent difficulty in the development of composites of nanocellulose without modification either in hydrophobic polymer matrix or in filler especially during melt-mixing process.

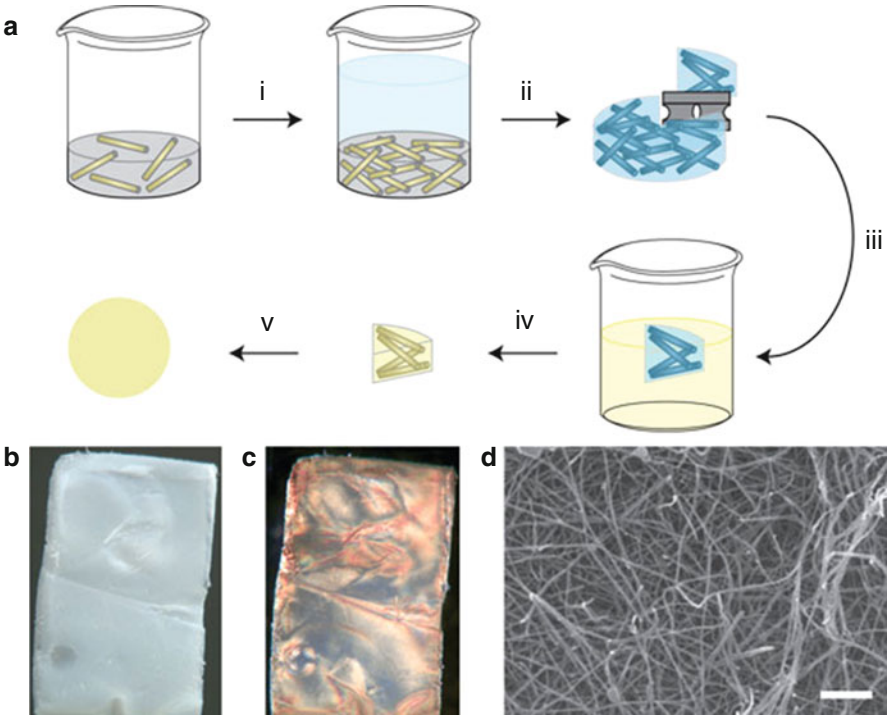

Fig. 11.4 (**a**) Schematic of this template approach to well-dispersed polymer/nanofiber composites. (*i*) A nonsolvent is added to a nanofiber dispersion in the absence of any polymer. (*ii*) Solvent exchange promotes the self-assembly of a nanofiber gel. (*iii*) The gelled nanofiber scaffold is imbibed with a polymer by immersion in a polymer solution, before the nanocomposite is dried (*iv*) and compacted (*v*). (**b**) Image of a cellulose whisker aerogel, prepared by supercritical extraction of a whisker acetone gel (**a**, *ii*) with a whisker density of 15 mg ml^{-1}. (**c**), Same object as in **b**, imaged through crossed polarizers. (**d**), SEM image of the same material (scale bar = 200 nm) (Reprinted (adapted) with permission from Capadona J.R., Van Den Berg O., Capadona L.A., Schroeter M., Rowan S.J., Tyler D.J., Weder C., Nature nanotechnology 2 (2007) 765, Ref. [23])

3 Summary

From the available literature, it appears that the uniform dispersion of nanocellulose in the matrix of polypropylene and polyethylene could not be achieved till today as in the case of water-soluble polymers. The agglomeration of chains is difficult to destroy during mixing with hydrophobic matrix. Partial stable suspension of nanocellulose in organic solvent may have potential to develop composites with polymer soluble in organic solvent at room temperature [24]. The use of surfactant must be given priority over the surface modification of cellulose crystals through chemical reactions to reduce the risk of degradation of polymer chains. Further, chemical reactions may generate the defects in the reinforcing chains reducing their

reinforcing capacity as defects are known to act as stress concentration points; those may cause the catastrophic failure of matrix during load.

It must be noted that the primary objective to fill such type of polymer matrix with natural nanofiller is to enhance their eco-friendly character to make them biodegradable. Although, a different discussion may be carried out on the biodegradation itself, as the definition of biodegradation is not always clear. Discussion on the definition of degradation/biodegradation seems out of scope of this book chapter. The careful evaluation of the environmental biodegradability of NC-based composites is an obviously key factor to enhance the spectrum of their importance as nanofiller. Few studies have been conducted toward this direction such as in the matrixes of natural rubber, polycaprolactone, and polylactic acid [3]; however, all of these matrixes are considered biodegradable under defined environment. Crystallinity has been known to alter the promotion of biodegradation when nanocellulose was filled in the matrix of natural rubber. Although a quantitative estimation on biodegradation was not conducted, still the increased water sorption behavior may be considered as positive indication of microbial adhesion, a primary step to initiate the biodegradation [25–29]. Indications of increased biodegradation were detected during soil burial test, when nanocellulose from bagasse was dispersed in the natural rubber [26]. Similar trends have been observed with the matrixes of polylactic acid and polycaprolactone under different testing conditions [27]. In general, it may be summarized that NC-based composites of polypropylene and polyethylene are in the infant stage of development and require extensive research to solve the dispersion and degradation issues.

Acknowledgements Support from Brain Pool Korea is gratefully acknowledged.

References

1. Pandey JK, Raghunatha RK, Pratheep KA, Singh RP (2005) An overview on the degradability of polymer nanocomposites. Polymer degradation and stability. Polym Degrad Stabil 88(2):234–250
2. Pandey JK, Misra M, Mohanty AK, Drzal LT, Palsingh R (2005) Recent advances in biodegradable nanocomposites. J Nanosci Nanotechnol 5(4):497–526
3. Pandey JK, Takagi H, Saini DR, Nakagaito AN, Ahn SH (2012) An overview on the cellulose based conducting composites. Compos B: Eng 43(7):2822–2826
4. Kolpak F, Blackwell J (1976) Determination of the structure of cellulose II. Macromolecules 9 (2):273–278
5. Stipanovic AJ, Sarko A (1976) Packing analysis of carbohydrates and polysaccharides. Molecular and crystal structure of regenerated cellulose II. Macromolecules 9(5):851–857
6. de Souza Lima MM, Borsali R (2004) Rodlike cellulose microcrystals: structure, properties, and applications. Macromol Rapid Commun 25(7):771–787
7. Siqueira G, Bras J, Dufresne A (2010) Cellulosic bionanocomposites: a review of preparation, properties and applications. Polymers 2(4):728–765
8. Araki J, Wada M, Kuga S, Okano T (1998) Flow properties of microcrystalline cellulose suspension prepared by acid treatment of native cellulose. Colloids Surf A Physicochem Eng Asp 142(1):75–82

9. Nair KG, Dufresne A, Gandini A, Belgacem MN (2003) Crab shell chitin whiskers reinforced natural rubber nanocomposites. 3. Effect of chemical modification of chitin whiskers. Biomacromolecules 4(6):1835–1842
10. Goussé C, Chanzy H, Excoffier G, Soubeyrand L, Fleury E (2002) Stable suspensions of partially silylated cellulose whiskers dispersed in organic solvents. Polymer 43(9):2645–2651
11. Grunert M, Winter WT (2002) Nanocomposites of cellulose acetate butyrate reinforced with cellulose nanocrystals. J Polym Environ 10(1–2):27–30
12. Gousse C, Chanzy H, Cerrada M, Fleury E (2004) Surface silylation of cellulose microfibrils: preparation and rheological properties. Polymer 45(5):1569–1575
13. Morandi G, Heath L, Thielemans W (2009) Cellulose nanocrystals grafted with polystyrene chains through surface-initiated atom transfer radical polymerization (SI-ATRP). Langmuir 25(14):8280–8286
14. Habibi Y, Goffin AL, Schiltz N, Duquesne E, Dubois P, Dufresne A (2008) Bionanocomposites based on poly (ε-caprolactone)-grafted cellulose nanocrystals by ring-opening polymerization. J Mater Chem 18(41):5002–5010
15. Jonoobi M, Harun J, Mathew AP, Hussein MZB, Oksman K (2010) Preparation of cellulose nanofibers with hydrophobic surface characteristics. Cellulose 17(2):299–307
16. Ifuku S, Nogi M, Abe K, Handa K, Nakatsubo F, Yano H (2007) Surface modification of bacterial cellulose nanofibers for property enhancement of optically transparent composites: dependence on acetyl-group DS. Biomacromolecules 8(6):1973–1978
17. Pandey JK, Chu W, Kim C, Lee C, Ahn S (2009) Bio-nano reinforcement of environmentally degradable polymer matrix by cellulose whiskers from grass. Compos B: Eng 40(7):676–680
18. Jonoobi M, Mathew AP, Abdi MM, Makinejad MD, Oksman K (2012) A comparison of modified and unmodified cellulose nanofiber reinforced polylactic acid (PLA) prepared by twin screw extrusion. J Polym Environ 20(4):991–997
19. Pandey JK, Lee S, Kim HJ, Takagi H, Lee C, Ahn SH (2012) Preparation and properties of cellulose-based nano composites of clay and polypropylene. J Appl Polym Sci 125(S1):E651–E660
20. Ljungberg N, Bonini C, Bortolussi F, Boisson C, Heux L, Cavaillé JY (2005) New nanocomposite materials reinforced with cellulose whiskers in atactic polypropylene: effect of surface and dispersion characteristics. Biomacromolecules 6(5):2732–2739
21. Wang B, Sain M (2007) Isolation of nanofibers from soybean source and their reinforcing capability on synthetic polymers. Compos Sci Technol 67(11):2521–2527
22. Bahar E, Ucar N, Onen A, Wang Y, Oksüz M, Ayaz O, Ucar M, Demir A (2012) Thermal and mechanical properties of polypropylene nanocomposite materials reinforced with cellulose nano whiskers. J Appl Polym Sci 125(4):2882–2889
23. Capadona JR, Van Den Berg O, Capadona LA, Schroeter M, Rowan SJ, Tyler DJ, Weder C (2007) A versatile approach for the processing of polymer nanocomposites with self-assembled nanofibre templates. Nature Nanotechnol 2(12):765–769
24. Beck-Candanedo S, Roman M, Gray DG (2005) Biomacromolecules 6:1048
25. Chuayjuljit S, Su-Uthai S, Tunwattanaseree C, Charuchinda S (2009) Preparation of microcrystalline cellulose from waste-cotton fabric for biodegradability enhancement of natural rubber sheets. J Reinf Plast Comp 28:1245–1254
26. Bras J, Hassan ML, Bruzesse C, Hassan EA, El-Wakil NA, Dufresne A (2010) Mechanical, barrier, and biodegradability properties of bagasse cellulose whiskers reinforced natural rubber nanocomposites. Ind Crop Prod 32(3):627–633
27. Poly(lactic acid)/natural rubber/cellulose nanocrystal bionanocomposites. Part II: Properties evaluation Natacha Bitinis Elena Fortunati Raquel Verdejo Julien Bras Jose Maria Kenny Luigi Torre Miguel Angel López- Carbohydrate Polymers 2013, 96, 2,621–627
28. Samir MASA, Alloin F, Dufresne A (2005) Review of recent research into cellulosic whiskers, their properties and their application in nanocomposite field. Biomacromolecules 6:612–626
29. Hassan ML, Bras J, Hassan EA, Fadel SM, Dufresne A (2012) Polycaprolactone/modified bagasse whisker nanocomposites with improved moisture-barrier and biodegradability properties. J Appl Polym Sci 125(Suppl 2):E10–E19

Electrospun Cellulose Composite Nanofibers

12

H. P. S. Abdul Khalil, Y. Davoudpour, A. H. Bhat, Enih Rosamah, and Paridah Md. Tahir

Contents

H.P.S. Abdul Khalil (✉) • Y. Davoudpour
School of Industrial Technology, Universiti Sains Malaysia, Penang, Malaysia
e-mail: akhalilhps@gmail.com; y.davoudpour@gmail.com

A.H. Bhat
Department of Fundamental and Applied Sciences, Universiti Teknologi Petronas, Perak, Malaysia
e-mail: aamir.bhat@petronas.com.my

E. Rosamah
Faculty of Forestry, Mulawarman University, Kelua Samarinda, East Kalimantan, Indonesia
e-mail: enihros@yahoo.com

P.M. Tahir
Biocomposite Technology Laboratory, Institute of Tropical Forestry and Forest Products, Universiti Putra Malaysia, Serdang, Selangor, Malaysia
e-mail: parida.introp@gmail.com

J.K. Pandey et al. (eds.), *Handbook of Polymer Nanocomposites. Processing, Performance and Application – Volume C: Polymer Nanocomposites of Cellulose Nanoparticles*,
DOI 10.1007/978-3-642-45232-1_61,

Abstract

This chapter deals with the structure, properties, and applications of electrospun-based cellulose composites. Extraction methods of cellulosic nanofibers from different sources are discussed in detail. Cellulose has the special advantage of high specific strength and sustainability, which make them ideal candidates for reinforcement in various polymeric matrices. Cellulose nanofibers find application in various fields, including construction, the automobile industry, and soil conservation. Cellulose, an eminent representative of nanomaterial obtained from various natural fibers, can be dissolved in various solvent systems, which are described in detail in this study. Thermoplastic-based electrospun cellulose nanocomposites and their applications are highlighted. This chapter describes current and future applications of electrospun cellulosic nanofibers in various fields.

Keywords

Cellulose • Electrospun • Polymer • Composite

1 Introduction

Science and technology continue to move toward renewable raw materials, such as plant fibers and biomass materials, and more environmentally friendly as well as sustainable resources and processes [3, 6, 7, 99]. Micron-size, nano-scale fibers exhibit several unique properties, such as higher surface area and surface functionalization [100, 154], and possess excellent mechanical, optical, and electrical properties [243], making them desirable for various applications.

There are many methods for fabricating polymeric nanofiber, including phase separation, drawing, self-assembly, template, and electrospinning [120]. The majority of these techniques suffer from disadvantages, for example, using limited polymer, noncontrollable orientation and diameter of fiber, and noncontinuous process [123]. Compared with other nanofiber production processes, electrospinning has gained considerable attention because of its control of fiber dimension, structures, alignment, and porosity [23]. Electrospinning is a straightforward technique for fabricating nanofibers using polymer solutions or melt in submicron diameters [84, 155, 231]. Briefly, in these processes nanofibers are generated by applying an electric field between opponent electrodes, which causes a whipping motion of solution, creating a stretched, charged polymer jet, evaporation of solvent, and solidifying of the jet to form fiber [20, 183]. The morphology and diameter of the nanofibers manufactured by electrospinning depend on several parameters: voltage, needle-to-target distance, solution concentration, surface tension, viscosity, environment conditions, and so on [90].

Electrospun nanofibers have broad potential for different applications such as sensors, filtrations materials, tissue engineering, and composites [52, 127]; this is because of their high porosity, large specific surface area, and tiny pore size [212]. In recent decades, research has focused on electrospinning of nanofibers [208] and composite nanofibers [13, 50, 137, 255] from natural resources in order to

utilize them in different fields, especially in composite. The key advantages of renewable fillers such as chitin, cellulose, and starch are their sustainability, accessibility, cheap price, small energy consumption, and excellent mechanical properties. Cellulose is an abundant, biodegradable, and biocompatible polymer [142] that recently came into researchers' consideration for electrospinning. Despite the above-mentioned properties, electrospinning of cellulose is restricted owing to its nonsolubility in common solvents and thermal degradation before melting [62, 214]. In addition, cellulose nanowhisker (CNW), obtained through an acid hydrolysis process of cellulose, is recognized as a new nano material to reinforce other materials [172]. Cellulose does dissolve in some solvents, such as lithium chloride-dimethylacetamide (LiCl/DMAc), *N*-methylmorpholine-*N*-oxide (NMMO), and ionic liquids (ILs) as a "green" solvent [1]. Obviously, each of these solvents has its own disadvantages. For example, NMMO requires elevated temperature and washing to eliminate residual NMMO; it also produces fibers with low uniformity [80].

The aim of this chapter is to investigate developments in the field of electrospinning of cellulose and cellulose composite nanofibers. Electrospun cellulose nanofibers have potential for use in a wide range of applications.

2 Electrospinning

2.1 Process

There are many methods for producing polymer nanofibers, including self-assembly, phase separation, and electrospinning [47, 156]. Electrostatic fiber spinning, or electrospinning, is a novel and interesting process for producing nano- to micro-fibers from solution or melt by electrostatic forces [144, 206]. Recently, it has gained increasing attention because of its simplicity and versatility in fabricating nanofibers [104, 220]. Formhal patented this method in 1934 [260]. Basically, there are two main differences between conventional fiber spinning and electrospinning. In traditional spinning, mechanical forces cause the production of microfibers, whereas electrospinning can produce fibers in nano size by electrical forces [221]. Electrospinning confers unique properties to nanofibers, such as large surface area, lower structural defect, and enhanced mechanical properties [88, 113]. Generally, the electrospinning apparatus comprises three main parts: a target to collect nanofibers, a high-voltage electric source that provides electric force for drawing the jet, and a syringe pump to carry the polymer solution [110]. Figure 12.1 displays a schematic of an electrospinning setup.

In a typical process, an electrostatic field between needle and collector is provided by a high-voltage electric source. Because of surface tension, the polymer drop remains at the tip of syringe [199]. High voltage induces charges to the solution [210]. In addition, ions act as an element to carry charges [188]. The polymer solution under the effect of electrostatic fields forms a conical-shaped droplet known as a Taylor cone at the tip of the capillary. At a critical value of applied voltage, electrostatic force overcomes the surface tension of the droplet and

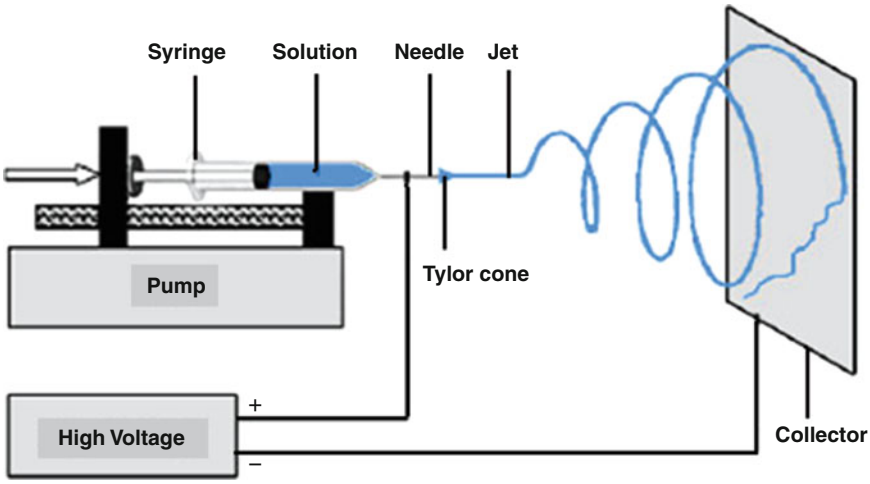

Fig. 12.1 Schematic of an electrospinning setup [259]

a fine, charged jet erupts from the cone tip [32, 118]. The polymer jet is only stable close to the tip of the capillary, after which it undergoes bending instability [182]. The electric field controls the path of the charged polymer jet. The jet is enlarged through spiraling loops. As the diameter of the loops grows, the jet becomes smaller in diameter and longer in length [43]. Finally, the solvent evaporates and solid nanofibers are deposited at the target [215]. Different structures of electrospun nanofibers, such as hollow, aligned, core-shell, and multilayer, can be fabricated by some modifications in the electrospinning setup [218].

Various forces impact the appearance of electrospun nanofibers. Viscoelastic forces are affected by solution concentration and viscosity as well as polymer molecular weight. Surface tension of electrospun nanofibers depends on surface tension of the solvent, average molecular weight of the polymer, and solution concentration. Gravitational forces are determined by the density of solution. Electrostatic forces change with electrostatic field and the conductivity of solution [235]. Columbic forces push apart neighboring charged species in the jet and cause drawing of the jet, while drag forces act between surrounding air and the jet. It is important to note that viscoelastic forces prohibit the jet from elongation, surface tension prevents from drawing of surface of the polymer jet, and electrostatic force is responsible for transferring the charged jet from the nozzle to target [158].

2.2 Parameters

One of the most important issues with regard to electrospinning is the morphology of resultant nanofibers, which depends on many factors. On the whole, these factors can be classified into three categories: processing parameters (voltage, flow rate, distance from nozzle to collector), solution characteristics (viscosity, polymer molecular

weight, concentration, surface tension, electrical conductivity), and ambient parameters (atmospheric pressure, temperature, and humidity) [60, 222, 226]. Morphology and characterization of electrospun nanofibers can be controlled by these conditions.

Polymer chain entanglement and, consequently, viscosity of the solution are determined by molecular weight. Furthermore, molecular weight is a crucial factor in choosing the lowest polymer concentration for electrospinning [217]. In general, when the molecular weight increases, the viscosity will be raised, and, therefore, higher chain entanglement leads to formation of a continuous polymer jet rather than droplets or beads [95]. Beads are generated in some conditions during the electrospinning process. Solution viscosity, surface tension, and charge density are the most important factors influencing the formation of beads [129, 140]. Spinnability of a polymer solution is determined by solution concentration. Concentration also has an effect on the surface tension and the viscosity of a polymer solution. Solutions that are too dilute form droplets, as a result of surface tension, prior to reaching the collector. On the other hand, polymer solution that is too concentrated cannot be electrospun because of high viscosity. Therefore, optimum concentration is required for producing nanofibers [207].

Solution viscosity plays an important role in determining the morphology and diameter of fibers. Generally, a solution with higher viscosity yields fibers with larger diameter. It has been documented that when viscosity is very low, no continuous fiber will form; with very high viscosity, the jet will eject with great difficulty. Maximum viscosities for spinning from 1 to 215 P have reported by researchers [28]. On the whole, if all other conditions remain constant, surface tension will determine the upper and lower limitations of electrospinning. Lower surface tension, which and is preferred for electrospinning, leads to lower electrostatic fields and helps to obtain fibers without beads [79].

The electrical conductivity of a solution is an important factor in electrospinning [115]. It reveals the charge density and repulsion in the polymer solution and, therefore, the amount of elongation a jet. Greater conductivity can cause the jet to carry more charges and smaller-diameters fibers will form [79, 173]. There is not a general pattern to follow for choosing specific values of parameters such as viscosity, conductivity, concentration, and surface tension because they change from one system (polymer-solvent) to another [75].

Choice of solvent is critical from two points of views: quick solvent evaporation and phase separation, which occurs before the fiber is deposited on the collector. Thus, the vapor pressure of solvent influences the rate of evaporation and the time required for drying of nanofibers [210].

Applied voltage or field strength is one of the most crucial parameters in the electrospinning process and has been studied widely. Increasing voltage causes a higher electric field. The effect of raising voltage on the diameter of resultant fibers is a controversial topic in electrospinning [42]. Several researchers have reported that increasing applied voltage leads to formation of thinner fibers because of increasing electrostatic forces [101, 160, 232]. Surprisingly, some authors showed that thicker fibers are produced by increasing voltage [46]. Other researchers have stated that there is no significant correlation between

Table 12.1 Effect of various electrospinning factors on the morphology of fibers [28]

Parameters	Effect on fiber morphology
Solution parameters	
Viscosity	Low causes bead generation; high increases fiber diameter, beads disappear
Concentration	Increase in fiber diameter with increase of concentration
Molecular weight	Reduction in the number of beads and droplets with increase of molecular weight
Conductivity	Decrease in fiber diameter with increase in conductivity
Surface tension	No conclusive link with fiber morphology, high surface tension results in instability of jets
Processing parameters	
Voltage	Decrease in fiber diameter with increase in voltage
Distance from needle to collector	Generation of beads with too small and too large distance, minimum distance required for uniform fibers
Flow rate	Decrease in fiber diameter with decrease in flow rate, generation of beads with too high flow rate
Ambient parameters	
Humidity	High humidity results in circular pores on the fiber
Temperature	Increase in temperature results in decrease in fiber diameter

fiber diameter and applied voltage [9, 14, 44]. This inconsistency can be explained as follows: in a conventional apparatus, the solution erupts downwards And, therefore, by increasing voltage, a greater electrostatic force is induced on the jet and the flow rate will boost. When gravitational force is accompanied by electrostatic force, this phenomenon will be reinforced. Sometimes, electrostatic and gravity forces can detach a drop prior to formation of an initiation cone [2]. In addition, increasing the applied voltage increases beaded fiber formation [260].

Distance from the nozzle to the target is one of the most studied parameters in the research. In the region where whipping instability occurs, the travel time and solvent evaporation rate can be changed by altering the distance from the tip to the collector. In short distances, the solvent cannot evaporate fully [108, 154]. Solution flow rate must be studied for the characterization of nanofibers. Typically, thinner fibers can be obtained by a lower solution feed rate. Flow rates that are too high may also cause formation of beads because of insufficient solvent evaporation before reaching the target [173].

A number of investigations have evaluated the effect of solution and processing parameters on electrospun nanofiber morphology. The influences of spinning environment conditions (like temperature, humidity, and pressure) need further study, however. In terms of the effect of temperature, it is accepted that by increasing solution temperature, nanofibers with smaller diameters can be produced because of the reduction in viscosity [229]. Humidity is another parameter that influences the evaporation rate of solvent, and has been observed that higher humidity leads to larger fiber diameter [82]. Table 12.1 describes the overall effect of electrospinning parameters on the morphology of nanofibers [28].

As stated in previous sections, electrospinning is a simple method for producing fibers in nano scale, and therefore many researchers have investigated

Table 12.2 Development of electrospinning

Year	Progress	References
1882	Balance of fluid conducting masses that are charged by electric potential	Lord Rayleigh [184]
1914	Electrical discharge from liquid points	Zeleny [250]
1934	Process and apparatus for fabricating artificial filaments	Formhal [65]
1955	Dispersibility of some liquids in aerosols using high voltage	Drozin [55]
1971	Acrylic microfibers produced by electrospinning	Baumgarten [26]
1981	Study electrospinning using polymer melts	Larrondo and Manley [125]
1996	Study electrospinning of various polymers	Reneker and Chun [187]
1997	Electrospinning of calf thymus Na-DNA with concentration from 0.3 % to 1.5 %	Fang and Reneker [61]
1998	Electrospinning of some polymer/solvent for producing ultrafine nanofibers	Jaeger et al. [96]
1999	Formation of beaded nanofibers in electrospinning of polyethylene oxide (PEO) solutions	Fong et al. ([64]
2000	A mathematical model for analysis of bending instability	Reneker et al. [189]
2001	Utilizing stability theory to forecast when electrospinning takes place	Hohman et al. [86]
2002	Electrospun membrane from cellulose acetate (CA) with three different solvents	Liu and Hsieh [139]
2003	Producing core-shell nanofibers by electrospinning	Sun et al. [213]
2004	Theoretical investigation of allometric scaling laws in various stages of electrospinning	He et al. [83]
2005	Effect of connection between concentration and viscosity on morphology of electrospun poly methyl methacrylate (PMMA)	Gupta et al. [76]
2006	Altering of energy in the alignment of molecules by computer simulation of EVOH (ethylene/vinyl alcohol copolymer) with different solvents	Lu et al. [143]
2007	Electrospinning of conductive microfluid approach to produce core/shell and hollow composite nanofibers by electrospinning	Srivastava et al. [209]
2008	Electrospinning of aligned nanofibers using nonconductive ferrite magnet target	Yang et al. [241]
2009	Co-electrospinning of thermoset polymer	Reddy et al. [185]
2010	Electrospinning of cyclodextrin as a non-polymeric system	Celebioglu and Uyar [37]
2011	Electrospun nylon-6 nanofibers using AFM probe as a tip	Gururajan et al. [77]
2012	Eliminating whipping motion and produce electrospun nanofiber from PEO and polystyrene (PS) with a fast-rotating collector	Kiselev and Rosell-Llompart [116]

about it. Table 12.2 shows the chronological events that take place in the development of electrospinning. It is undeniable that, during recent decades, electrospinning has gained more attention in different fields.

Electrospinning fabricates nanofibers with small diameter and, consequently, large surface area, high porosity, great pore interconnection [102], and higher mechanical

properties [119]. Based on these unique properties, electrospun nanofibers can be utilized in such fields as biomedical [18, 98, 135, 225, 252], filtration [24, 29, 180], sensors [53, 242], catalyst [45], energy and environment [219], and protective cloth [74, 128].

3 Cellulose

Cellulose forms the basic material of all plant fibers. It is generally accepted that cellulose is a linear condensation polymer consisting of D-anhydroglucopyranose units joined together by β-1, 4-glycosidic linkages. Cellulose is thus a 1, 4–βDglucan [164]. The molecular structure of cellulose, which is responsible for its supermolecular structure, determines many of its chemical and physical properties. In the fully extended molecule, the adjacent chain units are oriented by their mean planes at the angle of 180° to each other. Thus, the repeating unit in cellulose is the anhydro cellobiose unit, and the number of repeating units per molecule is half the Degree of Polymerization (DP). This may be as high as 14,000 in native cellulose. The mechanical properties of natural fibers depend on the cellulose type. Each type of cellulose has its own cell geometry, and the geometrical conditions determine the mechanical properties. Solid cellulose forms a microcrystalline structure with regions of high order (i.e., crystalline regions) and regions of low order (i.e., amorphous regions). Cellulose is also formed of slender rod-like crystalline microfibrils. The crystal nature (monoclinic sphenodic) of naturally occurring cellulose is known as cellulose I. Cellulose is resistant to strong alkali (17.5 wt%) but is easily hydrolyzed by acid to water-soluble sugars. Cellulose is relatively resistant to oxidizing agents.

Plant fibers are constituted of cellulose fibers consisting of helically wound cellulose microfibrils bound together by an amorphous lignin matrix. Lignin keeps the water in fibers, acts as protection against biological attack, and is a stiffener to give the stem its resistance against gravity forces and wind. Hemicellulose, found in natural fibers, is believed to be a compatibilizer between cellulose and lignin [81]. The cell wall in a fiber is not a homogenous membrane (Fig. 12.2) [191]. Each fiber has a complex, layered structure consisting of a thin primary wall that is the first layer deposited during cell growth encircling a secondary wall. The secondary wall is made up of three layers and the thick middle layer determines the mechanical properties of the fiber. The middle layer consists of a series of helically wound cellular microfibrils formed from long-chain cellulose molecules. The angle between the fiber axis and the microfibrils is called the microfibrillar angle. The characteristic value of microfibrillar angle varies from one fiber to another. These microfibrils have typically a diameter of about 10–30 nm and made up of 30–100 cellulose molecules in extended chain conformation that provide mechanical strength to the fiber.

The properties of cellulose fibers are affected by many factors, including variety, climate, harvest, maturity, retting degree, decortications, disintegration (mechanical, steam explosion treatment), fiber modification, textile, and technical processes (spinning and carding) [224]. In order to understand the properties of natural fiber-reinforced composite materials, it is necessary to know the mechanical, physical, and

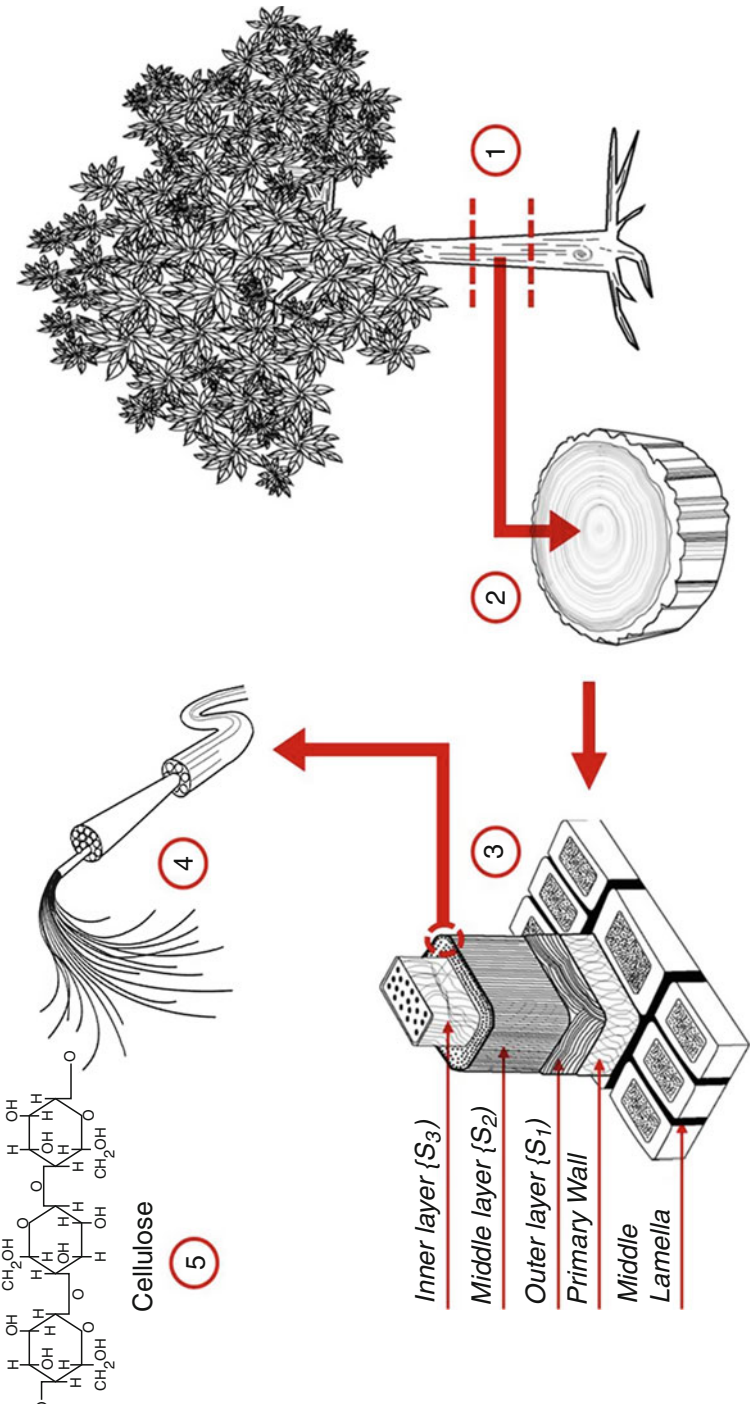

Fig. 12.2 Microscale to fiber bundles to cellulosic nanofibrils from plant fibers

chemical properties of natural fibers [4, 5]. Flax fibers are relatively strong fibers as compared to other natural fibers. The tensile strength of elementary fibers is in the range of 1,500 MPa and for technical fibers a value of approximately 800 MPa was observed at 3-mm clamp length [33]. Baley [25] and Lamy and Baley [124] investigated the modulus of flax fibers. The modulus of elementary fibers is dependent on the diameter of fiber and it ranges from 39 GPa for fibers having diameter approximately 35 μm to 78 GPa for fibers having 5-μm diameter. This variation is related to the variation in relative lumen size between fibers having different diameter. An average Young's modulus of 54 GPa was observed after numerous tensile tests on single flax fibers and the results are within the range of moduli measured on technical fibers. The mechanical, chemical, and physical properties of plant fibers are strongly harvest dependent, influenced by climate, location, weather conditions, and soil characteristics. These properties are also affected during the processing of fiber such as retting, scotching, bleaching, and spinning [97, 230].

4 Electrospun Cellulose Nanofibers

4.1 Cellulose Solvent Systems

Renewable biopolymers, particularly cellulose, have been attracted more attention in nanotechnology [70]. Owing to the fact that cellulose cannot be melted, it must be functionalized or prepared into solution form for electrospinning [68]. The hydrogen bond in cellulose is an obstacle for dissolving it in common solvents. However, some solvents, including NMMO/H_2O, LiCl/DMAc, and ionic liquids (ILs), have been utilized to direct dissolution of cellulose for electrospinning process (Lee et al. 2009). Some investigations related to direct dissolution of cellulose for electrospinning process are briefly described here.

4.1.1 *N*-methylmorpholine-*N*-oxide (NMMO)/H_2O

Monohydrated NMMO is probably the most used non-derivatizing solvent for cellulose in industry, and it is used in the manufacturing of man-made fibers [103]. NMMO belongs to the group of one-component tertiary amine oxide solvents for which the first reports on dissolution of cellulose appeared as early as 1939 (Fig. 12.3). It may be misleading to consider tertiary amine oxide solvents as true one-component solvent systems as they usually must be dissolved either in water or organic solvent (dimethyl formamide (DMF) or dimethyl sulfoxide (DMSO)) due to their solid and/or explosive nature at room temperature [31]. On the other hand, NMMO loses its capability to dissolve cellulose upon hydration by two or more water molecules [132].

The mechanism of cellulose dissolution in this family of solvents is accompanied by the strong intermolecular interaction between cellulose and a strong N → O dipole. The interaction may be interpreted as the formation of a hydrogen bond complex with a superimposed ionic interaction, as shown in Fig. 12.4 [63].

The earliest studies of electrospinning cellulose from NMMO water solutions [87] reported formation of fibers between 3 and 10 μm in diameter and noted

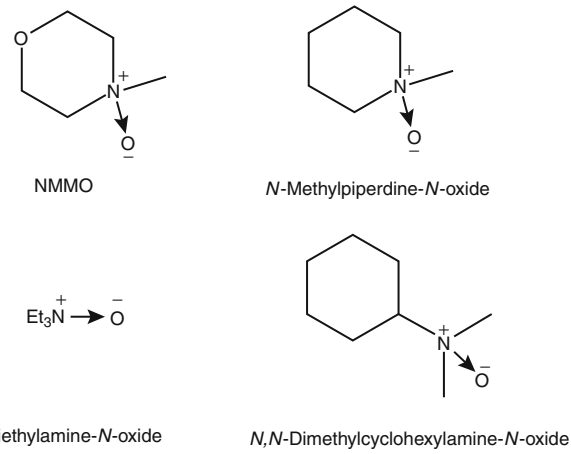

Fig. 12.3 Structures of one-component tertiary amine oxide solvents for dissolution of cellulose

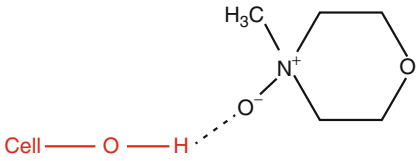

Fig. 12.4 A hydrogen bond complex between cellulose and NMMO during the dissolution

instability of fibers collected directly on a grounded surface. Fibers collected directly on a grounded surface would retain NMMO solvent and, over time, lose fiber shape and revert to film morphology. To overcome this difficulty, fibers were collected in a water bath and coagulated as excess solvent diffused into the bath. Finer fibers, with diameters ranging from 250 to 750 nm, were prepared by making two significant changes to the spinning apparatus [114]. First, the temperature of the spinning unit was carefully controlled between 70 °C and 110 °C, and increasing temperature was correlated with a measurable decrease in the spinning dope viscosity and a corresponding decrease in fiber diameter. Secondly, a rotating disk formed the grounded collector for the fibers.

Another approach to coagulating electrospun cellulose fibers was to use a flowing water bath [121]. Coagulation was found to be limited when fibers were electrospun directly onto a stationary water surface. Fibers would build up on the fiber surface and eventually spread into a film. The addition of a surfactant to the stationary bath allowed fibers to sink but did not prevent film formation. Incorporation of a moving bath prevented electrospun fibers from agglomerating and allowed fibers with diameters between 200 and 500 nm to be collected. Only Khil et al. [109] reported a successful collection of cellulose fibers electrospun from nNMMO/H_2O solution without incorporating a coagulation step. Fibers were successfully collected on a rotating, translating mandrel and washed with distilled water after the electrospinning process was complete.

4.1.2 Lithium Chloride (LiCl)/Dimethylacetamide (DMAc)

As stated previously, LiCl/DMAc is a common solvent system which can be applied for direct electrospinning of cellulose. However, this system has its own benefits and drawbacks. Various sources of cellulose can be dissolved in LiCl/DMAc with different range of concentrations without any side reactions, however, preparation of solution for electrospinning is challenging [202]. Frey et al. reported electrospinning of cellulose in LiCl/DMAc as a solvent system and produced a non-woven mat with diameter 250–750 nm [112]. They pretreated cellulose with water, then solvent was exchanged at 55 °C with DMAc before preparing the electrospinning solution. It was observed that with the combination of heated collector to remove the DMAc and water coagulant to eliminate LiCl, stable and dry cellulose fiber could be fabricated. No obvious degradation and no changes in thermal stability of cellulose were seen because of electrospinning. The authors claimed that these cellulose fibers have potential for filtration. In 2006, Kim et al. used the same process to produce cellulose nanofiber by the solvent system and obtained the same results [114]. They compared the solvent with NMMO/H_2O solvent and showed the amorphous structure for LiCl/DMAc in comparison with various amounts of crystallinity in the NMMO/H_2O system.

Two years later, a novel method was used to improve orientation of cellulose fibers to improve piezoelectricity of an electro-active paper actuator (EAPap) [247]. The procedure was composed of four steps: solution preparation (cellulose and LiCl/DMAc) and electrospinning, vacuum drying at ambient temperature, filling pores of electrospun cellulose with DMAc solution, and wet-drawing up to 10 % strain. Results of X-ray diffraction (XRD) and scanning electron microscopy (SEM) analysis exhibited greater crystalinity and multi-layer structure of electrospun cellulose compared with a spin-cast film of cellulose [247]. In line with previous work, Lee et al. fabricated electrospun cellulose membrane in LiCl/DMAc solvent at 2 wt% concentration (Lee et al. 2009). Hot air (around 80 °C) was utilized on a rotating collector to remove moisture and solvent. In addition, they used mechanical drawing to increase orientation and crystallinity of the membrane and therefore could use the membrane for an EAPap application.

4.1.3 Ionic Liquids (ILs)

The disadvantages of traditional processes for dissolution of cellulose, such as xanthate and cuprammonium processes, include environmental problems, high cost, use of uncommon solvents with great ionic strength [258], necessity of multiple steps pre-treatment, and prolonged stirring [69]. ILs are organic salts with low melting point, below 100 °C [126, 149]. They are used extensively to dissolve cellulose [186, 253]. Room-temperature ionic liquids (RTILs) consist of an inorganic or organic anion and an organic cation [162]. In 1934, Graenacher discovered that cellulose can be dissolved in molten salt. Some decades later, Roger and coworkers investigated the dissolution of cellulose in ILs, which could be melted in lower temperatures [228].

Several common ILs have been examined to dissolve cellulose and biopolymers: 1-butyl-3-methylimidazolium chloride (BMIMCl), 1-ethyl-3-methylimidazolium chloride (EMIMCl), 1-butyl-3-methylimidazolium acetate (BMIMAc), and 1-ethyl-3-methylimidazolium acetate (EMIMAc) [111, 117]. Liebert and Heinze reported that only ILs with imidazolium, pyridinium, and ammonium cations can dissolve cellulose [136]. In another words, they imply that cellulose only interacts with organic salt including asymmetric cations. Some researchers believe that particularly the anion parts of ILs can disrupt the hydrogen bonding of cellulose and dissolve it [216].

ILs exhibits notable and attractive characteristics, such as very low vapor pressure, great thermal stability, and capability to use at moderate or ambient temperatures. Because of nontoxicity and recyclability they are known as a "green solvents." In addition, by blending different anions and cations, some properties of ILs such as solubility, polarity, and viscosity can be changed [157, 237, 249]. For first time, in 2006, branched and smooth surface electrospun cellulose fibers of micron to nanometer size were prepared using BMIMCl [227]. Briefly, the solution was prepared by heating of IL to 70 °C, adding cellulose, and then irradiation with microwave for 4–5 min. They observed that there is not any N or S in elemental analysis (C, H, N, S) of resultant fibers, which means that no RTIL exists in the fibers using a bath containing ethanol coagulant. A thromboelastography (TEG) test, which measures clotting of human blood, was similar to control sample. Two years later, Xu et al. introduced DMSO as a co-solvent, which reduced surface tension and viscosity, increased conductivity, and improved spinability of a solution including native cellulose with 1-allyl-3-methylimidazolium chloride (AMIMCl) [240]. They also reported that fiber formation can be enhanced by using a rotating collector covered by copper wires and increasing environmental humidity. Furthermore, FT-IR and XRD analysis showed a mostly amorphous structure for electrospun cellulose fibers. Electrospinning of cellulose with AMIMCl was not possible.

After modifying an electrospinning apparatus by adding a chamber with constant temperature to the syringe and also using a water bath for coagulation of fibers, Quan et al. fabricated cellulose fibers with BMIMCl [181]. They claimed that addition of DMSO to the solvent leads to smooth fibers with smaller diameter in comparison to only using BMIMCl. By increasing concentration from 1.5 % to 5 %, the morphology of fibers changed from blocks to thin fibers (at 4 %) and then large fibers (at 5 %). Based on XRD test, crystallinity of electrospun fibers was higher than regenerated films, however, thermogravimetric analysis (TGA) revealed lower thermal stability for electrospun fibers (Fig. 12.5).

The effect of water bath compared with water/ethanol bath to remove EMIMAc solvent from electrospun cellulose fibers was the topic of another investigation [159]. Ribbon fibers that were produced by water bath had lower IL extraction rate and greater surface area compared with cylindrical fibers from a mixture of water/ethanol as coagulant. These ribbon fibers showed a bovine serum albumin (BSA) affinity adsorption capacity. In the same year, Freire et al. added 1-decyl-3-methylimidazolium chloride (C_{10}MIMCl) to the same ionic liquid and obtained

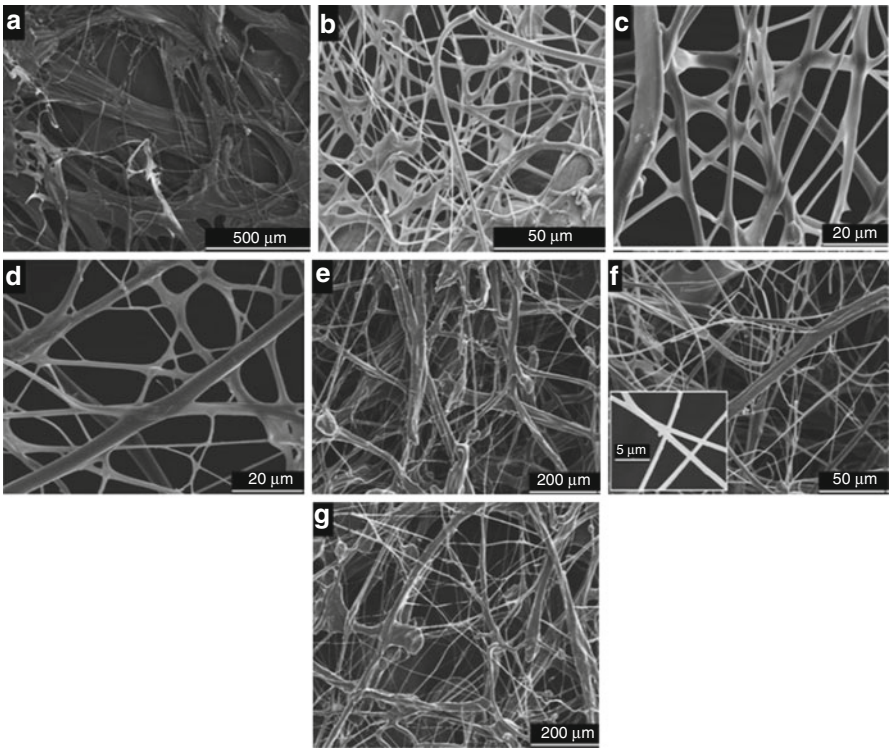

Fig. 12.5 SEM images of electrospun cellulose/BMIMCl with different cellulose concentrations:(**a**) 1.5 wt%, (**b**) 2.4 wt%, (**c**) 3 wt%, (**d**) 4 wt%, (**e**) 5 wt%, (**f**) 4 wt% with adding DMSO, (**g**) 5 wt% with adding DMSO [181]

fibers with more homogeneity and smaller diameters [66]. Fourier transform infrared spectroscopy (FT-IR) and XRD tests revealed lower crystallinity using a binary solvent system and also found that thermal stability of cellulose fibers by EMIMAc and EMIMAc/C_{10}MIMCl solvents was higher than regenerated cellulose casting film. Cellulose electrospun fibers and casting film were mostly amorphous with few crystalline parts.

The effect of three different co-solvents, DMAc, DMF, and DMSO, on the electrospinning of cellulose by EMIMAc was evaluated [78]. The viscosity of system based on DMSO was higher than two other systems, but by decreasing mole of IL solvent, the surface tension decreased. The binary solvent systems containing DMF and DMAc showed the highest and lowest conductivity, respectively. It was observed that the best cellulose fiber was formed by DMSO as a co-solvent. Ahn and co-workers increased spinnability of hemp fibres in EMIMAc by treatment of fibers with sodium hydroxide (NaOH) and sodium chlorite ($NaClO_2$) to reduce lignin content [11]. They obtained thinner fibers with uniform size distribution by decreasing lignin content. When lignin concentration was more than 6 %, only drops were formed. The author, in the same year, demonstrated that,

Table 12.3 Effect of different ionic liquids, coagulant, and collector on the diameter of electrospun cellulose nanofiber

Type of ionic liquid	Collector and coagulant	Nanofiber diameter	References
BMIMCl	Ethanol bath	Micro- to nanometer	Viswanathan et al. [227]
AMIMCl	Aluminum foil, aluminum foil in ethanol bath, rotating drum	100–800 nm	Xu et al. [240]
BMIMCl	Water bath, at constant temperature chamber (100 °C)	500–800 nm	Quan et al. [181]
EMIMAc	Coagulation bath filled with water or water/ethanol	100 nm	Miyauchi et al. [159]
EMIMAc and C_{10}MIMCl	Water coagulation bath	470 ± 110 nm for EMIMAc, 120 ± 55 nm for EMIMAc/C_{10}mimCl solvent	Freire et al. [66]
EMIMAc	Rotating collector submerged in water	–	Hardelin et al. [78]
EMIMAc	Rotating wired cylinder, ethanol as coagulant	–	Ahn et al. [11]
EMIMAc	Rotating wired cylinder, Ethanol as Coagulant	–	Ahn et al. [12]

in spite of the type of co-solvent (DMF or DMAc), higher concentration of co-solvent leads to thinner, uniform, high-crystalline fibers with more thermal stability in electrospinning solution of cellulose with EMIMAc [12]. Furthermore, it was observed that the influence of DMF on the diameter and crystallinity of fibers is more meaningful than DMAc (Table 12.3).

4.1.4 Trifluoroacetic Acid (TFA)

Ohkawa reported the first instance of electrospinning of two types of cellulose (cotton and wood pulp) with trifluoroacetic acid (TFA) or TFA/methylene dichloride (MC) as a solvent at room temperature [168]. The results showed that both solvents had similar effects. Also, FT-IR exhibited no residual solvent in fabrics, and XRD showed an amorphous structure of samples. In addition, electrospinning of pre-spun cellulose loaded with drugs indicated a large surface area of fabrics for releasing drugs and no phase separation between matrix and drugs. In line with Ohkawa's work, Montano-Leyva et al. used TFA, TFA/water, and TFA/acetic acid to prepare electrospun nanofiber from wheat straw [161]. They found that two binary solvent systems produce drops due to failure in solvent evaporation. Nonwoven fibers with tubular aggregates were fabricated by optimum condition of electrospinning (concentration 4 %, distance between needle to collector 7 cm, flow rate 1.5 mL/h, voltage 15 kV) with TFA. It was observed that the glass transition temperature of nanofibers was greater than cellulose, whereas degradation temperature was lower than cellulose. FT-IR showed formation of pure nanofibers and XRD exhibited reduction in crystallinity of nanofibers.

4.1.5 Other Direct Solvents

Ionic liquid solvents for cellulose, including BMIMCl, are touted as environmentally friendly solvents specifically because they are nonvolatile. Because evaporation of the solvent is not a possibility in electrospinning cellulose from ionic liquids, a coagulation bath is necessary. Cellulose fibers with diameters ranging from 500 nm to 10 μm have been formed by electrospinning cellulose from BMIMCl solution into an ethanol bath [227]. Cellulose solvents based on ethylene diamine/potassium thiocyanate (ED/KSCN) are similar to LiCl/DMAc in constituents of sufficiently volatile solvent and a salt. Diameters of fibers depended significantly on cellulose DP. Fibers spun from high molecular weight (DP. 1000) cotton cellulose had very fine segments with intermittent beads. Similar structures reported in LiCl/DMAc fibers [67] indicate that the nonvolatile salt component of the solvent may be incorporated in the beads. At low concentrations of lower molecular weight cellulose (DP ¼ 140), only droplets were formed. When a sufficient concentration of the low molecular weight cellulose was incorporated in the solvent, large fibers with a twisting structure were collected.

5 Electrospinning of Cellulose Composite Nanofibers

5.1 Polysaccharides

It is generally agreed that nanotechnology and new products such as nanocomposites from cellulose have the potential of to change the forestry industry and achieve new markets [58]. Cellulose and its particles have properties such as low cost and density, high strength and stiffness, renewability, availability, and biodegradability that make them attractive to use as a reinforcement for other materials [73, 148]. One type of cellulose particle is cellulose nanowhisker (CNW). By dissolving the amorphous region of cellulose via acid hydrolysis, rod-like CNW or cellulose nanocrystal (CNC) [85] with the length of few hundred nanometers and diameter of 5–20 nm can be obtained [27, 57].

5.1.1 Cellulose

Magalhaes et al. reported on a co-electrospinning process to generate nanofibers composed of cellulose in NMMO/H_2O in the shell and a CNC suspension in the core, using hot air (~120 °C) blown on the syringe and a stationary collector immersed in cold water (10 °C) [145]. It was found that with reduction of volume ratio of shell solution to core suspension, voltage and flow rate tend to fabricate individualized fibers. Lower viscosity of NMMO/H_2O led to easier electrospinning of CNC suspensions compared with a NMMO/DMSO solvent system. Interestingly, crystallinity and physical characterization of composite nanofibers were lower than that of electrospun neat cellulose. It was observed that absence of CNC causes greater crystallinity indices of FT-IR. The incorporation of this particle as a reinforcing

phase into a matrix and generation of nanocomposites is a result of this obvious improvement in mechanical characterization at very low concentration [35]. Finally, from differential thermogravimetric (DTG) thermograms and FT-IR test's Magalhaes et al. concluded that the concentration of CNC and the formulation of cellulose solution are two critical parameters during co-electrospinning of cellulose/CNC nanocomposites [145].

They also reported on a slightly modified process utilizing a rotating wire collector to fabricate oriented cellulose/CNC composite fibers and to prevent agglomeration [146]. They found that in co-electrospinning of this mixture, suitable dispersion of CNC in cellulose can be obtained by DMSO suspension in comparison with water suspension. It is worth mentioning that reinforced cellulose nanocomposite fibers had lower crystallinity, but greater alignment and adhesion of amorphous cellulose fibers resulted in higher tensile stress and modulus of elasticity of cellulose film reinforced with CNC.

5.1.2 Chitosan

Chitosan is a polysaccharide that is prepared from de-acetylation of chitin [153]. Chitin is extracted from crustaceans (shrimp and crabs) or is produced via a fungal fermentation [239]. Chitosan has promising properties such as good biocompatibility [167], wound healing characteristics, biodegradability, antimicrobial activity [71, 201], chemical-resistance, nontoxicity, and good film-forming ability [208], and has potential to be used in various industries. The rigidity and brittle properties of chitosan, along with its weak solubility, are the main reasons for restricted utilization of this polymer [200]. Because chitosan is powerfully interacting polymer, it can be blended with other materials [36, 59] like polylactic acid (PLA) [171], collagen (Chen et al. 2007), polyvinyl alcohol (PVA) [194], PEO [51], and polycaprolactone (PCL) [203]. Blending of cellulose and chitosan, similar to other mixing systems, yields the desirable advantages of both materials [56]. Because generating electrospun chitosan nanofiber with EMIMAc is difficult (because of its restricted solubility and cationic nature). Park et al. prepared electrospun hybrid nanofibers using EMIMAc, 0.25 wt% chitosan, and 0.5 wt% cellulose [170]. Energy-dispersive X-ray spectroscopy (EDS) nitrogen mapping showed homogeneous dispersion of chitosan on the surface. The micron-size composite nanofibers created a large surface area and can retain a good amount of water as a wound dressing.

5.2 Lignocellulosic Component

5.2.1 Lignin

Lignin is the most abundant phenolic polymer in the plant cell wall, which principally produced by the Kraft pulping method [138]. The two main types of lignin are guaiacyl and guaiacyl-syringyl [106]. Two approaches are applied to incorporate

lignin in polymer materials. The first one incorporates a large quantity of lignin to synthetic polymers, which leads to reduction of the mechanical characterization of the materials. The second approach is the addition of a lower concentration of lignin [178]. In general, lignin is a material with great recovery potential, low cost, low degree of pollution, and availability from different renewable resources [176]. In addition, it reinforces the middle layer of wood-plants and cell walls [8], conducts water, and defends plants against pathogens [196].

Ago and coworkers studied the effect of various compositions of CNC on the electrospinning of lignin-PVA matrix [10]. Lignin-PVA bead-free fibers were generated by weight ratio of 75 to 25. Furthermore, addition of lignin caused an increase in conductivity and viscosity and a decrease in surface tension of this bi-component solution. Three separated domains were obtained by a ternary diagram including beaded fiber, fibers without beads, and macro-size phase separation. Electrospinning of two component lignin-based composite nanofibers using PEO [49] and polyacrylonitrile (PAN) [204] have been reported. In the multi-component case (lignin/PVA/CNC), Ago's investigation revealed that, with addition of CNC, the viscosity and surface tension of solution increased due to the interaction between CNC and lignin, specifically at 75:25 of lignin to PVA [10]. They concluded that this interaction, basically from hydrogen bonding, led to better dispersion of CNC in the lignin-PVA matrix and improved thermal stability of the composite fibers.

5.3 Protein Polymer

5.3.1 *Bombyx mori* Silk Fibroin

Silk fiber is composed of fibroin cores surrounded by sericin [174]. The fibroin consists of heavy-chain and light-chain macro molecules linked together through a disulfide bond [93]. These fibers are rigid and strong, and they are generated from aqueous solution using silkworms at ambient temperature [17]. Some desirable characterizations of silk are low in vivo degradation rate, biocompatibility, easy chemical modification, and luster [190]. In the case of silk nanofibers, high surface area and surface energy, great strength, conductivity. and thermal properties make them good candidates for textile, biomedical. and electrical fields [21].

Huang et al. employed CNW to reinforce electrospun silk fibroin (SF) nanofiber [89]. They observed that the diameter of CNW-SF composite nanofibers is 77–160 nm because of increasing conductivity of solution, whereas in the case of unreinforced nanofibers it is 250 nm. The CNW oriented along the axis of fiber, was well dispersed in the matrix, and uniform and smooth composite nanofibers without bead were generated (Fig. 12.6).

In addition to blending CNW with silk, there has been extensive interest in expansion of nanofibers based on silk with other materials such as carbon nanotubes (CNT) [22, 105], chitosan [34], and hydroxyapatite [236]. Huang and co-workers displayed that the Young's modulus and tensile strength of CNW/SF nanofibers grew with an increase in the CNW concentration due to the formation of hydrogen

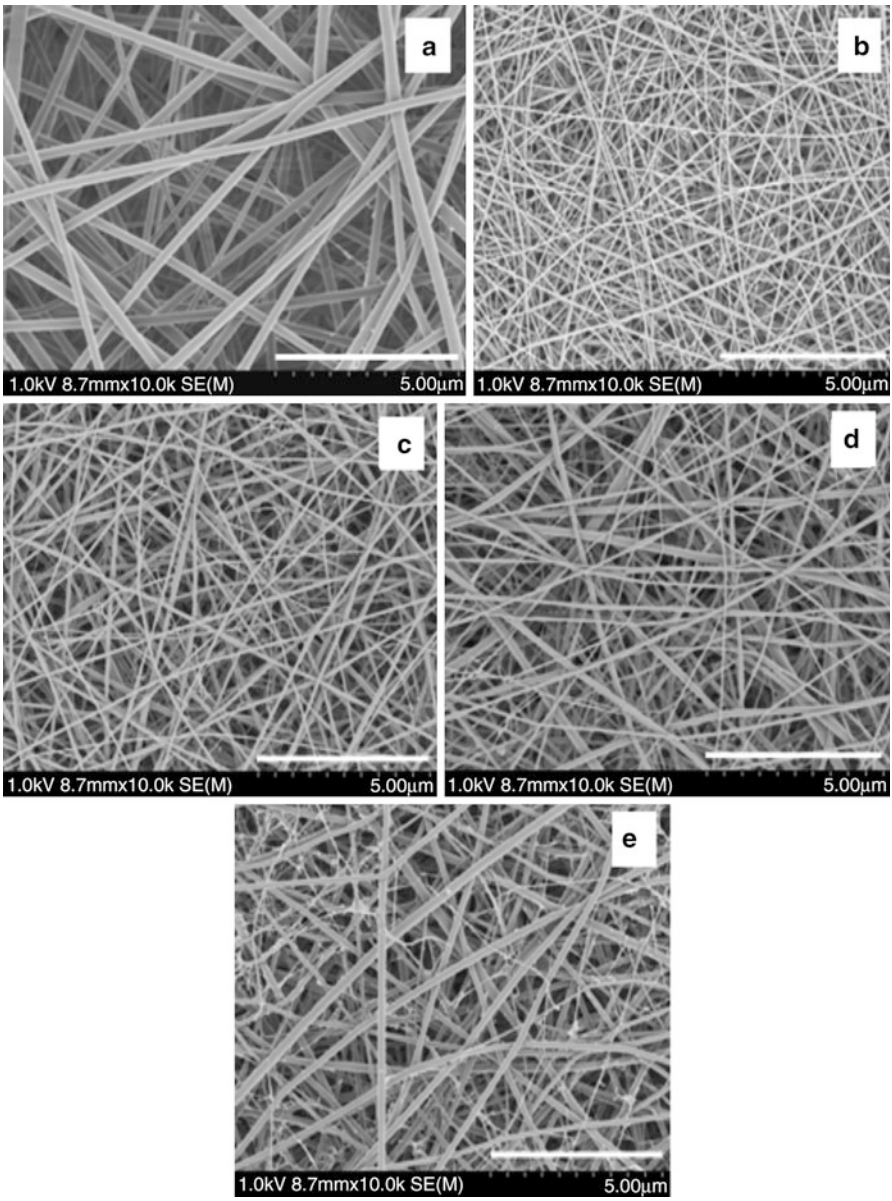

Fig. 12.6 FE-SEM micrographs of electrospun SF nanofiber with different CNW values: (**a**) 0, (**b**) 1, (**c**) 2, (**d**) 3, and (**e**) 4 w/w% [89]

bonds between hydroxyl groups of CNW and hydroxyl, amide, carboxyl, and amine groups of SF and good dispersion of CNW in SF [89]. They reported that the reduction in the strain at break is due to the needle structure of CNW and the semi-rigid structure of cellulose.

5.4 Synthetic Fiber

5.4.1 Meta-aramid

Aramids are classified as strong artificial and heat-resistant fibers [30]. Because of their high rigidity, backbone conjugation, and large amount of hydrogen bonding, meta-aramid (Ar) fibers can be difficult to dissolve in common solvents [244, 256]. Yao et al. prepared Ar-cellulose electrospun composite nanofiber using LiCl/DMAc solvent and compared it with electrospun composite nanofiber of Ar-CA [245]. The homogenous solution of Ar-cellulose and Ar-CA was formed due to new interactions between amide and hydroxyl groups of Ar and cellulose or CA. Also, by increasing the concentration and weight ratio of composite solution, the number of beads was reduced. It was found that higher viscosity and surface tension of Ar/cellulose made it less favorable for electrospinning than Ar-CA, and uniform nanofibers were formed by a solution containing 2:1 Ar/CA and 6:1 Ar/cellulose. Compared with the polymers, composite nanofibers exhibited less stable thermal properties because hydrogen bonds were broken and crystallinity was reduced after dissolving. The Ar/CA and Ar/cellulose showed three and two weight loss processes, respectively. By incorporation of cellulose or CA, new interactions were formed and led to increasing modulus and improvement in mechanical characteristics of composite nanofibers.

5.5 Thermoplastic Polymers

5.5.1 Poly(ethylene-co-vinyl alcohol) (EVOH)

Hybrid CNW and EVOH fibers generated by means of electrospinning have a more uniform morphology than pure polymer electrospun fibers. The treatment of purified bacterial cellulose with sulfuric acid is an effective way to extract cellulose nanowhiskers, consisting of highly crystalline cellulose I structures of nanofibrils aggregates. However, the thermal stability of the repeatedly washed cellulosic material was seen to decrease after the sulfuric acid treatment. A morphology of fewer beaded fibers, with the smallest diameter, was obtained with centrifuged CNWs and an increase in the concentration up to 8 wt%.

Taking into account the relative increase in the glass-transition temperature (Tg) as well as the degree of incorporation of CNW into the electrospun fibers calculated from the FT-IR spectra, it was confirmed that a more effective incorporation of nanowhiskers was achieved when adding them in the form of a centrifuged precipitate without applying sonication [152]. Sonication was found to more efficiently increase the Tg of the composite per filler content, probably due to stronger induced interfacial interaction of the CNWs with the matrix. Additionally, sonication improved the incorporation level of the nanofiller when added as a freeze-dried product, although it produced the contrary effect on centrifuged nanowhiskers. These results highlight the adequacy of the method developed for the incorporation and proper dispersion of CNW into EVOH matrixes, which yielded novel hybrid electrospun fibers.

5.5.2 Poly Methyl Methacrylate (PMMA)

Uniform fibers composed of PMMA reinforced with progressively increasing contents of CNC, up to 41 wt% CNC, have been successfully produced by electrospinning. The morphological, thermal, and nano-mechanical properties of the composite submicron fibers were investigated. The CNCs derived from wood pulp by sulfuric acid hydrolysis were well dispersed in solutions of PMMA and the processing solvent DMF prior to fiber formation. Well-formed fibers with controllable diameters were generated reproducibly at all CNC contents investigated. including 41 wt%. The orientation of the CNCs along the fiber axis was facilitated by the electrospinning process and was observed directly via microscopy examination. Shifts in thermal transitions of PMMA with increasing CNC content suggest hydrogen bonding interactions between CNC hydroxyl groups and carbonyl groups on the PMMA matrix. Nano-scale dynamic mechanical analysis (nanoDMA) was performed using nano indentation on single fibers perpendicular to the fiber axis. Many of the current challenges associated with single fiber nano indentation are addressed, such as fiber diameter range and minimum, depth to diameter ratio, and valid depth range under these experimental conditions. Fibers that contained 17 wt% CNCs showed a modest increase of 17 % in the storage modulus of PMMA, a high modulus polymer of interest for transparent composite applications [54].

The electrospinning process also facilitated alignment of CNCs along the fiber axis, making it feasible to use aligned electrospun fibers as an aid for CNC alignment in polymer composites. Thermal analysis revealed that the glass transition temperature of PMMA was increased with incorporation of CNCs, suggesting hydrogen bonding interactions between carbonyl in the ester groups of PMMA and hydroxyl groups on CNC surface. These studies present a method for incorporating evenly distributed CNCs into fibers, thin films, and composites in a manner that facilitates CNC alignment. The demonstrated alignment of CNCs along the fiber's long axis provides a new approach to orient CNCs with desired directions in polymer composites. For example, it may be feasible to achieve alignment of CNCs or whiskers in both thin-film and bulk polymer composites through application of pressure at an elevated temperature to layers of one-dimensional aligned nanocomposite fiber mats interspersed with the matrix polymer.

5.5.3 Polystyrene (PS)

PS is a thermoplastic polymer. It is a vinyl polymer that is one of the most widely used plastics; only polythene is more common. PS is an inexpensive and hard plastic with limited flexibility, and it is a colorless in pure conditions. The most serious deficiencies are its low impact strength and poor chemical resistance. It can be cast into moulds with fine detail. Solid polystyrene is used, for example, in plastic models, CD and DVD cases, packaging materials, insulation and foam drink cups, toys, and the housings of things like hairdryers, computers, and kitchen appliances. Table 12.4 lists the mechanical properties of PS.

The electrospinning process was performed at room temperature in a solution of cyclohexane, DMF, and tetrahydrofuran (THF) (70 %, 20 %, and 10 %, respectively), while the ratio of SEBS-g-MA to the solution was 10 %. An increase in

Table 12.4 Properties of PS

Properties	Polystyrene
Density	0.00800–2.14 g/cc
Hardness, shore D	36.0–83.0
Tensile strength, yield	10.3–539 MPa
Elongation at yield	0.600–75.0 %
Modulus of elasticity	0.00120–35.2 GPa

water content of the solution and a decrease of feeding rate resulted in deformation of nanofibers and thinning the fibers, respectively. The former was caused by aggregation of CNW and also slower evaporation of solvents in the presence of water contents [19]. In the parallel study, the same polymer as above was electrospun with cellulose CNW using two different methods. The single-nozzle method in which the polymer solution does not have any water content was preferable to the coaxial nozzle method with regard to thermal, mechanical, and morphological properties.

5.5.4 Polyethylene Oxide (PEO)

PEO is a synthetic polyether that is readily available in a range of molecular weights. Low molecular weight (Mw < 1,000) PEO is viscous and colorless liquid, while higher molecular weight PEO is a white solid with melting points proportional to molecular weight, to an upper limit of about 67 °C. It is a water-soluble thermoplastic resin, as well as being soluble in many organic solvents (e.g., methylene chloride, ethanol, toluene, acetone, and chloroform). PEO is used as a thickener in drug delivery, in tissue engineering scaffolds, and in other applications in many industries [257]. A series of PEO/CNC composite nanofibrous mats with different CNC loadings was successfully fabricated via an electrospinning process. A morphological investigation of the obtained nanofibrous mats demonstrated that the transition from homogeneousness to heterogeneousness in their microstructures was achieved by tailoring the concentration of electrospinning solutions from 5 to 7 wt%. PEO/CNC nanofibers became more uniform and finer with the increased CNC content because of the enhanced electric conductivity of electrospinning solutions (Fig. 12.7).

With the decrease in the needle diameter, as-spun nanofibers showed improved size uniformity. The heterogeneous composite mats were composed of rigid-flexible bimodal nanofibers. It was also indicated that CNCs effectively improved the mechanical properties of both types of nanofibrous mats. This was ascribed to the efficient stress transfer from PEO to CNCs, originating from their strong interactions and the uniform dispersion and high alignment of CNCs in the electrospun fibers. When a smaller diameter needle was used in the spinning of homogeneous network mats, enhanced thermal and mechanical properties were obtained. Moreover, the mechanical properties of heterogeneous nanofibrous mats were better than those of their homogeneous counterparts for all compositions (0–20 wt% CNC contents). It was demonstrated for the first time

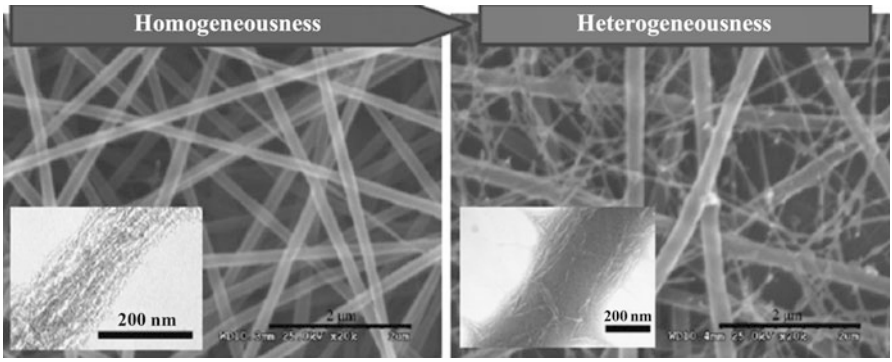

Fig. 12.7 SEM images of electrospun PEO

that the heterogeneous nanofibrous microstructure made of rigid-flexible bimodal nanofibers is especially beneficial to the mechanical properties of electrospun composite nanofibrous mats [75, 195, 223].

5.5.5 Polylactic Acid (PLA)

PLA/CNW composite nanofibers have been successfully produced by electrospinning through mixtures of cellulose whiskers with PLA solution. The effects of CNW on the microstructure and thermal behavior of electrospun PLA nanofibers have been investigated in this study [7]. The PLA/CNW composite nanofibers were successfully produced by electrospinning the mixtures of cellulose whiskers with PLA solution. The diameters of PLA and its composites were around 300 nm. Scanning electron micrographs showed that the CNWs do not protrude out of the outer surfaces of PLA nanofibers. The existence of CNWs in the electrospun PLA matrix nanofibers and the microstructural evolution were investigated using X-ray diffraction. FT-IR analysis showed various functional groups present in the PLA/CNW composites attributing to their chemical interactions [141]. The electrospun PLA and PLA/CNW composites revealed low crystallinity due to the rapid solvent evaporation and relatively slow crystallization kinetics characteristic of PLA. The electrospun nanofibers showed particularly different thermal behavior from that of the solution-cast films.

The nanofibers of pure PLA and PLA/CNW experience two consecutively overlapping crystallization processes. The CNWs act as heterogeneous sites for nucleation of PLA by decreasing the cold crystallization onset temperature. The incorporation of CNW into PLA nanofibers is expected to improve mechanical properties and bring new functionalities to the electrospun matrix nanofibers.

5.6 Carbon Nanotube (CNT)

Since the introduction of the CNT in 1991, it has the subject of many studies [92]. CNTs are fabricated by folding graphene sheets in a cylindrical form [38, 251]. Generally, there are two types of CNT: single-wall carbon nanotube (SWCNT) and

multi-wall carbon nanotube (MWCNT) [166, 246]. The nano diameter of CNT makes it more desirable than micrometer graphite fibers [198]. Geng et al. noticed that CNTs have 10,000 or higher aspect ratio, diameter of a few nanometers, 1–2 TPa elastic modulus, and higher electrical conductivity compared with copper wire [72]. In addition, they can be semi-conducting or metallic based on diameter and wrapping angle [150].

CNTs have potential applications in such fields such as electronics and sensors, specifically as a reinforcement in order to generate new, stronger composite materials [15, 147]. The surface nature of CNTs and interactions between them can cause agglomeration, so good dispersion of CNTs in the polymer matrix is necessary for better mechanical and thermal properties for nanocomposites [151]. In this perspective, various CNT-reinforced polymers have been fabricated by the electrospinning process with aliginate [94], PAN [179, 234], PVA [248], polybutylene terephthalate (PBT) [197], and PCL [192].

5.6.1 Multi-wall Carbon Nanotube (MWCNT)

Dry-jet-wet electrospinning was applied to fabricate smooth-surface white cellulose and black cellulose/MWCNT composite fibers with AMIMCl [254]. The storage modulus and tensile strength of composite nanofibers containing 4 wt% MWCNTs increased 2.5 times and 40 % at ambient temperature. In addition, the greatest conductivity was obtained in this composition. The results also displayed better mechanical properties with increasing temperature. MWCNT are composed of several sheets [48, 122] with graphene layer separation of 0.34 nm, 1 nm diameters, and large aspect ratio [177]. Zhang et al. reported that improved mechanical characteristics and thermal properties were related to good interaction of MWCNT and cellulose and, therefore, good distribution and alignment of MWCNT in the matrix [254].

Preparation of hybrid nanofibers with 200–500 nm diameter composed of 5 wt% bacterial cellulose (BC), AMIMCl, DMSO, and 0.02 wt% acid-treated MWCNTs by the electrospinning process was the main objective of an investigation conducted by Chen and his groups [41]. Acid treatment was done to create functional groups at the surface of MWCNT and to decrease its length. These fibers assembled on rotating parallel wires with a 1-cm gap and coagulated in ethanol. BC is a type of cellulose that can be produced using many microorganisms. Despite the properties of cellulose, BC shows its own particular properties such as great degree of polymerization [205], high purity, and high mechanical performance [163]. Chen et al. demonstrated that pure BC, electrospun BC, and electrospun BC/MWCNT have degradation temperatures around 203 °C, 237 °C and 260 °C, respectively [41]. It was noted that good dispersion, alignment, and addition of MWCNT leads to increasing modulus as well as the tensile strength of the hybrid fibers to around 290 % and 280 %. It was found that the conductivity of the BC/MWCNT composite nanofibers increased.

5.6.2 Single-wall Carbon Nanotube (SWCNT)

The SWCNT consists of a single sheet [165, 211] with 0.4–2 nm diameter, lengths up to 1.5 cm. and aspect ratio of over 10 million [16]. Factorial testing as well as design of experiments (DOE) were two means that Pankonian et al. used to

determine the optimum condition for electrospinning of cellulose and cellulose/SWCNT in DMAc [169]. For electrospinning of cellulose, they applied hot air blowing (around 90 °C) to the needle, while for cellulose/SWCNT an unheated setup was utilized. Desirable voltage and flow rate for electrospinning of cellulose were 20 kV and 0.90–1.50 mL/h, in contrast to 14 kV and 2.5–4.5 mL/h for cellulose embedded in SWCNT.

6 Applications of Electrospun Cellulose Composite Nanofibers

Over the past few years, increasing attention has been paid to composite materials based on natural fibers as a renewable resources instead of artificial fibers because of their lower cost and environmentally friend nature [107]. Among these renewable resources, cellulose has gained more consideration because of its abundance and notable characteristics [238]. The excellent mechanical properties of cellulose, which are derived from its strong hydrogen bonds [175], lead to increasing interest to incorporate cellulose with other materials for fabrication of composite fibers. As mentioned in previous sections, electrospinning is a simple and versatile method [233] that can be employed to produce continuous, long, highly oriented fibers with a good drawing rate [261], from micron to nanometer [91]. Many applications have been determined for electrospun hybrid fibers—filtration, energy, biotechnology, and sensors, to name a few [193]. Various applications have defined for electrospun cellulose composite nanofibers, including antibacterial textiles for wounds [170], filtration and catalysis [89], precursors for production of cellulose-based carbon fibers [254], and electrical and mechanical applications [41].

7 Conclusion

Recent advances in the field of electrospun nanofibers demonstrate their enormous potential in various applications. In this respect, Cellulose Nanofibers (CNFs) have been examined because of their properties such as renewability, biodegradability, and low cost. The main obstacle that must be overcome for effective electrospinning of cellulose is the need for a superior solvent, inasmuch as cellulose cannot be dissolved in common solvents. However, the use of different solvent systems like NMMO/H_2O, LiCl/DMAc, and ionic liquids has shown that electrospinning of cellulose is possible. A cellulose solution for electrospinning is prepared by dissolving a suitable amount of cellulose samples in various solvent systems and stirring until a homogenous solution is obtained. In spite of significant improvements, a comprehensive study is needed to overcome the disadvantages of the current solvent systems, including environmental problems, the high temperature required for electrospinning, and lack of control.

Cellulose's strong hydrogen bonds and the high surface area to volume ratio in nano cellulose lead to high mechanical strength of this material. For this reason, electrospun cellulose hybrid nanofibers have attracted much attention.

Briefly, solutions for electrospinning of cellulose composite nanofibers are prepared by incorporating the desired weight percentage of cellulose with various matrixes and suitable solvents, and then stirring to obtain an entirely transparent solution. Although much research has been concentrated on this concept, it is still a new subject that needs further studies.

References

1. Abbott A, Bismarck A (2010) Self-reinforced cellulose nanocomposites. Cellulose 17:779. http://link.springer.com/article/10.1007/s10570-010-9427-5
2. Abdel-Hady F, Alzahrany A, Hamed M (2011) Experimental validation of upward electrospinning process. ISRN Nanotechnol 2011:1
3. Abdul Khalil HPS, Issam AM, Ahmad Shakri MT, Suriani R, Awang AY (2007) Conventional agro-composites from chemically modified fibers. Ind Crop Prod 26:315
4. Abdul Khalil HPS, Siti Alwani M, Ridzuan R, Kamarudin H, Khairul A (2008) Chemical composition, morphological characteristics, and cell wall structure of Malaysian oil palm fibers. Polym Plast Technol Eng 47:273
5. Abdul Khalil HPS, Yusra AFI, Bhat AH, Jawaid M (2010) Cell wall ultrastructure, anatomy, lignin distribution, and chemical composition of Malaysian cultivated kenaf fiber. Ind Crop Prod 31:113
6. Abdul Khalil HPS, Bhat I, Ireana Yusra AF, Sanusi ZA, Hezri AA (2011) Broad perspective of palm oil for non- food applications for sustainable tomorrow. Nova Science, New York
7. Abdul Khalil HPS, Bhat AH, Ireana Yusra AF (2012) Green composites from sustainable cellulose nanofibrils: A review. Carbohydr Polym 87:963
8. Abreu HS, Latorraca JVF, Pereira RPW, Monteiro MBO, Abreu FA, Amparado KF (2009) Supramolecular proposal of lignin in structure and its relation with the wood proprieties. An Acad Bras Cienc 81:137
9. Adomaviciute E, Milasius R, Levinskas R (2007) The influence of main technological parameters on the diameter of poly (vinyl alcohol)(PVA) nanofibre and morphology of manufactured mat. Mater Sci 13:152
10. Ago M, Okajima K, Jakes JE, Park S, Rojas OJ (2012) Lignin-based electrospun nanofibers reinforced with cellulose nanocrystals. Biomacromolecules 13, pp 918–926
11. Ahn Y, Lee SH, Kim HJ, Yang YH, Hong JH, Kim YH, Kim H (2012) Electrospinning of lignocellulosic biomass using ionic liquid. Carbohydr Polym 88:395
12. Ahn Y, Hu DH, Hong JH, Lee SH, Kim HJ, Kim H (2012) Effect of co-solvent on the spinnability and properties of electrospun cellulose nanofiber. Carbohydr Polym 89:340. http://journals.ohiolink.edu/ejc/article.cgi?issn=01448617&issue=v89i0002&article=340_eocotsapoecn
13. Aluigi A, Vineis C, Varesano A, Mazzuchetti G, Ferrero F, Tonin C (2008) Structure and properties of keratin/PEO blend nanofibres. Eur Polym J 44:2465
14. Amiraliyan N, Nouri M, Haghighat Kish M (2009) Electrospinning of silk nanofibers. I. An investigation of nanofiber morphology and process optimization using response surface methodology. Fiber Polym 10:167
15. Ando T (2009) The electronic properties of graphene and carbon nanotubes. NPG Asia Mater 1:17
16. Arranz-Andreś J, Blau WJ (2008) Enhanced device performance using different carbon nanotube types in polymer photovoltaic devices. Carbon 46:2067
17. Asakura T, Yamane T, Nakazawa Y, Kameda T, Ando K (2001) Structure of Bombyx mori silk fibroin before spinning in solid state studied with wide angle x-ray scattering and 13C cross-polarization/magic angle spinning NMR. Biopolymers 58:521

18. Ashammakhi N, Ndreu A, Nikkola L, Wimpenny I, Yang Y (2008) Advancing tissue engineering by using electrospun nanofibers. Regen Med 3:547
19. Ayaz O, Ucar N, Bahar E, Oksuz M, Ucar M, Onen A, Demir A, Wang Y (2011) Production and analysis of composite nanofiber and heat applied nanofiber. In: International congress of innovative textiles, İstanbul, pp. 20–22
20. Ayaz O, Ucar N, Bahar E, Ucar O, Oksuz M, Onen A, Ucar M, İşmar E, Demir A (2012) Properties of composite nanofiber produced by single and coaxial nozzle method used for electrospinning technique. WASET 61:345
21. Ayutsede J, Gandhi M, Sukigara S, Micklus M, Chen HE, Ko F (2005) Regeneration of Bombyx mori silk by electrospinning. Part3: characterization of electrospun nonwoven mat. Polymer 46:1625
22. Ayutsede J, Gandhi M, Sukigara S, Ye H, Hsu CM, Gogotsi Y, Ko F (2006) Carbon nanotube reinforced Bombyx mori silk nanofibers by the electrospinning process. Biomacromolecules 7:208
23. Baji A, Mai YW, Wong SC, Abtahi M, Chen P (2010) Electrospinning of polymer nanofibers: effects on oriented morphology, structures and tensile properties. Compos Sci Technol 70:703
24. Balamurugan R, Sundarrajan S, Ramakrishna S (2011) Recent trends in nanofibrous membranes and their suitability for air and water filtrations. Membranes 1:232
25. Baley C (2002) Analysis of the flax fibres tensile behaviour and analysis of the tensile stiffness increase. Compos A 33:939
26. Baumgarten PK (1971) Electrostatic spinning of acrylic microfibers. J Colloid Interface Sci 36:71
27. Beck-Candanedo S, Roman M, Gray DG (2005) Effect of reaction conditions on the properties and behavior of wood cellulose nanocrystal suspensions. Biomacromolecules 6:1048
28. Bhardwaj N, Kundu SC (2010) Electrospinning: a fascinating fiber fabrication technique. Biotechnol Adv 28:325
29. Bjorge D, Daels N, Vrieze SD, Dejans P, Camp TV, Audenaert W, Hogie J, Westbroek P, Clerck KD, Hulle SWHV (2009) Performance assessment of electrospun nanofibers for filter applications. Desalination 249:942
30. Blascu V (2010) Aramid fibers for technical textiles II. Forms, availability and applications. Bul Inst Polit Iasi t LVI (LX) f.1: 9
31. Bochek A, Petropavlovsky G, Kallistov O (1993) Dissolution of cellulose and its derivatives in the same solvent, methylmorpholine-N-oxide and the properties of the resulting solutions. Cellul Chem Technol 27:137
32. Bognitzki M, Czado W, Frese T, Schaper A, Hellwig M, Steinhart M, Greiner A, Wendorff JH (2001) Nanostructured fibers via electrospinning. Adv Mater 13:70
33. Boss HL, Van Den Oever MJA, Peters OCJJ (2002) Tensile and compressive properties of flax fibres for natural fibre reinforced composites. J Mater Sci 37:1683
34. Cai ZX, Mo XM, Zhang KH, Fan LP, Yin AL, He CL, Wang HS (2010) Fabrication of chitosan/silk fibroin composite nanofibers for wound-dressing applications. Int J Mol Sci 11:3529
35. Cao X, Habibi Y, Magalhães WLE, Rojas OJ, Lucia LA (2011) Cellulose nanocrystals-based nanocomposites: fruits of a novel biomass research and teaching platform. Curr Sci 100:1172
36. Castro C, Gargallo L, Leiva A, Radic D (2005) Interactions in blends containing chitosan with functionalized polymers. J Appl Polym Sci 97:1953
37. Celebioglu A, Uyar T (2010) Cyclodextrin nanofibers by electrospinning. Chem Commun 46:6903
38. Charlier JC (2002) Defects in carbon nanotubes. Acc Chem Res 35:1063
39. Chen L, Bromberg L, Hatton TA, Rutledge GC (2007) Catalytic hydrolysis of *p*-nitrophenyl acetate by electrospun polyacrylamidoxime nanofibers. Polymer 48:4675
40. Chen Z, Mo X, Qing F (2007) Electrospinning of collagen–chitosan complex. Mater Lett 61:3490

41. Chen P, Yun YS, Bak H, Cho SY, Jin HJ (2010) Multiwalled carbon nanotubes-embedded electrospun bacterial cellulose nanofibers. Mol Cryst Liq Cryst 519:169
42. Chowdhury M, Stylios G (2010) Effect of experimental parameters on the morphology of electrospun Nylon 6 fibres. Int J Basic Appl Sci 10:116
43. Chronakis IS (2005) Novel nanocomposites and nanoceramics based on polymer nanofibers using electrospinning process–a review. J Mater Process Technol 167:283
44. Chung S, Moghe AK, Montero GA, Kim SH, King MW (2009) Nanofibrous scaffolds electrospun from elastomeric biodegradable poly (L-lactide-co-ε-caprolactone) copolymer. Biomed Mater 4:1
45. Cozza ES, Bruzzo V, Carniato F, Marsano E, Monticelli O (2012) On a novel catalytic system based on electrospun nanofibers and M-POSS. Appl Mater Interfaces 4:604
46. Cui W, Li X, Zhou S, Weng J (2007) Investigation on process parameters of electrospinning system through orthogonal experimental design. J Appl Polym Sci 103:3105
47. Dahlin RL, Kasper FK, Mikos AG (2011) Polymeric nanofibers in tissue engineering. Tissue Eng Part B Rev 17:349
48. Dai H (2002) Carbon nanotubes: Synthesis, integration, and properties. Acc Chem Res 35:1035
49. Dallmeyer I, Ko F, Kadla JF (2010) Electrospinning of technical lignins for the production of fibrous networks. J Wood Chem Technol 30:315
50. Deng XL, Xu MM, Li D, Sui G, Hu XY, Yang XP (2007) Electrospun PLLA-MWNTs-HA hybrid nanofiber scaffolds and their potential in dental engineering. Key Eng Mater 330–332:393
51. Desai K, Kit K, Li J, Zivanovic S (2008) Morphological and surface properties of electrospun chitosan nanofibers. Biomacromolecules 9:1000
52. Ding B, Li C, Hotta Y, Kim J, Kuwaki O, Shiratori S (2006) Conversion of an electrospun nanofibrous cellulose acetate mat from a super-hydrophilic to super-hydrophobic surface. Nanotechnology 17:4332
53. Ding B, Wang M, Yu J, Sun G (2009) Gas sensors based on electrospun nanofibers. Sensors 9:1609
54. Dong H, Strawhecker KE, Snyder JF, Orlicki JA, Reiner RS, Rudie AW (2012) Cellulose nanocrystals as a reinforcing material for electrospun poly (methyl methacrylate) fibers: Formation, properties and nanomechanical characterization. Carbohydr Polym 87:2488
55. Drozin VG (1955) The electrical dispersion of liquids as aerosols. J Colloid Sci 10:158
56. Du J, Hsieh YL (2009) Cellulose/chitosan hybrid nanofibers from electrospinning of their ester derivatives. Cellulose 16:247
57. Dufresne A (2008) Polysaccharide nano crystal reinforced nanocomposites. Can J Chem 86:484
58. Duran N, Lemes AP, Duran M, Freer J, Baeza J (2011) A minireview of cellulose nanocrystals and its potential integration as co-product in bioethanol production. J Chil Chem Soc 56, pp 672–677
59. El-Hefian EA, Nasef MM, Yahaya AH, Attakhan R (2010) Preparation and characterization of chitosan/agar blends: rheological and thermal studies. J Chil Chem Soc 55, pp 130–136
60. Evcin A, Kaya DA (2010) Effect of production parameters on the structure and morphology of aluminum titanate nanofibers produced using electrospinning technique. Sci Res Essays 5:3682
61. Fang X, Reneker DH (1997) DNA fibers by electrospinning. J Macromol Sci Phys 36:169
62. Feng H, Li J, Wang L (2010) Preparation of biodegradable flax shive cellulose-based superabsorbent polymer under microwave irradiation. BioResources 5:1484
63. Fink H-P, Weigel P, Purz H (2001) Structure formation from regenerated cellulose materials from NMMO solutions. Prog Polym Sci 26:1473
64. Fong H, Chun I, Reneker DH (1999) Beaded nanofibers formed during electrospinning. Polymer 40:4585
65. Formhals A (1934) US patent no 1,975,504

66. Freire MG, Teles ARR, Ferreira RAS, Carlos LD, Lopes-da-Silvac JA, Coutinho JAP (2011) Electrospun nanosized cellulose fibers using ionic liquids at room temperature. Green Chem 13:3173
67. Frenot A, Henriksson MW, Walkenstrom P (2007) Electrospinning of cellulose-based nanofibers. J Appl Polym Sci 103:1473
68. Frey MW (2008) Electrospinning cellulose and cellulose derivatives. Polym Rev 48:378
69. Fukaya Y, Hayashi K, Wadab M, Ohno H (2008) Cellulose dissolution with polar ionic liquids under mild conditions: Required factors for anions. Green Chem 10:44
70. Gardner DJ, Oporto GS, Mills R, Samir ASA (2008) Adhesion and surface issues in cellulose and nanocellulose. J Adhes Sci Technol 22:545
71. Geng X, Kwon OH, Jinho Jang J (2005) Electrospinning of chitosan dissolved in concentrated acetic acid solution. Biomaterials 26:5427
72. Geng HZ, Lee DS, Kim KK, Bae JJ, Lee YH (2008) Ect of carbon nanotube types in fabricating flexible transparent conducting films. J Korean Phys Soc 53:979
73. George J, Sreekala MS, Thomas S (2001) A review on interface modification and characterization of natural fiber reinforced plastic composites. Polym Eng Sci 41:1471
74. Gorji M, Jeddi AAA, Gharehaghaji AA (2012) Fabrication and characterization of polyurethane electrospun nanofiber membranes for protective clothing applications. J Appl Polym Sci 125, pp 4135–4141
75. Greiner A, Wendroff JH (2007) Electrospinning: a fascinating method for the preparation of ultrathin fibers. Angew Chem Int Ed 46:5670
76. Gupta P, Elkins C, Long TE, Wilkes GL (2005) Electrospinning of linear homopolymers of poly (methyl methacrylate): exploring relationships between fiber formation, viscosity, molecular weight and concentration in a good solvent. Polymer 46:4799
77. Gururajan G, Sullivan SP, Beebe TP, Chase DB, Rabolt JF (2011) Continuous electrospinning of polymer nanofibers of Nylon-6 using an atomic force microscope tip. Nanoscale 3:3300
78. Härdelin L, Thunberg J, Perzon E, Westman G, Walkenström P, Gatenholm P (2012) Electrospinning of cellulose nanofibers from ionic liquids: The effect of different cosolvents. J Appl Polym Sci 125, pp 1901–1909
79. Haghi AK, Akbari M (2007) Trends in electrospinning of natural nanofibers. Phys Stat Sol 204:1830
80. Han SO, Youk JH, Min KD, Kang YO, Park WH (2008) Electrospinning of cellulose acetate nanofibers using a mixed solvent of acetic acid/water: Effects of solvent composition on the fiber diameter. Mater Lett 62:759
81. Hansen CM, Bjorkman A (1998) The ultrastructure of wood from a solubility parameter point of view. Holzforschung 52:335
82. Hardick O, Stevens B, Bracewell DG (2011) Nanofibre fabrication in a temperature and humidity controlled environment for improved fibre consistency. J Mater Sci 46:3890
83. He JH, Wan YQ, Yu JY (2004) Application of vibration technology to polymer electrospinning. Int J Nonlin Sci Num 5:243
84. He JH, Wu Y, Pan N (2005) A mathematical model for AC-electrospinning. Int J Nonlin Sci Num 6:243
85. Herrera MA, Mathew AP, Oksman K (2012) Novel biorefinery: A residue from wood bioethanol production converted into cellulose nanocrystals. In: 6th EEIGM international conference on advanced materials research IOP publishing IOP conference series: materials science and engineering, vol 31, Nancy France
86. Hohman MM, Shin M, Rutledge G, Brenner MP (2001) Electrospinning and electrically forced jets. I. Stability theory. Phys Fluids 13:2221
87. Huang ZH, Kang FY, Zheng YP, Yang JB, Liang KM (2002) Adsorption of trace polar methy-ethyl-ketone and non-polar benzene vapors on viscose rayon-based activated carbon fibers. Carbon 40:1363

88. Huang ZM, Zhang YZ, Kotaki M, Ramakrishna S (2003) A review on polymer nanofibers by electrospinning and their applications in nanocomposites. Compos Sci Technol 63:2223
89. Huang J, Liu L, Yao J (2011) Electrospinning of Bombyx mori silk fibroin nanofiber mats reinforced by cellulose nanowhiskers. Fiber Polym 12:1002
90. Hur S, Kim WD (2006) The electrospinning process and mechanical properties of nanofiber mats under vacuum conditions. Key Eng Mater 326–328:393
91. Ignatova M, Manolova N, Markova N, Rashkov I (2009) Electrospun non-woven nanofibrous hybrid mats based on chitosan and PLA for wound-dressing applications. Macromol Biosci 9:102
92. Iijima S (1991) Helical microtubules of graphitic carbon. Nature 354:56
93. Inoue S, Tanaka K, Arisaka F, Kimura S, Ohtomo K, Mizuno S (2000) Silk fibroin of bombyx mori is secreted, assembling a high molecular mass elementary unit consisting of H-chain, L-chain, and P25, with a 6:6:1 molar ratio. J Biol Chem 275:40517
94. Islam MS, Ashaduzzaman M, Masum SM, Yeum JH (2012) Mechanical and electrical properties: electrospun alginate/carbon nanotube composite nanofiber. Dhaka Univ J Sci 60:125
95. Jacobs V, Anandjiwala RD, Maaza M (2010) The influence of electrospinning parameters on the structural morphology and diameter of electrospun nanofibers. J Appl Polym Sci 115:3130
96. Jaeger R, Bergshoef MM, Batlle CMI, Schönherr H, Julius Vancso G (1998) Electrospinning of ultra-thin polymer fibres. Macromol Symp 127:141
97. Jahn A, Schroder MW, Futing M, Schenzel K, Diepenbrock W (2002) Characterization of alkali treated flax fibres by means of FT Raman spectroscopy and environmental scanning electron microscopy. Spectrochim Acta Part A 58:2271
98. Jang JH, Castano O, Kim HW (2009) Electrospun materials as potential platforms for bone tissue engineering. Adv Drug Deliv Rev 61:1065
99. Jawaid M, Abdul Khalil HPS (2011) Cellulosic/synthetic fibre reinforced polymer hybrid composites: A review. Carbohydr Polym 86:1
100. Jayaraman K, Kotaki M, Zhang Y, Mo X, Ramakrishna S (2004) Recent advances in polymer nanofibers. J Nanosci Nanotechnol 4(1–2):52
101. Jia YT, Kim HY, Gong J, Lee DR (2006) Electrospun nanofibers of block copolymer of trimethylene carbonate and ε-caprolactone. J Appl Polym Sci 99:1462
102. Jian F, Tao NH, Tong L, XunGai W (2008) Applications of electrospun nanofibers. Chin Sci Bull 53:2265
103. Johnson D (1969) US patent 3,447,956 (Eastman Kodak Co)
104. Kanani AG, Bahrami SH (2010) Review on electrospun nanofibers scaffold and biomedical applications. Trends Biomater ArtRif Org 24:93
105. Kang MS, Yoon SH, Jin HJ (2006) Preparation of electrospun protein nanofibers with multiwalled carbon nanotubes. Key Eng Mater 326–328:1737
106. Karmanov AP, Monakov YB (2003) Lignin structural organisation and fractal properties. Russ Chem Rev 72:715
107. Khan MA, Ganster J, Fink HP (2009) Hybrid composites of jute and man-made cellulose fibers with polypropylene by injection moulding. Compos Part A 40:846
108. Khenoussi N, Schacher L, Adolphe DC (2012) Nanofiber production: Study and development of electrospinning device. Exp Tech 36:32
109. Khil MS, Kim HY, Kang YS, Bang HJ, Lee DR, Doo JK (2005) Preparation of electrospun oxidized cellulose mats and theirin vitro degradation behavior. Macromol Res 13:62
110. Kilic A, Oruc F, Demir A (2007) Effects of polarity on electrospinning process. Text Res J 00:1
111. Kilpelainen I, Xie H, King A, Granstrom M, Heikkinen S, Argyropoulos DS (2007) Dissolution of wood in ionic liquids. J Agric Food Chem 55:9142
112. Kim CW, Frey MW, Marquez M, Joo YL (2005) Preparation of submicron-scale, electrospun cellulose fibers via direct dissolution. J Polym Sci Part B Polym Phys 43:1673

113. Kim GM, Lach R, Michler GH, Chang YW (2005) The mechanical deformation process of electrospun polymer nanocomposite fibers. Macromol Rapid Commun 26:728
114. Kim CW, Kim DS, Kang SY, Marquez M, Joo YL (2006) Structural studies of electrospun cellulose nanofibers. Polymer 47:5097
115. Kirecci A, Özkoc U, Icoglu HI (2012) Determination of optimal production parameters for polyacrylonitrile nanofibers. J Appl Polym Sci 124:4961
116. Kiselev P, Rosell-Llompart J (2012) Highly aligned electrospun nanofibers by elimination of the whipping motion. J Appl Polym Sci 125:2433
117. Kosan B, Michels C, Meister F (2008) Dissolution and forming of cellulose with ionic liquids. Cellulose 15:59
118. Kowalewski TA, Blonski S, Barral S (2005) Experiments and modelling of electrospinning process. Bull Pol Acad Sci Chem Tech Sci 53:385
119. Kriegel C, Arrechi A, Kit K, McClements DJ, Weiss J (2008) Fabrication, functionalization, and application of electrospun biopolymer nanofibers. Crit Rev Food Sci Nutr 48:775
120. Kuan CY, Yee-Fung W, Yuen KH, Liong MT (2012) Nanotech: propensity in foods and bioactives. Crit Rew Food Sci 52:55
121. Kulpinski P (2005) Cellulose nanofibers prepared by the N-methylmorpholine-N-oxide method. J Appl Polym Sci 98:1855–1859
122. Kumar S, Asce F, Kolay P, Asce M, Malla S, Mishra S (2012) Effect of multiwalled carbon nanotubes on mechanical strength of cement paste. J Mater Civ Eng 24(1):84
123. Kumbar SG, Nukavarapu SP, James R, Hogan MV, Laurencin CT (2008) Recent patents on electrospun biomedical nanostructures: an overview. Recent Pat Biomed Eng 1:68
124. Lamy B, Baley C (2000) Stiffness prediction of flax fibers-epoxy composite materials. J Mater Sci Lett 19:979
125. Larrondo L, Manley SJ (1981) Electrostatic fiber spinning from polymer melts. I. Experimental observations on fiber formation and properties. J Polym Sci Polym Phys Ed 19:921
126. Laus G, Bentivoglio G, Schottenberger H, Kahlenberg V, Kopacka H, Röder T, Sixta H (2005) Ionic liquids: current developments, potential and drawbacks for industrial applications. Lenzinger Berichte 84:71
127. Lee S (2009) Developing UV-protective textiles based on electrospun zinc oxide nanocomposite fibers. Fibers Polym 10:295
128. Lee S, Obendorf SK (2007) Use of electrospun nanofiber web for protective textile materials as barriers to liquid penetration. Text Res J 77:696. http://scholar.google.com/citations?view_op=view_citation&hl=en&user=5W6EtHgAAAAJ&citation_for_view=5-W6EtHgAAAAJ:u5HHmVD_uO8C
129. Lee KH, Kim HY, Bang HJ, Jung YH, Lee SG (2003) The change of bead morphology formed on electrospun polystyrene fibers. Polymer 44:4029
130. Lee EH, Kim HM, Lim SK, Kim KS, Chin IJ (2009) Electro-active polymer actuator based on aligned cellulose nanofibrous membrane. Mol Cryst Liq Cryst 499:259[581]
131. Lee KY, Jeong L, Kang YO, Lee SJ, Park WH (2009) Electrospinning of polysaccharides for regenerative medicine. Adv Drug Deliv Rev 61:1020
132. Lewin M (2006) Handbook of fiber chemistry, 3rd edn. CRC Press, Boca Raton
133. Li P, Li Y, Ying B, Yang M (2009) Electrospun nanofibers of polymer composite as a promising humidity sensitive material. Sens Actuators B 141:390
134. Li Q, Zhou J, Zhang L (2009) Structure and properties of the nanocomposite films of chitosan reinforced with cellulose whiskers. J Polym Sci Part B Polym Phys 47:1069
135. Liao S, Li B, Ma Z, Wei H, Chan C, Ramakrishna S (2006) Biomimetic electrospun nanofibers for tissue regeneration. Biomed Mater 1:R45
136. Liebert T, Heinze T (2008) Interaction of ionic liquids with polysaccharides. 5. Solvents and reaction media for the modification of cellulose. BioResources 3:576
137. Lin Y-J, Cai Q, Li L, Li QF, Yang XP, Jin RG (2010) Co-electrospun composite nanofibers of blends of poly [(amino acid ester) phosphazene] and gelatin. Polym Int 59:610

138. Lisperguer J, Perez P, Urizar S (2009) Structure and thermal properties of lignins: characterization by infrared spectroscopy and differential scanning calorimetry. J Chil Chem Soc 54:460
139. Liu H, Hsieh YL (2002) Ultrafine fibrous cellulose membranes from electrospinning of cellulose acetate. J Polym Sci Part B Polym Phys 40:2119
140. Liu Y, He JH, Yu JY, Zeng HM (2008) Controlling numbers and sizes of beads in electrospun nanofibers. Polym Int 57:632
141. Liu D, Yuan X, Bhattacharyya D (2012) The effects of cellulose nanowhiskers on electrospun poly (lactic acid) nanofibres. J Mater Sci 47:3159
142. Lönnberg H, Zhou Q, Brumer H, Teeri TT, Malmstrom E, Hult A (2006) Grafting of cellulose fibers with poly (ε-caprolactone) and poly (L-lactic acid) via ring-opening polymerizations. Biomacromolecules 7:2178
143. Lu C, Chen P, Li J, Zhang Y (2006) Computer simulation of electrospinning. Part I. Effect of solvent in electrospinning. Polymer 47:915
144. Lyons J, Li C, Ko F (2004) Melt-electrospinning part I: processing parameters and geometric properties. Polymer 45:7597
145. Magalhães WLE, Cao X, Lucia LA (2009) Cellulose nanocrystals/cellulose core-in-shell nanocomposite assemblies. Langmuir 25:13250
146. Magalhãess WLE, Cao X, Ramires MA, Lucia LA (2011) Novel method for inducing the alignment of cellulose nanocrystals-reinforced cellulose nanofibers. Tappi J 10:19
147. Makar JM, Beaudoin JJ (2003) In: 1st international symposium on nanotechnology in construction, Paisley, Scotland
148. Marcovich NE, Auad ML, Bellesi NE, Nutt SR, Aranguren MI (2006) Cellulose micro/nanocrystals reinforced polyurethane. J Mater Res 21:870
149. Marsh KN, Boxall JA, Lichtenthaler R (2004) Room temperature ionic liquids and their mixtures–a review. Fluid Phase Equilib 219:93
150. Martel R, Schmidt T, Shea HR, Hertel T, Avourisa PH (1998) Single-and multi-wall carbon nanotube field-effect transistors. Appl Phys Lett 73
151. Martínez-Hernández AL, Velasco-Santos C, Castaño VM (2010) Carbon nanotubes composites: processing, grafting and mechanical and thermal properties. Curr Nanosci 6:12. http://scholar.google.com.mx/citations?view_op=view_citation&hl=en&user=megg-bIAAAAJ&citation_for_view=megg-bIAAAAJ:2osOgNQ5qMEC
152. Martínez-Sanz M, Olsson RT, Lopez-Rubio A, Lagaron JM (2011) Development of electrospun EVOH fibres reinforced with bacterial cellulose nanowhiskers. Part I: Characterization and method optimization. Cellulose 18:335
153. Martinová L, Lubasová D (2008) Electrospun chitosan based nanofibers. RJTA 12
154. Martins A, Reis RL, Neves NM (2008) Electrospinning: processing technique for tissue engineering scaffolding. Int Mater Rev 53:257
155. Matthews JA, Wnek GE, Simpson DG, Bowlin GL (2002) Electrospinning of collagen nanofibers. Biomacromolecules 3:232
156. Mazoochi T, Jabbari V (2011) Chitosan nanofibrous scaffold fabricated via electrospinning: The effect of processing parameters on the nanofiber morphology. Int J Polym Anal Charact 16:277. http://65.54.113.26/Publication/57595212/chitosan-nanofibrous-scaffold-fabricated-via-electrospinning-the-effect-of-processing-parameters
157. Meli L, Miao J, Dordick JS, Linhardt RJ (2010) Electrospinning from room temperature ionic liquids for biopolymer fiber formation. Green Chem 12:1883
158. Mit-uppatham C, Nithitanakul M, Supaphol P (2004) Ultrafine electrospun polyamide-6 fibers: effect of solution conditions on morphology and average fiber diameter. Macromol Chem Phys 205:2327
159. Miyauchi M, Miao J, Simmons TJ, Dordick JS, Linhardt RJ (2011) Lexible electrospun cellulose fibers as an affinity packing material for the separation of bovine serum albumin. J Chromatogr Separat Tech 2:110

160. Mo XM, Xu CY, Kotaki M, Ramakrishna S (2004) Electrospun P (LLA-CL) nanofiber: a biomimetic extracellular matrix for smooth muscle cell and endothelial cell proliferation. Biomaterials 25:1883
161. Montano-Leyva B, Rodriguez-Felix F, Torres-Chavez P, Ramirez-Wong B, Lopez-Cervantes J, Sanchez-Machado D (2011) Preparation and characterization of durum wheat (Triticum durum) straw cellulose nanofibers by electrospinning. J Agric Food Chem 59:870
162. Mora-Pale M, Meli L, Doherty TV, Linhardt RJ, Dordick JS (2011) Room temperature ionic liquids as emerging solvents for the pretreatment of lignocellulosic biomass. Biotechnol Bioeng 108:1229
163. Nakagaito AN, Iwamoto S, Yano H (2005) Bacterial cellulose: the ultimate nano-scalar cellulose morphology for the production of high-strength composites. Appl Phys A 80:93
164. Nevell TP, Zeronian SH (1985) Wiley, New York
165. Niyogi S, Hamon MA, Hu H, Zhao B, Bhowmik R (2002) Chemistry of single-walled carbon nanotubes. Acc Chem Res 35:1105
166. Nouri N, Ziaei-Rad S (2010) Mechanical property evaluation of carbon nanotube sheets. Trans F: Nanotechnol 17, pp 1600–1625
167. Ohkawa K, Cha D, Kim H, Nishida A, Yamamoto H (2004) Electrospinning of chitosan. Macromol Rapid Commun 25:1600
168. Ohkawa K, Hayashi S, Nishida A, Yamamoto H, Ducreux J (2009) Preparaiton of pure cellulose nanofiber via electrospinning. Text Res J 79:1396
169. Pankonian A, Ounaies Z, Yang C (2011) Electrospinning of cellulose and SWNT-cellulose nano fibers for smart applications. J Mech Sci Technol 25:2631
170. Park TJ, Jung YJ, Choi SW, Park H, Kim H, Kim E, Lee SH, Kim JH (2011) Native chitosan/cellulose composite fibers from an ionic liquid via electrospinning. Macromol Res 19:213
171. Peesan M, Rujiravanit R, Supaphol P (2006) Electrospinning of hexanoyl chitosan/polylactide blends. J Biomater Sci Polym Edn 17:547
172. Peng BL, Dhar N, Liu HL, Tam KC (2011) Chemistry and applications of nanocrystalline cellulose and its derivatives: a nanotechnology perspective. Can J Chem Eng 89:1191
173. Pham QP, Sharma U, Mikos AG (2006) Electrospinning of polymeric nanofibers for tissue engineering applications: a review. Tissue Eng 12:1197
174. Phillips DM, Drummy LF, Conrady DG, Fox DM, Naik RR, Stone MO, Trulove PC, Long HCD, Mantz RA (2004) Dissolution and regeneration of bombyx mori silk fibroin using ionic liquids. J Am Chem Soc 126:14350
175. Pinkert A, Marsh KN, Pang S, Staiger MP (2009) Ionic liquids and their interaction with cellulose. Chem Rev 109:6712
176. Popa VI, Capraru AM, Grama S, Malutan T (2011) Nanoparticles based on modified lignins with biocide properties. Cellul Chem Technol 45:221
177. Popov VN (2004) Carbon nanotubes: properties and application. Mater Sci Eng R 43:61
178. Pouteau C, Dole P, Cathala B, Averous L, Boquillon N (2003) Antioxidant properties of lignin in polypropylene. Polym Degrad Stab 81:9
179. Qiao B, Ding X, Hou X, Wu S (2011) Study on the electrospun CNTs/polyacrylonitrile based nanofiber composites. J Nanomater 2011, pp 1–7
180. Qin XH, Wang SY (2006) Filtration properties of electrospinning nanofibers. J Appl Polym Sci 102:1285
181. Quan SL, Kang SG, Chin IJ (2010) Characterization of cellulose fibers electrospun using ionic liquid. Cellulose 17:223
182. Ramakrishna S, Fujihara K, Teo WE, Yong T, Ma Z, Ramaseshan R (2006) Electrospun nanofibers: solving global issues. Mater Today 9:40
183. Rangkupan R, Reneker DH (2003) Electrospinning process of molten polypropylene in vacuum. J Met Mater Miner 12:81
184. Rayleigh L (1882) On the instability of jets. FRS Philos Mag Ser 5 14:184
185. Reddy CS, Arinstein A, Avrahami R, Zussman E (2009) Fabrication of thermoset polymer nanofibers by co-electrospinning of uniform core-shell structures. J Mater Chem 19:7198

186. Remsing RC, Swatloski RP, Rogers RD, Moyna G (2006) Mechanism of cellulose dissolution in the ionic liquid 1-n-butyl-3-methylimidazolium chloride: a 13C and 35/37Cl NMR relaxation study on model systems. Chem Commun 12:1271
187. Reneker DH, Chun I (1996) Nanometre diameter fibres of polymer, produced by electrospinning. Nanotechnology 7:216
188. Reneker DH, Yarin AL (2008) Electrospinning jets and polymer nanofibers. Polymer 49:2387
189. Reneker DH, Yarin AL, Fong H, Koombhongse S (2000) Bending instability of electrically charged liquid jets of polymer solutions in electrospinning. J Appl Phys 87:4531
190. Rockwood DN, Preda RC, Yücel T, Wang X, Lovett ML, Kaplan DL (2011) Materials fabrication from Bombyx mori silk fibroin. Nat Protoc 6:1612
191. Rong MZ, Zhang MQ, Liu Y, Yang GC, Zeng HM (2001) The effect of fiber treatment on the mechanical properties of unidirectional sisal-reinforced epoxy composites. Compos Sci Technol 61:1437
192. Saeed K, Park SY, Lee HJ, Baek JB, Huh WS (2006) Preparation of electrospun nanofibers of carbon nanotube/polycaprolactone nanocomposite. Polymer 47:8019
193. Sahay R, Kumar PS, Sridhar R, Sundaramurthy J, Venugopal J, Mhaisalkar SG, Ramakrishna S (2012) Electrospun composite nanofibers and their multifaceted applications. J Mater Chem 22:12953
194. Sajeev US, Anand KA, Menon D, Nair S (2008) Control of nanostructures in PVA, PVA/chitosan blends and PCL through electrospinning. Bull Mater Sci 31:343
195. Sakurai K, Maegawa T, Takahashi T (2000) Glass transition temperature of chitosan and miscibility of chitosan/poly (*N*-vinyl pyrrolidone) blends. Polymer 41:7051
196. Salazar-Valencia PJ, Pérez-Merchancano ST, Bolívar-Marinéz LE (2006) Optical properties in Biopolymers: lignin fragments. Braz J Phys 36, pp 840–843
197. Saligheh O, Arasteh R, Forouharshad M, Farsani RE (2011) Poly (Butylene Terephthalate)/single wall carbon nanotubes composite nanofibers by electrospinning. J Macromol Sci Phys 50:1031
198. Salvetat JP, Bonard JM, Thomson NH, Kulik AJ, Forró L, Benoit W, Zuppiroli L (1999) Mechanical properties of carbon nanotubes. Appl Phys A Mater Sci Proc 69:255
199. Samatham R, Kim KJ (2006) Electric current as a control variable in the electrospinning process. Polym Eng Sci 46:954
200. Sangsanoh P, Supaphol P (2006) Stability improvement of electrospun chitosan nanofibrous membranes in neutral or weak basic aqueous solutions. Biomacromolecules 7:2710
201. Schiffman JD, Schauer CL (2007) Cross-linking chitosan nanofibers. Biomacromolecules 8:2665
202. Schiffman JD, Schauer CL (2008) A review: electrospinning of biopolymer nanofibers and their applications. Polym Rev 48:317
203. Schueren LVD, Steyaert I, Schoenmaker BD, Clerck KD (2012) Polycaprolactone/chitosan blend nanofibres electrospun from an acetic acid/formic acid solvent system. Carbohydr Polym 88:1221
204. Seo DK, Jeun JP, Kim HB, Kang PH (2011) Preparation and characterization of the carbon nanofiber mat produced from electrospun PAN/lignin precursors by electron beam irradiation. Rev Adv Mater Sci 28:31
205. Shi Z, Zang S, Jiang F, Huang L, Lu D, Ma Y, Yang G (2012) In situ nano-assembly of bacterial cellulose–polyaniline composites. RSC Adv 2:1040
206. Shin YM, Hohman MM, Brenner MP, Rutledge GC (2001) Experimental characterization of electrospinning: the electrically forced jet and instabilities. Polymer 42:9955
207. Sill TJ, Recum HAV (2008) Electrospinning: applications in drug delivery and tissue engineering. Biomaterials 29:1989
208. Song R, Xue R, He LH, Liu Y, Xiao OL (2008) The structure and properties of chitosan/polyethylene glycol/silica ternary hybrid organic-inorganic films. Chin J Polym Sci 26:621

209. Srivastava Y, Marquez M, Thorsen T (2007) Multijet electrospinning of conducting nanofibers from microfluidic manifolds. J Appl Polym Sci 106:3171
210. Subbiah T, Bhat GS, Tock RW, Parameswaran S, Ramkumar SS (2005) Electrospinning of nanofibers. J Appl Polym Sci 96:557
211. Sui X, Wagner HD (2009) Tough nanocomposites: the role of carbon nanotube type. Nano Lett 9:1423
212. Sumin L, Kimura D, Yokoyama A, Lee KH, Park JC, Kim IS (2009) The effect of laundering on the thermal and water transfer properties of mass-produced laminated nanofiber web for use in wear. Text Res J 79:1085
213. Sun Z, Zussman E, Yarin AL, Wendorff JH, Greiner A (2003) Compound core–shell polymer nanofibers by co-electrospinning. Adv Mater 15:1929
214. Supaphol P, Neamnark A, Taepaiboon P, Pavasant P (2012) Effect of degree of acetylation on In vitro biocompatibility of electrospun cellulose acetate-based fibrous matrices. Chiang Mai J Sci 39:209
215. Suwantong O, Opanasopit P, Ruktanonchai U, Supaphol P (2007) Electrospun cellulose acetate fiber mats containing curcumin and release characteristic of the herbal substance. Polymer 48:7546
216. Swatloski RP, Spear SK, Holbrey JD, Rogers RD (2002) Dissolution of cellose with ionic liquids. J Am Chem Soc 124:4974
217. Tan SH, Inai R, Kotaki M, Ramakrishna S (2005) Systematic parameter study for ultra-fine fiber fabrication via electrospinning process. Polymer 46:6128
218. Tan S, Huang X, Wu B (2007) Some fascinating phenomena in electrospinning processes and applications of electrospun nanofibers. Polym Int 56:1330
219. Thavasi V, Singh G, Ramakrishna S (2008) Electrospun nanofibers in energy and environmental applications. Energy Environ Sci 1:205
220. Theron SA, Zussman E, Yarin AL (2004) Experimental investigation of the governing parameters in the electrospinning of polymer solutions. Polymer 45:2017
221. Theron SA, Yarin AL, Zussman E, Kroll E (2005) Multiple jets in electrospinning: experiment and modeling. Polymer 46:2889
222. Thompson CJ, Chase GG, Yarin AL, Reneker DH (2007) Effects of parameters on nanofiber diameter determined from electrospinning model. Polymer 48:6913
223. Unnithan AR, Barakat NAM, Nirmala R, Al-Deyab SS, Kim HY (2012) Novel electrospun nanofiber mats as effective catalysts for water photosplitting. Ceram Int 38, pp 5175–5180
224. Van De Velde K, Kiekens P (2001) Thermoplastic pultrusion of natural fibre reinforced composites. Compos Struct 54:355
225. Vasita R, Katti DS (2006) Nanofibers and their applications in tissue engineering. Int J Nanomedicine 1:15
226. Veleirinho B, Rei MF, Lopes-DA-Silva JA (2008) Solvent and concentration effects on the properties of electrospun poly (ethylene terephthalate) nanofiber mats. J Polym Sci Part B Polym Phys 46:460
227. Viswanathan G, Murugesan S, Pushparaj V, Nalamasu O, Ajayan PM, Linhardt RJ (2006) Preparation of biopolymer fibers by electrospinning from room temperature ionic liquids. Biomacromolecules 7:415
228. Vitz J, Erdmenger T, Haenscha C, Schubert US (2009) Extended dissolution studies of cellulose in imidazolium based ionic liquids. Green Chem 11:417
229. Vrieze SD, Camp TV, Nelvig A, Hagström B, Westbroek P, Clerck KD (2009) The effect of temperature and humidity on electrospinning. J Mater Sci 44:1357
230. Wan Nadirah WO, Jawaid M, Al Masri A, Abdul Khalil HPS, Suhaily SS, Mohamed AR (2012) Cell wall morphology, chemical and thermal analysis of cultivated pineapple leaf fibres for industrial applications. J Polym Environ 20:404
231. Wan YQ, Guo Q, Pan N (2004) Thermo-electro-hydrodynamic model for electrospinning process. Int J Nonlin Sci Num 5:5

232. Wang C, Hsu CH, Lin JH (2006) Scaling laws in electrospinning of polystyrene solutions. Macromolecules 39:7662
233. Wang C, Yan E, Huang Z, Zhao Q, Xin Y (2007) Fabrication of highly photoluminescent TiO2/PPV hybrid nanoparticle-polymer fibers by electrospinning. Macromol Rapid Commun 28:205
234. Wang K, Gu M, Wang JJ, Qin C, Dai L (2012) Functionalized carbon nanotube/polyacrylonitrile composite nanofibers: fabrication and properties. Polym Adv Technol 23:262
235. Wannatong L, Sirivat A, Supaphol P (2004) Effects of solvents on electrospun polymeric fibers: preliminary study on polystyrene. Polym Int 53:1851
236. Wei K, Li Y, Kim KO, Nakagawa Y, Kim BS, Abe K, Chen GQ, Kim LS (2011) Fabrication of nano-hydroxyapatite on electrospun silk fibroin nanofiber and their effects in osteoblastic behavior. J Biomed Mater Res A 97A:272
237. Wendler F, Kosan B, Krieg M, Meister F (2009) Cellulosic shapes from Ionic liquids modified by activated charcoals and nanosilver particles. Lenzinger Ber 87:106
238. Williamson RE, Burn JE, Hocart CH (2002) Towards the mechanism of cellulose synthesis. Trends Plant Sci 7:461
239. Wu CS (2005) A comparison of the structure, thermal properties, and biodegradability of polycaprolactone/chitosan and acrylic acid grafted polycaprolactone/chitosan. Polymer 46:147
240. Xu S, Zhang J, He A, Li J, Zhang H, Han CC (2008) Electrospinning of native cellulose from nonvolatile solvent system. Polymer 49:2911
241. Yang D, Zhang J, Zhang J, Nie J (2008) Aligned electrospun nanofibers induced by magnetic field. J Appl Polym Sci 110:3368
242. Yang DJ, Kamienchick I, Youn DY, Rothschild A, Kim ID (2010) Ultrasensitive and highly selective gas sensors based on electrospun SnO2 nanofibers modified by Pd loading. Adv Funct Mater 20:4258
243. Yang M, Cao K, Sui L, Qi Y, Zhu J, Waas A, Arruda EM, Kieffer J, Thouless MD, Kotov NA (2011) Dispersions of aramid nanofibers: a new nanoscale building block. AcsNano 5:6945
244. Yao L, Lee C, Kim J (2010) Fabrication of electrospun meta-aramid nanofibers in different solvent systems. Fibers Polym 11:1032. http://www.researchgate.net/publication/241053217_Fabrication_of_electrospun_meta-aramid_nanofibers_in_different_solvent_systems
245. Yao L, Lee C, Kim J (2011) Electrospun meta-aramid/cellulose acetate and meta-aramid/cellulose composite nanofibers. Fiber Polym 12:197
246. Yeo L, Friend JR (2006) Electrospinning carbon nanotube polymer composite nanofibers. J Exp Nanosci 1:177
247. Yun GY, Kim HS, Kim J, Kim K, Yang C (2008) Effect of aligned cellulose film to the performance of electro-active paper actuator. Sens Actuators A 141:530
248. Zamri MFMA, Zein SHS, Abdullah AZ, Basir NI (2011) Improved electrical conductivity of polyvinyl alcohol/multiwalled carbon nanotube nanofibre composite films with MnO_2 as filler synthesised using the electrospinning process. IJET-IJENS 11:20
249. Zavrel M, Bross D, Funke M, Büchs J, Spiess AC (2009) High-throughput screening for ionic liquids dissolving (ligno-) cellulose. Bioresour Technol 100:2580
250. Zeleny J (1914) The electrical discharge from liquid points, and a hydrostatic method of measuring the electric intensity at their surfaces. Phys Rev Second Ser 3:69
251. Zhang M, Li J (2009) Carbon nanotube in different shapes. Mater Today 12, pp 12–18
252. Zhang H, Qian XM (2010) The Applications of electrospun nanofibers in the medical materials. Adv Mater Res 148–149:1138
253. Zhang H, Wu J, Zhang J, He JS (2005) 1-Allyl-3-methylimidazolium chloride room temperature ionic liquid: a new and powerful nonderivatizing solvent for cellulose. Macromolecules 38:8272
254. Zhang H, Wang Z, Zhang Z, Wu J, Zhang J, He J (2007) Regenerated-cellulose/multiwalled-carbon-nanotube composite fibers with enhanced mechanical properties prepared with the ionic liquid 1-allyl-3-methylimidazolium chloride. Adv Mater 19:698

255. Zhao ML, Sui G, Deng XL, Lu JG, Ryu SK, Yang XP (2006) PLLA/HA electrospin hybrid nanofiber scaffolds: morphology, in vitro degradation and cell culture potential. Adv Mater Res 11–12:243
256. Zhao T, Wang H, Zhang Y, Wang B, Jiang J (2007) The preparation and characterization of poly(m-phenylene- isophthalamide) fibers using ionic liquids. Int J Mol Sci 8:680
257. Zhou C, Chu R, Wu R, Wu Q (2011) Electrospun polyethylene oxide/cellulose nanocrystal composite nanofibrous mats with homogeneous and heterogeneous microstructures. Biomacromolecules 12:2617
258. Zhu S, Wu Y, Chen O, Yu Z, Wang C, Jin S, Dinga Y, Wuc G (2006) Dissolution of cellulose with ionic liquids and its application: a mini-review. Green Chem 8:325
259. Ziabari M, Mottaghitalab V, Haghi AK (2009) Application of direct tracking method for measuring electrospun nanofiber diameter. Braz J Chem Eng 26:53
260. Zong X, Kim K, Fang D, Ran S, Hsiao BS, Chu B (2002) Structure and process relationship of electrospun bioabsorbable nanofiber membranes. Polymer 43:4403
261. Zucchelli A, Focarete ML, Gualandi C, Ramakrishna S (2011) Electrospun nanofibers for enhancing structural performance of composite materials. Polym Adv Technol 22:339

Nanomanifestations of Cellulose: Applications for Biodegradable Composites

13

Raed Hashaikeh, Parakalan Krishnamachari, and Yarjan Abdul Samad

Contents

Abstract

High-strength and high-stiffness nanocelluloses are extracted from native cellulose which is an abundant and sustainable material. Cellulose can come with different manifestations in terms of morphologies and microstructure. The variation of cellulose morphology at the nanoscale comes from the way the material is processed or extracted. We discuss four types of nanocellulose manifestations, namely, nanocrystalline cellulose, electrospun cellulose, microfibrillated cellulose, and bacterial cellulose. The low density and biodegradable nature of these cellulose manifestations make them very desirable material. Nanocomposites prepared from cellulose are of great interest, owing

R. Hashaikeh (✉) • P. Krishnamachari • Y.A. Samad
Materials Science and Engineering Program, Masdar Institute of Science and Technology, Abu Dhabi, United Arab Emirates
e-mail: rhashaikeh@masdar.ac.ae; krishpark01@gmail.com; yyarjan@masdar-alumni.ac.ae

J.K. Pandey et al. (eds.), *Handbook of Polymer Nanocomposites. Processing, Performance and Application – Volume C: Polymer Nanocomposites of Cellulose Nanoparticles*,
DOI 10.1007/978-3-642-45232-1_60,

to the many end-use applications. If they are to be used with hydrophobic polymers and ensure a good level of dispersion, chemical surface modification of nanocelluloses is necessary. In addition to the interfacial characteristics, the nanocellulose morphology can also dictate the processing method of the nanocomposites. In this chapter, we put particular emphasis on two important applications of nanocellulose-reinforced biodegradable polymers: packaging and tissue engineering.

Keywords
Cellulose • Nanomanifestations • Nanocomposites • Biodegradable • Packaging • Tissue engineering

Abbreviations

BC	Bacterial cellulose
CNs	Cellulose nanocrystals
HAp	Hydroxyapatite
MCC	Microcrystalline cellulose
MFC	Microfibrillated cellulose
NCC	Nanocrystalline cellulose
PCL	Polycaprolactone
PLA	Polylactic acid
TEMPO	2,2,6,6-Tetramethylpiperidine-1-oxyl
THF	Tetrahydrofuran

1 Introduction

With an annual production of 75G tons [1], cellulose is the most abundant polymer on earth. Native cellulose fibers consist of bundles of microfibrils. Different ordering of cellulose polymorphs such as cellulose 1 and 2 ordering of its chains gives nanocellulose unique properties such as high stiffness and strength. The elastic modulus of nanocrystalline cellulose has been approximated to be 138 GPa [2]. The most common methods of isolating nano-manifested cellulose from native cellulose fibers are acid/enzymatic hydrolysis and mechanical disintegration. In the literature, there are multiple descriptors for NCC, and they are often referred to as microcrystals, whiskers, cellulose nanocrystals, nanoparticles, microcrystallites, or nanofibers. Detailed descriptions of preparation and morphology of NCC can be found in several references [3–6].

Since the first publication related to the use of one of the nano-manifested cellulose, i.e., NCC, as reinforcing fillers in poly(styrene-*co*-butyl acrylate) (poly(S-*co*-BuA))-based nanocomposites by Favier et al. [7], nanocellulose has attracted a great deal of interest in the nanocomposite field due to their desirable intrinsic properties that include nanoscale dimensions, high surface

Table 13.1 Modulus and density of common reinforcing materials compared to nanocellulose

Material	Modulus (GPa)	Density (Mg m^{-3})	Specific modulus (GPaMg^{-1} m^3)	Cost/lb ($)	Source
Carbon fibers	300–800	1.75	170–450	5	(http://www.xgsciences.com/aboutxgnp.html)
Nanoclay	170	2.8	60	3–5	([99]; http://www.nanoclay.com/keyproperties.asp)
Carbon nanotubes	1,000–1,700	1.4	715–1,215	500	[100]
Glass	69	2.5	28	1	[2]
Crystalline cellulose	138	1.5	92	5–6	[2]
Microfibrillated cellulose	145	1.6	90	6–10	[2, 20, 101]
Bacterial cellulose	114	1.25	91	35	[102, 103]

area, unique morphology, low density, and high mechanical strength. For example, a 14 wt% loading of NCC maintained a modulus of poly (styrene-co-butyl acrylate) matrices well above the polymer glass transition temperature (T_g) [7]. NCC-reinforced silk fibroin nanocomposites showed a fivefold increase in tensile strength and ultimate strain [8]. Reinforcement of cellulose acetate butyrate with NCC resulted in the modulus increasing from 1 GPa (neat polymer) to 4 GPa at 25 wt% NCC content [9]. With the addition of 20 wt% NCC dissolved in NaOH-urea solutions yielded a nanocomposite with a modulus of 5.9 GPa [10].

The moduli of a number of commonly used engineering materials are listed in Table 13.1. It can be seen that the specific modulus (modulus/density) of crystalline cellulose exceeds that of nanoclay and glass and is comparable to carbon fibers.

2 Different Manifestations of Cellulose

2.1 Nanocrystalline Cellulose (NCC)

The most common method of NCC extraction has been acid hydrolysis [11–13]. Due to the fast hydrolysis kinetics of amorphous domains compared to crystalline ones, under strong acid treatment, amorphous (disordered) regions of cellulose are preferentially hydrolyzed, whereas the crystalline regions that have a higher resistance to acid attack remain intact (Fig. 13.1).

Typically in this method, cellulosic material is subjected to strong acid hydrolysis under strictly controlled conditions of temperature, agitation, and time.

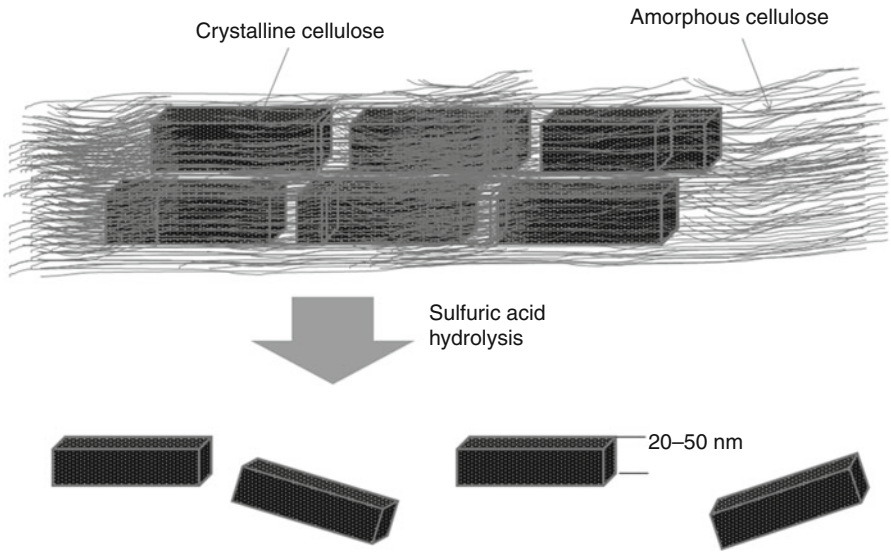

Fig. 13.1 Schematic representation of cellulose nanocrystal extraction using hydrolysis

The nature of the acid and the acid-to-cellulosic fiber ratio are also important parameters that affect the preparation of NCC [14]. While sulfuric and hydrochloric acids have been the most widely used for NCC preparation, phosphoric acid [15] and hydrobromic acid [16] also have been reported.

The resulting suspension after the hydrolysis is diluted with water and washed with successive centrifugations. The dialysis against distilled water is then performed to remove any free acid molecules from the dispersion. Additional steps such as filtration [17], differential centrifugation [18], or ultracentrifugation [19] also have been implemented.

2.2 Microfibrillated Cellulose (MFC) Manifestation of Cellulose

The natural fibers of cellulose are gathered together in a hierarchically ordered fashion. The nanosized fibrils composed of cellulose chains are called macrofibrils of cellulose [20]. The extraction of nano-/micro-sized fibrils can be done by breaking the hierarchical macrostructure of cellulose either mechanically or chemically. The most common methods of extracting MFC are mechanical shearing and enzymatic hydrolysis to produce nano-/microfibrils of cellulose [21] as shown in Fig. 13.2. MFC consists of crystalline cellulose 2 and amorphous regions different than the native cellulose crystal structure. The mechanical disintegration processes of making MFCs, usually energy-intensive processes, include but not limited to grinding, mechanical homogenization at

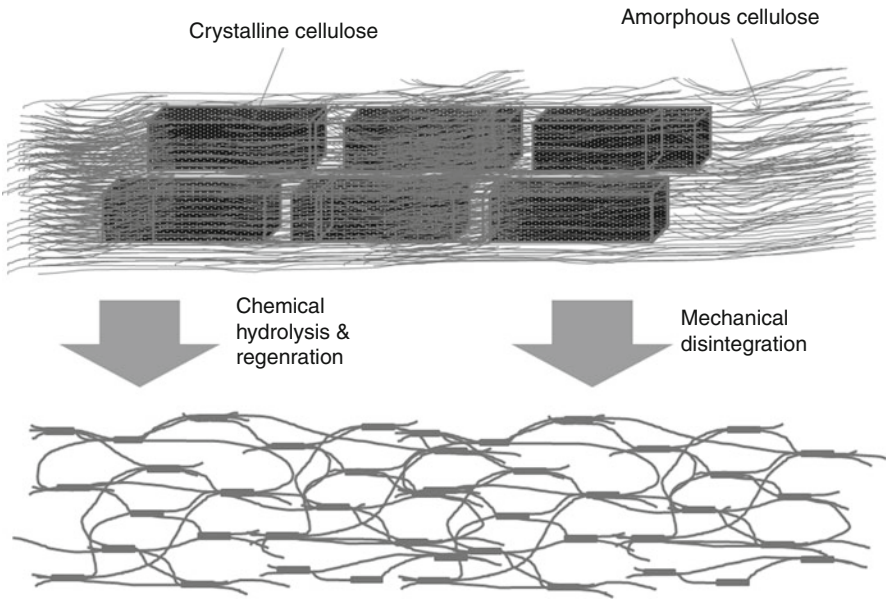

Fig. 13.2 Schematic representation of microfibrillated cellulose extraction using hydrolysis and mechanical disintegration

high pressures, mechanical filtration, and cryocrushing [22]. The chemical method usually consists of hydrolyzing natural cellulose fibers in high-concentration acid and subsequent regeneration of nano-/micro-sized fibrils in water or any other anti-solvent [21, 23]. Microfibrillated cellulose has found applications in several fields; however, one of the vital objectives of extracting micro-/nanofibrils of cellulose, by chemical or mechanical means, is to bring about a breakthrough in the performance of composites made from them. Cellulosic micro-/nano-fibrillated materials have garnered considerable attention for use in applications such as food, pharmaceutical, cosmetics, and also in paints and coatings [24]. MFCs have considerably higher interfibrillar adhesion and higher fibrillar strength than the natural cellulose fibers [25]. Major challenges faced by MFCs are their hydrophilic nature which prevents their use in nonpolar media and the tedious and costly extraction methods of MFC. The physical properties of MFCs depend on the method of formation and the source from which it is extracted [26, 27].

2.3 Bacterial Cellulose (BC)

Bacterial cellulose (BC) gels extracted by a family of bacteria *Gluconacetobacter xylinum* Aceto, an organism able to produce cellulose, consist of long and individual cellulose fibrils [28]. BC is similar in structure to the plant cellulose; however,

the extraction of cellulose micro-/nanofibers by disintegrating plant cellulose is quite difficult and expensive. In addition, BC fibers are lower in diameter and have a finer structure compared with that of the plant cellulose fibers [29]. BC fibers have, therefore, better mechanical properties than the natural cellulose fibers in wet state. High number of hydrogen bonds in BC makes them highly crystalline in nature creating a regular crystalline arrangement between the molecules [30]. Like other cellulosic derivatives, BC also is used in several applications in biomedicine and biotechnology. The major challenge in the industrialization of BC is its cost of production in mass quantity.

2.4 Electrospun Cellulose

Electrospinning deposits a solution of a material with the help of a large potential difference applied across the spinneret and the target where the material is to be deposited. The solution is injected through a syringe driver and a spinneret and is deposited on a counter electrode. The solution usually consists of a volatile solvent which evaporates, and fibers of the solute material are obtained in the form of a mat. Therefore, electrospun fibers of a polymer can be produced only if it's dissolved in a solvent. Nonetheless, due to the inter- and intramolecular hydrogen bonding and inflexible backbone, cellulose cannot be dissolved in conventional solvents. After decades of efforts by several researchers, a few successful solvents have been reported [31]. Ionic liquids with some polymer cosolvents are the most reported solvents, for the up-and-coming electrospinning of cellulose nanofibers, thus far [32, 33]. Fiber length, diameter, and morphology can be altered by changing parameters such as solvent composition and concentration and the voltage and feed rate of electrospinning. Thus, electrospun cellulose fibers can be made in a wide range of sizes and morphologies. Cellulose electrospun fibers can have applications such as wound dressing.

3 Surface Modification of Nano-manifested Cellulose

When added to nonpolar matrices, the highly polar surface of cellulose fibers results in some problems: low interfacial compatibility with the matrices, low moisture resistance/barrier, and interfiber aggregation by hydrogen bonding [34].

Chemical modification of nanocellulose surface becomes necessary if they are to be used with hydrophobic polymers and ensure a good level of dispersion. Because of a natural advantage of an abundance of hydroxyl groups at the surface of nanocellulose, different chemical modifications have been attempted, including esterification, etherification, oxidation, silylation, polymer grafting, etc. Noncovalent surface modifications, including the use of adsorbing surfactants and polymer coating, have also been studied. Chemical functionalization mainly aims to introduce stable negative or positive electrostatic charges on the surface of nanocellulose to obtain better dispersion [35–37]. The main challenge for the

chemical functionalization of nanocellulose is to facilitate changes on its surface while preserving the original morphology to avoid any polymorphic conversion and to maintain the integrity of the crystal structure [6]. Some of the common surface modification methods are listed in Table 13.2.

As clearly illustrated in the review paper by Hubbe et al. [38], surface-treated cellulosic materials can have negative influence on the cost of manufacturing of nanocomposites. The high surface area per unit mass of nanomaterials, which is their most attractive attribute, ironically also becomes a drawback when they have to be surface modified because of the cost of surface treatment.

4 Nanocellulose Composite Fabrication and Processing

There is a significant history of using cellulose fibers from plants as reinforcement in composite materials [22, 39, 40]; however, the application of nanocellulose for this purpose is relatively new. The properties of fiber-reinforced composites depend on many factors, including fiber size, fiber/matrix adhesion, volume fraction of fiber, fiber aspect ratio, fiber orientation, and stress/transfer efficiency through the interface. Fiber content in composites is a critical factor since fiber agglomeration through hydrogen bonding tends to occur at higher filler loadings [41, 42].

The various processing methods of the nanocomposites are dictated by factors such as morphology of the NCC, interfacial characteristics, degree of dispersion, and the eventual shape and form of the product that is desired. Habibi et al. [6] have listed several processing methods including solution casting, extrusion, sol–gel processing, and electrospinning. Eichhorn et al. [2] have also compiled a list of application-oriented processing done by prominent researchers in the area of nanocellulose. Some of the applications include reinforcing adhesives, electronic displays, etc. Commonly used processing methods for cellulose nanocomposites are listed in Table 13.3.

One of the popular theories for explaining the reinforcement mechanism of the nanocellulose is the formation of a so-called rigid percolating filler network that is cemented together by hydrogen bonds [43]. The matrix, the filler percolating network, and the nonpercolating filler all play a key role in determining the extent of reinforcement in a chosen method of processing and/or surface modification of the nanocellulose. The mechanical properties of composites are mainly affected by factors that influence or otherwise interfere with the formation of the percolated network such as the dimensions of nanocellulose and its interfacial interactions (among themselves or with the host polymer matrix). The conditions such as the processing rate and the viscosity of the system can have an effect on the ability of the percolating structure to be cemented or to withstand imposed stresses.

Due to the slow processing of the solution casting/solvent evaporation techniques, there is enough time for the nanocellulose to interconnect and form a percolation network. In the extrusion process however, the high melt viscosity

Table 13.2 Some common surface modification methods of cellulose

Method	Notes	References
Silylation	Isopropyl dimethylchlorosilane was used for surface silylation of cellulose microfibrils resulting from the homogenization of parenchymal cell walls. The microfibrils retained their morphology under mild silylation conditions and were dispersed in a non-flocculating manner into organic solvents	[104]
	MFC was hydrophobized via partial surface silylation. When silylation conditions were too harsh, partial solubilization of MFC and loss of nanostructure were observed	[105]
Application of coupling agents	MFC was modified by applying three different coupling agents, 3-aminopropyltriethoxysilane, 3-glycidoxypropyltrimethoxysilane, and a titanate coupling agent (Lica 38), in order to enhance the adhesion between microfibrils and epoxy resin polymer matrix. The surface modification changed the character of MFC from hydrophilic to hydrophobic, while the crystalline structure of the cellulose microfibrils remained intact	[106]
	The surface of chitin whiskers, prepared by acid hydrolysis of chitin from crab shells, was chemically modified using different coupling agents, namely, phenyl isocyanate (PI), alkenyl succinic anhydride (ASA), and 3-isopropenyl-α,α′-dimethylbenzyl isocyanate (TMI). Stable suspensions of these chemically modified chitin whiskers were obtained in toluene. The mechanical performances of the composites strongly decrease after the chemical modification	[107]
Grafting	Epoxy functionality was introduced onto the MFC surface by oxidation with cerium (IV) followed by grafting with glycidyl methacrylate. Reactive epoxy groups served as a starting point for further functionalization with ligands, which typically do not react with the surface hydroxyls present in native MFC	[108]
	N-octadecyl isocyanate (C18H37NCO) was applied as a grafting agent in order to improve MFC compatibility with polycaprolactone	[109]
	Cellulose nanofibers were treated using five different chemicals: ethylene acrylic acid, styrene maleic anhydride, guanidine hydrochloride, and Kelcoloid® HVF and LVF stabilizers (propylene glycol alginate). Bio-nanocomposites were prepared from PLA and PHB as matrices. Only partial dispersion was observed	[110]
	Functionality was added to microfibrillated cellulose film by covalently grafting the cellulose with octadecyldimethyl (3-trimethoxysilylpropyl) ammonium chloride (ODDMAC). The surface-modified MFC films showed antibacterial activity against both Gram-positive and Gram-negative bacteria	[111]
TEMPO oxidation	Never-dried native celluloses (bleached sulfite wood pulp, cotton, tunicin, and bacterial cellulose) were disintegrated into individual microfibrils after oxidation mediated by the 2,2,6,6-tetramethylpiperidine-1-oxyl (TEMPO) radical followed by a homogenizing mechanical treatment	[112]
	Excessive TEMPO-mediated oxidation resulted in a decrease of the crystal size due to the partial delamination of cellulose chains that are extant on the surface	[113]

(*continued*)

Table 13.2 (continued)

Method	Notes	References
Maleated polypropylene	Nanocomposite films of cellulose whiskers with a high dispersion level were obtained in an apolar matrix by incorporating surfactant-modified whiskers (SUWH) in atactic polypropylene (aPP)	[114]
Acetylation	BC was partially acetylated to modify its physical properties while preserving the microfibrillar morphology. The degree of acetyl substitution had a crucial influence on material properties	[115]
	Improvement of transparency and reduction of hygroscopicity were observed in BC/acrylic resin composite materials. However, the composites had an optimum degree of substitution (DS) and excessive acetylation reduced their properties	[116]
	Thermal degradation resistance of BC fibers was improved	[117]
	Fischer esterification of hydroxyl groups simultaneously with the hydrolysis of amorphous cellulose chains has been introduced as a viable one-pot reaction methodology that allows the isolation of acetylated CNs in a single-step process	[118, 119]
Esterification	Surface esterification of CNs led to highly substituted CN esters. The reaction of fatty acid chains was carried out on dried CNs via a gas-phase process	[120]
PVOH	Two feeding methods of polyvinyl alcohol and cellulose nanowhiskers were used and evaluated, dry-mixing with polylactic acid prior extrusion or pumping as suspension directly into the extruder. The relative small improvements in tensile modulus, tensile strength, and elongation to break for the nanocomposites indicated that it was principally the polyvinyl alcohol phase that was reinforced with whiskers and not the polylactic acid phase	[121]

Table 13.3 Processing methods for nanocomposite processing

Processing method	Polymer matrix/system	References
Extrusion	PLA	[121–123]
Solution casting	Cellulose acetate butyrate	[37, 124, 125]
	PCL	
	Poly(styrene-co-butyl acrylate) latex	
In situ polymerization	Elastomeric polyurethane	[126, 127]
	Polyphenol	
Electrospinning	PLA fibers	[128, 129]
	Biohybrid fiber yarns	[130]
	Poly(ethylene oxide)	[131]

during the compounding process is likely to hinder the mobility and as a result hinder the interconnection between nanocelluloses. But there are obvious merits in the extrusion process such as suitable for large amounts, easily duplicable for multiple systems, and absence of solvent – making it an economically and environmentally sound method.

5 Packaging Applications

Convenience, safety, low price, and good aesthetic qualities are among the major factors that make plastics useful for packaging. However, in recent years, environmental pollution has become a great concern due to the high impact of plastic waste from our daily use, which has grown rapidly. It is estimated that 47 % of all plastics used in the packaging industry are devoted to food packaging [44]. In general, these packaging materials are made from polyolefins and include polyethylene (PE), polypropylene (PP), polystyrene (PS), poly(vinyl chloride) (PVC), and polyesters like polyethylene terephthalate (PET). These polymers mostly produced from fossil fuels are used once and then discarded into the environment, ending up as nondegradable or slowly degrading waste, posing a serious global environmental problem.

New bio-based materials have been explored to develop edible and biodegradable films to tackle the issue of packaging waste [45]. However, the use of biodegradable polymers has been limited because of problems related to performance (such as brittleness, poor gas, and moisture barrier), processing (such as low heat distortion temperature), and cost. A review of biodegradable polymers in food packaging industry can be found elsewhere [46, 47]. The properties of some biodegradable and common polymers are reviewed here [48]. The application of nanotechnology to these polymers may open new possibilities for improving not only the properties but also the cost–price-efficiency.

Clay and inorganic solids have been the popular choice of additives for barrier property improvement, owing to their availability, low cost, significant enhancements, and ease of processing. The development of such polymer nanocomposites (using nanoclay) has been well documented by Ray et al. [49]. The layered silicates commonly used in nanocomposites consist of two-dimensional layers, which are 1 nm thick and several microns long depending on the particular silicate. Its presence in polymer formulations increases the tortuosity of the diffusive path for a penetrant molecule, providing excellent barrier properties [50–52].

NCC is an emerging candidate for packaging applications [53, 54]. Mechanical properties of cellulosic nanocomposites from some recent research are given in Table 13.4 [55]. It can be seen that PLA nanocomposites showed a significant increase in the Young's modulus and the cellulose acetate butyrate nanocomposite exhibiting more than 100 % increase in elongation at breaking point.

PLA, poly(lactic acid); CNW, cellulose nanowhiskers; CAB, cellulose acetate butyrate; MCC, microcrystalline cellulose; PVA, polyvinyl alcohol

Table 13.4 Average mechanical properties of cellulose nanocomposites

Material	Young's modulus (GPa)	Tensile strength (MPa)	Elongation at break %
PLA	2.0	58.0	4.2
PLA/CNW	2.6	57.0	3.3
CAB	0.3	30.3	17.0
CAB/MCC	0.2	39.5	40.0
PVA	2.3	43.0	–
PVA/5 % MCC	3.4	72.0	–
Lyocell	6.9	170.3	18.2
Lyocell/2 % MCC	12.6	218.6	10.6
Lyocell/3 % MCC	13.1	242.8	8.6

Moisture barrier of polymer films has been observed to be improved by cellulose nano-reinforcements [41, 56, 57]. The presence of crystalline fibers is thought to increase the tortuosity in the materials, leading to slower diffusion processes and, hence, to lower permeability. The barrier properties are enhanced if the filler is less permeable and has good dispersion in the matrix as well as a high aspect ratio [58]. Based on the tortuosity argument, Nielsen's model [59] is widely used to describe the permeability of filled polymers. Mechanical modeling and moisture diffusion modeling [60] on rodlike nanoparticle (typical morphology of NCC)-based nanocomposites have been studied to understand their impact on both mechanical and barrier properties.

Mechanical and water vapor barrier properties of chitosan films were improved by the addition of cellulose nanofibers. A nanocomposite film with 15 % cellulose nanofibers and plasticized with 18 % glycerol was comparable to synthetic polymers in terms of strength and stiffness, but their elongation and water vapor barrier were poorer, indicating that the film may be used only for applications that do not require a great flexibility and/or water vapor barrier [61].

6 Tissue Engineering

It is estimated that annually approximately one million fractures requiring hospitalization and medical attention occur in the USA. A significant fraction of which affect the load-bearing bones of the lower extremities [62]. Current treatments for severe bone injuries replace a nonunion defect with a permanent biomaterial that may corrode, wear, and cause infection [63, 64]. Additionally, these materials often possess mechanical strength far greater than bone, resulting in stress shielding and eventual bone resorption around the implant [65]. Thus, there is a significant need for a bone tissue engineering scaffold with tunable and predictable mechanical properties, similar to bone, that will gradually degrade, facilitate bone growth into the defect, and ultimately be replaced by natural bone tissue.

Polymers and especially those of the biodegradable variety find extensive use in the tissue engineering technology. Polymers provide great design flexibility, because the polymer composition and structure can be tailored to specific needs. In addition, biodegradable polymers can include chemical bonds that undergo hydrolysis upon exposure to body's aqueous environment or degrade by cellular or enzymatic pathways. The rate and extent of degradation are often a function of polymer properties such as hydrophobicity and crystallinity.

Degradable polymeric biomaterials are preferred candidates for developing therapeutic devices such as temporary prostheses, three-dimensional porous structures as scaffolds for tissue engineering, and as controlled/sustained release drug delivery vehicles. Each of these applications demands materials with specific physical, chemical, biological, biomechanical, and degradation properties to assure safe and efficient therapy.

Polymeric systems that have been investigated for bone regeneration include the poly(a-hydroxy esters) (poly(L-lactic acid) (PLLA), poly(glycolic acid) (PGA), poly(lactic-co-glycolic acid) (PLGA)), poly(propylene fumarate) [66], polydioxanone [67], poly(ethylene glycol) (PEG) [68], poly(orthoesters) [69], polyanhydrides [70], and polyurethane [71]. Poly(a-hydroxy esters), especially polylactic acid, have a long history of use as degradable surgical sutures, are approved for human use by the Food and Drug Administration, and are reasonably biocompatible. These polymers, by and large, serve as scaffolds that have appropriate three-dimensional structures on which osteoblasts will grow and deposit bone extracellular matrix (osteoid). The polymers degrade after the osteoid has become established. The polymeric materials may also serve as carrier vehicles for the delivery of bioactive molecules at the same time that they perform a structural function. A schematic displaying the interdisciplinary nature of tissue engineering study is displayed in Fig. 13.3.

However, it has been observed that the success that biodegradable polymers like PLA find in soft-tissue cell transplantation [72–74] has not been able to be duplicated in hard-tissue regeneration [75–78] due to weak mechanical properties. As the polymer scaffold matrix gradually degrades and simultaneously the resulting space is filled with the growing tissue, the scaffold structure should provide sufficient temporary mechanical support to withstand in vitro and in vivo stresses and loading in applications such as bone regeneration [79–81].

Nanocellulose application in tissue engineering is of growing interest [82, 83]. Predictable and high tensile modulus and strength under both wet and dry conditions are essential selection criteria for a bone tissue engineering material [84]. From a purely mechanical property point of view, nanocellulose's specific modulus makes it an attractive choice for bone repair covering a wide range of strength and strain typical of that of a native human bone [96]. Bacterial nanocellulose is especially distinguished by its biocompatibility and moldability during cultivation.

Microporous BC is a promising biomaterial for bone tissue engineering applications [85, 86]. Wan et al. [87] studied the HAp/BC nanocomposites with a three-dimensional (3-D) network were synthesized via a biological route.

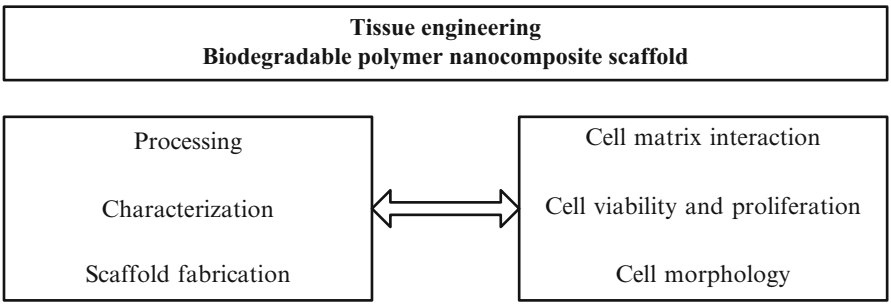

Fig. 13.3 Schematics of linkages and interdependencies in the field of tissue engineering

One of the key elements in bone tissue engineering is the three-dimensional biomaterial scaffold which provides structural support for cell attachment, spreading, migration, proliferation, and differentiation [88]. This scaffold should possess a network of interconnected pores to permit cell migration and the transport of nutrients to the cells. Zaborowska et al. [89] produced microporous bacterial cellulose scaffolds with a 300–500 μm pore size.

Rambo et al. [90] produced porous nanofibrous bacterial cellulose membranes. These membranes exhibited suitable macro- and microstructure and have potential for repairing tissue for cartilage and skin due to its nanofibrous network. The nanofibrous network could promote cell growth, and a porous network, which improves the oxygenation of the repairing tissue.

Czaja et al. [91] have discussed in detail the wide variety of biomedical applications of bacterial cellulose including scaffolds for tissue engineering. Cellulose scaffolds have also been shown to be capable growing structurally mature and functionally competent cardiac cell networks in culture [92].

Tissue engineering is a niche area where the high cost of manufacture of these nanocomposites can be justified. Microbial cellulose has already been shown to have excellent potential in this regard. In both tissue engineering and food packaging, it is very important to understand the underlying science of nanotechnology. New regulatory guidelines to accommodate nanotechnology-based products in contact with food and the body are likely to evolve from the fundamental understanding of these material [93–98], keeping in mind that nanoparticles behave very differently to their chemical analogues.

7 Conclusion

Cellulose is one of the most ubiquitous polymeric materials in the planet. Nanocellulose derived from cellulose through various mechanical and chemical ways presents opportunity for endless multitude of material applications. We review here the current research in two diverse and important fields of packaging

and tissue engineering. The manipulation of mechanical, thermal, and barrier properties that are provided by the reinforcement of nanocellulose is critical for both these applications.

It is clear that chemical modification of nanocellulose becomes necessary to expand the scope of its usage. This in turn has an adverse effect on the final cost of the product. This predicament can be overcome by directing more research towards cheaper methods of modification. A better understanding of nanocellulose-polymer matrix chemistry and reaction mechanisms is important to realize the full potential of these materials. We have reviewed the capabilities of nanocellulose to improve on properties of some existing polymers; however, nanocellulose's full potential has not been utilized yet. Nanocellulose surface modification, dispersion, and bonding with the polymer matrices are highlighted as major areas for research and development. Processing and methods of fabrication can also be a key in opening new applications and reducing the cost of production. Nanocellulose extraction processes are simple but unique at the same time, which allow investigating routes that are not common in industry for making and processing polymeric nanocomposites.

References

1. French AD, Bertoniere NR, Brown RM, Chanzy H, Gray D, Hattori K, Glasser W (2002) Cellulose. In: Encyclopedia of polymer science and technology. Wiley, New York. doi:10.1002/0471440264.pst042
2. Eichhorn S, Dufresne A, Aranguren M, Marcovich N, Capadona J, Rowan S, Weder C, Thielemans W, Roman M, Renneckar S, Gindl W, Veigel S, Keckes J, Yano H, Abe K, Nogi M, Nakagaito A, Mangalam A, Simonsen J, Benight A, Bismarck A, Berglund L, Peijs T (2010) Review: current international research into cellulose nanofibres and nanocomposites. J Mater Sci 45(1):1–33. doi:10.1007/s10853-009-3874-0
3. Azizi Samir MAS, Alloin F, Dufresne A (2005) Review of recent research into cellulosic whiskers, their properties and their application in nanocomposite field. Biomacromolecules 6(2):612–626. doi:10.1021/bm0493685
4. Dong XM, Kimura T, Revol JF, Gray DG (1996) Effects of ionic strength on the isotropic-chiral nematic phase transition of suspensions of cellulose crystallites. Langmuir 12:2076
5. Edgar CD, Gray DG (2003) Smooth model cellulose I surfaces from nanocrystal suspensions. Cellulose 10(4):299–306. doi:10.1023/a:1027333928715
6. Habibi Y, Lucia LA, Rojas OJ (2010) Cellulose nanocrystals: chemistry, self-assembly, and applications. Chem Rev 110(6):3479–3500. doi:10.1021/cr900339w
7. Favier V, Cavaille JY, Canova GR, Shrivastava SC (1997) Mechanical percolation in cellulose whisker nanocomposites. Polym Eng Sci 37(10):1732–1739. doi:10.1002/pen.11821
8. Noishiki Y, Nishiyama Y, Wada M, Kuga S, Magoshi J (2002) Mechanical properties of silk fibroin–microcrystalline cellulose composite films. J Appl Polym Sci 86(13):3425–3429. doi:10.1002/app.11370
9. Roman M, Winter William T (2006) Cellulose Nanocrystals for Thermoplastic Reinforcement: Effect of Filler Surface Chemistry on Composite Properties. In: Cellulose Nanocomposites, vol 938, ACS Symposium Series. American Chemical Society, Washington, DC, pp 99–113. doi:10.1021/bk-2006-0938.ch008
10. Qi H, Cai J, Zhang L, Kuga S (2009) Properties of films composed of cellulose nanowhiskers and a cellulose matrix regenerated from alkali/urea solution. Biomacromolecules 10(6):1597–1602. doi:10.1021/bm9001975

11. Marchessault RH, Morehead FF, Walter NM (1959) Liquid crystal systems from fibrillar polysaccharides. Nature 184:632–633
12. Revol J, Bradford H, Giasson J, Marchessault RH, Gray DG (1992) Helicoidal self-ordering of cellulose microfibrils in aqueous suspension. Int J Biol Macromol 14(3):170–172
13. Revol J, Godbout L, Dong XM, Gray DG, Chanzy H, Maret G et al (1994) Chiral nematic suspensions of cellulose crystallites; phase separation and magnetic field orientation. Liq Cryst 16(1):127–134
14. Dong XM, Revol J-F, Gray DG (1998) Effect of microcrystallite preparation conditions on the formation of colloid crystals of cellulose. Cellulose 5(1):19–32. doi:10.1023/a:1009260511939
15. Koshizawa T (1960) Degradation of wood cellulose and cotton linters in phosphoric acid. Kami Pa Gikyoshi, vol 14, pp 455–458
16. Sadeghifar H, Filpponen I, Clarke S, Brougham D, Argyropoulos D (2011) Production of cellulose nanocrystals using hydrobromic acid and click reactions on their surface. J Mater Sci 46(22):7344–7355. doi:10.1007/s10853-011-5696-0
17. Elazzouzi-Hafraoui S, Nishiyama Y, Putaux J-L, Heux L, Dubreuil F, Rochas C (2007) The shape and size distribution of crystalline nanoparticles prepared by acid hydrolysis of native cellulose. Biomacromolecules 9(1):57–65. doi:10.1021/bm700769p
18. Bai W, Holbery J, Li K (2009) A technique for production of nanocrystalline cellulose with a narrow size distribution. Cellulose 16(3):455–465. doi:10.1007/s10570-009-9277-1
19. de Souza Lima MM, Borsali R (2002) Static and dynamic light scattering from polyelectrolyte microcrystal cellulose†. Langmuir 18(4):992–996. doi:10.1021/la0105127
20. Nguyen XT, Tan Z (2003) Surface treatment with texturized microcrystalline cellulose microfibrils for improved paper and paper board. US Patent US7037405: (Submitted)
21. Henriksson M, Henriksson G, Berglund LA, Lindström T (2007) An environmentally friendly method for enzyme-assisted preparation of microfibrillated cellulose (MFC) nanofibers. Eur Polym J 43(8):3434–3441. doi:10.1016/j.eurpolymj.2007.05.038
22. Siró I, Plackett D (2010) Microfibrillated cellulose and new nanocomposite materials: a review. Cellulose 17(3):459–494. doi:10.1007/s10570-010-9405-y
23. Hashaikeh R, Abushammala H (2011) Acid mediated networked cellulose: preparation and characterization. Carbohydr Polym 83(3):1088–1094. doi:10.1016/j.carbpol.2010.08.081
24. Turbak AF, Snyder FW, Sandberg KR (1983) Microfibrillated cellulose, a new cellulose product: properties, uses, and commercial potential. J Appl Polym Sci Appl Polym Sympos 37(9):815–827
25. Gardner DJ, Oporto GS, Mills R, Samir MASA (2008) Adhesion and surface issues in cellulose and nanocellulose. J Adhes Sci Technol 22(5–6):545–567. doi:10.1163/156856108x295509
26. Habibi Y, Mahrouz M, Vignon MR (2009) Microfibrillated cellulose from the peel of prickly pear fruits. Food Chem 115(2):423–429. doi:10.1016/j.foodchem.2008.12.034
27. Spence K, Venditti R, Rojas O, Habibi Y, Pawlak J (2010) The effect of chemical composition on microfibrillar cellulose films from wood pulps: water interactions and physical properties for packaging applications. Cellulose 17(4):835–848. doi:10.1007/s10570-010-9424-8
28. Haigler CH, Weimer PJ (1990) Biosynthesis and biodegradation of cellulose. CRC Press, Boca Raton, Cambridge
29. Yoshinaga F, Tonouchi N, Watanabe K (1997) Research progress in production of bacterial cellulose by aeration and agitation culture and its application as a new industrial material. Biosci Biotechnol Biochem 61(2):219–224
30. Gardner KH, Blackwell J (1974) The structure of native cellulose. Biopolymers 13(10):1975–2001. doi:10.1002/bip.1974.360131005

31. John A. Cuculo NAaMWF (2001) Solvent spun cellulose fibers. In: Salem DR (ed) Structure formation in polymer fibers. ACS symposium series. Hanser Gardner Publications Inc., Ohio, pp 296–332
32. Freire MG, Teles ARR, Ferreira RAS, Carlos LD, Lopes-da-Silva JA, Coutinho JAP (2011) Electrospun nanosized cellulose fibers using ionic liquids at room temperature. Green Chem 13(11):3173–3180
33. Freire MG, Teles ARR, Rocha MAA, Schröder B, Neves CMSS, Carvalho PJ, Evtuguin DV, Santos LMNBF, Coutinho JAP (2011) Thermophysical characterization of ionic liquids able to dissolve biomass. J Chem Eng Data 56(12):4813–4822. doi:10.1021/je200790q
34. Freire CSR, Silvestre AJD, Neto CP, Gandini A, Martin L, Mondragon I (2008) Composites based on acylated cellulose fibers and low-density polyethylene: effect of the fiber content, degree of substitution and fatty acid chain length on final properties. Compos Sci Technol 68(15–16):3358–3364
35. Araki J, Wada M, Kuga S (2000) Steric stabilization of a cellulose microcrystal suspension by poly(ethylene glycol) grafting. Langmuir 17(1):21–27. doi:10.1021/la001070m
36. Goussé C, Chanzy H, Excoffier G, Soubeyrand L, Fleury E (2002) Stable suspensions of partially silylated cellulose whiskers dispersed in organic solvents. Polymer 43(9):2645–2651
37. Grunert M, Winter WT (2002) Nanocomposites of cellulose acetate butyrate reinforced with cellulose nanocrystals. J Polym Environ 10(1):27–30
38. Hubbe MA, Rojas OJ, Lucia LA, Sain M (2008) Cellulosic nanocomposites: a review. BioResources 3:929
39. Bledzki AK, Gassan J (1999) Composites reinforced with cellulose based fibres. Prog Polym Sci 24(2):221–274. doi:10.1016/s0079-6700(98)00018-5
40. Saheb DN, Jog JP (1999) Natural fiber polymer composites: a review. Adv Polym Technol 18(4):351–363
41. Sanchez-Garcia MD, Gimenez E, Lagaron JM (2008) Morphology and barrier properties of solvent cast composites of thermoplastic biopolymers and purified cellulose fibers. Carbohydr Polym 71(2):235–244
42. Tserki V, Matzinos P, Zafeiropoulos NE, Panayiotou C (2006) Development of biodegradable composites with treated and compatibilized lignocellulosic fibers. J Appl Polym Sci 100(6):4703–4710
43. Favier V, Chanzy H, Cavaille JY (1995) Polymer nanocomposites reinforced by cellulose whiskers. Macromolecules 28:6365
44. Fomin VA, Guzeev V (2001) Biodegradable polymers, their present state and future prospects. Prog Rubber Plastics Technol 17:186–204
45. Tharanathan RN (2003) Biodegradable films and composite coatings: past, present and future. Trends Food Sci Technol 14(3):71–78
46. Siracusa V, Rocculi P, Romani S, Rosa MD (2008) Biodegradable polymers for food packaging: a review. Trends Food Sci Technol 19(12):634–643
47. Sorrentino A, Gorrasi G, Vittoria V (2007) Potential perspectives of bio-nanocomposites for food packaging applications. Trends Food Sci Technol 18(2):84–95
48. Correlo V, Boesel L, Reis R, Bhattacharya M (2005) Material properties of biodegradable polymers. In: Biodegradable polymers for industrial applications, vol null. CRC Press, Boca Raton, Cambridge. doi:10.1201/9781439823699.ch13
49. Ray S, Easteal A, Quek SY, Chen XD (2006) The potential use of polymer–clay nanocomposites in food packaging. Int J Food Eng 2(4):art 5
50. Bharadwaj RK, Mehrabi AR, Hamilton C, Trujillo C, Murga M, Fan R, Chavira A, Thompson AK (2002) Structure–property relationships in cross-linked polyester-clay nanocomposites. Polymer 43(13):3699–3705
51. Cabedo L, Giménez E, Lagaron JM, Gavara R, Saura JJ (2004) Development of EVOH-kaolinite nanocomposites. Polymer 45(15):5233–5238

52. Mirzadeh A, Kokabi M (2007) The effect of composition and draw-down ratio on morphology and oxygen permeability of polypropylene nanocomposite blown films. Eur Polym J 43(9):3757–3765
53. Dufresne A, Dupeyre D, Paillet M (2003) Lignocellulosic flour-reinforced poly(hydroxybutyrate-co-valerate) composites. J Appl Polym Sci 87(8):1302–1315
54. Svagan AJ ASMaBL (2007) Biomimetic polysaccharide nanocomposites of high cellulose content and high toughness. Biomacromolecules 8(8):2556–2563
55. Tuomas H, Prof. Dr. Mark H, Dr.-Ing. Erwin B, Frank O, Tim H, Nina G, Prof. Dr.-Ing Jürg M, Eugen P, Martien van den O, Dr. Harriëtte B, Dr. Sanchita B-G, Dr. Subrata Bandhu G, Prof. Dr. Mohini S (2002) Composites. In: Prof. Dr.-Ing Jürg M (ed) Industrial applications of natural fibres. Wiley, pp 381–480
56. Paralikar SA SJaLJ (2008) Poly(vinyl alcohol)/cellulose nanocrystal barrier membranes. J Membr Sci 320(1–2):248–258
57. Svagan AJ HMaBL (2009) Reduced water vapour sorption in cellulose nanocomposites with starch matrix. Compos Sci Technol 69(3–4):500–506
58. Lagaron J, Catalá R, Gavara R (2004) Structural characteristics defining high barrier polymeric materials. Mater Sci Technol 20:1–7
59. Nielsen LE (1967) Models for the permeability of filled polymer systems. J Macromol Sci Chem 1(5):929–942
60. Picken SJ, Vlasveld DPN, Bersee HEN, Özdilek C, Mendes E (2007) Structure and mechanical Properties of nanocomposites with rod- and plate-shaped nanoparticles. Nanocomposites. Springer US, 143–173
61. Azeredo HMC, Mattoso LHC, Avena-Bustillos RJ, Filho GC, Munford ML, Wood D, McHugh TH (2010) Nanocellulose reinforced chitosan composite films as affected by nanofiller loading and plasticizer content. J Food Sci 75(1):N1–N7. doi:10.1111/j.1750-3841.2009.01386.x
62. Hall MJ, Owings MF (2002) National hospital discharge survey. CDC-National Center for Health Statistics, Atlanta
63. Petty W, Spanier S, Shuster J (1988) Prevention of infection after total joint replacement. Experiments with a canine model. J Bone Joint Surg Am 70:536–539
64. Petty W, Spanier S, Shuster J, Silverthorne C (1985) The influence of skeletal implants on incidence of infection: experimentsin a canine model. J Bone Joint Surg Am 67:1236–1244
65. Bobyn J, Mortimer ES, Glassman AH, Engh CA, Miller JE, Brooks CE (1992) Producing and avoiding stress shielding. Laboratory and clinical observations of noncemented total hip arthroplasty. Clin Orthop 1992:79–96
66. Miyamoto S, Takaoka K (1993) Bone induction and bone repair by composites of bone morphogenetic protein and biodegradable synthetic polymers. Ann Chir Gynaecol 82:69–75
67. Gerhart TNRA, Miller RL, Noecker RJ, Hayes WC (1989) In vivo histologic and biomechanical characterization of a biodegradable particulate composite bone cement. J Biomed Mater Res 23:1–16
68. Nichter LS, Yazdi M, Kosari K, Sridjaja R, Ebramzadeh E, Nimni ME (1992) Demineralized bone matrix/polydioxanone composite as a substitute for bone graft: a comparative study in rats. J Craniofac Surg 3:63–69
69. Solhcim E, Pinholt E, Bang G, Sudmann E (1992) Regeneration of calvarial defects by a composite of bioerodible polyorthoester and demineralized bone in rats. J Neurosurg 1992(76):275–279
70. Mathiowitz E, Amato C, Langer R (1990) Polyanhydride microspheres: 3. Morphology and characterization of systems made by solvent removal. Polymer 31:547–555
71. Nielsen F, Karring T, Gogolewski S (1992) Biodegradable guide for bone regeneration: polyurethane membranes tested in rabbit radius defects. Acta Orthop Scand 63:66–69
72. Cima LG, Vacanti J, Vacanti C, Ingber DE, Mooney DJ, Langer R (1991) Tissue engineering by cell transplantation using biodegradable polymer substrates. J Biomech Eng 113:143–151

73. Freed L, Marquis J, Nohria A, Emmanual J, Mikos A (1993) *Neocartilage* formation in vitro and in vivo using cells cultured on synthetic biodegradable polymers. J Biomed Mater Res 27:11–23
74. Mikos A, Bao Y, Cima L, Ingber D, Vacanti J, Langer R (1993) Laminated Three Dimensional Biodegradable Foams for use in Tissue Engineering. Biomater 14:323–330
75. Freyman T, Yannas I, Gibson L (2001) Cellular materials as porous scaffolds for tissue engineering. J Prog Mater Sci 46:273–282
76. Mikos A, Bao Y, Cima L, Ingber DE, Vacanti J, Langer R (1993) Preparation of poly(glycolic acid) bonded fiber structures for cell transplantation. J Biomed Mater Res 27:183–189
77. Nam Y, Park T (1999) Biodegradable polymeric microcellular foams by modified thermally induced phase separation method. Biomater 20:1783–1790
78. Nam Y, Yoon J, Park T (2000) A novel fabrication method of macroporous biodegradable polymer scaffolds using gas foaming salt as a porogen additive. J Biomed Mater Res 53:1–7
79. Hua F, Nam J, Lee D (2001) Preparation of a Macroporous Poly (L-lactide) Scaffold by Liquid-Liquid Phase Separation of a PLLA/1, 4-Dioxane/Water Ternary System in the presence of NaCl. Macromol Rapid Commun 22:1053–1057
80. Kikuchi M, Itoh S, Ichinose S, Shinomiya K, Tanaka J (2001) Self-organization mechanism in a bone-like hydroxyapatite/collagen nanocomposite synthesized in vitro and its biological reaction in vivo. Biomaterials 22:1705–1711
81. Kikuchi M, Tanaka J (2000) J Ceram Soc Jpn 108:643–645
82. Bodin A, Ahrenstedt L, Fink H, Brumer H, Risberg B, Gatenholm P (2007) Modification of nanocellulose with a xyloglucan–RGD conjugate enhances adhesion and proliferation of endothelial cells: implications for tissue engineering. Biomacromolecules 8(12):3697–3704. doi:10.1021/bm070343q
83. Klemm D, Schumann D, Kramer F, Heßler N, Hornung M, Schmauder H-P, Marsch S (2006) Nanocelluloses as innovative polymers in research and application. In: pp 49–96
84. Xu W (2009) Thesis: Development of laminated fiber-reinforced nanocomposites for bone regeneration
85. Bäckdahl H, Helenius G, Bodin A, Nannmark U, Johansson BR, Risberg B, Gatenholm P (2006) Mechanical properties of bacterial cellulose and interactions with smooth muscle cells. Biomaterials 27(9):2141–2149
86. Svensson A, Nicklasson E, Harrah T, Panilaitis B, Kaplan DL, Brittberg M, Gatenholm P (2005) Bacterial cellulose as a potential scaffold for tissue engineering of cartilage. Biomaterials 26(4):419–431
87. Wan YZ, Huang Y, Yuan CD, Raman S, Zhu Y, Jiang HJ, He F, Gao C (2007) Biomimetic synthesis of hydroxyapatite/bacterial cellulose nanocomposites for biomedical applications. Mater Sci Eng C 27(4):855–864
88. Hutmacher DW (2000) Scaffolds in tissue engineering bone and cartilage. Biomaterials 21(24):2529–2543
89. Zaborowska M, Bodin A, Bäckdahl H, Popp J, Goldstein A, Gatenholm P (2010) Microporous bacterial cellulose as a potential scaffold for bone regeneration. Acta Biomater 6(7):2540–2547. doi:10.1016/j.actbio.2010.01.004
90. Rambo CR, Recouvreux DOS, Carminatti CA, Pitlovanciv AK, Antônio RV, Porto LM (2008) Template assisted synthesis of porous nanofibrous cellulose membranes for tissue engineering. Mater Sci Eng C 28(4):549–554
91. Czaja WK, Young DJ, Kawecki M, Brown RM (2006) The future prospects of microbial cellulose in biomedical applications. Biomacromolecules 8(1):1–12. doi:10.1021/bm060620d
92. Entcheva E, Bien H, Yin L, Chung CYC-Y, Farrell M, Kostov Y (2004) Functional cardiac cell constructs on cellulose-based scaffolding. Biomaterials 25(26):5753–5762
93. Borm P, Robbins D, Haubold S, Kuhlbusch T, Fissan H, Donaldson K, Schins R, Stone V, Kreyling W, Lademann J, Krutmann J, Warheit D, Oberdorster E (2006) The potential risks of nanomaterials: a review carried out for ECETOC. Part Fibre Toxicol 3(1):11

94. Derfus AM, Chan WCW, Bhatia SN (2003) Probing the cytotoxicity of semiconductor quantum dots. Nano Lett 4(1):11–18. doi:10.1021/nl0347334
95. Hoet PH, Nemmar A, Nemery B (2004) Health impact of nanomaterials? Nat Biotechnol 22(1):19–19
96. http://www.feppd.org/ICBDent/campus/biomechanics_in_dentistry/ldv_data/mech/basic_bone.htm
97. TNFpM. http://www.nanosustain.eu
98. Oberdörster G, Oberdörster E, Oberdörster J (2005) Nanotoxicology: an emerging discipline evolving from studies of ultrafine particles. Environ Health Perspect 113(7):823–839
99. Southern Clay Products I http://www.scprod.com/home.asp
100. Lau K-t, Gu C, Hui D (2006) A critical review on nanotube and nanotube/nanoclay related polymer composite materials. Compos Part B Eng 37(6):425–436
101. Eichhorn SJ, Sirichaisit J, Young RJ (2001) Deformation mechanisms in cellulose fibres, paper and wood. J Mater Sci 36(13):3129–3135. doi:10.1023/a:1017969916020
102. Assessment USCOoT (1993) Biopolymers: making materials nature's way. Government Printing Office, Washington, DC
103. Guhados G, Wan W, Hutter JL (2005) Measurement of the elastic modulus of single bacterial cellulose fibers using atomic force microscopy. Langmuir 21(14):6642–6646. doi:10.1021/la0504311
104. Goussé C, Chanzy H, Cerrada ML, Fleury E (2004) Surface silylation of cellulose microfibrils: preparation and rheological properties. Polymer 45(5):1569–1575
105. Andresen M, Johansson L-S, Tanem BS, Stenius P (2006) Properties and characterization of hydrophobized microfibrillated cellulose. Cellulose 13(6):665–677. doi:10.1007/s10570-006-9072-1
106. Lu J, Askeland P, Drzal LT (2008) Surface modification of microfibrillated cellulose for epoxy composite applications. Polymer 49(5):1285–1296
107. Gopalan Nair K, Dufresne A, Gandini A, Belgacem MN (2003) Crab shell chitin whiskers reinforced natural rubber nanocomposites. 3. Effect of chemical modification of chitin whiskers. Biomacromolecules 4(6):1835–1842. doi:10.1021/bm030058g
108. Stenstad P, Andresen M, Tanem B, Stenius P (2008) Chemical surface modifications of microfibrillated cellulose. Cellulose 15(1):35–45. doi:10.1007/s10570-007-9143-y
109. Siqueira G, Bras J, Dufresne A (2008) Cellulose whiskers versus microfibrils: influence of the nature of the nanoparticle and its surface functionalization on the thermal and mechanical properties of nanocomposites. Biomacromolecules 10(2):425–432. doi:10.1021/bm801193d
110. Wang BSM (2007) The effect of chemically coated nanofiber reinforcement on biopolymer based nanocomposites. BioResources 2:371–388
111. Andresen M, Stenstad P, Møretrø T, Langsrud S, Syverud K, Johansson L-S, Stenius P (2007) Nonleaching antimicrobial films prepared from surface-modified microfibrillated cellulose. Biomacromolecules 8(7):2149–2155. doi:10.1021/bm070304e
112. Saito T, Nishiyama Y, Putaux J-L, Vignon M, Isogai A (2006) Homogeneous suspensions of individualized microfibrils from TEMPO-catalyzed oxidation of native cellulose. Biomacromolecules 7(6):1687–1691. doi:10.1021/bm060154s
113. Montanari S, Roumani M, Heux L, Vignon MR (2005) Topochemistry of carboxylated cellulose nanocrystals resulting from TEMPO-mediated oxidation. Macromolecules 38(5):1665–1671. doi:10.1021/ma048396c
114. Ljungberg N, Bonini C, Bortolussi F, Boisson C, Heux L, Cavaillé JY (2005) New nanocomposite materials reinforced with cellulose whiskers in atactic polypropylene: effect of surface and dispersion characteristics. Biomacromolecules 6(5):2732–2739. doi:10.1021/bm050222v
115. Kim D-Y, Nishiyama Y, Kuga S (2002) Surface acetylation of bacterial cellulose. Cellulose 9(3):361–367. doi:10.1023/a:1021140726936
116. Ifuku S, Nogi M, Abe K, Handa K, Nakatsubo F, Yano H (2007) Surface modification of bacterial cellulose nanofibers for property enhancement of optically transparent composites:

dependence on acetyl-group DS. Biomacromolecules 8(6):1973–1978. doi:10.1021/bm070113b
117. Nogi M, Abe K, Handa K, Nakatsubo F, Ifuku S, Yano H (2006) Property enhancement of optically transparent bionanofiber composites by acetylation. Appl Phys Lett 89(23):233123
118. Braun B, Dorgan JR (2008) Single-step method for the isolation and surface functionalization of cellulosic nanowhiskers. Biomacromolecules 10(2):334–341. doi:10.1021/bm8011117
119. Sobkowicz MJ, Braun B, Dorgan JR (2009) Decorating in green: surface esterification of carbon and cellulosic nanoparticles. Green Chem 11(5):680–682
120. Berlioz S, Molina-Boisseau S, Nishiyama Y, Heux L (2009) Gas-phase surface esterification of cellulose microfibrils and whiskers. Biomacromolecules 10(8):2144–2151. doi:10.1021/bm900319k
121. Bondeson D, Oksman K (2007) Polylactic acid/cellulose whisker nanocomposites modified by polyvinyl alcohol. Compos Part A Appl Sci Manuf 38(12):2486–2492
122. Mathew AP Chakraborty A, Oksman K, Sain M (2006) The structure and mechanical properties of cellulose nanocomposites prepared by twin screw extrusion. In: Oksman K, Sain M (eds) Cellulose nanocomposites: processing, characterization, and properties. American Chemical Society: Washington, DC 938:114–131
123. Oksman K, Mathew AP, Bondeson D, Kvien I (2006) Manufacturing process of cellulose whiskers/polylactic acid nanocomposites. Compos Sci Technol 66(15):2776–2784
124. Helbert W, Cavaillé JY, Dufresne A (1996) Thermoplastic nanocomposites filled with wheat straw cellulose whiskers. Part I: processing and mechanical behavior. Polym Compos 17(4):604–611. doi:10.1002/pc.10650
125. Morin A, Dufresne A (2002) Nanocomposites of chitin whiskers from riftia tubes and poly (caprolactone). Macromolecules 35(6):2190–2199. doi:10.1021/ma011493a
126. Li Z, Renneckar S, Barone J (2010) Nanocomposites prepared by in situ enzymatic polymerization of phenol with TEMPO-oxidized nanocellulose. Cellulose 17(1):57–68. doi:10.1007/s10570-009-9363-4
127. Wu Q LX, Berglund LA (2002) In: 23rd Risø international symposium on materials science, sustainable natural and polymeric composites-science and technology
128. Ramirez Vicèns MA (2010) Cellulose nanocrystals reinforced electrospun poly(lactic acid) fibers as potential scaffold for bone tissue engineering. Thesis
129. Chunhui Xiang MWFhhhn Nanocomposite fibers electrospun from biodegradable polymers
130. Olsson RT, Kraemer R, López-Rubio A, Torres-Giner S, Ocio MJ, Lagarón JM (2010) Extraction of microfibrils from bacterial cellulose networks for electrospinning of anisotropic biohybrid fiber yarns. Macromolecules 43(9):4201–4209. doi:10.1021/ma100217q
131. Park WI, Kang M, Kim HS, Jin HJ (2007) Electrospinning of poly(ethylene oxide) with bacterial cellulose whiskers. Macromol Symp 249–250(1):289–294. doi:10.1002/masy.200750347

Mechanical and Morphology Properties of Cellulose Nanocomposites

14

Mohamed H. Gabr, Kazuya Okubo, and Toru Fujii

Contents

Abstract

Cellulose nanofibers and their composites have a great deal of attention because of their abundance, biodegradability, high strength and stiffness, low weight, relatively low price, and the related characteristics such as a very large surface-to-volume ratio and outstanding mechanical, electrical, and thermal properties. Such new high-value materials are the subject of continuing research and are commercially interesting in terms of new products from the pulp and paper industry and the agricultural sector. This chapter summarizes (i) the progress in

M.H. Gabr (✉)
Department of Mechanical Engineering and Systems, Research and Development Center, Kanazawa Institute of Technology, Ishikawa, Kyoto, Japan

Faculty of Industrial Education, Sohag University, Sohag, Egypt
e-mail: mgabr@neptune.kanazawa-it.ac.jp

K. Okubo • T. Fujii
Department of Mechanical Engineering and Systems, Doshisha University, Kyotonabe, Kyoto, Japan
e-mail: kokubo@mail.doshisha.ac.jp; tfujii@mail.doshisha.ac.jp

J.K. Pandey et al. (eds.), *Handbook of Polymer Nanocomposites. Processing, Performance and Application – Volume C: Polymer Nanocomposites of Cellulose Nanoparticles*,
DOI 10.1007/978-3-642-45232-1_65,

nanocellulose preparation into polymer matrix with a particular focus on microfibrillated cellulose and also discusses recent developments in bio-nanocomposite fabrication based on nanocellulose, (ii) the progress in the reinforcement of the carbon fiber/epoxy composites using nanocellulose as a hybrid reinforcement, (iii) the improvement in the mechanical properties of carbon fiber/epoxy composites using nanocellulose as hybrid reinforcement, and (iv) the morphology of CF/epoxy composite reinforced with nanocellulose showing the effect of nanocellulose on the fiber/matrix adhesion.

1 Introduction

Composites are widely used in many applications, such as automotive, construction, packaging, etc., due to their combination of excellent stiffness and strength along with their low density. In recent years, the use of natural fibers as reinforcements in polymers and composites has attracted much attention due to the environmental concerns.

Natural fibers have many advantages, such as sustainability, renewability, recyclability, wide availability, low density, biodegradability, and, last but not least, low cost, which offer greater opportunities to develop a new class of lightweight, environmental friendly, and structural composites.

Cellulose, the most abundant natural homopolymer, is considered to be one of the most promising renewable resources and an environmentally friendly alternative to products derived from the petrochemical industry. Plant-derived cellulose has been widely used as either reinforcement [1–9] or matrix and even as the sole component to prepare all-cellulose composites [10, 11].

Recently the identification of nano-sized cellulose microfibrils increases the choices of fibers and expands their use because of their excellent mechanical properties in composites. Nano-sized cellulose fiber is called microfibrillated cellulose (MFC), which can be traced back to the early 1980s [12]. MFC is obtained through a homogenization process, at high shear, producing microfibrils with a diameter range of 10–100 nm, but with a weblike structure.

Besides cellulose from plants, cellulose is also secreted extracellularly as synthesized cellulose fibers by some bacterial species, which is called bacterial cellulose (BC). Compared with other natural plant cellulose, BC is a nanomaterial, which displays many unique properties including higher purity, higher crystallinity, higher degree of polymerization, higher water absorption and retaining capacity, higher tensile strength, higher Young's modulus, and stronger biological adaptability. BC has been widely used in foods and in acoustic diaphragms for audio speakers or headphones and for making unusually strong paper and has medical applications as wound dressings and artificial skins, artificial blood vessels, and tissue engineering scaffolds [13–16]. BC has been used as reinforcements for various composites due to its excellent mechanical performance [9, 17–22].

In this chapter, we are going to review the effect of nanocellulose on the tensile and fracture toughness properties of CF/epoxy composite with the carbon fiber fraction of volume 50 % of the composite. Because elastomeric modification is the accepted method for improving toughness properties of epoxy, we are going to discuss the effect of incorporating liquid rubber with nanocellulose on CF/epoxy composite. The composites reinforced with MFC and BC were prepared as the same as 56 and 57.

2 Progress in Reinforcing the Composites Using Nanocellulose as Reinforcement

Using MFC as reinforcement with polymer matrix gives significant effect on the mechanical properties for the composite [23–27]. Takagaki et al. [5, 6] showed that the static properties of MFC/CF/epoxy composite were slightly improved with the addition of 0.1, 0.3 wt% MF. They also stated that the fatigue life of the composite was improved significantly with the addition of MFC. Zimmerman et al. [28] reported that MFC-reinforced hydroxypropyl cellulose (HPC) prepared by film casting has three times higher tensile modulus and five times higher tensile strength compared with the matrix without reinforcement. Nakagaito and Yano [18] showed that nanocomposites produced by compression molding of MFC sheets impregnated with phenol formaldehyde (PF) resin have high bending strength and modulus comparable to magnesium alloy. Nanocomposite materials based on MFC and melamine formaldehyde (MF) resulted in high mechanical damping, showing their potential to be used as loudspeaker membranes [29]. Lisman Suryanegara et al. [30] showed that the addition of MFC increased the tensile modulus of crystallized neat polylactic acid (PLA) by 42 % and the strength by 14 % at an MFC content of 20 wt%.

However, the low interlaminar strength of composite laminates is one of the major disadvantages, which delayed the widespread use of composite laminates in primary aircraft structures. Interlaminar fracture is one of the major problems for fiber composites. Its occurrence greatly reduces the stiffness of a structure, often leading to catastrophic failure during service [31]. For this reason, many efforts have been made to improve the interlaminar strength. Kazuya Okubo et al. [32] stated that if a small amount of MFC is added into the bamboo fiber composite, tangled MFC fibers prevented the growth of microcrack along the interface between bamboo fiber and matrix. Kazuya Okubo et al. [33] showed significant improvements in the strain energy until fatal failure when the PLA matrix enhanced with 1 wt% of MFC. Yamashita Naoya et al. [34] showed that the addition of a small amount of MFC into polylactic acid/bamboo short fiber (PLA/BF) composites contributes to improve the fracture toughness and impact strength.

In this chapter, the epoxy resin was used as the matrix in the nanocomposites. Epoxy resins exhibit low shrinkage, excellent adhesion to a variety of substrate materials [35], high temperature performance, chemical resistance, and reactivity with a wide variety of chemical curing agents [36]. The resin forms a highly

cross-linked network structure having relatively high stiffness and glass transition temperature (T_g) with high chemical resistance. However, the inherent toughness of the network polymer is low. Elastomeric modification is one of the most frequently used and widely accepted methods for improving properties of epoxy networks. The copolymer of acrylonitrile and butadiene with end carboxyl functional groups, CTBN, can react with the epoxide groups and hence is popularly employed as a modifier to epoxy. A high level of interfacial adhesion and property improvements is achieved by this elastomer [37, 38]. Bussi and Ishida [39] studied the mechanical properties of blends of diglycidyl ether of bisphenol-A (DGEBA)-based epoxy resin and hydroxyl-terminated, internally epoxidized polybutadiene rubber. In order to improve mechanical properties, the epoxidized rubber was prereacted with an excess diepoxide to achieve better bonding between the rubber particles and the epoxy continuous phase. They also observed that without rubber prereaction, almost no improvement in the value of critical stress intensity factor, K_{IC} (fracture toughness), was achieved. However, K_{IC} increased with increasing prereacted rubber concentration. Nigam et al. [40] studied the changes in mechanical properties of epoxy cresol novolac (ECN) resin by liquid carboxyl-terminated copolymer of butadiene acrylonitrile (CTBN) modification. Tensile, flexural, and impact strength showed an increasing trend up to 10 % CTBN, beyond which a rapid fall took place. The great majority of the studies [41–43] involve the chemical modification of epoxy resin with reactive liquid rubber, particularly carboxyl-terminated butadiene acrylonitrile copolymer (CTBN). The micro structure formed consists of an elastomeric phase finely dispersed in the epoxy matrix with the elastomeric particle diameter of few micrometers or less. These particles enhance the toughness of the unmodified epoxy considerably with only a minimal modification to thermal and mechanical properties. Carbon fiber-reinforced plastic (CFRP) is a type of reinforcement which applied in this chapter. Carbon fibers offer the highest specific modulus and highest specific strength of all reinforcing fibers that make them suitable for such applications.

3 The Improvement in the Mechanical Properties of Carbon Fiber/Epoxy Composites Using Nanocellulose as Hybrid Reinforcement

3.1 Tensile Properties

The purpose of a tensile test is to determine the ultimate tensile stress and Young's modulus of a material. However, a closely observed test of a material under controlled conditions should provide a great deal more information about the way it behaves under load. A composite may split or delaminate, for instance, and studying the material as it is subjected to increasing load may give an insight into the ways in which damage initiates and develops. Finally, the nature of failure is seen; it may be brittle, with no warning, or it may be preceded by obvious audible or visible signs.

This section shows the effect of the nanocellulose fibers on the CF/epoxy composite and the modified composite with liquid rubber on the tensile properties. Young's modulus shows slight decrease with 0.5 wt% MFC followed by slight increase with 1 and 2 wt% MFC. The tensile strengths were almost constant at different MFC ratios. Qingzheng cheng et al. [44] prepared polyvinyl alcohol (PVA) nanocomposite reinforced with different types of cellulose fibrils. They reported that there is no significant difference for tensile strength and Young's modulus with the addition of 2 wt% MFC to PVA compared to neat PVA. The tensile strength and Young's modulus were 112 MPa and 6.3 GPa, respectively, for PVA reinforced with 2 wt% MFC, whereas 112 MPa and 5.7 GPa for neat PVA indicating slight increase for Young's modulus. The improvements of tensile strength as well as Young's modulus due to the addition of MFC were not as high as those of microfibers generated from wood pulp [45] and soybean [46]. The tensile strength was doubled (from 42 to 102 MPa), and the modulus was increased from 2.3 to 5.2 GPa by 5 % microfiber loading of wood microfibers-reinforced PVA [45]. The tensile strength was increased from 65 to 103 MPa; and the modulus was increased from 2.3 to 6.2 GPa by 5 % microfiber loading of soybean nanofibers-reinforced PVA [46].

Most reports have attributed the strong reinforcing effect of the cellulose to the formation of a networked structure above percolation threshold resulting from hydrogen bonding [47, 48]. In this work, possibly no network structure was formed at low MFC loadings due to relatively large diameter of microfiber aggregates. However, increasing MFC loadings in CF/epoxy composite, the carbon fiber cloth is deteriorated and lose its alignment during hand lay-up process. The reinforcing effect of MFC is a direct result of the interaction of the fiber and polymer, as well as the rigidity of the weblike structure. A higher concentration threshold is required to introduce interactions between fibrils so that a network can be formed [28]. As reported in Table 14.1, the tensile strength of these composite films displays almost a similar trend as the Young's modulus. The highest strength increase occurs at 2 wt% MFC by about 3 % which cannot consider significant increase. The results showed that the initiation of fatal failure under static load was not affected by the addition of MFC up to 2 wt%.

A gradual increase for composites filled with 1 % MFC and 0.5 and 1 % BC at 10 % CTBN was followed by a slight decrease with the addition of 20 % CTBN. This may be due to the increase in the relative amount of dissolved rubber as rubber content increases, which could be attributed to the fact that the strength and modulus of rubber is much lower than that of the epoxy matrix as well as carbon fiber [49]. In addition, low modulus rubber particles act as stress concentrators and decrease the yield strength. Although there is a tendency to increase strength for composite filled with the addition of MFC, the increase was not significant. The Young's modulus, determined from the typical stress–strain curve, showed little decrease for composites modified with 10 % CTBN followed by insignificant increase for composites filled with MFC at 20 % CTBN.

Table 14.1 Tensile properties for CF/epoxy composites reinforced with MFC and BC modified with CTBN

	MFC (%)	BC (%)	CTBN (%)	Tensile strength (MPa)	Young's modulus (GPa)
CF/epoxy/MFC_0/$CTBN_0$	0	0	0	669 ± 9.5	62.2 ± 4.1
CF/epoxy/MFC_0/$CTBN_{10}$	0	0	10	541 ± 35.9	53.8 ± 2.3
CF/epoxy/MFC_0/$CTBN_{20}$	0	0	20	604 ± 17.8	55.1 ± 1.9
CF/epoxy/$MFC_{0.5}$/$CTBN_0$	0.5	0	0	634.9 ± 16.6	55.5 ± 2.3
CF/epoxy/MFC_1/$CTBN_0$	1	0	0	593 ± 57.5	50 ± 2.9
CF/epoxy/$MFC_{0.5}$/$CTBN_{10}$	0.5	0	10	620 ± 22.7	57.4 ± 2.1
CF/epoxy/$MFC_{0.5}$/$CTBN_{20}$	0.5	0	20	664 ± 19.3	58.6 ± 3.4
CF/epoxy/MFC_1/$CTBN_{10}$	1	0	10	711 ± 25.2	56.7 ± 2.2
CF/epoxy/MFC_1/$CTBN_{20}$	1	0	20	698 ± 14.8	62.5 ± 2.6
CF/epoxy/MFC_2/$CTBN_0$	2	0	0	726 ± 27	57.2 ± 1.9
CF/epoxy/$BC_{0.5}$/$CTBN_0$	0	0.5	0	597 ± 21	58.95 ± 2.3
CF/epoxy/BC_1/$CTBN_0$	0	1	0	579 ± 4.3	59.85 ± 2.9
CF/epoxy/$BC_{0.5}$/$CTBN_{10}$	0	0.5	10	668 ± 31	54.85 ± 2.1
CF/epoxy/$BC_{0.5}$/$CTBN_{20}$	0	0.5	20	630 ± 4.7	53.05 ± 3.4
CF/epoxy/BC_1/$CTBN_{10}$	0	1	10	704 ± 11.1	51.15 ± 2.2
CF/epoxy/BC_1/$CTBN_{20}$	0	1	20	631 ± 5.3	51.8 ± 2.6

3.2 Mode I Interlaminar Fracture Toughness

This section discusses the effect of nanocellulose on the fracture toughness of the CF/epoxy composites. The typical load displacement curves recorded during the interlaminar fracture test for CF/epoxy composite filled with MFC contents are shown in Fig. 14.1. Step by step variations in the crack opening load of all specimens are observed. Severe steps are clearly observed for unfilled CF/Epoxy. It's seen that the specimens filled with MFC contents showed more stable and gradual crack growth than unfilled specimens. It was more pronounced that at 2 % MFC, the crack propagates more stable and gradually as well as almost all peaks rather than the first peak showed closed values which could be attributed to higher crack closure force exerted with the addition of MFC.

The delamination resistance curves (R-curves) are drawn between crack length (a) and the corresponding fracture toughness as shown in Fig. 14.2. The G_{IC} value corresponding to the first crack initiation is determined from the load point at which the initiation of delamination is microscopically observed on the specimen edge. High deviations are noted for all fabric composites, probably as a consequence of the complex translaminar crack growth mechanism acting in the material.

Both delamination initiation and delamination propagation mode I fracture toughness values are plotted in Fig. 14.3. The delamination initiation mode I fracture toughness values reported to the first peak load in the load–crack opening displacement curves, while the delamination propagation mode I fracture toughness values are taken from the plateau region of the R-curves [50, 51].

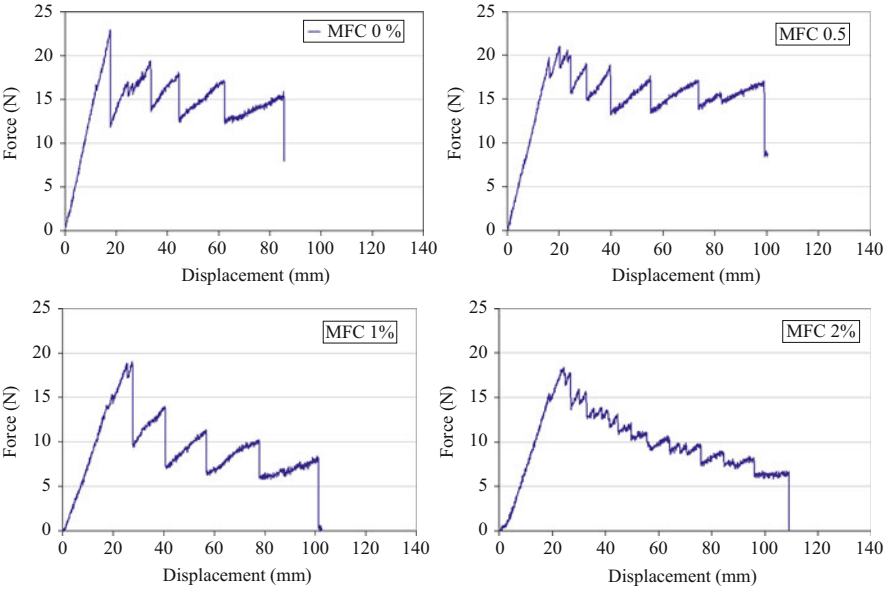

Fig. 14.1 Force–displacement curves for CF/epoxy composites reinforcement with different ratios of MFC

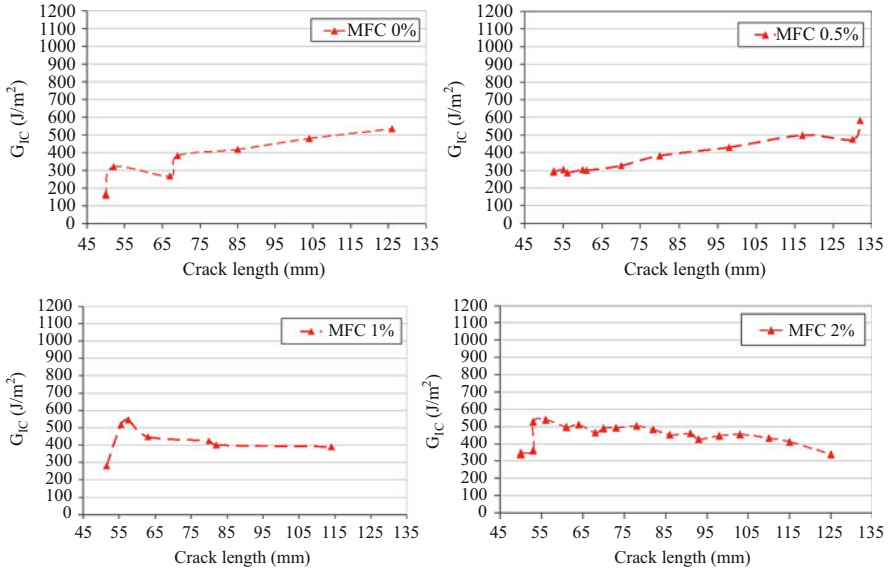

Fig. 14.2 R-curves for CF/epoxy composites reinforcement with different ratios of MFC

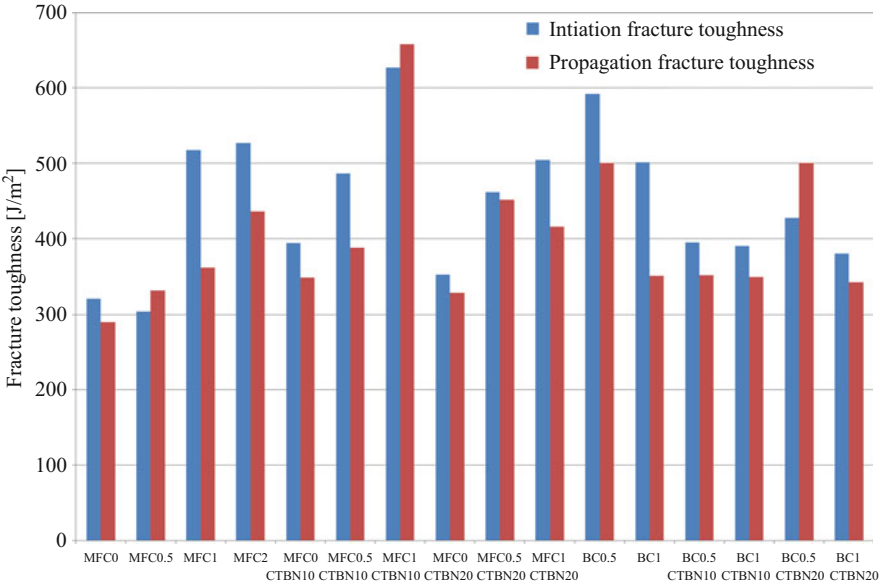

Fig. 14.3 Initiation and propagation fracture toughness of modified and unmodified CF/epoxy composite reinforcement with different ratios of MFC

Various reasons such as intralaminar delamination, fiber bridging, microcracking, residual stresses, or a combination of these effects of lamina at interface caused the development of transverse intralaminar and unstable crack propagation in DCB tests [52].

In general, a number of mechanisms contribute to the fracture toughness and it is often very difficult to determine the dominant mechanism [53]. With the addition of fibers, those toughening mechanisms related to the fibers begin to act which results in more superficial area and consequently larger fracture energy. The experimental of initiation and propagation G_{IC} results obtained from modified compliance calibration (MCC) method for different ratios of nanocellulose is shown in Fig. 14.3.

The addition of MFC to CF/epoxy composite affects the initiation and propagation G_{IC}, as shown in Fig. 14.3. It is clear that fracture delimitation improved significantly with addition of MFC; the initial fracture toughness was increased by about 61 % from 320 J/m^2 for neat composite to 517 J/m^2 for 1 %wt MFC. The propagation fracture toughness for the same content was increased by about 25 % from 295 J/m^2 for neat composite to 368 J/m^2. A more significant increase was observed for the initial fracture toughness at 2 wt% MFC; the initial fracture toughness increased about 56 % from 320 J/m^2 for neat composite to 499 J/m^2; the propagation fracture toughness for the same content was increased by about 44 % from 295 J/m^2 for neat composite to 424.4 J/m^2 which is a better indicator of the reinforcing effect of MFC for improving interlaminar fracture toughness.

The incorporation of MFC with liquid rubber to the CF/epoxy composites affects the G_{IC} and G_{IP} as shown in Fig. 14.3. With the addition of 10 % of CTBN, the fracture toughness was increased by 23 % from 320 J/m^2 for neat composite CF/epoxy to 394 J/m^2. The improved interlaminar fracture toughness is attributed to improved fracture toughness of rubber-modified adhesives, originating from the additional toughening mechanisms provided by the rubber particles, such as tearing, cavitation, shear band formation, and fracture of rubber particles [54]. Although the rubber-modified composite showed increase in fracture toughness of the composite, it imparted only moderate improvements in interlaminar fracture toughness. An established explanation for the poor translation of the toughness of rubber-modified resin into composite interlaminar fracture toughness is mainly due to the suppression of the toughening effect in a thin resin film between reinforcing fibers or between substrates, which constrain plastic deformation near the crack tip [55].

A more significant increase was observed for the initial fracture toughness with the addition of 1 % MFC, and with the addition of 10 % of CTBN, the initial fracture toughness increased about 96 % from 320 J/m^2 for neat CF/epoxy to 627.4 J/m^2. The propagation fracture toughness was further improved by 127 % from 289 J/m^2 for neat CF/epoxy to 657 J/m^2. This increase could be attributed to crack deflection processes at nanofiber obstacles in a matrix which proposed to play an important role in the toughening [56]. The theory was described by Faber and Evans [57, 58]. It is assumed that a crack can be deflected at an obstacle and that it is forced to move out of the initial propagation plane by tilting and twisting. Tilting and twisting subsequently continues at further particles if the crack follows a three-dimensional pathway. Therefore, an increase in total fracture toughness of a composite can be expected if this mechanism holds. However, the crack deflection theory cannot fully explain the toughening effect provided especially by the nanofibers, while, with the addition of 20 % of CTBN, the fracture toughness decreased. This may be attributed to the lowering of cross-linking density in the modified samples. During the curing of epoxy resin, phase-separated rubber domains shall occupy the space in between the reaction sites, thereby impairing the cross-linking reaction at that particular site. This, in turn, reduces the cross-linking density of cured systems. Thus, the overall cross-linking density changes by the incorporation of more rubber.

As mentioned in the introduction in this chapter, cellulose is also secreted extracellularly as synthesized cellulose fibers by some bacterial species, which is called bacterial cellulose (BC). The experimental results show that the addition of BC to CF/epoxy composite affects the G_{IC} and G_{IP}. With the addition of 0.5 % of BC to the CF/epoxy composite, the fracture toughness improved significantly by 84 % which increased from 320 J/m^2 for neat CF/epoxy to 592 J/m^2. Also, the propagation fracture toughness for the same content improved by 72 % from 289 J/m^2 for neat CF/epoxy to 501 J/m^2. This increase could be attributed to crack deflection processes at nanofiber obstacles in a matrix which is explained above.

4 The Morphology of CF/Epoxy Composites Using Nanocellulose as Hybrid Reinforcement

4.1 Morphology of the Fracture Ends of the Tensile Specimens

SEM is considered an important tool in the study of composites since it can supply essential information about the degree of fiber–matrix adhesion and fiber dispersion in the matrix. Figure 14.4 shows scanning electron microscope images of the fracture ends of the tensile specimens for the CF/Epoxy, MFC_1/CF/Epoxy, and MFC_1/$CTBN_{10}$/CF/epoxy composites, respectively. The figure shows clearly fiber pull-out at the fracture surface of carbon fiber as well as carbon fiber breakage. The most distinct feature of the fracture surface with the addition of 1 wt% MFC and 10 % CTBN is extensive matrix deformation between clean fibers devoid of the matrix. Although there is an extensive matrix deformation, the tensile strength wasn't improved significantly by the addition of MFC. It is worth noting that the presence of nanoparticles plays a major role in determining the strength of the interface. This could be attributing to the dependence of the tensile properties of nano CF/epoxy interface to the carbon fibers which is characterized by high tensile strength.

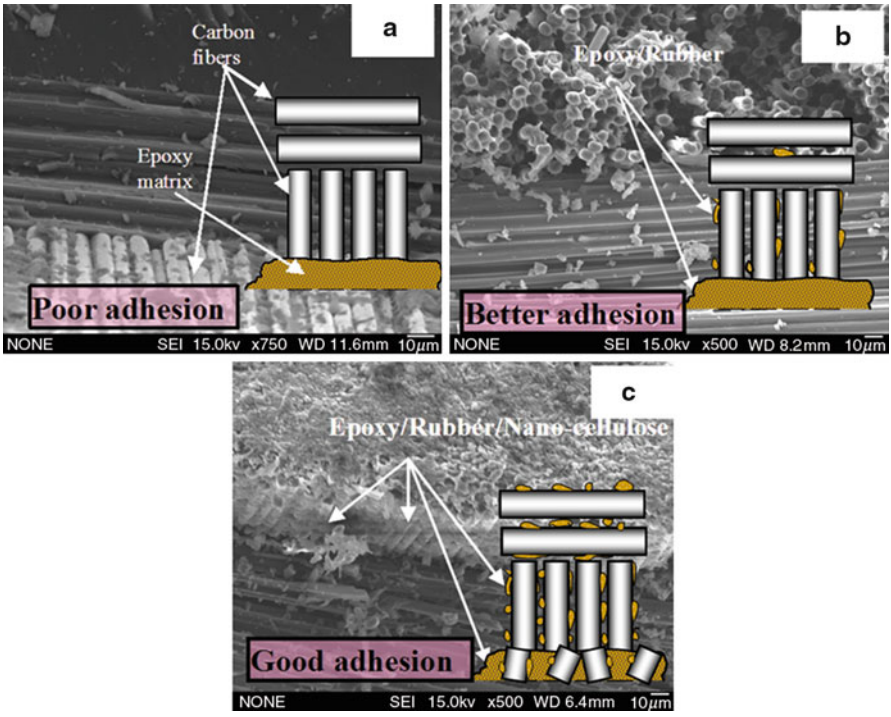

Fig. 14.4 SEM images for CF/epoxy composites at fracture surface of tensile testing specimens; (**a**) neat CF/epoxy, (**b**) CF/epoxy/MFC_1, and (**c**) CF/epoxy/MFC_1/$CTBN_{10}$

4.2 Morphology of the Fracture Toughness Specimen

The micrographs in Fig. 14.5 shows stepwise topography at the end of the insert film and fiber/matrix interface debonding of the fracture toughness specimen. Apparently, large areas are covered by the epoxy adhesive indicative of the reduction in delamination resistance for neat CF/epoxy composite (Fig. 14.5a).

The fracture surface for CF/epoxy/MFC_1, CF/epoxy/$MFC_{0.5}$/$CTBN_{20}$, and CF/epoxy/$BC_{0.5}$/$CTBN_{10}$ appeared similar as regards to the plastic deformation associated with the shear lip formation of the fracture surface. The fracture surface in front of the tip consists mainly of resin microflow lines and river patterns, which are characteristic of brittle cleavage matrix fracture. In the fracture surface of the CF/Epoxy/$BC_{0.5}$/$CTBN_{20}$ (Fig. 14.5d), the coalescing direction of the river lines coincides with the macroscopic crack direction. However, the river marks in the matrix fracture area of the composite appear not to coincide with the macroscopic crack growth direction, which may indicate various directions of local microcrack growth due to the interference of fibers during interlaminar crack growth.

The matrix failure with the addition of 10 % CTBN to CF/Epoxy/BC_1 in Fig. 14.5e appears very similar to the plastic deformation associated with shear lip formation of CF/epoxy/$BC_{0.5}$/$CTBN_{20}$ fracture surface (see Fig. 14.5d). Although a few isolated areas of the cohesive matrix fracture consisting of river patterns and patch patterns can be found, the extensive matrix deformation between fibers with interfacial debonding remains the dominant fracture feature. Increasing the CTBN content to 20 wt% for CF/Epoxy/BC_1, larger cavities remaining within the carbon cloth layer and matrix appear as interwoven bundles and aggregates of up to several tens of microns in diameter (Fig. 14.5f). Therefore, between the carbon cloths, cracks are easily initiated and propagated, spreading along the weak interface where they are blocked, leading to less required fracture energy.

Two distinct regions exist in Fig. 14.5g showing micrograph of CF/Epoxy/MFC_1/$CTBN_{10}$; the first is the rough region showing reinforced adhesion, while the second one in front of the tip of film insert contains remnants of the CFRP substrate. The rough areas of the CFRP suggest a stronger bond exists at the interface as a result of the strengthening effect resulting from the dispersed nanofillers with liquid rubber. In front of the tip, fiber breakage takes place during initiation delamination. Fiber breakage results from fiber–polymer interaction, fiber–fiber interaction, and fiber contact with surfaces of processing equipment. Fiber–polymer interaction promoted a large number of carbon fiber to break at the fracture surfaces resulting in consuming substantial fracture energy.

The images in Fig. 14.5h, i show the SEM for CF/Epoxy/MFC_2 and CF/Epoxy/$BC_{0.5}$/$CTBN_{10}$, in which two distinct regions exist: the first is the region showing exposed fibers of the CFRP substrate, while the second shows cohesive matrix fracture surfaces in the resin-rich areas of the CF/epoxy composite. However, the distinct feature of the fracture surface is matrix deformation between clean fibers devoid of the matrix, indicating tearing (or drawing) of the matrix and interfacial debonding. Significant matrix deformation has been identified as one of the major energy contributions enhancing the interlaminar fracture toughness.

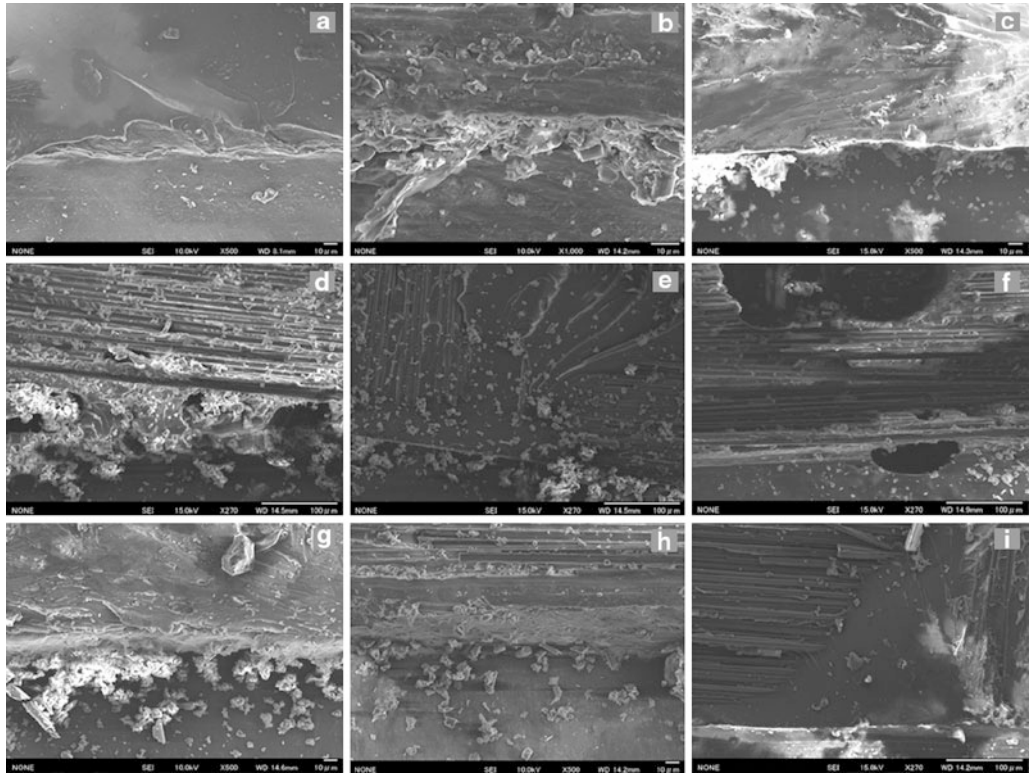

Fig. 14.5 SEM images for CF/epoxy composites at fracture surface of fracture toughness testing specimens; (**a**) neat CF/epoxy, (**b**) CF/epoxy/MFC_1, (**c**) CF/epoxy/$MFC_{0.5}$/$CTBN_{20}$, (**d**) CF/epoxy/$BC_{0.5}$/$CTBN_{20}$, (**e**) CF/epoxy/BC_1/$CTBN_{10}$, (**f**) CF/epoxy/BC_1/$CTBN_{20}$, (**g**) CF/epoxy/MFC_1/$CTBN_{10}$, (**h**) CF/epoxy/MFC_2, (**i**) CF/epoxy/$BC_{0.5}$/$CTBN_{10}$

References

1. Bledzki AK, Gassan J (1999) Composites reinforced with cellulose based fibers. Prog Polym Sci 24:221
2. Angles MN, Dufresne A (2001) Plasticized starch/tunicin whiskers nanocomposite materials. 2. Mechanical behavior. Macromolecules 34:2921
3. Darder M, Aranda P, Ruiz-Hitzky E (2007) Bionanocomposites: a new concept of ecological, bioinspired, and functional hybrid materials. Adv Mater 19:1309
4. Mottershead B, Eichhorn SJ (2007) Deformation micromechanics of model regenerated cellulose fiber–epoxy/polyester composites. Compos Sci Technol 67:2150
5. Takagaki N, Okubo K, Fujii T (2008) Improvement of fatigue strength and impact properties of plain-woven CFRP modified with micro fibrillated cellulose. Adv Mater Res 47:133
6. Takagaki N, Okubo K, Fujii T (2008) Improvement of fatigue strength and impact properties of plain-woven CFRP modified with micro fibrillated cellulose. In: Proceedings of the 6th Asia-Australasian conference on composite materials (ACCM/6). Kumamouto, p 499
7. Gabr MH, Okubo K, Elrahman MA, Fujii T (2010) Effect of microfibrillated cellulose on mechanical properties of plain woven CFRP reinforced epoxy. Compos Struct 92:1999
8. Gabr MH, Elrahman MA, Okubo K, Fujii T (2010) Interfacial adhesion improvement of plain woven carbon fibre reinforced epoxy filled with micro-fibrillated cellulose by addition liquid rubber. J Mater Sci 45:3841
9. Gabr MH, Elrahman MA, Okubo K, Fujii T (2010) A study on mechanical properties of bacterial cellulose/epoxy reinforced by plain woven carbon fiber modified with liquid rubber. J Compos A 1263
10. Soykeabkaew N, Arimoto N, Nishino T, Peijs T (2008) All-cellulose composites by surface selective dissolution of aligned ligno-cellulosic fibers. Compos Sci Technol 68:2201
11. Gabr MH, Matsouka K, Okubo K, Fujii T (2010) Effect of different types of aramid fibres on mechanical and thermal properties of nano-cellulose composites for vehicle applications. Int J Vehicle Noise Vibration 6:118
12. Turbak A, Snyder F, Sandberg K (1983) Suspensions containing microfibrillated cellulose. US Patent 4,378,381
13. Fontana JD, Joerke CG, Baron M, Maraschin M, Ferreira AG, Torriani I, Souza AM, Scares MB, Fontana MA, Guimaraes MF (1997) Acetobacter cellulosic biofilms search for new modulators of cellulogenesis and native membrane treatments. Appl Biochem Biotechnol 63:327
14. Wan YZ, Hong L, Jia SR, Huang Y, Zhu Y, Wang YL, Jiang HJ (2006) Synthesis and characterization of hydroxyapatite-bacterial cellulose nanocomposites. Compos Sci Technol 66:182
15. Czaja WK, Young DJ, Kawecki M, Brown RM (2007) The future prospects of microbial cellulose in biomedical applications. Biomacromolecules 8:1–12
16. Wan YZ, Huang Y, Yuan CD, Raman S, Zhu Y, Jiang HJ, He F, Gao C (2007) Biomimetic synthesis of hydroxyapatite/bacterial cellulose nanocomposites for biomedical applications. Mater Sci Eng 27:855
17. Gindl W, Keckes J (2004) Tensile properties of cellulose acetate butyrate composites reinforced with bacterial cellulose. Compos Sci Technol 64:2407
18. Nakagaito AN, Iwamoto S, Yano H (2005) Bacterial cellulose: the ultimate nano-scalar cellulose morphology for the production of high-strength composites. Appl Phys A Mater 80:93
19. Yano H, Sugiyama J, Nakagaito AN, Nogi M, Matsuura T, Hikita M, Handa K (2005) Optically transparent composites reinforced with networks of bacterial nanofibers. Adv Mater 17:153
20. Ifuku S, Nogi M, Abe K, Handa K, Nakatsubo F, Yano H (2007) Surface modification of bacterial cellulose nanofibers for property enhancement of optically transparent composites: dependence on acetyl-group DS. Biomacromolecules 8:1973

21. Martins IMG, Magina SP, Oliveira L, Freire CSR, Silvestre AJD, Neto CP, Gandini A (2009) New biocomposites based on thermoplastic starch and bacterial cellulose. Compos Sci Technol 69:2163
22. Wan YZ, Luo H, He F, Liang H, Huang Y, Li XL (2009) Mechanical, moisture absorption, and biodegradation behaviours of bacterial cellulose fiber-reinforced starch biocomposites. Compos Sci Technol 69:1212
23. Abdelmouleh M, Boufi S, Belgacem MN, Dufresne A, Gandini A (2005) Modification of cellulose fibers with functionalized silanes: effect of the fiber treatment on the mechanical performances of cellulose–thermoset composites. J Appl Polym Sci 98:974
24. Iwatake A, Nogi M, Yano H (2008) Cellulose nanofiber-reinforced polylactic acid. Compos Sci Technol 68:2103
25. Lu J, Wang T, Drzal LT (2008) Preparation and properties of microfibrillated cellulose polyvinyl alcohol composite materials. Compos Part A 39:738
26. Lu J, Askeland P, Drzal LT (2008) Surface modification of microfibrillated cellulose for epoxy composite applications. Polymer 49:1285
27. Nakagaito AN, Yano H (2005) The effect of fiber content on the mechanical and thermal expansion properties of biocomposites based on microfibrillated cellulose. Cellulose 15:555
28. Zimmermann T, Pohler E, Geiger T (2004) Cellulose fibrils for polymer reinforcement. Adv Eng Mater 6:754
29. Svagan AJ, Samir MASA, Berglund LA (2007) Biomimetic polysaccharide nanocomposites of high cellulose content and high toughness. J Polym Environ 8:2556
30. Suryanegara L, Nakagaito AN, Yano H (2009) The effect of crystallization of PLA on the thermal and mechanical properties of microfibrillated cellulose-reinforced PLA composites. Compos Sci Technol 69:1187
31. Todo M, Jar P-YB, Takahashi K (2000) Initiation of a mode-II interlaminar crack from an insert film in the end-notched flexure composite specimen. Compos Sci Technol 60:263
32. Okubo K, Fujii T, Yamashita N (2005) Improvement of interfacial adhesion in bamboo polymer composite enhanced with micro-fibrillated cellulose. JSME Int J Series A 48:199
33. Okubo K, Fujii T, Thostenson ET (2009) Multi-scale hybrid biocomposite: processing and mechanical characterization of bamboo fiber reinforced PLA with microfibrillated cellulose. Compos Part A 40:469
34. Naoya Y, Kazuya O, Fujii T (2004) Improvement of bending strength, fracture toughness and impact strength of bamboo fiber composites by adding micro-fibrillated cellulose as an enhancer. Bamboo J 21:35
35. Mazumdar SK (2002) Composites manufacturing: materials, product, and process engineering. CRC Press LLC, Boca Raton
36. Thomas R, Yumei D, Yuelong H, Le Y, Moldenaers P, Weimin Y, Czigany T, Thomas S (2008) Miscibility, morphology, thermal, and mechanical properties of a DGEBA based epoxy resin toughened with a liquid rubber. Polymer 49:278
37. Verchere D, Sautereau H, Pascault JP, Moschiar SM, Riccardi CC, Williams RJJ (1990) J Appl Polym Sci 41:467
38. Chen TK, Jan YH (1991) Effect of rubber/matrix interfacial modifications on the properties of a rubber-toughened epoxy resin. Polym Eng Sci 31:577
39. Bussi P, Ishida H (1994) Partially miscible blends of epoxy resin and epoxidized rubber: structural characterization of the epoxidized rubber and mechanical properties of the blends. J Appl Polym Sci 53:441
40. Nigam V, Setua DK, Mathur GN (1999) Characterization of liquid carboxy terminated copolymer of butadiene acrylonitrile modified epoxy resin. Polym Eng Sci 39:1424
41. Pearson AF, Yee AF (1989) Toughening mechanisms in elastomer-modified epoxies. Part 3: The effect of cross-link density. J Mater Sci 24:2571
42. Thomas R, Abraham J, Thomas S (2004) Influence of carboxyl-terminated (butadiene-co-acrylonitrile) loading on the mechanical and thermal properties of cured epoxy blends. J Polym Sci B 42:2531

43. Shukla D, Srivastava S (2006) Blends of modified epoxy resin and carboxyl-terminated polybutadiene. I. J Appl Polym Sci 100:1802
44. Cheng S, Wang S, Rials TG (2009) Poly(vinyl alcohol) nanocomposites reinforced with cellulose fibrils isolated by high intensity ultrasonication. Compos Part A 40:218
45. Chakraborty A, Sain M, Kortschot M (2006) Reinforcing potential of wood pulpderived microfibres in a PVA matrix. Holzforschung 60(1):53–58
46. Wang B, Sain M (2007) Isolation of nanofibers from soybean source and their reinforcing capability on synthetic polymers. Compos Sci Technol 67:2521
47. Dubief D, Samain E, Dufresne A (1999) Polysaccharide microcrystals reinforced amorphous poly(β-hydroxyoctanoate) nanocomposite materials. Macromolecules 32:5765
48. Azizi Samir AS, Alloin F, Dufresne A (2005) Review of recent research into cellulosic whiskers, their properties and their application in nanocomposite field. Biomacromolecules 6:612
49. Tripathi G, Srivastava D (2007) Effect of carboxyl-terminated poly(butadiene co-acrylonitrile) (CTBN) concentration on thermal and mechanical properties of binary blends of diglycidyl ether of bisphenol-a (DGEBA) epoxy resin. Mater Sci Eng A443:262
50. Shah Khan MZ, Mouritz AP (1996) Fatigue behaviour of stitched GRP laminates. Compos Sci Technol 56(6):695–701
51. Velmurugan R, Solaimurugan S (2007) Improvements in mode I interlaminar fracture toughness and in-plane mechanical properties of stitched glass/polyester composites. Compos Sci Technol 67:61
52. Ray D, Sarkar BK, Bose NR (2002) Impact fatigue behaviour of vinylester resin matrix composites reinforced with alkali treated jute fibers. Compos Part A Appl Sci Manuf 33:233
53. Silva RV, Spinelli D, Bose Filho WW, Claro Neto S, Chierice GO, Tarpan JR (2006) Fracture toughness of natural fibers/castor oil polyurethane composites. Compos Sci Technol 66:1328
54. Gao B, Kim J-K, Leung CKY (2003) Effect of rubber modifier on interlaminar fracture toughness of CFRP-concrete interface. Compos Sci Technol 63:883
55. Jordan WM, Bradley WL (1987) Micromechanisms of fracture in toughened graphite-epoxy laminates. In: Johnston NJ (ed) Toughened composites, ASTM special technical publication 937. ASTM, Philadelphia, p 95
56. Wetzel B, Rosso P, Haupert F, Friedrich K (2006) Epoxy nanocomposites – fracture and toughening mechanisms. Eng Fracture Mech 73:2375
57. Faber KT, Evans AG (1983) Crack deflection processes – I. Theory. Acta Metall 31:565
58. Faber KT, Evans AG (1983) Crack deflection processes – II. Experiment. Acta Metall 31:577

Characterization and Processing of Nanocellulose Thermosetting Composites

15

Ronald C. Sabo, Rani F. Elhajjar, Craig M. Clemons, and Krishna M. Pillai

Contents

Abstract

Fiber-reinforced polymer composites have gained popularity through their advantages over conventional metallic materials. Most polymer composites are traditionally made with reinforcing fibers such as carbon or glass. However, there has

Book Chapter in, "Technological advancement in polymer nano- composites of cellulose nanoparticle: processing, performance and applications"

R.C. Sabo (✉) • C.M. Clemons
USDA Forest Products Laboratory, Madison, WI, USA
e-mail: rsabo@fs.fed.us; cclemons@fs.fed.us

R.F. Elhajjar • K.M. Pillai
College of Engineering & Applied Science, University of Wisconsin, Milwaukee, WI, USA
e-mail: elhajjar@uwm.edu; krishna@uwm.edu

J.K. Pandey et al. (eds.), *Handbook of Polymer Nanocomposites. Processing, Performance and Application – Volume C: Polymer Nanocomposites of Cellulose Nanoparticles*,
DOI 10.1007/978-3-642-45232-1_64,

been recent interest in sourcing these reinforcing fibers from renewable, natural resources. Nanocellulose-based reinforcements constitute a new class of these naturally sourced reinforcements. Some unique behavior of nanocellulose creates both opportunities and challenges. This chapter reviews the progress and some of the remaining issues related to the materials, processing, and performance of nanocellulose reinforced thermosetting composites.

Keywords
Nanocellulose • Thermosets • Mechanical properties • Nonmechanical properties • Applications

1 Introduction

Fiber-reinforced polymer composites have gained popularity through their advantages over conventional metallic materials. The composites can be tailored to achieve desirable characteristics including low weight, high mechanical properties, and low temperature processing [1]. Most polymer composites are traditionally made with reinforcing fibers such as carbon or glass. However, there has been recent interest in sourcing these reinforcing fibers from renewable, natural resources. For example, composite manufacturers are seeking to take advantage of the favorable balance of properties (e.g., low density, good mechanical properties) by using bast fibers from plants in composite applications in automotive, packaging, sporting goods, and furniture applications [2–6].

Nanocellulose-based reinforcements constitute a new class of these naturally sourced reinforcements. Trees, plants, some marine creatures such as tunicates, and certain bacteria and algae form microfibrils from cellulose molecules [7]. These microfibrils have a complex structural hierarchy and often act as the main reinforcing element in their respective organisms. These fibrils are about 5–50 nm in diameter and several microns in length [7]. In part, it is the high reinforcing potential of native crystalline cellulose within these microfibrils that has recently led researchers to extract nanocellulose from them for use in composites. Table 15.1 compares the

Table 15.1 Comparison of crystalline cellulose with other selected reinforcements

Material	Density (g cm^{-3})	Strength (GPa)	Elastic modulus (GPa)	Strain to failure (%)	References
Crystalline cellulose	1.6	7.5–7.7	110–220	–	[7]
E-glass fiber	2.6	3.5–3.8	69–72	4.5–4.9	[142]
S-2 glass fiber	2.5	4.6–4.8	86–90	5.4–5.8	[142]
K-49 aramid fiber	1.4	–	124–131	2.5–2.9	[142]
AS4 carbon fiber	1.8	–	221–234	1.5–1.6	[142]

Fig. 15.1 Luminescence of an organic light-emitting diode deposited onto a flexible, low coefficient of thermal expansion (CTE) and optically (Reprinted from Okahisa et al. [17], with permission from Elsevier)

mechanical properties of crystalline cellulose with other reinforcements. The listed properties for crystalline cellulose represent a range of values from a survey of mechanical performance by different researchers and techniques and do not reflect the actual inherent variability of the properties. While not as high performance as some reinforcements such as carbon nanotubes, crystalline cellulose is derived from natural resources, and its reinforcing potential is sufficiently high that there is considerable interest in finding ways to economically extract it and efficiently use it in composite materials. However, reinforcement is not the only reason for adding nanocellulose to polymers. Others are trying to make transparent, dimensionally stable cellulose nanocomposites for electrical applications [8–17] or exploit other features of nanocellulose such as its good barrier properties [18–21]. Figure 15.1 shows an organic light-emitting diode on a flexible nanocellulose-based composite. Different types of nanocellulose materials have been investigated for use in polymer composites. These are briefly described below, but more detailed information can be found elsewhere in this book or in recent reviews [7, 22–28].

Cellulose nanocrystals (CNCs), also called *cellulose whiskers, nanow*hiskers, or *nanorods*, are produced by transverse cleavage of cellulose by acid hydrolysis. This results in high modulus, rodlike structures with aspect ratios of around 10–100 but which depend on the source of the cellulose and the exact preparation conditions [7]. Plant-based sources yield crystallites with diameters of about 5 nm and lengths of about 100–400 nm. Tunicate and algae yield crystallites with diameters of 10–20 nm and length up to several micrometers [29]. A transmission electron micrograph of CNCs is shown in Fig. 15.2.

Other forms of nanocellulose are also being investigated as polymer reinforcements. For example, severe, mechanical refining of highly purified pulps results in a fibrillated form of cellulose with fibril widths on the same order of magnitude as the cellulose microfibrils in the original pulp. This *microfibrillated cellulose* (MFC) has more of a network structure than CNCs (see Fig. 15.3) and often forms gels in water even at low concentrations (e.g., less than 1 % by weight). Certain preprocessing steps (e.g., enzymatic or chemical pretreatments) can be used to weaken hydrogen bonding and facilitate processing. *Nanofibrillated cellulose*, *cellulose nanofibrils*, and *cellulose*

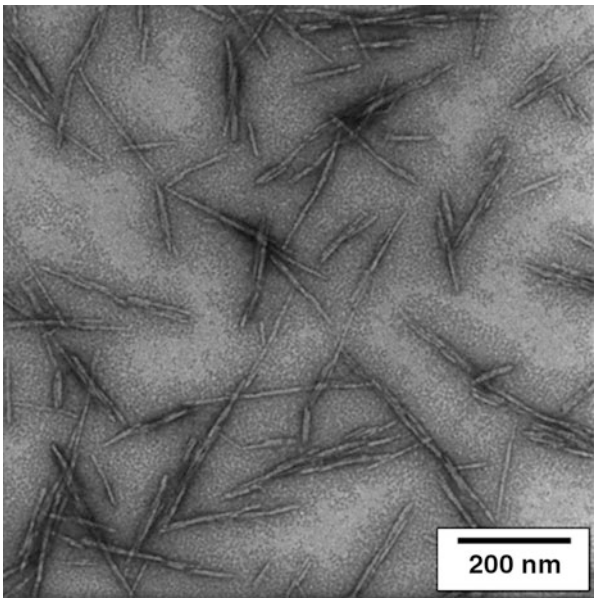

Fig. 15.2 TEM of CNCs from wood [7]

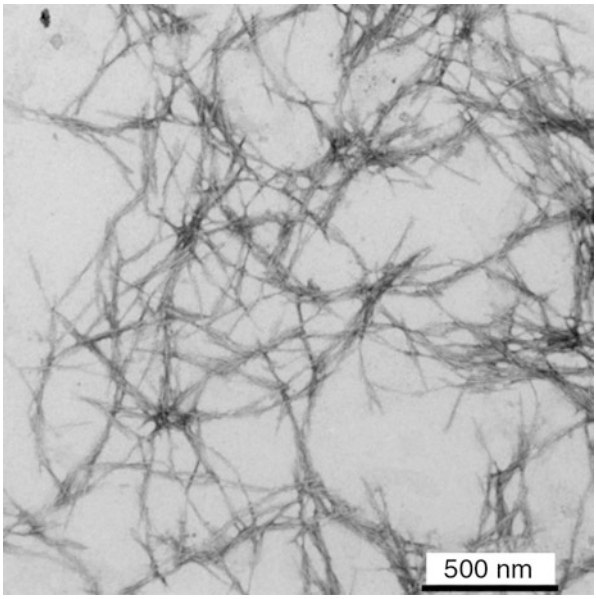

Fig. 15.3 TEM of NFC

nanofibers are terms that are sometimes used to describe fibrillated cellulose with a finer structure or to reflect that the fibril diameters are of nano-scale dimension. However, the use of the terms is inconsistent, and the variability between samples of fibrillated cellulose due to differences in preparation methods, starting materials, etc. or

even variability within samples makes clear distinction between fibril diameters difficult. In this chapter, we use the term nanofibrillated cellulose (NFC) for this type of nanocellulose. Besides from pulps, nano-scale, cellulose reinforcements have also been produced from cellulose secreted by certain bacteria (e.g., *Gluconacetobacter xylinus*) under special culturing conditions [7]. They are usually specifically referred to as *bacterial cellulose microfibrils* or *bacterial cellulose nanofibers* to distinguish them from their pulp-derived counterparts.

Some unique behavior of nanocellulose creates both opportunities and challenges. For example, preparation of nanocellulose results in aqueous gels or suspensions that may need to be dried into a fiber and film or otherwise converted into a form more useful for reinforcing thermosets. Nanocellulose's strong tendency to hydrogen bond can lead to challenges in redispersing them if they are dried but can also result in fairly strong and stiff films that can be used in laminated composites [30]. Nanocellulose is very hydrophilic, which can create difficulties in dispersing them and bonding them to some thermosets and can lead to swelling during composite manufacture.

The use of nanocellulose as a reinforcement in polymer composites is in its infancy. While much recent progress has been made, there are many challenges remaining to efficiently and economically use nanocellulose as a reinforcement. This chapter reviews the progress and some of the remaining issues related to the materials, processing, and performance of nanocellulose reinforced thermosetting composites.

2 Materials

Various forms of nanocellulose have been incorporated into numerous thermoset resins using a wide range of forms and techniques. An overview of the types of nanocellulose used, the various forms of reinforcement, and the types of resins used to make composites will be provided in this section.

These different types of nanocellulose can be used as is or converted into various forms of reinforcement, including distributed reinforcements, planar reinforcements, or continuous networked structures. Each type of nanocellulose has certain advantages and limitations for these various reinforcement structures. One recurring challenge for creating these reinforcements is to remove the water from the hydrophilic nanocellulose while retaining properties favorable for incorporation into resins, which are typically hydrophobic. Some of the approaches for creating these reinforcements, along with their physical and mechanical properties, are discussed below.

2.1 Dispersed Fibrous or Particulate Reinforcements

Nanocellulose materials have been mixed or dispersed in various resins using a variety of processing techniques. While these techniques vary in complexity, they typically involve physically mixing and dispersing the nanocellulose and resin in a solvent system. In many cases, solvent exchange techniques are used, often

along with surface modification of nanocellulose to make it compatible with organic solvents and/or the resin system. Here, an overview of various techniques to blend, modify, or prepare nanocellulose for distribution in resins is provided.

Nanocellulose is typically produced in aqueous suspensions, so removal of the water is critical for producing composite materials, and since most resins are hydrophobic, the water is typically removed prior to mixing nanocellulose with resins. Methods of delivering dried nanocellulose for incorporation into composites are highly desirable and thus the subject of numerous research and development efforts [31–37]. These methods typically involve freeze-drying or spray-drying of modified or unmodified nanocellulose. Because nanocellulose tends to agglomerate during drying, the redispersibility and morphology of the dried material are often different than the original material, although recent work has shown that the negative impact of these drying techniques can be minimized by optimizing processing conditions and/or surface modification [32–34]. For example, CNC dispersions neutralized with sodium hydroxide were found to be much more readily dispersible after drying than CNCs without sodium counter ions [33]. The drying rate, duration, temperature, and method are all factors that affect the dispersibility and morphology of nanocellulose, and practical methods for delivering dried nanocellulose are emerging.

Numerous research studies have reported the modification of nanocellulose for compatibility in nonpolar solvents and hydrophobic polymers [38–45]. Although many of these modifications were made with the aim of incorporating nanocellulose into thermoplastics, the hydrophobization of these CNCs and NFCs is equally applicable for distribution in thermoset resins. For example, Ljungberg et al. found that CNCs with an adsorbed surfactant (phosphoric ester of polyoxyethylene (9) nonylphenyl ether) dispersed in toluene [40]. Various methods of chemically reacting compounds with nanocellulose surfaces have also been used to facilitate compatibility and dispersion of nanocellulose in hydrophobic polymers [41, 42]. Goussé et al. modified CNCs with chlorosilanes resulting in stable suspensions in organic solvents [41]. The chlorosilanes were found to be reactive with the CNCs provided that water was removed from the solvent. However, if the reactions were carried out too far, the integrity of the CNCs was destroyed. Therefore, the CNCs were not able to be dispersed in solvents, such as toluene, with polarity lower than that of tetrahydrofuran (THF). Tunicin CNCs were acylated using aqueous alkenyl succinic anhydride (ASA) emulsions by mixing the two materials, freeze-drying, and heating to 105 °C [38]. The length of heating was crucial to the degree of substitution achieved. After approximately 1 hour at 105 °C, the modified CNCs were dispersible in low-polarity solvents including 1,4-dioxane [38]. NFCs have also been chemically modified to change the surface properties and to facilitate their dispersion in nonpolar media [42, 46–48]. For instance, polycaprolactone (PCL) was grafted to NFCs via ring-opening polymerization [46]. The resulting grafted material was stable in nonpolar solvents and had excellent thermal stability. Siqueira et al. found that modification of nanocellulose with *n*-octadecyl isocyanate improved their dispersion in organic solvents [42]. Silane chemistry also has enormous potential as a surface modifier for NFCs, and such modifications

have been explored [47]. Another approach being explored is the in situ modification of nanocellulose during spray-drying [49]. However, clear and practical strategies for modifying NFCs for incorporation into polymers have not been established.

2.2 Planar Reinforcements

Planar nanocellulose reinforcements or films are typically made from NFCs either by casting or by using a papermaking-like process. These films have been coined "nanopaper" and have been touted as the "strongest cellulose-based material made by man" [50, 51]. Films or sheets from CNCs are rarely used as a reinforcing phase because of their brittleness and difficulty in handling. Some of the methods of producing these NFC films and their properties are discussed here.

Dewatering NFC solutions presents a practical challenge because of their affinity for water. Casting is a slow process and not readily scalable, so NFC films (Fig. 15.4) are often formed by filtering NFC solutions with membranes or fine filters and drying the wet mats under pressure. Press conditions vary throughout the literature, but wet films are commonly pressed for days at temperatures of 55–70 °C and low pressures [52, 53]. For example, Nakagaito and Yano produced films by vacuum filtering a solution of NFC, separating the wet mats from filter papers, and drying the sheets between metal plates at 70 °C for 48 h followed by vacuum drying for another 5 h at 70 °C [53]. Films are also often simply cast by slowly evaporating the water from the NFC suspension [54]. Sehaqui et al. developed an accelerated

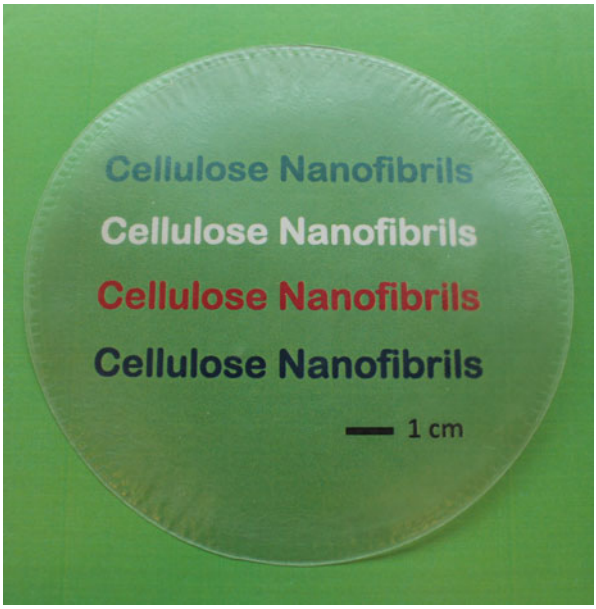

Fig. 15.4 Nanofibrillated cellulose film

procedure similar to papermaking, which resulted in the production of NFC sheets about 60 μm thick in 1–2 h [55]. This process for making NFC films is similar to the process for making paper, and efforts to develop pilot-scale processes for producing continuous NFC films are underway [56].

The mechanical properties of NFC films are dictated by a variety of factors, and the effects of these variables are difficult to discern based on results in the literature. The tensile strengths of NFC films range from about 70 MPa to over 300 MPa, and tensile moduli range from about 3 GPa to nearly 20 GPa [23]. Stelte and Sanadi showed that softwood pulp resulted in cellulose nanofiber sheets with higher tensile strength than those from hardwood pulp, whereas the effect of species was reversed for tensile modulus [57]. However, they also demonstrated that the softwood pulps required extremely reduced levels of refining and homogenizing to yield NFC. On the other hand, some of the highest tensile strengths of cellulose nanofiber sheets reported in the literature are those made from hardwood fibers. For example, cellulose nanofiber sheets prepared from TEMPO-oxidized hardwood fibers resulted in sheets having tensile strength of over 300 MPa [58], which is the highest reported value found for unoriented NFC films.

Orientation of nanocellulose has been shown to significantly enhance the mechanical properties of films along the direction of orientation [30, 59]. For example, Sehaqui et al. produced NFC films with as high as 89 % degree of orientation parallel to the plane of the film by cold drawing wet NFC films [30]. The wet films, or "hydrogel cakes" containing 70–90 % water, were oriented by stretching them in a tensile testing machine at constant elongation, resulting in enhanced tensile stiffness and strength compared to randomly oriented films. The modulus of the films increased from about 10 GPa with no drawing to about 33 GPa with a draw ratio of 1.6. The strength of random films was about 185 MPa, which is typical of other reports in the literature, while the strength of oriented films reached over 400 MPa in one case. The optimum achievable mechanical properties for aligned nanocellulose structures and composites are not known, but oriented NFC reinforcements clearly have potential.

2.3 Continuous Fibrous Forms

Most fibrous reinforcements (e.g., carbon, glass) for advanced composites are continuous fibers or yarns, fabrics, and preforms made from them, which allow broad flexibility in design and manufacturing approaches. Recently, there has been increasing interest in using plant-based materials, which use cellulose as their main structural component, as a source for continuous polymer reinforcements. A potentially promising area of investigation is the use of nanocellulose (e.g., CNC, NFC) as continuous fiber reinforcement in polymers. However, it is useful to first review other approaches for producing plant-based continuous reinforcements for comparison.

One obvious approach to producing continuous, plant-based reinforcements is to simply extract fibers from the plants directly and spin them into yarns.

Table 15.2 Comparison of the properties of selected natural fibers and continuous glass fibers

Material	Density (g cm^{-3})	Strength (GPa)	Elastic modulus (GPa)	Strain to failure (%)	References
E-glass fiber	2.6	3.5–3.8	69–72	4.5–4.9	[142]
S-2 glass fiber	2.5	4.6–4.8	86–90	5.4–5.8	[142]
Flax[a]	1.4–1.5	0.5–0.9	50–70	1.5–4.0	[143]
Hemp[a,b]	1.5	0.3–0.8	30–60	2–4	[143]
Jute[a]	1.3–1.5	0.2–0.5	20–55	2–3	[143]
Softwood	1.4	0.1–0.2	10–50	–	[143]

[a]Fiber bundles
[b]Industrial hemp is listed as a controlled substance in the United States and cannot be used in commercial production of composites

The composition and mechanical properties of several natural fibers from plants are shown in Table 15.2 along with more common continuous reinforcing fibers. Flax and hemp bast fibers have the highest mechanical performance of the fibers listed partly due to their high cellulose content. Not surprisingly, they are some of the most investigated natural fibers for polymer reinforcement [4, 6]. Natural fibers such as flax, hemp, and jute have sufficiently long fibers that they can readily be made into continuous reinforcing yarns or rovings using textile technologies. Modifications to existing textile technologies (e.g., to produce low-twist rovings) are often made to better target composite applications [6]. While the mechanical performance of these yarns or rovings fall short of the more commonly used continuous synthetic fibers, they are of interest because of their specific properties (i.e., property divided by density) and their damping abilities, for example. These roving or yarns can be sold as reinforcement directly or fabricated into mats, fabrics, and prepregs for use in composites for automotive, sporting goods, or boating applications [6, 60]. However, the potential of these reinforcements in advanced composites is somewhat limited by their inherent variability in structure and composition.

Regenerated cellulose fibers have been made for over a 100 years [61], and although they have been traditionally been used in textiles, there has been growing interest in their use as polymer reinforcements as well [62, 63]. These fibers are attractive partly due to their lower variability than natural fibers such as flax [62]. Regenerated fibers are made by several technologies that first dissolve cellulose and then recrystallize it during fiber production. Their mechanical performance is typically less than glass fiber (Table 15.3). However, new regenerated cellulose fibers with high orientation and crystallinity have been recently developed and show significant improvements. For example, Bocell fiber, an experimental regenerated cellulose fiber, has a tensile modulus and strength of 46.6 ± 6.5 GPa and 1,170 ± 165 MPa, respectively (Table 15.3). Since its density is only about 1.5 g cm^{-3}, its specific modulus is comparable to some glass fibers. However, the crystalline structure of regenerated cellulose (referred to as Cellulose II) is different from that of cellulose in its native state (i.e., Cellulose I). While reported values for

Table 15.3 Average tensile properties of continuous, regenerated cellulose fibers

Fiber	Strength (GPa)	Elastic modulus (GPa)	Strain to failure (%)	References
Viscose	0.34 ± 0.07	10.8 ±2.5	15.4 ± 2.2	[62]
Modal	0.44 ± 0.07	13.2 ± 2.2	10.4 ± 1.8	[62]
Lyocell	0.56 ± 0.08	23.4 ± 3.9	8.7 ± 1.6	[62]
Rayon tirecord	0.78 ± 0.06	22.2 ± 1.0	10.7 ± 1.4	[62]
Bocell	1.17 ± 0.17	46.6 ± 6.5	6.1 ± 0.8	[144]

the mechanical performance of these two types of crystal structures vary considerably and depend on the measurement technique, the values for Cellulose I are clearly considerably higher [7]. This is one of the reasons that researchers have recently begun investigating spinning continuous fibers from nanocellulose, which maintains its Cellulose I crystal structure when it is produced [64, 65].

To date, approaches for reinforcing thermosets with nanocellulose have largely focused on (1) dispersing CNCs or NFC into thermosets and then casting composites [66–68] or (2) preparing films from nanocellulose and then laminating or impregnating them [8, 9, 14, 69–73]. However, until very recently, there has been no work in the literature on producing continuous fibers from nanocellulose [64, 65] despite the considerable efforts of doing so with other nano-scale reinforcements such as carbon nanotubes [74].

Ideally, these fibers would have high crystallinity, high orientation, and a fine, homogeneous structure with no defects. From a spinning standpoint, nanocellulose lies between natural fibers and regenerated cellulose in that the starting point for spinning is neither comprised of macro-scale fibers (as with spinning natural fibers into yarns or tows) nor molecular-scale solutions (as with spinning of regenerated cellulose). Instead they are usually aqueous gels or dispersions of nanocellulose particles with very different characteristics depending on their method of preparation, both in terms of structure and chemistry. For example, NFCs tend to form more of a network structure compared to the rigid rodlike structure of CNCs. This allows their gels to stretch somewhat without breaking in order to induce some alignment but also limits the ultimate alignment that can be achieved. NFCs form thick aqueous gels at lower concentrations than CNCs, and their higher viscosities and water content need to be considered. Different surface chemistries result from different methods of nanocellulose preparation, which have a significant effect on approaches to spinning. For example, CNC production most often results in sulfated surfaces, while NFCs often have carboxylated surfaces, for instance, due to chemical pretreatment.

Continuous fibers have been readily spun from NFC and coagulated using acetone or ethanol followed by drying [64, 65]. Unfortunately, the tensile properties of the fibers resulting from this approach are below those of commercial regenerated celluloses, even if some alignment is induced [64]. However, this research area is very much in its infancy, and improved spinning methods (e.g., that result in better alignment) and new approaches are likely. Optimizing methods for extracting nanocellulose that result in characteristics more favorable for spinning fibers

(e.g., higher crystallinity) may also improve the situation. Also, other characteristics besides mechanical performance (e.g., transparency, biodegradability) may prove useful in a composite system, or other functionalities may be achieved through chemical modification (e.g., electrical conduction, magnetism) [65]. As with other types of continuous reinforcements, surface treatments will likely be necessary for optimal performance for a given resin type, processing method, and application.

Because of the limitations imposed by the structure and chemistry of nanocellulose gels and dispersions, other materials may very well need to be added to produce a dope that is easily spun and has high performance. For example, adding a different polymer may improve gel elasticity and result in better alignment or allow different approaches to coagulation. Small amounts of nanocellulose have been added to wet spun [75, 76] or electrospun [77–79] polymer fibers. While somewhat beyond the scope of this chapter, these investigations may offer some insight into the production of continuous nanocellulose fibers. Because of high surface area and low percolation thresholds of nanocellulose, some of the issues related to spinning at high nanocellulose content (e.g., control of hydrogen bonding) are present even when little nanocellulose is used.

2.4 Thermoset Resins

Polymers are generally divided into thermoplastic and thermosetting varieties. The advantage of using thermosets stems from distinct advantages in mechanical properties and processing. Thermosetting composites can be cured with low or no heat applied, which can be advantageous since nanocellulose has limited thermal stability. Thermosetting plastics are polymer materials that irreversibly cure. The curing maybe initiated through heat, through radiation, or through a chemical reaction (e.g., a two-part epoxy). Uncured thermosetting materials have low viscosities, which is a critical feature in the construction of composites that allows for infiltration and wetting of the fibers. However, once the curing is complete, the thermoset cannot be melted into a liquid form as can be done with a thermoplastic material.

A variety of thermosets, including epoxies and various formaldehydes, have been investigated for use in nanocellulose composites. Epoxy-based nanocellulose composites, for example, have the potential for wide application partly due to the relatively high mechanical properties. Epoxy is a thermosetting copolymer, also known as polyepoxide, formed from reaction of an epoxide "resin" with polyamine "hardener." Bio-based resins have been explored for the manufacturing of macroscopic, cellulose-based composites and are of interest in nanocellulose composites. These resins have the benefit of reducing the amount of petrochemical-based materials used. Resins from soybean-based oil and methacrylic anhydride-modified soybean oil (MMSO) were used as matrices and were combined with various flax fibers. Lactic acid-based thermosets have also been proposed for use in cellulose-based composites for creating prepreg-type reinforcement for use in sheet molding compound applications [80]. Fiber volume fractions of near 70 % have been reported in the literature [81]. Similar resins are of interest for use in nanocellulose composites.

Adekunle et al. [82] used a soybean oil-based thermosetting matrix in their composites. Despite the bio-content and processing improvements, these thermosets still have the detrimental property of not being as readily recyclable as thermoplastics.

Chemical compatibility between the filler and the matrix plays a critical role in the filler dispersion within the matrix and in the adhesion between both phases. Part of the issue arises from the hydrophobic nature of many matrices and the hydrophilic nature of the cellulose materials. The use of cellulose in nanocomposites with hydrophobic matrices often results in weak filler–matrix interactions, low moisture resistance, and interfiber aggregation. Another limitation to the application of NFCs related to the hydrophilic nature is the high water absorption capacity, which is undesirable in many potential applications [83]. Abdelmouleh et al. [84] used silane-treated cellulose fibers in unsaturated polyester and epoxy resin matrices, but the immersion into water induced a large loss of mechanical properties of the materials indicating that the silane treatment was insufficient for preventing cellulose from water absorption. Lu et al. [85] reported successful surface treatments of NFC with three different coupling agents: 3-aminopropyltriethoxysilane(APS), 3-glycidoxypropyltrimethoxysilane, and a titanate coupling agent. These were incorporated into an epoxy resin using an acetone solvent. Better and stronger adhesion between the NFC and the epoxy polymer matrix was observed resulting in a modulus increase for APS-treated material from 10 MPa to over 65 MPa at 130 °C [85]. The results of the surface treatments show no consensus on the best treatment and remain an open area of investigation.

3 Processing of Nanocellulose Composites

Challenges remain in the ability to integrate the nanocellulose reinforcements into composite structures using composite processing techniques. As mentioned earlier in this chapter, nanofibrillated cellulose has incredible potential as a reinforcement material. However, such materials have seen limited use to date as a polymer reinforcements and methods for producing scalable cellulose nanofiber reinforcements are lacking. Moreover, there are a number of challenges in using nanofibrillated cellulose for reinforcement in traditional liquid composite molding (LCM) processes, including the dense structure of the fiber networks in these films as well as the swelling of such networks due to liquid absorption during their wetting by resins during processing. Here, some of the approaches for incorporating nanocellulose into thermoset resins are described.

3.1 Dispersed Fibrous or Particulate Reinforcements

The incorporation of distributed nanocellulose reinforcements into resins presents many challenges, and a number of approaches have been proposed to overcome them. These typically involve casting the composite from some type of solvent. Much of the

research in thermosetting nanocellulose composites has focused on methods of dispersing the various nanocellulose forms in the matrix. In the simplest cases, unmodified nanocellulose is simply blended with water-soluble resins or resin-in-water emulsions. In some cases, the aqueous dispersions of nanocellulose are solvent exchanged to a solvent compatible with the resin, and the resin and nanocellulose are blended together in the solvent. In other cases, freeze-dried nanocellulose, often modified, has been mixed directly into solvents and blended with the resin. Capadona et al. describe a sol–gel process by which nanocellulose can be dispersed in hydrophobic polymers [86]. The process involved converting an aqueous dispersion of CNCs into a "three-dimensional template of well-individualized nanofibers, which is filled with any polymer of choice." The water in which the CNCs are dispersed is replaced by a miscible but weaker hydrogen-bonding solvent forming a gel with dispersed but networked CNCs. This gel is then placed in a polymer solution, allowing the polymer to diffuse into the gel, and the gel can be dried and cast.

Casting methods have been employed with a variety of thermoset systems. For example, Lu et al. [85] reported using epoxy (EPON™ Resin 863) with a polyether amine (D-230) curing agent for making NFC composites. This resin system has a low viscosity (300 cP at 25 °C) and a gel time of 6 h at 33 °C. In their procedure, the epoxy was added to an acetone suspension, sonicated, and then stirred. The curing agent was then added followed by further mixing [85]. The suspension was poured into dishes, and the solvent was evaporated with mild heating, which facilitated simultaneous curing of the resin. The results from differential scanning calorimetry showed that the nanocellulose has a catalytic effect on the epoxy–amine cure and increased the glass transition temperature and the heat of reaction at a low level of NFC reinforcement [67]. Epoxy resin was also used by Ruiz et al. [87] but in the form of an aqueous suspension.

3.2 Planar Reinforcements

Composites from planar NFC reinforcements have been made using a variety of methods, often using a wet lay-up type of approach. Films or "nanopaper" of NFCs have also shown superior mechanical properties and have been used as a reinforcement phase in composites. Masoodi et al. [88] used a bio-based epoxy (Super Sap 100/1000) made by Entropy Bio-Resins Co [89]. The bio-based epoxy is an epoxy resin that is made from up to 37 % bio-content obtained as coproducts of other green industries including wood pulp and biofuel production. The resin has a total calculated biomass of 50 %. NFC films were used as reinforcements and were integrated into the composites using a hand lay-up technique. The resin was degassed using a degassing chamber prior to application for a period of 5 min to allow for the volatiles and voids introduced during the mixing of the hardener and resin to dissipate. However, as discussed later in this chapter, the use of such films is not ideal for composite processing and can result in less-than-desirable stress transfer between the layers. Thus, the ability to use nanocellulose reinforcements in more traditional liquid molding processes is desirable.

3.3 Liquid Molding Processes: Resin Transfer Molding and Its Derivatives

Liquid composite molding (LCM) processes, which include technologies such as resin transfer molding (RTM), vacuum-assisted RTM (VARTM), and vacuum-assisted resin infusion, are used to produce net-shaped composites parts (see Fig. 15.5). For LCM processes, a preform is first created from reinforcing fibers, typically in the form of random, woven, or stitched fiber mats made from carbon, glass, or other materials. Next, the preform is inserted in a mold that matches the dimensions of the desired part, and the mold is closed (in case of the rigid mold processes such as RTM) or covered with a flexible sheet (in case of the soft mold processes such as VARTM). Then, a low viscosity thermosetting resin such as epoxy, polyester, phenolic, or vinyl ester resin is mixed with a hardener and injected under pressure (in the case of the RTM-like processes) or imbibed under vacuum (in the case of the VARTM-like processes) into a closed mold containing the preform. The resulting part is cured at room temperature or under a strictly controlled mold-temperature cycle till the end of the curing reaction. Finally, the cured hardened part is extracted and ready for use after minimal machining.

Of the different LCM processes, RTM is characterized by small cycle times and is appropriate for mass-producing medium-sized parts with good dimensional control. VARTM, on the other hand, is a method of choice for producing large composites parts such as boat hulls; however, it is hampered by large cycle times. The resin and fibrous reinforcements for LCM processes are usually obtained from artificial, man-made sources.

Swelling of fibers, used as reinforcing materials, affects the porosity and permeability of fiber mats; thus, swelling plays an important role in the mold-filling simulations. Swelling reduces pore size and porosity, which results in a reduction in permeability. The thickness growth or swelling measurement can enable mold designers to estimate the porosity and permeability change during the mold-filling processes such as LCM. In the swelling tests on nanocellulose films [72], the thickness of NFC films increased up to averages of 242 % and 159 % for water and the bio-derived epoxy after 2 min. The rate of the increase is significant at the initiation of the soaking procedure then stabilizes within a minute of the initiation of the swelling tests (Fig. 15.6). The variability in the thickness within the sheet, which results in different starting points for each specimen can be attributed to some of the variability observed. The main reason for higher swelling rate of NFC films in water is hydrogen bonding of water molecules to the free OH groups present in cellulose molecules.

Recently NFCs in the form of aerogel-like or scaffolds with elaborate structures at different scales have been produced [90–94]. Such structures with high porosities and large surface area for NFCs suggest a way forward for the use of NFCs as composite reinforcement in the form of LCM preforms. If successful, such an approach will lead to a new way of producing scalable nanocomposites through the LCM technology.

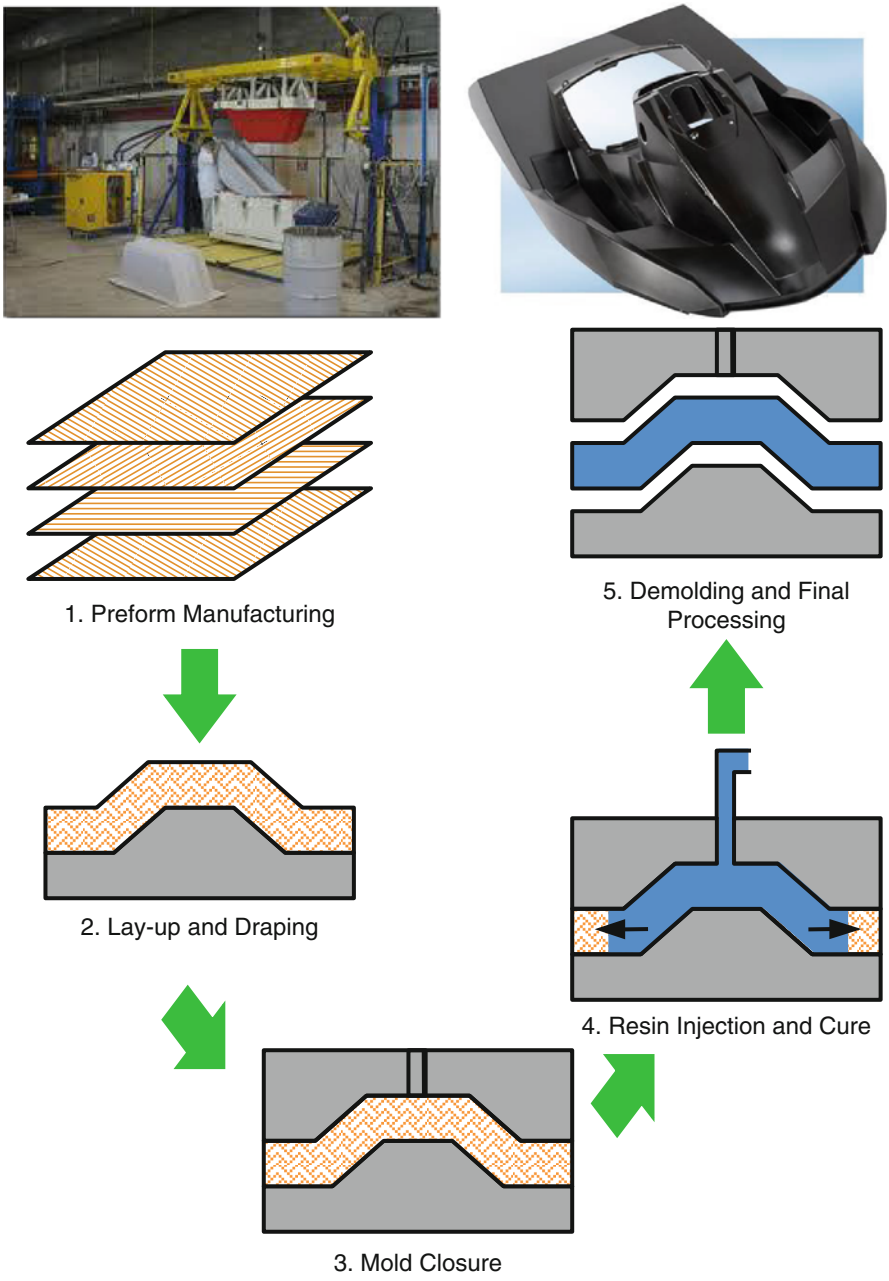

Fig. 15.5 (*Top left*) An example of RTM setup. (*Top right*) A Jet-Ski part made using RTM. (*Bottom*) The main process steps while making the RTM part

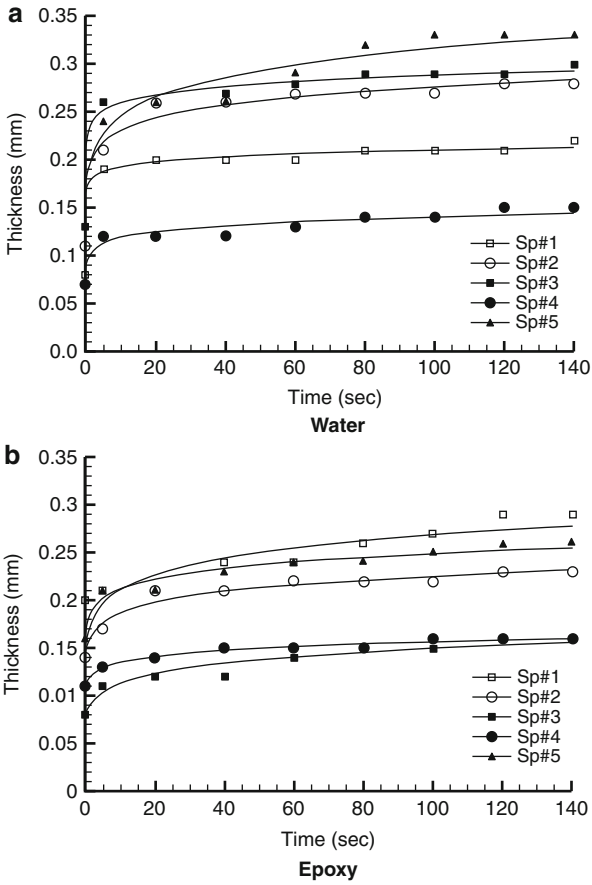

Fig. 15.6 Swelling of cellulose nanopaper in water and epoxy (Reprinted from Masoodi et al. [88], with permission from Elsevier)

Some preliminary studies were conducted by the authors to test the effectiveness of using a NFC aerogel-like structure as a reinforcement in LCM processes. First, we investigated whether the pore space inside the spongelike NFC reinforcement was interconnected and hence amenable to complete wetting through a forced resin flow inside an RTM/VARTM mold. An effort was made to study the morphology of pores through a micro-CT scan of the aerogel samples where significant interconnection of pores was observed. The use of liquid hexane with its low surface energy enabled it to be spontaneously imbibed ("wicked") into the reinforcement (Fig. 15.7, left). A fairly high degree of saturation with the liquid behind a sharp liquid front indicated the presence of a large fraction of interconnected micro-sized pores and pointed to its suitability as an LCM preform. Later, a small RTM mold was prepared, and slices of NFC aerogels created through the freeze-drying process were placed inside the mold and closed. Later an epoxy resin was injected in order to completely impregnate the NFC preform and was allowed to cure. The dog-bone specimen extracted

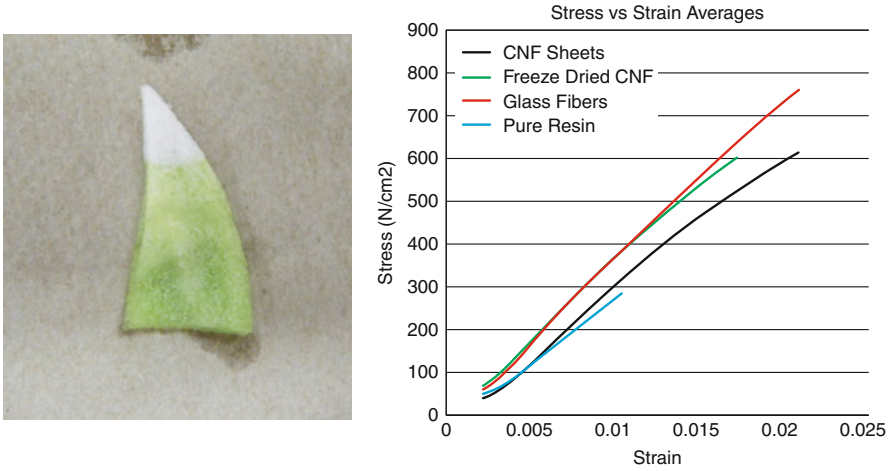

Fig. 15.7 (*Left*) A wicking test done with a freeze-dried NFC preform created at Forest Products Lab, Madison, shows the clear movement of a green-dyed hexadecane through the porous specimen, thereby demonstrating the interconnection of pores and the possibility of creating polymer composites by impregnating the specimen with resin using the RTM technology. (*Right*) A comparison of the uniaxial tension test results indicates that the freeze-dried NFC is performing as well as glass fiber in reinforcing the epoxy-based composite

from the mold was subjected to a uniaxial tension tests according to ASTM standards. Figure 15.7 (right) compares the stress–strain curves for the freeze-dried NFC sample vis-à-vis the glass and pure resin samples for different volume fractions. These results may indicate that freeze-dried NFC structures or aerogels are capable of creating large NFC nanocomposites parts using the LCM technology.

3.4 Outlook on Process Modeling LCM for Making NFC Composites

In any LCM process, complete filling of the mold with adequate wetting of fibers is the mold designer's primary objective [95]. Incomplete filling in the mold leads to the production of defective parts with dry spots. It is also important for the mold designer to minimize fill time and fluid pressure buildup during the filling process (especially in RTM) to make the technology cost-effective in a manufacturing environment. Many factors affect the filling of a mold, including the permeability of the fiber mats, the presence of gaps in the mold, the positions of inlet and outlet gates, and the rates of resin injection from different inlet ports. Often, it is not possible for the mold designer to visualize and design an adequate system for resin infusion by intuition alone; as a result, mold-filling simulations are used to optimize mold performance [96–107]. Numerical simulations allow designers to optimize mold design in virtual space quickly and economically.

The trend of using LCM for making natural-fiber composites is beginning to grow [108–111] due to the short cycle time and automation friendliness of the process that lends itself particularly well to use in the high-volume automotive sector; however, unlike synthetic fibers, natural fibers absorb liquid and swell, thereby exhibiting a very different response during LCM mold filling. Until recently, the conventional approaches to model mold filling in natural-fiber mats involve changing the permeability of fiber mats in an ad hoc manner [109]. However, Masoodi and Pillai [112] were the first to propose a completely new set of flow governing equations for isothermal conditions (under low curing rate and test conditions) that were derived using the rigorous and reputed volume-averaging method for natural-fiber mats. Pillai et al. were also the first to incorporate these equations into their finite element/control volume-based LCM mold-filling simulation [96]. The new mold-filling physics developed for swelling LCM preforms, when rigorously tested against experiments, was found to be superior to the conventional flow physics used for non-swelling preforms [112, 113].

Until very recently, NFCs have been produced in very small quantities, thereby rendering them exorbitantly expensive for mass production-type engineering applications; hence, there had been little attempt to use them as reinforcement in LCM processes until now. However, due to the establishment of several pilot plants around the world (including one at Forest Products Lab, Madison) for the production of NFC, the cost of NFC is likely to come down drastically and its availability is being ramped up. As a result, it may become economically feasible to use NFC reinforcements in LCM for making industrial-scale green composites. Consequently there have been some attempts to study the swelling and liquid-absorbing properties of NFC reinforcements [114] as well as develop mathematics for modeling resin flow in liquid-absorbing, swelling porous media created by NFC inside an LCM mold [115]. The future will witness a rapid development of the processing science for producing NFC-based thermoset composites using NFC reinforcements with LCM processes.

4 Mechanical Characterization

Thermoplastic materials have been previously used with nanocellulose materials and offer important advantages of recyclability and high fracture toughness [116–118], and a review of the mechanical properties of these composites can be found elsewhere, for example, in Siró et al. [23]. In this section, we discuss some of the mechanical characterization results of nanocellulose thermosetting composites. Continuous nanocellulose reinforcements have not progressed sufficiently that they have been used in composites yet and are not discussed. A summary of the properties reported for thermosetting materials is shown in Table 15.4.

4.1 Stiffness and Strength Properties

The stiffness and strength properties are highly dependent on the form of nanocellulose reported. The mechanical testing in the literature is mainly for thermoplastic resins;

Table 15.4 Survey of mechanical properties of several thermosetting NFC composites

Resin	Nanocellulose form	Process	Strength (MPa)	Initial elastic modulus (GPa)	Strain to failure (%)	References
Phenol formaldehyde	NFC film (5–20 %wt fibers)	Press	201–216	4.16–4.84	12.6–14.7	[145]
Phenol formaldehyde	NFC (14.4–27.9 %wt resin)	Press	300–375 (bending)	16–20 (bending)	–	[146]
Melamine formaldehyde	NFC film (13 % wt fiber)	Press	142	16.6	0.81	[147]
Epoxy	NFC film (0–5 % fiber vol.)	Press	–	1.5–2.9	–	[88]

however, limited work has been reported. Of these studies reported, using a hot press process is generally the most preferred. Distributed or particulate composites based on nanocellulose benefit from the interactions with the resin and relatively high aspect ratios of the cellulose particles or fibers. In work by Ruiz et al. [87] on composites from NFC and aqueous suspensions of epoxy, NFC displayed large aspect ratios and an ability to associate by means of H-bonds. Using an aqueous suspension of epoxy avoided the problem of high viscosity that would result if a conventional, reactive epoxy was simply mixed with the CNCs. The reinforcement benefits were linked to strong interactions between the CNCs and epoxy network and the percolating network linked by H-bonds between the NFC. The effect of fiber content on the mechanical and thermal expansion properties of biocomposites based on NFC has also been reported [119]. A linear increase in Young's modulus was observed at fiber contents up to 40 wt%, using a phenolic resin. The results also showed a correlation between the coefficients of thermal expansion (CTE) relative to fiber content, indicating the effective reinforcement attained by the NFC.

The incorporation of NFC into epoxy has been found to greatly increase the glassy storage modulus. At 30 °C, this modulus increases from 2.6 GPa for neat epoxy to 3.1 GPa for 5 wt% NFC–epoxy film [85]. Higher increases are reported for temperatures above the glass transition temperature temperatures. The rubbery storage modulus at 130 °C increases from 9.7 MPa for neat epoxy to 37.3 MPa for 5 wt% NFC–epoxy film. In another example, Ruiz et al. found that adding NFC up to about 2 % in an epoxy resin increased the mechanical properties, but further addition of NFC led to agglomeration and reduced thermal and mechanical properties [87]. The pressing method has been found to be the most common in the literature for processing of thermosetting composites with NFC reinforcements. Nakagaito and Yano [120] used a compression molding technique of NFC sheets impregnated with phenol formaldehyde to achieve a Young's modulus and bending strength of up to 19 GPa and 370 MPa, respectively. Compared to a starch matrix with 70 wt% NFC which showed a modulus of 6.2 GPa and a tensile strength of 160 MPa [121]. The differences between regular cellulose and NFC and their relationship to pressing

pressure have been previously examined [53]. Processing the same pulp to NFC, the researchers found increased modulus and strength from the NFC-based composites when combined with a phenol formaldehyde matrix. The Young's modulus of NFC-based and pulp-based composites using phenolic resin as binder was very similar, around 18–19 GPa; however, the bending strength peaked at 370 and 260 MPa for NFC and pulp-based composites, respectively [88, 120]. The planar NFC reinforcements also result in significant amounts of porosity (~10 %) that can affect the stiffness values [52]. Improving the processing of these composites can yield some improvements in the matrix-dominated properties.

4.2 Fracture Properties

Although the tensile properties are commonly tested, the amount of research on fracture properties of nanocellulose composites is limited. Researchers have proposed hierarchical systems of reinforcement incorporating NFC to take advantage of the fracture toughness benefits provided at different length scales. While not in a thermosetting resin material, Okubo et al. [122] dispersed NFC reinforcement around bamboo fibers in a polylactic acid (PLA) matrix and showed that the additional NFC improved the fracture properties by preventing sudden crack growth. Adding 1 wt% of NFC resulted in an increase of the fracture energy by 200 %. Although this approach has not been investigated in thermosets, hybrid systems incorporating NFC have also been proposed for carbon fibers reinforced with an epoxy matrix [123]. Adding 2 wt% of NFC resulted in improved fracture toughness and higher glass transition temperatures but with limited increases in the tensile strength and modulus. Fracture testing on NFC sheet-reinforced composites panels has also been reported [88]. Figure 15.8 shows the lack of fiber bridging observed in the propagating crack in a layered NFC/epoxy composite [88]. The crack is retarded manually by not having a self-similar growth behavior. The fracture surface does not show significant mechanical interlocking between the two surfaces. Increasing the fracture energy required to separate the surfaces across

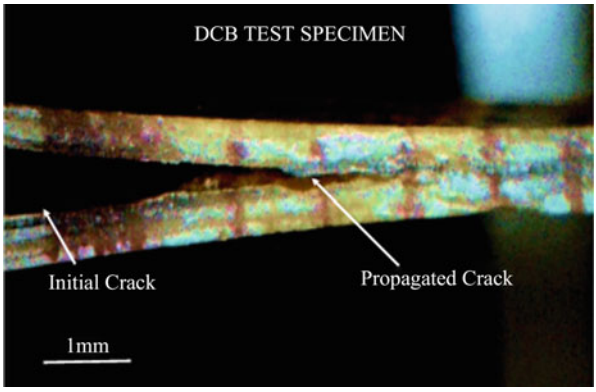

Fig. 15.8 Crack propagation in a nanopaper composite specimen (Reprinted from Masoodi et al. [88], with permission from Elsevier)

the NFC sheets will result in a larger fracture toughness of the NFC composite and overcome the limitations associated with discrete layers of the nanocellulose material. The planar reinforcements clearly have benefits when loaded in the in-plane directions; however, out of plane stresses show the potential for the crack growth in between the planar layers.

5 Nonmechanical Characteristics

The benefits of nanocellulose are not restricted to mechanical property improvements of composites. Researchers have envisioned that, with proper processing, they can lead to environmentally safe, lightweight composites with unique properties (e.g., transparency and barrier properties) for application in automotive manufacturing, packaging, medicine, energy storage devices, sensors, and electronics [16, 23, 124]. Nanocellulose films could be used as barrier materials, or conversely, high-porosity aerogels could be used to allow flow of gases while absorbing moisture due to their hydrophilic nature [125]. Nystrom et al. [126] coated wood-based nanocellulose with polypyrrole using in situ chemical polymerization to obtain an electrically conducting composite. Many of these applications are in their infancy as work continues to better characterize the behavior of these materials. Some of the attributes that highlight the potential of nanocellulose for these various applications are discussed here.

Nanocellulose composites can offer transparency for a variety of potential applications ranging from flexible display devices to armor applications. The small cross section of the fibers does not result in light scattering even at high reinforcement ratios; thus, strong, transparent composites are possible using NFC. Excellent transparency of 80 % or more has been reported for neat NFC films [12, 127] and NFC composites [8, 17]. Polishing or coating NFC films with resins has been used as a method to increase the transparency by eliminating the surface scattering [12, 17]. For example, Okahisa et al. [17] studied the use of optically transparent wood–cellulose nanocomposite as a base substrate for flexible organic light-emitting diode displays. Acrylic resins were used to achieve the desirable combination of high flexibility and low coefficient of thermal expansion.

Low coefficient of thermal expansion (CTE) in composites is desirable in electronic applications as expansion can lead to device failure [16, 17]. Okahisa et al. suggest CTE values should be below about 20 ppm K^{-1} for printed OLED displays, whereas many foldable plastics have CTE values more than an order of magnitude higher than this target [17], and polyethylene terephthalate (PET) has a CTE of about 50 ppm K^{-1}. Okahisa et al. achieved a coefficient of thermal expansion of 12.1 ppm K^{-1} by removing excess surface resin layers from the NFC composite. CTE values of less than 10 ppm K^{-1} for NFC composites have also been reported [12]. Such low CTE values, along with high transparency, suggest that NFC composites may be useful for a wide variety of applications including substrates for flexible electronics or display devices.

Nanocellulose films have been shown to exhibit excellent barrier properties, especially at low levels of humidity [18–21, 128]. The water vapor barrier of

polymer films has been observed to be improved by cellulose nanoreinforcements [129]. The mechanism is related to creating a more complex path leading to a slower diffusion and lower permeability. Azeredo et al. [130] studied the barrier properties of a nanocomposite film with 15 % NFC and plasticized with 18 % glycerol and compared to synthetic polymer films. The strength and stiffness were found to be comparable to the synthetic polymer. The water vapor barrier properties were enhanced but not to the level of the synthetic materials. The surface rather than the core dominated the diffusion process. CNC film was found to be much more permeable to gases than NFC [131]. Related to this is application of nanocellulose in the area of active packaging. In this application, cellulose nanocomposites have been proposed where nanoparticles can be used for scavenging purposes in removing oxygen and odor chemicals or to release preservatives or color where and when required [132]. Biodegradable cellulose nanocomposites are a potential material for replacing synthetic materials in the food packaging industry. They can be used to improve the mechanical and barrier properties of bio-polymers and also provide antimicrobial activity, enzyme immobilization, and biosensing [133].

Cellulose nanocrystals, like many polysaccharides, are self-ordering and thus produce a number of interesting optical properties. The birefringence of cellulose nanocrystals has long been known, and ordered chiral nematic phases were seen to be preserved in films of cellulose and cellulose derivatives more than two decades ago [134, 135]. Gray and colleagues observed that when solidified by evaporation, cellulose nanocrystal films produced "helicoidal structures resembling those in various biological skeletal structures" [136]. Revol et al. describe cellulose nanocrystal films that have helicoidal arrangement of nanocrystals and that reflect polarized light [137, 138]. The wavelength of light reflected by these films was reported to be controllable across the visible, infrared, and ultraviolet spectrum. The colors were reported to change with viewing angle, thus making them suited for security papers and other applications.

6 Future Trends

With changing consumer perceptions, increased ecological considerations, and technological advances, recent trends in sourcing materials from rapidly renewable, natural resources are likely to continue. From a composites perspective, this includes not only the polymer matrices and additives but the reinforcements as well. Reinforcements from nanocellulose offer one interesting possibility. Nanocellulose reinforcements offer potential advantages in specific properties related to their lower density and other advantages such as low CTE, transparency, barrier properties, etc.

However, the use of nanocellulose as a reinforcement is in its infancy, and the full reinforcing potential of these materials has yet to be realized partly because of issues related to scaling manufacturing processes. To date, the availability of significant quantities of nanocellulose has prevented more rapid wide-scale research and development efforts related to their use. However, recent

announcements of commercial and government pilot- and plant-scale production facilities will likely improve the situation [139]. NFCs have begun receiving additional attention as a reinforcement material because of reductions in the energy requirements for breaking down cellulose fibers to NFC [140]. While much recent progress has been made, there are many challenges remaining to efficiently and economically use it as reinforcement. More efficient and effective strategies need to be found for producing nanocellulose with optimal characteristics. Widespread application of these materials will require additional research to address the issues related to their hydrophilic nature in many applications. Techniques and appropriate chemistry are needed to adequately disperse nanocellulose reinforcements or convert them into a useful form for incorporation into a variety of matrices and strongly bond them to it. More efficient control of structure on multiple scales is needed to tailor performance. For example, better control of the porosity and fiber volume is likely to result in improvements in strength, stiffness, and fracture behavior. Development of new analytical methods is necessary for simulation of processing and also prediction of the mechanical properties of nanocellulose-based structures. The process modeling effort will be required to link the modeling of NFC distributions to optimize properties. Appropriate applications need to be identified, investigated, and demonstrated. Health and safety issues related to nano-scale size need to be understood and addressed as well.

It is unlikely that these developments will occur in isolation and will need to be incorporated in to larger infrastructures. For example, paper mills could be repurposed for the production of biofuels and materials that could potentially mitigate climate change through the reduction of greenhouse gas emissions [141]. If high-value applications can be found, it may be possible to integrate nanocellulose production into the material flow of these biorefineries, where it could potentially help improve economics [141].

References

1. Mohseni Languri E, Moore RD, Masoodi R, Pillai KM, Sabo R (2010) An approach to model resin flow through swelling porous media made of natural fibers. Paper presented at the the 10th international conference on flow processes in composite materials (FPCM10), Monte Verità, 11–15 Jul 2010
2. Goutianos S, Peijs T, Nystrom B, Skrifvars M (2006) Development of flax fibre based textile reinforcements for composite applications. Appl Compos Mater 16:199–215. doi:10.1007/s10443-006-9010-2
3. Nickel J, Riedel U (2003) Activities in biocomposites. Mater Today 6:44–48. doi:10.1016/S1369-7021(03)00430-9
4. Summerscales J, Dissanayake N, Virk A, Hall W (2010) A review of bast fibres and their composites. Part 2 – composites. Compos Part A 42:1336–1344. doi:10.1016/j.compositesa.2010.05.020
5. Bledski AK, Gassan J (1999) Composites reinforced with cellulose based fibres. Prog Polym Sci 24:221–274
6. Reux F, Verpoest I (eds) (2012) Flax and hemp fibres: a natural solution for the composite industry, 1st edn. JEC Composites, Paris

7. Moon RJ, Martini A, Nairn J, Simonsen J, Youngblood J (2011) Cellulose nanomaterials review: structure, properties and nanocomposites. Chem Soc Rev 40(7):3941–3994. doi:10.1039/c0cs00108b
8. Iwamoto S, Nakagaito AN, Yano H (2007) Nano-fibrillation of pulp fibers for the processing of transparent nanocomposites. Appl Phys A Mater 89(2):461–466. doi:10.1007/s00339-007-4175-6
9. Iwamoto S, Nakagaito AN, Yano H, Nogi M (2005) Optically transparent composites reinforced with plant fiber-based nanofibers. Appl Phys A Mater 81(6):1109–1112. doi:10.1007/s00339-005-3316-z
10. Nogi M, Handa K, Nakagaito AN, Yano H (2005) Optically transparent bionanofiber composites with low sensitivity to refractive index of the polymer matrix. Appl Phys Lett 87(24). Art No 243110, doi:10.1063/1.2146056
11. Nogi M, Ifuku S, Abe K, Handa K, Nakagaito AN, Yano H (2006) Fiber-content dependency of the optical transparency and thermal expansion of bacterial nanofiber reinforced composites. Appl Phys Lett 88(13). Art No 133124, doi:10.1063/1.2191667
12. Nogi M, Iwamoto S, Nakagaito AN, Yano H (2009) Optically transparent nanofiber paper. Adv Mater 21:1595–1598. doi:10.1002/adma.200803174
13. Nogi M, Yano H (2008) Transparent nanocomposites based on cellulose produced by bacteria offer potential innovation in the electronics device industry. Adv Mater 20:1849–1852. doi:10.1002/adma.200702559
14. Nogi M, Yano H (2009) Optically transparent nanofiber sheets by deposition of transparent materials: a concept for a roll-to-roll processing. Appl Phys Lett 94. doi:10.1063/1.3154547
15. Nogia M, Abe K, Handa K, Nakatsubo F, Ifuku S, Yano H (2006) Property enhancement of optically transparent bionanofiber composites by acetylation. Appl Phys Lett 89. doi:10.1063/1.2403901
16. Sabo R, Seo J-H, Ma Z (2012) Cellulose nanofiber composite substrates for flexible electronics. In: 2012 TAPPI international conference on nanotechnology for renewable materials, Montreal
17. Okahisa Y, Yoshida A, Miyaguchi S, Yano H (2009) Optically transparent wood–cellulose nanocomposite as a base substrate for flexible organic light-emitting diode displays. Compos Sci Technol 69(11,Äì12):1958–1961. doi:10.1016/j.compscitech.2009.04.017
18. Minelli M, Baschetti MG, Doghieri F, Ankerfors M, Lindström T, Siró I, Plackett D (2010) Investigation of mass transport properties of microfibrillated cellulose (MFC) films. J Membr Sci 358(1–2):67–75. doi:10.1016/j.memsci.2010.04.030
19. Syverud K, Stenius P (2009) Strength and barrier properties of MFC films. Cellulose 16(1):75–85. doi:10.1007/s10570-008-9244-2
20. Fukuzumi H, Saito T, Iwata T, Kumamoto Y, Isogai A (2008) Transparent and high gas barrier films of cellulose nanofibers prepared by TEMPO-mediated oxidation. Biomacromolecules 10(1):162–165. doi:10.1021/bm801065u
21. Aulin C, Gällstedt M, Lindström T (2010) Oxygen and oil barrier properties of microfibrillated cellulose films and coatings. Cellulose 17(3):559–574. doi:10.1007/s10570-009-9393-y
22. Berglund L (2005) Cellulose-based nanocomposites. In: Mohanty AK, Misra M, Drzal LT (eds) Natural fibers, biopolymers, and biocomposites. Taylor & Francis, Boca Raton, pp 807–832
23. Siró I, Plackett D (2010) Microfibrillated cellulose and new nanocomposite materials: a review. Cellulose 17(3):459–494. doi:10.1007/s10570-010-9405-y
24. Eichorn SJ (2011) Cellulose nanowhiskers: promising materials for advanced applications. Soft Matter 7:303–315. doi:10.1039/C0SM00142B
25. Habibi Y, Lucia LA, Rojas OJ (2010) Cellulose nanocrystals: chemistry, self-assembly, and applications. Chem Rev 110:3479–3500
26. Peng BL, Dhar N, Liu HL, Tam KC (2011) Chemistry and applications of nanocrystalline cellulose and its derivatives: a nanotechnology perspective. Can J Chem Eng 89:1191–1206. doi:10.1002/cjce.20554

27. Samir MASA, Alloin F, Dufresne A (2005) Review of recent research into cellulosic whiskers, their properties and their application in nanocomposite field. Biomacromolecules 6:612–626
28. Eichhorn SJ, Dufresne A, Aranguren M, Marcovich NE, Capadona JR, Rowan SJ, Weder C, Thielemans W, Roman M, Renneckar S, Gindl W, Veigel S, Keckes J, Yano H, Abe K, Nogi M, Nakagaito AN, Mangalam A, Simonsen J, Benight AS, Bismarck A, Berglund LA, Peijs T (2010) Review: current international research into cellulose nanofibres and nanocomposites. J Mater Sci 45(1):1–33. doi:10.1007/s10853-009-3874-0
29. Beck-Candanedo S, Roman M, Gray DG (2005) Effect of reaction conditions on the properties and behavior of wood cellulose nanocrystal suspensions. Biomacromolecules 6(2):1048–1054
30. Sehaqui H, Ezekiel Mushi N, Morimune S, Salajkova M, Nishino T, Berglund LA (2012) Cellulose nanofiber orientation in nanopaper and nanocomposites by cold drawing. ACS Appl Mater Interfaces 4(2):1043–1049. doi:10.1021/am2016766
31. Viet D, Beck-Candanedo S, Gray D (2007) Dispersion of cellulose nanocrystals in polar organic solvents. Cellulose 14(2):109–113. doi:10.1007/s10570-006-9093-9
32. Eyholzer C, Bordeanu N, Lopez-Suevos F, Rentsch D, Zimmermann T, Oksman K (2010) Preparation and characterization of water-redispersible nanofibrillated cellulose in powder form. Cellulose 17(1):19–30. doi:10.1007/s10570-009-9372-3
33. Beck S, Berry RM, Bouchard J (2012) Dispersing dried nanocrystalline cellulose in water. Paper presented at the 2012 TAPPI nanotechnology conference for renewable materials, Montreal
34. Peng Y, Gardner D, Han Y (2012) Drying cellulose nanofibrils: in search of a suitable method. Cellulose 19(1):91–102. doi:10.1007/s10570-011-9630-z
35. Gardner DJ, Han Y, Peng Y (2011) Methods for drying cellulose nanofibrils. US Patent 0,260,348, A1
36. Mertaniemi H, Laukkanen A, Teirfolk J-E, Ikkala O, Ras RHA (2012) Functionalized porous microparticles of nanofibrillated cellulose for biomimetic hierarchically structured superhydrophobic surfaces. RSC Adv 2(7):2882–2886
37. Herrick FW (1984) Redispersable microfibrillated cellulose. US Patent 4,481,076
38. Yuan H, Nishiyama Y, Wada M, Kuga S (2006) Surface acylation of cellulose whiskers by drying aqueous emulsion. Biomacromolecules 7:696–700
39. Heux L, Chauve G, Bonini C (2000) Nonflocculating and chiral-nematic self-ordering of cellulose microcrystals suspensions in nonpolar solvents. Langmuir 16:8210–8212
40. Ljungberg N, Bonini C, Bortolussi F, Boisson C, Heux L, Cavaillé JY (2005) New nanocomposite materials reinforced with cellulose whiskers in atactic polypropylene: effect of surface and dispersion characteristics. Biomacromolecules 6(5):2732–2739
41. Goussé C, Chanzy H, Excoffier G, Soubeyrand L, Fleury E (2002) Stable suspensions of partially silylated cellulose whiskers dispersed in organic solvents. Polymer 43(9):2645–2651
42. Siqueira G, Bras J, Dufresne A (2009) Cellulose whiskers versus microfibrils: influence of the nature of the nanoparticle and its surface functionalization on the thermal and mechanical properties of nanocomposites. Biomacromolecules 10:425–432
43. Sabo R, Clemons C, Reiner R, Agarwal U (2008) Cellulose nanocrystal reinforced polyolefin composites. In: TAPPI-FPS international conference on nanotechnology for the Forest Products Industry, St. Louis
44. Bondeson D, Oksman K (2007) Dispersion and characteristics of surfactant modified cellulose whiskers nanocomposites. Compos Interfaces 14(7–9):617–630. doi:10.1163/156855407782106519
45. Azizi Samir MAS, Alloin F, Dufresne A (2005) Review of recent research into cellulosic whiskers, their properties and their application in nanocomposite field. Biomacromolecules 6(2):612–626. doi:10.1021/bm0493685

46. Lönnberg H, Fogelström L, Azizi Samir MAS, Berglund L, Malmström E, Hult A (2008) Surface grafting of microfibrillated cellulose with poly(e-caprolactone) – synthesis and characterization. Eur Polym J 44:2991–2997
47. Goussé C, Chanzy H, Cerrada ML, Fleury E (2004) Surface silylation of cellulose microfibrils: preparation and rheological properties. Polymer 45(5):1569–1575
48. Lu J, Askeland P, Drzal L (2008) Surface modification of microfibrillated cellulose for epoxy composite applications. Polymer 49:1285–1296
49. Han Y, Gardner DJ, Peng Y (2011) A new processing method for production of dried cellulose nanofibrils with in situ surface modification and their thermoplastic composites. Paper presented at the 11th international conference on wood and biofiber plastic composites & nanotechnology in wood composites symposium, Madison, 18 May 2011
50. Ankerfors M, Lindström T (2007) On the manufacture and use of nanocellulose. In: Ninth international conference on wood and biofiber plastic composites, Madison, 21–23 May 2007
51. Ankerfors M, Lindström T (2009) Nanocellulose developments in Scandinavia. In: Paper and coating chemistry symposium, Hamilton
52. Henriksson M, Berglund LA, Isaksson P, Lindström T, Nishino T (2008) Cellulose nanopaper structures of high toughness. Biomacromolecules 9(6):1579–1585. doi:10.1021/bm800038n
53. Nakagaito AN, Yano H (2005) Novel high-strength biocomposites based on microfibrillated cellulose having nano-order-unit web-like network structure. Appl Phys A Mater Sci Process 80(1):155–159. doi:10.1007/s00339-003-2225-2
54. Zimmermann T, Bordeanu N, Strub E (2010) Properties of nanofibrillated cellulose from different raw materials and its reinforcement potential. Carbohydr Polym 79(4):1086–1093. doi:10.1016/j.carbpol.2009.10.045
55. Sehaqui H, Liu A, Zhou Q, Berglund LA (2010) Fast preparation procedure for large, flat cellulose and cellulose/inorganic nanopaper structures. Biomacromolecules 11(9):2195–2198. doi:10.1021/bm100490s
56. Kunnari V, Tammelin T, Kaljunen T, Vartiainen J, Hippi U, Salminen A (2012) Transparent plastic-like flim material from birch fibril pulp. In: 12th international conference on biocomposites, Niagara Falls, 6–8 May 2012
57. Stelte W, Sanadi AR (2009) Preparation and characterization of cellulose nanofibers from two commercial hardwood and softwood pulps. Ind Eng Chem Res 48(24):11211–11219. doi:10.1021/ie9011672
58. Saito T, Hirota M, Tamura N, Kimura S, Fukuzumi H, Heux L, Isogai A (2009) Individualization of nano-sized plant cellulose fibrils by direct surface carboxylation using TEMPO catalyst under neutral conditions. Biomacromolecules 10(7):1992–1996. doi:10.1021/bm900414t
59. Gindl W, Keckes J (2007) Drawing of self-reinforced cellulose films. J Appl Polym Sci 103(4):2703–2708
60. Bledski AK, Jaszkiewicz A, Murr M, Sperber VE, Lötzendorf R, Reuβmann T (2008) Processing techniques for natural- and wood-fibre composites. In: Pickering KL (ed) Properties and performance of natural-fibre composites. Woodhead, Cambridge, pp 163–192
61. Woodings C (2001) A brief history of regenerated cellulose fibres. In: Calvin W (ed) Regenerated cellulose fibres. Woodhead, Boca Raton, pp 1–21
62. Adusumali R-B, Reifferscheid M, Weber H, Roeder T, Sixta H, Gindl W (2006) Mechanical properties of regenerated cellulose fibres for composites. Macromol Symp 244:119–125
63. Ganster J, Fink H-P (2006) Novel cellulose fibre reinforced thermoplastic materials. Cellulose 13(3):271–280. doi:10.1007/s10570-005-9045-9
64. Iwamoto S, Isogai A, Iwata T (2011) Structure and mechanical properties of wet-spun fibers made from natural cellulose nanofibers. Biomacromolecules 12(3):831–836. doi:10.1021/bm101510r

65. Walther A, Timonen JV, Diez I, Laukkanen A, Ikkala O (2011) Multifunctional high-performance biofibers based on wet-extrusion of renewable native cellulose nanofibrils. Adv Mater 23(26):2924–2928. doi:10.1002/adma.201100580
66. Bruce DM, Hobson RN, Farrent JW, Hepworth DG (2005) High-performance composites from low-cost plant primary cell walls. Compos Part A 36:1486–1493. doi:10.1016/j.compositesa.2005.03.008
67. Omrani A, Simon LC, Rostami AA (2008) Influences of cellulose nanofiber on the epoxy network formation. Mater Sci Eng A 490:131–137. doi:10.1016/j.msea.2008.01.012
68. Matos Ruiz M, Cavaillé JY, Dusfresne A, Graillat C, Gérard J-F (2001) New waterborne epoxy coatings based on cellulose nanofillers. Macromol Symp 169:211–222
69. Henriksson M, Berglund LA (2007) Structure and properties of cellulose nanocomposite films containing melamine formaldehyde. J Appl Polym Sci 106:2817–2824. doi:10.1002/app.26946
70. Nakagaito AN, Yano H (2004) The effect of morphological changes from pulp fiber towards nano-scale fibrillated cellulose on the mechanical properties of high-strength plant fiber based composites. Appl Phys A Mater 78(4):547–552. doi:10.1007/s00339-003-2453-5
71. Nakagaito AN, Yano H (2005) Novel high-strength biocomposites based on microfibrillated cellulose having nano-order-unit web-like network structure. Appl Phys A Mater 80(1):155–159. doi:10.1007/s00339-003-2225-2
72. Masoodi R, El-Hajjar RF, Pillai KM, Sabo R (2012) Mechanical characterization of cellulose nanofiber and bio-based epoxy composite. Mater Des 36:570–576. doi:10.1016/j.matdes.2011.11.042
73. Nogi M, Abe K, Handa K, Nakatsubo F, Ifuku S, Yano H (2006) Property enhancement of optically transparent bionanofiber composites by acetylation. Appl Phys Lett 89. doi:10.1063/1.2403901
74. Behabtua N, Green MJ, Pasquali M (2008) Carbon nanotube-based neat fibers. Nano Today 3(5–6):24–34
75. Uddin AJ, Araki J, Gotoh Y (2011) Characterization of the poly(vinyl alcohol)/cellulose whisker gel spun fibers. Compos Part A Appl Sci Manuf 42(7):741–747. doi:10.1016/j.compositesa.2011.02.012
76. Uddin AJ, Araki J, Gotoh Y (2011) Toward "strong" green nanocomposites: polyvinyl alcohol reinforced with extremely oriented cellulose whiskers. Biomacromolecules 12(3):617–624. doi:10.1021/bm101280f
77. Lu P, Hsieh Y-L (2009) Cellulose nanocrystal-filled poly(acrylic acid) nanocomposite fibrous membranes. Nanotechnology 20:1–9
78. Peresin MS, Habibi Y, Zoppe JO, Pawlak JJ, Rojas OJ (2010) Nanofiber composites of polyvinyl alcohol and cellulose nanocrystals: manufacture and characterization. Biomacromolecules 11:674–681
79. Peresin MS, Habibi Y, Vesterinen A-H, Rojas OJ, Pawlak JJ, Seppala JV (2010) Effect of moisture on electrospun nanofiber composites of poly(vinyl alcohol) and cellulose nanocrystals. Biomacromolecules 11:2471–2477
80. Akesson D, Skrifvars M, Hagstrom B, Walkenstrom P, Seppala J (2009) Processing of structural composites from biobased thermoset resins and natural fibres by compression moulding. J Biobased Mater Bio 3(3):215–225. doi:10.1166/Jbmb.2009.1036
81. Akesson D, Skrifvars M, Walkenstrom P (2009) Preparation of thermoset composites from natural fibres and acrylate modified soybean oil resins. J Appl Polym Sci 114(4):2502–2508. doi:10.1002/App.30773
82. Adekunle K, Akesson D, Skrifvars M (2010) Biobased composites prepared by compression molding with a novel thermoset resin from soybean oil and a natural-fiber reinforcement. J Appl Polym Sci 116(3):1759–1765. doi:10.1002/App.31634
83. Hubbe MA, Rojas OJ, Lucia LA, Sain M (2008) Cellulosic nanocomposites: a review. Bioresources 3(3):929–980

84. Abdelmouleh M, Boufi S, Belgacem MN, Dufresne A, Gandini A (2005) Modification of cellulose fibers with functionalized silanes: effect of the fiber treatment on the mechanical performances of cellulose–thermoset composites. J Appl Polym Sci 98(3):974–984. doi:10.1002/app.22133
85. Lu J, Askeland P, Drzal LT (2008) Surface modification of microfibrillated cellulose for epoxy composite applications. Polymer 49(5):1285–1296. doi:10.1016/j.polymer.2008.01.028
86. Capadona JR, Van Den Berg O, Capadona LA, Schroeter M, Rowan SJ, Tyler DJ, Weder C (2007) A versatile approach for the processing of polymer nanocomposites with self-assembled nanofibre templates. Nat Nano 2(12):765–769. http://www.nature.com/nnano/journal/v2/n12/suppinfo/nnano.2007.379_S1.html
87. Ruiz MM, Cavaille JY, Dufresne A, Gerard JF, Graillat C (2000) Processing and characterization of new thermoset nanocomposites based on cellulose whiskers. Compos Interfaces 7(2):117–131
88. Masoodi R, El-Hajjar RF, Pillai KM, Sabo R (2012) Mechanical characterization of cellulose nanofiber and bio-based epoxy composite. Mater Des 36:570–576. doi:10.1016/j.matdes.2011.11.042
89. Entropy R (2010) Entropy resins. http://www.entropyresins.com/sites/default/files/SuperSap-100_1000_TDS.pdf. Accessed 5 Jan 2012
90. Pääkkö M, Vapaavuori J, Silvennoinen R, Kosonen H, Ankerfors M, Lindström T, Berglund LA, Ikkala O (2008) Soft Matter 4:2492
91. Pääkkö M, Ankerfors M, Kosonen H, Nykänen A, Ahola S, Österberg M, Ruokolainen J, Laine J, Larsson PT, Ikkala O, Lindström T (2007) Biomacromolecules 8:1934
92. Turbak AF, Snyder FW, Sandberg KR (1983) J Appl Polym Sci Appl Polym Symp 37:815
93. Henriksson M, Henriksson G, Berglund LA, Lindström T (2007) Eur Polym J 43:3434
94. Hüsing N, Schubert U (1998) Angew Chem Int Ed 37:45
95. Tan H, Pillai KM (2010) Processing polymer matrix composites composites for blast protection. In: Uddin N (ed) Blast protection of civil infrastructures and vehicles using composites. Woodhead Publishing Limited, Cambridge
96. Tan H, Pillai KM (2010) PORE-FLOW – a software to model the flow of liquids in single- and dual-scale porous media. http://www4.uwm.edu/porous
97. Jiang S, Yang L, Alsoliby S, Zhou G (2007) PCG solver and its computational complexity for implicit control-volume finite-element method of RTM simulation. Compos Sci Technol 67(15–16):3316–3322
98. Soukane S, Trochu F (2006) Application of the level set method to the simulation of resin transfer molding. Compos Sci Technol 66(7–8):1067–1080
99. Shojaei A, Gaffarian SR, Karimian SMH (2002) Numerical simulation of three-dimensional mold filling process in resin transfer molding using quasi-steady state and partial saturation formulations. Compos Sci Technol 62(6):861–879
100. Mohan RV, Ngo ND, Tamma KK (1999) On a pure finite-element-based methodology for resin transfer mold filling simulations. Polym Eng Sci 39(1):26–43
101. Wu CH (1998) Simulation of reactive liquid composite molding using an Eularian-Lagrangian approach. Int Polym Process 4:398
102. Phelan FR Jr (1997) Simulation of the injection process in resin transfer molding. Polym Compos 18(4):460–476
103. Bruschke MV, Advani SG (1991) RTM filling simulation of complex three dimensional shell-like structures. SAMPE Q 23(1):2–11
104. Young WB, Han K, Fong LH, Lee LJ, Liou MJ (1991) Analysis of resin injection molding in molds with preplaced fiber mats. Polym Compos 12:391–403
105. Young WB, Rupel K, Han K, Lee LJ, Liou MJ (1991) Analysis of resin injection molding in molds with preplaced fiber mats, II: numerical simulation and experiments of mold filling. Polym Compos 12:30–38

106. Fracchia CA, Castro J III (1989) CLT A finite element/control volume simulation of resin transfer molding. In: Proceedings of the American Society for Composites fourth technical conference. Technomic, Lancaster, pp 157–166
107. Molnar J, Trevino L, Lee LJ (1989) Liquid flow in molds with prelocated fiber mats. Polym Compos 10:414–423
108. O'Donnell A, Dweib MA, Wool RP (2004) Natural fiber composites with plant oil-based resin. Compos Sci Technol 64:1135–1145
109. Umer R, Bickerton S, Fernyhough A (2007) Wood fiber mats as reinforcements for thermosets. In: Handbook of engineering biopolymers. Hanser Gardner, Munich, pp 693–713
110. Richardson MOW, Zhang ZY (2000) Experimental investigation and flow visualization of the resin transfer moulding process for non-woven hemp reinforced phenolic composites. Compos Pt A 31:1303–1310
111. Rowell R, O'Dell J, Basak RK, Sarkar M (1997) Applications of jute in resin transfer molding. http://www.fpl.fs.fed.us/documents/pdf1997/rowel97h.pdf
112. Masoodi R, Pillai KM (2011) Modeling the processing of natural fiber composites made using liquid composites molding. In: Pilla S (ed) Handbook of bioplastics and biocomposites engineering applications. Scrivener Publishing, LLC, Salem, Massachusetts
113. Masoodi R, Pillai KM, Grahl N, Tan H (2012) Numerical simulation of LCM mold-filling during the manufacture of natural fiber composites. J Reinf Plast Compos 31(6)
114. Masoodi R, Javadi A, Pillai KM, Sabo R (2011) An experimental study on swelling of cellulose nano-fiber films in epoxy resins and water. Paper presented at the 2011 Spring SAMPE technical conference and exhibition – state of the industry: advanced materials, applications, and processing technology, Long Beach
115. Javadi A, Pillai KM, Sabo R (2012) An experimental estimation of liquid absorption coefficient for cellulose nano-fiber films. Paper presented at the 11th international conference on flow processes in composite materials (FPCM11), Auckland, 9–12 Jul 2012
116. Floros M, Hojabri L, Abraham E, Jose J, Thomas S, Pothan L, Leao AL, Narine S (2012) Enhancement of thermal stability, strength and extensibility of lipid-based polyurethanes with cellulose-based nanofibers. Polym Degrad Stab. doi:10.1016/j.polymdegradstab.2012.02.016
117. Lemahieu L, Bras J, Tiquet P, Augier S, Dufresne A (2011) Extrusion of nanocellulose-reinforced nanocomposites using the Dispersed Nano-Objects Protective Encapsulation (DOPE) process. Macromol Mater Eng 296(11):984–991. doi:10.1002/Mame.201100015
118. Tang X, Alavi S (2011) Recent advances in starch, polyvinyl alcohol based polymer blends, nanocomposites and their biodegradability. Carbohydr Polym 85(1):7–16. doi:10.1016/j.carbpol.2011.01.030
119. Nakagaito AN, Yano H (2008) The effect of fiber content on the mechanical and thermal expansion properties of biocomposites based on microfibrillated cellulose. Cellulose 15(4):555–559
120. Nakagaito A, Yano H (2005) Novel high-strength biocomposites based on microfibrillated cellulose having nano-order-unit web-like network structure. Appl Phys A Mater Sci Process 80(1):155–159
121. Svagan AJ, Samir MASA, Berglund LA (2007) Biomimetic polysaccharide nanocomposites of high cellulose content and high toughness. Biomacromolecules 8(8):2556–2563
122. Okubo K, Fujii T, Thostenson ET (2009) Multi-scale hybrid biocomposite: processing and mechanical characterization of bamboo fiber reinforced PLA with microfibrillated cellulose. Compos Part A Appl Sci Manuf 40(4):469–475. doi:10.1016/j.compositesa.2009.01.012
123. Gabr MH, Elrahman MA, Okubo K, Fujii T (2010) Effect of microfibrillated cellulose on mechanical properties of plain-woven CFRP reinforced epoxy. Compos Struct 92(9):1999–2006. doi:10.1016/j.compstruct.2009.12.009
124. (2012) EMPA Wood Laboratory researchers develop production process for nanocellulose powder. Addit Polym 2012 (1):2–3. doi:10.1016/s0306-3747(12)70003-9

125. Agbenyega J (2010) Nanopaper: nanotechnology. Mater Today 13(10):12. doi:10.1016/s1369-7021(10)70179-6
126. Nystrom G, Mihranyan A, Razaq A, Lindstrom T, Nyholm L, Stromme M (2010) A nanocellulose polypyrrole composite based on microfibrillated cellulose from wood. J Phys Chem B 114(12):4178–4182. doi:10.1021/Jp911272m
127. Zhu JY, Sabo R, Luo X (2011) Integrated production of nano-fibrillated cellulose and cellulosic biofuel (ethanol) by enzymatic fractionation of wood fibers. Green Chem 13(5):1339–1344
128. Qing Y, Sabo R, Wu Y, Cai Z (2013) Resin impregnation of cellulose nanofibril films facilitated by water swelling. Cellulose (Submitted Aug 2012) 20:303–313
129. Paralikar SA, Simonsen J, Lombardi J (2008) Poly(vinyl alcohol)/cellulose nanocrystal barrier membranes. J Membr Sci 320(1–2):248–258. doi:10.1016/j.memsci.2008.04.009
130. Azeredo HMC, Mattoso LHC, Avena-Bustillos RJ, Ceotto G, Munford ML, Wood D, McHugh TH (2010) Nanocellulose reinforced chitosan composite films as affected by nanofiller loading and plasticizer content. J Food Sci 75(1):N1–N7. doi:10.1111/J.1750-3841.2009.01386.X
131. Belbekhouche S, Bras J, Siqueira G, Chappey C, Lebrun L, Khelifi B, Marais S, Dufresne A (2011) Water sorption behavior and gas barrier properties of cellulose whiskers and microfibrils films. Carbohydr Polym 83(4):1740–1748. doi:10.1016/j.carbpol.2010.10.036
132. Bradley EL, Castle L, Chaudhry Q (2011) Applications of nanomaterials in food packaging with a consideration of opportunities for developing countries. Trends Food Sci Technol 22(11):604–610. doi:10.1016/j.tifs.2011.01.002
133. de Azeredo HMC (2009) Nanocomposites for food packaging applications. Food Res Int 42(9):1240–1253. doi:10.1016/j.foodres.2009.03.019
134. Charlet G, Gray DG (1987) Solid cholesteric films cast from aqueous (hydroxypropyl) cellulose. Macromolecules 20(1):33–38. doi:10.1021/ma00167a007
135. Giasson J, Revol J-F, Ritcey AM, Gray DG (1988) Electron microscopic evidence for cholesteric structure in films of cellulose and cellulose acetate. Biopolymers 27(12):1999–2004. doi:10.1002/bip.360271210
136. Revol JF, Bradford H, Giasson J, Marchessault RH, Gray DG (1992) Helicoidal self-ordering of cellulose microfibrils in aqueous suspension. Int J Biol Macromol 14(3):170–172. doi:10.1016/S0141-8130(05)80008-X
137. Revol J-F, Godbout D, Gray D, G (1997) Solidified liquid crystals of cellulose with optically variable properties. US Patent 5,629,055, 13 May 1997
138. Revol J-F, Godbout L, Gray GD (1998) Solid self-assembled films of cellulose with chiral nematic order and optically variable properties. J Pulp Pap Sci 24(5)
139. Walker C (2012) Thinking small is leading to big changes. Paper 360° vol Jan/Feb 2012. TAPPI
140. Siro I, Plackett D (2010) Microfibrillated cellulose and new nanocomposite materials: a review. Cellulose 17(3):459–494
141. Zhu JY, Sabo R, Luo X (2011) Integrated production of nano-fibrillated cellulose and cellulosic biofuel (ethanol) by enzymatic fractionation of wood fibers. Green Chem 13:1339–1344. doi:10.1039/c1gc15103g
142. Advanced materials – solutions for demanding applications (2004) Pub. No. LIT-2004-341 (03/04). Aiken
143. Lilholt H, Lawther JM (2000) Natural organic fibers. In: Chou T-W (ed) Comprehensive composite materials, vol 1, Fiber reinforcements and general theory of composites. Elsevier, New York, pp 1–23
144. Gindl W, Reifferscheid M, Adusumalli R-B, Weber H, Röder T, Sixta H, Schöberl T (2008) Anisotropy of the modulus of elasticity in regenerated cellulose fibres related to molecular orientation. Polymer 49:792–799

145. Qing Y, Sabo R, Wu Y, Cai Z (2012) High-performance cellulose nanofibril composite films. Bioresources 7(3):3064–3075
146. Nakagaito A, Yano H (2004) The effect of morphological changes from pulp fiber towards nano-scale fibrillated cellulose on the mechanical properties of high-strength plant fiber based composites. Appl Phys A Mater Sci Process 78(4):547–552
147. Henriksson M, Berglund LA (2007) Structure and properties of cellulose nanocomposite films containing melamine formaldehyde. J Appl Polym Sci 106(4):2817–2824

Poly(vinyl Alcohol)-Cellulose and Nanocellulose Composites

16

Maha M. Ibrahim and Waleed K. El-Zawawy

Contents

Abstract

The development of micro/nanofibers has attracted significant interest in the last few decades due to the unique properties they endow. Cellulose nanocrystals (CNs) are a promising material and have been widely studied over the past two decades. This material is interesting as nanofiller due to its nanoscale dimensions, high specific area, and highly rigid crystalline structure. Poly(vinyl alcohol), PVA, is water soluble, semicrystalline, fully biodegradable, nontoxic, and biocompatible, and therefore, it finds use in a broad applications. PVA-based fibers have been considered as an attractive choice in tissue scaffolding, filtration materials, membranes, optics, protective clothing, enzyme immobilization, drug release, and so on. Preparation and morphological features of PVA–nanocelluloses are discussed in this chapter. Their incorporation in

M.M. Ibrahim (✉) • W.K. El-Zawawy
Cellulose and Paper Department, National Research Center, Giza, Egypt
e-mail: mwakleed@hotmail.com; mwakleed@yahoo.com; wkzawawy@yahoo.com

J.K. Pandey et al. (eds.), *Handbook of Polymer Nanocomposites. Processing, Performance and Application – Volume C: Polymer Nanocomposites of Cellulose Nanoparticles*,
DOI 10.1007/978-3-642-45232-1_77,

nanocomposite materials including processing methods and properties such as thermal gravimetric analysis (TGA), differential scanning calorimetry (DSC), mechanical performances, dynamic mechanical analysis (DMA), and membrane properties are also presented.

Keywords
Cellulose nanocrystals • Poly(vinyl) alcohol • PVA-based fibers • Nanocomposites • Thermal gravimetric analysis • Dynamic mechanical analysis

1 Introduction

Natural fibers are pervasive throughout the world in plants such as grasses, reeds, stalks, and woody vegetation. They are also referred to as cellulosic fibers, related to the main chemical component cellulose, or as lignocellulosic fibers, since the fibers usually also contain a natural polyphenolic polymer, lignin, in their structure [113].

The use of lignocellulosic fibers derived from annually renewable resources as a reinforcing phase in polymeric matrix composites provides positive environmental benefits with respect to ultimate disposability and raw material use [40].

Many researchers are investigating the performances of adding cellulosic reinforcements in polymeric matrices to create versatile new composites. These new materials are widely used in medicinal, aerospace, food, and cosmetic industries. The behavior of cellulose surfaces in different media as well as their interaction with different chemicals is of great importance in their current and future applications (papermaking, composites, and nanocomposites). The mechanical performance of composites is dependent on the degree of dispersion of the fibers in the matrix polymer and the nature and intensity of fiber–polymer adhesion interactions.

As most of the present-day polymers used for preparing nanocomposites are synthetic materials, their processability, biocompatibility, and biodegradability are much more limited than those of natural polymers. Compared to the studies in the field of conventional microcomposites and nanocomposites based on synthetic nonbiodegradable materials, only limited work has been reported in the area of bionanocomposites. Another advantage of the natural nanofillers is their availability and their resulting lower cost in comparison to synthetic nanofillers.

Various polymers, including polyolefins, polyamides, polyesters, polyurethanes, polypeptides, and polysaccharides, have successfully been electrospun into micro- and nanofiber mats [46]. Poly(vinyl alcohol) (PVA), a commonly used polymer obtained by controlled hydrolysis of poly(vinyl acetate) (PVAc), can also be used to produce fibers via electrospinning. PVA is water soluble, semicrystalline, fully biodegradable, nontoxic, and biocompatible, and therefore, it finds use in a broad spectrum of applications [44]. Furthermore, PVA-based fibers have been considered as an attractive choice in tissue scaffolding, filtration materials, membranes, optics, protective clothing, enzyme immobilization, drug release, and so on [99].

A common feature of PVA fibers is their low mechanical strength and integrity, which have triggered alternatives such as posttreatment [70], cross-linking [74, 33],

and blending [34, 64]. Furthermore, the use of nanofillers, such as carbon nanotubes [69, 136], inorganic nanoparticles based on hydroxyapatite [78], gold [11], silver [63], clay [2, 71, 112], silica [116], cellulose nanofibrils [94, 144], and chitin whiskers [76], has been reported.

Electrospun fibers produced from PVA have been extensively studied over the past few years with regard to the effects of production parameters [41, 80, 87, 142], molecular weight [74, 81, 87], concentration [32, 72], solvent, and pH [120], as well as the presence of additives [75, 88]. Also, the mechanical and thermal properties, as well as the structural stability of PVA fibers, have been studied [52, 96].

Currently, numerous efforts are focused on the use of materials from renewable resources as reinforcement agents in nanocomposites. Among such materials readily available, cellulose nanocrystals (CNs) have attracted great interest due to their renewability, biodegradability, and spectacular mechanical properties. In this chapter, we will describe the manufacture of nanocomposites based on PVA mats reinforced with CNs. The study will include the morphology of the resulting fibers analyzed by transmission electron microscopy (TEM) and scanning electron microscopy (SEM). Also, the enhancement of the thermomechanical properties of PVA nonwoven mats will be included by thermal gravimetric analysis (TGA), differential scanning calorimetry (DSC), and dynamic mechanical analysis (DMA).

2 Structure of Cellulose

Cellulose, the most widespread biopolymer, is known to occur in a wide variety of living species from the worlds of plants, animals, and bacteria as well as some amoebas. In many of these, the main function of cellulose is to act as a reinforcement material. This is, for instance, the case in plant cells where the osmotic pressure of the inner cell has to be counterbalanced by the tight winding of the cellulose within the cell wall. Cellulose is the main component of plant cell walls and the basic building block for many textiles and for paper [54, 92, 140]. In the primary (growing) plant cell wall (Fig. 16.1) [18], the major carbohydrates are cellulose, hemicellulose, and pectin. It has been estimated that globally between 10^{10} and 10^{11} tons of cellulose is synthesized and also destroyed each year [62].

The links in the cellulose chain are a type of sugar: ß-D-glucose. The sugar units are linked when water is eliminated by combining the –OH group and H (Fig. 16.2) [138]. Linking just two of these sugars produces a disaccharide called cellobiose. Cellulose is a polysaccharide produced by linking additional sugars in exactly the same way. The length of the chain varies greatly, from a few hundred sugar units in wood pulp to over 6,000 for cotton.

In nature, cellulose chains have a DP of approximately 10,000 glucopyranose units in wood cellulose and 15,000 in native cellulose cotton [118]. However, chain lengths of such large, insoluble molecules are difficult to measure due to enzymatic and mechanical degradation which may occur during analysis. A specific characteristic of

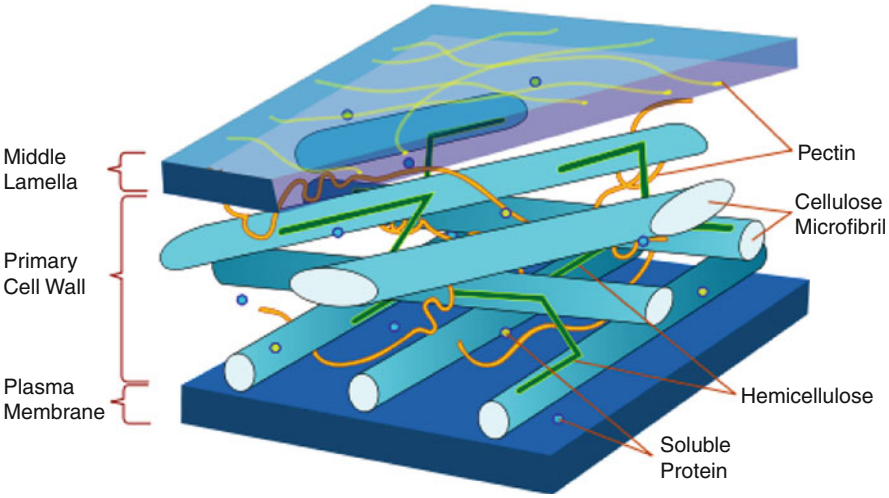

Fig. 16.1 Location and arrangement of cellulose microfibrils in the plant cell wall (From [18])

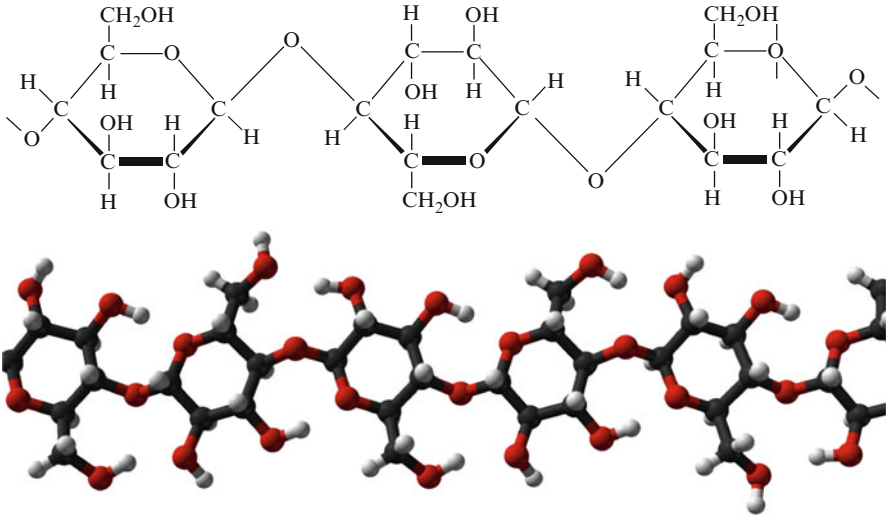

Fig. 16.2 Chemical structure of cellulose (From [138])

lignocellulosic compounds is the high density of hydroxyl groups which provides the hydrophilic nature of these materials.

Cellulose has a strong affinity to itself and hydroxyl-containing materials. Based on the preponderance of hydroxyl functional groups, cellulose is very reactive with water. At common ambient environmental conditions, cellulose will have at least a monomolecular layer and up to several molecular layers of water associated with it [119].

Cellulose fibers on the nanoscale are prepared in four different ways: (1) bacterial cellulose nanofibers, (2) cellulose nanofibers by electrospinning, (3) microfibrillated cellulose plant cell fibers, and (4) nanorods or cellulose whiskers. Processing techniques have a significant impact on the adhesion properties of the resulting cellulose nanofibers in composite material applications [35].

2.1 Electrospun Cellulose

Cellulose needs to be in solution form to facilitate electrospinning [73, 131]; some of the solvents used have been *N*-methylmorpholine-*N*-oxide (NMMO), *N,N*-dimethylacetamide (DMAc), and lithium chloride (LiCl)/DMAc [73, 77, 84, 91, 131]. In addition to the solvent, other important factors to consider in the intrinsic properties of the solution for the cellulose electrospinning process are the cellulose molecular weight, solution viscosity, net charge density, surface tension of the cellulose solution, and solution conductivity. Some of the operational conditions depend on the applied voltage, spinning temperature, flow rate, and distance between the nozzle and collector. The humidity and temperature of the surroundings may also play an important role in determining the morphology and diameter of electrospun nanofibers [137]. The polymer solution must have a concentration high enough to cause polymer entanglements yet not so high that the viscosity prevents polymer motion induced by the electric field. The solution must also have a surface tension low enough, a charge density high enough, and a viscosity high enough to prevent the jet from collapsing into droplets before the solvent has evaporated [29].

Kim et al. [77] studied the effect of solvent system, degree of polymerization (DP), processing conditions, and post-spinning treatment on the microstructure of submicrometer scale, electrospun cellulose fibers. Also, they utilized electrospun cellulose fibers to develop highly oxidized cellulose with HNO_3/H_3PO_4 and $NaNO_2$ having a large surface area. The particular interest was to study how the degree of crystallinity of electrospun fibers was influenced by these parameters. They demonstrated that nonwoven mats of submicronized cellulose fibers of 250–750 nm in diameter could be obtained using the electrospinning process. They showed that cellulose fibers obtained from LiCl/DMAc were mostly amorphous, whereas the degree of crystallinity of cellulose fibers from NMMO/water could be controlled by the process conditions. Some pictures of electrospun cellulose are presented in Fig. 16.3. Liu and Tang [91] used cellulose acetate with the same acetyl concentration (39.8 %), but different molecular weights ranging from 3.0×10^4 to 5.0×10^4, to prepare cellulose acetate nanofibers and nanofibrous membranes in several conventional solvents such as acetone, acetone/DMAc, and acetone/water. They produced nanofibers with mean diameters less than 265 nm, but nanofibers from low molecular weight cellulose acetate had a larger amount of spindle-like beads on fibers and a broader fiber size distribution compared to those produced from high molecular weight which showed uniform and smooth fiber structure without defects. Joo and co-workers [73] obtained cellulose nonwoven

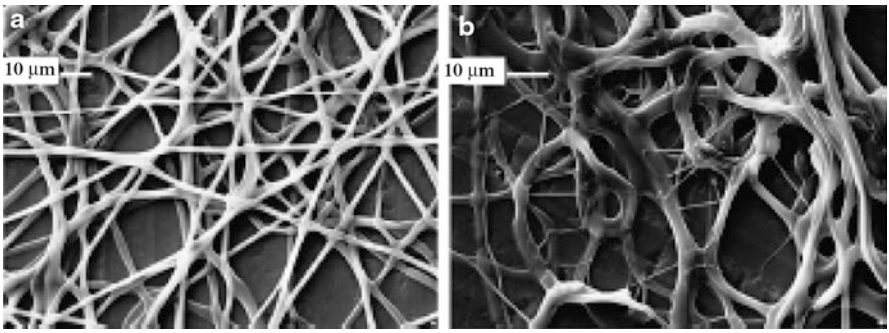

Fig. 16.3 SEM images of electrospun fibers from 9 wt% DP 210 cellulose/NMMO/water solution with a rotating collector at (**a**) 1.2 rpm and (**b**) 6 rpm. Flow rate was kept at 0.03 ml/min (From [77])

mats of submicrometer-sized fibers (150–500 nm in diameter) by electrospinning cellulose solutions. The solvent system used was based on LiCl and DMAc. They evaluated the effect of temperature of the collector, type of collector (aluminum mesh and cellulose filter media), and post-spinning treatment, such as coagulation with water, on the morphology of electrospun fibers. Ethyl cellulose has also been used to study the diameter distribution and surface morphology of electrospun nanofibers previously dissolved in a multicomponent solvent system (tetrahydrofuran, THF, and DMAc) [65].

Walkenstrom et al. [131] used electrospinning to process mixtures of poly (ethylene oxide) (PEO) and cellulose derivatives of carboxymethyl cellulose (CMC) sodium salt, hydroxypropyl methylcellulose (HPMC), methylcellulose (MC), and enzymatically treated cellulose. They found that the substitution pattern of carboxymethyl groups on the CMC derivatives proved to be crucial for the appearance of the nanoweb as well as for the morphology of individual nanofibers.

On the other hand, electrospun fibers have been successfully used for reinforced thermoplastic polymers by Fink and Ganster [45]. They developed a double pultrusion technique for compounding thermoplastic polymers and electrospun fibers (from viscose and lyocell) for injection molding applications. They increased the final mechanical properties of the composites up to three times compared to the initial matrix.

2.2 Microfibrillated Cellulose

Microfibrillated cellulose (MFC) is a material derived by disintegrating digested cellulose through a homogenizing process, exposing the underlying microfibrils. This new morphology was developed by Turbak et al. [128] in the early 1980s. This process usually starts with wood pulp; however, Samir et al. [114] describe how microfibrillated cellulose can be extracted from sugar beets. Regardless of the starting material, the process always involves a homogenization process.

Nakagaito and Yano [97, 98] describe the homogenizing process as subjecting the cellulose to a reciprocating motion producing a high pressure drop resulting in shearing and impact forces. The shearing and impact forces are responsible for exposing the substructural cellulose microfibrils.

The production of MFC by fibrillation of cellulose fibers into nanoscale elements requires intensive mechanical treatment. However, depending upon the raw material and the degree of processing, chemical treatments may be applied prior to mechanical fibrillation. These chemical processes are aimed to produce purified cellulose, such as bleached cellulose pulp, which can then be further processed. Depending upon the raw materials and fibrillation techniques, the cellulose degree of polymerization, morphology, and nanofiber aspect ratio may vary [124].

Although the thickness of MFC nanoelements could, in principle, be as small as 3–10 nm, it is typically in the range of 20–40 nm since MFC usually consists of aggregates of cellulose microfibrils [125]. Through the homogenization process, the cellulose bundles are split and degraded leaving microfibrillated cellulose strands with dimensions of 10–100 nm. Various terms are used to describe MFC in the literature, including microfibril [6, 7, 10, 27], microfibril aggregates [57, 58, 68], microfibrillar cellulose [121, 126, 135], nanofibril [4, 56], nanofiber [1, 12, 121], nanofibrillar cellulose [3, 4, 103, 121, 126], or fibril aggregates [59, 67, 130].

When subjected to acid hydrolysis, cellulose microfibrils undergo transverse cleavage along the amorphous regions, and the use of sonication results in a rodlike material with a relatively low aspect ratio referred to as "cellulose whiskers" [111]. The typical diameter of these whiskers is around 2–20 nm, but there is a wide length distribution from 100 to 600 nm and in excess of 1 μm in some cases [66]. Due to the near-perfect crystalline arrangement of cellulose whiskers, this form of nanocellulose has a high modulus and therefore significant potential as a reinforcing material [40].

Elementary kraft fibers are on the order of 10's of μm's wide and are rodlike [98], whereas MFC is a network of interconnected microfibrils with little order on the nanometer scale. Although a combination of microscopic techniques with image analysis can provide information on MFC nanofiber widths, it is more difficult to determine nanofiber lengths because of entanglements and difficulties in identifying both ends of individual nanofibers. It is often reported that MFC suspensions are not homogeneous and that they consist of cellulose nanofibers and nanofiber bundles. In addition, suspensions may contain a certain amount of larger fiber fragments and unfibrillated fibers [5, 6]. The evolution of larger nanofiber agglomerates is due to the high density of hydroxyl groups on the surface of the microfibrils, which can strongly interact and lead to agglomeration [143]. The network of single nanofibers with superimposed fibers can be seen in the TEM micrograph of an MFC gel (Fig. 16.4).

Besides microscopic techniques, the extent of fibrillation can be assessed indirectly by other measurements. Degree of cellulose polymerization (DP) is reported to correlate strongly with the aspect ratio of the nanofibers; longer fibrils are

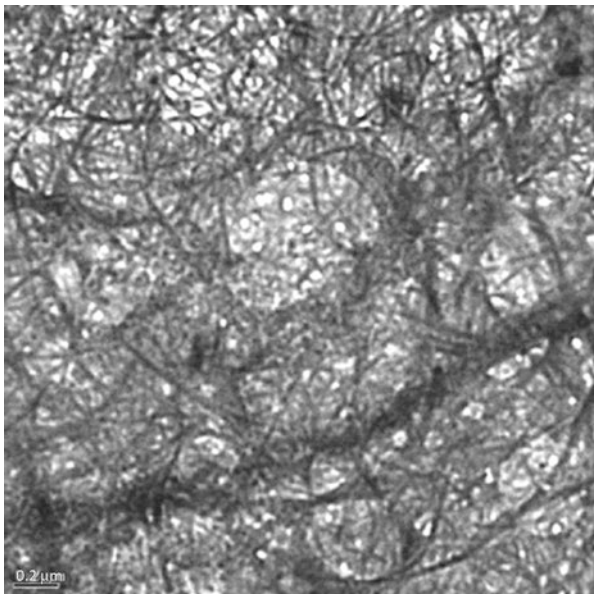

Fig. 16.4 TEM image of MFC gel showing cellulose nanofibers and nanofiber bundles. Scale bar corresponds to 0.2 µm (From [117])

associated with higher cellulose DP. The DP for the raw material (sulfite pulp) is often reported to be around 1,200–1,400, while mechanical isolation of nanofibers may result in about 30–50 % decrease in DP [58]. Depending on the nature of the starting material, the DP of MFC may be even lower.

2.3 Cellulose Nanorods or Whiskers of Cellulose

Whiskers of cellulose, the needlelike structure of the cellulose crystallite, have been mainly studied for their liquid crystalline behavior in concentrated aqueous suspensions [5, 49, 50, 93] and for their reinforcing effect when added to a polymeric matrix giving rise to very strong and tough percolating networks of hydrogen-bonded whiskers [22, 23, 43, 47, 60, 82, 101]. Whiskers of cellulose are renewable materials which possess high availability, light weight, and high mechanical properties. They consist of slender parallelepiped rods, and, depending on their origin, the lateral dimensions range from about 2 to 50 nm in diameter for length than can reach several tens of micrometers [39]. According to these dimensions, they possess high aspect ratios and high specific surface area of about 150 m^2/g [25]. Figure 16.5 shows an example of whiskers of cellulose [102].

Several raw materials have been used for producing whiskers of cellulose. These include sugar beet pulp, tunicin from tunicates (a sea animal) [36, 43, 61], mantle of the tunicates [59], valonia, sulfite wood pulp [48, 143], wheat straw [38], cotton filter paper [16, 31], bacterial cellulose (BC) [51], sisal [37], kraft pulp, hemp, flax [12], and microcrystalline cellulose (MCC) [100]. Some sources for obtaining cellulose nanocrystals and their characteristics are listed in Table 16.1. The method

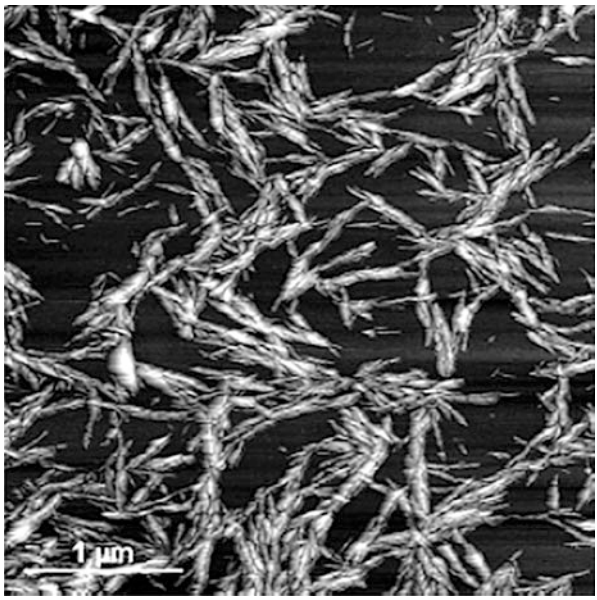

Fig. 16.5 AFM topography image of cellulose nanowhiskers from a dried water suspension (From [102])

Table 16.1 Characteristics of whiskers of cellulose from different sources (From [25, 39, 48])

Cellulose source	Length (nm)	Cross section (nm)
Tunicate[a]	100–several microns	15
Algal (Valonia)	> 1,000	10–20
Bacterial	100–several microns	5–10 by 30–50
Wheat straw	220	5
Cotton	200–350	5–15
Wood	100–300	3–5
Sugar beet pulp	210	15

[a]Marine animal from the Mediterranean Sea

primarily utilized for obtaining the whiskers has been acid hydrolysis, which consists basically in removing the amorphous regions present in the cellulose fibrils leaving the crystalline regions intact; therefore, the dimensions of the cellulose whiskers obtained after hydrolysis are mainly dependent on the percentage of amorphous regions that varies for each organism. Traditionally the yields of cellulose whiskers by acid hydrolysis have been quite low (2–3 %); however, in a recent study by Oksman et al. [100], the process was optimized to reach yields up to 30 % and suspensions of nanocrystals with a length between 200 and 400 nm and a width less than 10 nm.

Hydrochloric acid also has been used for obtaining cellulose whiskers; however, the use of sulfuric acid leads to more stable whiskers aqueous suspensions [8, 15, 25, 82] because the whiskers present a higher negative charge on their surface

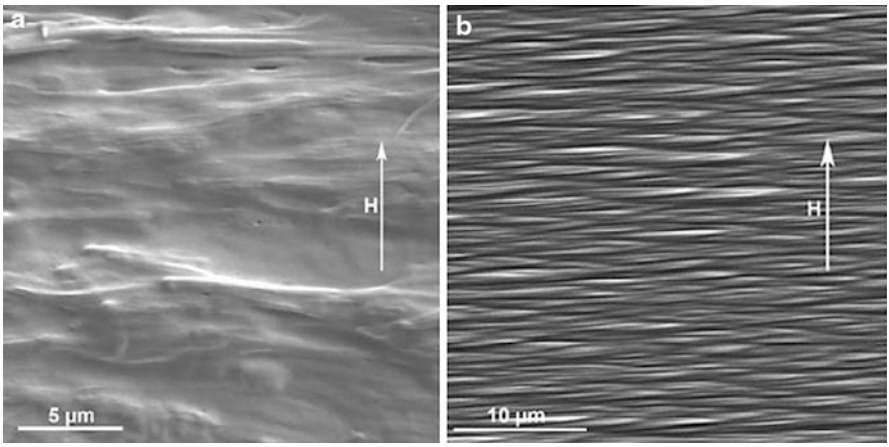

Fig. 16.6 FESEM pictures of (**a**) a fracture surface and (**b**) an etched surface of the CNW nanocomposite showing a highly oriented structure

compared with those prepared with HCl [113]; the repulsion forces are then also higher and the flocculation between the nanoparticles is reduced. Another way to achieve charged whiskers consists of the oxidation of the whisker's surface [9, 129] or through an acylation process [83].

It has been reported that cellulose whiskers in suspension can be oriented by superconducting magnets [123], by shearing forces [139], and by an electric field [14]. The magnetic orientation of a whisker with its long axis perpendicular to the field was explained due to the negative diamagnetic anisotropy of cellulose [14, 123].

Kvien et al. [85] aimed to study the utilization and the capability of cellulose nanowhiskers (CNWs) to align in a magnetic field in order to prepare a unidirectional, reinforced nanocomposite. In this novel study they align CNWs in a polymeric matrix and present the dynamic mechanical behavior of the nanocomposite in the aligned and transverse directions. The structure analysis indicated that the CNWs oriented perpendicular to the direction of the magnetic field. The field emission scanning electron microscope (FESEM) image of a fracture surface of the nanocomposite indicated aligned CNWs perpendicular to the field direction as seen from the underlying structure in Fig. 16.6. Moreover, the dynamic mechanical thermal analysis showed that the dynamic modulus of the nanocomposite transverse to the field direction was around 2 GPa higher than along the field direction at room temperature, which further indicated aligned cellulose nanowhiskers.

3 Cellulose as Reinforcement in Nanocomposites

In recent years, nanocomposites have attracted significant scientific attention because of their phenomenal electrical barrier and mechanical properties.

They are defined as composite materials for which one of the phases has at least one dimension in the nanometer range (1–100 nm). A large variety of nanocomposites have been prepared using PVA as a matrix and nanoreinforcement like layered silicate [24, 79, 122, 134, 141], silica [106–108], cadmium sulfide nanoparticles [133], and carbon nanotubes [95, 104, 127]. The preparation methods are usually solution casting or in situ polymerization. As most of the present-day nanofillers used to prepare nanocomposites are inorganic, their processability, biocompatibility, and biodegradability are much more limited than those of naturally organic ones.

Nanocomposite films either by film casting (water evaporation) or by freeze drying, followed by classical compression or extrusion, have been prepared to study cellulose whiskers reinforcing properties in thermoplastics [19–21, 53] or thermoset matrices [23]. Water suspensions of whiskers have been preferred in nanocomposite films because of their high stability and the expected high level of dispersion of the whiskers within the host matrix in the resulting films. This behavior, however, restricts the choice of the matrix to hydrosoluble polymers. The utilization of latexes, which allows the use of hydrophobic polymers as matrix, is a practical alternative and ensures a good dispersion level of the filler required for homogeneous composite processing [19, 36]. The simplest technique to process a composite material from latex and aqueous suspension of whiskers consists in mixing and casting the two aqueous suspensions. A solid nanocomposite film can be then obtained by water evaporation and particle coalescence at a temperature higher than the glass transition temperature of the matrix [39]. Some polymer latexes used for film nanocomposites include those obtained by copolymerization of styrene and butyl acrylate [36, 39, 42] and poly(hydroxyoctanoate). Another alternative to processing nanocomposites using whiskers consists in dispersing them in an organic medium.

4 Poly(vinyl alcohol) Nanocomposites Reinforced with Cellulose Fibrils

Poly(vinyl alcohol) or PVA is water soluble, has excellent chemical resistance, and is biocompatible and biodegradable. There is therefore interest in a wide range of practical applications for this polymer [34]. PVA is the largest synthetic water-soluble polymer produced in the world [110]. It is prepared by the hydrolysis of polyvinyl acetate. The degree of solubility and the biodegradability as well as other physical properties can be controlled by varying the molecular weight (M_W) and the degree of hydrolysis (saponification) of the polymer [13]. Indeed, the chemical characteristics of these polymers, e.g., the reactivity of the numerous hydroxyl groups, depend strongly on the residual acetyl group content or the degree of hydrolysis. In particular, PVA is an ideal candidate for biomedical applications including tissue reconstruction and replacement, cell entrapment and drug delivery, soft contact lens materials, and wound covering bandages for burn victims [55, 105].

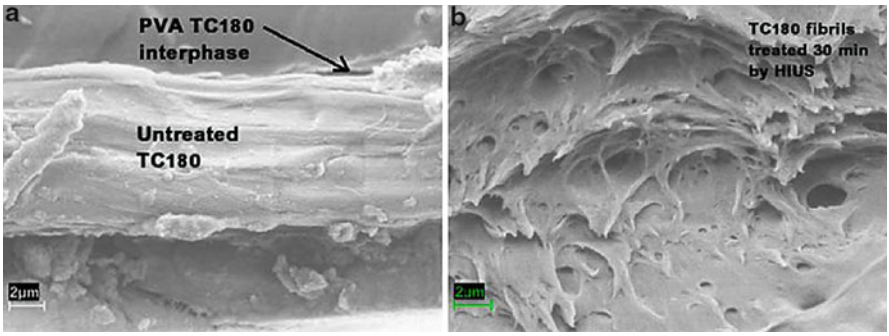

Fig. 16.7 SEM images of the fractured cross sections of PVA composites reinforced with untreated PCF (TC180) and separated small PCF fibrils (From [26])

4.1 Morphological Structure

Cheng et al. [26] studied the scanning electron microscopy (SEM) images of PVA composites reinforced with 2 % of untreated pure cellulose fiber (PCF) and small PCF fibrils as shown in Fig. 16.7. From the fracture surfaces of untreated PCF, Cheng et al. [26] demonstrated the presence of clear gaps between fibers and polymer which are responsible for the lower tensile strength for the composites reinforced with both untreated and treated fibers compared to the pure PVA. They also mentioned that the small PCF fibrils from the cross section were not clear (Fig. 16.7b), where the fibril dispersion in the PVA matrix could be more uniform than that of untreated PCF.

On the other hand, Cheng et al. [26] had investigated the geometrical characteristics of the fibrils by the polarized light microscopy (PLM), where Fig. 16.8 shows the PLM images of surface and cross sections (inset) of PVA composites reinforced with small regenerated cellulose fibrils (RCF) and microfibrillated cellulose MFC (as reference). They indicated that the dispersions from the surfaces of both RCF and MFC fibrils were uniform, but SEM images of fracture surface after tensile test (Fig. 16.9) and atomic force microscopy AFM images of cross sections after cut by microtome (Fig. 16.10) from the PVA composites reinforced by small RCF fibrils demonstrated that the dispersion of fibrils from the cross section was not absolutely uniform, where some fibrils were aggregated and some were pulled out after tensile test. Moreover, they showed in Fig. 16.11 the SEM images of the fractured cross sections of PVA composites reinforced with 2 % and 10 % of RCF fibrils. They have mentioned that the relative fiber and fibril dispersion in 10 % loading was worse, which demonstrated that more filler may be not further reinforcing PVA composites.

4.2 Mechanical Properties

Although PVA hydrogels can have mechanical properties similar to some soft biological tissues, in order to mimic other tissues and, in particular, for medical device applications, improvement of PVA durability is required. One approach is to

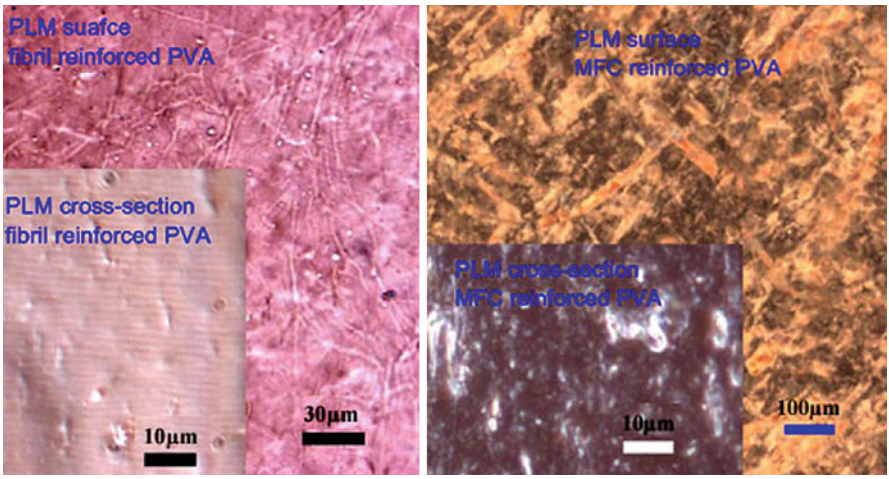

Fig. 16.8 PLM images of surface and cross sections (*inset*) of PVA composites reinforced with small RCF fibrils and MFC (From [26])

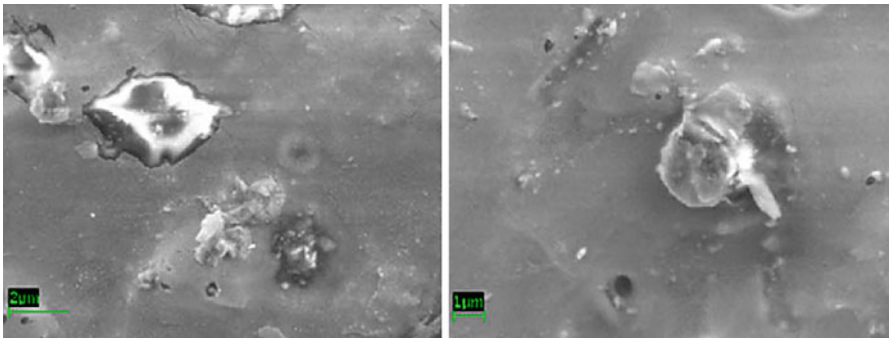

Fig. 16.9 SEM images of the fractured cross sections of PVA composites reinforced with small RCF fibrils (From [26])

create a PVA-based nanocomposite that possesses the required properties. A number of applications using MFC for reinforcing PVA have been reported. For example, Zimmermann et al. [143] dispersed MFC into PVA and generated fibril-reinforced PVA nanocomposites (fibril content 20 wt%) with up to three times higher E-modulus and up to five times higher tensile strength when compared to the reference polymer.

A blend containing 10 % cellulose nanofibers obtained from various sources, such as flax bast fibers, hemp fibers, kraft pulp, or rutabaga, and 90 % PVA was used by Bhatnagar et al. [12] for making nanofiber reinforced composite material by a solution casting procedure. Both tensile strength and Young's modulus were improved compared to neat PVA film, with a pronounced four- to fivefold increase

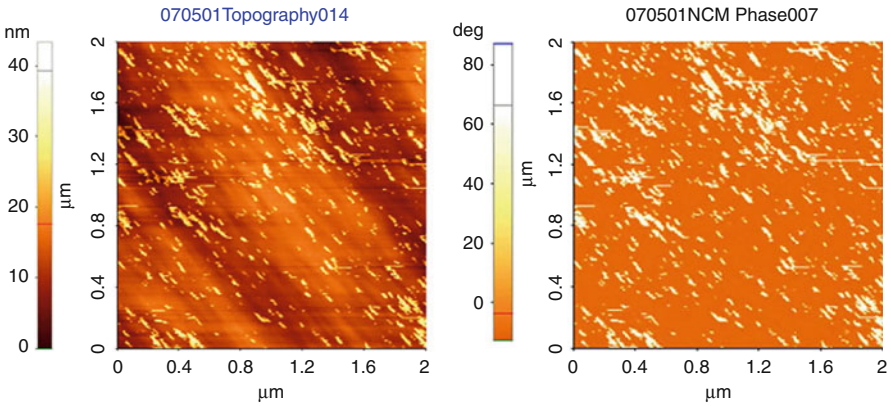

Fig. 16.10 AFM topography and phase images of the cross sections of PVA composites reinforced with small RCF fibrils (From [26])

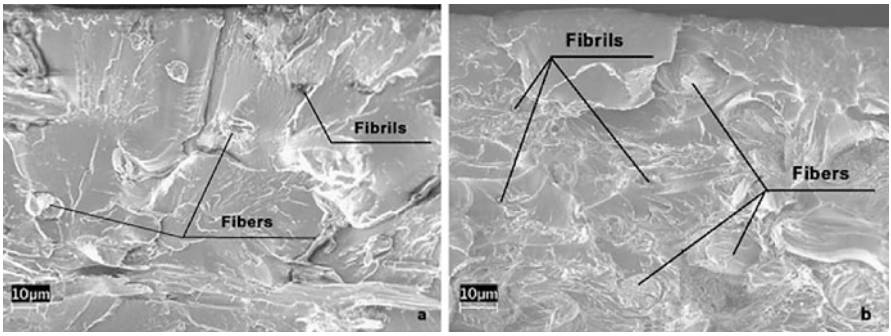

Fig. 16.11 SEM images of the fractured cross sections of PVA composites reinforced with 2 % (**a**) and 10 % (**b**) treated RCF fibers (From [26])

in Young's modulus observed. Similarly, Bruce et al. [17] reported approximately five times higher tensile strength for PVA containing 50 wt% MFC when compared to the neat polymer. Such improvement in mechanical properties can be explained by strong interfacial bonding between the cellulose nanofibers and PVA.

Leitner et al. [89] prepared PVA nanocomposites with a range of nanocellulose contents (0–90 wt%). At a cellulose content of 50 wt%, the modulus of elasticity of PVA increased by a factor of 20 and tensile strength increased by a factor of 3.5. Both parameters increased further at cellulose contents of 70 and 90 wt%, respectively. It was also reported that tensile strength increased linearly as a function of filler content, which suggests that cellulose content was the major determinant of strength in these composites.

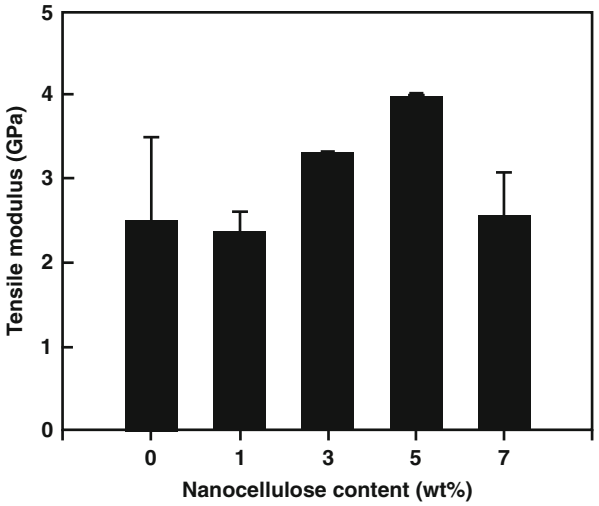

Fig. 16.12 Tensile modulus of PVA nanocomposite as the function of the nanocellulose content (From [28])

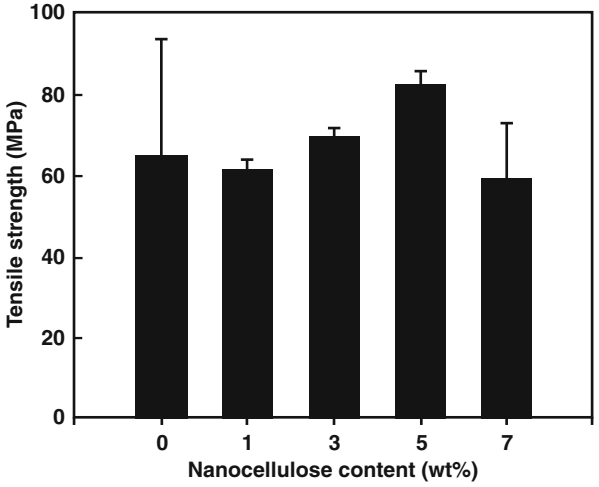

Fig. 16.13 Tensile strength of nanocellulose-reinforced PVA nanocomposites as function of the nanocellulose content (From [28])

Cho et al. [28] studied the tensile properties of the nanocomposites reinforced by the nanocellulose of 1, 3, 5, and 7 wt% loading. As seen in Figs. 16.12 and 16.13, they have mentioned that the tensile modulus decreases at 1 wt% and then increases with an increase in the nanocellulose content up to 5 wt%, followed by leveling off at higher nanocellulose content. At the 5 wt% nanocellulose content, the tensile modulus of the nanocomposite increases by 60 %. Also, as shown in Fig. 16.13, it was mentioned that the tensile strength of these nanocomposites displayed a similar trend to the tensile modulus.

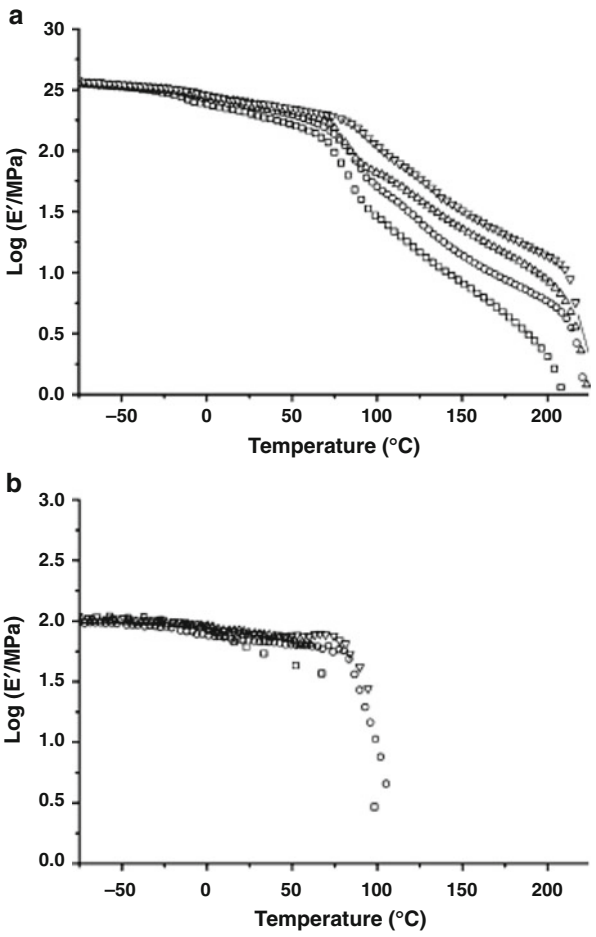

Fig. 16.14 Storage modulus of electrospun nanofiber mats versus temperature for fully hydrolyzed PVA-98 (**a**) and partially hydrolyzed PVA88 (**b**) with different loadings of cellulose nanocrystals (CN) (□ 0 %, ○ 5 %, Δ 10 %, and ▽ 15 %) (From [109])

Peresin et al. [109] mentioned that to evaluate the mechanical properties of nanofiber mats obtained after electrospinning of PVA polymers and the corresponding nanocomposites with CN, longer electrospinning collection times had to be used to produce thicker mats suitable for dynamic mechanical analysis (DMA). They noticed that the mechanical analyses were performed by DMA in linear tensile mode, and the main results can be presented in Fig. 16.14.

It was noticed by Peresin et al. [109] that all composites based on the partially hydrolyzed PVA-88 displayed the typical behavior of amorphous polymers due to the low degree of crystallinity, while in contrast to the electrospun nanofiber mats based on PVA88, the storage modulus of all CN-loaded PVA-98 (fully hydrolyzed PVA) nanocomposites displayed the typical behavior of partially crystalline polymers, with their three distinctive zones. An additional important feature was observed in that the modulus of the nanocomposite mats increased significantly upon CN loading in PVA-98. Because a decrease in the crystallinity would be

expected to induce a reduction in the storage modulus, it is therefore concluded that the observed strength enhancement in CN-loaded PVA mats can only be related to the reinforcing effect of the dispersed phase, via the percolation network held by hydrogen bonds. Peresin et al. [109] estimated the enhancement in mechanical strength to be more than threefold when composites with 15 % CN loading are compared to the respective neat PVA. These results demonstrate efficient stress transfer between CN and PVA-98 polymer in the electrospun fibers due to an existence of strong interactions between the reinforcing CN phase and the fully hydrolyzed PVA-98 continuous phase.

4.3 Thermal Properties

Thermogravimetric analysis (TGA) and differential scanning calorimetry (DSC) were used to investigate the effect of CN on the thermal stability of the composites and also to obtain deeper insights on the interactions between the dispersed and continuous phases of the nanofibers. The stability of PVA polymer during the electrospinning process was investigated by Peresin et al. [109] by comparing samples of bulk, "as-received" PVA with electrospun PVA. They observed that the difference in the TGA's first-order derivative before and after electrospinning was negligible; therefore, they concluded that the electrospinning process did not affect the structure of the matrix polymer.

On the other hand, Cho et al. [28] used the TGA to examine the thermal stability of the PVA-based nanocomposite. According to the TGA curves obtained (Fig. 16.15), major degradation temperature was noticed to occur between 280 °C and 500 °C. They have noticed that the degradation temperature of the nanocomposites increased as the nanocellulose content increased, and the major degradation peak temperature was shifted to higher temperature. In the case of the 1 and 3 wt% nanocellulose loadings, there was no significant influence to the thermal stability. However, the thermal stability of the nanocomposite increased above these loading levels of nanocellulose, especially at the 5 wt% loading.

Moreover, Cho et al. [28] studied the storage modulus (E′) versus temperature curves for neat PVA film and the nanocellulose-reinforced nanocomposites (Fig. 16.16). They noticed that the reinforcing effect of the nanocellulose appeared even at low temperature. When the 3 wt% nanocellulose was incorporated into the PVA matrix, Cho et al. [28] observed that the E′ of the resultant nanocomposite greatly increased. The E′ for 3 and 5 wt% nanocellulose-reinforced PVA nanocomposite increased 74 % and 69 %, respectively, compared to that of the neat PVA film at 25 °C. Also, according to Favier et al. [43], these improved properties were ascribed to a mechanical percolation phenomenon, yielded by cellulosic nanoparticle interactions through hydrogen bond forces.

Differential scanning calorimetric analyses were carried out by Peresin et al. [109] on both PVA polymers, before and after electrospinning, as well as after adding CNs at different loadings. Their results were gathered in Table 16.2 which indicates the measured melting temperature and degree of crystallinity

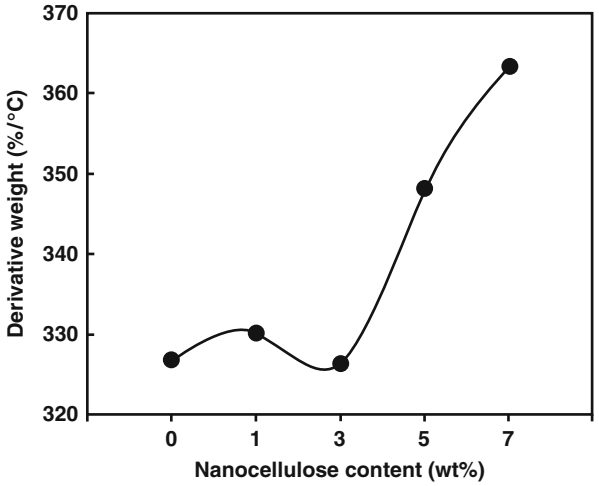

Fig. 16.15 The peak temperature of PVA nanocomposites as the function of the nanocellulose content (From [28])

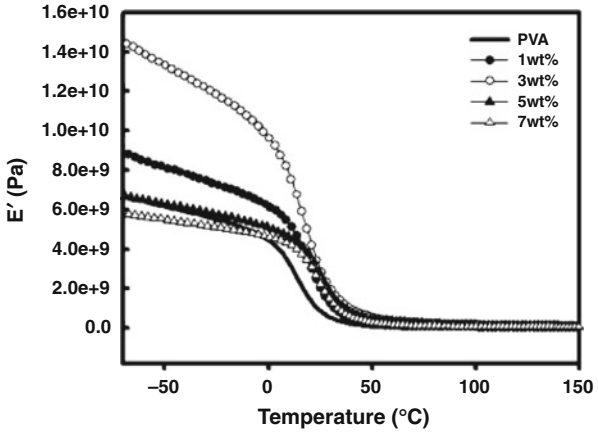

Fig. 16.16 Storage tensile modulus E′ versus the temperature (°C) for nanocellulose-reinforced PVA nanocomposites (From [28])

for all materials studied. They observed that after electrospinning, the degree of crystallinity of both PVA neat polymers increased significantly. The corresponding melting temperature also increased slightly, by about 2 °C, for each PVA polymer. These effects were explained by Peresin et al. [109] as the result of alignment and enhanced crystallization of the polymer chains within the individual PVA fibers that were subjected to very high shear stresses during electrospinning. On the other hand, the melting temperature T_m of electrospun fibers containing CN at different loadings remained fairly constant for both sets of the PVA samples.

Table 16.2 Effect of electrospinning and CN loading on the melting temperature (T_m) and degree of crystallinity (χ_c) of composite nanofibers[a]

Sample	CN content (wt%)	T_m (°C)	ΔH_m (J/g)	χ_c
PVA-98, as received	0	220.7	79.0	0.50
PVA-98, electrospun	0	222.8	111.3	0.70
	5	222.6	106.3	0.70
	10	221.5	80.4	0.56
	15	221.1	72.8	0.54
PVA-98, as received	0	191.7	43.9	0.32
PVA-98, electrospun	0	193.7	56.1	0.40
	5	193.3	60.0	0.45
	10	193.7	37.4	0.30
	15	193.5	50.3	0.42

[a] $\chi_c = (\Delta H_m)/(\Delta H_m^0 \times \omega)$, with ΔH_m^0 is the heat of fusion for the 100 % crystalline polymer, which is estimated to $\Delta H_m^0 = 158$ J/g for PVA-98 and $\Delta H_m^0 = 139$ J/g for PVA-88; ω is the weight fraction of polymeric material in the respective composite (From [109])

4.4 Membrane Properties

Poly(vinyl alcohol) (PVA) has been extensively investigated as a controlled drug release hydrogel, a membrane material for chemical separations, barrier membrane for food packaging, pharmaceutical component, manufacturing material for artificial human organs, and as a biomaterial [86, 90, 115, 132].

A unique study was carried out by Çifci et al. [30] to prepare composite PVA/cellulose membranes by coating PVA mixture solutions on the filter paper to be used as composite membranes in a batch stirred ultrafiltration for metal removal from aqueous solution. From the SEM, they investigated the morphologies of composite membranes made by solutions of different PVA concentrations. They have seen that when concentration of PVA solutions increased, a large amount of PVA is coated on the cellulose filter (Fig. 16.17).

The prepared PVA/cellulose composite membranes were used in the filtration to study the removal of Fe(III) and Cu(II) ions from aqueous solutions. Alginic acid (AA) and PVA were used as complexing agents to enhance the retention of metal ions. Çifci et al. [30] studied the effects of applied pressure and pH of solution on percent retention and flux for Fe(III) and Cu(II) solutions. They found that the water flux increased with increasing applied pressure for the membrane covered by 0.5(w/v)% PVA and with decreasing PVA content of membrane for the same applied pressure (10 psi) (Fig. 16.18). Also, they noticed that the permeate flux increased and percent retention stayed constant with increasing applied pressure for filtration of Fe(III)–PVA solutions between pressure of 45 and 60 psi (Fig. 16.19). Moreover, they noticed that as the pH increased, the permeate flux decreased and percent retention of metal ions increased for filtration of metal–AA complex solutions (Fig. 16.20).

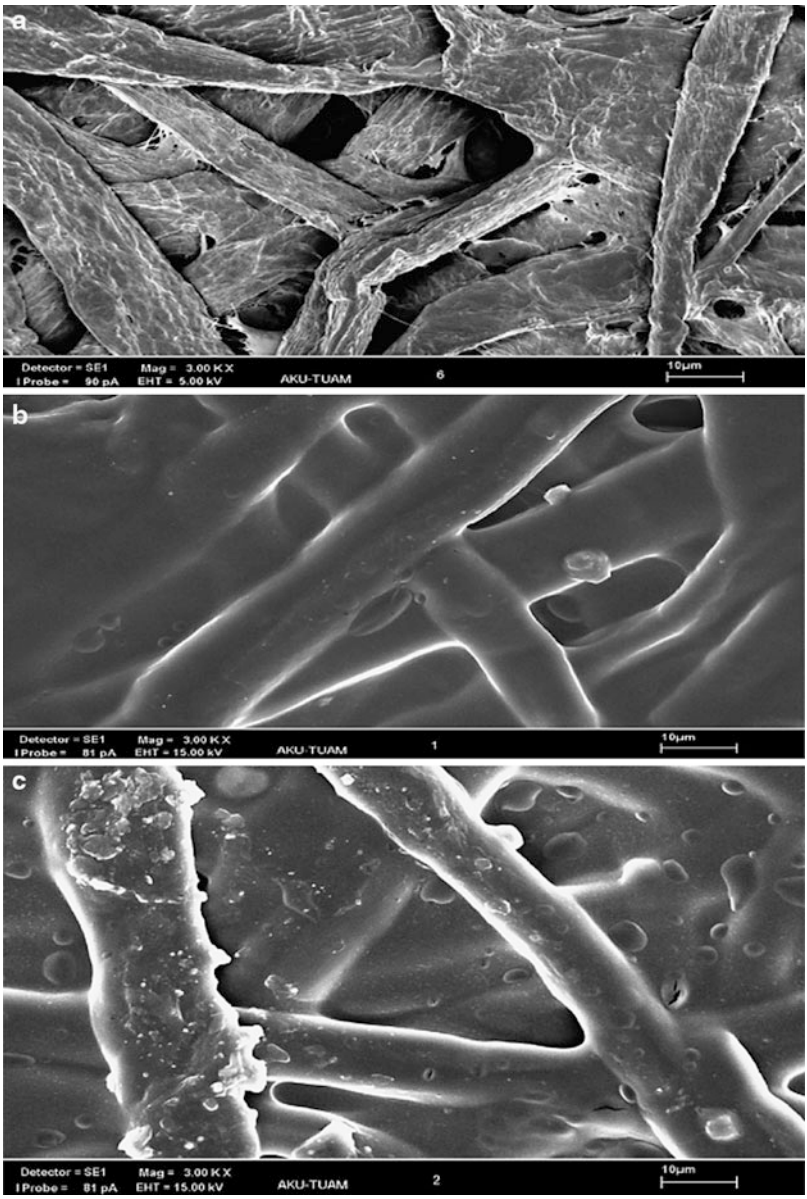

Fig. 16.17 SEM of the composite PVA/cellulose membranes prepared by coating with different PVA concentration: (**a**) 0(w/v)% PVA, (**b**) 0.25(w/v)% PVA, and (**c**) 0.35(w/v)% PVA. Magnification, 3,000× for (**a**), (**b**), and (**c**) (From [30])

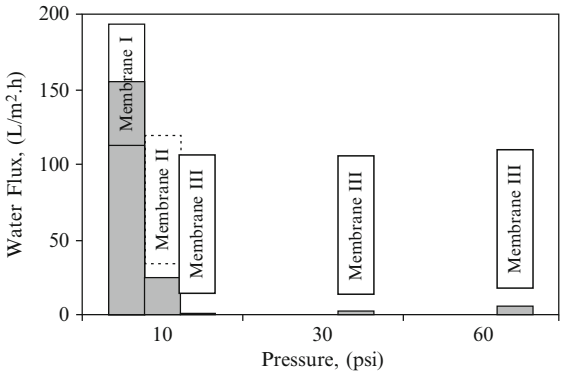

Fig. 16.18 Effect of applied pressure on water flux of membranes (From [30])

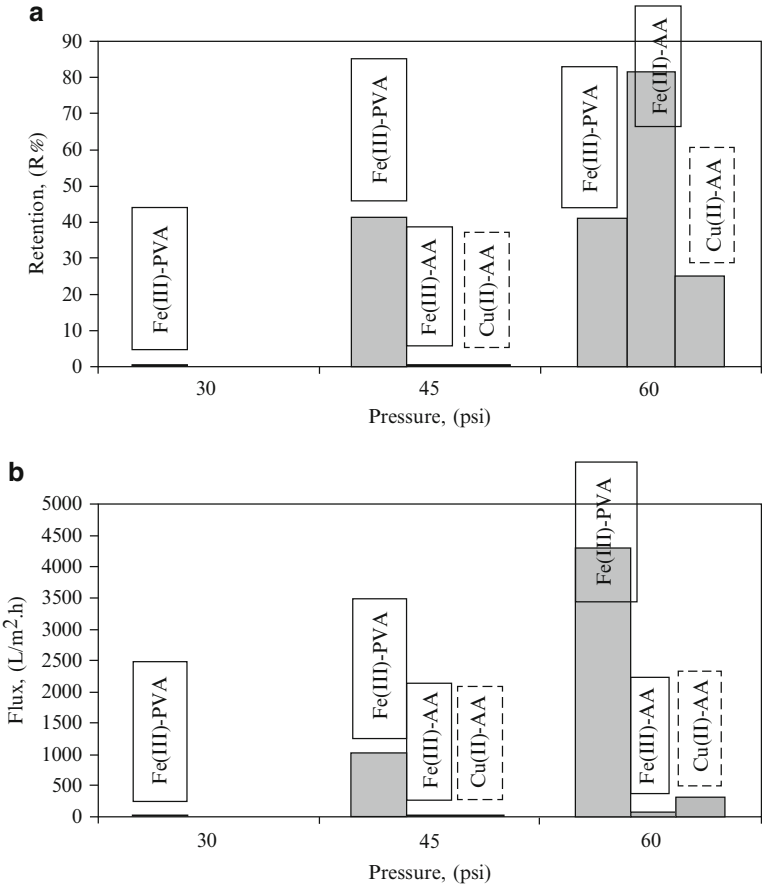

Fig. 16.19 Effect of applied pressure on (**a**) percent retention of metal ions and (**b**) flux ($C_{Fe(III)} = C_{Cu(II)} = 1 \times 10^{-4}$ M, $C_{AA} = C_{PVA} = 2 \times 10^{-4}$ g/L, pH = 3.0 for Fe(III), pH = 6.0 for Cu(II), membrane I) (From [30])

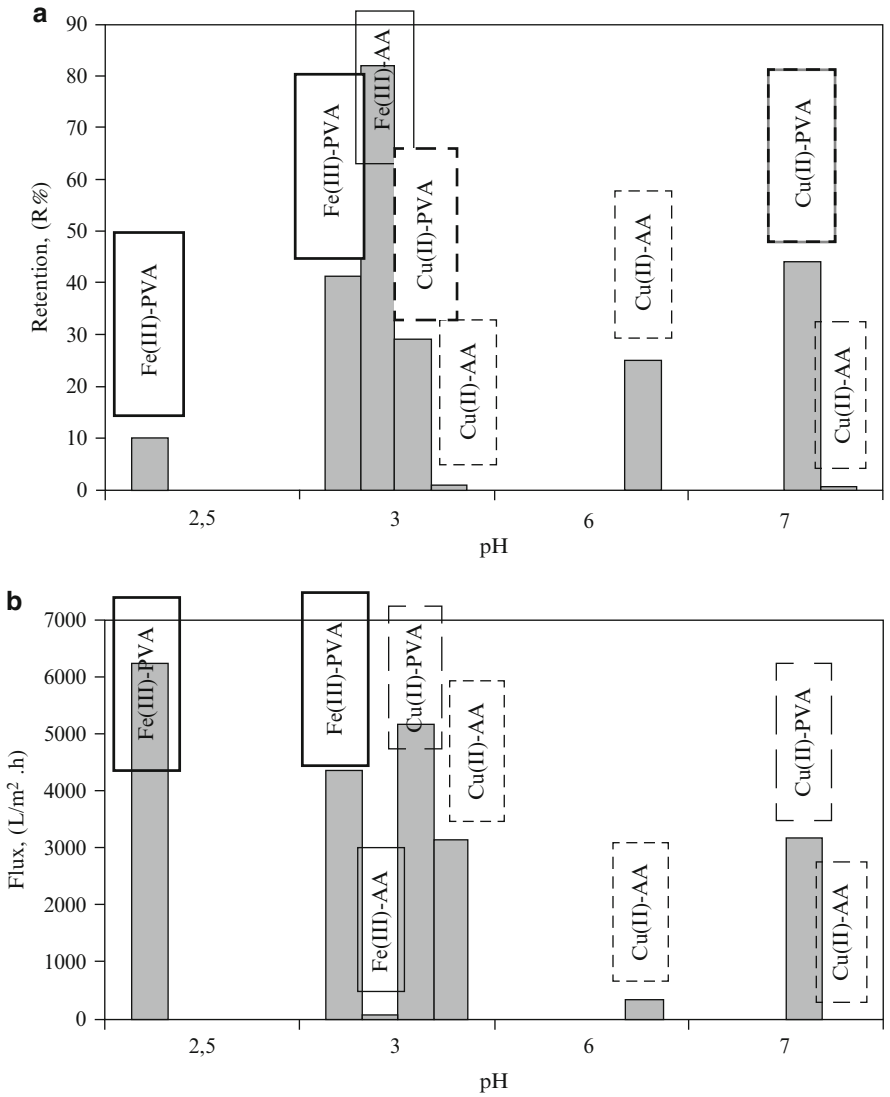

Fig. 16.20 Effect of pH on (**a**) percent retention of metal ions and (**b**) flux ($C_{Fe(III)} = C_{Cu(II)} = 1 \times 10^{-4}$ M, $C_{AA} = C_{PVA} = 2 \times 10^{-4}$ g/L, membrane I, $P = 60$ psi) (From [30])

The maximum percent retention was found by Çifci et al. [30] to be 82 % for Fe(III) solution at pressure of 60 psi, pH of 3 in the presence of AA as complexing agent by using a PVA/cellulose composite membrane containing 0.9 ml of PVA solution 0.25(w/v)% per cm^2 of the membrane. For Cu(II) solution the maximum percent retention was found to be 44 % at pressure of 60 psi, pH of 7 in the presence of PVA as complexing agent by using 0.25(w/v)% PVA/cellulose composite membranes.

5 Conclusions

It has been shown that cellulose nanofibers have an exciting potential as reinforcements in nanocomposites. They also, due to their size and the ability to chemically modify their surface, have great potential for a wide variety of applications. A number of methods have been reviewed that enable cellulose nanofibers to be extracted from different sources. The potential mechanical properties of cellulose nanofibers compete well, and this could be useful in high-end technological applications. Cellulose nanowhiskers have a high surface area to volume ratio. This means that the surface plays a dominant role in not only the mechanical efficiency of stress transfer in a nanocomposite but also the ability to modify the surface chemistry.

In order to achieve improved mechanical properties in polymer nanocomposites, good filler–matrix interaction is essential. Due to compatibility problems of nanocellulosic materials and hydrophobic matrices, it can be anticipated that nanocomposites based on hydrophilic matrix polymers will be easier to commercialize. Poly(vinyl alcohol) has a domain usage in different applications. It is a hydrophilic polymer contributing hydroxyl group on each of its repeating units, which permits the development of hydrogen bonds with hydroxyl groups of cellulose fibers and enhances strength properties. Consequently, more research targeting novel methods, as well as an understanding of the mechanism of reactions occurring at the cellulose nanofiber polymer matrix interface, is required.

References

1. Abe K, Iwamoto S, Yano H (2007) Biomacromolecules 8:3276
2. Adanur S, Ascioglu B (2007) J Ind Text 36:311
3. Ahola S, Österberg M, Laine J (2008) Cellulose 15:303
4. Ahola S, Salmi J, Johansson LS, Laine J, Österberg M (2008) Biomacromolecules 9:1273
5. Andresen M, Johansson LS, Tanem BS, Stenius P (2006) Cellulose 13:665
6. Andresen M, Stenius P (2007) J Disper Sci Technol 28:837
7. Andresen M, Stenstad P, Moretro T, Langsrud S, Syverud K, Johansson LS, Stenius P (2007) Biomacromolecules 8:2149
8. Araki J, Wada M, Kuga S, Okano T (1998) Colloids Surf A 142:75
9. Araki J, Wada M, Kuga S (2001) Langmuir 17:21
10. Aulin C, Varga I, Claesson PM, Wågberg L, Lindström T (2008) Langmuir 24:2509
11. Bai J, Li Y, Yang S, Du J, Wang S, Zheng J, Wang Y, Yang Q, Chen X, Jing X (2007) Solid State Commun 141:292
12. Bhatnagar A, Sain M (2005) J Reinf Plast Compos 24:1259
13. Bohlmann GM (2005) Handbook of biodegradable polymers: General characteristics, processability, industrial applications and market evolution of biodegradable polymers, Bastioli, C. (ed.). Shawbury, Shrewsbury, Shropshire, UK, Rapra Technology Limited
14. Bordel D, Outaux JL, Heux L (2006) Langmuir 22:4899
15. Borsali R, De Souza Lima MM (2004) Macromol Rapid Commun 25:771
16. Borsali R, Ebeling T, Paillet M, Diat O, Dufresne A, Cavaillé JY, Chanzy H (1999) Langmuir 15:6123
17. Bruce DM, Hobson RN, Farrent JW, Hepworth DG (2005) Compos Part A Appl Sci Manufact 36:1486

18. Buchanan BB, Gruissem W, Jones RL (2000) Biochemistry & molecular biology of plants, 1st edn. American society of plant physiology, Cellulose - Wikipedia, the free encyclopedia (en.wikipedia.org/wiki/Cellulose)
19. Cavaillé JY, Chazeau L, Canova G, Dendievel R, Boutherin B (1999) J Appl Polym Sci 71:1797
20. Cavaillé JY, Chazeau L, Paillet M (1999) J Polym Sci Part B Polym Phys 37:2151
21. Cavaillé JY, Chazeau L, Perez J (2000) J Polym Sci Part B Polym Phys 38:383
22. Cavaillé JY, Favier V, Chanzy H (1995) Macromolecules 28:6365
23. Cavaillé JY, Ruiz MM, Dufresne A, Gerard JF, Graillat C (2000) Compos Interface 7:117
24. Chang JH, Jang TG, Ihn KJ, Sur GS (2003) J Appl Polym Sci 90:3204
25. Chazeau L, Terech P, Cavaillé JY (1999) Macromolecules 32:1872
26. Cheng Q, Wang S, Rials TG (2009) Compos Part A 40:218
27. Cheng Q, Wang SQ, Rials TG, Lee SH (2007) Cellulose 14:593
28. Cho M-J, Park B-D (2011) J Ind Eng Chem 17:36
29. Chronakis IS, Frenot A (2003) Curr Opin Colloid Interface Sci 8:64
30. Çifci C, Kaya A (2010) Desalination 253:175
31. De Souza Lima MM, Wong JT, Paillet M, Borsali R, Pecora R (2003) Langmuir 19:24
32. Ding B, Kim H-Y, Lee S-C, Lee D-R, Choi K-J (2002) Fibers Polym 3:73
33. Ding B, Kim H-Y, Lee S-C, Shao C-L, Lee D-R, Park SJ, Kwag G-B, Choi K-J (2002) J Polym Sci Part B Polym Phys 40:1261
34. Ding B, Kimura E, Sato T, Fujita S, Shiratori S (2004) Polymer 45:1895
35. Gardner DJ, Oporto GS, Mills R, Samir MASA (2008) J Adhes Sci Technol 22:545
36. Dufresne A, Azizi Samir MAS, Alloin F, Sanchez JY, El Kissi N (2004) Macromolecules 37:1386
37. Dufresne A, Garcia de Rodriguez N, Thielemans W (2006) Cellulose 13:261
38. Dufresne A, Helbert W, Cavaillé JY (1996) Polym Compos 17:604
39. Dufresne A (2006) J Nanosci Nanotechnol 6:322
40. Eichhorn SJ, Baillie CA, Zafeiropoulos N, Mwaikambo LY, Ansell MP, Dufresne A, Entwistle KM, Herrera-Franco PJ, Escamilla GC, Groom L, Hugues M, Hill C, Rials TG, Wild PM (2001) J Mater Sci 36:2107
41. Erika Adomaviciute RM (2007) Fibres Text East Eur 15:69
42. Favier V, Canova GR, Cavaillé JY, Chanza H, Dufresne A, Gauthier C (2003) Polym Adv Technol 6:351
43. Favier V, Cavaillé JY, Canova GR, Chanzy H, Dufresne A, Gauthier C (1995) Polym Adv Technol 6:351
44. Finch CA (1973) Poly Vinyl alcohol; properties and applications. Wiley Interscience, New York
45. Fink H-P, Ganster J (2006) Cellulose 13:271
46. Frenot A, Chronakis IS (2003) Curr Opin Colloid Interface Sci 8:64
47. Gindl W, Keckes J (2005) Polymer 46:10221
48. Gray DG, Beck-Candanedo S, Roman M (2005) Biomacromolecules 6:1048
49. Gray DG, Chen W (2002) Langmuir 18:633
50. Gray DG, Cranston ED (2006) Sci Technol Adv Mater 7:319
51. Grunert M, Winter WT (2002) J Polym Environ 10:27
52. Guerrini LM, de Oliveira MP, Branciforti MC, Custodio TA, Bretas RES (2009) J Appl Polym Sci 112:1680
53. Hajji P, Favier V, Gauthier C, Vigier G (1996) Polym Compos 17:612
54. Hanley SJ, Revol J-F, Godbout L, Gray DG (1997) Cellulose 4:209
55. Hassan CM, Peppas NA (2000) Polym Nanocompos 153:37
56. Henriksson M, Berglund LA, Isaksson P, Lindström T, Nishino T (2008) Biomacromolecules 9:1579
57. Henriksson M, Berglund LA (2007) J Appl Polym Sci 106:2817
58. Henriksson M, Henriksson G, Berglund LA, Lindström T (2007) Eur Polym J 43:3434
59. Heux L, Bonini C, Cavaillé JY, Linder P, Dewhurst C, Terech P (2002) Langmuir 18:3311

60. Heux L, Chauve G, Bonini C (2000) Langmuir 16:8210
61. Heux L, Ljungberg N, Cavaillé JY (2006) Polymer 47:6285
62. Hon DNS (1994) Cellulose 1:1
63. Hong KH (2007) Polym Eng Sci 47:43
64. Huang CC, Lin CK, Lu CT, Lou CW, Chao CY, Lin JH (2009) Fibres Text East Eur 17:34
65. Huang Y, Wu X, Wang L, Yu H (2005) J Appl Polym Sci 97:1292
66. Hubbe MA, Rojas OJ, Lucia LA, Sain M (2008) BioResour 3:929
67. Hult EL, Larsson PT, Iversen T (2001) Polymer 42:3309
68. Iwamoto S, Nakagaito AN, Yano H (2007) Appl Phys A Mater Sci Process 89:461
69. Jeong JS, Moon JS, Jeon SY, Park JH, Alegaonkar PS, Yoo JB (2007) Thin Solid Films 515:5136
70. Jeun J-P, Jeon Y-K, Nho Y-C, Kang P-H (2009) J Ind Chem Eng 15:430
71. Ji HM, Lee HW, Karim MR, Cheong IW, Bae EA, Kim TH, Islam MS, Ji BC, Yeum JH (2009) Colloid Polym Sci 287:751
72. Jia Z, Li Q, Liu J, Yang Y, Wang L, Guan Z (2008) J Polym Eng 28:87
73. Joo YL, Kim C-W, Frey M, Marquez M (2005) J Polym Sci Part B Polym Phys 43:1673
74. Joon Seok Lee KHC, Ghim HD, Kim SS, Chun DH, Kim HY, Lyoo WS (2004) J Appl Polym Sci 93:1638
75. Jung YH, Kim HY, Lee DR, Park SY, Khil MS (2005) Macromol Res 13:385
76. Junkasem J, Rujiravanit R, Supaphol P (2006) Nanotechnology 17:4519
77. Kim C-W, Kim D-S, Kang S-Y, Marquez M, Joo YL (2006) Polymer 47:5097
78. Kim G-M, Asran AS, Michler GH, Simon P, Kim J-S (2008) Bioinspir Biomim 3:046003/1
79. Kokabi M, Sirousazar M, Hassan ZM (2007) Eur Polym J 43:773
80. Kong C-S, Lee T-H, Lee K-H, Kim H-S (2009) J Macromol Sci B 48:77
81. Koski A, Yim K, Shivkumar S (2003) Mater Lett 58:493
82. Kotov NA, Podsiadlo P, Choi SY, Shim B, Lee J, Cuddihy M (2005) Biomacromolecules 6:2914
83. Kuga S, Yuan H, Nishiyama Y, Wada M (2006) Biomacromolecules 7:696
84. Kulpinski P (2005) J Appl Polym Sci 98:1855
85. Kvien I, Oksman K (2007) Appl Phys A 87:641
86. Lange J, Wyser Y (2003) Packag Technol Sci 16:149
87. Lee HW, Karim MR, Park JH, Bae DG, Oh W, Cheong IW, Yeum JH (2009) Polym Polym Compos 17:47
88. Lee HW, Karim MR, Park JH, Ghim HD, Choi JH, Kim K, Deng Y, Yeum JH (2009) J Appl Polym Sci 111:132
89. Leitner J, Hinterstoisser B, Wastyn M, Keckes J, Gindl W (2007) Cellulose 14:419
90. Li W, Yue J, Liu S (2012) Ultrason Sonochem 19:479
91. Liu H, Tang C (2007) Polym J 39:65
92. Liu R, Yu H, Huang Y (2005) Cellulose 12:25
93. Matthews S, Fleming K, Gray D, Prasannan S (2000) J Am Chem Soc 122:5224
94. Medeiros E, Mattoso L, Offeman R, Wood D, Orts WJ (2008) Biobased Mater Bioenergy 2:1
95. Mi Y, Zhang X, Zhou S, Cheng J, Liu F, Zhu H, Dong X, Jiao Z (2007) Compos Part A 38:2041
96. Munir MM, Iskandar F, Khairurrijal OK (2009) Rev Sci Instrum 80:026106-3
97. Nakagaito AN, Yano H (2004) Appl Phys A 78:547
98. Nakagaito AN, Yano H (2005) Appl Phys A 80:155
99. Nishiyama M (1997) Chem Fibers Int 47:296
100. Oksman C, Bondeson D, Mathew A (2006) Cellulose 13:171
101. Oksman K, Petersson L (2006) Compos Sci Technol 66:2187
102. Oskman K, Kvien I (2007) Appl Phys A 87:641
103. Pääkkö M, Vapaavuori J, Silvennoinen R, Kosonen H, Ankerfors M, Lindström T, Berglund LA, Ikkala O (2008) Soft Matter 4:2492
104. Paiva MC, Zhou B, Fernando KAS, Lin Y, Kennedy JM, Sun Y-P (2004) Carbon 42:2849

105. Paradossi G, Cavalieri F, Chiessi E (2003) J Mater Sci Mater Med 14:687
106. Peng Z, Kong LX, Li SD (2005) Synthetic Met 152:25
107. Peng Z, Kong LX, Li SD (2005) Synthetic Met 152:321
108. Peng Z, Kong LX (2007) Polym Degrad Stabil 926:1061
109. Peresin MS, Habibi Y, Zoppe JO, Pawlak JJ, Rojas OJ (2010) Biomacromolecules 11:674
110. Ramaraj B (2007) J Appl Polym Sci 103:909
111. Ranby BG (1952) Tappi 35:53
112. Ristolainen N, Heikkila P, Harlin A, Seppala J (2006) Macromol Mater Eng 291:114
113. Samir MASA, Alloin F, Dufresne A (2005) Biomacromolecules 6:612
114. Samir MASA, Dufresne A, Alloin F, Paillet M (2004) Macromolecules 37:4313
115. Schmedlen R, Masters K, West J (2002) Biomaterials 23:4325
116. Shao C, Kim H-Y, Gong J, Ding B, Lee D-R, Park S-J (2003) Mater Lett 57:1579
117. Siró I, Plackett D (2010) Cellulose 17:459
118. Sjoström E (1993) Wood chemistry fundamentals and applications. Academic, New York
119. Skaar C (1988) Wood–Water Relations, New York, NY: Springer Verlag (Springer Series in Wood Science)
120. Son WK, Youk JH, Lee TS, Park WH (2005) Mater Lett 59:1571
121. Stenstad P, Andresen M, Tanem BS, Stenius P (2008) Cellulose 15:35
122. Strawhecker KE, Manias E (2000) Chem Mater 12:2943
123. Sugiyama J, Chanzy H, Maret G (1992) Macromolecules 25:4232
124. Svagan AJ, Samir MASA, Berglund LA (2008) Adv Mater 20:1263
125. Svagan AJ, Samir MASA, Berglund LA (2007) Biomacromolecules 8:2556
126. Syverud K, Stenius P (2009) Cellulose 16:75
127. Tsai Y-C, Huang J-D (2006) Electrochem Commun 8:956
128. Turbak AF, Snyder FW, Sandberg KR (1983) J Appl Polym Sci Appl Polym Symp 37:815
129. Vignon MR, Habibi Y, Chanzy H (2006) Cellulose 13:679
130. Virtanen T, Maunu SL, Tamminen T, Hortfing B, Liitia T (2008) Carbohydr Polym 73:156
131. Walkenstrom P, Frenot A, Henriksson MW (2007) J Appl Polym Sci 103:1473
132. Wan W, Campbell G, Zhang Z, Hui A, Boughner D (2002) J Biomed Mater Res 63:854
133. Wang H, Fang P, Chen Z, Wang S (2007) Appl Surf Sci 253:8495
134. Wang Y, Wang Y, Yan D (2003) Polym Prep 44:1102
135. Werner O, Persson L, Nolte M, Fery A, Wågberg L (2008) Soft Matter 4:1158
136. Wong KKH, Zinke-Allmang M, Hutter JL, Hrapovic S, Luong JHT, Wan W (2009) Carbon 47:2571
137. Xia Y, Li D (2004) Adv Mater 16:1151
138. Yoshiharu N, Paul L, Henri C (2002) J Am Chem Soc 124:9074
139. Yoshiharu N, Shigenori K, Masahisa W, Takeshi O (1997) Macromolecules 30:6395
140. Yu H, Liu R, Shen D, Jiang Y, Huang Y (2005) Polymer 46:5689
141. Yu YH, Lin CY, Yeh JM, Lin WH (2003) Polymer 44:3553
142. Zhang C, Yuan X, Wu L, Han Y, Sheng J (2005) Eur Polym J 41:423–432
143. Zimmermann T, Pohler E, Geiger T (2004) Adv Eng Mater 6:754
144. Zoppe JO, Peresin MS, Habibi Y, Venditti RA, Rojas OJ (2009) ACS Appl Mater Interfaces 1:1996

Polymer Nanofibers Reinforced with Cellulose Nanocrystals

17

Hong Dong

Contents

Abstract

Cellulose nanocrystals (CNCs) have been used as effective reinforcing nanofillers for a variety of polymer nanofibers, taking advantage of their high-modulus and high-strength mechanical properties. Continuous polymer nanofibers incorporated with various contents of CNCs were fabricated using a simple and versatile electrospinning technique driven by a high-voltage electric field. Prior to the electrospinning process, CNCs were dispersed with polymers in solutions. Effects of the addition of CNCs on solution properties

H. Dong
Macromolecular Science and Technology Branch, U.S. Army Research Laboratory, Aberdeen, MD, USA
e-mail: hong.dong.ctr@mail.mil

J.K. Pandey et al. (eds.), *Handbook of Polymer Nanocomposites. Processing, Performance and Application – Volume C: Polymer Nanocomposites of Cellulose Nanoparticles*,
DOI 10.1007/978-3-642-45232-1_66,

were investigated and correlated with the morphology and diameter of the nanofibers. Polymer nanocomposite fibers, usually several hundreds of nanometers in diameter, were produced as either randomly oriented porous mats or uniaxially aligned mats. CNCs were highly aligned along the fiber long axis. Thermal analysis suggested that the incorporation of CNCs influences thermal behaviors of polymer nanofibers, such as glass transition temperatures and melting enthalpies. Increases in tensile strength, Young's modulus, and elastic modulus have been demonstrated from mechanical studies of the nanocomposite fibers containing CNCs.

Keywords
Cellulose nanocrystals • Polymer nanofibers • Electrospinning • Nanocomposites • Reinforcement

1 Introduction

Over the years, a large number of polymers have been processed into nanofibers using a simple and cost-effective electrospinning technique driven by a high-voltage electric field [1]. Polymer fibers with a range of diameters from several micrometers down to tens of nanometers have been electrospun from various synthetic polymers, natural polymers, or blends of both. The nanofiber mats produced by this process offer many advantages like high surface area-to-volume ratio, tunable porosity, and the ability to manipulate nanofiber composition to achieve desired properties and functionalities [1, 2]. Therefore, electrospun nanofibers have been widely investigated as potential candidates for applications in areas including tissue engineering, drug delivery, filtration, catalysis, sensors, energy storage, and functional textiles [1–4]. Over the past several decades, there has been extensive research in electrospinning from various aspects. Many review articles have been published recently. Some of them provide overviews of the electrospinning technique, electrospun fibers, properties, and applications [1–4]. Some of them summarized specific topics on electrospinning, such as electrospinning jet [5], electrospinning design and nanofiber assemblies [6, 7], chemistry on electrospun nanofibers [8], and biomedical applications [9].

The electrospinning process of fabricating polymer nanofibers from solutions or melts utilizes the potential difference of an applied electric field as driving force to propel a jet from the spinning nozzle. A typical lab electrospinning setup is shown in Fig. 17.1. Generally, an electrospinning setup consists of three components: a high-voltage power supply, a spinneret, and an electrically conductive collecting plate (either grounded or connected with opposite voltage polarity). Polymer solution is introduced via the syringe and fed through spinneret using a syringe pump. When the applied electric field reaches a critical value, the repulsive electrical forces in polymer solution overcome the surface tension forces, and thus, a charged jet of the solution is ejected from the tip of the Taylor cone at the spinneret [5]. The charged fluid jet extends in straight flow lines and then undergoes

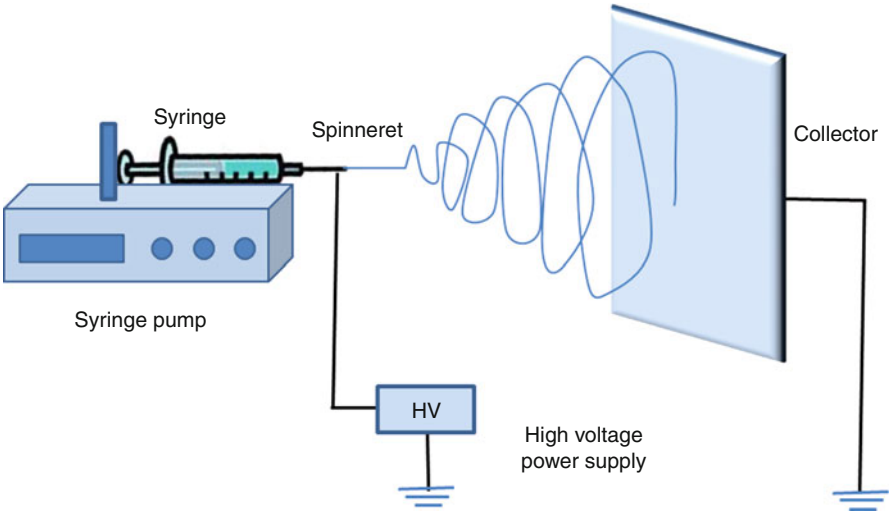

Fig. 17.1 Schematic diagram of a typical laboratory setup for electrospinning

vigorous whipping motion caused by electrohydrodynamic instabilities [5]. As solvent in the jet solution evaporates, polymer is collected to form a randomly oriented nonwoven mat or network. By utilizing special electrospinning design, ordered nanofiber assemblies such as aligned fiber and patterned fiber structures have been fabricated [6]. To scale up the electrospinning process, high-throughput electrospinning units have been developed for mass production of nanofibers, which further open the opportunities for electrospun nonwovens.

Incorporation of stiff nanofillers such as carbon nanotubes [10–13] and nanoclays [14, 15] into electrospun nanofibers has been studied as an effective approach to enhance mechanical strength, thermal property, or electrical conductivity of the electrospun fibers. It was demonstrated that the high electrostatic forces and shear force experienced by the jet during electrospinning aligned the high aspect ratio fillers along the fiber axis [12, 14]. Distribution of nanotubes in the polymer matrix and interfacial adhesion between nanotubes and polymers were considered to be two major factors that determine the reinforcement effect of carbon nanotubes in polymer fibers [11].

Utilizing cellulose nanocrystals (Fig. 17.2) as a reinforcing phase for developing new nanocomposite materials has been investigated [16–20]. Cellulose nanocrystals (CNCs) as a reinforcing phase have several advantages over other types of nanofillers. They are easily modified, inexpensive, renewable, and biocompatible and have a low density [16]. Most importantly, CNCs are highly crystalline and possess impressive mechanical properties. For example, the elastic modulus of tunicate CNCs extracted by acid hydrolysis was 151 $\pm$ 29 GPa measured by AFM three-point bending [21]. The rodlike or whisker-shaped particles have also been named as nanocrystalline cellulose, nanowhiskers, or whiskers. CNCs can be isolated by acid hydrolysis from a variety of renewable sources including

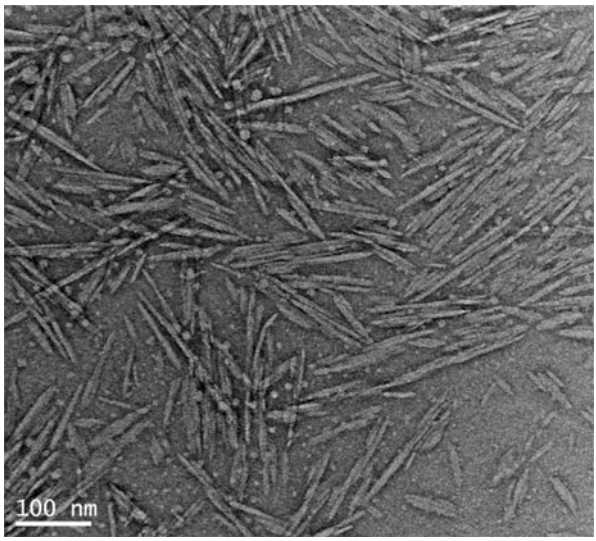

Fig. 17.2 Transmission electron micrograph (TEM) of cellulose nanocrystals produced from wood pulp

wood, plants, algae, bacteria, and sea animals called tunicates [19]. The dimension of CNCs varies based on the source of the cellulose, but the width is typically on the order of a few nanometers and the length is generally several hundreds of nanometers [18]. A notable feature of CNCs is hydrophilicity, which makes them suitable for reinforcing hydrophilic polymers. Surface modifications of CNCs using various methods [18, 19] have been explored to improve compatibility, especially when used as reinforcement nanofillers in nonpolar or hydrophobic matrices.

The incorporation of cellulose nanocrystals to the electrospun nanofibers has shown promise for improving mechanical properties of the nanofibers that are required in many applications. Especially, because CNCs are nontoxic, biocompatible, and biodegradable, they have a significant potential in developing strong and fully biodegradable polymer nanocomposite fibers for biomedical applications, such as tissue engineering and wound healing. For hydrophobic synthetic biopolymers, such as poly(lactic acid) (PLA) and poly(ε-caprolactone) (PCL), addition of biocompatible cellulose nanocrystals is also expected to improve wettability, which favors living cell adhesion on the fiber scaffolds in tissue engineering applications [22, 23].

Cellulose nanocrystals have successfully been used as effective reinforcing nanofillers for various electrospun natural and synthetic polymer nanofibers. As shown in Table 17.1, polymer nanocomposite fibers incorporated with cellulose nanocrystals have been produced from polyethylene oxide (PEO) [24–26], poly(acrylic acid) (PAA) [27], poly(vinyl alcohol) (PVA) [28–31], lignin/poly(vinyl alcohol) [32], poly(lactic acid) (PLA) [23, 33], poly(ε-caprolactone) (PCL) [22], cellulose acetate (CA) [34], ethylene vinyl alcohol [35, 36], silk fibroin [37], polystyrene (PS) [38], and poly(methyl methacrylate) (PMMA) [39, 40]. Sources of cellulose nanocrystals include bacterial cellulose, ramie, cotton, wood pulp, tunicate, microcrystalline

Table 17.1 Electrospun polymer nanofibers reinforced with cellulose nanocrystals

Polymer	CNC content (%)	Source of CNCs	Solvent for electrospinning	Mechanical property investigated	Reference
Poly(vinyl alcohol)	0, 5, 10, 15	Ramie fibers	H_2O	Storage modulus E' (DMA)	[29, 30]
	6.6	Whatman cellulose fiber	H_2O	Tensile properties	[28]
	0–15	Whatman filter paper	H_2O	Tensile properties of aligned and isotropic fiber mats	[31]
Lignin/poly(vinyl alcohol)	0, 5, 10, 15	Cotton	H_2O	None	[32]
Polyethylene oxide	0, 5, 10, 20	Microcrystalline cellulose	H_2O	Tensile properties	[25]
	0, 5, 10, 15	Tunicate	H_2O	Storage modulus E' (DMA) of aligned fiber mats	[24]
Cross-linked poly(ethylene oxide)	0, 5, 10, 20	Cotton	H_2O	Tensile properties	[26]
EVOH (ethylene vinyl alcohol)	0, 1, 5, 8	Bacterial cellulose	2-propanol/H_2O	None	[35]
	0, 5, 15, 20, 25, 40	Bacterial cellulose	2-propanol/H_2O	None	[36]
Cellulose acetate	0–5	Microcrystalline cellulose	Acetic acid/acetone	Storage modulus E' (DMA)	[34]
Poly(acrylic acid)	0, 5, 10, 15, 20	Cotton	Ethanol	Tensile properties	[27]
Poly(ε-caprolactone)	0, 2.5, 5.0, 7.5	Ramie fibers	DMF/dichloromethane	Storage modulus E' (DMA)	[22]
Poly(lactic acid)	0, 1, 10	Microcrystalline cellulose	DMF	Tensile properties	[33]
	0, 2.5, 5.0, 7.5	Bacterial cellulose	DMF/THF	None	[23]
Polystyrene	PS-CNC of 94:6 and 91:9	Cellulose filter paper	THF	Storage modulus E' (DMA)	[38]
Poly(methyl methacrylate)	0, 5, 9, 17, 23, 33, 41	Soft wood pulp	DMF	Storage modulus E' (nanoindentation)	[40]
	0, 1, 3.5, 7, 14, 20	Bacterial cellulose	DMF/THF	None	[39]
Silk fibroin	0, 1, 2, 3, 4	Mulberry branch bark	Formic acid	Tensile properties	[37]

cellulose, and cellulose filter papers. Additionally, CNC/cellulose core-in-shell nanocomposite fibers have been fabricated by co-electrospinning a cellulose solution as the shell and a CNC water suspension as the core [41]. In this article, we aim to present a brief overview on currently reported work of electrospun polymer fibers reinforced with CNCs. The development and properties of nanocomposite fibers containing CNCs are described in terms of preparation, effects of addition of CNCs on electrospun solution properties, fiber morphologies, alignment, thermal behaviors, and mechanical properties.

2 Dispersion and Solution Properties

2.1 Dispersion of CNCs in Polymer Solutions

The electrospun solutions for fabricating polymer/CNCs fibers were prepared by dispersing CNCs and dissolving polymers in the same solvents that were suitable for electrospinning. Good dispersion of CNCs in the polymer as well as in the processing solvent is essential for preparing polymer/CNC nanocomposite fibers that have significant mechanical reinforcement. Owing to the highly hydrophilic nature of cellulose, stable dispersions of CNCs with negatively charged sulfate groups have only been obtained in water or some polar organic solvents, as recently reported, *N*,*N*-dimethylformamide (DMF), dimethyl sulfoxide, *N*-methyl-2-pyrrolidone, formic acid, and m-cresol [42, 43]. Considering that the "as-produced" CNCs are water dispersive, the development of an all-aqueous system for electrospinning based on a combination of CNCs with water-soluble polymers offers advantages in avoiding the use of organic solvents [25]. Nanocomposite fibers of CNCs with hydrophilic polymers such as PVA [28–32] and PEO [24–26] have been prepared by directly mixing cellulose nanocrystals with the polymer in aqueous solutions followed by electrospinning. DMF, a "good" processing solvent for electrospinning, was used for incorporating CNCs into hydrophobic matrix polymers, such as PMMA [40]. Solvent exchange of CNCs from aqueous dispersion to DMF was applied to avoid the limited dispersibility of freeze-dried CNCs in DMF. Dried CNCs can easily disperse in formic acid, which is also a solvent for silk fibroin. Therefore, formic acid was used as a solvent for producing silk fibroin/CNC fibers [37]. The use of a nonionic surfactant has also been explored to improve the dispersibility of freeze-dried CNCs in tetrahydrofuran (THF) and hydrophobic polystyrene [38]. In addition to single-solvent systems, a mixture of solvents has been employed for achieving good dispersions of CNCs in polymer solutions as well as continuous electrospinning process. Examples of these include 2-propanol/water (70/30) for ethylene vinyl alcohol copolymer [35, 36], acetic acid/acetone (1:1) for cellulose acetate [34], and DMF/THF for PLA [23] and PMMA [39].

2.2 Solution Properties

The electrospun solution properties such as concentration, polymer molecular weight, viscosity, surface tension, and conductivity play important roles in forming a stable spinning jet and determining the morphologies of electrospun fibers, and these effects have been well studied [1, 9, 44]. Continuous spinning and uniform fibers are achieved by adjusting these solution parameters to be in the optimum range. Solutions of high electrical conductivity usually lead to thinner fibers and less bead formation. On the other hand, solutions of low electrical conductivity are subject to insufficient elongation by electrical forces on the fluid jet, and beads may be observed [1]. Viscosity correlates with concentration and polymer molecular weight. Smooth fibers are obtained when the solution has a sufficient viscosity to form a continuous jet and to avoid splitting. Generally, the high surface tension of a solution inhibits the electrospinning process because of instability of the jets and the generation of sprayed droplets. By lowering the surface tension of the solution, the bead formation in the fibers can be reduced [1].

The changes of solution properties upon addition of CNCs to a polymer solution have been investigated in many studies and were correlated with the morphology and diameter of the fibers. Typically, the conductivity of CNC/polymer dispersion increased with the addition of CNCs as a result of the negative charges from the sulfate groups on CNC surfaces, which were grafted via sulfuric acid hydrolysis during CNC production. The increased conductivity can effectively prevent formation of beads and promote continuous spinning of smaller diameter fibers. The surface tension of the PVA/CNC [29] and PEO/CNC [25] systems was not significantly affected by the addition of CNCs. The effects of the addition of CNCs on viscosity of the suspensions varied depending greatly on the matrix polymer. The viscosities of PEO/CNC and PAA/CNC suspensions decreased after CNCs were added, because CNCs disrupt the PEO or PAA intermolecular interactions and chain entanglement [25, 27]. On the contrary, the viscosities of lignin-PEO/CNC [32] and cross-linked PEO/CNC [26] increased with increasing contents of CNCs. Viscosity of PVA/CNC [29] suspensions was not significantly affected by the addition of CNCs.

Shear viscosity of the PEO/CNC, lignin-PVA/CNC, and cross-linked PEO/CNC were also investigated using a rheometer. All these suspensions exhibited a typical shear-thinning behavior across the investigated range of shear rates. The shear-thinning behavior of lignin-PVA/CNC was explained by the fluctuating structure of the dispersion disrupted under shear producing CNC alignment along the flow direction [32]. PEO/CNC suspensions exhibited more shear-thinning behavior with increased CNC contents, which was attributed to the strong interaction between PEO and CNCs increasing the solution inertia [25].

3 Formation of Nanocomposite Fibers

3.1 Electrospinning

Nanofiber mats of polymer and polymer incorporated with various loadings of CNCs were produced by electrospinning. The suspension of polymer/CNC was loaded in a disposable plastic syringe with flow rate controlled by a syringe pump. The needle of the syringe was connected to one electrode of a power supply. A plate covered by aluminum foil, either grounded or connected with the opposite electrode of the power supply, was used as a collector (Fig. 17.1). In addition to solution properties, the processing parameters, such as applied voltage, flow rate, types of collectors, and tip-to-collector distance, and ambient parameters, such as humidity, influence fiber morphologies [1, 9]. In the preparation of PVA/CNC nanofibers [28], effects of process variables, such as applied voltage, injection rate, tip-to-collector distance, rotation speed of the collector, and relative humidity, as well as polymer concentration on fiber morphology were investigated. It was concluded that decreasing polymer concentration and injection rate, increasing rotational speed of the collector and relative humidity tended to form thin fibers, whereas very high applied voltage favored the formation of beaded fibers.

Typically, the operating parameters used in electrospinning of polymer/CNC nanocomposite fibers have an applied voltage in the range of 10–30 kV, a tip-to-collector distance of 10–25 cm, and a flow rate that is able to generate a continuous and stable jet under applied electric field. Electrospinning process is usually performed at room temperature and in some studies at a controlled humidity.

3.2 Morphology of the Fibers

The nanocomposite fibers collected on the plate exhibited randomly oriented form, and the diameters were usually hundreds of nanometers. By adding a low content of CNCs, fibers with decreased average diameter and improved uniformity were produced, as compared to the unfilled polymer nanofibers. The diameter reduction was attributed to the increased conductivity of the electrospinning solutions in the presence of CNCs [25, 26, 29]. Incorporating a high content of CNCs to the same concentration of polymer solution, however, induced fibers with thick diameters. When the effect of increased viscosity on the diameter of nanofibers was greater than the enhanced electrical conductivity, elongation of the jet between the needle tip and collector weakened; therefore, thicker fibers were obtained [26]. While most of the nanocomposite fibers of polymer/CNC have homogenous microstructures, heterogeneous microstructure consisting of the primary nanofibers and secondary ultrafine nanofibers exhibited a bimodal size distribution in 7 % PEO/CNC nanofibers as well as 7 % PEO nanofibers [25].

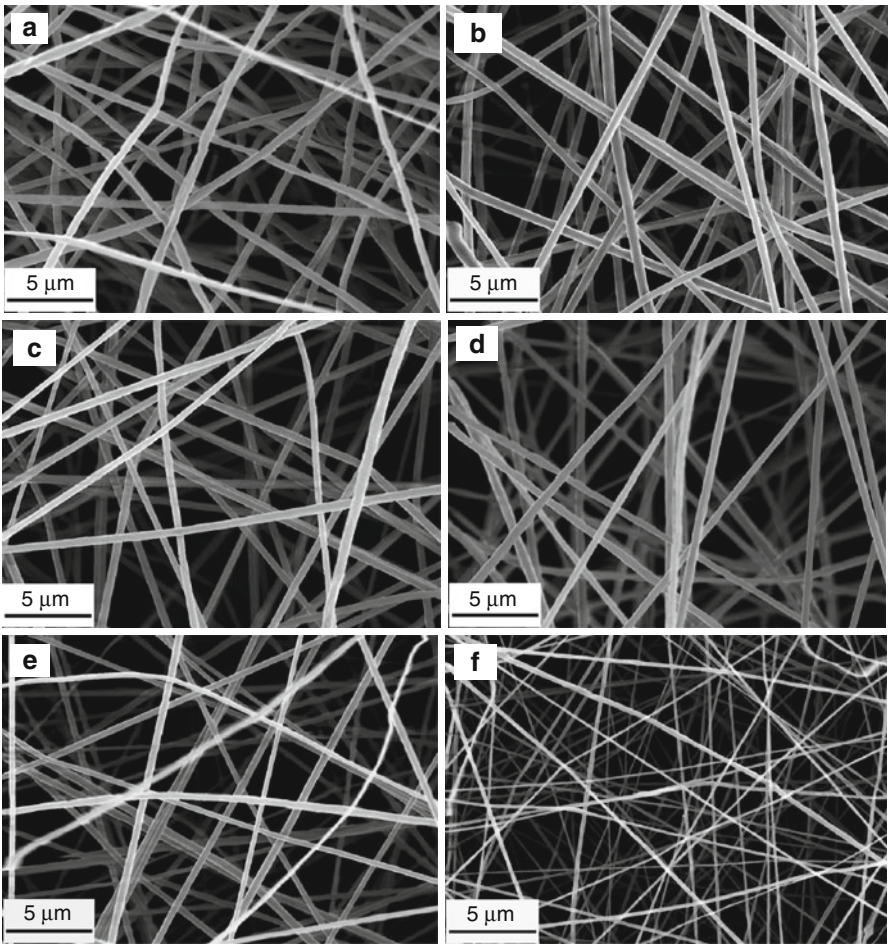

Fig. 17.3 Scanning electron micrographs (SEM) of (**a**) PMMA fibers and (**b–f**) PMMA/CNC fibers at various w/w percentages of CNCs in fibers: (**b**) 5 % CNC, (**c**) 9 % CNC, (**d**) 17 % CNC, (**e**) 23 % CNC, and (**f**) 41 % CNC

The content of CNCs included in the fibers was usually less than 20 wt%. The systems with a higher content of CNCs than 20 % were highly viscous and gel-like and could not form a stable jet during electrospinning. To incorporate high loadings of the CNC fillers, a low concentration of polymer solution is necessary to obtain a less viscous, spinnable solution. Various contents of CNCs have been incorporated into electrospun PMMA fibers with weight up to 41 % [40]. Ultrathin fibers and well-formed fiber mats were produced at the all investigated CNC contents (Fig. 17.3). The concentration of PMMA in DMF started with 90 mg/mL for PMMA/5 % CNC and decreased to 40 mg/mL for PMMA/41 % CNC to reduce viscosity.

The formation of PMMA/CNC fibers at high CNC percentages took account of factors such as low concentrations of PMMA solutions, conductivity increased with CNC content, and a good dispersion of CNCs in PMMA/DMF [40].

3.3 Alignment of Nanocomposite Fibers

Aligned fibers or arrays of fibers can be obtained by collecting the fibers on specially designed collector systems. Mechanical and electrostatic methods to control the electrospinning process, such as rotating drum, parallel electrodes, rotating wire drum collector, and disk collector, have been used to achieve highly ordered aligned fibers [6, 7]. Aligned fibers are important in many engineering applications, such as tissue engineering, sensors, nanocomposites, filters, and electronic devices [7]. For instance, cells cultured on aligned nanofiber scaffolds have been shown to proliferate in the direction of the fiber orientation [45].

Among the commonly used alignment techniques, a high-speed rotating metal drum [31, 40], an aluminum frame with opening gaps [24], and two pieces of metal sheet separated by an insulating gap [34] have been applied to acquire aligned fibers of polymers with CNCs. By controlling the rotation speed of the metal drum, fibers of PMMA/CNC [40] showed significant alignment along the axis of rotation direction (Fig. 17.4). Fiber arrays of PEO/CNC [24] with varied CNC contents were deposited in a uniaxially aligned manner across the gap of electrically charged aluminum frame. Aligned fibers of cellulose acetate/CNC [34] were collected on two separated metal sheets, and the alignment was found to be affected by the gap distance, the voltage, and the collection time. Nanofiber webs of PVA/CNC [31] with different alignment degrees were fabricated using a rotating collector with variable linear velocity. The relative alignment degree was analyzed using a fast Fourier transform method. The morphology and mechanical properties of aligned electrospun PVA/CNC fiber webs were investigated and compared with isotropic nanofiber webs.

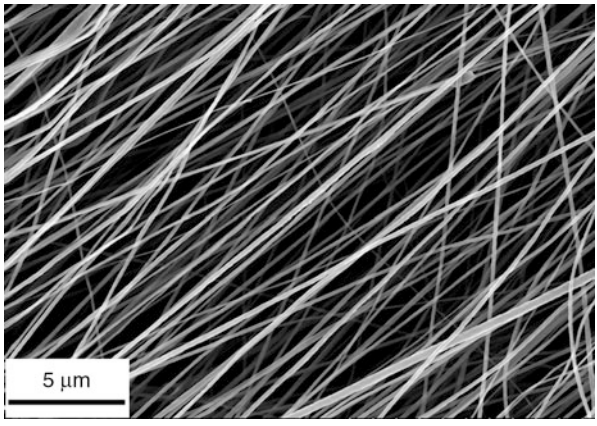

Fig. 17.4 SEM image of PMMA/33 wt% CNC fibers aligned using a rotating metal drum (Reprinted with permission from [40]. Copyright 2012, Elsevier)

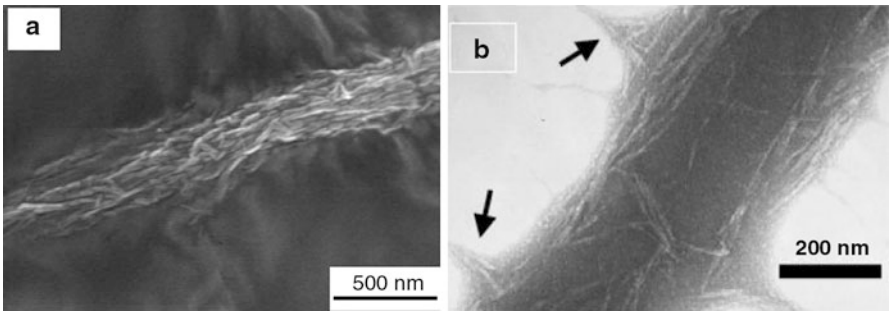

Fig. 17.5 (**a**) FESEM image of CNCs aligned along fiber axis direction that was revealed by solvent etching of PMMA (Reprinted with permission from [40]. Copyright 2012, Elsevier). (**b**) TEM image of 7-PEO/CNC-20 composite nanofibers (*arrows* pointing to secondary nanofibers) (Reprinted with permission from [25]. Copyright 2011, American Chemical Society)

3.4 Orientation of CNCs in the Fibers

The orientation of CNCs along the nanofiber axis was demonstrated in several studies. The orientation of CNCs embedded in a PMMA/CNC fiber was investigated by solvent-etching PMMA from fibers with THF. Highly aligned CNCs were revealed along the fiber axis after etching using field emission scanning microscopy (FESEM), as displayed in Fig. 17.5a [40]. TEM was also used to investigate the orientation of CNCs in the composite fibers. The fibers were directly collected on TEM grids and stained with uranyl acetate to enhance the contrast between CNCs and polymer. Figure 17.5b shows that CNCs aligned along the PEO nanofiber long axis, suggesting that CNCs obtained a high degree of orientation through a high electric field [25]. This phenomenon was also observed when other types of nanofillers were used to reinforce electrospun polymer fibers, such as carbon nanotubes. The alignment of nanofillers along the fiber axis is mainly induced by high shear forces when the solution is ejected from small diameter needles. Other factors may also contribute, such as nanoscale confinement effect, large electric field, and polymer chain orientation during electrospinning [13].

3.5 Characterization of the Nanocomposite Fibers

Chemical characterization of electrospun nanocomposite fibers to confirm the presence of CNCs was performed using Fourier transform infrared spectroscopy (FT-IR). Spectra of the composite fibers with different contents of CNCs were collected and compared with the spectra of CNCs and pure polymer fibers. The characteristic absorbance of CNCs includes broad bands in the range of 3,500–3,300 cm^{-1}, which are characteristic absorptions of the free hydroxyl and the hydrogen-bonded hydroxyl groups of cellulose [40]. The presence of CNCs may also influence the shape and intensity of the main peaks of the polymer due to the

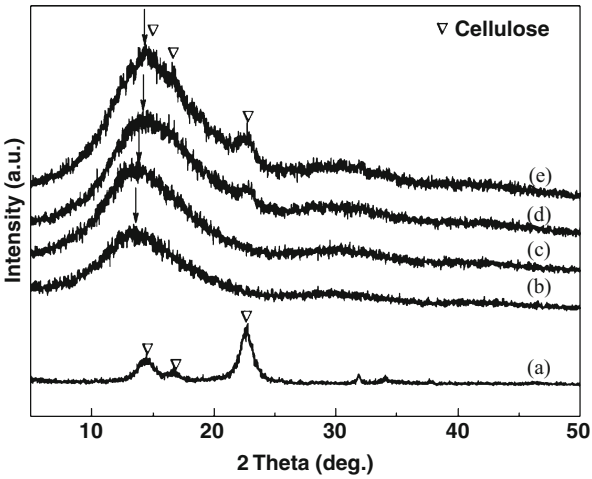

Fig. 17.6 X-ray diffraction patterns of (*a*) CNCs, (*b*) pure PLA mat, (*c*) PLA with 2.5 wt%, (*d*) PLA with 5.0 wt%, and (*e*) PLA with 7.5 wt% CNC mats (Reproduced with permission from [23]. Copyright 2012, Springer)

hydrogen bonding between the hydrophilic CNCs and the PVA continuous polymer matrix [29]. Analysis of FT-IR spectra indicated that the nanocomposite fibers contained both components from the electrospun solutions. Because of high crystallinity of cellulose crystals, X-ray diffraction has been used to examine the presence of the nanofillers in the fibers. X-ray diffraction on nanocomposite fibers showed a small peak at 2θ ~23° (Fig. 17.6), which was attributed to the [200] plane of the cellulose crystals, indicating the presence of CNCs [23, 25, 27, 34, 35, 39]. To directly reveal the presence of CNCs in the fibers, the cross sections of the electrospun fiber were examined using FESEM, and the images showed CNCs embedding in the fiber matrix [29, 37, 39].

4 Thermal Behaviors

The effects of CNCs on thermal behaviors of the polymer, such as thermal glass transition temperature (T_g), melting temperature (T_m), enthalpy of fusion, and degree of crystallinity, were investigated by differential scanning calorimetry (DSC) studies on the pure polymer and the polymer/CNC fiber mats. The thermal glass transition temperatures of the PEO/CNC and PMMA/CNC fibers were found slightly increased with increased contents of CNCs [25, 40]. The effects of addition of CNCs on T_g of the matrix polymer PEO or PMMA were explained by the interactions between CNCs and the polymer limiting the molecular chain movement. On the contrary, the T_g of PS fibers with added CNCs (and surfactant) tended to decrease with the CNC loading, which is caused by the plasticizing effect of the surfactant [38].

For fibers of PEO/CNC [25], lignin-PVA/CNC [32], EVOH/CNC [36], and PCL/PCL-grafted CNC [22], the incorporation of CNCs decreased the melting

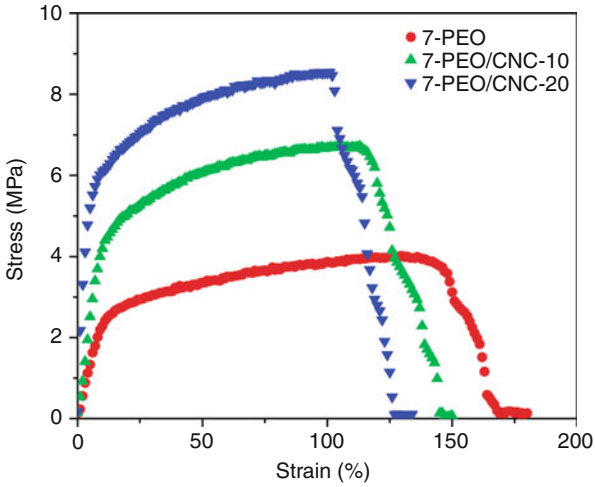

Fig. 17.7 Stress-strain curves of electrospun 7 % PEO and 7 % PEO/CNC nanofibrous mats (Reprinted with permission from [25]. Copyright 2011, American Chemical Society)

temperatures, the melting enthalpies, and the crystallinities of the matrix polymers in the nanocomposite fibers. The interactions between the dispersed CNCs and the matrix hindered the organization of polymer molecular chains into ordered structures on the surfaces of CNCs during the electrospinning process, causing a lower overall crystallinity [25, 32]. For fibers of PVA/CNC [29], the degree of crystallinity in the composite nanofibers decreased, while the melting temperature T_m of fibers containing different loadings of CNCs remained fairly constant. On the other hand, the addition of CNCs increased the crystallinity of PLA fibers, because CNCs acted as nucleation sites for PLA [23, 33].

5 Mechanical Properties

5.1 Tensile Properties of CNC-Reinforced Nanofiber Mats

In general, incorporation of CNCs to polymer fibers yields higher Young's modulus and tensile strength but lower elongation than the pure polymer fibers. Several studies have investigated the tensile properties of polymer nanofiber mats incorporated with various contents of CNCs. For example, Zhou et al. [25] investigated the tensile properties of PEO/CNC fabricated from 7 % PEO in H_2O with increased CNC content from 0 to 20 wt%. The maximum tensile stress and Young's modulus increased from 4 MPa for 0 % to 8.52 MPa for 20 % CNCs and 23.8 to 59.6 MPa, respectively, whereas the elongation at break decreased from 168 % to 125 % (Fig. 17.7). Huang et al. [37] showed that as little as 2 % of CNCs could improve the tensile strength and Young's modulus of silk fibroin nanofiber mat significantly, which were about 2 times higher than those of unreinforced nanofiber. However, the strain at break dropped gradually with

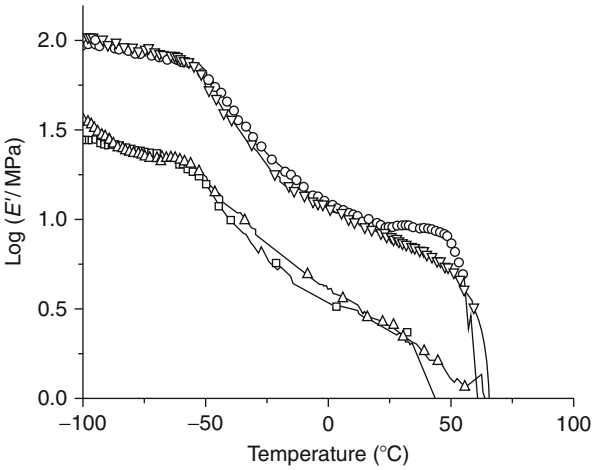

Fig. 17.8 Storage modulus curves for the nanofiber webs of neat PCL (□) and PCL loaded with 2.5 % (O), 5 % (Δ), and 7.5 % (▽) of unmodified CNCs (Reprinted with permission from [22]. Copyright 2009, American Chemical Society)

increase of CNCs. Tensile properties of cross-linked PEO/CNC fiber mats and PAA/CNC fiber mats have also been studied. The overall improvement in Young's modulus and tensile strength was significant by CNC loading in the electrospun polymer mats.

The effect of alignment on tensile properties of CNC-reinforced nanofibers was examined in the mechanical study of the aligned and isotropic PVA/CNC nanofiber webs [31]. Oriented electrospun webs showed 30–45 % higher in tensile strength and modulus than isotropic electrospun webs, regardless of CNC contents. CNCs had a more reinforcement effect on the aligned PVA/CNC webs than on the isotropic PVA/CNC webs. While 15 wt% CNC loaded isotropic PVA electrospun fiber webs had 86 % higher tensile and 105 % higher modulus, aligned PVA electrospun fiber webs with 15 wt% CNCs had 95 % higher tensile and 118 % higher modulus [31].

5.2 Storage Modulus of CNC-Reinforced Nanofiber Mats

The storage modulus of the fiber mats after incorporation of CNCs was investigated using dynamic mechanical analysis (DMA) in tensile mode. The reinforcing effects of CNCs on the storage modulus at temperatures either above or below T_g were demonstrated from several nanocomposite fibers. The storage modulus of fibers of PCL with several loadings of CNCs (Fig. 17.8) was investigated, and the reinforcement effect was related to both loading of CNCs and the fiber diameter [22]. A significant increase in the storage modulus was observed in PCL fibers filled with unmodified CNCs (2.5 % and 7.5 %) in comparison to the neat PCL. The reinforcement of 2.5 % CNCs was attributed to both the filler loading and the smaller fiber diameters than PCL fibers resulting in higher interfiber bonding area.

The increased storage modulus at 7.5 % CNC loading was brought about by the reinforcing contribution of CNCs within the fiber, despite the diameter of the nanocomposite fiber being larger than that of the neat PCL fibers.

In another study, uniaxially oriented arrays of PEO/CNC fibers were prepared with CNC contents of 5 %, 10 %, and 15 % [24]. All the fibers have similar diameters in the range of 400–500 nm. The reinforcement of CNCs on fibers of PEO was apparent, and the storage moduli of the PEO/CNC nanofiber arrays along the fiber axis were 1.5–2 times greater than the neat PEO fiber array. It is worth noting that the effect of interfiber bonding on mechanical properties was largely eliminated because of disconnection among fibers in the transverse direction.

5.3 Nanomechanical Properties of Single CNC-Reinforced Nanofibers

Owing to the small size and difficulty in handling single nanofibers, the mechanical properties were usually tested on the fiber mats consisted of entangled nanofibers. Aside from the composition and diameter of the fibers, the mechanical properties measured on fiber mats depend strongly on fiber orientation within the material, bonding between fibers, and slippage of one fiber over the other, and these effects can superimpose the material-specific properties of the nanofibers that compose the fiber mat [46]. Thus, nanoscale mechanical testing methods have been developed to investigate the properties of single nanofibers. Tensile test methods using commercial nanotensile testing or the atomic force microscope (AFM) cantilever, bending test methods, and nanoindentation have been applied on mechanical testing of single electrospun nanofibers [14, 46–48].

To investigate the reinforcement of CNCs on PMMA fibers, nanoscale dynamic mechanical analysis (nano-DMA) was performed using nanoindentation on single fibers of PMMA and PMMA/CNC perpendicular to the fiber axis [40]. Challenges associated with single fiber nanoindentation were addressed, such as fiber diameter range and minimum, depth to diameter ratio, and valid depth range under these experimental conditions [40]. In order to compare fibers of slightly different diameter, the indentation depth (h) was normalized to the fiber diameter (D), h/D, resulting in a relative depth. Figure 17.9 shows the nano-DMA modulus data of fibers with various CNC contents obtained from 0.2 to 0.3 (h/D) relative indentation depth. Fibers that contained 17 wt% CNCs showed a modest increase of 17 % in the storage modulus of PMMA, considering that the glassy matrix PMMA had a high modulus of 5.4 GPa.

Nanomechanical properties of single PEO nanofibers reinforced with network-forming microfibrillated cellulose (MFC) were investigated by AFM three-point bending method and compared with macrotensile testing of aligned fiber mats [49]. Highly filled fibers (6.5–21 wt%) showed an enhancement of Young's modulus up to a factor of 10 compared to pure PEO fiber by using AFM techniques. The conventional tensile testing of aligned fiber mats resulted in lower Young's

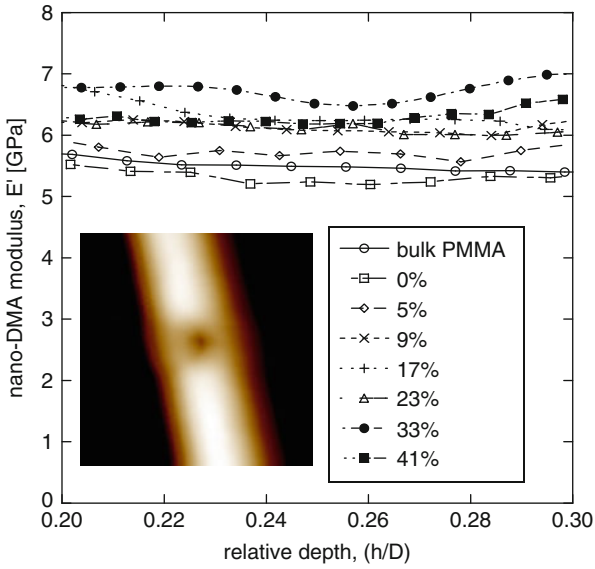

Fig. 17.9 Nano-DMA storage modulus data for bulk PMMA film, PMMA fibers, and PMMA/CNC fibers. *Insert*: topographic image of a fiber after a shallow indent was performed (Adapted from [40]. Copyright 2012, Elsevier)

modulus than AFM testing on single fibers, which was explained by the non-fully aligned fibers and the high porosity within the mat. However, nanotensile investigation of single CNC-reinforced nanofibers has rarely been reported.

6 Conclusions

Reinforcing electrospun polymer nanofibers with naturally derived cellulose nanocrystals is a relatively new and rapidly evolving research area. It has been shown that cellulose nanocrystals have an exciting potential as reinforcements in polymer nanofibers. Particularly, the combination of biodegradable cellulose nanocrystals and biocompatible polymers is attractive for developing strong nanofibers for biomedical applications. Uniform nanofibers with various contents of CNCs, either randomly oriented or aligned, have been produced by optimizing electrospun solution properties and processing parameters. Mechanical studies of the nanocomposite fibers showed increases in tensile strength, Young's modulus, and elastic modulus.

Despite the advantages and success of using CNCs as nanofillers for electrospun polymer fibers, the hydrophilic nature of CNCs limits processability and compatibility with many hydrophobic polymers. Surface modifications of CNCs to enhance dispersion in common organic solvents as well as filler-matrix interactions with hydrophobic polymers are expected to widen the scope of research into CNC reinforcement of polymer nanofibers.

References

1. Bhardwaj N, Kundu SC (2010) Electrospinning: A fascinating fiber fabrication technique. Biotechnol Adv 28:325
2. Lu XF, Wang C, Wei Y (2009) One-dimensional composite nanomaterials: Synthesis by electrospinning and their applications. Small 5:2349
3. Huang Z-M, Zhang Y-Z, Kotakic M, Ramakrishnab S (2003) A review on polymer nanofibers by electrospinning and their applications in nanocomposites. Compos Sci Technol 63:2223
4. Greiner A, Wendorff JH (2007) Electrospinning: A fascinating method for the preparation of ultrathin fibers. Angew Chem Int Ed 46:5670
5. Reneker DH, Yarin AL (2008) Electrospinning jets and polymer nanofibers. Polymer 49:2387
6. Teo WE, Ramakrishna S (2006) A review on electrospinning design and nanofibre assemblies. Nanotechnology 17:R89
7. Baji A, Mai Y-W, Wong S-C, Abtahi M, Chen P (2010) Electrospinning of polymer nanofibers: Effects on oriented morphology, structures and tensile properties. Compos Sci Technol 70:703
8. Agarwal S, Wendorff JH, Greiner A (2010) Chemistry on electrospun polymeric nanofibers: Merely routine chemistry or a real challenge?. Macromol Rapid Commun 31:1317
9. Sill TJ, von Recum HA (2008) Electrospinning: Applications in drug delivery and tissue engineering. Biomaterials 29:1989
10. Ko F, Gogotsi Y, Ali A, Naguib N, Ye HH, Yang GL, Li C, Willis P (2003) Electrospinning of continuons carbon nanotube-filled nanofiber yarns. Adv Mater 15:1161
11. Ye HH, Lam H, Titchenal N, Gogotsi Y, Ko F (2004) Reinforcement and rupture behavior of carbon nanotubes–polymer Nanofibers. Appl Phys Lett 85:6
12. Hou HQ, Ge JJ, Zeng J, Li Q, Reneker DH, Greiner A, Cheng SZD (2005) Electrospun polyacrylonitrile nanofibers containing a high concentration of well-aligned multiwall carbon nanotubes. Chem Mater 17:967
13. Chen D, Liu TX, Zhou XP, Tjiu WC, Hou HQ (2009) Electrospinning fabrication of high strength and toughness polyimide nanofiber membranes containing multiwalled carbon nanotubes. J Phys Chem B 113:9741
14. Li L, Bellan LM, Craighead HG, Frey MW (2006) Formation and properties of nylon-6 and nylon-6/montmorillonite composite nanofibers. Polymer 47:6208
15. Roghani-Mamaqani H, Haddadi-Asl V, Najafi M, Salami-Kalajahi M (2011) Preparation of nanoclay-dispersed polystyrene nanofibers via atom transfer radical polymerization and electrospinning. J Appl Polym Sci 120:1431
16. Samir MASA, Alloin F, Dufresne A (2005) Review of recent research into cellulosic whiskers, their properties and their application in nanocomposite field. Biomacromolecules 6:612
17. Eichhorn SJ, Dufresne A, Aranguren M, Marcovich NE, Capadona JR, Rowan SJ, Weder C, Thielemans W, Roman M, Renneckar S, Gindl W, Veigel S, Keckes J, Yano H, Abe K, Nogi M, Nakagaito AN, Mangalam A, Simonsen J, Benight AS (2010) Review: current international research into cellulose nanofibres and nanocomposites. J Mater Sci 45:1
18. Habibi Y, Lucia LA, Rojas OJ (2010) Cellulose nanocrystals: Chemistry, self-assembly, and applications. Chem Rev 110:3479
19. Moon RJ, Martini A, Nairn J, Simonsen J, Youngblood J (2011) Cellulose nanomaterials review: Structure, properties and nanocomposites. Chem Soc Rev 40:3941
20. Khalil HPSA, Bhat AH, Yusra AFI (2012) Green composites from sustainable cellulose nanofibrils: A review. Carbohydr Polym 87:963
21. Iwamoto S, Kai WH, Isogai A, Iwata T (2009) Elastic modulus of single cellulose microfibrils from tunicate measured by atomic force icroscopy. Biomacromolecules 10:2571
22. Zoppe JO, Peresin MS, Habibi Y, Venditti RA, Rojas OJ (2009) Reinforcing poly(ε-caprolactone) nanofibers with cellulose nanocrystals. ACS Appl Mater Interf 1:1996

23. Liu DY, Yuan XW, Bhattacharyya D (2012) The effects of cellulose nanowhiskers on electrospun poly(lactic acid) nanofibres. J Mater Sci 47:3159
24. Changsarn S, Mendez JD, Shanmuganathan K, Foster EJ, Weder C, Supaphol P (2011) Biologically inspired hierarchical design of nanocomposites based on poly(ethylene oxide) and cellulose nanofibers. Macromol Rapid Commun 32:1367
25. Zhou CJ, Chu R, Wu R, Wu QL (2011) Electrospun polyethylene oxide/cellulose nanocrystal composite nanofibrous mats with homogeneous and heterogeneous microstructures. Biomacromolecules 12:2617
26. Zhou CJ, Wang QW, Wu QL (2012) UV-initiated crosslinking of electrospun poly(ethylene oxide) nanofibers with pentaerythritol triacrylate: Effect of irradiation time and incorporated cellulose nanocrystals. Carbohydr Polym 87:1779
27. Lu P, Hsieh Y-L (2009) Cellulose nanocrystal-filled poly(acrylic acid) nanocomposite fibrous membranes. Nanotechnology 20:415604
28. Medeiros ES, Mattoso LHC, Ito EN, Gregorski KS, Robertson GH, Offeman RD, Wood DF, Orts WJ, Imam SH (2008) Electrospun nanofibers of poly(vinyl alcohol) reinforced with cellulose nanofibrils. J Biobased Mater Bioenergy 2:231
29. Peresin MS, Habibi Y, Zoppe JO, Pawlak JJ, Rojas OJ (2010) Nanofiber composites of polyvinyl alcohol and cellulose nanocrystals: Manufacture and characterization. Biomacromolecules 11:674
30. Peresin MS, Habibi Y, Vesterinen A-H, Rojas OJ, Pawlak JJ, Seppälä JV (2010) Effect of moisture on electrospun nanofiber composites of poly(vinyl alcohol). Biomacromolecules 11:2471
31. Lee J, Deng YL (2012) Increased mechanical properties of aligned and isotropic electrospun PVA nanofiber webs by cellulose nanowhisker reinforcement. Macromol Res 20:76
32. Ago M, Okajima K, Jakes JE, Park S, Rojas OJ (2012) Lignin-based electrospun nanofibers reinforced with cellulose nanocrystals. Biomacromolecules 13:918
33. Xiang CH, Joo YL, Frey MW (2009) Nanocomposite fibers electrospun from poly(lactic acid)/cellulose nanocrystals. J Biobased Mater Bioenergy 3:147
34. Herrera NV, Mathew AP, Wang LY, Oksman K (2011) Randomly oriented and aligned cellulose fibres reinforced with cellulose nanowhiskers, prepared by electrospinning. Plast Rubber Compos 40:57
35. Martínez-Sanz M, Olsson RT, Lopez-Rubio A, Lagaron JM (2011) Development of electrospun EVOH fibres reinforced with bacterial cellulose nanowhiskers. Part I: Characterization and method optimization. Cellulose 18:335
36. Martínez-Sanz M, Olsson RT, Lopez-Rubio A, Lagaron JM (2012) Development of bacterial cellulose nanowhiskers reinforced EVOH composites by electrospinning. J Appl Polym Sci 124:1398
37. Huang J, Liu L, Yao JM (2011) Electrospinning of bombyx mori silk fibroin nanofiber mats reinforced by cellulose nanowhisker. Fibers Polym 12:1002
38. Rojas OJ, Montero GA, Habibi Y (2009) Electrospun nanocomposites from polystyrene loaded with cellulose nanowhiskers. J Appl Polym Sci 113:927
39. Olsson RT, Krämer R, López-Rubio A, Torres-Giner S, Ocio MJ, Lagarón JM (2010) Extraction of microfibrils from bacterial cellulose networks for electrospinning of anisotropic biohybrid fiber yarns. Macromolecules 43:4201
40. Dong H, Strawhecker KE, Snyder JF, Orlicki JA, Reiner RS, Rudie AW (2012) Cellulose nanocrystals as a reinforcing material for electrospun poly(methyl methacrylate) fibers: Formation, properties and nanomechanical characterization. Carbohydr Polym 87:2488
41. Magalhães WLE, Cao XD, Lucia LA (2009) Cellulose nanocrystals/cellulose core in-shell nanocomposite assemblies. Langmuir 25:13250
42. van den Berg O, Capadona JR, Weder C (2007) Preparation of homogeneous dispersions of tunicate cellulose whiskers in organic solvents. Biomacromolecules 8:1353
43. Viet D, Beck-Candanedo S, Gray DG (2007) Dispersion of cellulose nanocrystals in polar organic solvents. Cellulose 14:109

44. Dong H, Nyame V, Macdiarmid AG, Jones WE (2004) Polyaniline/poly(methyl methacrylate) coaxial fibers: The fabrication and effects of the solution properties on the morphology of electrospun core fibers. J Polym Sci B Polym Phys 42:3934
45. Xu CY, Inai R, Kotaki M, Ramakrishna S (2004) Aligned biodegradable nanofibrous structure: A potential scaffold for blood vessel engineering. Biomaterials 25:877
46. Wang M, Jin H-J, Kaplan DL, Rutledge GC (2004) Mechanical properties of electrospun silk fibers. Macromolecules 37:6856
47. Tan EPS, Ng SY, Lim CT (2005) Tensile testing of a single ultrafine polymeric fiber. Biomaterials 26:1453
48. Bazbouz MB, Stylios GK (2010) The tensile properties of electrospun nylon 6 single nanofibers. J Polym Sci B Polym Phys 48:1719
49. Fortunato G, Zimmermann T, Lubben J, Bordeanu N, Hufenus R (2012) Reinforcement of polymeric submicrometer-sized fibers by microfibrillated cellulose. Macromol Mater Eng 297:576

Optically Transparent Nanocomposites

18

Antonio Norio Nakagaito and Hitoshi Takagi

Contents

Flexible circuit boards are ubiquitous components in electronic products, and eventually the substrate of image displays will soon be made of flexible materials as well. Plastics are prospective candidates due to their inherent flexibility and optical qualities, but they also present large thermal expansion. The expansion of the substrate has to be compatible with those of the active layers deposited on it, to avoid damages during the thermal cycles involved in the display manufacture. One way to reduce the thermal expansion of plastics is to reinforce them with nanofibers, without significant loss of transparency. Nanofibers are available in large amounts in the form of cellulose in nature, being produced by plants and animals. Here some of the researches to produce optically transparent composites based on natural nanofibers for use in flexible displays are presented and discussed.

A.N. Nakagaito (✉)
Department of Mechanical Engineering, Graduate School of Engineering, The University of Tokushima, Tokushima, Japan
e-mail: nakagaito@tokushima-u.ac.jp

H. Takagi
Advanced Materials Division, Institute of Technology and Science, The University of Tokushima, Tokushima, Japan
e-mail: takagi@tokushima-u.ac.jp

J.K. Pandey et al. (eds.), *Handbook of Polymer Nanocomposites. Processing, Performance and Application – Volume C: Polymer Nanocomposites of Cellulose Nanoparticles*,
DOI 10.1007/978-3-642-45232-1_68,

1 Introduction

Flexible circuits have a longer history than usually thought. As early as in the beginning of the twentieth century, electrical conductors deposited on flat substrates were considered for use in telephony switching for exchanging lines and to replace complex wire harnesses in radios. The nascent electronics industry was seeking circuit technologies for automated mass production. These early rigid substrates later evolved and became flexible, and nowadays flexible electronics are present in virtually any electrical or electronic product where space, shape constraints, or electrical connection of moving parts is are required. As flexible electronics progresses, soon flexible substrates will be used in solar panels that can be wrapped to the surfaces of buildings and in displays that can be rolled for portability or integrated in garments.

Displays require switching of the individual pixels by a thin-film transistor (TFT) circuit that provides a controlled current source to turn the pixels on or off. For that, displays require an inorganic TFT backplane deposited on the substrate, which means it is subjected to thermal stress cycles during panel manufacture, hence requiring extremely low coefficient of thermal expansion (CTE) for the substrate material. The use of flexible plastic substrates instead of the traditional rigid glass brings the possibility to make tough, thin, and lightweight panels that flex, bend, and conform to various shapes. Cost-effective roll-to-roll processing becomes a possibility in manufacturing as well. However, plastic substrates still have to offer the high transparency, surface smoothness, barrier capacity, solvent resistance, thermal and dimensional stability, and reduced thermal expansion of glass. Bottom-emissive displays in which images are viewed through the substrate require a total light transmittance greater than 85 % over the visible spectrum (400–800 nm), with a haze of less than 0.7 % [1]. The barrier and solvent resistance can be achieved by applying a hard coating, whereas the surface smoothness is obtained through a scratch-resistant coating. The thermal and dimensional stabilities are properties intrinsic to the material, so a proper selection of the type of plastics is needed in order to resist the high temperatures and thermal cycles during the deposition of coatings and active layers during manufacture. However, the required CTE should be typically below $2.0 \times 10^{-5}\ ^{\circ}C^{-1}$ to avoid any mismatch in thermal expansion relative to the device layers deposited on the substrate, otherwise they would be strained and damaged during a thermal cycle [1].

From an atomistic view of materials, thermal expansion and Young's modulus are both correlated to the depth of the atomic bond energy function, but the relationship between the two properties is inversely proportional. Therefore, flexible plastics having low modulus exhibit intrinsically high CTEs. To reduce the CTE of plastics while preserving its flexibility, one possibility is to reinforce it with fibers possessing low CTE. However, the inclusion of elements even at micrometer sizes reduces the transparency, unless the refractive indexes of fibers and plastic material are exactly matched. A better approach is to use tinier nanofibers instead of microfibers, with lateral dimensions much smaller than the wavelength of

the visible light. This required dimension should be an order of magnitude smaller than the wavelength of visible light, meaning sizes in the order of 40–80 nm or lower. Such nanofibers are already available in nature as renewable resources and in large quantities, in the form of a biopolymer called cellulose.

This chapter will give a brief overview of the studies on transparent nanocomposites based on cellulose nanofibers, especially on the efforts to reduce the thermal expansion of polymeric resins aiming the application as substrates in flexible electronics.

2 Cellulose Nanofiber-Reinforcement to Restrict the Thermal Expansion of Transparent Plastics

Cellulose nanofibers consist of semicrystalline cellulose molecular chains arranged parallel to their axes. In the crystalline domains, the cellulose chains are lined up and laterally connected to each other by hydrogen bonds, forming a highly ordered crystalline structure. Each molecule of cellulose consists of glucose rings joined together without foldings, just as the benzene rings are joined in aramid, and therefore even the density and the modulus of the two materials are very similar [2]. The Young's modulus of the cellulose nanofiber is close to that of a perfect cellulose crystal, at 138 GPa [3], and the estimated tensile strength is well beyond 2 GPa. The first report of a transparent nanocomposite reinforced by cellulose nanofibers is due to Yano et al. in 2005 [4], in which cellulose nanofibers synthesized by bacteria, called bacterial cellulose (BC), were used as the reinforcing phase of a transparent resin matrix. BC consists of a network of ribbon-shaped fibrils less than 100 nm in width and, because of the huge exposed hydrophilic surface area, contains about 99 wt% of water. These were compressed to remove the excess water and completely dried; impregnated with acrylic, epoxy, and phenol-formaldehyde resins; and cured by UV light or hot pressed depending on the matrix. The obtained composites had fiber contents between 60 and 70 wt%.

Despite the high nanofiber content, the total light transmittance in the visible wavelength between 500 and 800 nm was greater than 80 %. The reduction of light transmittance relative to the neat matrix resin due to the reinforcement was less than 10 percentage points. In conventional microcomposites, the light transmittance is primarily controlled by the matching of the refractive indexes of the fibers and the matrix, and so transparency is severely reduced if there is a slight mismatch. At a temperature of 23 °C, the refractive index of cellulose is 1.618 along the fiber and 1.544 in the transverse direction, whereas that of the impregnated phenol-formaldehyde, for instance, is 1.483 at 587.6 nm. Similar differences hold for the other types of resin employed. The high transparency is due primarily to the reduced lateral size of the reinforcing elements, because the scattering of light is prevented by nanofibers much smaller than the wavelength of light.

In terms of mechanical properties, the CTE of the BC/epoxy composite was largely reduced from the $120 \times 10^{-6}\,K^{-1}$ of the epoxy matrix to just $6 \times 10^{-6}\,K^{-1}$.

The CTE of BC/phenol-formaldehyde was even lower at 3×10^{-6} K^{-1}. The tensile strength reached 325 MPa with a modulus around 20–21 GPa. Despite the high modulus, BC nanocomposites are flexible, light, and highly transparent.

To study the extent of the effects caused by the mismatch between the refractive indexes of matrix and nanofibers, Nogi et al. [5] evaluated the changes in transparency of BC nanocomposites in relation to the refractive index of the matrix acrylic resin. At a wavelength of 590 nm, the total and regular transmittances were above 85 % and 75 %, respectively, when the refractive index of the resin varied from 1.492 to 1.636. Similarly the regular transmittance of composites did not vary when the matrix refractive index varied by 0.014 due to a temperature variation from room temperature to 80 °C, as shown in Fig. 18.1. In BC-reinforced acrylic resin [6], the transmittance is linearly reduced with increasing fiber contents, but the reduction is just 13.7 percentage points from the neat resin to the composite at a fiber content of 66 wt%. Meanwhile, the coefficient of thermal expansion is suppressed with the addition of BC nanofibers, from 86×10^{-6} K^{-1} of the neat acrylic resin to just 15×10^{-6} K^{-1} at around 30 wt% fiber content, and to 10×10^{-6} K^{-1} at a 50 wt% fiber content.

Despite the good characteristics, an intrinsic drawback of cellulose is the high hygroscopicity due to the presence of hydroxyl groups in their molecular chains, making cellulose-based materials highly hydrophilic. To reduce the susceptibility of BC nanocomposites to moisture, Nogi et al. [7] and Ifuku et al. [8] acetylated the BC nanofibers, replacing the hydroxyl groups on the surface of the fibers with acetyl groups. When exposed to a 55 % relative humidity at room temperature, the untreated BC composite at 60 wt% fiber content had a 3.12 % moisture content, whereas the acetylated BC composite had the moisture content reduced to 1.33 % at a fiber load of 66 wt%. Besides, the CTE of the BC sheet improved from 3×10^{-6} K^{-1} of untreated to just 0.8×10^{-6} K^{-1} of the acetylated sheet, even though the Young's modulus was reduced from 23.1 to 17.3 GPa. This reduction in CTE might be due to the better compatibility of the less hydrophilic acetylated BC with the hydrophobic matrix. The regular transmittance in one of the BC/acrylic resin combinations revealed that the acetylated BC had increased transparency in the wavelength around 400 nm, keeping unchanged the transparency in the rest of the spectrum. The scanning electron microscopy images showed that the untreated BC sheet is densely packed, whereas the acetylated one shows nanofibers separated from each other, implying that the presence of acetyl groups in the surface of fibrils prevented their aggregation through hydrogen bonds, keeping the uniformity of the individualized nanosized lateral dimensions of the nanofibers. The resistance to thermal degradation in terms of optical transparency was also improved as the acetylated BC nanocomposite showed a lower drop in transmittance than the untreated BC nanocomposite when both were exposed to a temperature of 200 °C for several hours.

To further decrease the thermal expansion of composites, especially at a fiber content as low as 5 wt%, BC was combined with a low Young's modulus transparent resin [9]. As the modulus of the resin was only 25 MPa, the resulting composite had a modulus of 355 MPa, in the order of high-density polyethylene.

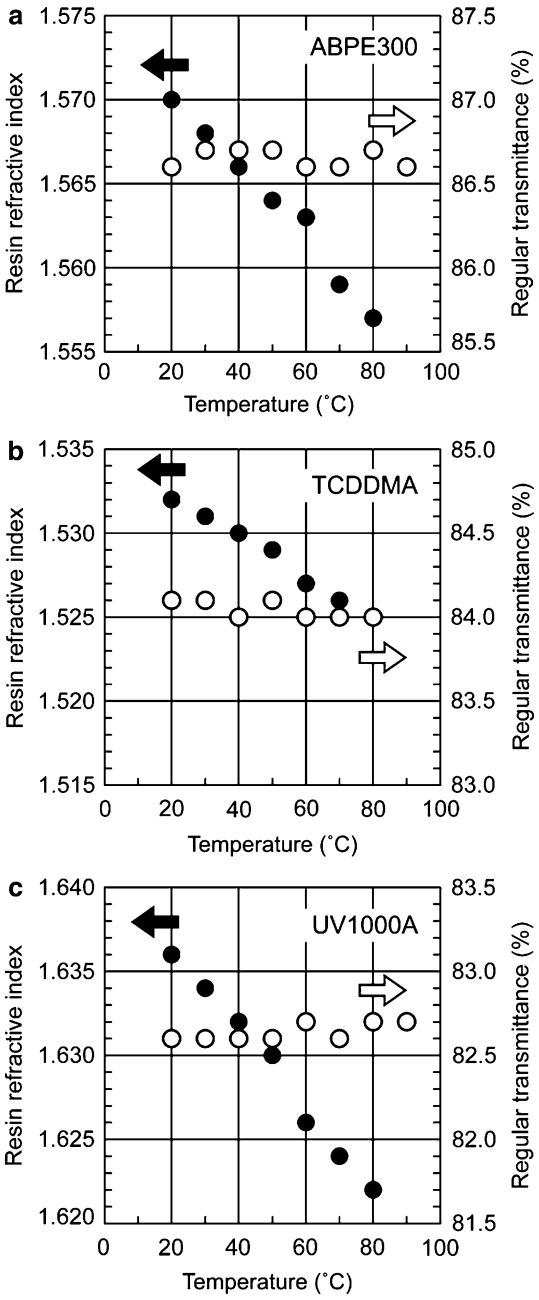

Fig. 18.1 Light transmittances of bacterial cellulose-based composites and corresponding refractive indexes of matrix resin as a function of temperature. Three different matrixes are shown, with large variations in refractive index, but the transmittance of composites is constant [5]

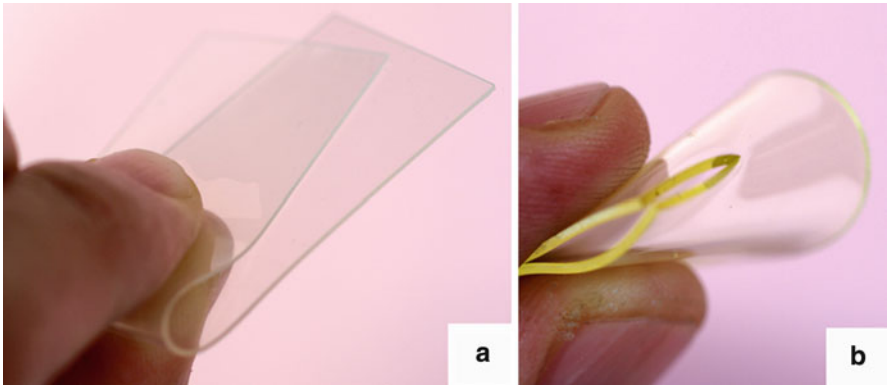

Fig. 18.2 Bacterial cellulose-reinforced composite being folded (*left*), compared to fragile neat resin (*right*) [9]

This low modulus made the composite not only extremely flexible but even foldable without causing damage (Fig. 18.2). Despite the low modulus, the in-plane CTE was unusually low at just 4×10^{-6} K^{-1}. In general, higher Young's moduli translate into lower CTEs, so the phenomenon was explained by the unique structure of BC pellicles consisting of multiple layers of nanofiber networks which form strong in-plane networks but are weakly connected along the thickness direction of the pellicles. Even at low contents, fibers are able to restrain the small stresses generated by the expansion of the low modulus matrix in the in-plane direction, while in the thickness direction, the material is free to expand. This anisotropic behavior results in ultra-low in-plane CTE but also allows enhanced flexibility for the material to be folded.

Bacterial cellulose appears to be a good source of nanofibers to produce transparent composites, but the fermentation processes employed to produce BC are extremely slow. An alternative resource would be the more abundant wood or plant fibers, but the nanofibers have to be extracted before use. Cellulose nanofibers are found embedded in a matrix of hemicelluloses and lignin in the fiber cell wall of plants, in a fairly complex structure (Fig. 18.3). In order to fibrillate wood pulp fibers and reduce the size of fibril bundles to a greater extent.

Iwamoto et al. started with a commercially available cellulose morphology known as microfibrillated cellulose (MFC), obtained by refining and high-pressure homogenization processes. He complemented the refining/high-pressure homogenization steps with an additional grinding treatment [10]. MFC obtained by 14 passes through the homogenizer has a wide distribution of fibrils width, from some tens of nanometers to some micrometers, that produces composites significantly less transparent than BC-based composites. The reduced transparency is attributed to light scattering caused by the thicker fibril elements. The 14 passes through homogenizer MFC was supplemented with a grinding treatment, in a total of 10 passes through the grinder, resulting in fibril bundles with

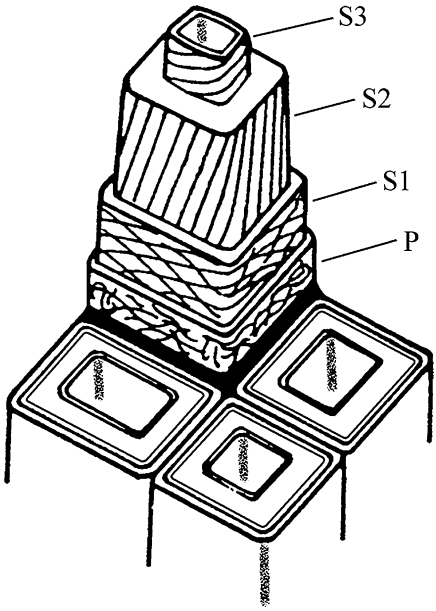

Fig. 18.3 Multilayered structure of a wood fiber cell wall. The fine lines seen in layers labeled *P*, *S1*, *S2*, and *S3* represent cellulose nanofibers [24]

dimensions 50–100 nm in width. This grinder-fibrillated MFC was dispersed in water and the suspension was vacuum filtered, producing a thin sheet. Sheets were oven dried, impregnated with acrylic resin, and cured by UV light, and the light transmittance of grinder-fibrillated fiber/acrylic resin composite, pure acrylic resin, BC/acrylic resin, and homogenizer-fibrillated fiber/acrylic resin was measured. At the wavelength of 600 nm, grinder-fibrillated fiber/acrylic composites with 70 wt% fiber content showed a total transmittance of 70 %, meaning a transmission reduction of just 20 percentage points from the transmittance of the pure acrylic resin. In contrast, the light transmittance of homogenizer-fibrillated fiber/acrylic composites at a 62 wt% fiber content was only 30 %. The BC/acrylic resin showed the highest transmittance of all, but as plant fibers consist of elementary cellulose microfibrils 4 nm by 4 nm in cross section, an improved fibrillation process might lead to higher light transmittances, or even exceed those of BC composites. The CTE of the matrix resin was reduced from $86 \times 10^{-6}\ K^{-1}$ of neat resin to $17 \times 10^{-6}\ K^{-1}$. The Young's modulus of 7 GPa was lower than the modulus of BC composites, but a lower modulus means a more flexible material.

In order to extract higher-quality nanofibers by grinding, Abe et al. [11] developed a new protocol that produced uniform nanofibers with 15 nm in diameter by only one pass through the grinder to minimize the damage to the nanofibers. In previous studies by Iwamoto et al., the severity of mechanical shear applied by the grinder to fibrillate was evaluated based on the mechanical properties of the final nanocomposites [12]. Although the transparency of composites increased up to

five passes through the grinder and above it, neither transparency nor the morphology of the nanofibers had changed. But the tensile and thermal expansion properties were significantly reduced, due to the decrease of crystallinity and degree of polymerization of cellulose. The role of hemicelluloses on nanofibrillation [13] was also clarified. When pulp fibers are dried, the presence of hemicelluloses impedes the formation of irreversible hydrogen bonds between the cellulose microfibrils. And by rewetting, hemicelluloses are plasticized by absorbing water, facilitating posterior nanofibrillation. Abe chose to keep the fiber in a water-swollen state after chemical removal of hemicelluloses and lignin, skipping the drying process in a typical pulp production that would generate strong hydrogen bonds between the nanofibers. Okahisa et al. [14] later fabricated an optically transparent film made of a low Young's modulus resin reinforced with cellulose nanofibers extracted from wood by the new method, using it as a substrate on which an organic light-emitting diode (OLED) layer was deposited.

An even simpler method to extract cellulose nanofibers by chemical means was reported by Saito et al. [15]. By oxidizing the surface of the nanofibers by a 2,2,6,6-tetramethylpiperidine-1-oxyl (TEMPO) radical catalyzed process, C6 hydroxyl groups of cellulose on the surface of the nanofibers were converted into negatively charged sodium carboxylate groups. The electrostatic repulsion loosened the mutual adhesion of the nanofibers so that a posterior mechanical agitation by a Waring blender was enough to individualize the original fibers into nanofibers 3–5 nm in diameter. The films obtained by filtration of these nanofibers [16] were optically transparent, with transmittances above 85 % over the visible spectrum. The tensile strength of the films was similar to that of cellulose nanofiber paper of Nogi et al. [17], while the coefficient of thermal expansion was as low as $2.7 \times 10^{-6}\ K^{-1}$, even though the Young's modulus was around half of Nogi's paper. The films exhibited high oxygen-barrier properties as well. When nanofibers were composed with polystyrene resin [18] at a 10 wt% fiber load, the light transmittance of composite at 600 nm dropped only 3 percentage points from the 89 % of neat resin. Meanwhile the CTE was reduced from $116 \times 10^{-6}\ K^{-1}$ to $63.7 \times 10^{-6}\ K^{-1}$. These relative reductions are similar to values reported by Nogi et al. [6] on bacterial cellulose-reinforced acrylic resin, at a comparable fiber content. Nonetheless, these nanofibers obtained by TEMPO-mediated oxidation are finer in diameter and produced by less energy-intensive extraction than mechanical methods and extracted by faster means than fermentation methods to produce bacterial cellulose.

Another approach to overcome the costly extraction process of nanofibers is producing them through electrospinning. Liu et al. [19] used a mixture of acetone and *N*,*N*-dimethylacetamide (DMAc) as solvent for cellulose acetate and spun it into continuous fibers with nanoscale diameter. These cellulose acetate nanofibers were additionally treated to hydrolyze the acetyl groups and regenerate the hydroxyl groups, to obtain cellulose nanofibers. Composites were prepared using polyvinyl alcohol (PVA) as the matrix resin, and optically transparent films were obtained [20]. To evaluate the parameters affecting transparency [21], PVA was reinforced with cellulose acetate nanofibers and regenerated cellulose nanofibers with diameters in the range of 250–940 nm, and regenerated cellulose

nanofibers of smaller diameter and narrower range of 160–290 nm. The neat PVA showed a transmittance of about 92 % in the middle of the visible spectrum. The cellulose acetate nanofiber composite at 20 wt% fiber content had the transmittance reduced to about 80 %, dropping to only 18 % at 50 wt% fiber load. Meanwhile, the regenerated cellulose nanofiber counterpart with the same diameter exhibited a transmittance over 85 % at fiber contents up to 30 wt%, reducing to 38 % at 50 wt% fiber content. The smaller regenerated cellulose nanofiber-reinforced PVA films, however, exhibited transmittance of 90 % for fiber loads up to 30 wt%, staying in the 85–88 % range at 40 wt% fiber content, reaching 55 % at a fiber content of 60 wt%. This study confirmed the relevance of the size of fibers but also drew attention to their interfacial adhesion with the matrix resin. Cellulose acetates are more hydrophobic than regenerated cellulose, thus less compatible with hydrophilic PVA. Light reflections and refractions are reduced by stronger fiber-matrix adhesion of cellulose-PVA interfaces that produces gradual variation in optical impedances, resulting in enhanced transparency.

An optically transparent paper was later developed, without the use of matrix resins. It was called by Nogi et al. [17] "cellulose nanofiber paper", and it is strictly made of the same chemical constituents of conventional paper, but with a physical difference in the size of the fibers, the nanofibers obtained by the protocol developed by Abe et al. [11]. The only difference from ordinary paper resides in the morphology of cellulose. A nanofiber aqueous suspension was filtered and dried, turning into nanofiber paper with a density of 1.53 g/cm^3, quite close to the 1.59 g/cm^3 of the cellulose crystallite [22]. The small interfibrillar cavities were practically eliminated, what was confirmed by scanning electron microscopy observations. This paper was initially just translucent, but once the roughness of its surfaces was minimized by careful polishing, the transparency at 600 nm wavelength reached 71.6 %. The coefficient of thermal expansion of 8.5×10^{-6} K^{-1} was similar to that of glass, along a tensile modulus of 13 GPa and a strength of 223 MPa. Authors also coated the cellulose nanofiber paper with transparent resins to smooth out the surfaces [23] and suggested the possibility of continuous roll-to-roll manufacturing methods.

3 Conclusions and Prospects

Cellulose is produced by nature in the form of nanofibers to make remarkably useful nanocomposites for specific purposes of living matter, as wood in the trunk of trees, plant fibers in stems and leafs, bacterial cellulose, tunicates, and so forth. Humans can extract these nanofibers and reconstitute them to make new composites with different properties, destined to applications not intended by their natural evolution. As once happened with the prosaic paper that serves our everyday needs, cellulose offers again the potential to become the reinforcing phase of transparent plastics for flexible electronic-based devices. Whether this potential becomes a commercial reality or not, the fundamental research so far realized will serve as the basis for other new materials to come.

References

1. McDonald BA, Rollins K, MacKerron D, Rakos K, Eveson R, Hashimoto K, Rustin B (2005) Engineered films for display technologies. In: Crawford GP (ed) Flexible flat panel displays. Wiley, Society for Information Display, New York, pp 11–34
2. Gordon JE (1976) The new science of strong materials. Princeton University Press, New Jersey, p 201
3. Nishino T, Takano K, Nakamae K (1995) Elastic modulus of the crystalline regions of cellulose polymorphs. J Polym Sci Part B Polym Phys 33:1647
4. Yano H, Sugiyama J, Nakagaito AN, Nogi M, Matsuura T, Hikita M, Handa K (2005) Optically transparent composites reinforced with networks of bacterial nanofibers. Adv Mater 17:153
5. Nogi M, Handa K, Nakagaito AN, Yano H (2005) Optically transparent bionanofiber composites with low sensitivity to refractive index of the polymer matrix. Appl Phys Lett 87:243110
6. Nogi M, Ifuku S, Abe K, Handa K, Nakagaito AN, Yano H (2006) Fiber-content dependency of the optical transparency and thermal expansion of bacterial nanofiber reinforced composites. Appl Phys Lett 88:133124
7. Nogi M, Abe K, Handa K, Nakatsubo F, Ifuku S, Yano H (2006) Property enhancement of optically transparent bionanofiber composites by acetylation. Appl Phys Lett 89:233123
8. Ifuku S, Nogi M, Abe K, Handa K, Nakatsubo F, Yano H (2007) Surface modification of bacterial cellulose nanofibers for property enhancement of optically transparent composites: dependence on acetyl-group DS. Biomacromolecules 8:1973
9. Nogi M, Yano H (2008) Transparent nanocomposites based on cellulose produced by bacteria offer potential innovation in the electronics device industry. Adv Mater 20:1849
10. Iwamoto S, Nakagaito AN, Yano H, Nogi M (2005) Optically transparent composites reinforced with plant fiber-based nanofibers. Appl Phys A Mater Sci Process 81:1109
11. Abe K, Iwamoto S, Yano H (2007) Obtaining cellulose nanofibers with a uniform width of 15 nm from wood. Biomacromolecules 8:3276
12. Iwamoto S, Nakagaito AN, Yano H (2007) Nano-fibrillation of pulp fibers for the processing of transparent nanocomposites. Appl Phys A Mater Sci Process 89:461
13. Iwamoto S, Abe K, Yano H (2008) The effect of hemicelluloses on wood pulp nanofibrillation and nanofiber network characteristics. Biomacromolecules 9:1022
14. Okahisa Y, Yoshida A, Miyaguchi S, Yano H (2009) Optically transparent wood-cellulose nanocomposite as a base substrate for flexible organic light-emitting diode displays. Compos Sci Technol 69:1958
15. Saito T, Nishiyama Y, Putaux JL, Vignon M, Isogai A (2006) Homogeneous suspensions of individualized microfibrils from TEMPO-catalyzed oxidation of native cellulose. Biomacromolecules 7:1687
16. Fukuzumi H, Saito T, Wata T, Kumamoto Y, Isogai A (2009) Cellulose nanofibers prepared by TEMPO-mediated oxidation of native cellulose. Biomacromolecules 10:162
17. Nogi M, Iwamoto S, Nakagaito AN, Yano H (2009) Optically transparent nanofiber paper. Adv Mater 21:1595
18. Fujisawa S, Ikeuchi T, Takeuchi M, Saito T, Isogai A (2012) Superior reinforcement effect of TEMPO-oxidized cellulose nanofibrils in polystyrene matrix: optical, thermal, and mechanical studies. Biomacromolecules 13:2188
19. Liu HQ, Hsieh HL (2002) Ultrafine fibrous cellulose membranes from electrospinning of cellulose acetate. J Polym Sci Part B Polym Phys 40:2119
20. Tang C, Liu HQ (2008) Cellulose nanofiber reinforced poly(vinyl alcohol) composite film with high visible light transmittance. Compos Part A 39:1638
21. Tang C, Wu M, Wu Y, Liu HQ (2011) Effects of fibers surface chemistry and size on the structure and properties of poly(vinyl alcohol) composite films reinforced with electrospun fibers. Compos Part A 42:1100

22. Sugiyama J, Vuong R, Chanzy H (1991) Electron diffraction study on the two crystalline phases occurring in native cellulose from an algal cell wall. Macromolecules 24:4168
23. Nogi M, Yano H (2009) Optically transparent nanofiber sheets by deposition of transparent materials: A concept for a roll-to-roll processing. Appl Phys Lett 94:233117
24. Nakagaito AN, Yano H (2005) Novel high-strength biocomposites based on microfibrillated cellulose having nano-order-unit web-like network structure. Appl Phys A Mater Sci Process 80:155

Applications of Cellulose Acetate Nanofiber Mats

19

Orawan Suwantong and Pitt Supaphol

Contents

Abstract

Electrospinning is an efficient process for fabrication of polymeric ultrafine fibers with diameters ranging from sub-micrometer to nanometer. It involves the application of a strong electric field across a conductive capillary attaching to a polymer liquid-containing reservoir and a collector. The obtained ultrafine fibers exhibit several interesting characteristics, e.g., high surface area to mass or volume ratio, high porosity, vast possibilities for surface functionalization, etc. These unique characteristics make them used in various applications such

O. Suwantong (✉)
School of Science, Mae Fah Luang University, Muang, Chiang Rai, Thailand
e-mail: o.suwantong@gmail.com

P. Supaphol
The Petroleum and Petrochemical College (PPC) and The Center of Excellence on Petrochemical and Materials Technology (PetroMAT), Chulalongkorn University, Pathumwan, Bangkok, Thailand
e-mail: pitt.s@chula.ac.th

J.K. Pandey et al. (eds.), *Handbook of Polymer Nanocomposites. Processing, Performance and Application – Volume C: Polymer Nanocomposites of Cellulose Nanoparticles*,
DOI 10.1007/978-3-642-45232-1_70,

as biomedical, pharmaceutical, and industrial applications, etc. Cellulose acetate, the acetate ester of cellulose, has been widely used as fibers. Recently, the electrospinning of cellulose acetate has been attracted due to its good thermal stability, chemical resistance, biocompatibility, biodegradability, etc. These properties render it suitable for use in various applications including tissue engineering, drug delivery system, wound dressing, separation membrane, etc. This chapter covers research related to electrospinning of cellulose acetate and the potential applications of cellulose acetate fibers.

Keywords
Electrospinning • Cellulose acetate • Wound dressing • Tissue engineering • Drug delivery system • Membrane • Sensor

1 Introduction

1.1 Electrospinning

In the past decade, electrospinning or the electrostatic spinning technique has been recognized as the most interesting technique to produce continuous ultrafine fibers with diameters ranged from microns down to nanometers. In the electrospinning process, a polymer solution held by its surface tension at the end of a capillary tube is subjected to an electric field. Charge is induced on the liquid surface by an electric field. Mutual charge repulsion causes a force directly opposite to the surface tension. As the intensity of the electric field is increased, the hemispherical surface of the solution at the tip of the capillary tube elongates to form a conical shape known as the Taylor cone. When the electric field reaches a critical value at which the repulsive electric force overcomes the surface tension force, a charged jet of the solution is ejected from the tip of the Taylor cone. As the jet travels in air, the solvent evaporates, leaving behind a charged polymer fiber which lays itself randomly on a collecting metal screen. Thus, continuous fibers are laid to form a nonwoven fabric [1–3]. The three major components of electrospinning process are (1) a polymer reservoir attached to a small capillary tube, (2) a high-voltage power supply, and (3) a screen collector (Fig. 19.1) [4].

Various parameters can affect the formation and morphology of the obtained electrospun fibers. These parameters can be divided into two major classes which are system and process parameters. The system parameters affecting the formation and structure of the obtained electrospun fibers are polymer concentration [5, 6], solvent volatility [7, 8], and solution conductivity [9, 10], while the process parameters are applied voltage [11, 12], polymer flow rate [8, 13], and capillary-collector distance [14, 15]. The obtained electrospun fibers from this process exhibit several interesting characteristics such as a high surface area to mass or volume ratio, high porosity of the nonwoven mat, vast possibilities for surface functionalization, etc. These unique characteristics make these electrospun fibers as candidates for use in various applications such as biomedical, pharmaceutical, and

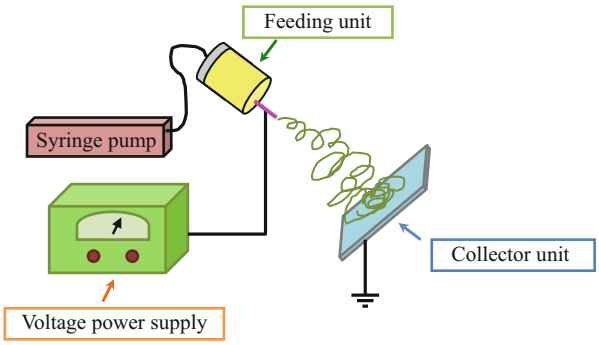

Fig. 19.1 Schematic drawing of electrospinning process [4]

Table 19.1 General properties of CA (40.4 % acetyl content) [25]

Properties	Details
Chemical structure	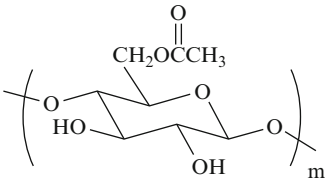
Melting point (°C)	306
Char point (°C)	315
Density (g/ml)	1.28
Tensile strength (MPa)	71.6

industrial applications, etc. [16–20]. Moreover, since electrospinning is a simple process, various natural and synthetic polymers have been electrospun to apply in various applications [21–24].

1.2 Cellulose Acetate

Cellulose acetate (CA) is the acetate ester of cellulose, the primary structural component of the cell wall of green plants and one of the most common biopolymers on earth. In general, CA is prepared from cellulose by a solution process employing sulfuric acid as the catalyst with acetic anhydride in an acetic acid solvent. The acetylation reaction is heterogeneous and topochemical [25]. General properties of CA are shown in Table 19.1.

The properties of CA can be affected by the number of acetyl groups per anhydroglucose unit of cellulose and the degree of polymerization. Fewer acetyl groups per anhydroglucose unit (increased hydroxyl content) increase the solubility in polar solvent and decrease moisture resistance [25].

Solubility characteristics of CA with various acetyl contents are shown in Table 19.2.

Table 19.2 Solubility characteristics of CA [25]

Acetyl, %	Soluble in	Insoluble in
43.0–44.8	Dichloromethane	Acetone
37–42	Acetone	Dichloromethane
24–32	2-methoxymethanol	Acetone
15–20	Water	2-methoxymethanol
<13	None of the above	All of the above

CA is one of the most commercially important cellulose derivatives. It has been used in various applications such as textile fibers, plastics, films, sheeting, membrane separation, cigarette industries, and lacquers. In biomedical applications, CA had been used in drug delivery systems [26–30] wound dressings [31–33], and tissue engineerings [34, 35].

2 Electrospinning of Cellulose Acetate

There are several techniques used for fabricating the ultrafine fibers. Among of them, electrospinning has been interested as the simple technique and can produce the ultrafine fiber from several materials. The electrospinning of CA has been attracted due to its good thermal stability, chemical resistance, biocompatibility, biodegradability, etc. These properties render it suitable for use in various applications including tissue engineering, drug delivery system, wound dressing, membrane, etc. Liu and Hsieh [36] fabricated the ultrafine CA fiber mats as well as regenerated cellulose membranes by electrospinning. Three solvents (acetone, acetic acid, and *N*,*N*-dimethylacetamide (DMAc)) were used for electrospinning of CA. The results showed that none of these solvents alone can produce fibers. An improvement in the electrospinning of CA was achieved when 2:1 v/v acetone/DMAc was used as the solvent system. This mixture allowed the resulting CA solutions with concentration in the range of 12.5–20 wt% to be continuously spun into fibers with diameters ranging between ~100 nm and ~1 μm [36]. In 2004, Son et al. successfully prepared the electrospun CA fiber mats by using a mixture of acetone/water with the water content in the range of 10–15 wt%. Moreover, they found that the electrospinning of a CA solution in acetone/water in an acidic condition produced larger fibers, while that in a basic condition produced much finer ones [37]. The blend electrospun fiber mats of CA and poly(vinyl alcohol) (PVA) were successfully prepared by multi-jet electrospinning [38]. The weight ratio of CA/PVA in the blend electrospun fiber mats could be controlled by changing the number ratio of jets of CA/PVA, since it was difficult to find a good solvent for preparing the blend solution of CA and PVA. The 10 wt% of CA solutions in 2:1 of acetone to DMAc and the 10 wt% of PVA solution in distilled water at 80 °C were used to prepare the blend electrospun fiber mats of CA/PVA [38]. Tungprapa et al. [39] studied the effects of solvent system, solution concentration, and applied electrostatic field strength on the morphology and size of the electrospun CA fiber mats. The CA solutions for electrospinning

were prepared in two systems: the single-solvent system (acetone, chloroform, *N*,*N*-dimethylformamide (DMF), dichloromethane (DCM), methanol (MeOH), formic acid, and pyridine) and the mixed-solvent systems (acetone-DMAc, chloroform-MeOH, and DCM-MeOH). The results showed that the smooth fibers were achieved from 16 % (w/v) CA solution in 1:1, 2:1, and 3:1 (v/v) acetone-DMAc, 14–20 % (w/v) CA solutions in 2:1 (v/v) acetone-DMAc, and 8–12 % (w/v) CA solution in 4:1 (v/v) DCM-MeOH. Moreover, the average diameters of the electrospun CA fibers from the CA solutions in acetone-DMAc ranged between 0.14 and 0.37 μm, while that from the CA solutions in DCM-MeOH ranged between 0.48 and 1.58 μm [39]. Zhang and Hsieh [40] investigated the effect of polymer molecular weight, concentration, mixing composition, and solvent system to the formation of the CA and poly(ethylene oxide) (PEO) bicomponent fibers by electrospinning of binary mixtures of these polymers. The polymer solutions of CA and PEO and their mixtures were prepared in DMF or 1:1 DMF/dioxane mixture. The total polymer concentrations ranged between 5 and 30 wt% and the CA/PEO compositions were 70/30, 50/50, and 30/70 mass ratio. The results showed that the threshold molecular weights of CA and PEO to obtain fiber formation from electrospinning of 20 wt% solutions in DMF were 50 kDa and 100 kDa, respectively. Moreover, the fiber formation could be improved by longer polymer chain lengths of 60 kDa CA and 600 kDa PEO. Addition of a low dielectric constant cosolvent, dioxane, helped the fiber formation from CA alone at a lower 30 kDa and from binary systems with one low molecular weight polymer [40]. A new solvent system for the electrospinning of electrospun CA fiber mats was investigated by Han et al. [41]. The CA solutions were electrospun at a positive voltage of 25 kV, a tip-to-collector distance of 10 cm, and a solution flow rate of 3 $mL \cdot h^{-1}$. Long uniform electrospun CA fibers with an average diameter of 180 nm were obtained from a 17 wt% CA solution in mixed solvent containing acetic acid/water at a ratio of 75:25 by weight. Moreover, the average diameters of the electrospun CA fibers could be controlled from 160 nm to 1,280 nm by changing the composition of the mixed solvent [41]. In 2010, Wongsasulak et al. [42] prepared the edible electrospun fibrous thin films from the blend solutions of CA and egg albumen (EA) by electrospinning. The 20 wt% of CA in 85 % acetic acid and 12 wt% of EA in 50 % formic acid were blended at various ratios (100/0, 91/9, 77/23, 66/34, and 0/100). The results showed that only EA could not be formed the electrospun fiber since it had very high surface tension. Thus, the addition of CA and surfactant (Tween 40®) to the blend solutions facilitated the formation of electrospun CA-EA blend fibers since it decreased both the electrical conductivity and the surface tension of the blends [42]. The effect of thermal and alkali treatment on the structural stability of electrospun cellulose fiber mats prepared by electrospinning was investigated by Greish et al. [43]. Since cellulose was difficult to dissolve in traditional solvents, electrospinning of 10–20 wt% of CA in 2:1 of acetone/DMAc solvent mixtures followed by regeneration of cellulose was more convenient method. They found that thermal treatment of the electrospun CA fiber mats followed by deacetylation in alkaline solution damaged the morphology of fibers [43]. The ultrafine polyethylene glycol (PEG)/CA composite fibers with various PEG contents were fabricated as phase change fibers by electrospinning [44]. A 15 wt% of CA solution in 2:1 of

acetone/DMAc was mixed with PEG at various contents (i.e., 10, 20, 30, 40, 50, 60, 70 wt%). The blend solutions were electrospun at a positive voltage of 14 kV, a tip-to-collector distance of 15 cm, and a solution flow rate of 3 mL · h^{-1}. The results showed that the obtained morphology and average diameter of the composite fibers varied with PEG content [44]. In 2011, Baek et al. [45] fabricated the electrospun CA/poly(butyl acrylate) (PBA) fiber mats by electrospinning. They used CA as a matrix and PBA as an adhesive. The 18 wt% of CA solutions in 8:2 of acetone/DMF were mixed with PBA at various ratio (i.e., 10/90, 20/80, and 30/70). Moreover, 2 wt% of isocyanate which acts as heat hardener was added into the blend solutions with respect to amounts of the PBA. The blend solutions were electrospun at a positive voltage of 15 kV, a tip-to-collector distance of 18 cm, and a solution flow rate of 1 μL · min^{-1}. The results showed that the morphology of the blend fiber mats with different PBA concentrations exhibited the point-bonded fiber uniformly distributed throughout the fiber mats [45].

3 Applications of Cellulose Acetate Nanofiber Mats

3.1 Tissue Engineering

There are several considerations for using electrospun fibers in tissue engineering, including type and morphology of material, porosity, surface modification, and tissue application. Almost all of the human tissues and organs have fibrous network to provide mechanical integrity to them. For the treatment of injured or defective tissues or organs, biocompatible materials are designed and fabricated to form structure that mimics the structure and biological functions of extracellular matrix (ECM). As a result, electrospun fiber mats act as temporary supports for cells to regenerate the cellular matrix that has been destroyed by disease, injury, or defects. In addition, the electrospun fiber mats should be biocompatible, biodegradable, and porous for allowing cell attachment and proliferation. The electrospinning of CA solutions containing alkannin and shikonin (A/S) was reported by Kontogiannopoulos et al. [34], since alkannin and shikonin (A/S) are naturally occurring hydroxynaphthoquinones. Moreover, they had various properties including with wound healing, antimicrobial, anti-inflammatory, antioxidant, and antitumor activity. They varied the shikonin concentrations ranging 0 %, 1 %, 2 %, 3 %, 4 %, 5 %, and 10 % wt. (based on the weight of CA) to incorporate into the electrospun CA fiber mats. Since the incorporation of A/S mixture into the electrospun CA fiber mats resulted in lower costs of the final materials, the varied concentrations (e.g., 3 %, 5 %, and 10 % wt.) of the A/S mixture were incorporated into the electrospun CA fiber mats. They found that the incorporation of drugs did not affect the morphology of fibers and their mean diameter size varied from 315 to 670 nm. The release characteristics of the electrospun CA fiber mats containing shikonin and derivatives showed an initial rapid release of the drug followed by a slower second stage until reaching a plateau after 48 h. Therefore, these electrospun fiber mats could be the potential tissue engineering scaffolds for repairing and regenerating tissues and mainly skin [34].

Gouma et al. [35] prepared the electrospun CA fiber mats containing nano-hydroxyapatite (n-HA) as an artificial bone tissue scaffolds. They found that these scaffolds promoted adhesion and growth of osteoblasts and also stimulated the cells to exhibit functional activity of bone cells. Hence, these scaffolds could be considered as a promising candidate for bone tissue engineering application [35].

3.2 Drug Delivery Systems

Drug delivery systems are used to improve therapeutic efficiency and safety of drugs by delivering them a rate dictated by the need of the physiological environment over a period of treatment to the site of action. Electrospinning has great flexibility in selecting materials; several biocompatible polymeric materials have been used to produce the fiber matrices for drug delivery. Moreover, it has several advantages over the cast films due to its high surface area to volume ratio. In 2007, the electrospun CA fiber mats containing vitamin A acid (Retin-A) and vitamin E (Vit-E) have been reported by Taepaiboon et al. [28]. Retin-A or Vit-E in an amount of 5 % or 0.5 % wt. (based on the weight of CA) was incorporated into the CA spinning solutions to prepare the vitamin-loaded spinning solutions. The obtained electrospun fibers from these solutions were cross-sectionally round with smooth surface, with their average diameters ranging between 247 and 265 nm. The release characteristics of these vitamin-loaded CA fiber mats and films were investigated by immersion in the acetate buffer solution containing either 0.5 vol% Tween 80 (nonionic surfactant) or 0.5 vol% Tween 80 and 10 vol% methanol. The results showed that the vitamin-loaded CA fiber mats exhibited a gradual release over the time periods, whereas the vitamin-loaded CA films exhibited a burst release of the vitamins [28]. Tungprapa et al. (2007) [29] prepared the electrospun CA fiber mats containing four different types of model drugs, i.e., naproxen (NAP), indomethacin (IND), ibuprofen (IBU), and sulindac (SUL). The amount of the drugs in the solutions was fixed at 20 % wt. based on the weight of CA powder. The obtained morphology of the drug-loaded electrospun CA fiber mats was smooth without drug aggregated on the surfaces of these fibers suggesting that the drugs were incorporated well within the fibers. Moreover, the release characteristics of the drug-loaded electrospun CA fiber mats and films were investigated by the total immersion method in the acetate buffer solution at 37 °C. The results showed that the release of the drugs from these fiber mats was greater than that from films at any given immersion time point. In addition, the maximum release of the drugs from both the drug-loaded electrospun CA fiber mats and films could be found in the following order: NAP > IBU > IND > SUL [29]. Suwantong et al. [30] fabricated the curcumin-loaded electrospun CA fiber mats for use as carriers for topical or transdermal drug delivery of curcumin. Various amounts (i.e., 5–20 wt% based on the weight of CA powder) of curcumin were incorporated into the CA spinning solutions to prepare the curcumin-loaded electrospun CA fiber mats. The obtained fibers were smooth without curcumin aggregates on the surface of the fibers. The average diameters of the curcumin-loaded electrospun CA fiber

mats ranged between 314 and 340 nm. The release characteristics of the curcumin-loaded electrospun CA fiber mats were carried out by the total immersion method and the transdermal diffusion through a pig skin method in the acetate buffer solution containing Tween 80 and methanol. The results showed that in total immersion method, almost all of the curcumin loaded in the curcumin-loaded electrospun CA fiber mats was released in the medium, while small amount of curcumin was obtained when the curcumin-loaded electrospun CA fiber mats were placed on top of a pig skin. In addition, the release amount of curcumin from the curcumin-loaded electrospun CA fiber mats was greater than that from films at any given immersion time point in both investigated techniques [30]. In 2011, the fibrous membranes of CA, poly(vinylpyrrolidone) (PVP), and composite membranes of these polymers were fabricated by coaxial electrospinning [46]. Amoxicillin is in a class of antibiotics called penicillin. It is used to treat certain infections caused by bacteria. The effect of the pH (i.e., pH 3.0 and pH 7.2) on the controlled release of amoxicillin was investigated. The results showed that the release characteristics of amoxicillin from these fibrous membranes were dependent on the pH of the medium. The released amount of amoxicillin from these fibrous membranes in the medium at pH 7.2 was three times greater than that in the medium at pH 3.0. These results could be due to the greater interactions of amoxicillin with the components of the membrane at pH 3 resulting in lower drug release [46].

3.3 Wound Dressing

Wound dressing from the electrospun fiber mats potentially offers several advantages over conventional processes. With its high surface area and porous structure, the electrospun fiber mats could quickly start signaling pathway and attract fibroblast to the derma layer, which can excrete important extracellular matrix components such as collagen and several cytokines, to repair damaged tissue. Moreover, the electrospun fiber mats should not only serve as a substrate for wound healing but also may deliver suitable bioactive agents, including drugs (e.g., antibiotic agent), within a controlled manner during healing. Son et al. [31] prepared the electrospun CA fiber mats containing 0.5 wt% of $AgNO_3$. When the electrospun CA fiber mats containing 0.5 wt% of $AgNO_3$ were irradiated with UV light at 245 nm, Ag nanoparticles were generated on the surface of the CA fibers and their average size was 21 nm after UV irradiation for 240 min. While when the electrospun CA fiber mats containing 0.5 wt% of $AgNO_3$ were irradiated with UV light at 365 nm, the photoreduction of the Ag^+ ions was delayed and the average size of the Ag nanoparticles was 12 nm. From the antimicrobial activity results, the Ag nanoparticles with an average size of 21 nm showed strong antimicrobial activity [31]. In 2008, the electrospun CA fiber mats containing chlorhexidine (CHX) as a bactericidal agent were successfully prepared by Chen et al. [32]. A small amount of PEO was incorporated into CA solutions to improve the elasticity of the CA solutions and facilitate the formation of fibers. The CHX-loaded CA fiber

mats were cured by an organic titanate Tyzor® TE (TTE) in the presence of water vapor to create covalent links between CA and CHX. The CHX-loaded CA fiber mats showed bactericidal properties. Moreover, the bactericidal properties were also obtained by post-spin treatment of the CA-PEO fibers to immobilize CHX on the fibers via titanate linkers. From the results, they concluded that a post-spin treatment of fiber could result in higher CHX loading on the fiber surface and may enhance the bactericidal properties of the fiber mats [32]. Asiaticoside (AC) is one of the four major triterpenoid components (i.e., asiatic acid, asiaticoside, madecassic acid, and madecassoside) of the *Centella asiatica* extracts. It is supposed to be the most active compound associated with the healing of wounds. Thus, Suwantong et al. [33] prepared the electrospun CA fiber mats containing AC in the form of either a pure substance (PAC) or a crude extract (CACE) at concentration of 40 wt% (based on the weight of CA powder) by electrospinning. The obtained average diameters of these fibers were 485 and 545 nm, respectively. The release characteristics of AC from both the PAC- and the CACE-loaded electrospun CA fiber mats were carried out by the total immersion and the transdermal diffusion through a pig skin method in acetate or phosphate buffer solution that contained methanol at either 32 °C or 37 °C, respectively. The results showed that the lower amounts of AC were released into both types of the releasing medium, when these fiber mats were placed on the top of a pig skin. Moreover, the potential use of these fiber mats as topical/transdermal or wound dressing patches was investigated by the indirect cytotoxicity of these fiber mats against normal human dermal fibroblasts [33].

3.4 Sensor

Shuiping et al. [47] prepared the electrospun CA fiber mats containing 1′,3′,3′-trimethyl-6-nitrospiro (NO_2SP) as photochromic fiber mats. They found that incorporation of NO_2SP did not affect the fiber morphology. In addition, incorporation of NO_2SP into the electrospun CA fiber mats could provide good photochromic and fluorescent properties of these fiber mats to be a great potential in optical devices and/or biosensors applications [47]. The nanocomposite multilayers were deposited on the electrospun nanofiber mats by an electrostatic layer-by-layer (LBL) self-assembly technique [48]. The positively charged water-insoluble 2,9,16,23-tetraaminophthalocyanine copper (CuTaPc) and the negatively charged water-soluble poly(acrylic acid) (PAA) were alternately deposited on the surface of the electrospun cellulose fiber mats. The templates of the electrospun cellulose fiber mats were obtained from the alkaline hydrolysis of the electrospun cellulose acetate fiber mats. The formation and the morphology of the LBL films containing CuTaPc/PAA films coated on the surface of the electrospun cellulose fiber mats were controlled by controlling the number of CuTaPc/PAA deposition bilayers. These LBL multilayer films on the electrospun cellulose fiber mats showed great potential applications as catalysts and sensors [48].

3.5 Membrane

The electrospun CA fiber mats as affinity membrane were prepared by Ma et al. (2005) [49]. These fiber mats were heat treated under 208 °C for 1 h to improve structural integrity and mechanical strength and then treated in alkaline solution for 24 h to obtain regenerated cellulose (RC) fiber mats. The RC fiber mats were surface functionalized with Cibacron Blue F3GA (CB, a general dye ligand) for separation of various biomolecules. The CB-derived RC fiber mats showed abilities to capture BSA or bilirubin with capacities of 13 and 4 mg/g, respectively. These results showed that these RC fiber mats could be a great potential for affinity membrane application [49]. Ritcharoen et al. [50] prepared the electrospun CA membrane as a support for coating with polyelectrolyte multilayers of chitosan (CHI)/sodium alginate (SA) and CHI/poly(styrene sulfonate) sodium salt (PSS). The results showed that the morphology of the CHI/SA-coated CA membrane was denser than the CHI/PSS-coated CA membrane. These composite membranes were characterized for its water permeability. The results showed that the electrospun CA membrane had a high water flux, due to the highly porous nature of the membrane. While the deposition of the polyelectrolyte bilayers decreased the water flux. Moreover, the desalination property of the CHI/SA-coated membranes showed better than that of the CHI/PSS-coated membranes [50]. Zhang et al. [51] prepared adsorptive membranes made from the electrospun CA fiber mats as an ion-exchange medium for protein separation. The electrospun CA fiber mats were hydrolyzed/deacetylated to form regenerated cellulose fibers which were then surface functionalized with diethylaminoethyl (DEAE) anion-exchange ligand. The RC microfiber adsorption medium, the commercially available RC adsorptive membrane, and the bleached adsorbent cotton balls were treated and evaluated to compare with the functionalized electrospun cellulose fiber felts. The results showed that the functionalized CA fiber felts had the highest static binding capacity of 40.0 mg $\cdot$ g^{-1} for bovine serum albumin (BSA), while the functionalized commercial membranes, cellulose microfiber mediums, and cotton balls had 33.5, 14.5, and 15.5 mg $\cdot$ g^{-1}, respectively [51]. The molecularly imprinted nanofiber membranes were prepared from CA and a derivative of optically pure glutamic acid, such as N-α-benzyloxycarbonyl-D-glutamic acid (Z-D-Glu) or N-α-benzyloxycarbonyl-L-glutamic acid (Z-L-Glu), by an alternative molecular imprinting and an electrospray deposition [52]. The results showed that these molecularly imprinted nanofiber membranes increased both permselectivity and flux. Hence, these membranes have potential use for chiral separation [52]. The electrospun CA membranes for heavy metal ions adsorption in water treatment were prepared by electrospinning and surface modification with poly(methacrylic acid) (PMMA) using Ce^{4+} -initiated radical graft copolymerization [53]. The adsorption of heavy metal ions (Cu^{2+}, Hg^{2+}, and Cd^{2+}) on these membranes was studied. The adsorption capacity increased with the increasing of initial pH value in the system. Moreover, these membranes showed high adsorption selectivity especially for Hg^{2+} and could be easily de-adsorbed from the surface of membrane by

using ethylenedinitrilo tetraacetic acid solution. Hence, these membranes could be reused for the metal ion adsorption [53]. Huang et al. [54] fabricated the immobilization of Candida rugosa lipase on the electrospun CA fiber mats by electrospinning of CA and then treated with alkaline hydrolysis to convert the surface of fiber mats into RC. The RC fiber mats were then oxidized by $NaIO_4$ to generate aldehyde groups for reacting with lipase. From the results, they found that the enzymatic activity of these fiber mats was 29.6 $U \cdot g^{-1}$. Moreover, the immobilized lipase exhibited significantly higher thermal stability and durability than equivalent free enzyme [54]. The ZnO nanoparticles-loaded electrospun CA fiber mats with optical, bactericidal, and water-repellent properties have been prepared by Anitha et al. [55]. They found that the optical property of these fiber mats was no significant change in the emission characteristics even with addition of ZnO. Moreover, the ZnO nanoparticles-loaded electrospun CA fiber mats exhibited a better water-repellent property than the pure electrospun CA fiber mats. In addition, the ZnO nanoparticles-loaded electrospun CA fiber mats showed strong antibacterial activity against the *S. aureus*, *E. coli*, and *Citrobacter* [55].

4 Conclusions

The application of the electrospun CA fiber mats has been promisingly attracted in various fields, since the electrospun CA fiber mats exhibit several interesting characteristics. Moreover, CA has suitable characteristics such as good thermal stability, chemical resistance, biocompatibility, biodegradability, etc., for use in many applications including tissue engineering, drug delivery system, wound dressing, sensor, membrane, etc.

References

1. Formhals A (1934) Process and apparatus for preparing artificial threads. US Patent 1975504
2. Doshi J, Reneker DH (1995) Electrospinning process and applications of electrospun fibers. J Electrostat 35:151
3. Reneker DH, Chun I (1996) Nanometre diameter fibres of polymer, produced by electrospinning. Nanotechnology 7:216
4. Supaphol P, Suwantong O, Sangsanoh P, Neamnark A (2011) Electrospinning in drug delivery. In: Reisner DE (ed) Bionanotechnology II: global prospects. Boca Raton, CRC Press, p 455
5. Teo WE, Ramakrishna S (2006) A review on electrospinning design and nanofibre assemblies. Nanotechnology 17:R89
6. Greiner A, Wendorff JH (2007) Electrospinning: A fascinating method for the preparation of ultrathin fibers. Angew Chem 46:5670
7. Lannutti J, Reneker D, Ma T, Tomasko D, Farson D (2007) Electrospinning for tissue engineering scaffolds. Mater Sci Eng C 27:504
8. Sill TJ, von Recum HA (2008) Electrospinning: Applications in drug delivery and tissue engineering. Biomaterials 29:1989

9. Baumgarten P (1971) Electrostatic spinning of acrylic microfibers. J Colloid Interface Sci 36:71
10. Hayati I, Bailey AI, Tadros TF (1987) Investigations into the mechanisms of electrohydrodynamic spraying of liquids: Effect of electric-field and the environment on pendant drops and factors affecting the formation of stable jets and atomization. J Colloid Interface Sci 117:205
11. Deitzel JM, Kleinmeyer J, Harris D, Tan NCB (2001) The effect of processing variables on the morphology of electrospun nanofibers and textiles. Polymer 42:261
12. Meechaisue C, Dubin R, Supaphol P, Hoven VP, Kohn J (2006) Electrospun mat of tyrosine-derived polycarbonate fibers for potential use as tissue scaffolding material. J Biomat Sci Polym E 17:1039
13. Megelski S, Stephens JS, Chase DB, Rabolt JF (2002) Micro- and nanostructured surface morphology on electrospun polymer fibers. Macromolecules 22:8456
14. Deitzel JM, Kleinmeyer J, Hirvonen JK, Beck TNC (2001) Controlled deposition of electrospun poly(ethylene oxide) fibers. Polymer 42:8163
15. Jaeger R, Bergshoef MM, Batlle CMI, Schonherr H, Vancso GJ (1998) Electrospinning of ultra-thin polymer fibers. Macromol Symp 127:141
16. Jia H, Zhu G, Vugrinovich B, Kataphinan W, Reneker DH, Wang P (2002) Enzyme-carrying polymeric nanofibers prepared via electrospinning for use as unique biocatalysts. Biotechnol Prog 18:1027
17. Khil M-S, Cha D-I, Kim H-Y, Kim I-S, Bhattarai N (2003) Electrospun nanofibrous polyurethane membrane as wound dressing. J Biomed Mater Res A 67:675
18. Kim K, Luu YK, Chang C, Fang DF, Hsiao BS, Chu B, Hadjiargyrou M (2004) Incorporation and controlled release of a hydrophilic antibiotic using poly(lactide-co-glycolide)-based electrospun nanofibrous scaffolds. J Control Release 9:47
19. Ma Z, Kotaki M, Inai R, Ramakrishna S (2005) Potential of nanofiber matrix as tissue-engineering scaffolds. Tissue Eng 11:101
20. Ma Z, Kotaki M, Ramakrishna S (2006) Surface modified nonwoven polysulphone (PSU) fiber mesh by electrospinning: A novel afffinity membrane. J Membrane Sci 272:179
21. Luu YK, Kim K, Hsiao BS, Chu B, Hadjiargyrou M (2003) Development of nanostructured DNA delivery scaffold via electrospinning of PLGA and PLA-PEG block copolymers. J Control Release 89:341
22. Wang Y, Hsieh Y-L (2004) Enzyme immobilization to ultra-fine cellulose fibers via amphiphilic polyethylene glycol spacers. J Polym Sci Pol Chem 42:4289
23. Riboldi SA, Sampaolesi M, Neuenschwander P, Cossu G, Mantero S (2005) Electrospun degradable polyesterurethane membranes: Potential scaffolds for skeletal muscle tissue engineering. Biomaterials 26:4606
24. Wu L, Yuan X, Sheng J (2005) Immobilization of cellulase in nanofibrous PVA membranes by electrospinning. J Membrane Sci 250:167
25. Mark HF, Bikales NM, Overberger CG, Menges G (1985) Encyclopedia of polymer science and engineering. Wiley-Interscience, New York
26. Lu EX, Jiang ZQ, Zhang QZ, Jiang XG (2003) A water-insoluble drug monolithic osmotic tablet system utilizing gum arabic as an osmotic, suspending and expanding agent. J Control Release 92:375
27. Makhija SN, Vavia PR (2003) Controlled porosity osmotic pump-based controlled release systems of pseudoephedrine I. Cellulose acetate as a semipermeable membrane. J Control Release 89:5
28. Taepaiboon P, Rungsardthong U, Supaphol P (2007) Vitamin-loaded electrospun cellulose acetate nanofiber mats as transdermal and dermal therapeutic agents of vitamin A acid and vitamin E. Eur J Pharm Biopharm 67:387
29. Tungprapa S, Jangchud I, Supaphol P (2007) Release characteristics of four model drugs from drug-loaded electrospun cellulose acetate fiber mats. Polymer 48:5030

30. Suwantong O, Opanasopit P, Ruktanonchai U, Supaphol P (2007) Electrospun cellulose acetate fiber mats containing curcumin and release characteristic of the herbal substance. Polymer 48:7546
31. Son WK, Youk JH, Park WH (2006) Antimicrobial cellulose acetate nanofibers containing silver nanoparticles. Carbohydr Polym 65:430
32. Chen L, Bromberg L, Hatton TA, Rutledge GC (2008) Electrospun cellulose acetate fibers containing chlorhexidine as a bactericide. Polymer 49:1266
33. Suwantong O, Ruktanonchai U, Supaphol P (2008) Electrospun cellulose acetate fiber mats containing asiaticoside or *Centella asiatica* crude extract and the release characteristics of asiaticoside. Polymer 49:4239
34. Kontogiannopoulos KN, Assimopoulou AN, Tsivintzelis I, Panayiotou C, Papageorgiou VP (2011) Electrospun fiber mats containing shikonin and derivatives with potential biomedical applications. Int J Pharm 409:216
35. Gouma P, Xue R, Goldbeck CP, Perrotta P, Balázsi C (2012) Nano-hydroxyapatite-Cellulose acetate composites for growing of bone cells. Mater Sci Eng C 32:607
36. Liu H, Hsieh YL (2002) Ultra-fine fibrous cellulose membranes from electrospinning of cellulose acetate. J Polym Sci Pol Phys 40:2119
37. Son WK, Youk JH, Lee TS, Park YH (2004) Electrospinning of ultrafine cellulose acetate fibers: Studies of a new solvent system and deacetylation of ultrafine cellulose acetate fibers. Polym Sci Pol Phys 42:5
38. Ding B, Kimura E, Sato T, Fujita S, Shiratori S (2004) Fabrication of blend biodegradable nanofibrous nonwoven mats via multi-jet electrospinning. Polymer 45:1895
39. Tungprapa S, Puangparn T, Weerasombut M, Jangchud I, Fakum P, Semongkhol S, Meechaisue C, Supaphol P (2007) Electrospun cellulose acetate fibers: effect of solvent system on morphology and fiber diameter. Cellulose 14:563
40. Zhang L, Hsieh Y-L (2008) Ultra-fine cellulose acetate/poly(ethylene oxide) biocomponent fibers. Carbohydr Polym 71:196
41. Han SO, Youk JH, Min KD, Kang YO, Park WH (2008) Electrospinning of cellulose acetate nanofibers using a mixed solvent of acetic acid/water: Effects of solvent composition on the fiber diameter. Mater Lett 62:759
42. Wongsasulak S, Patapeejumruswong M, Weiss J, Supaphol P (2010) Electrospinning of food-grade nanofibers from cellulose acetate and egg albumen blends. J Food Eng 98:370
43. Greish YE, Meetani MA, Al Matroushi EA, Al Shamsi B (2010) Effects of thermal and chemical treatments on the structural stability of cellulose acetate nanofibers. Carbohydr Polym 82:569
44. Chen C, Wang L, Huang Y (2011) Electrospun phase change fibers based on polyethylene glycol/cellulose acetate blends. Appl Energy 88:3133
45. Baek W-I, Pant HR, Nam K-T, Nirmala R, Oh H-J, Kim I, Kim H-Y (2011) Effect of adhesive on the morphology and mechanical properties of electrospun fibrous mat of cellulose acetate. Carbohydr Res 346:1956
46. Castillo-Ortega MM, Nájera-Luna A, Rodríguez-Félix DE, Encinas JC, Rodríguez-Félix F, Romero J, Herrera-Franco PJ (2011) Preparation, characterization and release of amoxicillin from cellulose acetate and poly(vinyl pyrrolidone) coaxial electrospun fibrous membranes. Mater Sci Eng C 31:1772
47. Shuiping L, Lianjiang T, Weili H, Xiaoqiang L, Yanmo C (2010) Cellulose acetate nanofibers with photochromic property: Fabrication and characterization. Mater Lett 64:2427
48. Mao X, Ding B, Wang M, Yin Y (2010) Self-assembly of phthalocyanine and polyacrylic acid composite multilayers on cellulose nanofibers. Carbohydr Polym 80:839
49. Ma Z, Kotaki M, Ramakrishna S (2005) Electrospun cellulose nanofiber as affinity membrane. J Membrane Sci 265:115
50. Ritcharoen W, Supaphol P, Pavasant P (2008) Development of polyelectrolyte multilayer-coated electrospun cellulose acetate fiber mat as composite membranes. Eur Polym J 44:3963

51. Zhang L, Menkhaus TJ, Fong H (2008) Fabrication and bioseparation studies of adsorptive membranes/felts made from electrospun cellulose acetate nanofibers. J Membrane Sci 319:176
52. Sueyoshi Y, Fukushima C, Yoshikawa M (2010) Molecularly imprinted nanofiber membranes from cellulose acetate aimed for chiral separation. J Membrane Sci 357:90
53. Tian Y, Wu M, Liu R, Li Y, Wang D, Tan J, Wu R, Huang Y (2011) Electrospun membrane of cellulose acetate for heavy metal ion adsorption in water treatment. Cabohydr Polym 83:743
54. Huang X-J, Chen P-C, Huang F, Ou Y, Chen M-R, Xu Z-K (2011) Immobilization of *Candida rugosa* lipase on electrospun cellulose nanofiber membrane. J Mol Catal B Enzym 70:95
55. Anitha S, Brabu B, Thiruvadigal DJ, Gopalakrishnan C, Natarajan TS (2012) Optical, bactericidal and water repellent properties of electrospun nano-composite membranes of cellulose acetate and ZnO. Carbohydr Polym 87:1065

Application of Membranes from Cellulose Acetate Nanofibers

20

Masakazu Yoshikawa and Kalsang Tharpa

Contents

Abstract

We have to reduce our dependence on oil so that we can construct sustainable environment and society. To this end, we should utilize naturally occurring or "green polymers," their derivatives, and wastes from food industries and so forth as resources of polymeric materials. Cellulose acetate is not only a derivative of naturally occurring raw material but also one of the promising alternatives to polymers, at the moment, produced from oil. Cellulose acetate has been utilized

M. Yoshikawa (✉)
Department of Biomolecular Engineering, Kyoto Institute of Technology, Matsugasaki, Kyoto, Japan
e-mail: masahiro@kit.ac.jp

K. Tharpa
Department of Chemistry, University of Mysore, Manasagangothri, Mysore, Karnataka, India

J.K. Pandey et al. (eds.), *Handbook of Polymer Nanocomposites. Processing, Performance and Application – Volume C: Polymer Nanocomposites of Cellulose Nanoparticles*,
DOI 10.1007/978-3-642-45232-1_71,

as membrane materials for desalination, which supplies pure drinking water from brackish or seawater. Cellulose and its derivatives, such as cellulose acetate and so forth, contain functional moieties for molecular recognition of chemicals of use to our daily life. In this chapter, the application of cellulose derivatives to membrane separation of racemic mixtures, which are required to be divided into each optically pure enantiomers in connection with diverse fields, such as pharmaceuticals, agrochemicals, foods, perfumes, and so forth. In the present chapter, the author would like to reveal that the membrane form of nanofiber fabrics gave both higher permselectivity and throughput (flux).

Keywords
Chiral separation • Electrospray deposition: Membrane • Molecular imprinting • Molecularly imprinted nanofiber membrane • Nanofiber membrane • Optical resolution

1 Introduction

In the chemical industries, synthesis and purification of a target material are a couple of key processes. Among those two important processes, the purification of the target chemical from mixtures containing by-products, starting materials, solvents, catalysts, and so forth is essential, since the value of target product is greatly dependent on its purity. Among various separation techniques, membrane separation is an emerging technology and regarded as follows:

- Membrane separation can be carried out continuously under mild conditions.
- Membrane separation is economically and ecologically competitive to other separation methods.
- Upscale is relatively easy.
- No additives are required.

As mentioned above, membrane separation is a promising separation method and expected to spread out various separation processes. However, at the moment, suitable membrane materials applicable to practical membrane separation in chemical industries have not appeared excepting filtration, desalination, and ion exchange membranes.

Membrane separation consists of a couple of mechanism, such as incorporation of permeant into a given membrane and diffusion (migration) of permeant within the membrane from the feed side to the permeate side [1–3]. In the case of a membrane transport through a nonporous dense membrane, such transport mechanism is called "solution-diffusion mechanism," while that through a porous membrane, "partition-diffusion mechanism." Diffusion of permeant within the membrane would be dominantly governed by its dimension and/or shape. From this, the control of permselectivity by diffusivity would be intrinsically limited. Contrary to this, incorporation of permeant into a given membrane is theoretically expected to range from naught to infinity. In order to improve permselectivity of membranes, introduction of molecular recognition sites, in other words, specific binding sites, which rigorously discriminate the target material and others, into a given membrane is crucial.

Introduction of molecular recognition sites into polymeric membrane is a time-consuming, costly, and awkward experimental work. Against this, molecular imprinting technique [4–7] would introduce molecular recognition sites into polymeric membranes without such a laborious work mentioned above. Molecular imprinting is regarded as the most facile way to give polymeric membranes substrate specificity [8–11].

Among molecular imprinting methods, an alternative molecular imprinting is a facile and easy way to introduce molecular recognition sites into polymeric membranes. In the present chapter, first molecular imprinting and alternative molecular imprinting are briefly surveyed and then the application of alternative molecular imprinting to cellulose acetate to convert it to chiral separation membrane is mentioned. In the last part in the present chapter, it will be described that the membrane form of molecularly imprinted nanofiber membrane is an ultimate membrane form to give a relatively high throughput without concurrent reduction in permselectivity.

2 Molecular Imprinting

Molecular imprinting is a method to introduce molecular recognition sites into polymeric materials. In other words, the molecular memory, which is both the shape of the target molecule and alignment of the functional moieties to interact with those in the target molecules, is memorized in the polymeric materials for the recognition or separation of target molecule during formation of the polymeric materials.

The concept of imprinting polymer stems from silica imprinting materials, first developed by Polyakov [12] and later modified by Dickey [13]. Due to the instability and non-reproducibility of the silica imprinted material, the research in this field has declined steadily. However, more recently, the researchers are re-exploring silica imprinting materials [14].

It was in the early 1970s that the groups of Klotz, Takagishi, and Wulff presented the first examples of molecular imprinting in synthetic organic polymers [15–17]. The covalent imprinted polymer for template molecule (phenyl-α-D-mannopyranoside) was synthesized by using two molecules of 4-vinylbenzeneboronic acid as functional monomer, bound by diester linkages, was successful in separating D– and L– enantiomer with α values between 3.5 and 6.0. Although covalent MIP is known to yield less heterogeneous polymer and stoichiometric reaction, its application is limited because of the reason that the template molecule should have functional group capable of forming covalent bond with the functional monomer and it often involves drastic chemical reaction prior to template rebinding process. A more versatile technique called non-covalent MIP was first introduced by Arshady and Mosbach [18]. It is based on the stabilization of multiple weak non-covalent interactions between the template and the functional monomers in which a wide range of template molecule can be employed and,

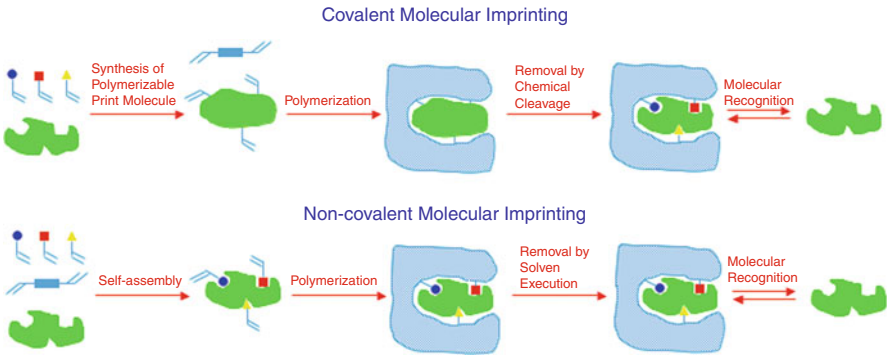

Fig. 20.1 Schemes of covalent and non-covalent molecular imprinting. (Molecularly imprinted materials are synthesized by polymerization of functional monomer and cross-linker in the presence of print molecule)

however, at the same time extensive selectivity study of MIP is required. The first report on non-covalent MIP is based on hydrogen bond formation between Z-glutamic acid and methacrylic acid in a nonpolar porogen. Later, the template is cleaved by treating with polar solvent, prior to rebinding in the polymerization solvent. Soon, a group of Whitecombe et al. [19] combines the advantages of both covalent and non-covalent imprinting polymer. It is known as covalent sacrificial imprinting or "covalent binding followed by non-covalent rebinding" process. In it, 4-vinylphenyl carbonate ester of cholesterol functions as a covalently bound template monomer and at the same time is easily cleaved hydrolytically with the loss of CO_2 to give non-covalent recognition site bearing a phenolic residue for cholesterol (a template molecule) to form hydrogen bonding in nonpolar solvents.

The scheme for the covalent and non-covalent molecular imprinting is given in Fig. 20.1. In brief, as can be seen in the figure, molecularly imprinted materials are prepared from a print molecule, which is a target molecule or a target molecule analogue; a functional monomer with functional moieties, which forms covalent or non-covalent bonds with the print molecule adopted; and cross-linkers. Functional monomers are assembled around the print molecule and consequently predetermined orientation of the functional moieties is achieved. In the next step, the complex mixtures are polymerized to form highly cross-linked polymers such that the molecular shape of the print molecule and alignment of the functional moieties are retained in the formed molecularly imprinted materials. In the final step, the print molecule is removed from the imprinted polymers so that complementary molecular recognition sites are constructed in the molecularly imprinted polymeric materials.

Non-covalent molecular imprinting is simpler than covalent molecular imprinting. Most molecularly imprinted materials are nowadays prepared by non-covalent molecular imprinting. Selective adsorption materials for metal ions were also prepared by non-covalent molecular imprinting [20].

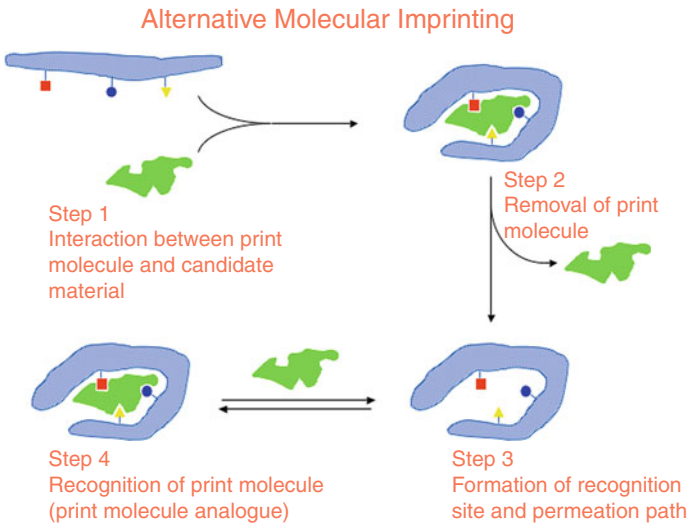

Fig. 20.2 Scheme of alternative molecular imprinting. (Molecularly imprinted materials are directly prepared from polymeric materials in the presence of print molecule)

3 Alternative Molecular Imprinting

Molecularly imprinted materials can be obtained directly from polymers instead of functional monomers and cross-linkers. This method is named "alternative molecular imprinting," which was proposed in 1994 [8, 10, 21]. The concept of alternative molecular imprinting is shown in Fig. 20.2. In step 1, the polymeric material, which is a candidate material to construct molecular recognition sites, is interacted with a print molecule by specific interaction before and during the formation process of molecular recognition materials so that molecular memory can be incorporated into the polymeric materials. In step 2, the print molecule is extracted from the molecularly imprinted materials. When the molecularly imprinted material thus constructed is in contact with the print molecule or print molecule analogue, the molecular recognition sites preferentially interact with them or incorporate them into the molecular recognition sites (step 3 and step 4). Contrary to the pioneering molecular imprinting method, molecular recognition sites are formed at the same time as the molecularly imprinted materials are prepared from polymer solution or polymer melt. In other words, any polymeric materials, such as synthetic polymers [22], oligopeptide derivatives [23, 24], derivatives of natural polymer [25], and natural polymers [26], can be directly converted into a molecular recognition material by applying the alternative molecular imprinting without any tedious and laborious laboratory work. It might go so far as to say that someone, who has no experience of doing chemical experiment, can prepare molecularly imprinted materials from polymeric materials and print molecules by applying the alternative molecular imprinting.

A similar approach was proposed by Michaels and his colleagues in 1962 [27]. The paper reported pervaporation separation of *p*-xylene with polyethylene membranes conditioned by *p*-xylene as a print molecule. This study is regarded as not only the first report on the alternative molecular imprinting but also the first application of molecularly imprinted polymeric membranes to membrane separation. Michaels' paper that appeared in 1962 is the commemorable paper in molecular imprinting and membrane separation.

4 Application of Molecularly Imprinted Polymeric Membranes to Membrane Separation

As mentioned above, application of molecular imprinting to membrane separation was first reported by Michaels and his research group in 1962 [27]. In addition to this, molecularly imprinted polymeric membranes prepared by non-covalent molecular imprinting technique were reported in 1990 [28]. Since then, various molecularly imprinted membranes were studied by adopting non-covalent molecular imprinting [29, 30]. Molecularly imprinted membranes (materials) were directly converted from polymeric materials by applying an alternative molecular imprinting [21, 31]. A wet phase inversion process was applied to an alternative molecular imprinting to prepare asymmetric membranes [32, 33] soon after molecularly imprinted membranes prepared by an alternative molecular imprinting had been reported [31].

As described above, the application of molecular imprinting to obtain separation membrane is one of the most facile ways to introduce molecular recognition sites into polymeric membranes. However, at the moment, neither flux nor permselectivity is enough for practical application. In membrane separation, not only permselectivity but also flux (throughput) is a couple of important factors. In a sense, development of synthetic membranes with high flux values is more important than that with high permselectivity. A flux for a given membrane and the corresponding permselectivity often show a trade-off relationship. In other words, the enhancement of a flux for a given membrane often leads to the concurrent reduction in permselectivity and *vice versa*. Membranologists perceived that simultaneous enhancement of both flux and permselectivity is an unsolved problem and/or unsolvable problem in membrane separation.

Membrane form of nanofiber mat, which is fabricated by electrospray deposition, is expected to solve a trade-off relationship in membrane separation. Nanofiber mat gives higher surface area and higher porosity [34, 35]. This is expected to lead a higher permselectivity and an enhancement of flux. The enhancement of both the flux and permselectivity was proved in chiral separation of racemic mixtures with molecularly imprinted nanofiber membranes [36–38]. In the next chapter, possibility of the breakthrough in membrane separation will be described adopting cellulose acetate nanofiber membrane as an example. Cellulose acetate has been successfully used for constructing polymeric membrane (Table 20.1) [25, 37, 39–45].

Table 20.1 Molecular imprinted membrane involving cellulose acetate

Template	Monomer mixture	Imprinting/ polymerization technique	Mobility	Selectivity factor (α)	Remark	References
N-α-*Z*-D-glutamic acid (Z-D-Glu) *N*-α-*Z*-L-glutamic acid (Z-L-Glu)	Cellulose acetate	Alternative molecular imprinting/solvent evaporation	–	$\alpha_{(Z\text{-D-Glu}/Z\text{-L-Glu})} = \alpha_{(Z\text{-L-Glu}/Z\text{-D-Glu})} =$ 2.3 below 2.5 V	–	[25]
N-benzyloxycarbonyl-d-glutamic acid (Z-D-Glu) or N-benzyloxycarbonyl-l-glutamic acid (Z-L-Glu)	Cellulose acetate	Alternative molecular imprinting/electrospray deposition	1.04×10^{-9} mol cm cm^2 J^{-1} h^{-1} (0.5×10^{-3} mol dm^{-3}, Z-D-Glu); 2.49×10^{-9} mol cm cm^2 J^{-1} h^{-1} (0.5×10^{-3} mol dm^{-3}, Z-L-Glu)	$\alpha_{(Z\text{-D-Glu}/Z\text{-L-Glu})} =$ 1.27 $\alpha_{(Z\text{-L-Glu}/Z\text{-D-Glu})} =$ 1.34	–	[37]
6-benzyladenine (BA) 6-(furfurylamino) purine (KT), selectivity test analogue molecule	MAA and EGDMA on cellulose acetate support	Bulk polymerization on CA membrane filter/ photo initiation	9.41 ± 0.3 n mol cm^{-2} h^{-1} (2×10^{-3} mol dm^{-3}, BA) 13.63 ± 0.3 n mol cm^{-2} h^{-1} (2×10^{-3} mol dm^{-3}, KT)	Difference in the permeation of KT is more in BA imprinted membrane than in non-imprinted membrane	The flexibility and mechanical strength of the membrane are by CA porous support	[39]
Rhodamine B	Blend of CA and sulfonated polysulfone (SPS) in the presence of polyethylene glycol	Blend of SPS and CA/solvent casting using DMSO	DMSO as solvent yielded highest flux among the solvent studied. Flux increases with addition of polyethylene glycol	Not studied	Binding capacity of about 72 % in the case of MIP	[40]
					CA/SPS (95/5) blend membranes	[41]
S-propranolol HCl R-propranolol HCl as selectivity test analogue	MA and EGDMA on CA support	Bulk polymerization on the surface of functionalized cellulose membrane/thermal initiation	1.73 ± 0.25 μg cm^{-2} h^{-1}	$\alpha_{(S\text{-propranolol}/R\text{-propranolol})} = 0.037$	Potential of enantioselective-controlled release system of MIP cellulose membrane was supported by the in vivo results	[42]

(*continued*)

Table 20.1 (continued)

Template	Monomer mixture	Imprinting/ polymerization technique	Mobility	Selectivity factor (α)	Remark	References
S-propranolol HCl R-propranolol HCl as selectivity test analogue	MAA, EGDMA, perfluoro polymeric surfactant (PFPS), and perfluoro (methylcyclohexane)	Suspension polymerization, integrated nanoparticle MIP onto cellulose membrane/photo initiation	(S-propranolol) 0.43 ± 0.09 μg $cm^{-2}h^{-1}$ (R-propranolol) 0.57 ± 0.08 μg $cm^{-2}h^{-1}$	S/R flux ratio = 1.2	Integrated nanoparticle MIP cellulose membrane displayed greater enantioselectivity than membrane polymer of either granules or microspheres MIP	[43]
α-Tocopherol δ-Tocopherol as selectivity test analogue	α-Tocopherol methacrylate and divinylbenzene	Covalent bulk polymerization/scaffold polymerization by phase inversion technique	–	$\alpha_i = 0.49$ (in ethanol) and $\alpha_i = 0.28$ (in n-hexane)	CA-hybrid MIP membrane shows highest K_a value as well as binding capacity in comparison to polysulfone and nylon hybrid MIP membrane	[44]
Thymine (T) Other analogue substrates are uracil(U), cytosine(C), adenine(A), and guanine(G)	9-vinyladenine, diethylene glycol dimethacrylate	Bulk polymerization on porous cellulosic membrane/UV irradiation	–	$\alpha_{T/U} = 0.98$, $\alpha_{T/C} = 1.31$, $\alpha_{T/A} = 1.45$, $\alpha_{T/G} = 1.44$	Template molecule diffused relatively faster than C, A, and G but not U	[45]

5 Cellulose Acetate Nanofiber Membranes

5.1 Molecularly Imprinted Cellulose Acetate Membranes

The research group of MY developed membranes from various naturally occurring or "green polymers," their derivatives, and wastes from food industries as resources for membrane material so that we can construct sustainable environment and society. To this end, they developed membranes from various raw materials, such as cellulose acetate for optical resolution [25, 46], egg shell membranes for chiral separation [47], agarose for pervaporation [48, 49], gelatin for vapor permeation [50], proteins from *Geobacillus thermodenitrificans* DSM465 for vapor permeation [51] and molecular recognition [26, 52], DNA for gas [53] and chiral separation [54–56], chitosan for chiral [57] and vapor permeation [58], optical resolution with molecularly imprinted nanofiber membranes from cellulose acetate [37], keratin for optical resolution [59], and chitin nanofiber for chiral separation [60].

As a link in the chain of the utilization of renewable polymers as membrane materials, cellulose acetate, a derivative of natural polymer of cellulose, was adopted as candidate material for molecularly imprinted membranes for chiral separation [25, 46]. In the present study, cellulose acetate (CA) with acetyl content of 40 mol% was adopted as candidate material. *N*-α-Benzyloxycarbonyl-D-glutamic acid (Z-D-Glu) or *N*-α-benzyloxycarbonyl-L-glutamic acid (Z-L-Glu) was adopted as a print molecule. Chemical structures of CA and the print molecules are shown in Fig. 20.3. There can be found asymmetric carbon in CA. However, both print molecules, such as that with D-isomer and L-isomer, worked well as print molecules, contrary to the results of oligopeptide derivatives [24]. In other words, the molecularly imprinted CA membrane imprinted by Z-D-Glu adsorbed D-Glu in preference to the antipode and *vice versa* [25].

From CA and print molecules, such as Z-D-Glu or Z-L-Glu, two types of molecularly imprinted membrane were obtained; in other words, the membrane imprinted by

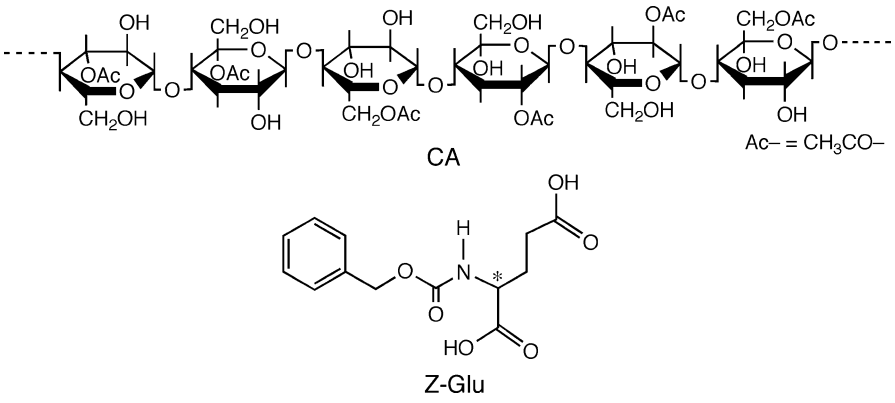

Fig. 20.3 Chemical structures of cellulose acetate (*CA*) and print molecule (Z-Glu)

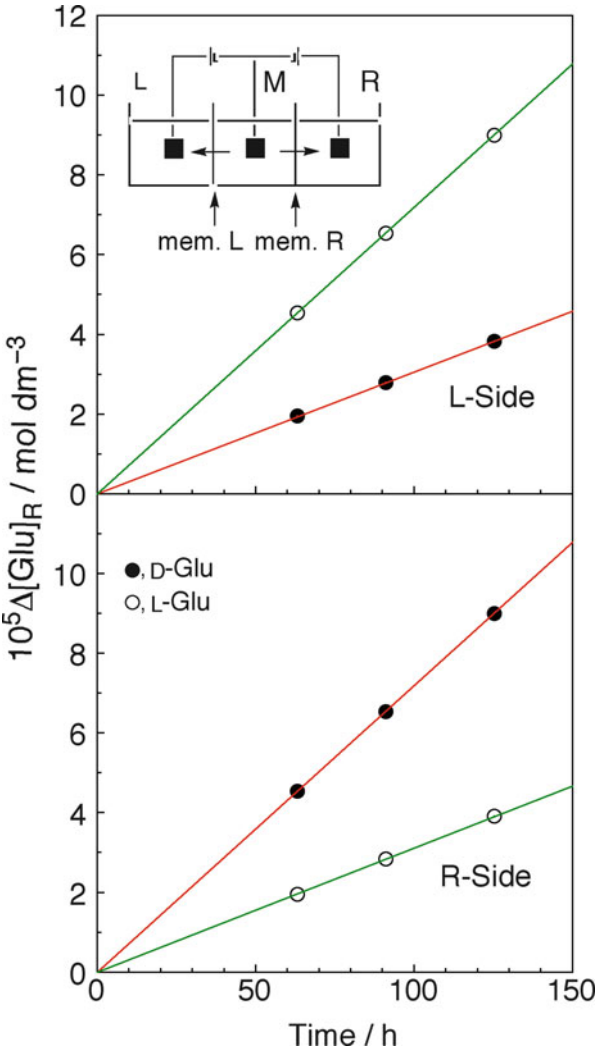

Fig. 20.4 Time-transport curves of racemic mixture of Glu by dual direction enantioselective electrodialysis at $\Delta E = 2.5$ V. [(Z-D-Glu)/(CA) = (Z-L-Glu)/(CA) = 0.5; $[D\text{-Glu}]_0 = [L\text{-Glu}]_0 = 1.0 \times 10^{-3}$ mol dm^{-3}]

Z-D-Glu selectively transported D-Glu at the optimally applied potential as a driving force for membrane transport and *vice versa*. Using those two types of molecularly imprinted membrane at the same time as depicted in Fig. 20.4, D-Glu was selectively transported toward the right side (R) and L-Glu preferentially moved toward to the opposite side (L) from the middle feed chamber (M). The dual direction enantioselective membrane transport is one of interesting membrane separation systems.

As can be seen, applying molecular imprinting, such as conventional molecular imprinting or alternative molecular imprinting, molecular recognition sites can be introduced into membranes with ease. From this, it is relatively easy to enhance permselectivity of a given membrane by applying those molecular

imprinting techniques. However, neither flux nor permselectivity of those membranes was enough for practical application. The enhancement of flux was especially indispensable so that those membranes could be applicable to industries. Molecularly imprinted membranes with higher surface area and higher porosity are requisite to give both higher flux and higher permselectivity. Molecularly imprinted membranes with a membrane form of nanofiber are a suitable or best membrane morphology to give both high flux and high permselectivity. Electrospray deposition is expected to give such membranes.

5.2 Preparation of Molecularly Imprinted Nanofiber Membranes by Electrospray Deposition

Electrospray and electrospinning (combination of two techniques – electrospray and spinning) are widely used in the generation of polymeric materials with a diameter ranging from sub-micrometer to nanometer. The fundamentals and historical development of electrospinning [34], the experimental setup [61], its applications [61, 62], and ever-increasing patents on electrospinning nanofiber [63], have been reviewed. The inherent high surface to volume ratio of nanofiber with fiber fineness ranging from 1 to 10^{-4} denier will have major applications in the field of molecularly imprinted membrane. This was first envisioned by imprinting 2,4-dichlorophenoxyacetic acid using electrospinning technique [64]. The feasibility of encapsulation of molecularly imprinted nanoparticles within electrospun nanofiber has also been demonstrated [65]. In this chapter, the applications and advantages of alternative molecularly imprinted polymeric membrane prepared using electrospray deposition will be demonstrated.

The molecular imprinting ratio, which was the mole ratio of print molecule to constitutional repeating unit of CA in the membrane preparation process, was fixed to be 0.50 so that the results for nanofiber membrane can be compared with the previous usual membrane [25]. *N,N*-Dimethylformamide (DMF) was adopted as a solvent and the polymer concentration was fixed to be 30.0 wt%. Polymer solution containing either one of the print molecule or polymer solution without print molecule was electrosprayed at ambient temperature using an applied voltage of 30.0 kV. The syringe used in the present study had a capillary tip of 0.52 mm diameter. The feeding rate was fixed to be 1.0 $mm^3\ min^{-1}$. A grounded aluminum foil used as a counter electrode was placed 10 cm from the tip of the capillary. Schematic setup of electrospray deposition is shown in Fig. 20.5. It consisted of syringe to keep the polymer solution, a couple of electrodes, and DC voltage supply. As can be seen, the setup for the fabrication of nanofiber mat is simple and the operation is relatively easy under ambient conditions.

An example of scanning electron microscope (SEM) images of electrosprayed nanofiber membrane is shown in Fig. 20.6. The nanofiber membrane was electrosprayed in the presence of Z-D-Glu. The nanofiber membrane imprinted by the L-isomer and the control nanofiber membrane, which was electrosprayed without print molecule, gave similar morphology like that shown in Fig. 20.6.

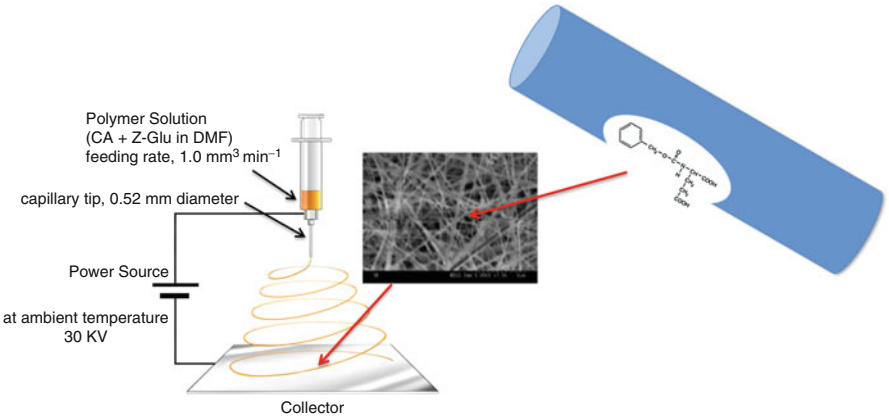

Fig. 20.5 Schematic setup of electrospray deposition to fabricate molecularly imprinted nanofiber membrane

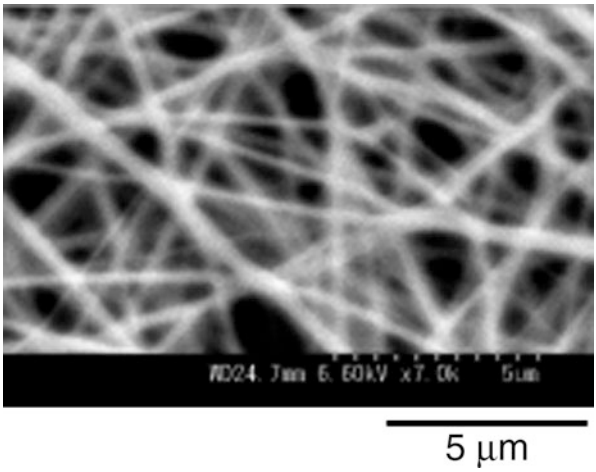

Fig. 20.6 SEM image of surface of Z-D-Glu molecularly imprinted nanofiber membrane. [(Z-D-Glu)/(CA) = 0.50]

The diameters of molecularly imprinted nanofiber membranes were determined to be 200–500 nm and that of the control membrane to be 300–800 nm.

5.3 Adsorption Selectivity

First, adsorption selectivity of those three types of membrane toward racemic mixture of Glu will be described. The membrane samples were immersed in a racemic mixture of Glu solution. The adsorption selectivity was studied at various

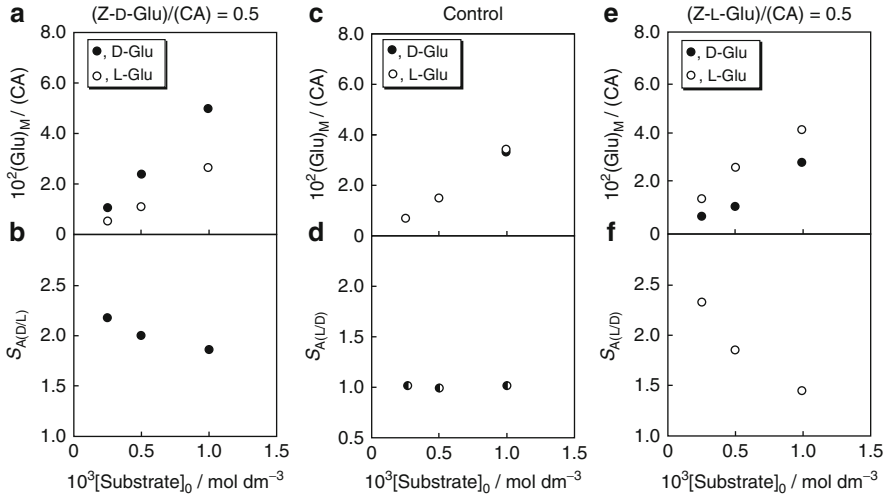

Fig. 20.7 Effect of the substrate concentrations on Glu adsorption (**a**, **c**, and **e**) and adsorption selectivity (**b**, **d**, and **f**) for Z-D-Glu imprinted membrane (**a** and **b**), control one (**c** and **d**), and Z-L-Glu imprinted one (**e** and **f**). (The two data of Glu adsorption in (**c**) are superimposed and not distinguishable)

concentrations, such as 2.50×10^{-4}, 5.00×10^{-4}, and 1.00×10^{-3} mol dm^{-3}, respectively. The results for those membranes are shown in Fig. 20.7. In Fig. 20.7a, c, and e, each amount of Glu adsorbed by the membrane is given as a relative value, which is relative to that of the constitutional repeating unit of CA. Figure 20.7b, d, and f show adsorption selectivities for those nanofiber membranes. The adsorption selectivity $S_{A(i/j)}$ is defined as

$$S_{A(i/j)} = ((i\text{-Glu})/(j\text{-Glu}))/([i\text{-Glu}]/[j\text{-Glu}]) \tag{20.1}$$

where (i-Glu) and [i-Glu] are the amount of i-Glu adsorbed in the membrane and concentration in the solution after equilibrium had been reached, respectively. Two types of molecularly imprinted nanofiber membrane showed adsorption selectivity, in other words, chiral recognition ability, while the control nanofiber membrane hardly showed adsorption selectivity. The molecularly imprinted nanofiber membrane imprinted by Z-D-Glu recognized D-Glu in preference to the corresponding antipode and *vice versa*, as observed in molecularly imprinted CA membranes [25]. CA consists of $\beta(1 \rightarrow 4)$ linked D-glucose with asymmetric carbon. Against expectation, both print molecules, such as the D-isomer of Z-Glu and the Z-L-Glu, equally worked as print molecules. Contrary to this, cellulose triacetate (CTA), of which hydroxyl groups are mostly acetylated, showed different results, though the results are unpublished. In the case of CTA, the L-isomer of the print molecule worked well to construct molecular recognition sites, while it seems to be hard for

the D-isomer of print molecule to convert CTA to molecular recognition materials toward the D-isomer.

The dependence of adsorption selectivity on the substrate concentration is shown in Fig. 20.7b, d, and f. The adsorption selectivities for both molecularly imprinted nanofiber membranes ($S_{A(i/j)}$) increased with the decrease in the substrate concentrations from 1.00×10^{-3} to 2.50×10^{-4} mol dm^{-3}, implying that there can be found molecular recognition sites, which were constructed by the presence of the print molecule, Z-D-Glu or Z-L-Glu, during the electrospray deposition process, in the electrosprayed nanofiber membranes. Contrary to this, the adsorption selectivity for the control nanofiber membrane was hardly dependent on the substrate concentration as shown in Fig. 20.7d. The explanation for the dependence of adsorption selectivity on substrate concentration will be described in the coming Section.

5.4 Substrate Specificity

The adsorption isotherm for optically pure enantiomer will provide us more precise data concerning interaction mode between the substrate and membrane. The membrane samples were in contact with various concentrations of optically pure D-Glu or L-Glu solution and the amounts of each enantiomer adsorbed in the membrane after equilibrium were determined. The concentration of Glu in the membrane was determined adopting the amount of Glu adsorbed in the membrane and the volume of membrane phase, including that of membrane and that of the solution in the membrane.

The adsorption isotherms for the molecularly imprinted nanofiber membranes are shown in Fig. 20.8. The adsorption isotherms for L-Glu in Fig. 20.8a and that for D-Glu in Fig. 20.8b are straight lines passing through origin, implying that the L-isomer in the D-isomer selective adsorption nanofiber membrane (Fig. 20.8a) and the D-isomer in the L-isomer selective adsorption one (Fig. 20.8b) were adsorbed without any specific interaction with membrane. This can be anticipated from the results that the Z-D-Glu molecularly imprinted nanofiber membrane showed D-isomer adsorption selectivity, while the Z-L-Glu molecularly imprinted one recognized L-Glu in preference to the corresponding D-isomer as shown in Fig. 20.7. The isotherm of Glu adsorbed nonspecifically in the nanofiber membrane can be represented by the following equation:

$$[\text{j-Glu}]_M = k_A[\text{j-Glu}] \tag{20.2}$$

where j means the enantiomer of Glu adsorbed nonspecifically in the nanofiber membrane, $[\text{j-Glu}]_M$ is the concentration of j-isomer of Glu adsorbed nonspecifically in the membrane, k_A denotes the adsorption constant, and [j-Glu] is the concentration of j-isomer of Glu in the solution equilibrated with the nanofiber membrane.

On the other hand, the adsorption isotherm of D-Glu in Fig. 20.8a and that of L-Glu in Fig. 20.8b gave dual adsorption isotherms. Those target molecules were selectively adsorbed in each molecularly imprinted nanofiber membrane.

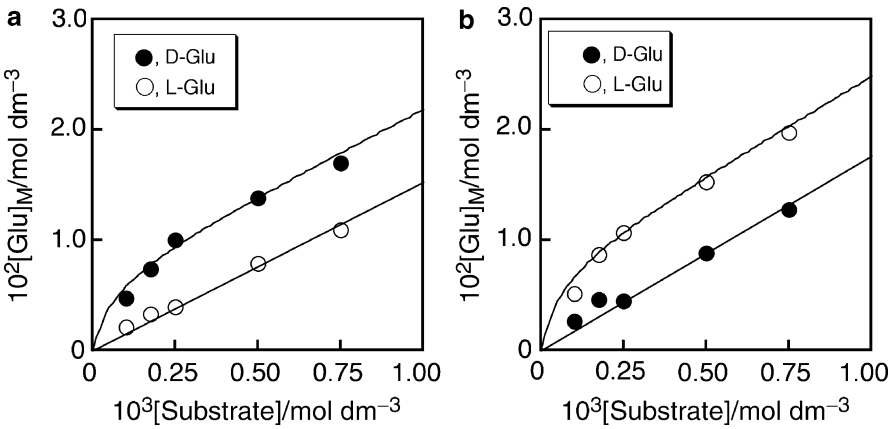

Fig. 20.8 Adsorption isotherms of D-Glu and L-Glu in the nanofiber membrane imprinted by Z-D-Glu (**a**) and the nanofiber membrane imprinted by Z-L-Glu (**b**). The mole ratio of print molecule to CA in the electrospray deposition process was fixed to be 0.50: $k_A = 1.5 \times 10$; $[\text{Site}]_0 = 7.0 \times 10^{-3}$ mol dm^{-3}; $K_S = 1.6 \times 10^4$ mol^{-1} dm^3 for (**a**) and $k_A = 1.8 \times 10$; $[\text{Site}]_0 = 8.0 \times 10^{-3}$ mol dm^{-3}; $K_S = 1.7 \times 10^4$ mol^{-1} dm^3 for (**b**)

The straight lines over the substrate concentration of 5.0×10^{-4} mol dm^{-3} are almost parallel to those of enantiomers nonspecifically adsorbed in each membrane. And the extension of those straight lines does not pass through origin and has positive intercept. Those dual adsorption isotherms consist of nonspecific adsorption and adsorption on specific recognition sites toward the D-isomer (Fig. 20.8a) or the L-isomer (Fig. 20.8b).

The isotherm of Glu adsorbed specifically in the membrane can be represented by the following equation:

$$[\text{i-Glu}]_M = k_A[\text{i-Glu}] + K_S[\text{Site}]_0[\text{i-Glu}]/(1 + K_S[\text{i-Glu}]) \tag{20.3}$$

where $[\text{i-Glu}]_M$ means the concentration of i-isomer of Glu adsorbed preferentially in the molecularly imprinted nanofiber membrane, K_S is the affinity constant between the i-isomer and the molecular recognition site, $[\text{Site}]_0$ is the concentration of molecular recognition site in the membrane, and [i-Glu] denotes the concentration of i-isomer of Glu in the solution equilibrated with the nanofiber membrane. Two parameters in those adsorption equations (Eqs. 20.2 and 20.3), which were determined to fit each adsorption isotherm in Fig. 20.8 best, are summarized in Table 20.2 together with those for usual molecularly imprinted CA membranes [25].

The concentration of molecular recognition sites, which were constructed by the presence of the print molecule during the electrospray deposition process, for the Z-D-Glu molecularly imprinted nanofiber membrane was determined to be 7.0×10^{-3} mol dm^{-3} and that for the Z-L-Glu imprinted one to be

Table 20.2 Parameters for adsorption isotherms

	Z-D-Glu imprinted mem.		Z-L-Glu imprinted mem.	
	MIPM[a]	MINFM[b]	MIPM[a]	MINFM[b]
k_A	1.9×10^3	1.5×10	2.0×10^3	1.8×10
$[\text{Site}]_0$ / mol dm^{-3}	3.4	7.0×10^{-3}	3.4	8.0×10^{-3}
K_S / mol^{-1} dm^3	3.1×10^3	1.6×10^4	3.1×10^3	1.7×10^4

[a]Molecularly imprinted membrane; the data were cited from Ref. [25]
[b]Molecularly imprinted nanofiber membrane; the data were cited from Ref. [37]

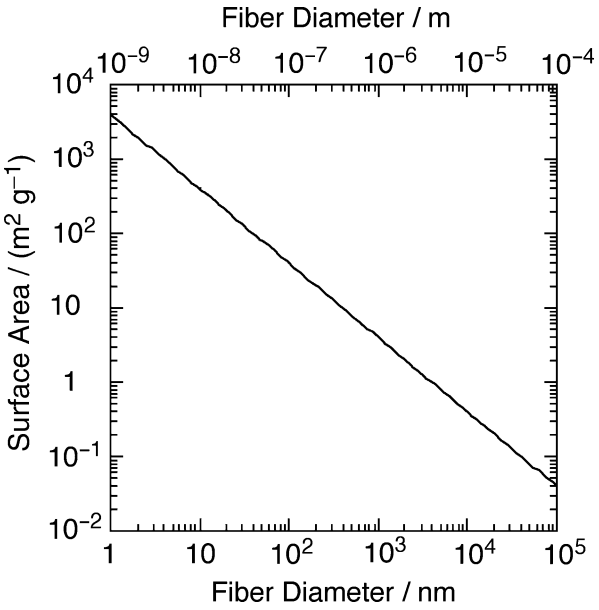

Fig. 20.9 Relationship between surface area of nanofiber membrane and its diameter. (Calculation was carried out, assuming the density of the polymer being 1.0 g cm^{-3})

8.0×10^{-3} mol dm^{-3}, respectively. On the other hand, the concentration of the molecular recognition site for the molecularly imprinted usual CA membranes was determined to be 3.4 mol dm^{-3} [25]. Figure 20.9 shows the relationship between surface area of nanofiber membrane and its diameter, assuming the density of the candidate polymer being 1.0 g cm^{-3}. Against expectation, the numbers of molecular recognition sites in the molecularly imprinted nanofiber membranes were lower than that for the usual molecularly imprinted CA membrane, even though the surface area of the nanofiber membrane was higher than that for the usual dense membrane. This led to the conclusion that the amount of Z-D-Glu or Z-L-Glu, which effectively worked as a print molecule in electrospray deposition process, was less than that in the previous study to obtain usual molecularly imprinted CA membranes [25]. This can be explained as follows: as schematically shown in Fig. 20.10,

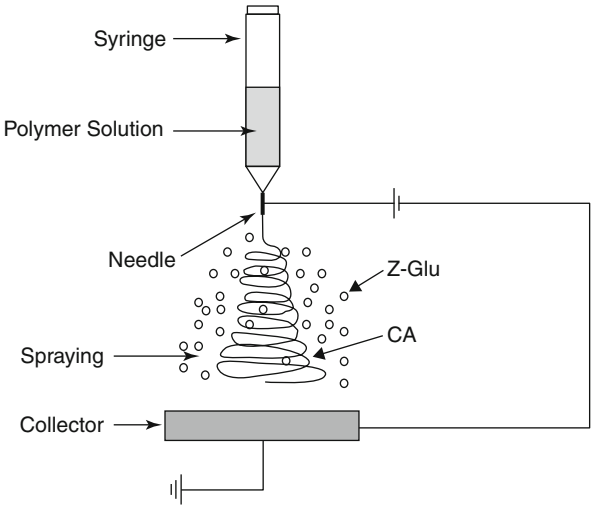

Fig. 20.10 Tentative scheme of electrospray deposition, where CA and Z-Glu were simultaneously electrosprayed

in the electrospray deposition process of CA and Z-D-Glu or Z-L-Glu, most print molecule Z-Glu was solely sprayed toward the counter electrode of grounded aluminum foil accompanying with no CA molecule. As a result, small amount of the print molecule was electrosprayed together with CA molecule toward the collector. In other words, the molecular imprinting ratio, which is the mole ratio of the print molecule to the constitutional repeating unit of CA, for the preparation of the molecularly imprinted nanofiber CA membrane was lower than that for the previous molecularly imprinted CA membrane.

The above speculation can be supported by the affinity constants for those two types of membrane, such as molecularly imprinted nanofiber membrane and usual molecularly imprinted membrane. The affinity constant K_S for the molecularly imprinted nanofiber membranes were determined to be 1.6×10^4 mol^{-1} dm^3 for the Z-D-Glu molecularly imprinted nanofiber membrane and 1.7×10^4 mol^{-1} dm^3 for the Z-L-Glu imprinted one, respectively. Those for the molecularly imprinted usual membranes were determined to be 3.1×10^3 mol^{-1} dm^3 [25], which were less than 20 % of those for the molecularly imprinted nanofiber membranes. As schematically depicted in Fig. 20.11, the affinity constant for the molecular recognition site constructed by the print molecule and the target molecule would be greatly dependent on the molecular imprinting condition (molecular imprinting ratio) and K_S was increased with the decrease in the molecular imprinting ratio (Z-Glu)/(CA) [66]. At the low molecular imprinting ratio, more functional groups interacted with one print molecule, resulting in a higher affinity constant. As a result, the affinity constant gave higher values with the decrease in the molecular imprinting ratio. This means that the amount of the print molecule effectively worked during the electrospray deposition process was lower than that during the usual molecular imprinting process.

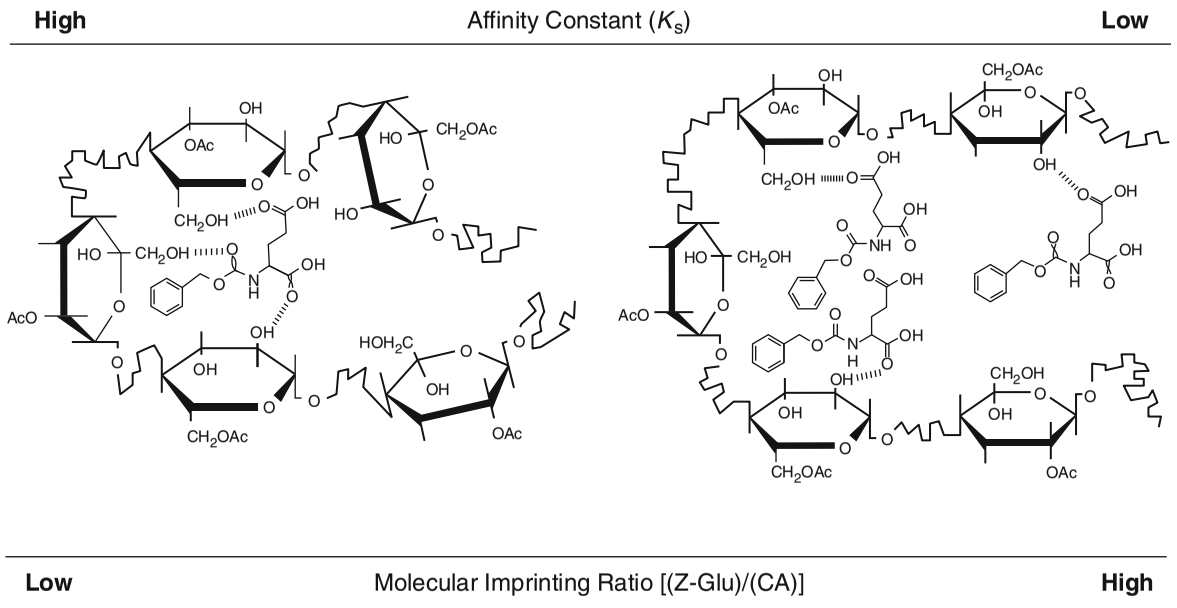

Fig. 20.11 Schematic image of the relationship between molecular imprinting ratio and affinity constant

The parameters in the adsorption equations were determined by using adsorption isotherms shown in Fig. 20.8. Those parameters could be determined by adopting the experimental data obtained in the adsorption selectivity study shown in Fig. 20.7. Since the molecular recognition site, which was constructed by the presence of the print molecule, incorporated the enantiomer, of which absolute configuration was the same as that of the print molecule. Contrary to this, the antipode was not incorporated into the constructed molecular recognition site. Nonspecific adsorption of each enantiomer of Glu, which was an adsorption without any specific interaction, occurred without the interference of nonspecific adsorption of antipode.

Substituting Eqs. 20.2 and 20.3 into Eq. 20.1 and rearranging yield Eq. 20.4:

$$S_{A(i/j)} = k_{A,i}/k_{A,j} + K_S[\text{Site}]_0/k_{A,j}(1 + K_S[\text{i-Glu}]) \tag{20.4}$$

where $k_{A,i}$ denotes the adsorption constant for the i-isomer and $k_{A,j}$ is that for j-isomer, respectively. If the feed is the solution of racemic mixture and the adsorption constant for i-isomer ($k_{A,i}$) and that for j-isomer ($k_{A,j}$) are same (k_A), as is the case here, the adsorption selectivity can be represented as follows:

$$S_{A(i/j)} = 1 + K_S[\text{Site}]_0/k_A(1 + K_S[\text{Glu}]) \tag{20.5}$$

where [Glu] denotes the concentration of each enantiomer in the racemic mixture ([i-Glu] = [j-Glu] = [Glu]). From Eq 20.5, in the case that i-isomer is incorporated into the membrane following the dual adsorption equation and the antipode j-isomer nonspecifically adsorbed, the adsorption selectivity will be dependent on substrate concentration and increased with the decrease in the substrate concentration as observed in Fig. 20.7.

5.5 Chiral Separation

From adsorption selectivity and adsorption isotherm studied, those two types of molecularly imprinted CA nanofiber membrane were expected to show enantioselective transport ability. To this end, enantioselective transport of racemic Glu through those two types of molecularly imprinted nanofiber membrane and the control nanofiber membrane was studied. As expected from the previous study on nanofiber membranes [36], the present membranes would give relatively high flux. From this, concentration gradient was adopted as a driving force for membrane transport. As examples of time-transport curves for those membranes, those for the initial feed concentration of 2.50×10^{-4} mol dm^{-3} are shown in Fig. 20.12. As expected from previous results [25] and adsorption phenomena shown in Figs. 20.7 and 20.8, D-Glu was transported through the Z-D-Glu molecularly imprinted nanofiber membrane in preference to the corresponding antipode L-Glu and *vice versa*. In other words, the Z-L-Glu molecularly imprinted nanofiber membrane selectively transported the L-isomer of Glu. The permselectivity

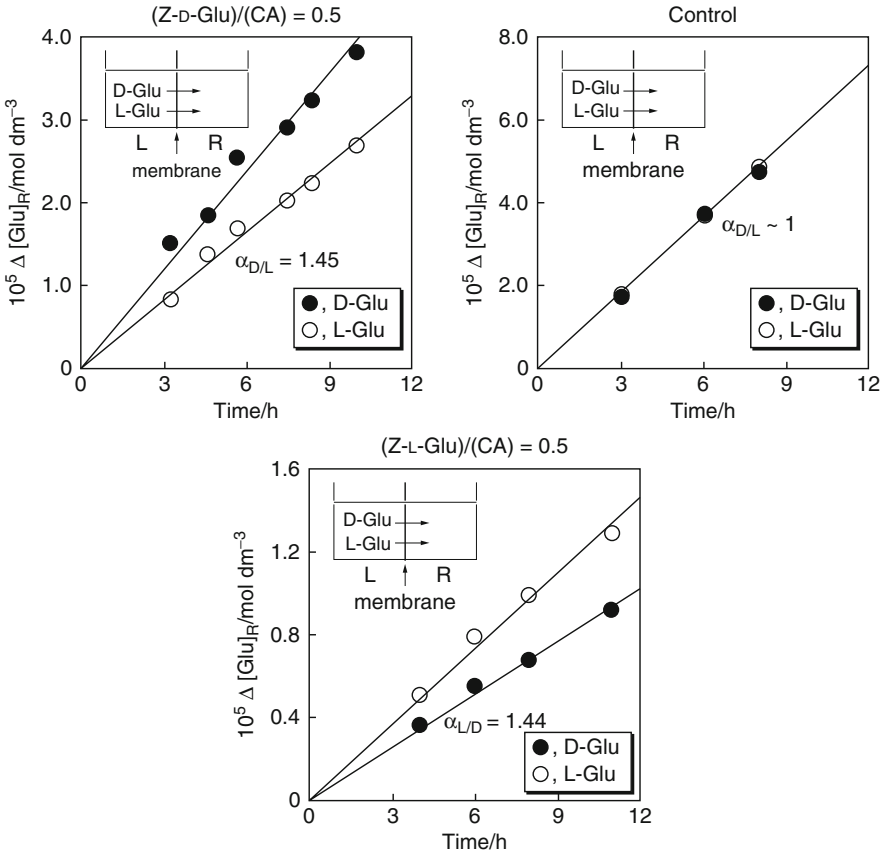

Fig. 20.12 Time-transport curves of racemic Glu through the molecularly imprinted and control nanofiber membranes. (The molecular imprinting ratio, (Z-Glu)/(CA), was fixed to be 0.50; $[\text{D-Glu}]_{L,0} = [\text{L-Glu}]_{L,0} = 2.50 \times 10^{-4}$ mol dm^{-3})

$\alpha_{i/j}$ is defined as the flux ratio, J_i/J_j, divided by the initial concentration ratio $[\text{i-Glu}]_0/[\text{j-Glu}]_0$.

$$\alpha_{i/j} = \left(J_i/J_j\right)/\left([\text{i-Glu}]_0/[\text{j-Glu}]_0\right) \tag{20.6}$$

The flux J (mol cm cm^{-2} h^{-1}) is defined as

$$J = Q\delta/At \tag{20.7}$$

where Q [mol] is the amount of transported Glu, δ [cm] is the membrane thickness, A [cm^2] is the membrane area, and t [h] means membrane transport time. The permselectivity toward D-Glu for the Z-D-Glu molecularly imprinted nanofiber

membrane was determined to be 1.45, while that toward L-Glu for the Z-L-Glu molecularly imprinted nanofiber membrane to be 1.44. Contrary to this, as anticipated, the control nanofiber membrane, which was fabricated by electrospray deposition without a print molecule, hardly showed permselectivity toward racemic mixture of Glu. The dependence of permselectivity on the initial feed concentration will give us the insight into the transport mechanism like that of adsorption phenomena gave important results.

From Eqs. 20.3 and 20.7, the flux of i-isomer, which was incorporated into the membrane following the dual adsorption equation, can be represented as follows:

$$J_{\mathrm{i}} = D_{\mathrm{n,i}} k_{A,\mathrm{i}} [\text{i-Glu}] \quad + \quad D_{\mathrm{s,i}} K_{\mathrm{S}} [\mathrm{Site}]_0 [\text{i-Glu}] / (1 + K_{\mathrm{S}} [\text{i-Glu}]) \tag{20.8}$$

$$= D_{\mathrm{n,i}} k_{A,\mathrm{i}} [\text{i-Glu}] \{1 + \mathrm{FK} / (1 + K_{\mathrm{S}} [\text{i-Glu}])\} \tag{20.9}$$

$$F = D_{\mathrm{s,i}} / D_{\mathrm{n,i}}, K = K_{\mathrm{S}} [\mathrm{Site}]_0 / k_{A,\mathrm{i}}$$

where $D_{\mathrm{n,i}}$ is the diffusion coefficient of i-Glu nonspecifically incorporated into the membrane and $D_{\mathrm{s,i}}$ means the diffusion coefficient of i-Glu preferentially incorporated into the molecular recognition sites. The flux for J_{j} is represented as follows:

$$J_{\mathrm{j}} = D_{\mathrm{n,j}} k_{A,\mathrm{j}} [\text{j-Glu}] \tag{20.10}$$

where $D_{\mathrm{n,j}}$ denotes the diffusion coefficient of j-Glu nonspecifically adsorbed in the membrane. Substituting Eqs. 20.9 and 20.10 into Eq. 20.6 and rearranging yield Eq. 20.11:

$$\alpha_{\mathrm{i/j}} = \left(D_{\mathrm{n,i}} k_{A,\mathrm{i}} / D_{\mathrm{n,j}} k_{A,\mathrm{j}} \right) \left\{ 1 + FK / (1 + K_{\mathrm{S}} [\text{i-Glu}]) \right\} \tag{20.11}$$

If the feed is the solution of racemic mixture and the adsorption constant for i-isomer ($k_{\mathrm{A,i}}$) and that for j-isomer ($k_{\mathrm{A,j}}$) are same (k_{A}), as is the case here, the permselectivity can be represented as follows:

$$\alpha_{\mathrm{i/j}} = \left(D_{\mathrm{n,i}} / D_{\mathrm{n,j}} \right) \{1 + FK / (1 + K_{\mathrm{S}} [\mathrm{Glu}])\} \tag{20.12}$$

$$F = D_{\mathrm{s,i}} / D_{\mathrm{n,i}}, K = K_{\mathrm{S}} [\mathrm{Site}]_0 / k_{\mathrm{A}}$$

From Eq. 20.12, the permselectivity would be expected to increase with the decrease in feed concentration. Figure 20.13 shows the dependence of permselectivity on initial feed concentration. As can be seen, permselectivity of molecularly imprinted nanofiber membranes was increased with the decrease in feed concentration, implying that the molecular recognition sites in the molecularly imprinted nanofiber membrane contributed to enantioselective transport. On the other hand, permselectivity for the control nanofiber membrane was hardly

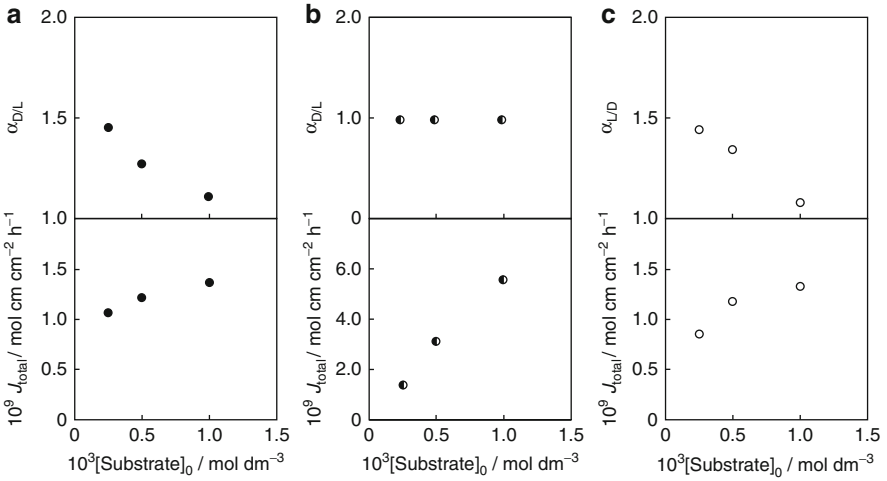

Fig. 20.13 Effect of substrate concentrations on the transport of racemic Glu through Z-D-Glu molecularly imprinted nanofiber membrane (**a**), control nanofiber membrane (**b**), and Z-L-Glu molecularly imprinted nanofiber membrane (**c**)

dependent on the feed concentration and gave unity at any initial feed concentrations. The dependence of flux on initial feed concentration also supported the transport mechanism described above; in other words, the flux through the molecularly imprinted nanofiber membranes showed nonlinear relationship to substrate concentration. The slope of the flux dependence on substrate concentration decreased with the increase in the feed concentration and reached asymptotically to a certain value. Contrary to this, the flux through the control nanofiber membrane was linearly increased with the substrate concentration and the relationship passed through origin.

5.6 Comparison of Membrane Performances

In membrane separation, not only permselectivity but also flux is an important membrane performance as mentioned before. In a sense, the enhancement of flux is more important than that of permselectivity. In the present chapter, membrane performance for molecularly imprinted CA nanofiber membranes and molecularly imprinted usual CA membranes will be compared. In the membrane transport with molecularly imprinted CA nanofiber membranes, the membrane performances were studied adopting concentration gradient as a driving force for membrane transport, while potential difference was adopted as a driving force for membrane transport in the membrane transport through molecularly imprinted usual CA membranes. Molar mobility, u (mol cm cm^{-2} J^{-1} h^{-1}), of permeant Glu is a suitable parameter to compare flux values for those membranes each other. From Nernst-Planck equation, a flux can be represented by the following equation [67]:

Table 20.3 Results of chiral separation with molecularly imprinted nanofiber membranes (MINFM's)[a]

	Z-D-Glu imprinted MINFM		Control NFM		Z-L-Glu imprinted MINFM	
$10^3\Delta c$[b] mol dm^{-3}	$\alpha_{D/L}$	u[c]	$\alpha_{D/L}$	u[c]	$\alpha_{L/D}$	u[c]
0.25[d]	1.45	1.96×10^{-9} (290)	~1	1.98×10^{-9} (293)	1.44	3.81×10^{-9} (564)
0.50[d]	1.27	1.04×10^{-9} (154)	~1	2.04×10^{-9} (302)	1.34	2.49×10^{-9} (368)
1.00[d]	1.11	5.49×10^{-10} (81.2)	~1	1.70×10^{-9} (251)	1.07	1.32×10^{-9} (195)
ΔE[e]	2.30	6.76×10^{-12} (1)			2.30	6.76×10^{-12} (1)

[a]Figures in parentheses are the relative values, the u value for ΔE being set as unity
[b]A concentration gradient was applied as a driving force for membrane transport
[c]$u = (-J/c)/(\mathrm{d}\mu/\mathrm{d}x)$ [{(mol cm cm^{-2}h^{-1})/(mol cm^{-3})}/(J mol^{-1}cm^{-1}) = mol cm cm^{2}J^{-1}h^{-1}]
[d]A concentration difference was applied as a driving force for membrane transport, cited from Ref. [37]
[e]A potential difference was applied as a driving force for membrane transport, cited from Ref. [25]

$$J = -ucRT[(\mathrm{d}\ln c/\mathrm{d}x) + (zF/RT)(\mathrm{d}\phi/\mathrm{d}x) + (v/RT)(\mathrm{d}P/\mathrm{d}x)] \tag{20.13}$$

where J denotes the sum of D-Glu and L-Glu fluxes, c is the concentration of each Glu in the feed side, R means universal gas constant, T denotes absolute temperature, $\mathrm{d}c/\mathrm{d}x$ is the concentration gradient at that point, z is valence of permeant, F means the Faraday constant, $\mathrm{d}\phi/\mathrm{d}x$ denotes electrical potential gradient at that point, v is partial molar volume of permeant, and $\mathrm{d}P/\mathrm{d}x$ is the pressure gradient at that point. In the present study, membrane transport experiments were carried out under isothermal and isobar conditions. From this, the third term in Eq. 20.13 was left out. In the case of membrane transport adopting concentration gradient as a driving force, the flux J can be represented by just first term in Eq. 20.13; the flux by using potential gradient as a driving force can be represented by just second term in Eq. 20.13.

The molar mobility is simply the flux per unit membrane area, per unit membrane thickness, per unit concentration, per unit driving force. In the calculation of the chemical potential due to the concentration gradient, the concentration of Glu in the permeate side was determined to be 1.0×10^{-8} mol dm^{-3}, since the lowest limit of the detection of Glu in the present study was the concentration of around 1.0×10^{-8} mol dm^{-3}. Table 20.3 summarizes membrane performances for two types of CA membranes, such as molecularly imprinted nanofiber and molecularly imprinted usual membranes. In the parentheses in the table, the relative molar mobility for each membrane, which is relative to that of molecularly imprinted usual membrane, is also given for convenience.

As can be seen in Table 20.3, flux values for the molecularly imprinted CA nanofiber membranes were one to two orders of magnitude higher than those for molecularly imprinted usual CA membranes. In the membrane separation, a flux value and the corresponding permselectivity often show a trade-off relationship.

Against this, the molecularly imprinted CA nanofiber membranes still gave permselectivity as observed in chiral separation with molecularly imprinted nanofiber membranes from carboxylated polysulfone [36].

6 Conclusions

Molecularly imprinted nanofiber membranes, which are expected to open a door to novel separation membranes, were fabricated from cellulose acetate (CA) and a derivative of optically pure glutamic acid, such as Z-D-Glu or Z-L-Glu, as a print molecule by simultaneously applying an alternative molecular imprinting and an electrospray deposition. The molecularly imprinted CA nanofiber membranes revealed that those membranes enhance both permselectivity and flux, which are generally perceived to show a trade-off relationship.

The flux values for the molecularly imprinted CA nanofiber membranes were about two orders of magnitude higher than those for molecularly imprinted usual CA ones. However, the molecularly imprinted CA nanofiber membranes still showed permselectivity. The present study revealed that molecularly imprinted nanofiber membranes have potential that both permselectivity and flux can be simultaneously enhanced.

References

1. Ho WSW, Sirkar KK (eds) (1992) Membrane handbook. Chapman & Hall, New York
2. Mulder M (1996) Basic principles of membrane technology, 2nd edn. Kluwer Academic, Dordrecht
3. Baker RW (2004) Membrane technology and applications, 2nd edn. Wiley, West Sussex
4. Bartsch RA, Maeda M (eds) (1998) Molecular and ionic recognition with imprinted polymers. ACS symposium series, vol 703. ACS, Washington, DC
5. Sellergren B (ed) (2001) Molecularly imprinted polymers man-made mimics of antibodies and their applications in analytical chemistry. Elsevier, Amsterdam
6. Komiyama M, Takeuchi T, Mukawa T, Asanuma H (2003) Molecular imprinting. Wiley-VCH, Weinheim
7. Alexander C, Andersson HS, Andersson LI, Ansell RJ, Kirsch N, Nicholls IA, O'Mahony J, Whitcombe MJ (2006) J Mol Recognit 19:106
8. Yoshikawa M (1998) Molecularly imprinted polymeric membranes for optical resolution. In: Bartsch RA, Maeda M (eds) Molecular and ionic recognition with imprinted polymers. ACS symposium series, vol 703. ACS, Washington, DC, p 170
9. Piletsky SA, Panasyuk TL, Piletskaya EV, Nicholls IA, Ulbricht M (1999) J Membr Sci 157:263
10. Yoshikawa M (2002) Bioseparation 10:277
11. Ulbricht M (2004) J Chromatogr B 804:113
12. Polyakov MV (1931) Zhur Fiz Khim 2:799
13. Dickey FH (1949) Proc Natl Acad Sci USA 35:227
14. Katz A, Davis ME (2000) Nature 403:286
15. Klotz IM, Harris JU (1971) Biochemistry 10:923
16. Takagishi T, Klotz IM (1972) Biopolymers 11:483

17. Wulff G, Sarhan A (1972) Angew Chem Int Ed 11:341
18. Arshady R, Mosbach K (1981) Makromol Chem 182:687
19. Whitecombe MJ, Rodrequez ME, Villar P, Vulfson EN (1995) J Am Chem Soc 117:7105
20. Nishide H, Tsuchida E (1976) Makromol Chem 177:2295
21. Yoshikawa M, Izumi J, Kitao T, Koya S, Sakamoto S (1994) Preprints for the 16th annual meeting of the Membrane Society of Japan, Tokyo. p 73
22. Yoshiakwa M, Izumi J, Ooi T, Kitao T, Guiver MD, Robertson GP (1998) Polym Bull 40:517
23. Yoshikawa M, Izumi J, Kitao T, Sakamoto J (1996) Macromolecules 29:8197
24. Yoshikawa M, Izumi J (2003) Macromol Biosci 3:487
25. Yoshikawa M, Ooi T, Izumi J (1999) J Appl Polym Sci 72:493
26. Yoshikawa M, Kawamura K, Ejima A, Aoki T, Sakurai S, Hayashi K, Watanabe K (2006) Macromol Biosci 6:210
27. Michaels AS, Baddour RF, Bixler HJ, Choo CY (1962) Ind Eng Chem Process Des Dev 1:14
28. Piletskii SA, Dubei IY, Fedoryak DM, Kukhar VP (1990) Biopolim Kletka 6:55
29. Mathew-Klotz J, Shea KJ (1996) J Am Chem Soc 118:8154
30. Yoshikawa M, Tanioka A, Matsukoto H (2011) Curr Opin Chem Eng 1:18, and ref. 27–42 herein
31. Yoshikawa M, Izumi J, Kitao T, Koya S, Sakamoto S (1995) J Membr Sci 108:171
32. Trotta F, Drioli E, Baggiani C, Lacopo D (2002) J Membr Sci 201:77
33. Yoshikawa M, Tanioka A, Matsukoto H (2011) Curr Opin Chem Eng 1:18, and ref. 43–49 herein
34. Greiner A, Wendorff JG (2007) Angew Chem Int Ed 46:5670
35. Chu B, Hsiao BS (2009) J Polym Sci B Polym Phys 47:2431
36. Yoshikawa M, Nakai K, Matsumoto H, Tanioka A, Guiver MD, Robertosn GP (2007) Macromol Rapid Commun 28:2100
37. Sueyoshi Y, Fukushima C, Yoshikawa M (2010) J Membr Sci 357:90
38. Sueyoshi Y, Utsunomiya A, Yoshikawa M, Robertson GP, Guiver MD (2012) J Membr Sci 89:401
39. Qu XJ, Meng QX, Ai SY, Zhoum J, Zhu LS (2008) J Anal Chem 63:999
40. Ramamoorthy M, Ulbrich M (2003) J Membr Sci 217:207
41. Ramamoorthy M, Ulbric M (2004) Sep Pur Tech 39:211
42. Suedee R, Bodhibukkana C, Naruedom T, Amnuaikit C, Kaewnopparat S, Srichana TJ (2008) Control Release 129:170
43. Jantarat C, Tangthong N, Sarunyoo S, Martin GP, Suedee R (2008) Int J Pharm 349:212
44. Faizal CKM, Takaomi K (2008) Pol Eng Sci 46:1085
45. Xiang-Jin Q, Chang-Bao C, Jie Z, Chun-Hui W (2007) Chin J Chem 25:213
46. Izumi J, Yoshikawa M, Kitao T (1997) Membrane 22:149
47. Kondo Y, Yoshikawa M (2001) Membrane 26:228
48. Yoshikawa M, Yoshioka T, Fujime J, Murakami A (2000) J Membr Sci 178:75
49. Yoshikawa M, Masaki K, Ishikawa M (2002) J Membr Sci 205:293
50. Yoshikawa M, Higuchi A, Ishikawa M, Guiver MD, Robertson GP (2004) J Membr Sci 243:89
51. Yoshikawa M, Kawamura K, Ejima A, Aoki T, Watanabe K, Guiver MD, Robertson GP (2004) Membrane 29:384
52. Yoshiakwa M, Kawamura K, Watanabe K (2007) Membrane 32:40
53. Matsuura T, Sada T, Yoshiakwa M, Ogata N (2006) Membrane 31:281
54. Yoshikawa M, Maruhashi M, Iwamoto Y, Ogata N (2007) Macromol Symp 557:249
55. Yoshikawa M, Maruhashi M, Iwamoto Y, Ogata N (2007) Polym J 39:1193
56. Iwamoto Y, Maruhashi M, Yoshiakwa M, Ogata N (2009) Membrane 34:281
57. Iwamoto Y, Yoshikawa M, Yamaoka K, Ogata N (2010) Desalination Water Treat 17:268
58. Iwamoto Y, Shimizu T, Murai Y, Yoshikawa M, Ogata N (2010) Membrane 35:201
59. Sueyoshi Y, Hashimoto T, Yoshikawa M, Watanabe K (2011) Waste Biomass Valor 2:303
60. Sueyoshi Y, Hashimoto T, Yoshikawa M, Ifuku S (2012) Sustain Agric Res 1:42

61. Agarwal S, Wendorff JH, Greiner A (2008) Polymer 49:5603
62. Huang ZM, Zhang YZ, Kotaki M, Ramakrishna S (2003) Comp Sci Tech 63:2223
63. Sangamesh GK, Syam PN, Roshan J, MaCalus VH, Cato TL (2008) Recent Patent Biomed Eng 1:68
64. Chronakis IS, Jakob A, Hagstrom B, Ye L (2006) Langmuir 22:8960
65. Chronakis IS, Milosevic B, Frenot A, Ye L (2006) Macromolecules 39:357
66. Taniwaki K, Hyakutake A, Aoki T, Yoshikawa M, Guiver MD, Robertson GP (2003) Anal Chim Acta 489:191
67. Schultz SG (1980) Basic principles of membrane transport. Cambridge University Press, Cambridge

Electrical and Optical Properties of Nanocellulose Films and Its Nanocomposites

21

Hyun-Joong Kim, Hyeok-Jin Kwon, Sera Jeon, Ji-Won Park, Jackapon Sunthornvarabhas, and Klanarong Sriroth

Contents

Book Chapter in, "The potential of nanocomposites composed of nanocellulose in various applications requiring optical transparency and electrical conductivity"

H.-J. Kim (✉)
College of Agriculture and Life Sciences, Seoul National University, Seoul, Republic of Korea
e-mail: hjokim@snu.ac.kr

H.-J. Kwon • S. Jeon • J.-W. Park
Laboratory of Adhesion & Bio-Composites, Program in Environmental Materials Science, Seoul National University, Seoul, Republic of Korea
e-mail: hjk00153@snu.ac.kr; serajeon@snu.ac.kr; rooroun7@snu.ac.kr

J. Sunthornvarabhas
Laboratory of Adhesion & Bio-Composites, Program in Environmental Materials Science, Seoul National University, Seoul, Republic of Korea

Cassava and Starch Technology Research Unit, National Center for Genetic Engineering and Biotechnology, Bangkok, Thailand
e-mail: jackapon.sun@biotec.or.th

K. Sriroth
Kasetsart Agricultural and Agro-Industrial Product Improvement Institute, Department of Biotechnology, Kasetsart University, Bangkok, Thailand
e-mail: aapkrs@ku.ac.th

J.K. Pandey et al. (eds.), *Handbook of Polymer Nanocomposites. Processing, Performance and Application – Volume C: Polymer Nanocomposites of Cellulose Nanoparticles*,
DOI 10.1007/978-3-642-45232-1_74,

Keywords
Nano-cellulose • Bacterial cellulose • Nanocellulose Whisker • Microfibrillated Cellulose • Optical properties • Thermal stability • Conductivity • Nano-composites • Carbon nano tube

1 Introduction

Cellulose is one of the most abundant and common natural resources around us. The production of nanoscaled cellulose fibers and their application in composite materials have gradually got increasing attention during the last decades because nanocellulose has many advantages (i.e., high crystallinity, high tensile strength, high melting temperature, 200 times more surface area, finer weblike network, stiffness combined with low weight, and biodegradability). Nanocomposites with cellulosic nanofibers as reinforcing material appeared 15 years ago [1]. Due to these advantages, nanocelluloses were applied in various fields of technologies [2]. Nanocellulose can be classified into four kinds according to production method and material source. Figure 21.1 shows categories of nanocellulose.

Table 21.1 compares mechanical properties of nanocellulose with other selected hard materials. It shows that nanocellulose exceeds other materials on some properties. These unique properties of nanocellulose open the possibility of applications to various industrial fields.

Nanocellulose has been attended for an excellent candidate material to substitute rigid glass. The flat-panel display (FPD) are generally manufactured by the deposition of functional materials such as metal wiring, transparent conductive films, and gas barrier films on large glass substrates and then divided into commercial sizes. But, the processing of continuous roll-to-roll is expected to substitute

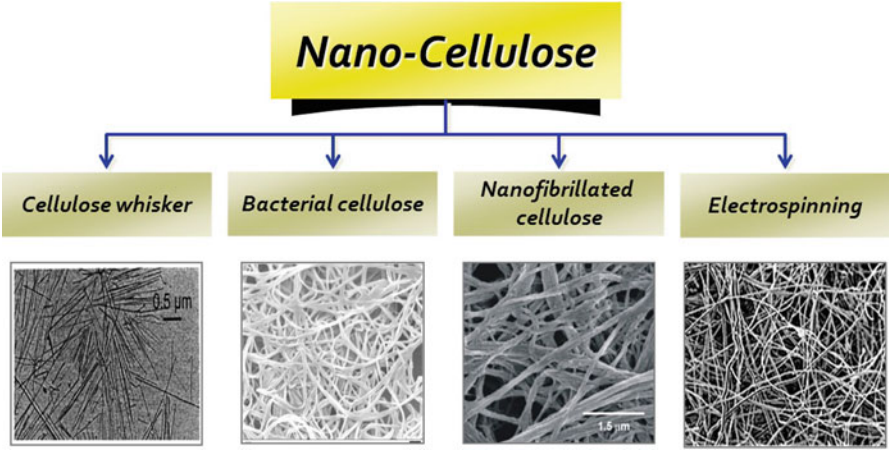

Fig. 21.1 Classification of nanocellulose; this figure was adapted from [3]

Table 21.1 Moduli of engineering materials compared to nanocellulose [1]

Material	Modulus [GPa]	Density [g cm^{-2}]	Specific modulus [GPa g^{-1} cm^{-3}]
Aluminum	69	2.7	26
Steel	200	7.8	26
Glass	69	2.5	28
Crystalline nanocellulose	138	1.5	92

the conventional bath processing of glass substrates, resulting in simpler process and cost-effective production. The substituted materials for the glass need many requirements, such as optical properties, flexibility, and thermal expansion, to be processed by continuous roll-to-roll. Therefore, nanocellulose-reinforced nanocomposites are anticipated proper substitution material for glass. Table 21.2 shows properties of nanocellulose-based nanocomposites [4–7].

Two primary important properties of flat film for electronic display are optical properties and electrical properties. Conducting polymers (i.e., polypyrrole, polyaniline, polyacetylene, etc.) and the conducting nanoparticles (i.e., single-walled carbon nanotubes, double-walled carbon nanotubes, multiwalled carbon nanotubes) were introduced to nanocellulose in order to enhance electrical properties; more details will be discussed in later part of this chapter.

The conducting polymers were chosen based on required properties of electric instrument and application. Because of diverse chemical structure of conductive polymers as shown in Fig. 21.2, wide range of materials have been developed and studied. Table 21.3 compares benefit and limitation of conductive polymers, metal, and CNT-based materials.

Giving electrical properties to nanocellulose provides chance to pioneer technological application, including electromagnetic interference (EMI) shielding and microwave absorbing as other potential applications [9–11].

2 Optical Properties of Nanocomposites

Nanocomposites in general are two-phase materials in which one of the phases has at least one dimension in the nanometer range or between 1 and 100 nm. The advantages of nanocomposite materials comparing with conventional composites are their superior thermal, mechanical, and barrier properties at low reinforcement levels around 2 $\sim$ 10 % by weight as well as their better recyclability, transparency, and low weight [12]. But, the most difficult to get good material homogeneity and property consistency of nanocomposites is the lack of interfacial adhesion between the hydrophilic fillers and hydrophobic polymer matrix or vice versa. Many researchers strived to improve the interfacial adhesion by introducing the use of coupling agents and chemical modification by using alkali and acid to improve filler and matrix adhesion.

Table 21.2 Properties of nanocellulose-based nanocomposites [4]

Source of cellulose	Fibrillation method	Matrix resin	Fiber content (wt%)	Regular transmittance 500 ~ 800 nm (%)	CTE (ppm K^{-1})	Tensile Young's modulus (GPa)	Tensile strength (MPa)
Bacterial	–	Epoxy	60 ~ 70	80 ~ 90	6	20 ~ 21	>300
		Low modulus acrylic	5	75 ~ 95	4	0.36	20
Kraft pulp	High-pressure homogenization + grinding	Acrylic	70	60 ~ 75	17	21	–
Softwood	Never-dried pulp grinding	Acrylic	60 ~ 85	85 ~ 90	13	13	216
Softwood (acetylated)	Never-dried pulp grinding	Low modulus acrylic	35 ~ 40	80 ~ 85	12.1	3.7	90
Softwood	Never-dried pulp grinding	–	100	65 ~ 80	8.5	13	223

2.1 Materials

2.1.1 Bacterial Cellulose (BC)

Cellulose fibers are extracellularly produced by bacteria belonging to the genera Acetobacter, Agrobacterium, Alcaligenes, Pseudomonas, Rhizobium, or Sarcina. The most efficient producer of bacterial cellulose (BC) is *Acetobacter xylinum* (or *Gluconacetobacter xylinus*), a gram-negative strain of acetic-acid-producing bacteria. Figure 21.3 shows synthesis process of cellulose by *Acetobacter xylinum*.

Bacterial cellulose is secreted as a ribbon-shaped fibril, less than 100 nm wide, which is composed of much finer 2 ~ 4 nm nanofibrils. Growing mechanism can be identified as three stages. First, bacterial cellulose accepts glucose into the cell of bacteria. Second, nanocellulose that is passed on metabolic pathway by cellulose synthase is discharged outward the cell wall. Finally, the nanocellulose aggregates into pellicle.

BC has been getting more attention during the past decade. This material can be categorized into nanocellulose based on its three dimensions, and there are important structural differences between bacterial cellulose to cellulose from other sources, for example, wood–cellulose. In contrast to the existing methods for obtaining nanocellulose through mechanical or chemo-mechanical processes, bacterial cellulose is produced by bacteria, cellulose biosynthesis, that is, building up microfibril bundles. BC has been employed in several applications such

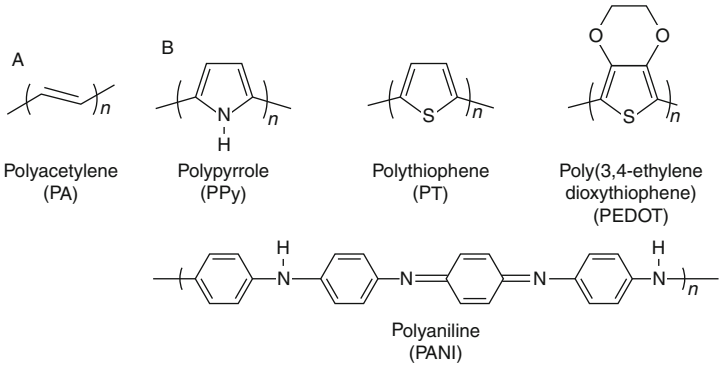

Fig. 21.2 Chemical structures of common conductive polymers [8]

Table 21.3 Compared conductive polymer with metal and CNT-based materials [9–11]

Material	Examples	Advantages	Disadvantages
Conductive polymers	Polyacetylene	Flexible	Low solubility
	Polypyrrole	Light-weighted, inexpensive	Mechanical weakness
	Polyaniline		
Metal	Cu, Al	High electrical conductivity	Highly susceptible to acid
CNT-based materials	CNT	High mechanical properties	Toxic, expensive
	Graphene		
	Graphite		

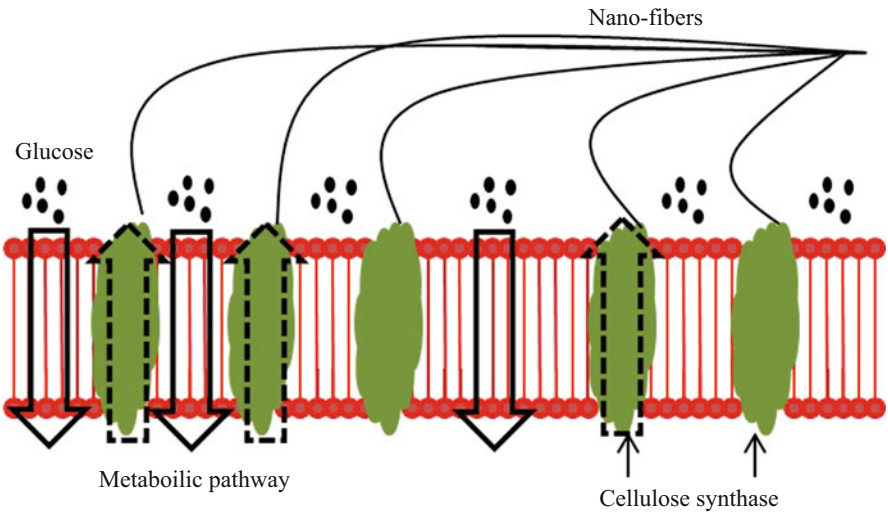

Fig. 21.3 Synthesis process of cellulose by *Acetobacter xylinum* [13]

as acoustic diaphragms, paper, wound dressings, artificial skin, and reinforced composites. It was a result of its unique properties, for instance, high crystallinity, high purity, high Young's modulus, biodegradability, large water holding capacity, etc.

There are two options for BC cultivation process: static or agitated cultivation. BC which is got by thesis method contains some impurities, such as bacteria itself. So, BC purification process is needed after cultivation process. The method of purification process was selected based on type of cultivation process. The cellulose pellicle produced in the Erlenmeyer flask was immersed repeatedly in a 0.25 M aqueous sodium hydroxide solution (NaOH) for 24 h at room temperature to remove the residual bacteria and culture medium from celluloses. The pH was then decreased to 7.0 by repeatedly washing with distilled water. The purified cellulose pellicles were stored in distilled water at 4 °C to prevent drying. For agitated culture method, purification is carried out by transferring the bacteria into a liquid medium in a flask, where it is then agitated for several days. The culture liquid is transferred into a liquid medium in a Roux flask where it is cultivated under continuous agitation for several days.

Benefit of static culture method is to prevent cellulose-deficient mutation that is interfered with the fermentation of BC [9, 14]; thus this technique is normally applied to investigate the production of BC.

Figure 21.4a shows that BC produced by the static cultivation yields smooth cellulose pellicle. On the other hand, Fig. 21.4b shows that BC produced by the static cultivation has an irregularly shaped aggregation.

2.1.2 Nanocellulose Whisker (Nano-whisker)

Making nanocomposites composed of cellulose whiskers was firstly attempted many years ago by Favier [15]. The process of making cellulose whiskers from shells of tunicate (a worm-like sea animal) was produced by dividing into small

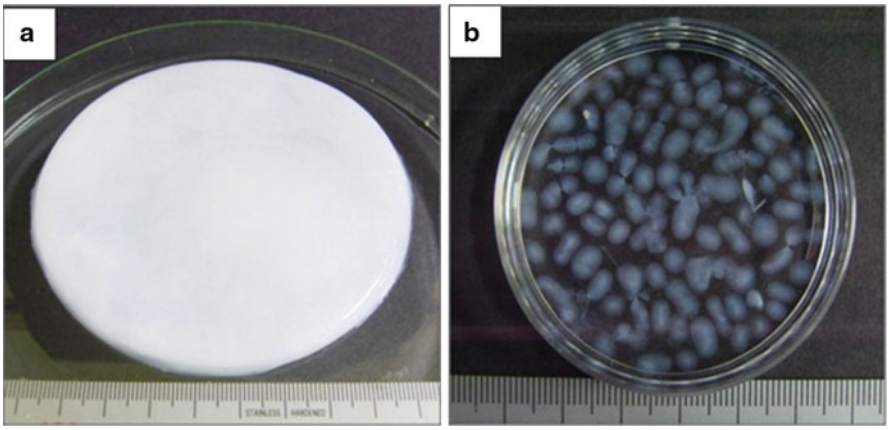

Fig. 21.4 BC pellicle formed through static cultivation (**a**) and BC pellets formed through agitated cultivation (**b**) [14]

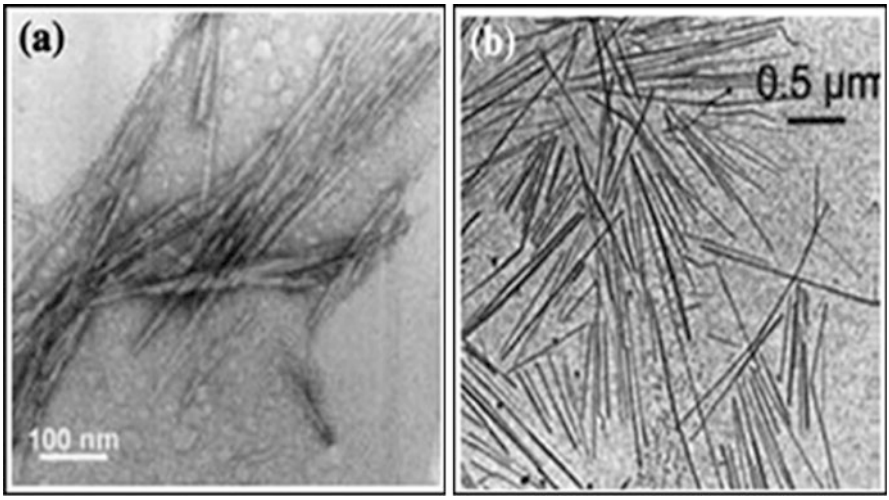

Fig. 21.5 Transmission electron microscope images of cellulose whiskers, obtained from acid hydrolysis of microstalline cellulose (**a**) and tunicate (**b**) [16]

fragments and bleached, followed by a disintegration process using a blender and a Gaulin laboratory homogenizer, and then the suspension process was hydrolyzed with 55 % sulfuric acid (H_2SO_4). Figure 21.5 indicated nanocellulose whiskers composed of rodlike cellulose crystals, with widths and lengths of 5 $\sim$ 70 nm and between 100 and 3,000 nm [3, 16].

Principle of the nanocellulose whisker processing is in Fig. 21.6. It shows breaking of crystalline regions of the semicrystalline cellulosic fibers by hydrolysis

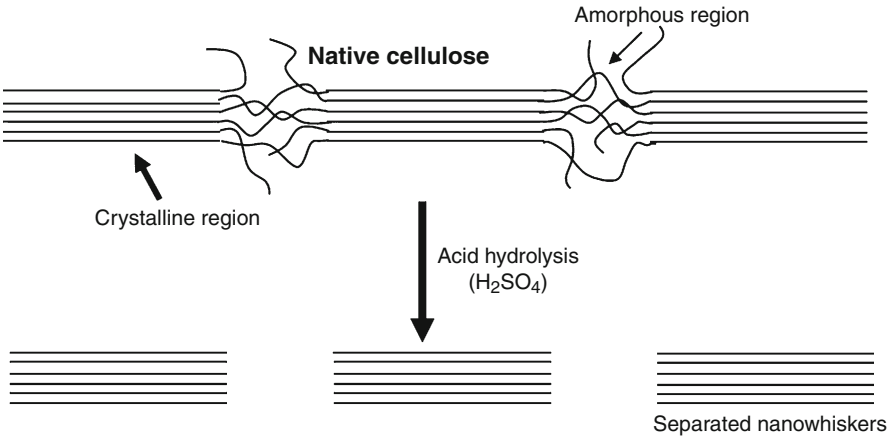

Fig. 21.6 Schematic diagram of nanocellulose separation during acid hydrolysis

with mineral acids. The polysaccharides bound at the fibril surface are firstly eliminated, and the rodlike crystalline cellulose sections are easily separated from amorphous regions. When crystalline and semicrystalline cellulose are completely separated, the acidic mixture is diluted, and the residual acids and impurities are fully removed by repeated centrifugation and extensive dialysis. After the hydrolysis, the mechanical process such as sonication disperses the nanocrystals in order to get uniform stable suspension. The formed nanocellulose whiskers have many interests including biocompatibility, biodegradability, and unique chemical and reactive surface properties [3, 17].

The nanocellulose whiskers have great potentials and are gaining interest in the fields of composites as reinforcement as well as in pharmaceutical and optical industries as additives [18].

2.1.3 Microfibrillated Cellulose (MFC)

Herrick et al. firstly attempted to isolate cellulose microfibrils through using a Gaulin laboratory homogenizer [19]. This extracted cellulose microfibril was named microfibrillated cellulose (MFC). MFC is composed of inhomogeneous material characteristics which include fibers, fiber fragments, fines, and fibrils. The production of MFC is affected by the applied treatment to the fibers before homogenization, the number of passes through the homogenizer, and the pressure applied during homogenization as shown in Fig. 21.7. When fibers are subjected to high pressure by homogenizer, the cellulose is effectively fibrillated. An increase in the transparencies of the MFC materials owing to the generation of optically inactive fibrils can indicate higher degree of fibrillation. On the other hand, in case of forming dense and compact fiber-forming structure, material exhibits low light-scattering potential or opaque behavior [20, 21].

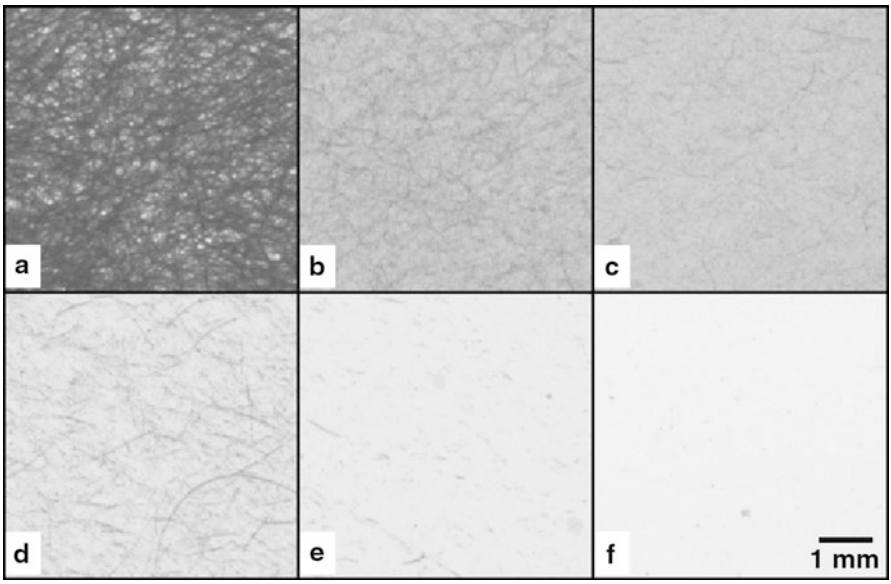

Fig. 21.7 (**a**) Control film made of 100 % *Pinus radiata* pulp fibers. (**b**) Film made of MFC, homogenized with three passes and 1,000 bar pressure. (**c**) Film made of MFC, homogenized with five passes and 1,000 bar pressure. (**d**) Film made of MFC produced with TEMPO-pretreated fibers, three passes, and 200 bar pressure. (**e**) Film made of MFC produced with TEMPO-pretreated fibers, three passes, and 600 bar pressure. (**f**) Film made of MFC produced with TEMPO-pretreated fibers, five passes, and 1,000 bar pressure. Dark threadlike structures indicate poorly fibrillated fibers or fiber fragments. Lighter local areas indicate high level of transparency [20]

Energy consumption of homogenization from 200 to 600 bar is noticeable and without any reduction in the transparency levels. Figure 21.8 shows that it is possible to design a given procedure for producing nanofibrils with a given morphology and utilizing acceptable energy levels.

Another method for making MFC is using the grinder. The mechanism of the grinder method similars with the homogenizer. The shear strength that is generated by the grinder destroys the cell wall composed of nanofibers that are connected by hydrogen bonding [23]. Contrary to nanocellulose whiskers whose shape is straight and rodlike, the structure of MFC is long and flexible nanosize object.

MFC is composed of more or less individualized cellulose microfibrils, presenting lateral dimensions in the order of 10–100 nm and length generally in the micrometer scale. Its morphology consists of alternation between crystalline and amorphous domains. Comparing with nanocellulose from BC, MFC has a weblike structure [21]. Figure 21.9 presents cellulose nanocrystal morphology from transmission electron micrographs [3], and Table 21.4 summarizes their distinctive characteristics.

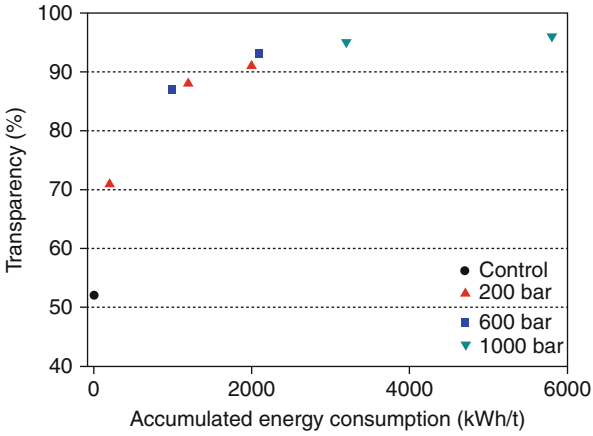

Fig. 21.8 Transparency levels of films as a function of pressure utilized during the homogenization of *P. radiata* pulp fibers, pretreated with TEMPO. The control sample corresponds to films made of *P. radiata* pulp fibers, which were not homogenized [22]

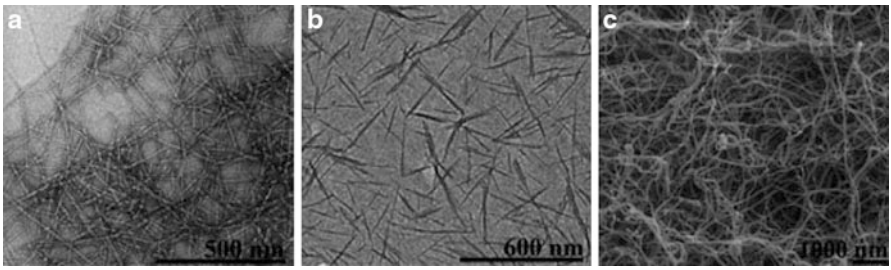

Fig. 21.9 Transmission electron micrographs of MFC (**a**), nanocellulose whiskers (**b**), and scanning electron micrograph of BC (**c**) [3]

Table 21.4 The characters of nanocellulose materials [3]

Type of nanocellulose	Typical sources	Formation and average size
Bacterial cellulose (BC)	Low-molecular-weight sugars and alcohols	Bacterial synthesis
		Diameter: 20 ~ 100 nm, different types of nanofibers networks
Nanocellulose whiskers	Wood, cotton, hemp, flax, wheat straw, mulberry bark, ramie, tunicin, cellulose from algae and bacteria	Acid hydrolysis of cellulose from many sources
		Diameter: 5 ~ 70 nm
		Length: 100 ~ 250 nm (from plant celluloses), 100 nm to several micrometers (from celluloses of tunicates, algae, bacteria)
Microfibrillated cellulose (MFC)	Wood, sugar beet, potato tuber, hemp, flax	Delamination of wood pulp by mechanical pressure before and/or after chemical or enzymatic treatment
		Diameter: 5 ~ 60 nm
		Length: several micrometers

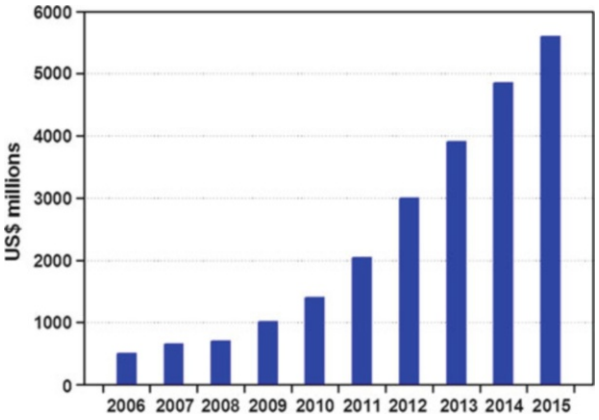

Fig. 21.10 OLED display revenue forecast [24]

2.2 Important Factor for Optically Transparent Application

Organic light-emitting diode (OLED) display is one of flat-panel displays that are currently receiving attention. Figure 21.10 shows OLED market size that is anticipated to increase to $ 5.5 million by 2015. This anticipation of growth of OLED market is because OLED is applied in larger displays for desktop monitor, laptop, tablet, and mobile devices [24, 25].

To meet this situation, the nanocellulose has received much attention as a component of flexible display. The process of flat-panel display (FPD) is transforming continuous roll-to-roll from bath process owing to importance of production cost. The conventional process is produced by piling up on large substrate, which is mostly glass. Then cut the panel into various sizes depending on equipment purpose. So, the cost-effective was been conducting by making various size of glass in a conventional process. In case of continuous roll-to-roll process, the plastics are used as substrate instead of glass because of its flexibility. When process is not in operational, a flexibility of plastic enables folding and rolling up for storage. As such, roll-to-roll process gives many advantages including cost-effectiveness, convenience to distribute functional material over substrates, and storage of product in Fig. 21.11 [4, 26, 27].

To become a substrate in roll-to-roll process, there are three requirements. Firstly, the high coefficient of thermal expansion (CTE) is essentially demanded to be lower than 3 ppm K^{-1}. But, CTE of plastics is large CTEs (about 50 ppm K^{-1}). Furthermore, flexible or foldable plastics have extremely large CTEs (about 200 ppm K^{-1}). The difference between CTE of functional materials and plastics can destroy and damage functional materials in the assembly and mounting process. Secondly, the flexibility allows the devices to be flexed or bent but also suggests the cost-effectiveness. But, the plastic is sensitive to small cracks so to enable to be torn in rolling process. Thirdly, a high optical transparency is needed to apply in diverse applications [5, 7].

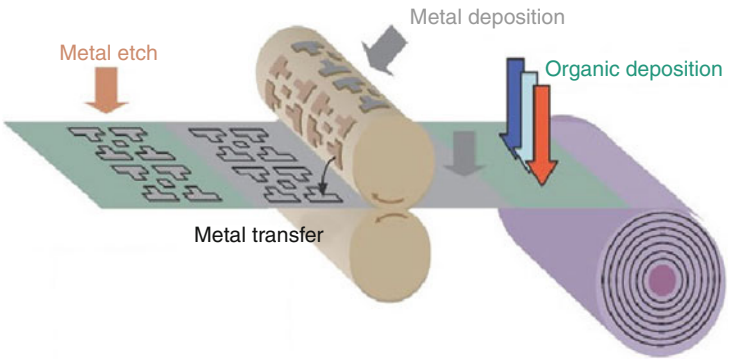

Fig. 21.11 Conceptual diagram of continuous roll-to-roll process [26]

Table 21.5 The basic properties of films used for base substrates [28]

Base polymer	PET	PEN	PC	PES	PAR	PCO	PI
CTE (from −55 to 85 °C) ppm/°C	15	13	60 ~ 70	54	53	74	30 ~ 60
Transmission (400 ~ 700 nm) %	>85	0.85	>90	90	90	91.6	Yellow
Water absorption (%)	0.14	0.14	0.4	1.4	0.4	0.03	1.8

2.2.1 Coefficients of Thermal Expansion (CTE)

The CTE is very important in roll-to-roll process. If the substrate cannot endure the high temperature within the process, the functional materials deposited onto substrates would be damaged and destroyed by mismatching between CTE of materials. In case of glass used as substrates, the CTE of glass is enough to ensure temperature of manufacturing process, but the glass is very fragile and un-foldable. The substitution of glass for plastics is demanded as low CTE as silicon crystal (3 ppm K^{-1}). However, general plastics have high CTEs (exceeding 50 ppm K^{-1}); moreover, CTEs of foldable plastics are higher than 200 ppm K^{-1}. Table 21.5 indicates basic properties of films used for base substrates.

To improve CTE of plastics, reinforcements are needed to add in plastics. When reinforcements are added into plastic, reinforcements give low CTE to plastics without loss of optical transmission. The low CTE, which is affiliated to nanocellulose, complements the high CTEs of plastics. On the other hand, the low Young's modulus, which is affiliated to plastics, complements the high Young's modulus of nanocellulose. To use nanocomposites composed of nanocellulose and plastics, many studies are in development. The CTEs of nanocomposites are varied dependent on variation of reinforcements, plastics, and chemical treatments. Optically transparent composites composed of fibrillated kraft pulp and acrylic resin were fabricated by the dried mats of fibrillated pulp immersed in neat acrylic resin. And then impregnated mats were cured by UV light. The composites show lower CTE (17 ppm K^{-1}) than CTE of pure acrylic resin (86 ppm K^{-1}). This result indicates that the fibrillated pulp acted as reinforcement in nanocomposites [29].

Table 21.6 CTEs of the sheets and composites made with cellulose nanofibers from immature and mature bamboo. The density of the sheets for both conditions is in a range of $0.8 \sim 0.9\ g^{-1}\ cm^{-3}$ [7]

	Immature bamboo	Mature bamboo 1	Mature bamboo 2	Acrylic resin
Sheet (ppm K^{-1})	10.4	12.3	16.4	–
Composite (ppm K^{-1})	17.5	18.9	41.1	213.0

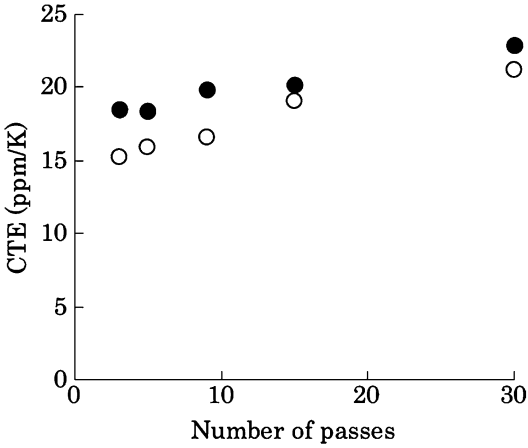

Fig. 21.12 CTE of sheets (○) and composites (●) made with fibrillated pulp fibers as a function of the number of passes through the grinder [23]

Nanofibers extracted from bamboos, which were prepared with a treatment to leach extractives, had been introduced as reinforcement in acrylic resin. The nanocomposites were fabricated through impregnating the dried nanofiber sheet in acrylic resin. The nanocomposites made of nanofibers extracted from bamboo and resin showed that CTEs of the nanocomposites were lower than CTE of pure resin (in Table 21.6.). One of the interesting points is that CTEs of composites composed of mature bamboo containing lignin were higher than absence of lignin, since the CTE of lignin is high (58.1 ppm K^{-1}) [7].

The relation between degree of crystallinity, CTE, and modulus was studied by Yano et al. [23]. Figures. 21.12 and 21.13 showed that CTEs and degree of crystallinity of the sheets composite as the number of passes increased. The intermolecular hydrogen bonding between cellulose molecular chains is increased when increasing the degree of crystallinity. Because intermolecular hydrogen bonding restricts the thermal expansion, the high degree of crystallinity indicates the low CTE. In case of increasing the number of passes through the grinder, excessive grinder causes the degradation and destruction of fibrillated fibers. In conclusion, the degree of crystallinity affects CTEs and modulus of materials [23].

Moreover, cellulose consists of nanofibers are hard to be separated by mechanical process (i.e., grinding, homogenizing, etc.) because these nanofibers connect through hydrogen bonding between intermoleculars. To separate and divide into microfibril without destruction and damage, Fukuzumi et al. [30] converted most of the hydroxyl groups of cellulose into negatively charged sodium carboxylate groups through

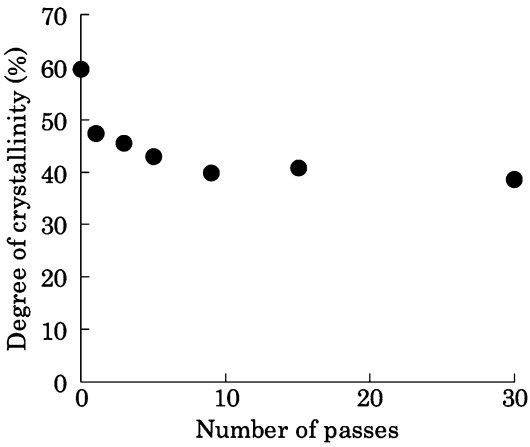

Fig. 21.13 Degree of crystallinity of the pulp fibers as a function of the number of passes through the grinder [23]

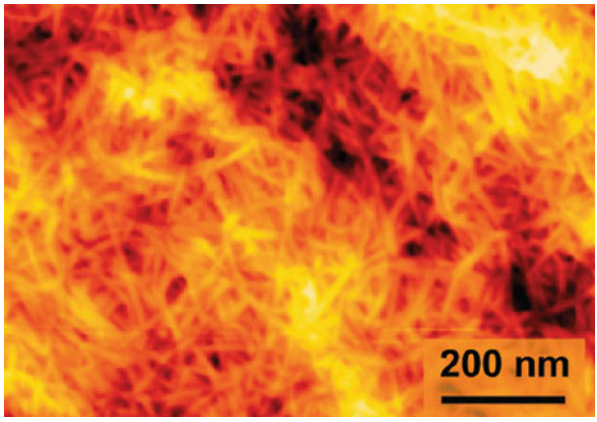

Fig. 21.14 AFM image of surface of a nanofiber film prepared from TEMPO-oxidized softwood cellulose [30]

2,2,6,6-tetramethylpiperidine-1-oxyl radical (TEMPO). They could get TEMPO-oxidized cellulose nanofiber (TOCN) by a blender-type homogenizer (in Fig. 21.14) [30]. The CTEs (2.7 ppm K^{-1}) of formed TOCN were lower than glass (about 9 ppm K^{-1}) compared with silicon (about 3 ppm K^{-1}) (in Fig. 21.15) [30].

In addition, an excessive acetylation which is one of the chemical treatments to cause a negatively affects CTEs of nanocomposites including BC. In case of Fig. 21.16, CET of BC sheets gradually decreased with increase in DS by 0.6, and CTE within range from DS 0.23 to 0.6 was lower than 1 ppm K^{-1}, because the introduction of bulky acetyl groups restricted mobile and thermal expansion of BC when the surface and amorphous region was firstly substituted by acetyl groups.

But, the CTEs of nanocomposites, which made by impregnation method, were stayed around 1 ppm K^{-1} in ranges of $0 \sim 0.82$. When the hydroxyl groups of BC were substituted by acetyl groups from acetylation, the hydrogen bonding between cellulose molecular chains became weak. As a result, the nanocomposites

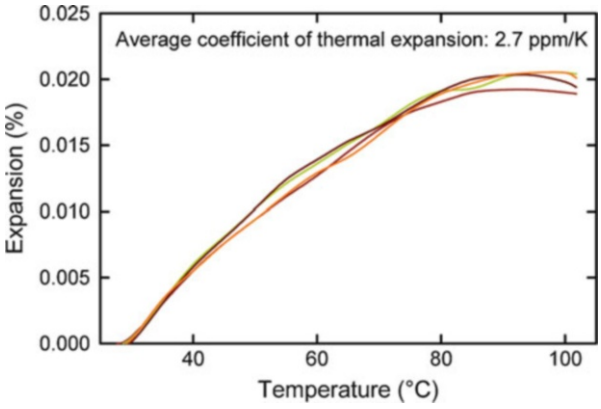

Fig. 21.15 Thermal expansion behavior of nanofiber film prepared from TEMPO-oxidized softwood cellulose obtained in a dry nitrogen atmosphere after drying at 120 °C for 40 min. Four different specimens were measured, and the data are shown as different colors [30]

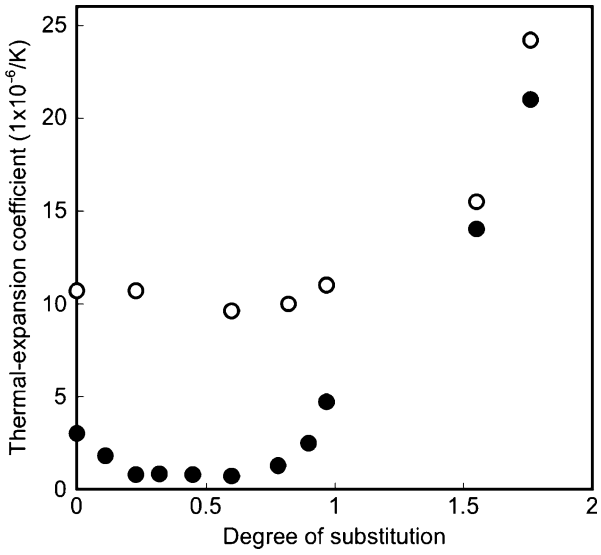

Fig. 21.16 The CTE of a series of acetylated BC samples (●) and their nanocomposites (○) [31]

compose of acetylated BC and polymer were readily deformed by thermal expansion of polymer [31]. In case of using BC to act as reinforcement, the CTEs of nanocomposites would be affected by layer direction within BC. The reason of existing layers is because cell growth is unable to maintain their activity only bacteria near the surface of the culture media (in Fig. 21.17). The CTEs of plane direction for BC nanocomposites were found to be 4 ppm K^{-1} because hydrogen bonding between nanofibers consisting of dense and finely branched fibers is strong. On the other hand, The CTEs of thickness direction for BC nanocomposites were found to be 555 ppm K^{-1}. It was expected that BC in the thickness direction consist of multiple layers of planar nanofiber networks, with more weak interaction between them than planer direction (in Fig. 21.18) [6, 23].

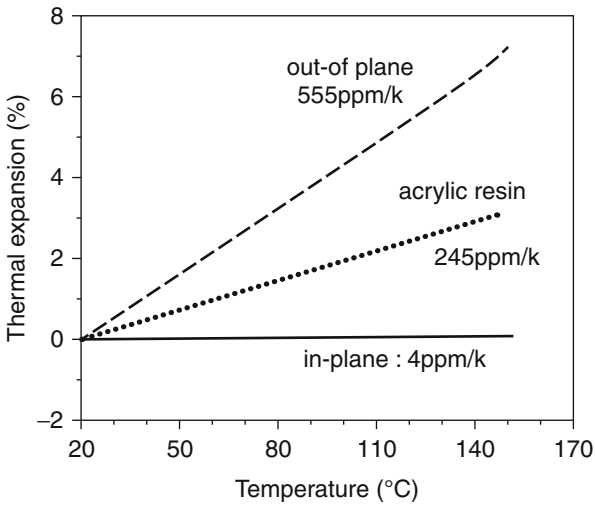

Fig. 21.17 Thermal expansion behavior of nanocomposites composed of acrylic resin and BC [6]

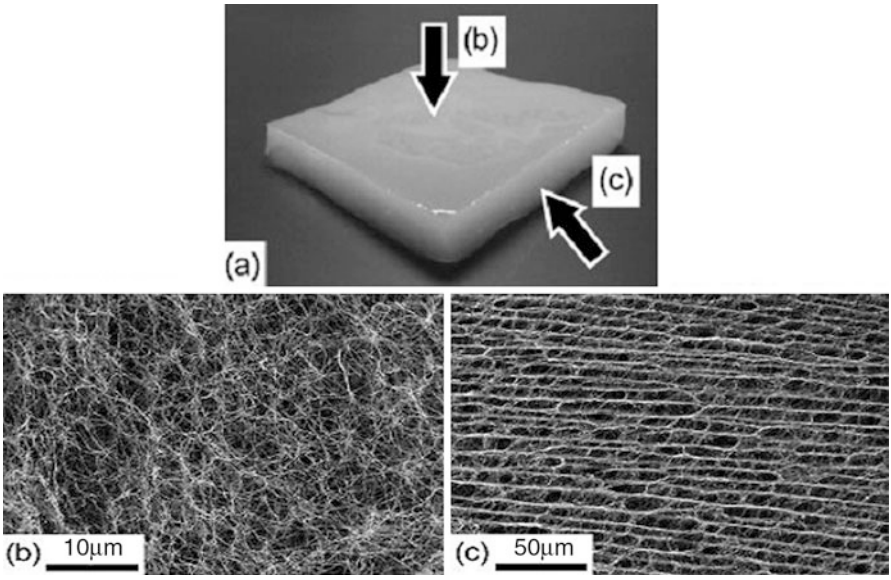

Fig. 21.18 Macroscopy of BC pellicles (**a**) shows the planer direction (**b**) and show thickness direction (**c**) [6]

2.2.2 Optically Transparent

The nanofibers can suppress light scattering if the cellulose nanofibers are densely formed and the pores between the fibers are small, while the dried BC sheets were translucent for surface light scattering. Figure 21.19 shows transparent degree of smooth surface of nanocellulose sheets. The transparency was increased by treating

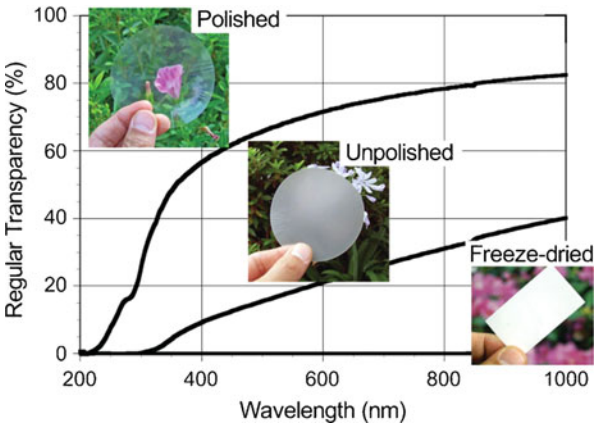

Fig. 21.19 Light transmittance of the cellulose nanofiber sheets dependent on using emery paper [32]

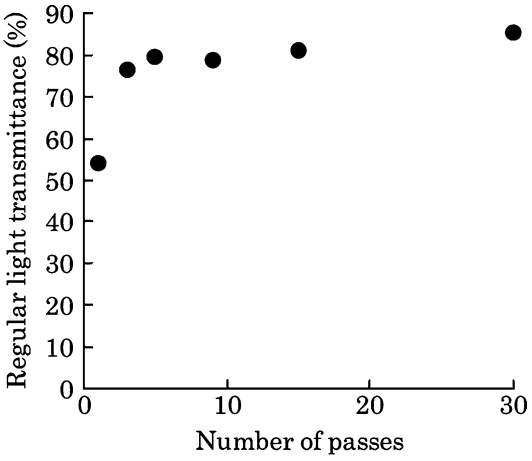

Fig. 21.20 Regular light transmittances at a 600 nm wavelength of composites made with fibrillated pulp fibers dependent on the number of passes through the grinder [23]

emery paper. To improve light surface scattering, the uniformly smooth surface of nanocellulose is needed. The methods that are smoothing surface of nanocellulose exist some ways. The first method is lamination of optically transparent plastics on nanocellulose sheets. The second method which has been mainly used is impregnation in plastics [32].

The indication of total light transmission in bottom-emissive displays where one sees through the substrate film is more than 85 % (over the visible spectrum of 400–800 nm) [4]. Figures. 21.20 and 21.21 indicate increasing CTE of substrate makes optical transparency of substrate to reduce.

Because diameter of nanocellulose is smaller than the wavelength of visible light, the nanocomposites composed of nanocellulose and plastics appear highly optical transparent (in Fig. 21.21). To improve light transmittance of nanocomposite, difference between refractive index (RI) of nanocellulose and plastic is minimized. Because RI of plastics is diverse, as a result, RI of nanocellulose needs to be

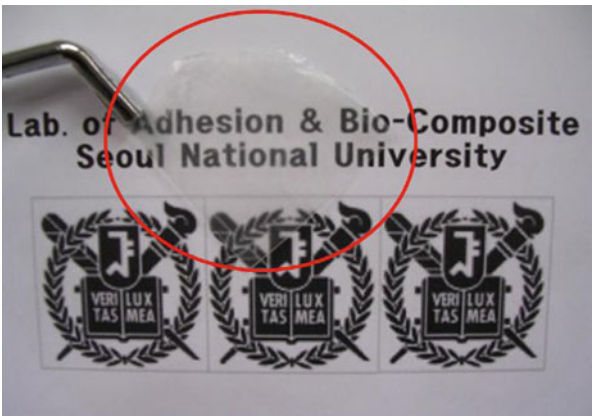

Fig. 21.21 Photograph of optically transparent acetylated BC/PLA nanocomposite film [9]

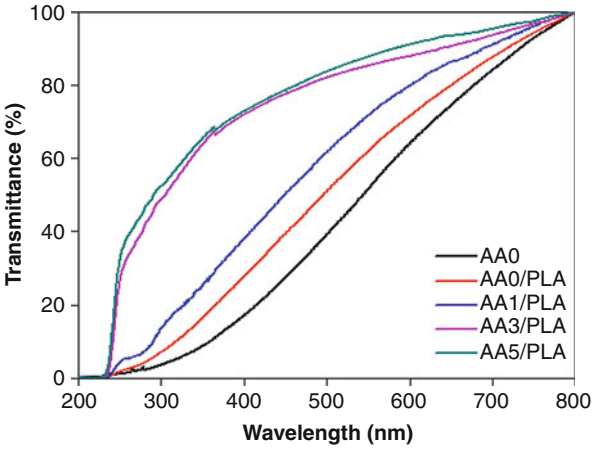

Fig. 21.22 Regular light transmittances or a series of acetylated BC/PLA nanocomposite films (AA0 = anhydride contents 1 mL, AA3 = 3 mL, AA5 = 5 mL)

Table 21.7 Transmittance at 550 nm of nanocomposite films

Samples	Transmittance at 550 nm
AA0	51.8
AA0/PLA	62.0
AA1/PLA	71.9
AA3/PLA	85.3
AA5/PLA	90.5

controlled. The RI of nanocellulose is adjusted by chemical treatments. Therefore, CTE and optical transparency of substrate should be properly controlled, and the most common method of chemical treatment is acetylation. Figure 21.22 and Table 21.7 show that transmittance was increased with increasing degree of substitution (DS).

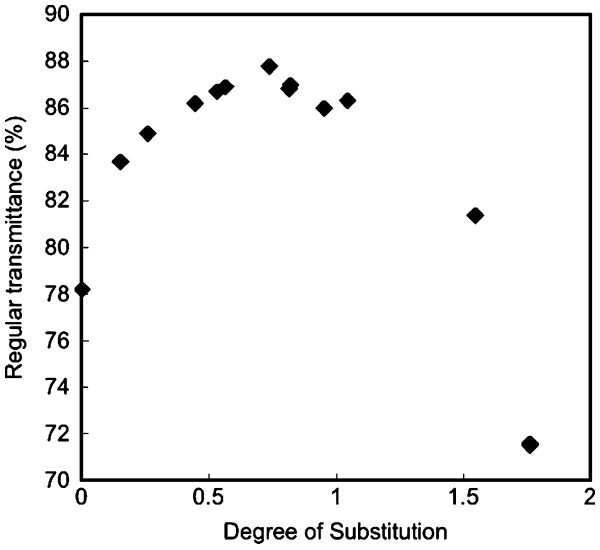

Fig. 21.23 Regular transmittance of a series of acetylated BC nanocomposite at 580 nm [31]

Results showed that the higher DS of PLA in BC affects both light transmission and porosity as PLA filled in pores in BC networks, as shown in Figs. 21.23 and 21.24. Also, because RI of BC was decreased with increasing DS, nanocomposites containing BC with high DS showed high transmittance. Moreover, acetylated BC was effectively impregnated by plastics because of improving between cellulose and plastics through acetylation. However, the high of DS negatively affected transmittance and CTE (in Fig. 21.23, [4]). Figure 21.24 shows the introduction of bulky acetyl groups to nanocellulose caused thickness of cellulose to become thicker so that these thicken nanocellulose may interface with transmittance. In addition, RI of excessively acetylated nanocellulose would be lower than plastics [31].

The transparency of different nanocellulose-reinforced nanocomposites can be compared as shown by Figs. 21.25 and 21.26. Appearances of grinder-treated pulp/acrylic resin sheet and BC/acrylic resin sheet show optically transparency. On the other hand, appearance of homogenizer-treated pulp/acrylic resin sheet shows translucency. Generally, the transparency of nanocomposites up to 30 pass through refiner later cannot be improved, while additional treatment such as grinder can improve transparency through more fibrillated.

2.2.3 Flexibility

The flexibility of substrates gives many advantages including convenience of storage and processing. As mentioned earlier, relation between flexibility and CTE is contrary. The foldable and flexible substrates indicate low modulus and high elongation at break. Figure 21.27 indicates flexibility of nanocomposites that is given by plastics. The elongation at break is very high in case of pure acrylic resin, but the sheet is torn which results from material sensitivity to small cracks

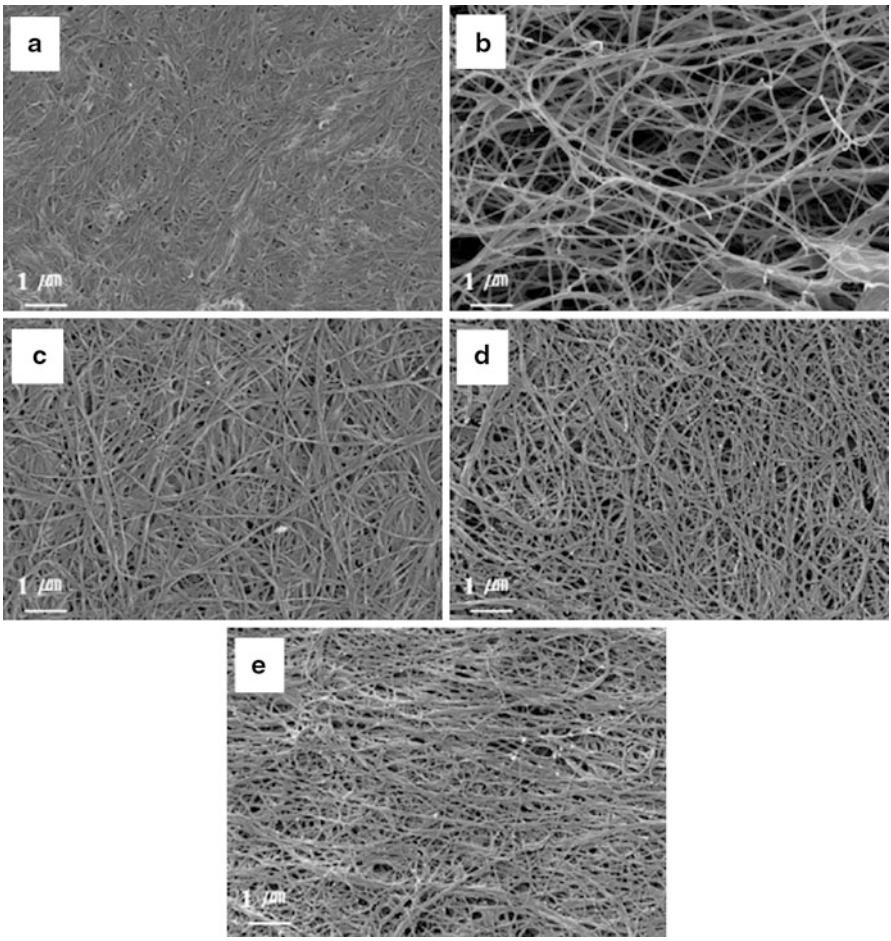

Fig. 21.24 SEM images of bacterial cellulose, AA0 (**a**), freeze-dry (**b**), AA1 (**c**), AA3 (**d**), and AA5 (**e**) bacterial cellulose [9]

when pure acrylic resin sheet was folded (in Fig. 21.28b). Figure 21.28a shows that the nanocomposites are possible to fold without cracking because nanocellulose (BC) interrupts crack propagation in nanocomposites [6].

The BC nanocomposites composed of nanoparticulate boehmite and epoxy-modified siloxane showed difference in flexibility according to BC used, never-dried or in dried state. Figure 21.29 shows the mechanical properties of nanocomposites dependent on dried or never-dried BC.

In case of using never-dried BC, the nanocomposites were observed, and results showed that tensile strength and Young's modulus increase with decreasing in the elongation at break because of the good interaction between boehmite–GPTS sol and the BC microfibrils; and water acts as plasticizer. Contrastively, the elongation

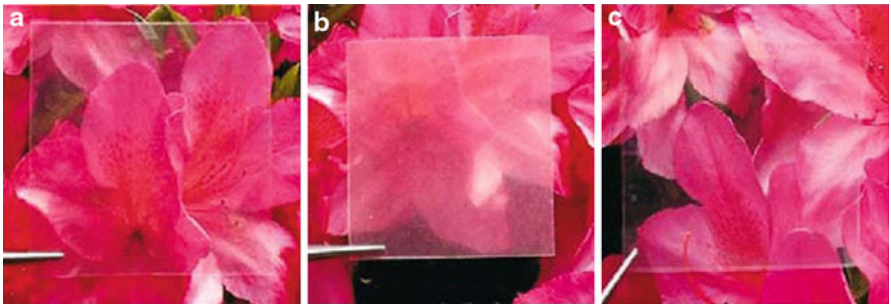

Fig. 21.25 Appearance of nanocomposites dependent on treated method of nanocellulose: appearance of grinder-treated pulp/acrylic resin sheet (**a**), appearance of homogenizer-treated pulp/acrylic resin sheet (**b**), appearance of bacteria cellulose/acrylic resin sheet (**c**) [29]

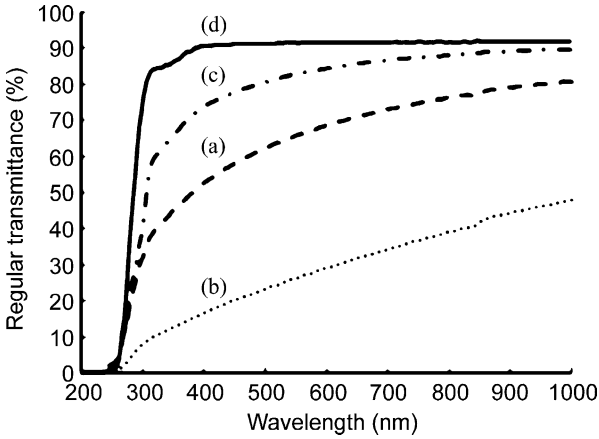

Fig. 21.26 Regular transmittance of different nanocellulose-reinforced nanocomposite [29]

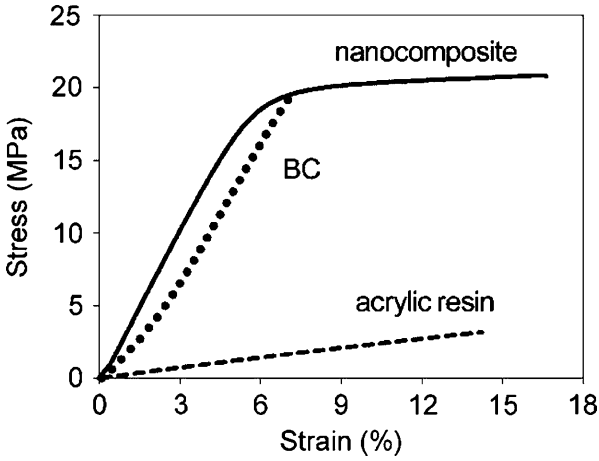

Fig. 21.27 Physical properties of neat acrylic resin matrix, BC sheet (density 0.1 g cm^{-3}), and composite containing 5 wt% fiber tensile stress–strain behavior [6]

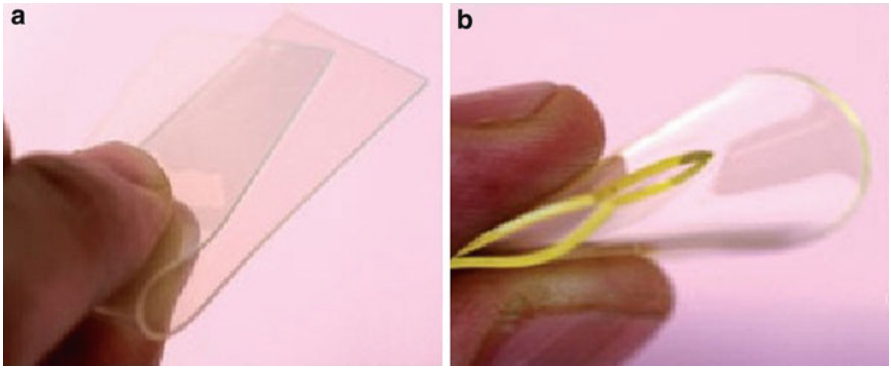

Fig. 21.28 Foldable transparent nanocomposites reinforced with bacterial cellulose (**a**) and more fragile neat acrylic resin sheet of the same thickness (**b**) [6]

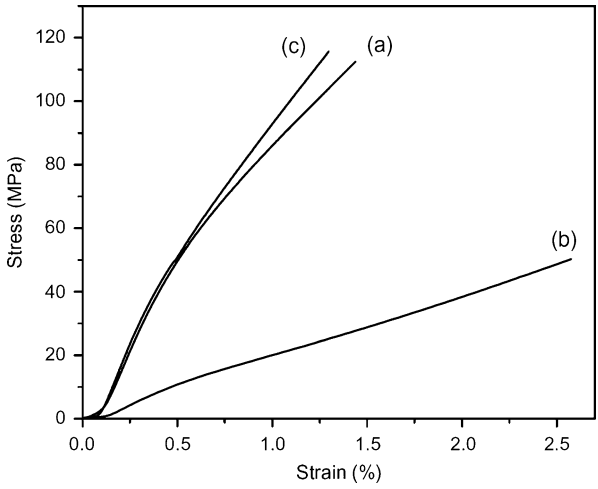

Fig. 21.29 Stress–strain curves for pure BC (**a**), nanocomposite containing dried BC (**b**) and containing never-dried BC (**c**) [33]

at break increases with decreasing of tensile strength and increasing of Young's modulus when using in dried BC [33]. Method of plastic introduction into BC is also important to properties of nanocomposite containing BC. The first way to introduce is "in situ" method which directly adds plastics into the medium of the growing BC. The second way to introduce is "impregnation" method which impregnates BC into plastic solution. According to methods of making nanocomposites, the ribbon-shaped structure of nanocellulose is different from each other (in Fig. 21.30a).

Mechanical properties of BC composite from different technique were evaluated (Fig. 21.30b). When compared with pure BC, the elongation at break was improved which is caused by interruption of hydrogen bonding between nanofibers due to PVA coated onto surface of BC [34].

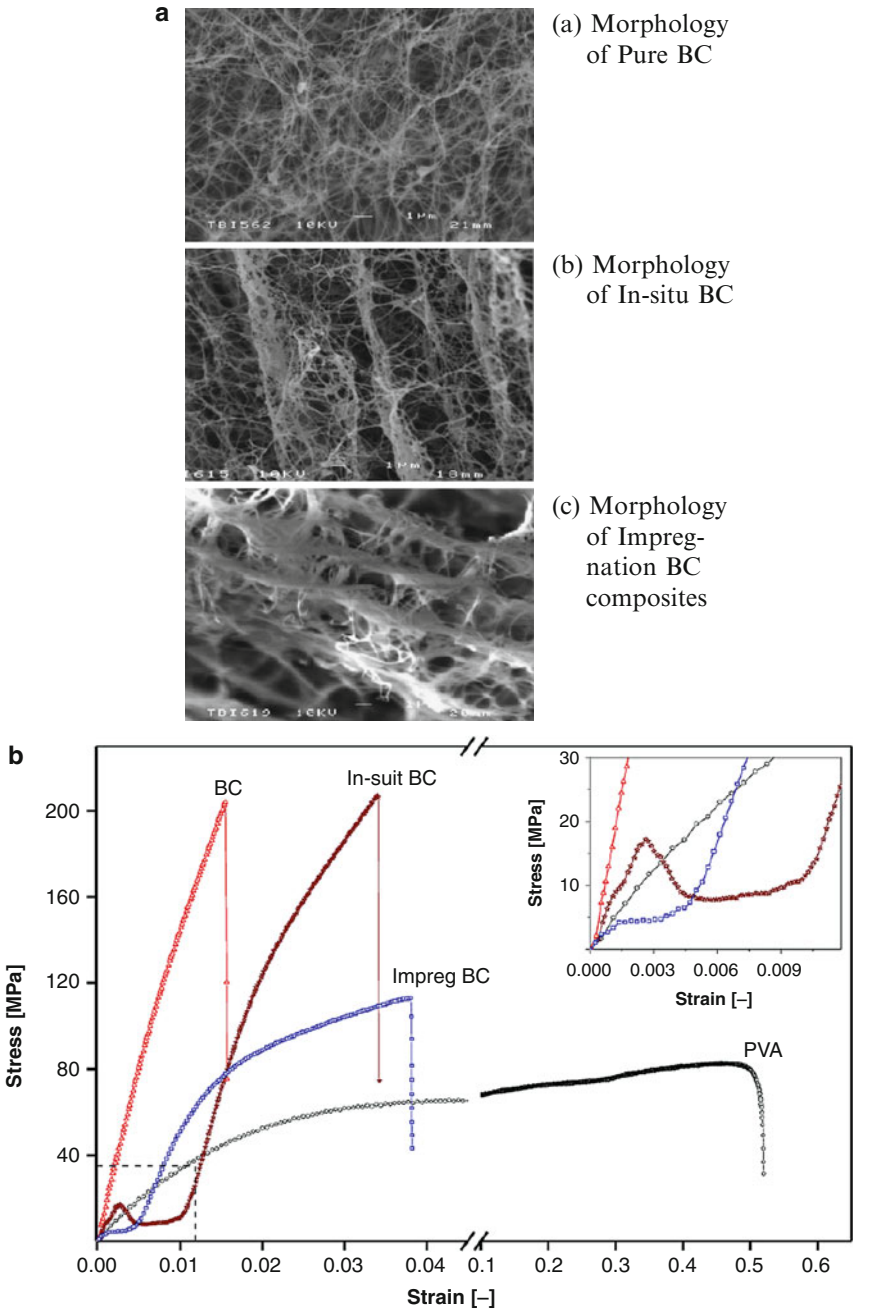

Fig. 21.30 (**a**) SEM micrographs of dependent on introducing plastics into BC [34]. (**b**) Stress–strain curves of pure BC compared with in situ BC and impreg BC composites. The inset graph show in greater detail the stress–strain behavior at small deformations [34]

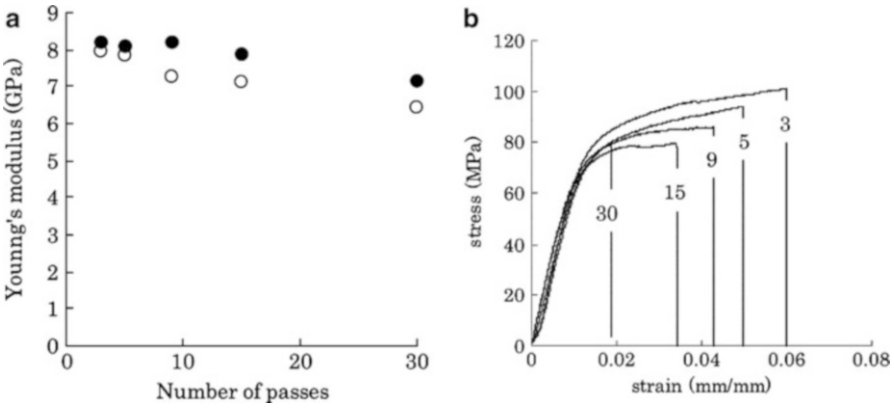

Fig. 21.31 (**a**) Young's moduli of sheets (○) and composites (●) made with fibrillated pulp fibers as a function of the number of passes through the grinder [23]. (**b**) The typical stress–strain curves of composites made with fibrillated pulp fibers at various numbers of passes through the grinder [23]

In case of MFC, Young's modulus and yield strain are affected by the number of pass through grinder. Increasing the number of pass decreases young's modulus and yield strain (in Fig. 21.31a, b).

These results indicated that the fibrillated fibers through pass number and hydrogen bonding between intermoleculars were related. The reasons of decreasing in yield strain were caused by morphology of fiber. Firstly, the degradation of the fibrillated fibers occurred owing to further grinder treatments, at same time increasing hydrogen bonding. Secondly, aspect ratio of fiber was decreased because the length of fiber was short by shear force [23].

3 Conductivity

3.1 Conductive Polymers

Alan MacDiarmid, Hideki Shirakawa, and Alan Heeger reported a ten million-fold increase in the conductivity of polyacetylene doped with iodine that the first inherently conductive polymer is recognized [35]. Although polyacetylene, a noncyclic polyene, is still one of the most studied polymers in this field, it has significant limitations, such as difficulty with processing and high instability in air environment. Consequently, the development of such aromatic conducting polymers for different applications had received much attention. Polyheterocycles, such as polypyrrole, polythiophene (PT), polyaniline (PANi), and poly (3,4-ethylenedioxythiophene) (PEDOT), emerged as another class of conducting polymers which exhibit good stabilities, conductivities, and ease of synthesis [23]. Polyacetylene was the one that actually launched a new field of research on

Table 21.8 Conductivity of common conducting polymers regenerated from [36]

Conducting polymer	Conductivity [S cm^{-1}]	Type of doping
Polyacetylene (PA)	200 ~ 1,000	n, p
Polyparaphenylene (PPP)	500	n, p
Polyparaphenylene sulfide (PPS)	3 ~ 300	P
Polyparavinylene (PPv)	1 ~ 1,000	P
Polypyrrole (PPy)	40 ~ 200	P
Polythiophene (PT)	10 ~ 100	P
Polyisothionaphthene (PITN)	1 ~ 50	P
Polyaniline (PANi)	1 ~ 50	n, p

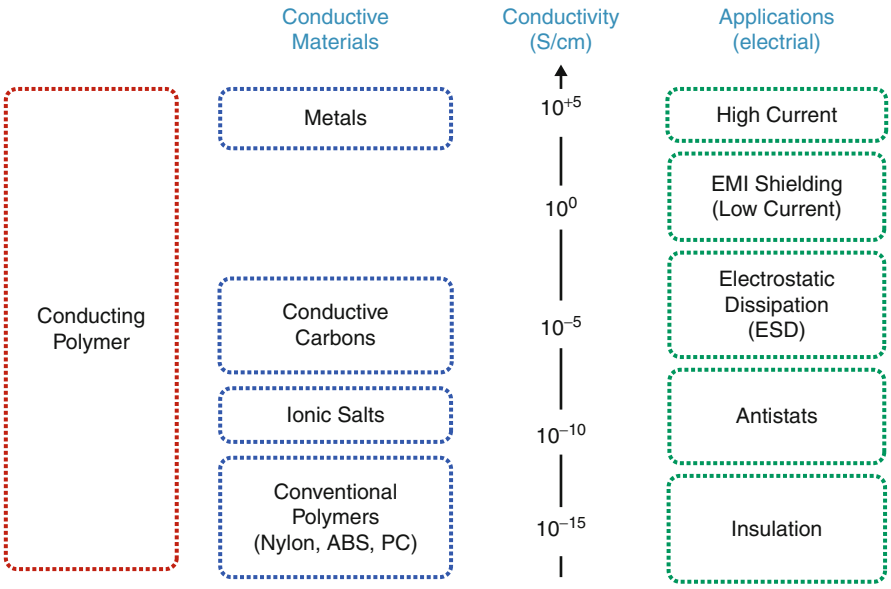

Fig. 21.32 Conductivity spectrum of conductive material [38]

conductive polymer. Other polymers that were studied extensively since the early 1980s include polypyrrole, polythiophene, polyphenylene vinylene, and polyaniline. Polyacetylene remains the most crystalline-conductive polymer, but it was not the first conductive polymer to be commercialized. This is because it is easily oxidized by the oxygen in air and is also sensitive to humidity. Polypyrrole and polythiophene differ from polyacetylene most notably in that they may be synthesized directly in the doped form and are very stable in air. Table 21.8 shows their conductivities. Even though they have low conductivity, only 10^4 S m^{-1}, this is sufficient for many practical purposes [37]. Figure 21.32 shows range of material and its application based on conductivity [38].

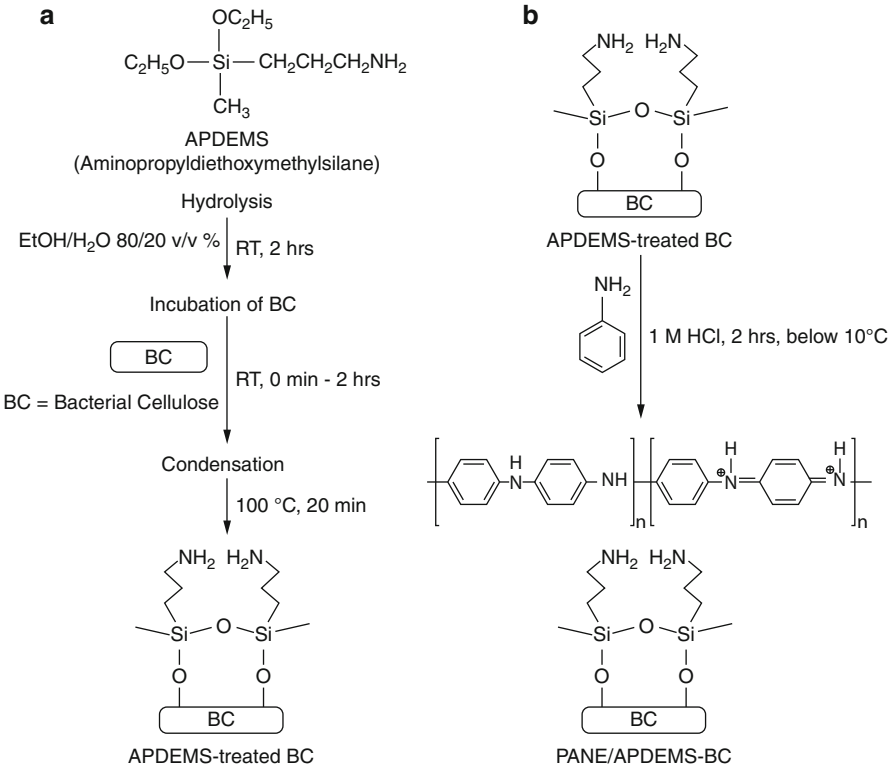

Fig. 21.33 Hydrolysis and condensation procedures applied to BC by treatments of APDEMS (**a**) and polymerization of aniline on aminosilylated BC by APDEMS (**b**) [11]

3.1.1 Method

To improve electrical properties of nanocomposites cooperating with bacterial cellulose, nanocellulose needs some method like pretreatment, oxidant, and dopant to improve its properties and material compatibility.

Aminosilane Treatment of Bacterial Cellulose to Improve Electrical Conductivity

Among the group of conjugated polymers, polyaniline (PANi) has many advantages such as controllability of doping/dedoping chemistry, its facile synthesis, and its high conductivity which recaptured the extensive attention since 1980s [11].

A conductive polyaniline (PANi) layer was assembled on aminosilylated bacterial cellulose (BC) surface. The process of modification is based on a chemical polymerization of aniline which is bound to the amine moieties from 3-aminopropyldiethoxymethylsilane (APDEMS) (in Fig. 21.33a, b). The amines were prepared by hydrolysis and condensation reaction between silanol and hydroxyl groups on BC under catalyzed conditions [11].

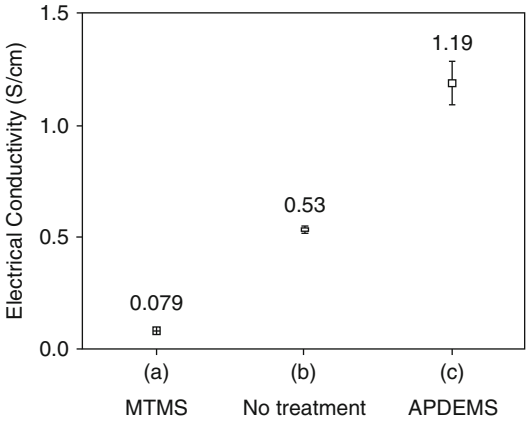

Fig. 21.34 Electrical conductivity of PANi-/MTMS-treated BC (**a**), PANi on untreated BC (**b**), and PANi-/APDEMS-treated BC (**c**); PANi was synthesized on BC pretreated with APDEMS under the base- catalyzed condition. PANi on all surfaces were synthesized by conventional chemical oxidation [11]

For PANi synthesized on untreated BC, the electrical conductivity was 5.3×10^{-1} S cm^{-1} with small variation. This value is relatively higher than that of PANi/BC composites reported before [39, 40]. For PANi synthesized on APDEMS-treated BC surface, the electrical conductivity is the highest compared to other systems examined in this study. The PANi synthesized on MTMS-treated BC showed an electrical conductivity only up to 7.9×10^{-2} S cm^{-1}. The improvement in electrical conductivity from 5.3×10^{-1} S cm^{-1} to 1.2 S cm^{-1} was attained by synthesizing PANi on APDEMS-treated surfaces under the base-catalyzed condition. Based on this improvement, it is highly possible that aniline in acidic solutions and aminosilylated BC surfaces prepared under base-catalyzed conditions are bonded through hydrogen bonding or electrostatic interaction (in Fig. 21.34). The enhanced deposition of PANi leads to improvement in electrical conductivity, reaching 1.2 S cm^{-1} for BC pretreated with APDEMS under base-catalyzed condition [11].

Oxidant and Dopant

The bacterial cellulose was fully encapsulated with polyaniline by direct polymerization of the respective monomers using APS as an oxidant and p-TSA as a dopant. These bacterial cellulose/polyaniline nanocomposite film materials exhibited the inherent properties of both components. BC/PANi1 was composed of bacterial cellulose and polyaniline with p-TSA (dopant). BC/PANi2 was made up of bacterial cellulose and polyaniline without p-TSA. The calculated electrical conductivities were 1.3 S cm^{-1} (BC/PANi1) and 0.8 S cm^{-1} (BC/PANi2), respectively, whereas the bacterial cellulose film was insulating. This considerable increase in electrical conductivity from insulating to semiconducting is significant. It was reported that the electrical conductivity of polyaniline depends on the degree of doping, oxidation state, particle morphology, crystallinity, interior intrachain interactions, molecular weight, etc. [9, 41–43].

Cyclic voltammetry was used to measure the electrochemical redox properties of the nanocomposite films and to determine their thermodynamic stability.

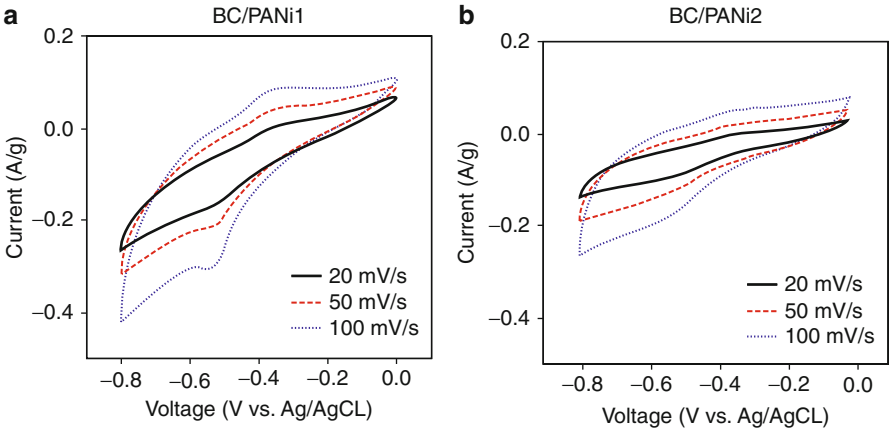

Fig. 21.35 Cyclic voltagram recorded at the displayed different voltage scan rates 20, 50, and 100 mV s^{-1} of BC/PANi1 (**a**) and BC/PANi2 nanocomposite films (**b**) [9]

Figure 21.35 shows the cyclic voltagrams of the BC/polyaniline nanocomposite films on Pt in 2 M NaCl. In these voltagrams, the current was normalized to the mass of the nanocomposite films used as the working electrode in the cyclic voltammetry experiment. When the scan rate of the cyclic voltagrams for the nanocomposite film was changed from 20 to 100 mV s^{-1}, the redox peaks of electrochemical transitions in the voltagrams were maintained in both the BC/PANi1 and BC/PANi2 nanocomposite films [9]. These results indicated that the polyaniline polymer is thermodynamically stable [44]. The oxidant and dopant had a significant effect on the electrical conductivity and thermal stability of the nanocomposites.

PANi Synthesis by Interfacial Polymerization

Recent development showed a general chemical route to polyaniline nanofibers by using interfacial polymerization at an aqueous/organic interface [45, 46]. The reactants – aniline, ammonium peroxydisulfate, and a doping acid such as HCl – are separated by the interface between an organic solvent containing aniline and an aqueous phase containing the oxidant plus the doping acid. The polyaniline product, polymerized at the interface, contains almost exclusively nanofibers with relatively uniform diameters. The nanofiber diameters were determined by the doping acid used in the polymerization [46].

Procedure in Fig. 21.36 is analogous to the "drop-by-drop" titration used in traditional synthesis but with a precisely controlled feeding rate.

Interfacial polymerization represents one effective method to suppress secondary growth (in Fig. 21.37). Since the monomer aniline and the initiator ammonium peroxydisulfate are separated by the boundary between the aqueous and the organic phase, polymerization occurs only at this interface where all the components needed for polymerization mixed together [45, 46, 48]. Polyaniline then forms as nanofibers. Since these newly formed nanofibers are in the doped emeraldine salt

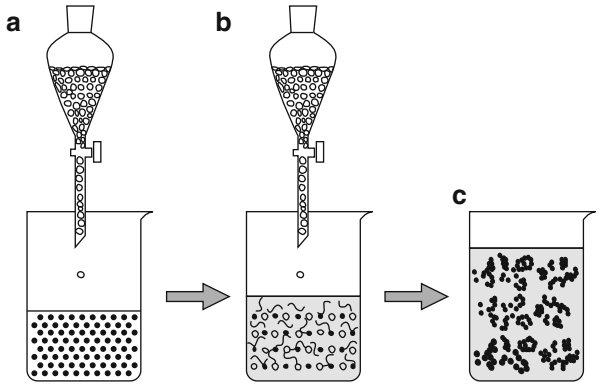

Fig. 21.36 Schematic diagram illustrating the formation of polyaniline agglomerates during conventional chemical synthesis. (**a**) The oxidant (*open circle*) dopant solution is added slowly to the aniline (*solid circles*) dopant solution. (**b**) Polyaniline nanofibers form as soon as the polymerization begins. Since the nanofibers are exposed to aniline and oxidant, they are subject to secondary growth. (**c**) Agglomerates of polyaniline particles plus a few nanofibers are found because of severe secondary growth [47]

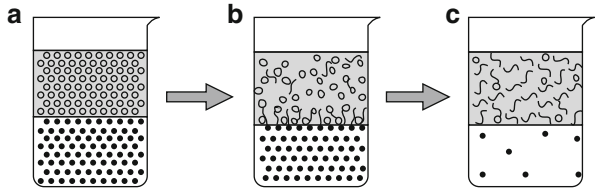

Fig. 21.37 Schematic illustration of the synthesis of polyaniline nanofibers by using interfacial polymerization. (**a**) An interface is set up between an organic phase containing dissolved aniline (*solid circles*) and an aqueous phase containing the oxidant (*open circles*). (**b**) Polyaniline nanofibers form at the interface, where aniline meets the oxidant and diffuses into the water phase. Note that this carries the nanofibers away from the reactive interface, so they are not subject to further secondary growth. (**c**) As the polymerization proceeds, nanofibers accumulate in aqueous phase [47]

form, they are hydrophilic and can rapidly move away from the interface and diffuse into the water layer (in Fig. 21.37b). In this way, as the nanofibers form, they are continuously withdrawn from the reaction front; thus avoiding secondary growth and allowing new nanofibers to grow at the interface. This effect explains nanofiber behavior that is obtained of no matter which solvent is used as the organic phase in interfacial polymerization. Hence, the interface between the immiscible aqueous/organic layers does not contribute directly to the formation of nanofibers; it simply separates nanofiber formation from secondary growth [47]. With the knowledge to synthesizing polyaniline nanofibers in order to prevent secondary growth, it is possible to design a new and simpler method to make pure polyaniline nanofibers (in Fig. 21.38). The idea is that if all the reactants can be consumed

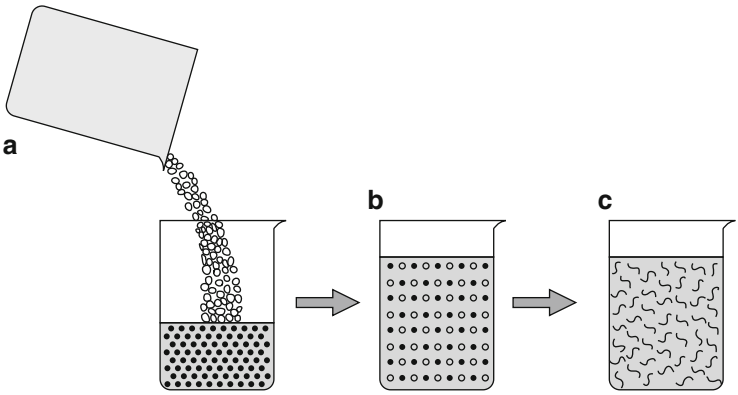

Fig. 21.38 Schematic illustration of the synthesis of polyaniline nanofibers in a rapidly mixed reaction. (**a**) The oxidant (*open circles*) dopant solution is quickly added into the aniline (*solid circles*) dopant solution and mixed. (**b**) A homogenous solution is obtained where all the aniline and oxidant molecules are evenly distributed, thus leading to fast polymerization across the entire solution. (**c**) Since all the reactants are consumed in the formation of nanofibers, secondary growth is suppressed [47]

during the formation of nanofibers, secondary growth will be greatly suppressed since no reactants will be available for further reaction. To achieve this goal, the initiator solution (ammonium peroxydisulfate in 1 M HCl) was added into the monomer solution (aniline in 1 M HCl) all at once (in Fig. 21.38a), rather than slowly feeding it in by titration or pyringe- pumping. Sufficient mixing can be achieved with a magnetic stirrer or shaker to evenly distribute the initiator and monomer molecules before polymerization (in Fig. 21.38b). As the polymerization begins, the initiator molecules induce the formation of nanofibers by rapidly polymerizing aniline monomers in their vicinity. Therefore, all the initiator molecules are consumed to form polyaniline nanofibers, thus suppressing the secondary growth of polyaniline.

Figure 21.39 shows that the diffusion and polymerization starting from the boundary between organic and aqueous phase could be observed in a few minutes. Because interfacial polymerization is diffusion-controlled reaction, leaving reaction to occur overnight was sufficient to complete the reaction. This similar phenomenon was also observed in the case of interfacial polymerization of PANi nanofibers without any substrate or template [47, 49]. Anilinium hydrochloride monomer at the interface acted like a surfactant having a polar hydrophilic part and an organic hydrophobic part. The generation of radicals was occurred when these monomers interacted with APS in aqueous phase and initiated polymerization, while hydrophilic PANi chains act as interfacial stabilizers. This separation leads to suppress unwanted side reactions such as ortho-coupling reactions between reactive chain ends [50]. Interfacial polymerization can be the effective method to suppress secondary growth of PANi by carrying the polymerized species from the reactive interface to diffusion into aqueous phase [47, 49].

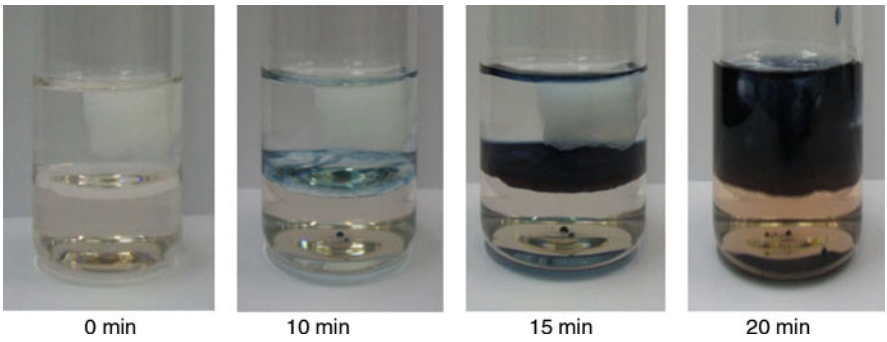

Fig. 21.39 Snapshots taken during 20 min after interfacial polymerization of sample 1 commenced. 0.08 M of aniline was used for preparation of sample 1 [10]

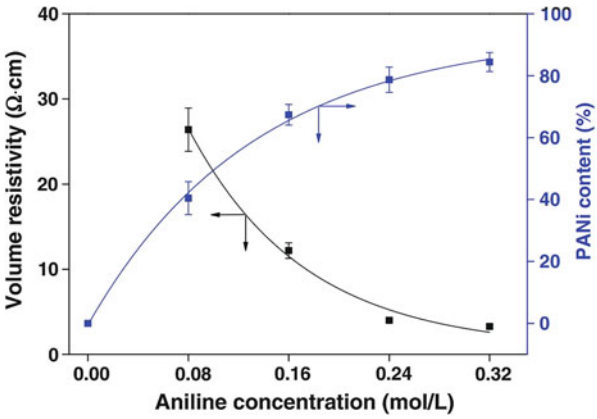

Fig. 21.40 Dependence of PANi content and volume resistivity of PANi/BC composites on the aniline concentration [10]

PANi pretreatment concept is mainly about the increasing of BC that absorbs water and the possibility to form hydrogen bond with amines of aniline. This phenomenon can be explained by the better adsorption of never-dried BC which can contain more reagents such as aniline, contributing to the improvements in electrical conductivity as well (in Fig. 21.40) [10].

The effect of monomer concentration on these two properties is not significant above the point at which 0.32 M of aniline was used. The volume resistivity of PANi/BC composites was converted to electrical conductivity (σ, S cm^{-1}) and mentioned in Table 21.9 [10]. By interfacial polymerization, PANi/BC composites were fabricated successfully without the help of surfactants or template; the nanosized PANi on BC was synthesized. The nanostructured BC provided a good substrate environment which expanded its surface area and absorbency. As a function of aniline concentration, the PANi content and electrical conductivity of PANi/BC composites were traced. There was an optimum point which those two properties do not increase significantly after 0.3 M of aniline was used.

Table 21.9 Composition of pure BC and PANi/BC composites [10]

Sample	M [mol L^{-1}]		PANi content [%]	Maximum tensile stress [MPa]	Electrical conductivity [S cm^{-1}]
	Oxidant	Monomer			
Pure BC	–	–	–	2.08×10^{-1}	–
1	0.1	0.08	40.46	5.07×10^{-1}	3.81×10^{-2}
2	0.2	0.16	67.40	4.81×10^{-1}	1.03×10^{-1}
3	0.3	0.24	78.69	3.75×10^{-1}	3.12×10^{-1}
4	0.4	0.32	84.42	2.73×10^{-1}	3.82×10^{-1}

The electrical conductivity reached up to 3.8×10^{-1} S cm^{-1} which is relatively higher than the conductivity reported before, resulting from the better affinity to reagents and absorbency of wet BC.

3.2 CNT-Based Materials

Carbon nanotubes (CNTs) recently emerged as the wonder materials of the new century and are being considered for a whole host of applications ranging from large-scale structures in automobiles to nanometer-scale electronics [51]. The benefit of CNT-based material is their electrical properties. In addition to the advantages conferred by miniaturization, carbon-based nanoelectronics promise greater flexibility compared to conventional silicon electronics, one example being the extraordinarily large variety of carbon structures exemplified in organic chemistry [52]. Consequently, nanotubes are also considered as candidates for molecular electronics [53]. Several remarkable properties, peculiar to low dimensionality, can be harnessed in CNT structures and gainfully employed.

The aim of this review, in addition to enumerating the electrical properties of CNT-derived structures, is to encourage the integration of a diverse set of electrical phenomena into a multifunctional CNT-based device. While large-scale assembly of CNTs, at a level that would be impressive to a systems designer, is still challenging, it was predicted that such a device would encourage applications where power savings, radiation hardness, and reduced heat dissipation are major considerations [51]. This will include significant features of electrical transport, which impact interpretation of measurements and suitability in advanced electronics. Basic issues involving doping to control nanotube properties, methods of contact from higher dimensional contacts/environment, and sensitivity to ambient conditions are relevant topics of concern. Briefly, single-walled and multiwalled CNTs (SWNTs and MWNTs) have been synthesized by various methods, e.g., by arc discharge and laser ablation methods, which seem to have a higher degree of structural perfection, due to the high temperatures (>3,000 ºC) involved in the synthesis [54]. Nanotubes are also grown through chemical vapor deposition (CVD) at a lower temperature (<1,000 ºC) with a higher defect density, which in turn adversely affects the electrical and thermal characteristics along with the structural properties [55].

Fig. 21.41 HUD navigation installed in K9 (Kia Motor) for the first time in Korea [56]

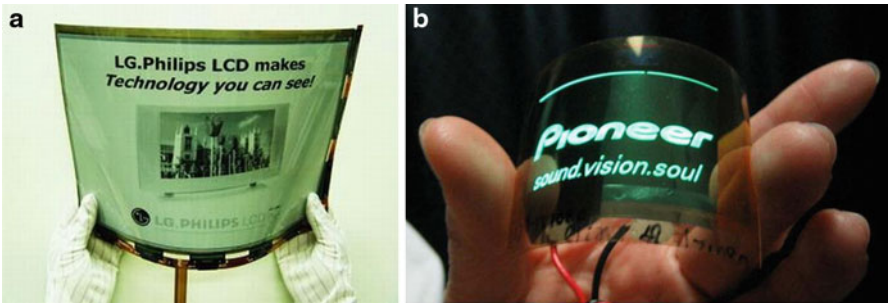

Fig. 21.42 (**a**) Flexible display (LG. Philips) [58] (**b**) Luminescence of an organic light-emitting diode deposited onto a flexible, low-CTE, and optically transparent wood–cellulose nanocomposite [59]

3.3 Applications

Transparent nanocomposites acted as substrates in OLED can be applied in diverse vision-area applications which are containing architectural windows, automotive windshields for navigation, and warning systems. Recently, this characteristic in automotive has been applying in head-up display (HUD) navigation (in Fig. 21.41). In addition, the flexibility of nanocomposites has a potential to apply cell phones and PDAs and tablet PC and be sewn into cloth integrating computer chip, cell phone, and GPS receiver [57].

Also, transparent nanocomposites acted as substrates in OLED can be flexible and foldable so that flexible display using nanocomposites is possible to create (in Figs. 21.33 and 21.42) [58, 59].

In order to be used as industrial product, current manufacture processing requires an improvement. Some defect such as crack can be founded on substrate surface from bad manufacturing of nanocomposite. Contamination from air and water can also easily damage display surface. Some of these problems can be solved easily by using transparent nanocomposites as packing material (in Fig. 21.43).

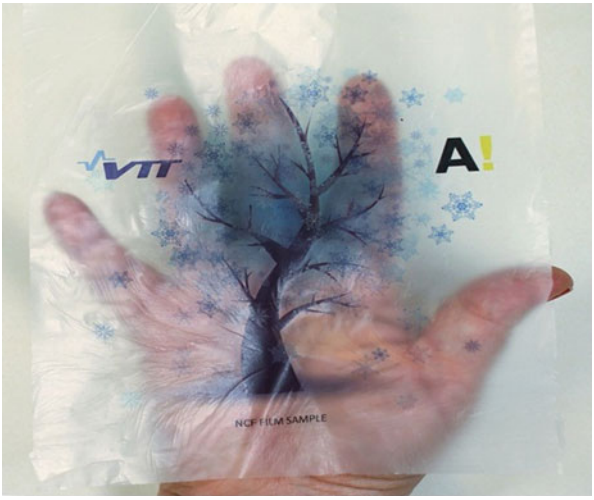

Fig. 21.43 Transparent nanocomposite composed of nanofibrillated cellulose packaging film [60]

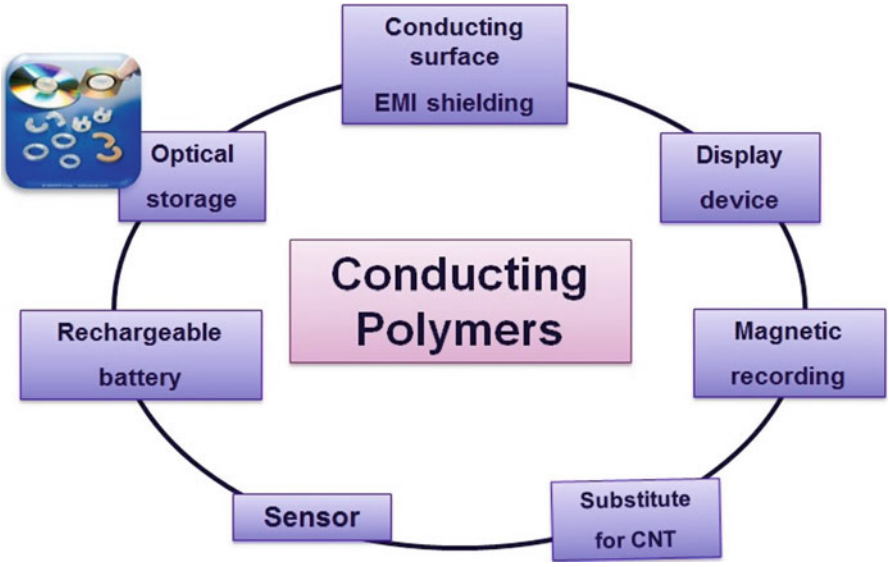

Fig. 21.44 Application of conducting polymer [38]

It is possible to manufacture through coating fibril cellulose on plastics. The manufacture processes and its improvements do not require addition investment; these can be manufactured through already-existing technology in the industry [60].

Electromagnetic shielding, depending on the conductivity of conductive polymer, can be applied to optical devices, display devices, sensors, batteries, etc. (in Fig. 21.44) [38].

One of the first applications of conducting polymers, which was in the center of attention worldwide, was light-weight batteries. While a lot of the conjugated polymers were experimented, most of them failed to exhibit the desired properties, specifically with respect to stability. However, batteries made using either polypyrrole or polyaniline as the positive electrode (cathode) and lithium–aluminum alloy as the negative electrode (anode) exhibited much more respectable properties. The electrolytes in these cases were either $LiCLO_4$ or $LiBF_4$ in propylene carbonate. During the battery discharge, electrons move from oxidized lithium alloy, as Li^+ from anode and BF_4^- from the cathode enter the electrolyte.

4 Conclusion

The fact that nanocellulose is a promising material that implements and enhances product properties, due to its intrinsic properties such as high crystallinity, high tensile strength, high melting temperature, high surface area-to-volume ratio, finer weblike network architecture, stiffness, and biodegradability has been demonstrated and discussed. Potential uses of nanocellulose composite involve diverse applications, due to its broad range properties as mentioned earlier, from electrical instrument, sensor, display panel, and bio-packaging product. As it has been stressed throughout an entire chapter on the importance of nanocellulose in electronic application mainly electronic display, considering nanocellulose composite's excellent optical and electrical conductivity properties, the use of this nanocellulose composite greatly improves film-display technology development. Including high expectation of growing market in the near future, which guarantee the promising future of this material. It is to be expected that the significance of nanocellulose composite has been a major role in electronic equipment application development.

References

1. Eichhorn SJ, Aranguren A, Marcovich NE, Dufresne A, Capadona JR, Rowan SJ, Weder C, Thielemans W, Roman M, Renneckar S (2010) Review: current international research into cellulose nanofibres and nanocomposites. J Mater Sci 45:1
2. Byoung-Ho Lee (2011) Preparation and characterization of bacterial cellulose nanofiber-based nanocomposite films. Doctoral dissertation, Seoul National University
3. Klemm D, Kramer F, Moritz S, Lindstrm T, Ankerfors M, Gray D, Dorris A (2011) Nanocelluloses: a new family of nature-based materials. Angew Chem Int Ed 50:5438
4. Nakagaito AN, Nogi M, Yano H (2010) Displays from transparent films of natural nanofibers. MRS Bull 35:214
5. Yano H, Sugiyama J, Nakagaito AN, Nogi M, Matsuura T, Hikita M, Handa K (2005) Optically transparent composites reinforced with networks of bacterial nanofibers. Adv Mater 17:153
6. Nogi M, Yano H (2008) Transparent nanocomposites based on cellulose produced by bacteria offer potential innovation in the electronics device industry. Adv Mater 20:1849

7. Okahisa Y, Abe K, Nogi M, Nakagaito AN, Nakatani T, Yano H (2011) Effects of delignification in the production of plant-based cellulose nanofibers for optically transparent nanocomposites. Compos Sci Technol 71:1342
8. Guimard NK, Gomez N, Schmidt CE (2007) Conducting polymers in biomedical engineering. Prog Polym Sci 32:876
9. Lee BH, Kim HJ, Yang HS (2012) Polymerization of aniline on bacterial cellulose and characterization of bacterial cellulose/polyaniline nanocomposite films. Curr Appl Phys 12:75
10. Lee HJ, Chung TJ, Kwon HJ, Kim HJ, Tze WTY (2012) Fabrication and evaluation of bacterial cellulose-polyaniline composites by interfacial polymerization. Cellulose 19:1251
11. Lee HJ (2012) Aminosilane treatment of bacterial cellulose and its application to improve electrical conductivity. Master thesis. Seoul National University
12. Oksman K, Mathew AP, Bondeson D, Kvien I (2006) Manufacturing process of cellulose whiskers/polylactic acid nanocomposites. Compos Sci Technol 66:2776
13. Yoon SH, Jin HJ, Kook MC, Pyun YR (2006) Electrically conducting polymer composites films prepared by bacterial celluloses and carbon nanotubes. Biomacromolecules 7:1280
14. Chen P, Cho SY, Jin HJ (2010) Modification and applications of bacterial celluloses in polymer science. Macromol Res 18:309
15. Favier V, Chanzy H, Cavaille JY (1995) Polymer nanocomposites reinforced by cellulose whiskers. Macromolecules 28:6365
16. Khalil HPSA, Bhat AH, Yusra AFI (2012) Green composites from sustainable cellulose nanofibrils: a review. Carbohydr Polym 87:963
17. Liu D, Yuan X, Bhattacharyya D (2012) The effects of cellulose nanowhiskers on electrospun poly (lactic acid) nanofibres. J Mater Sci 47:3159
18. Li R, Fei J, Cai Y, Li Y, Feng J, Yao J (2009) Cellulose whiskers extracted from mulberry: a novel biomass production. Carbohydr Polym 76:94
19. Herrick FW, Casabier RL, Hamilton JK, Sandberg KR (1983) Microfibrillated cellulose: morphology and accessibility. J Appl Polym Sci Appl Polym Symp 37:797
20. Carrasco GC (2011) Cellulose fibres, nanofibrils and microfibrils: the morphological sequence of MFC components from a plant physiology and fibre technology point of view. Nanoscale Res Lett 6:1
21. Gilberto S, Bras J, Dufresne A (2010) Review cellulosic bionanocomposites: a review of preparation, properties and applications. Polymers 2:728
22. Syverud K, Carrasco GC, Toledo J, Toledo PG (2011) A comparative study of *Eucalyptus* and *Pinus radiata* pulp fibres as raw materials for production of cellulose nanofibrils. Carbohydr Polym 84:1033
23. Iwamoto S, Nakagaito AN, Yano H (2007) Nano-fibrillation of pulp fiber for the processing of transparent nanocomposites. Appl Phys A Mater Sci Process 89:461
24. http://www.oled-display.net/oled-revenues-forecast
25. Jeong DY (2007) Industry report: OLED, next-generation display, heat up. http://seriworld. org/
26. Forrest SR (2004) The path to ubiquitous and low-cost organic electronic appliances on plastic. Nature 428:911
27. Reuss RH, Chalamala BR, Moussessian A, Kane MG, Kumar A, Zhang DC, Rogers JA, Hatalis M, Temple D, Moddel G, Eliasson BJ, Estes MJ, Kunze J, Handy ES, Harmon ES, Salzman DB, Woodall JM, Alam MA, Murthy JY, Jacobsen SC, Olivier M, Markus D, Campbell PM, Snow E (2005) Macroelectronics: perspectives on technology and applications. P IEEE 93:1239
28. MacDonald WA (2004) Engineered films for display technologies. J Mater Chem 14:4
29. Iwamoto S, Nakagaito AN, Yano H, Nogi M (2005) Optically transparent composites reinforced with plant fiber-based nanofibers. Appl Phys A Mater Sci Process 81:1109
30. Fukuzumi H, Saito T, Iwata T, Kumamoto Y, Isogai A (2009) Transparent and high gas barrier films of cellulose nanofibers prepared by TEMPO-mediated oxidation. Biomacromolecules 10:162

31. Ifuku S, Nogi M, Abe K, Handa K, Nakatsubo F, Yano H (2007) Surface modification of bacterial cellulose nanofibers for property enhancement of optically transparent composites: dependence on acetyl-group DS. Biomacromolecules 8:1973
32. Nogi M, Iwamoto S, Nakagaito AN, Yano H (2009) Optically transparent nanofiber paper. Adv Mater 21:1595
33. Barud HS, Caiut JMA, Dexpert-Ghys J, Messaddeq Y, Ribeiro SJL (2012) Transparent bacterial cellulose-boehmite-epoxi-siloxane nanocomposites. Composites 43:973, Part A
34. Gea S, Bilotti E, Reynolds CT, Soykeabkeaw N, Peijs T (2010) Bacterial cellulose–poly(vinyl alcohol) nanocomposites prepared by an in-situ process. Mater Lett 64:901
35. Shirakawa H, Louis EJ, Macdiarmid AG, Chiang CK, Heeger AJ (1977) Synthesis of electrically conducting organic polymers: halogen derivatives of polyacetylene. J Chem Soc Chem Commun 16:570
36. Collier JH et al (2000) Synthesis and characterization of polypyrrole-hyaluronic acid composite biomaterials for tissue engineering applications. J Biomed Mater Res 50:574, Part A
37. Norden B, Krutmeijer E (2000) Conductive polymers: The Royal Swedish Academy of Sciences, Information Department, Stockholm, Sweden
38. Lee BH (2011) Preparation and characterization of bacterial cellulose nanofiber-based nanocomposite films. Doctoral dissertation, Seoul National University
39. Hu WL, Chen SY, Yang ZH, Liu LT, Wang HP (2011) Flexible electrically conductive nanocomposite membrane based on bacterial cellulose and polyaniline. J Phys Chem B 115:8453
40. Marins JA, Soares BG, Dahmouche K, Ribeiro SJL, Barud H, Bonemer D (2011) Structure and properties of conducting bacterial cellulose-polyaniline nanocomposites. Cellulose 18:1285
41. Stafström S, Brédas JL, Epstein AJ, Woo HS, Tanner DB, Huang WS, MacDiarmid AG (1987) Polaron lattice in highly conducting polyaniline: Theoretical and optical studies. Phys Rev Lett 59:1464
42. Zhang Z, Wei Z, Wan M (2002) Nanostructures of Polyaniline Doped with Inorganic Acids. Macromolecules 35:5937
43. Abdiryim T, Jamal R, Nurulla I (2007) Doping effect of organic sulphonic acids on the solid-state synthesized polyaniline. J Appl Polym Sci 105:576
44. Kelly FM, Johnston JH, Borrmann T, Richardson MJ (2007) Functionalised hybrid materials of conducting polymers with individual fibres of cellulose. Eur J Inorg Chem 2007:5571
45. Huang J, Virji S, Weiller BH, Kaner RB (2003) Polyaniline Nanofibers: Facile Synthesis and Chemical Sensors. J Am Chem Soc 125:314
46. Huang J, Kaner RB (2004) A General Chemical Route to Polyaniline Nanofibers. J Am Chem Soc 126:851
47. Huang J, Kaner RB (2004) Nanofiber formation in the chemical polymerization of aniline: a mechanistic study. Angew Chem 116:5941
48. Huang J, Virji S, Weiller BH, Kaner RB (2004) Nanostructured polyaniline sensors. Chem Eur J 10:1314
49. Huang J, Kaner R (2004) A general chemical route to poly-aniline nanofibers. J Am Chem Soc 126:851
50. Lee K, Cho S, Park SH, Heeger AJ, Lee CW, Lee SH (2006) Metallic transporting polyaniline. Nature 441:65
51. Koh WC, Chandra P, Kim DM, Shim YB (2011) Electropolymerized self-assembled layer on gold nanoparticles: detection of inducible nitric oxide synthase in neuronal cell culture. Anal Chem 83:6177
52. McGehee DG, Topinka MA (2006) Solar cells: pictures form the blended zone. Nat Mater 5:675
53. Yoon JH, Kim DM, Yoon SS, Won MS, Shim YB (2011) Comparison of solar cell performance of conducting polymer dyes with different functional groups. J Power Sources 196

54. Shiddiky MJA, Rahman MA, Shim YB (2007) Hydrazine-catalyzed ultrasensitive detection of DNA and proteins. Anal Chem 79:6886
55. Bandaru PR (2007) Electrical properties and applications of carbon nanotube structures. J Nanosci Nanotechnol 7:1239
56. http://blog.naver.com/HUD_KIA
57. http://www.ent.mrt.ac.lk/Oled
58. http://linepic.blogspot.kr/Flexible_display_by_Jang,H
59. Okahisa Y, Yoshida A, Miyaguchi S, Yano H (2009) Optically transparent wood–cellulose nanocomposite as a base substrate for flexible organic light-emitting diode displays. Compos Sci Technol 69:1958
60. Tammelin T (2012) Transparent plastic-like packaging material from birch fibril pulp
61. Hong SY, Marynick DS (1992) Understanding the conformational stability and electronic structures of modified polymers based on polythiophene. Macromolecules 25(18), pp 4652–4657

Poly(Vinyl Alcohol) Cellulose Nanocomposites

22

Qingzheng Cheng, Siqun Wang, and Zhaohui Tong

Contents

Q. Cheng (✉)
Forest Products Development Center, Auburn University, Auburn, AL, USA

Agricultural & Biological Engineering, University of Florida, Gainesville, FL, USA
e-mail: chenggq@hotmail.com

S. Wang
Center for Renewable Carbon, University of Tennessee, Knoxville, TN, USA
e-mail: swang@utk.edu

Z. Tong
Agricultural & Biological Engineering, University of Florida, Gainesville, FL, USA
e-mail: ztong@ufl.edu

J.K. Pandey et al. (eds.), *Handbook of Polymer Nanocomposites. Processing, Performance and Application – Volume C: Polymer Nanocomposites of Cellulose Nanoparticles*,
DOI 10.1007/978-3-642-45232-1_69,

Abstract

Cellulose is the most abundant natural biopolymer in the world. Cellulose fibrils in micro- and nanoscales are attractive materials to replace man-made fibers such as glass and aramid fibers. They can be used as the reinforced additives or fillers to produce environmentally friendly materials. Poly(vinyl alcohol) (PVA) is a biodegradable polymer, which has many advantages including the resistance to solvents, being able to chemically bond with cellulose and soluble in hot water. The water solubility of PVA allows it to be fabricated with other water-soluble materials (e.g., nanocellulose solution) to form a nanocomposite by film casting method. In the introduction of this chapter, we overviewed the recently developed methods to generate cellulose fibril in a micro- or nanoscale, the characterization of nanocrystals and nanofibers, and the fabrication methods for PVA/cellulose nanocomposites. As an example, commercial microfibrillated cellulose (MFC) was used to reinforce PVA through film casting method in this chapter. The morphologies and sizes of the MFC were detected by scanning electronic microscopy (SEM). The effects of MFC on mechanical and thermal properties and surface morphologies of composites were studied. The introduction of MFC increased both tensile modulus and tensile strength of neat PVA. The composite had a higher thermal degradation temperature compared to neat PVA. The SEM images indicated the existence of interbonding between PVA and cellulose fibrils.

Keywords

Cellulose • Mechanical and thermal properties • Nanocomposite • Poly(Vinyl Alcohol) • Surface morphology

1 Introduction

In the past decades, biodegradable products from renewable materials are becoming increasingly more attractive due to the escalating price of the crude oil and the shortage of petroleum resources. Cellulose, the most abundant natural biopolymer in the world, is synthesized in biomass through photosynthesis. The cellulosic fibers and their derivatives (e.g., fibrils in micro- and nanoscales, cellulose crystals/whiskers) have many advantages including biodegradable, renewable, relatively low cost and density, nonabrasive, and high specific strength and modulus. Therefore, these cellulosic materials are used as reinforced materials or fillers to produce environmentally friendly products.

Nano-sized materials (e.g., nanocellulose) are defined as the materials that have at least one dimension in a nanometer scale (1–100 nm) [1]. Microfibers are defined as the fibers with 0.1–1 μm in diameter and a corresponding minimum length of 5–50 μm [2]. Cellulose fibrils in micro- and nanoscales have much higher mechanical properties compared with original fibers [3, 4]. It is still very challengeable

for a low-cost process to isolate fibrils and to further fabricate nanocomposites with the improving strength and stiffness as expected. Chemical and mechanical processes are two common methods to obtain cellulose fibrils. Strong acid hydrolysis is one of the primary chemical methods that remove the amorphous regions of cellulose fibers to produce cellulose nanocrystals or nanowhiskers. The mechanical method utilizes strong shear forces to disintegrate cellulose fibers into fibril bundles. Many terms, including microfibrillated cellulose (MFC), cellulose nanocrystal, cellulose nanofibril, cellulose whisker, and cellulose nanofibers, have been used to describe different types of cellulosic fibrils in micro- and nanoscales. In this chapter, we use cellulose nanofibers for mechanically isolated fibrils and nanocrystals for chemical isolated fibrils after removing amorphous parts using strong acids. Bacterial cellulose fibrils can also be used to reinforce PVA, but it will not be discussed in this chapter [5, 6].

Poly(vinyl alcohol) (PVA) is a biodegradable polymer, which has many advantages including resistance to solvents, being able to chemically bond with cellulose. It is soluble in hot water, which enables the formation of films by first mixing water suspensions of PLA and cellulose nanofibers and nanocrystals followed by a casting process. PVA has also been broadly used as protective colloids in the manufacture of polymer emulsions, for bindings of pigments and fibers, and for the production of detergents and cleansing agents, adhesives, emulsion paints, and solution cast films [7, 8]. However, it has relatively low mechanical strength and integrity. Therefore, recently many researchers have focused on using cellulose nanofibers and nanocrystals to reinforce PVA to improve its mechanical and thermal properties.

This chapter will review the processes to isolate cellulose fibrils in micro- and nanoscales, the characteristics of recently developed cellulose fibrils, and the properties of its reinforced PVA nanocomposites in the introduction. As a comparison, commercial microfibrillated cellulose (MFC) was used to reinforce PVA as well. The morphologies and the average sizes of MFC were estimated by scanning electronic microscopy. The effects of MFC on mechanical and thermal properties and surface morphologies of the PVA nanocomposites were investigated.

1.1 The Isolation of Cellulose Nanocrystals by Chemical Methods

Strong acid hydrolysis, as one of the primary chemical methods, has been used to remove the amorphous regions of cellulose fibers and then generate cellulose nanocrystals, also called cellulose whiskers. Figure 22.1 shows typical chemical isolation procedures for the cellulose nanocrystal generation from raw lignocellulosic materials (wood residues or other biomass) and from other cellulosic materials. Generally, when raw lignocellulosic materials were used, the lignin and hemicellulose have to be removed before acid hydrolysis process [9–11]. After lignin removal, the procedure to prepare cellulose nanocrystals from pure cellulose

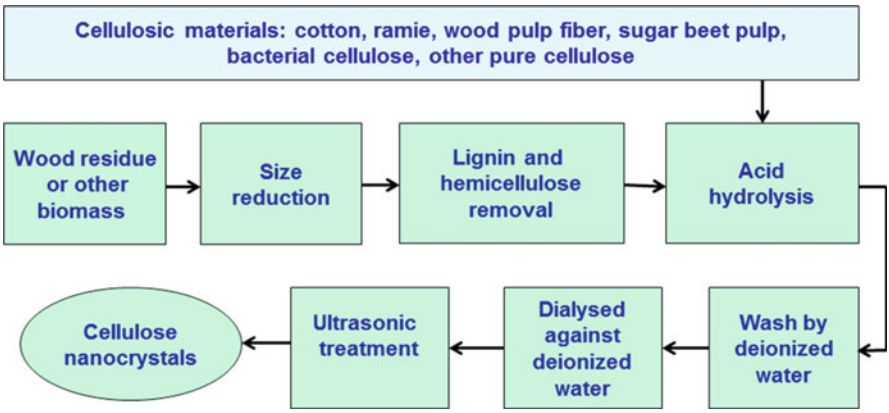

Fig. 22.1 Typical chemical isolation procedure of cellulose nanocrystals from wood residues or other biomass and from cellulose materials

normally includes five steps: acid hydrolysis, centrifugation and neutralization, washing with deionized water, further disintegration by ultrasonic treatment, and ultrafiltration to remove any remaining ions (Fig. 22.1) [11, 12]. Cellulose nanocrystals have been obtained from many cellulose materials, such as wood pulp fibers, cotton, ramie, tunicate mantles, sugar beet pulp, and bacterial cellulose [10, 13–26]. The properties and morphologies of cellulose nanocrystals are significantly affected by acid reaction conditions [17].

1.2 The Isolation of Cellulose Nanofibers by Mechanical Methods

The most common mechanical method utilizes strong shear forces, such as the shear force generating from a homogenizer, to disintegrate cellulose fibers to fibrils in a micrometer scale. This method can be used to generate cellulose microfibril or bundles, commonly called microfibrillated cellulose (MFC) [14, 27, 28]. A high-pressure refiner or super grinder treatment can also be used to generate cellulose nanofibers [18, 29]. Another method is a process that generates the shear force from high-intensity ultrasonication (HIUS). A HIUS processor can be used to isolate fibrils from several cellulosic resources, such as regenerated cellulose fiber, pure cellulose fiber, microcrystalline cellulose, and pulp fiber [30–32]. HIUS produces a very strong mechanical oscillating power from ultrasonic waves, which forms hydrodynamic forces to separate cellulose fibrils [33]. A mixture suspension of fibers and fibrils with a diameter ranging from tens of nanometers (nm) to microns (μm) was obtained after HIUS treatment. SEM and AFM images can be used to observe the structure and appearance of the regenerated cellulose fibrils isolated by HIUS (Figs. 22.2 and 22.3). The diameters of the fibrils were in a wide range of tens-to-hundreds nanometers and have a wide range of aspect ratios.

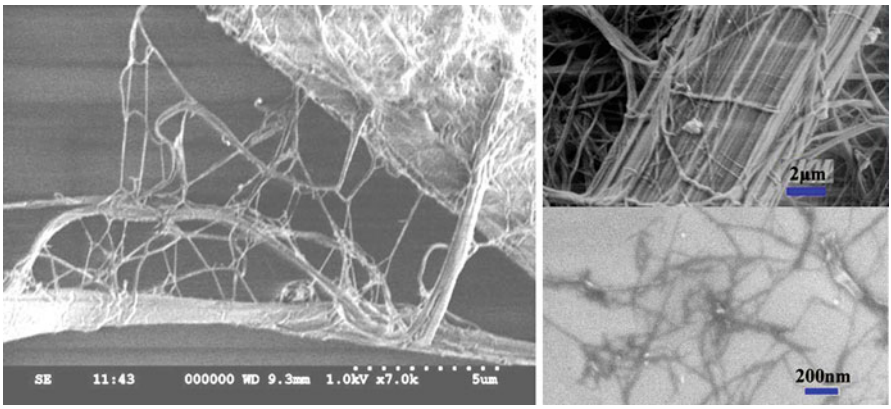

Fig. 22.2 SEM images of cellulose fibers and fibrils isolated by ultrasonic treatment (Reprinted from [31] with permission from Wiley)

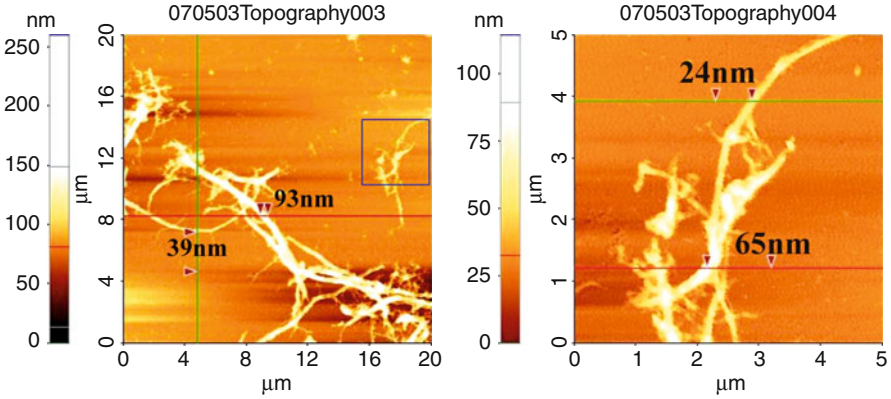

Fig. 22.3 AFM images of cellulose fibrils isolated by ultrasonic treatment (Reprinted from [31] with permission from Wiley)

1.3 Characterizations of Cellulose Nanocrystals and Nanofibers

Cellulose fibrils can be characterized by morphological observation, degree of fibrillation, crystalline measurement, and mechanical tests. Several technologies can be used for morphological observation, such as a scanning electron microscope (SEM), an atomic force microscope (AFM), and a transmission electron microscopy (TEM) [12, 16, 18, 34–36]. The degree of fibrillation of the cellulose fibers can be evaluated by water retention value (WRV) [27, 28, 30, 31, 37–39]. The crystallinity of the cellulose fibrils can be studied through wide-angle X-ray diffraction (WAXD) [2, 34, 38, 40] or Fourier transform infrared spectroscopy (FTIR) [31].

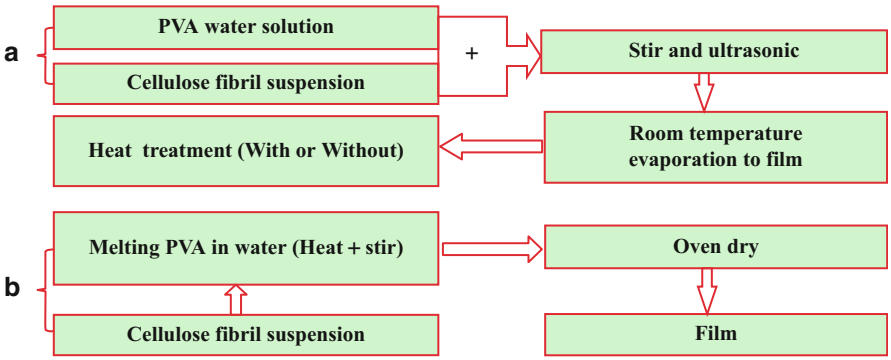

Fig. 22.4 Typical fabrication procedure of PVA cellulose nanocomposites: (**a**) PVA solution and cellulose fibril suspension mixture process, (**b**) cellulose fibril suspension added in melting PVA process

Mechanical properties, especially the elastic modulus of the crystalline region of cellulose, have been determined either experimentally or theoretically using Raman spectroscopy and X-ray diffraction [6, 13, 41, 42]. AFM three-point bending test can be used to measure mechanical properties of single cellulose nanofibers [3, 43–45].

1.4 Fabrication and Characterization of PVA Cellulose Nanocomposites

The most frequently used method for cellulose nanocomposite fabrication is solvent evaporation casting, using water-soluble and other solvent-soluble polymers. For example, cellulose nanocomposites can be produced by a solvent casting method in Teflon or propylene dishes [29, 46]. Nanocomposites can also be obtained through a hot-pressing method using freeze-drying fibrils [47]. An optically transparent composite reinforced with plant fiber-based cellulose microfibrils can be produced by a mat formation at first, followed by a resin immersion and curing by UV light [48], or followed by a hot press with high pressures [49], or compression molding [50].

The film casting method is a commonly used method that produces PVA cellulose nanocomposites because PVA is a hot-water-soluble polymer. Figure 22.4 shows two fabrication procedures for the formation of PVA cellulose nanocomposites. In procedure (a), PVA was dissolved in water under heating and then mixed with cellulose fibril suspension. Then the mixture was treated by untrasonification and followed by a film casting process [4, 38]. In procedure (b), PVA powder was dissolved in hot water under heating and continuous stirring at first. Then nanofiber suspension was added to the hot PVA solution and heated until the solution became viscous. The formed mixture solution was poured onto dishes and then heated in a 50 °C in an oven to cast films [36].

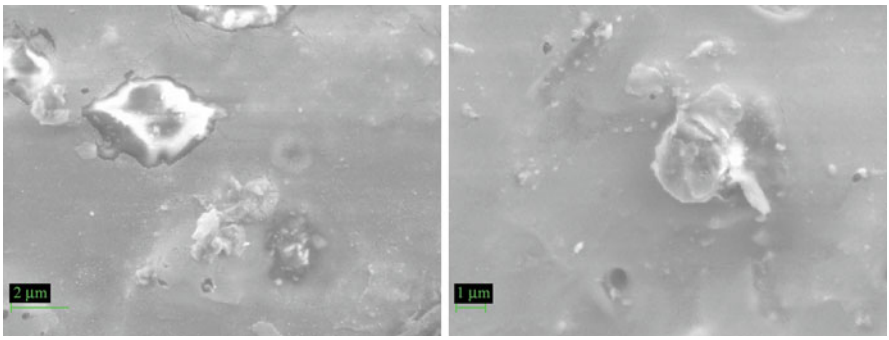

Fig. 22.5 SEM images of the fractured cross sections of PVA composites reinforced with small cellulose fibrils (Reprinted from [4] with permission from Elsevier)

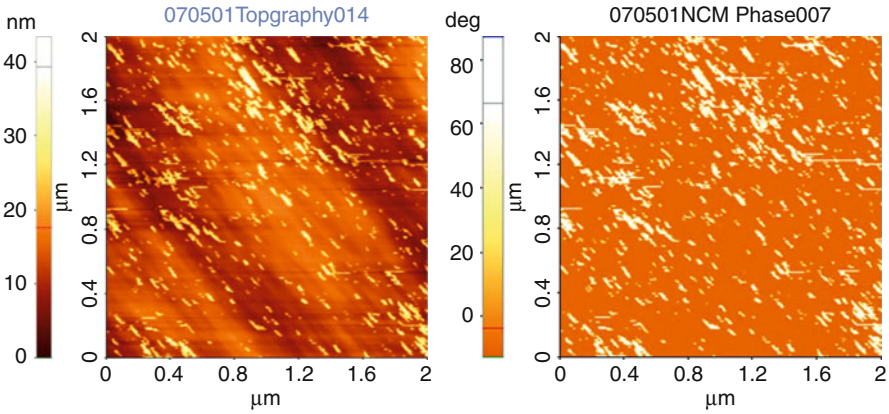

Fig. 22.6 AFM topography and phase images of the cross sections of PVA composites reinforced with small cellulose fibrils (Reprinted from [4] with permission from Elsevier)

Many instruments have been used to investigate the mechanical, morphological, and thermal properties of cellulose nanocomposites. The mechanical properties can be measured by tensile and bending tests [4, 5, 10, 12, 23, 24, 29, 34, 38, 49, 51–53]. Dynamic mechanical analysis (DMA) tests can also be used to evaluate composite performance under various conditions of temperature and relative humidity [12, 46, 53]. AFM, SEM, and TEM are common tools for morphological characterizations of nanocomposites [3, 16, 19, 21, 29, 32, 51]. Figures 22.5 and 22.6 show SEM images of fracture surfaces of nanocomposites after tensile testing and AFM images of cross sections after cutting by microtome from the PVA nanocomposites reinforced by a small number of cellulose fibrils. Differential scanning calorimetry (DSC), thermogravimetric analyzer (TGA), and DMA have been used to evaluate thermal properties of cellulose nanocomposites [10, 11, 22, 23, 25, 27, 32, 53–57].

2 Materials and Methods

2.1 Materials

Poly(vinyl alcohol) (PVA) was purchased from Acros Organics (99–100 % hydrolyzed, average M.W. 86000) and used as the matrix material in the composites. Microfibrillated cellulose (MFC, 10 % solid slurry, Daicel Chemical Industries Ltd., Japan) was used for PVA reinforcement.

The MFC morphological structure was observed by field emission gun-scanning electron microscopy (FEI XL-40 FEG-SEM, Tokyo, Japan). All samples were coated with Au-Pd (~10 nm) before the SEM observation and the operating voltage was 15 kV.

2.2 MFC Nanocomposite Fabrication

Solid PVA was dissolved in water to prepare the solution with 10 wt% of solid content under heating [4, 8]. MFC water suspension (1 wt%) and the PVA water solution (10 wt%) were mixed together and stirred manually and then treated by ultrasonification (Model 300 V/T, BioLogics, Inc., Manassas, VA) for 3 min at a power level of 50 % and under a continuous mode. The cellulose nanocomposites with four MFC loading levels (0 wt%, 2 wt%, 5 wt%, and 10 wt%) were fabricated by the film casting method. The mixtures were degassed in a desiccator using vacuum and then evaporated in Petri dishes at room temperature with relative humidity (RH) of ~30 % until films were formed. The films were then heated in an oven at 70 °C for more than 4 h. The samples were kept in a desiccator with magnesium nitrate $Mg(NO_3)_2$ saturated solution (RH about 53 % at ~22 °C) more than 3 days before mechanical and thermal properties were tested in accordance to ASTM D1708 conditioning conditions (RH is 50 ± 5 % and time is more than 40 h) [58]. The nominal thickness of the nanocomposite films was 127 μm.

2.3 Characterization of PVA and PVA MFC Nanocomposites

An Instron test machine (Model 5566, load cell capacity of 100 N, Grove City, PA) was used to test the mechanical properties of the films. The crosshead speed was 10 mm/min and the crosshead extension was used as specimen deformation. All samples were cut to dog-bone shapes with widths of 5 mm and lengths of 20 mm for the narrow portions. Five specimens for each MFC level film were tested in accordance to ASTM D1708 [58]. Tensile elastic modulus of all films was determined from the linear portion of the stress-strain curves. Multiple comparisons by the Statistical Analysis System (SAS) (t-tests (LSD)) were used to detect the overall significant differences of MFC influences on the tensile elastic modulus and strength of composites ($\alpha = 0.05$).

A thermogravimetric analyzer (TGA/DSC1, Stare system, Mettler Toledo, Schwerzenbach, Switzerland) was used to determine the thermal behaviors of the

PVA MFC nanocomposite films, neat PVA and neat MFC. The sample weight was approximately 10 mg and heated from 50 °C to 500 °C at a 20 °C/min heating rate. The tests were conducted under nitrogen gas with a flow rate of 20 ml/min to avoid oxidation. Scanning electron microscopy (SEM; same process was used as described above) was also used to examine the topography of sample fracture surfaces after tensile test.

3 Results and Discussion

3.1 SEM Observation of MFC

Figure 22.7 shows the SEM images of MFC in micro- and nanoscales. The MFC diameters were ranged from tens of nanometer (nm) up to approximately hundreds of nm, but most of them were less than 100 nm. The MFC lengths were ranged from several micrometers (μm) up to tens of μm. It is estimated that the MFC aspect ratio (length/diameter) could be up to 100. Microfibers and nanofibers with high aspect ratios could greatly improve the mechanical properties of neat PVA [2, 4, 36].

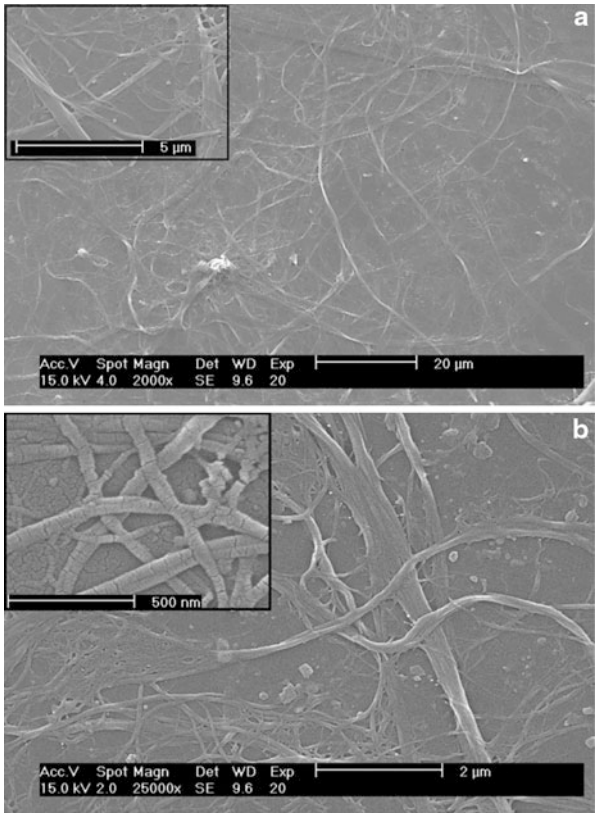

Fig. 22.7 SEM images of microfibrillated cellulose (MFC) with low ((**a**) scale = 20 μm and the insert scale = 5 μm) and high ((**b**) scale = 2 μm and the insert scale = 500 nm) magnifications

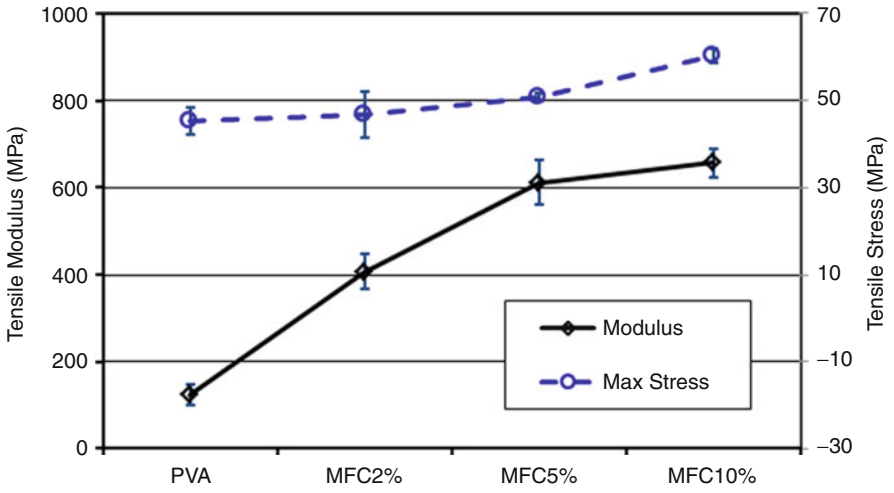

Fig. 22.8 Tensile modulus and max stress of PVA and PVA MFC nanocomposites with 2 %, 5 %, and 10 % MFC loadings

Table 22.1 Statistical analysis data of tensile modulus, max stress, and max strain at break of PVA and its MFC nanocomposites with 2 %, 5 %, and 10 % MFC loadings

		Max stress (MPa)		Modulus (MPa)		Max strain (%)	
Sample	Specimen number	Mean	t grouping[a]	Mean	t grouping[a]	Mean	t grouping[a]
PVA	5	45.3	C	123.4	C	3.63	A
MFC2	5	46.8	BC	406.8	B	2.68	B
MFC5	5	50.9	B	611.8	A	1.59	C
MFC10	5	60.2	A	656.4	A	0.69	D

[a]Means with the same letter are not significantly different

3.2 Tensile Mechanical Properties of the Nanocomposites

Figure 22.8 shows the tensile moduli and tensile strengths (max stress) of neat PVA and PVA MFC nanocomposites with 2, 5, and 10 wt% MFC loadings, and the statistical analysis data are shown in Table 22.1. The tensile modulus of neat PVA was increased 230 %, 396 %, and 432 % in the substitution of 2 %, 5 %, and 10 wt% MFC, respectively. These results indicated that MFC could significantly improve PVA modulus. The modulus increased with the enhancement of MFC loading levels. However, as the substitution of 10 wt% of MFC, the modulus of MFC composite was not significantly different with that of MFC composite with 5 wt% (Fig. 22.8, Table 22.1). This is partially caused by the aggregation of small fibrils at a high fibril loading. It has been reported that the aggregation of smaller cellulose fibrils under a high loading level of fibrils may affect the reinforcement of their composites [4, 38].

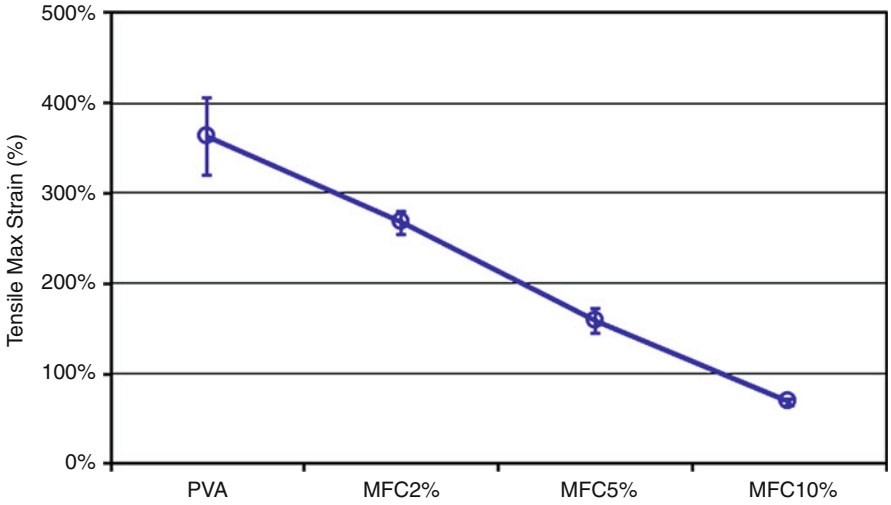

Fig. 22.9 Tensile max strain at break of PVA and PVA MFC nanocomposites with 2 %, 5 %, and 10 % MFC loadings

The tensile strength (max stress) of neat PVA could also be improved as the substitution of MFC, and it increased with the enhancement of MFC loading levels. Although the substitution of 2 wt% MFC did not significantly increase the tensile strength of neat PVA, at a 5 wt% and 10 wt% loading level, the tensile strengths were significantly improved according to the statistical analysis under 95 % confidence ($\alpha = 0.05$ %) (Table 22.1). The reinforcement could be attributed to a high aspect ratio of MFC.

Figure 22.9 shows the tensile max strain (elongation) of neat PVA and PVA MFC nanocomposites as the substitution of 2, 5, and 10 wt% of MFC. The max strain at break of neat PVA was significantly decreased by all three MFC loadings, and it was decreased with the incensement of the MFC loading levels (Fig. 22.9, Table 22.1). It may be caused by the brittle property of MFC, the aggregation of small-sized MFC, and the uneven MFC distribution in the polymer matrix [4, 38].

3.3 Thermal Properties of the Nanocomposites

Thermal properties of neat PVA and the PVA MFC nanocomposites were analyzed using thermogravimetric analysis (TGA). The TGA and derivative TGA (DTGA) thermograms are shown in Fig. 22.10. Basically, we observed three weight-loss regions. The first region exhibited an initial weight loss from 70 °C to 150 °C due to the evaporation of water. The second degradation region was the max weight-loss region from 250 °C to 400 °C with a weight loss from 50 % to 75 % depending on the different materials, which were mainly attributed to the degradation of the PVA

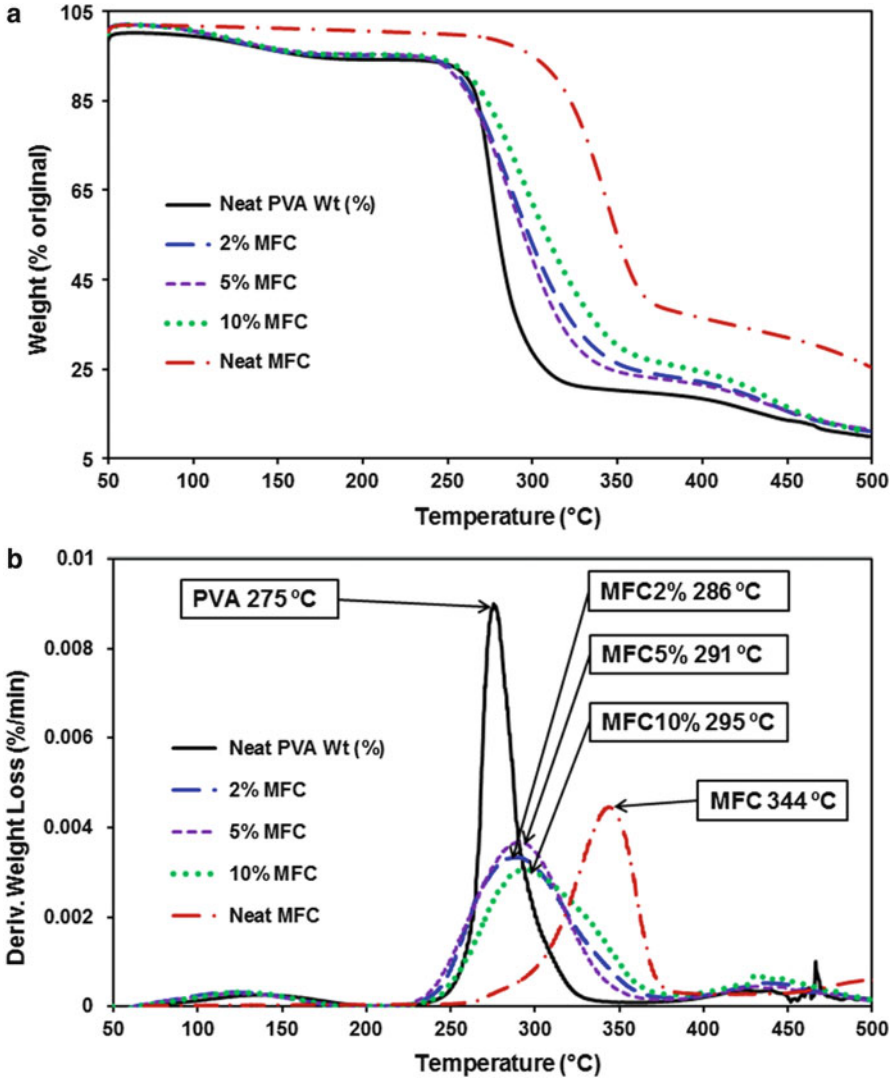

Fig. 22.10 TGA (**a**) and DTGA (**b**) diagrams of neat PVA, MFC, and PVA MFC nanocomposites with 2 %, 5 %, and 10 % MFC loadings

and its composites. The third region of weight loss occurred above 400 °C, which was mainly caused by the decomposition of carbonaceous matters from the PVA and cellulose [59, 60].

Water content has significant effects on the mechanical properties. The water content of MFC was lower than PVA and its composites because it was not conditioned after drying. The PVA and all nanocomposites had relative high water contents (∼2 %) since they were conditioned at the RH of 53 % for more

than 3 days (Fig. 22.10a). The water has strong plasticizing effect and improves the movement of PVA chains [60]. This could be the main reason that the tensile modulus and strength shown in Fig. 22.8 were not as high as those of PVA and its composites without 50 % RH conditioning [4].

Neat PVA thermally degraded at a lower temperature than neat MFC (Fig. 22.10a). The PVA/MFC nanocomposites had a lower degradation temperature than the neat MFC but a higher temperature than the neat PVA. DTGA curves further confirm these results (Fig. 22.10b). As shown in Fig. 22.10, the max degradation temperature of PVA was increased about 11 °C, 16 °C, and 20 °C by adding 2 %, 5 %, and 10 % MFC, respectively. It was caused by the higher degradation temperature of cellulose (315–400 °C) compared to that of polyvinyl alcohol (200–300 °C) [61, 62].

3.4 SEM Observation of the Composites Fracture Surfaces

The SEM images of fractured cross sections of PVA and its MFC nanocomposites after tensile test are shown in Fig. 22.11. It was observed that the fracture surfaces of nanocomposites were rough (Fig. 22.11a–c) compared to the relatively smooth surface of the neat PVA film (Fig. 22.11d). The MFC fibrils were well dispersed in the PVA matrix, but they were not uniformly distributed in the matrix (Fig. 22.11c).

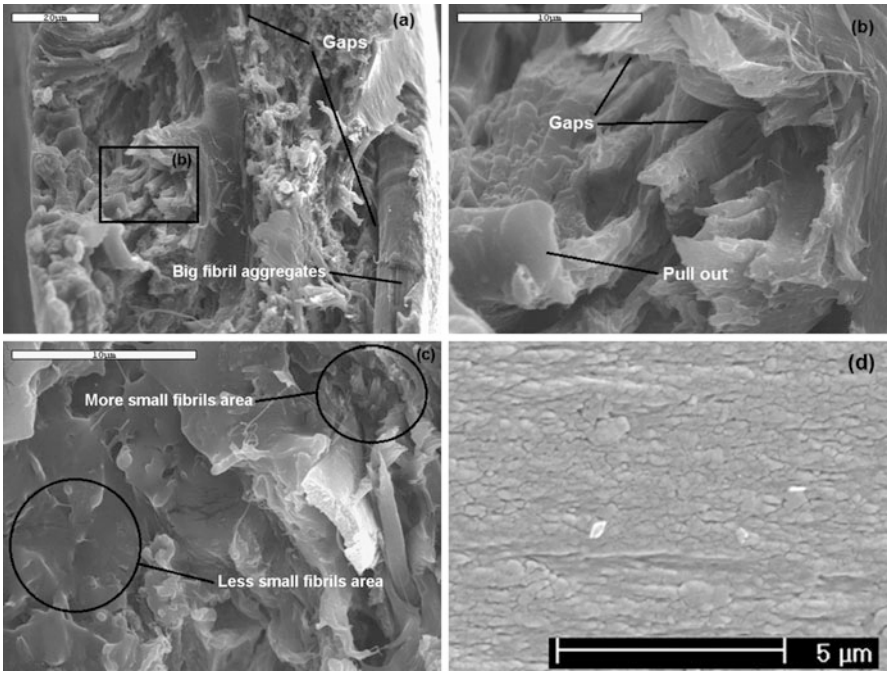

Fig. 22.11 SEM images of the fractured cross sections of PVA MFC nanocomposites with 5 % MFC loading ((**a**) scale = 20 µm; (**b**) scale = 10 µm; (**c**) scale = 10 µm) and neat PVA (**d**)

There were some clear gaps between MFC fibrils (especially large fibril aggregations) and the PVA matrix (Fig. 22.11a, b). Some MFC fibrils could be pulled out during tensile test (Fig. 22.11b). These could be the main reasons that the tensile strength (max stress) of PVA was not increased much by adding MFC and the max strain at break of the MFC nanocomposites was significantly decreased compared with neat PVA (Fig. 22.8) [4].

4 Conclusions

Cellulose fibrils in micro- and nanoscales (nanofibers or nanocrystals) can be generated by mechanical or chemical methods. Both cellulose nanofibers and nanocrystals can be used to reinforce PVA to produce biodegradable nanocomposites by film casting methods. Commercial microfibrillated cellulose (MFC) with diameters ranged from tens of nanometer to hundreds of nm was used to reinforce PVA in this chapter as an example. Both tensile modulus and tensile strength of neat PVA were significantly improved with the substitution of the MFC from 2 wt% to 5 wt%. However, the PVA max tensile strain was decreased significantly. Thermal gravimetric data revealed that the MFC-reinforced nanocomposites had higher thermal degradation temperatures compared with neat PVA. The entire nanocomposites are biodegradable and environmentally friendly.

Acknowledgment The authors thank Dr. Seung-Hwan Lee at the National Institute of Advanced Industrial Science and Technology (AIST) for proving the commercial microfibrillated cellulose (MFC).

References

1. Jordan J, Jacob KI, Tannenbaum R, Sharaf MA, Jasiuk I (2005) Mater Sci Eng A Struct Mater Prop Microstruct Process 393:1
2. Chakraborty A, Sain M, Kortschot M (2006) Holzforschung 60:53
3. Cheng Q, Wang S, Harper D (2009) Comp A Appl Sci Manuf 40:583
4. Cheng Q, Wang S, Rials T (2009) Comp A Appl Sci Manuf 40:218
5. Gea S, Bilotti E, Reynolds CT, Soykeabkeaw N, Peijs T (2010) Mater Lett 64:901
6. Qiu K, Netravali AN (2012) J Mater Sci 47:6066
7. Finch CA (1987) Poly(vinyl alcohol): properties and applications. Wiley, New York
8. Hassan CM, Peppas AN (2000) Adv Polym Sci 153:37–65
9. Wise LE, Murphy M, Addieco AA (1946) Pap Trade J 122:35
10. Kamphunthong W, Hornsby P, Sirisinha K (2012) J Appl Polym Sci 125:1642
11. Wang J, Cheng Q, Adebayo AB, Difazio S (2012) Poly(vinyl alcohol) nanocomposites reinforced with cellulosic nanofibers isolated from juvenile poplar. In: Cheng Q (ed) Fiber-reinforced composites. Nova Science, New York, p 91
12. Choi YJ, Simonsen J (2006) J Nanosci Nanotechnol 6:633
13. Sakurada I, Nukushina Y, Ito T (1962) J Polym Sci 57:651
14. Dufresne A, Cavaille JY, Vignon MR (1997) J Appl Polym Sci 64:1185
15. Edgar CD, Gray DG (2002) Macromolecules 35:7400
16. Zimmermann T, Pohler E, Geiger T (2004) Adv Eng Mater 6:754

17. Beck-Candanedo S, Roman M, Gray DG (2005) Biomacromolecules 6:1048
18. Chakraborty A, Sain M, Kortschot M (2005) Holzforschung 59:102
19. Kvien I, Tanem BS, Oksman K (2005) Biomacromolecules 6:3160
20. Lu YS, Weng LH, Cao XD (2005) Macromol Biosci 5:1101
21. Pu Y, Zhang J, Elder T, Deng Y, Gatenholm P, Ragauskas A (2007) Comp B Engine 38:360
22. Peresin MS, Habibi Y, Zoppe JO, Pawlak JJ, Rojas OJ (2010) Biomacromolecules 11:674
23. Cho MJ, Park BD (2011) J Ind Eng Chem 17:36–40
24. Uddin AJ, Araki J, Gotoh Y (2011) Biomacromolecules 12:617
25. Uddin AJ, Araki J, Gotoh Y (2011) Comp A Appl Sci Manuf 42:741
26. Uddin AJ, Araki J, Gotoh Y (2011) Polym Int 60:1230
27. Herrick FW, Casebier RL, Hamilton JK, Sandberg KR (1983) J Appl Polym Sci Appl Polym Symp 37:797
28. Turbak AF, Snyder FW, Sandberg KR (1983) J Appl Polym Sci Appl Polym Symp 37:815
29. Taniguchi T, Okamura K (1998) Polym Int 47:291
30. Wang S, Cheng Q (2009) J Appl Poly Sci 113:1270
31. Cheng Q, Wang S, Han Q (2010) J Appl Poly Sci 115:2756
32. Li W, Yue J, Liu S (2012) Ultrason Sonochem 19:479
33. Abramov O (1998) High-intensity ultrasonic theory and industrial applications. Gordon and Breach Science Publishers, Amsterdam
34. Bhatnagar A, Sain M (2005) J Reinf Plast Comp 24:1259
35. Bondeson D, Mathew A, Oksman K (2006) Cellulose 13:171
36. Wang B, Sain M (2007) Compos Sci Technol 67:2521
37. Yano H, Nakahara S (2004) J Mater Sci 39:1635
38. Cheng Q, Wang S, Rials T, Lee SH (2007) Cellulose 14:593
39. Cheng Q, Wang J, McNeel J, Jacobson P (2010) BioResources 5:1945
40. Gindl W, Keckes J (2005) Polymer 46:10221
41. Wiley JH, Atalla RH (1987) Carbohydr Res 160:113
42. Matsuo M (1990) Macromolecules 23:13
43. Tan EPS, Lim CT (2004) Appl Phys Lett 84:1603
44. Wan WK, Hutter JL, Millon L, Guhados G (2006) Bacterial cellulose and its nanocomposites for biomedical applications. In: Oksman K, Sain M (eds) Cellulose nanocomposites: processing, characterization, and properties. American Chemical Society, Washington, DC, p 221
45. Cheng Q, Wang S (2008) Comp A Appl Sci Manuf 39:1838
46. Favier V, Canova GR, Cavaillé JY, Chanzy H, Dufresne A, Gauthier C (1995) Polym Adv Technol 6:351
47. Dufresne A, Cavaille J, Helbert W (1997) Polym Comp 18:198
48. Iwamoto S, Nakagaito AN, Yano H, Nogi M (2005) Appl Phys A Mater Sci Process 81:1109
49. Nakagaito AN, Yano H (2005) Appl Phys A Mater Sci Process 80:155
50. Cheng Q, Wang S, Zhou D, Zhang Y, Rials T (2007) J Nanjing Forestry Univ 31:21
51. Zimmermann T, Pohler E, Schwaller P (2005) Adv Eng Mater 7:1156
52. Peresin MS, Habibi Y, Vesterinen AH, Rojas OJ, Pawlak JJ, Seppala JV (2010) Biomacromolecules 11:2471
53. Srithep Y, Turng LS, Sabo R, Clemons C (2012) Cellulose 19:1209
54. Orts WJ, Shey J, Imam SH, Glenn GM, Guttman ME, Revo JF (2005) J Polym Environ 13:301
55. Ljungberg N, Cavaille JY, Heux L (2006) Polymer 47:6285
56. Samir M, Alloin F, Dufresne A (2006) Compos Interfac 13:545
57. Kadokawa J, Takegawa A, Mine S, Prasad K (2011) Carbohydr Polym 84:1408
58. ASTM (2002) American Society for Testing and Materials, West Conshohocken. D 1708–2002a
59. Lee SY, Mohan DJ, Kang IA, Doh DH, Lee S, Han SO (2009) Fibers Polym 10:77
60. Frone AN, Panaitescu DM, Donescu D, Spataru CI, Radovici D, Trusca R (2011) BioResources 6:487
61. Yang H, Yan R, Chen H, Lee DH, Zheng C (2007) Fuel 86:1781
62. Holland BJ, Hay JN (2011) Polymer 42:6775

Cellulose Nanofiber-Protein Composite

23

Ruilai Liu, Chunyi Tang, and Haiqing Liu

Contents

Abstract

Cellulose and protein are the two most abundant naturally occurring polymers. Both polymers are renewable and biodegradable. The exploration of various applications of these two polymers is vital to sustaining development of our society as far as the environment and resource are concerned. Due to the strong mechanical strength and modulus and high aspect ratio, nanocellulose in the form of a nanowhisker and nanofiber has been extensively studied as reinforcing fibers. The nanocellulose/protein composite has been attracted much research

R. Liu • H. Liu (✉)
Fujian Provincial Key Laboratory of Polymer Materials, College of Materials Science and Technology, Fujian Normal University, Fuzhou, China
e-mail: haiqing.liu@gmail.com

C. Tang
College of Biological and Chemical Engineering, Guangxi University of Science and Technology, Liuzhou, China

J.K. Pandey et al. (eds.), *Handbook of Polymer Nanocomposites. Processing, Performance and Application – Volume C: Polymer Nanocomposites of Cellulose Nanoparticles*,
DOI 10.1007/978-3-642-45232-1_63,

attention to make fully biodegradable materials. The good chemical structure compatibility of the cellulose fiber and the protein matrix imparts strong interfacial interaction and hence resulting in great improvement of mechanical properties. Another unique property of the protein composite films reinforced with nanocellulose of <500 nm in diameter is the high optical transparency even though the fiber content is as much as 30 wt%. Because of the superhigh length-to-diameter ratio of nanocellulose, cellulose nanofibers or whiskers and protein matrix readily form an interpenetrating network (IPN) alike composite material. Such a structure enhances the thermal stability and barrier properties and reduces the moisture absorption and water swelling ratio of the nanocellulose/protein composite materials.

Keywords
Cellulose • Nanostructure • Protein • Composite

1 Introduction

Fiber-reinforced composite materials display excellent mechanical properties and low density giving them high specific strength and stiffness, so they have been applied in many areas such as aircraft and automotive parts, constructing materials, medical applications, sporting goods, etc. The two components, i.e., fiber and matrix, of most commercialized composite materials are from petroleum chemicals. With concerns of diminishing fossil fuels, and of the pollutions (e.g., poor degradability, emission of toxic gases) upon dumping in landfills or incineration for energy recycling, these composites are not environmentally benign materials. Consequently, there are growing research interest and practical demands in developing bio-composites or "green" composites using fully sustainable, biodegradable, and yearly renewable fibers and resins [1–4]. In terms of the cost and abundance, cellulose fibers and plant proteins are the most promising fiber and matrix candidates for the fully green composite materials, among the many biodegradable fibers and resins [5–7].

Due to the abundance, renewability, easy availability, low cost, biodegradability, biocompatibility, and high mechanical strength, cellulose fibers have long been applied as reinforcing fibers for the manufacturing of composites [8, 9]. Particularly, cellulose nanofibers with one nanoscale dimension have aroused many research interests as reinforcing fillers because their mechanical properties are superior to microfibers [10], for instance, the elastic modulus and mechanical strength of cellulose nanowhiskers are in the order of 100–150 and 10 GPa [11–13], respectively; additionally, nanocelluloses have larger surface area and consequently more surface atoms than their microscale counterparts because of their nanosize, leading to better contact with matrix at the interfaces. Moreover, a well dispersion of nanocellulose in the matrix would effectively induce a percolating nanocellulose network in the composite and therefore efficiently improving the properties of a nanocomposite, such as their superior thermal, mechanical, and barrier properties

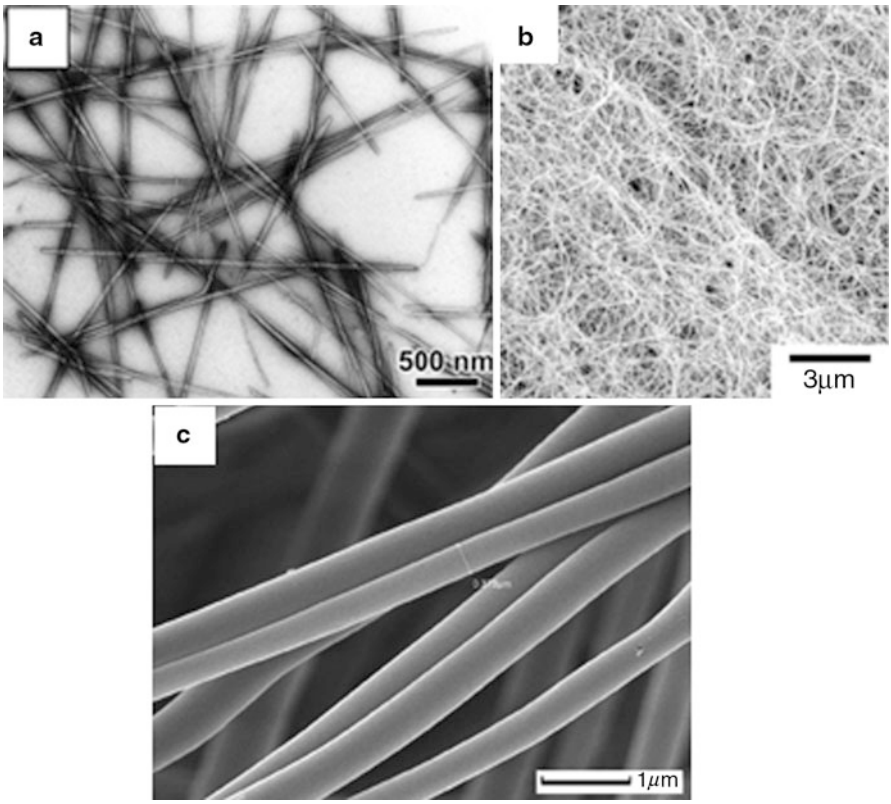

Fig. 23.1 Nanocelluloses in the form of (**a**) cellulose nanowhisker, (**b**) bacterial cellulose, (**c**) electrospun cellulose nanofiber (Reproduced from Ref. [18, 27, 34])

even at a very low reinforcement content (<5 wt%), added to a better recyclability and low weight [14, 15].

Nanocelluloses in forms of cellulose nanowhisker (CNW) and cellulose nanofibers including bacterial cellulose nanofibers (BCNF) and electrospun cellulose nanofibers (eCNFs) have been frequently studied as reinforcing fibers in composites [12, 16, 17]. Figure 23.1 shows the morphology of these nanostructured celluloses. The CNWs are prepared by acid hydrolysis of raw celluloses [18]. The length and width are around respective 100–2,000 nm and 3–60 nm for most CNWs: thus, their aspect ratios (L/d, L: length and d: diameter) are in the range of 1–100 [18]. BCNF is produced by bacteria, like *Acetobacter xylinum*. The length of BCNF is up to several tens micrometers, which is much longer than CNWs, and their diameter and crystallinity are 20–50 nm and 60–75 % [16], respectively. Young's modulus (E) of BCNF is 116 GPa [19]. The newly developed eCNFs from electrospinning are tens to hundreds nanometers in diameter and about several centimeters in length [20]. Thus, their L/d values are >10,000, orders of magnitude more than that of CNWs. The top-down electrospinning method can easily fabricate

plenty of nanofibers to meet the needs for practical applications [21]. Due to the characteristic ultrafine fiber diameter, ultrahigh specific surface areas, and aspect ratios, eCNFs have also found application in the composite materials [17, 22, 23].

Soy protein is an agricultural coproduct with relatively low cost, abundant availability, and renewability [24]. It contains 18 different amino acids. Among them, glutamic acid and aspartic acid contain carboxyl groups; lysine and arginine contain amino groups; and serine, threonine, and tyrosine contain polar hydroxyl groups. The amino acids are connected through peptide (amide) bonds to form polypeptide chains [1]. These functional groups on the chains cannot only be utilized to chemically modify soy proteins but interact with other polymers through hydrogen bonding and therefore providing convenient ways to improve their properties. Soy protein is easily processed both in solution and in melt state. Away from its isoelectric point pH 4.5–5, in either direction, the soy protein molecules are water soluble [1]. In the presence of plasticizers like water and glycerol, it can be hot pressed into plastic sheets [24, 25]. As a result, soy protein has been extensively studied as a fully sustainable and biodegradable resin. However, broad applications of the neat soy protein film are restricted due to disadvantages such as brittleness, poor gas and moisture barrier, and bad water resistance. The addition of plasticizers is able to make flexible soy protein film, while an impregnation of nanofillers such as chitin whisker and nanocellulose can effectively reinforce and toughen soy protein plastics. Additionally, the water resistance of soy protein is improved as well [26].

From the viewpoints of strong mechanical properties of fibers, the processability of matrix, and the structural compatibility between fiber and matrix, nanocellulose/protein is a good pair for the fabrication of green composites. Such composites may display not only improved mechanical properties (strength, stiffness, and toughness), but also enhanced thermal stability, water resistivity, and moisture barrier ability [15, 24]. Specifically, the nanocellulose/soy protein composites can maintain the optical transparence of soy protein film even though the nanocellulose content is as high as 50 wt% [27]. This property is the most significant difference from the microfiber/soy protein composite.

In this chapter the preparation methods including solution casting, hot pressing, and electrospinning of nanocellulose/protein composites are briefly described. Their mechanical, thermal, optical, and water absorption properties are discussed in relation to the fiber morphology and size, dispersion in the matrix, and fiber/matrix interfacial structure. Due to the excellent properties of the nanocellulose/protein composites, they can be promisingly utilized in areas of packaging materials, structural materials, and biomaterials.

2 Preparation Method of Nanocellulose/Soy Protein Composites

2.1 Solvent-Casting Processing

Protein shows good solubility in weak basic aq. solutions (pH $\geq$ 8). Nanocelluloses were dispersed into film-forming protein solutions, followed by casting and drying.

Homogeneous dispersion of nanofibers in solutions should be reached in order to efficiently improve the properties of the resulting nanocomposite. Pereda et al. [15] fabricated CNW/sodium caseinate (SC) composite films by the solvent-casting method. The CNWs were dispersed in water by ultrasonication then mixed with the SC aq. solution. They were poured into Teflon Petri dishes and dried at 35 °C in a convection oven to evaporate excess water; the composite films were then obtained. In the case of nanofibrous mats used as reinforcing fibers, the mats were placed flatly in a quadrate poly(tetrafluoroethylene) (PTFE) trough, into which soy protein isolate (SPI)/H_2O solutions were then added. The mixture was air-dried at ambient conditions to remove most of the water and then dried at 50 °C for 36 h [27]. For the solvent-casting method, about 95 wt% of the mixture solution is water. Therefore, a large amount of energy is consumed in the drying process. Additionally, the sedimentation of nanocellulose in the film-forming solution in the period of drying may occur, resulting in a nonuniform distribution of nanocellulose in the films.

2.2 Hot-Pressing Method

Soy protein displays thermoplasticity, so it can be conveniently processed by the hot-pressing method, through which Wang et al. [24] fabricated CNW/soy protein isolate (SPI) composite films. The CNWs (size: 1.2 mm × 90 nm, aspect ratio *l*/*d*: 13.3) and SPI ($M_w = 2.05 \times 10^5$) were dispersed separately in distilled water and stirred for 30 min at room temperature. They were then mixed and stirred for 2 h to obtain a homogeneous dispersion. The resulting dispersion was freeze-dried, and 30 wt% of glycerol was added. The mixture was then placed in a mold, covered with two polished stainless steel plates, as shown in the setup (Fig. 23.2). The temperature of the mold was controlled to 140 °C, and the pressure was quickly increased to 20 MPa. The sample was kept at 140 °C for 10 min and then

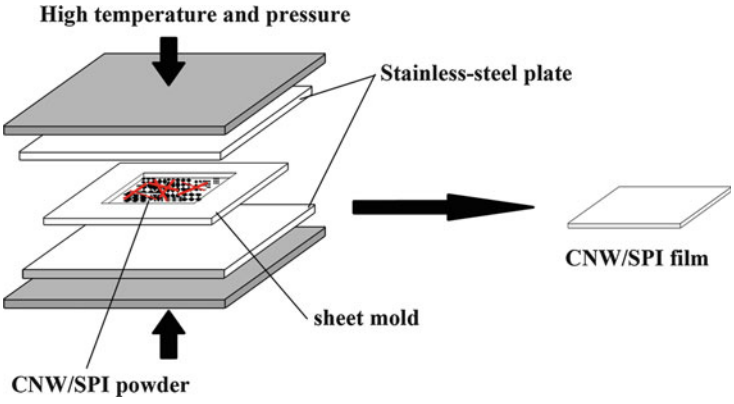

Fig. 23.2 Nanocellulose/soy protein composite film prepared through hot pressing

wind-cooled to room temperature. In a similar procedure, soy protein concentrate (SPC) films reinforced with micro-/nano-fibrillated celluloses (MFC) were reported by Huang and coauthors [28, 29]. They prepared SPC/H_2O and MFC/H_2O suspensions separately, then mixed them under strong stirring to reach even dispersion. The mixture solution was adjusted to pH 8.0 and stirred in air at 75 °C for precuring. The precured resin was then poured in a PTFE-coated mold and dried in an airflowing oven at 35 °C to get specimens in a sheet form, followed by hot pressing at 120 °C and 8 MPa to obtain MFC/SPC composite film. Compared to the time-consuming solvent-casting method, the hot-pressing method is quick.

2.3 Electrospinning Method

In the method of electrospinning, the charged fluid at the tip of the nozzle forms a Taylor cone under electrostatic force and surface tension. A polymer jet is ejected from the cone when the surface tension is overcome by the electrostatic force. The jet is solidified with solvent evaporation and thinned under whipping instability. Fibers with diameter down to tens of nanometers are fabricated. Moreover, the top-down electrospinning method can easily fabricate massive nanofibers to meet the needs for practical applications. *Bombyx mori* silk fibroin (SF) nanofiber mats reinforced with CNWs were fabricated through electrospinning [30] (Fig. 23.3). The electrospinning solution was prepared by dissolving SF in 98 % formic acid, followed by adding the concentrated CNW aq. suspension. Under the stretching of electrostatic force, CNWs in the composite nanofibers predominantly align in the longitudinal fiber axis.

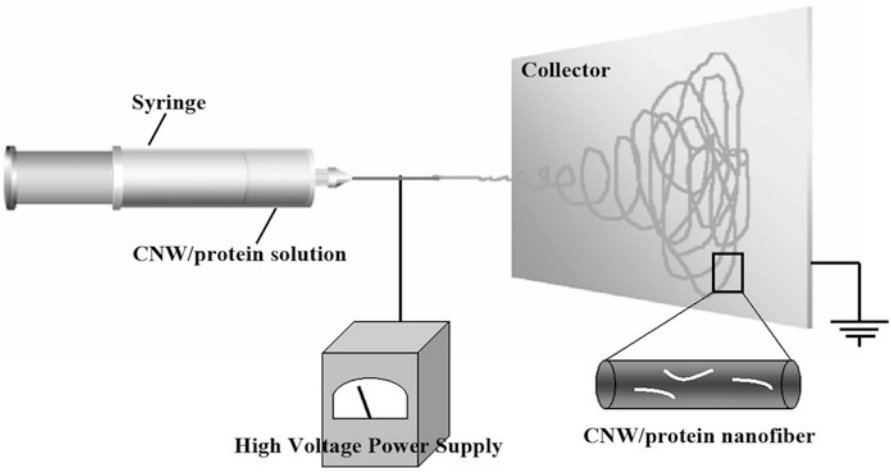

Fig. 23.3 Electrospinning setup for the preparation of CNW/silk fibroin composite nanofiber

3 Properties of Nanocellulose/Protein Nanocomposite Film

3.1 Mechanical Properties

The primary objective of embedding of nanocellulose in protein films or fibers is to improve their mechanical properties. The high specific surface area, aspect ratio, high tensile strength, and Young's modulus of nanocellulose are dedicated to provide effective reinforcing abilities [12, 18]. In the case of CNW/SC composite films, an addition of only 3 wt% CNWs gave more than a twofold increase in the tensile modulus of the composites, due to an even dispersion of CNW in the SC matrix and the strong interfacial interaction between CNW and caseinate. Nevertheless, the strain at break (ε_b) decreased with increasing CNW content in the composites [15]. For CNW/SPI composite films prepared from hot pressing, the tensile strength at break (σ_b) and E increased respectively from 5.8 to 8.2 MPa and from 44.7 to 90.6 MPa at 43 % relative humidity (RH) when the CNW content increased from 0 to 20 wt%, indicating that the incorporation of CNWs into the SPI matrix improved the mechanical properties of the SPI, as a result of high mechanical strength and modulus of the CNWs and the strong interfacial interactions caused by hydrogen bonds between the CNWs and the SPI [24]. As for the MFC-reinforced SPC specimens [29], the E of the composite film increased significantly from 589 MPa for SPC containing 15 parts of glycerol to 2,346 MPa for SPC containing 15 parts of glycerol and 40 parts of MFC. This is almost a fourfold increase. A same trend was observed for their fracture stress, which increased from 21.7 to 71.2 MPa, which is about 3.3 times higher than the control SPC film. Additionally, their toughness increased from 2.7 to 5.3 MPa, an increase of about 100 %. Such an effective reinforcement is related to the good interfacial adhesion between MFC and SPC. The rich hydroxyl groups on the MFC provide the condition for a good interfacial adhesion between MFC and soy protein molecules through hydrogen bonding. Though the interfacial strength of nanocellulose/soy protein has not been known yet, Jansson et al. [31] reported that the interfacial shear strength between soy protein and ramie cellulose fiber (microfiber) was as high as 29.8 MPa. In addition, the fine diameter and rough surface of the MFC fibrils provided significantly large areas for interfacial interaction with the SPC resin. Therefore, the MFC fibrils can effectively increase the load transfer efficiency in the composites, resulting in good mechanical properties of the MFC/SPC composite films [29].

The reinforcing efficiency of CNW on the mechanical strength and modulus of the electrospun silk protein nanofiber was obvious as well [30]. Though the mechanical property of an individual CNW/SF nanofiber was not measured to directly show the enhancement, the σ_b and E of the CNW/SF composite nanofibers increased with the CNW content. The σ_b and E of the neat SF nanofibrous mat were 12.5 and 309 MPa, respectively. The σ_b and E of the CNW/SF composite nanofibrous mats with 4 wt% CNWs were 38.5 and 1,237 MPa, which were about three and four times higher than that of the neat SF nanofibrous mat, respectively, while its ε_b significantly dropped to 4.8 % (Fig. 23.4a–b).

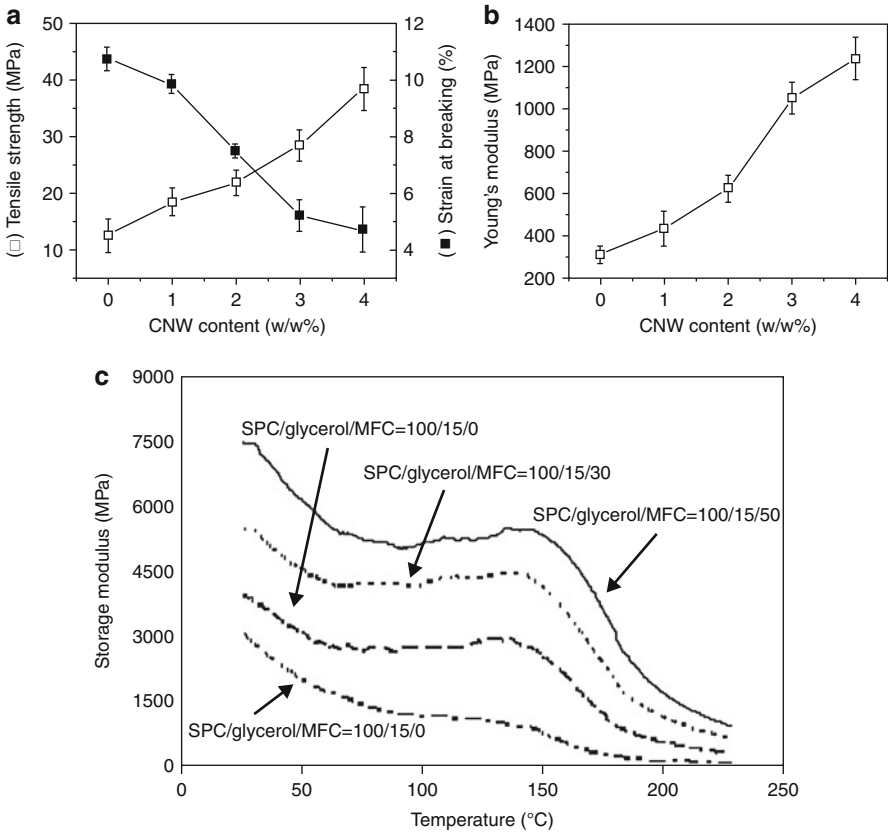

Fig. 23.4 (**a**) Tensile strength and strain at breaking and (**b**) Young's modulus of electrospun CNW/silk fibroin nanofiber mats as a function of CNW content; (**c**) storage moduli of SPC resins reinforced with MFC, glycerol as plasticizer (Reproduced from Ref. [29, 30])

The cellulose have abundant hydroxyl groups on its molecular chains, while the SF molecules are rich in amine, amide, carboxyl, and hydroxyl groups, so CNWs and SF matrix can form hydrogen bonds at the interfaces in the composite nanofibers. Therefore, the authors thought that the even distribution of CNWs in the SF matrix and interfacial adhesion between CNWs and SF play important roles in improving the mechanical properties of CNW/SF composite nanofibers.

For the SPI composites reinforced with eCNF mats, the σ_b and E increased substantially with eCNF content in the composite films [27]. It was 13 times the σ_b of the neat SPI film for the composite film with eCNF content of 22 %. And the E of eCNF/SPI with 22 wt% eCNF was 200 MPa, a substantial increment from 30 MPa of the neat SPI film. During stretching, the loading on the SPI matrix transfers to the reinforced fiber. Moreover, composite films cannot rupture easily because the reinforcement cellulose nanofibers act as bridges inhibiting the propagation of crack. Thus, eCNF can reinforce the mechanical strength of composite materials.

With more reinforcing nanofibers impregnated in the SPI resin, higher volume of nanofibers per unit cross-section area of the composite contributes to the enhancement of stress and modulus. The increasing of modulus follows the rule of mixtures as in a composite. In a uniform strain situation, the fiber and matrix combine to give the overall modulus according to E(comp) = E(fiber) * V + E(matrix) * (1 − V). As V goes up, the stiffer phase (the fiber) dominates the mechanical properties. With the embedding of as small as 7.5 % eCNF in the SPI matrix plasticized with glycerol, the failure strain of composite film decreased significantly from 275 % to 25 %. In the eCNF/SPI composite films, the rigid reinforcing cellulose nanofibers restrain the elongation of composite film. As a result, the strain of eCNF/SPI composite film is relatively low.

3.2 Thermal Properties

The thermal stability of nanocellulose/protein composites is generally improved as compared to the neat proteins, partly because of (i) the more thermally stable nature of cellulose than that of proteins, (ii) percolating nanocellulose network in the protein matrix, and (iii) strong interfacial interaction. As demonstrated by Huang and coauthors [29], the MFC/SPC composites showed an improved thermal property compared with the neat SPC resin. SPC with 15 parts of glycerol has a decomposition onset temperature at about 236 °C, which increased to about 257 °C after the addition of 40 parts of MFC.

However, the effect of nanocellulose on the glass transition temperature (T_g) of protein matrix is controversial for various composite systems. In the case of CNW/SC composites [15], a T_g increase was found as compared to the neat SC. Due to the hydrogen-bonding interaction at the interfaces, the CNWs could restrict the mobility of SC chains in the vicinity of the interfacial areas, resulting in a red shift of T_g. However, the authors pointed out that not only the moisture content of the films is decreasing in the testing process but also that cross-linkage in SC films can be induced simply by heating. These two conditions would also contribute to the increase of the Tg. The Tg of MFC/SPC composites increased as well [29]. As measured by the dynamical mechanical analysis (DMA), the T_g increased from about 165 °C for SPC containing 1.5 parts of glycerol to 180 °C for SPC containing 1.5 parts of glycerol and 40 parts of MFC. These findings are similar to the T_g increasing effect of nanocellulose on the CNW/poly(L-lactic acid) nanocomposite [32].

However, in other studies the effect of nanocellulose reinforcement on T_g was the opposite. For the CNW/SPI composites, the T_g of SPI decreased from −44.3 °C to −51.5 °C as the CNW content increased from 0 to 15 wt% [24]. Due to the ultrahigh specific surface areas and nanometer size of CNW, a strong hydrogen-bonding interaction between the CNW and SPI at the interfaces is generated, leading to an improvement of the SPI molecular chain segments mobility in the matrix. As a result, T_g decreased with the addition of CNW in the SPI. Some other polymer matrices such as CNW/starch composites showed this similar phenomenon [33]. The incorporation of nanocellulose in protein matrices has been found to significantly increase the

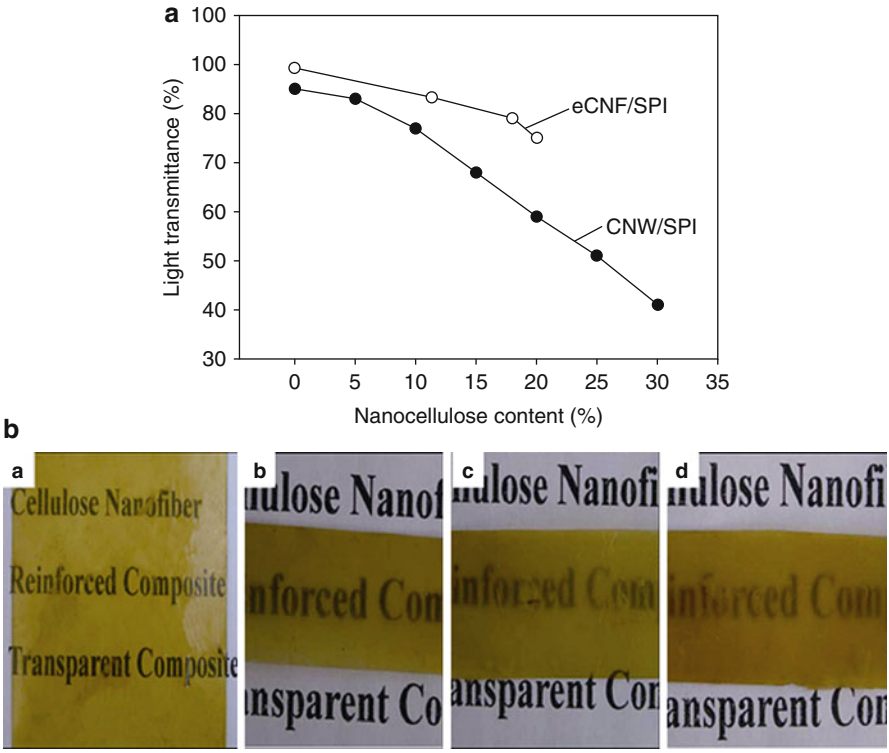

Fig. 23.5 (**A**) Light transmittance of CNW/SPI composite films at 800 nm and eCNF/SPI composite films at 700 nm. (**B**) Appearance of eCNF/SPI composite films with eCNF content of (*a*) 0 %, (*b*) 7.7 %, (*c*) 12.6 %, (*d*) 30.5 % (Reproduced from Ref. [24, 27, 35])

storage modulus (*E'*) of proteins, especially when the working temperature is over T_g, as demonstrated by the MFC/SPC composites [29] (Fig. 23.4c).

3.3 Light Transmittance of Nanocellulose/Soy Protein Composite Films

The incorporation of nanocellulose in protein matrices has been reported to cause transmitted light loss mainly due to the light refraction/reflection at the nanocellulose/protein interfaces. The CNW/SC composite films became less transparent as the nanocellulose content increased [15]. With an increase of the CNW content from 0 to 20 wt%, the light transmittance at 800 nm for the CNW/SPI composite films decreased from 85.1 % to 58.8 % and further dropped to 40.7 % when the CNW content increased to 30 wt% (Fig. 23.5A). The obvious reduction in the light transmittance was regarded as a resultant of phase separation causing severe light scattering at the interfaces [24].

Chen et al. reported an optically transparent SPI composite film reinforced with high content of eCNF [27]. The light transmittance of pure SPI film at 700 nm was 89 %. The eCNF film is white in color with light transmittance of ca 7.5 % at 700 nm. The impregnation of 20 wt% eCNF in the composite film reduced the transmitted light to 75 % at 700 nm, indicating that the embedding of as high as 20 wt% eCNF in the composite film did not result in significant loss of transmitted light (Fig. 23.5A). In view of the possible more light scattering on the much larger eCNF (200–940 nm) than that on the CNW (90 nm), the surprisingly more transmitted light of eCNF/SPI than that of CNW/SPI with 20 wt% nanocellulose suggests a more even distribution of eCNF in the SPI matrix. A digital photo of SPI and eCNF/SPI composite films placed on letters was shown in Fig. 23.5B. The neat SPI film is highly transparent. With impregnation of eCNF in SPI resin matrix, letters under the composite films can still be seen clearly, though the clarity decreases with the increasing of eCNF content. Because of the refractive index (RI) difference between the reinforcing eCNF and the SPI matrix, severe light refraction and reflection at the large amount of fiber/SPI interfaces are supposed to occur. Thus the composite films with 20 wt% fiber content are expected to show poor light transmittance. However, the eCNF/SPI composite films showed good light transmittance. This should be attributable to (i) the ultrafine diameter of the fibers. The light scattering is small when it strikes fibers with a diameter smaller than the visible light wavelength [16, 34–37]; (ii) the good eCNF/SPI interfacial structure reduces the light loss caused by the light scattering and reflectance at the interfaces. It should be pointed out that the eCNF/SPI composite film with 20 wt% eCNF is not optically transparent. In order to improve the light transmittance of eCNF-reinforced composite materials, the diameter of nanofiber should be much smaller than 400 nm. In a similar work, it is very impressive that the poly(vinyl alcohol) (PVA) film reinforced with 40 wt% eCNF fibers of 250 nm in diameter was still optically transparent with 85–88 % light transmittance. Additionally, the light transmittance of eCNF/PVA was insensitive to temperature [34]. More astonishingly, it was reported that BCNF-reinforced epoxy composite film is optically transparent even fiber content is as high as 70 % in the composite [16], when the diameter of BCNF is less than 50 nm.

3.4 Water Resistivity of Nanocellulose/Protein Composite Films

SPI is a hygroscopic polymer due to the presence of amine, amide, carboxyl, and hydroxyl groups. Thus, it is readily to adsorb moisture and swell in aq. solution. Obviously, this characteristic would certainly hinder its application in a wet state. The neat SPI sheet with 30 wt% glycerol absorbed nearly 40 wt% water. However, the water uptake of the CNW/SPI composites with 30 wt% CNW content decreased to 25 wt%, indicating an improvement in the water resistivity. Huang et al. [24] regarded that the strong interaction between the CNW and SPI leads to an enhancement of water resistance of the composite.

For the MFC/SPC composite films, the moisture content of the SPC resin (15 parts of glycerol and 40 parts of MFC) decreased to 13.1 % from 15.2 %

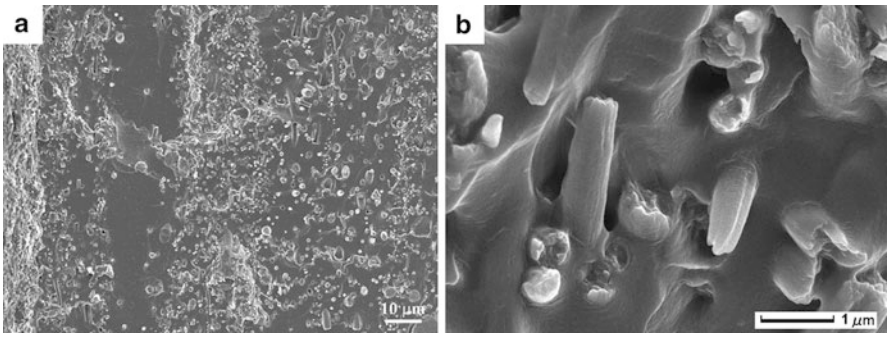

Fig. 23.6 SEM images of fractured eCNF/SPI composite films at different magnifications (Reproduced from Ref. [27])

moisture content of the neat SPC resin (15 parts of glycerol) [29]. The highly crystalline nature of the MFC cannot absorb significant amount of moisture in spite of its highly hydrophilic nature. Nevertheless, the decreased moisture content in the protein composite would contribute to the increased stiffness and decreased elongation at break since water is an effective plasticizer for soy protein.

The embedding of nanocellulose in polymer matrices is able to improve the moisture barrier of protein films. The presence of nanocellulose is thought to increase the tortuosity in the materials leading to slower diffusion processes and, hence, to lower permeability [15]. The poor permeability, high aspect ratio of nanocellulose, and its even dispersion in the matrix would enhance the barrier properties of the composite films. It was found that the addition of CNW to the neat SC films produced an initial increase in the barrier properties to water vapor, and then, the permeability decreased as CNW content increased.

By impregnation of eCNF in the SPI matrix, the swelling ability of SPI decreased steadily with eCNF content [27]. The swelling ratio of composite film reduced substantially from 106 % to 12.7 % as eCNF content increased from 0 % to 21.3 %. Besides the widely accepted conception of strong eCNF/SPI interfacial interaction, the IPN structure also contributes to the reduction of water swelling. As shown in the cross-section SEM images of CNM/SPI composite (Fig. 23.6a), a large number of eCNFs interpenetrate through the SPI matrix to form an IPN alike network. The swelling of SPI filling in the pores within the eCNF mat is restricted by the dimensionally stable eCNF network, resulting in low swelling ratio of CNM/SPI composite film.

3.5 Interfacial Structure and Its Effect on the Properties of Composite Films

The dispersion of nanocellulose in the soy protein matrix plays a critical role in the macro-properties like mechanical, thermal, and optical properties of the composites.

Due to the hydrophilic nature of cellulose and soy protein, a relatively even distribution of nanocellulose in soy protein matrix can be normally achieved without dependence on the preparation methods. For instance, Wang et al. [24] reported a homogeneous dispersion of CNW in the SPI composite prepared from hot pressing. For the protein composite nanofiber from electrospinning, the FE-SEM and TEM of fractured SF nanofiber mat reinforced with 4 wt% CNW showed that the CNW was evenly dispersed in the SF matrix and aligned along the fiber axis [30].

The SEM image of the cross-sectional surface of eCNF/SPI composite films displayed random distribution of eCNF in the SPI matrix. Some broken fiber ends protruded out the fractured surface, while a few fibers flatly layered on the surface. There were also some very shallow cylindrical cavities (Fig. 23.6b), which were generated from the pullout of eCNFs whose end is very near the fractured surface. No obvious delamination was observed at the interfaces of eCNF/SPI; adherence of SPI on the broken fibers was obvious. These results indicated that the reinforcing eCNF and SPI resin matrix has excellent interfacial interaction [38]. The energy consumed by fibril pulling-out and breaking contributes to the increased toughness of nanocellulose/protein nanocomposites.

Nanocellulose is rich of hydroxyl groups on the surface, while soy protein has plenty of amine, amide, carboxyl, and hydroxyl groups on the molecular chains. Therefore, the nanocellulose filler should have structure miscibility with soy protein matrix through hydrogen-bonding interaction. The strong interfacial adhesion was demonstrated by the soy protein remnant on the micro-ramie cellulose fiber [39]. This interaction force should become much stronger because of the very large specific surface areas of cellulose nanofibers making more hydroxyl groups available to form more hydrogen bonds.

4 Perspectives of Nanocellulose/Soy Protein Nanocomposite

The excellent mechanical properties and low density of nanocellulose/protein composites impart them high specific strength and stiffness. Such weight savings are highly desirable for applications in aerospace and transportation to reduce weight and associated fuel consumption [1]. The environmental benign SPC-based “advanced green composites” should find applications from sports gear to auto parts and from electronics to primary structural parts for housing. The biocompatibility of CNW/SPC membranes was confirmed by cell culture and in vivo implantation experiments. The results revealed that human umbilical vein endothelial cells (ECV304) grew well on this biomaterial. In comparison with the pure cellulose membrane, because of the incorporation of SPI and the resultant alteration of microstructure, the SPI-modified membranes showed an improved in vivo biocompatibility and biodegradability in the implantation experiments. These cellulose/SPI membranes warrant further explorations in biomedical fields [40].

However, much research work should be done before they are capable of replacing some of the traditional microfiber-reinforced composite materials. Due to the ultrashort length of CNW and BCNF, they are difficult to be assembled or aligned in one direction, leading to a random distribution in the protein matrix. Thus, they can hardly be engineered to obtain required properties in different directions by appropriate fiber placing in different layers of the laminated structure like using microfibers [1]. Additionally, though individual nanocellulose shows high mechanical properties, its reinforcing efficiency is far below expectation mainly due to the weak percolating nanocellulose networks which is formed by the physical contact among the short nanocelluloses. As a result, their applications are restricted to only noncritical and non-load-bearing parts, such as packaging, casings, etc. They are inapplicable for the load-bearing structural applications where high strength and stiffness are required [1, 9]. In order to substantially improve the mechanical strength and to reduce the water uptake of protein composites, the soy protein matrix should be chemically and/or physically modified, and a novel plasticizer instead of glycerol for the soy protein composite has to be developed.

Acknowledgment This work is supported by the National Natural Science Foundation of China (No. 50973019), the National Basic Research Program of China (2010CB732203), the Natural Science Foundation of Fujian Province (2010 J06017), and the Research Fund for the Doctoral Program of Higher Education of China (20123503110003).

References

1. Netravali AN, Huang X, Mizuta K (2007) Advanced 'green' composites. Adv Compos Mater 16:269
2. John MJ, Thomas S (2008) Biofibres and biocomposites. Carbohydr Polym 71:343
3. Satyanarayana KG, Arizaga GGC, Wypych F (2009) Biodegradable composites based on lignocellulosic fibers-An overview. Prog Polym Sci 34:982
4. Yu L, Dean K, Li L (2006) Polymer blends and composites from renewable resources. Prog Polym Sci 31:576
5. Siro I, Plackett D (2010) Microfibrillated cellulose and new nanocomposite materials: a review. Cellulose 17:459
6. Song F, Tang D-L, Wang X-L, Wang Y-Z (2011) Biodegradable Soy Protein Isolate-Based Materials: A Review. Biomacromolecules 12:3369
7. Zhang H, Mittal G (2010) Biodegradable Protein-based Films from Plant Resources: A Review. Environ Prog Sustain Energy 29:203
8. Bledzki AK, Gassan J (1999) Composites reinforced with cellulose based fibres. Prog Polym Sci 24:221
9. Mohanty AK, Misra M, Hinrichsen G (2000) Biofibres, biodegradable polymers and biocomposites: An overview. Macromol Mater Eng 276:1
10. Eichhorn SJ, Dufresne A, Aranguren M, Marcovich NE et al (2010) Review: current international research into cellulose nanofibres and nanocomposites. J Mater Sci 45:1
11. Sakurada I, Nukushima Y (1962) Experimental determination of the elastic modulus of a crystalline regions in oriented polymers. J Polym Sci 57:651

12. Azizi Samir MAS, Alloin F, Dufresne A (2005) Review of recent research into cellulosic whiskers, their properties and their application in nanocomposite field. Biomacromolecules 6:612
13. Sturcova A, Davies JR, Eichhorn SJ (2005) Elastic Modulus and Stress-Transfer Properties of Tunicate Cellulose Whiskers. Biomacromolecules 6:1055
14. Oksman K, Mathew AP, Bondeson D, Kvien I (2006) Manufacturing process of cellulose whiskers/polylactic acid nanocomposites. Compos Sci Technol 66:2776
15. Pereda M, Arnica G, Racz I, Marcovich NE (2011) Structure and properties of nanocomposite films based on sodium caseinate and nanocellulose fibers. J Food Eng 103:76
16. Yano H, Sugiyama J, Nakagaito AN, Nogi M, Matsumura K, Hakita M, Handa K (2005) Optically transparent composites reinforced with networks of bacterial nanofibers. Adv Mater 17:153
17. Liao H, Wu Y, Wu M, Zhan X, Liu H (2012) Aligned electrospun cellulose fibers reinforced epoxy resin composite films with high visible light transmittance. Cellulose 19:111
18. Habibi Y, Lucia LA, Rojas OJ (2010) Cellulose Nanocrystals: Chemistry, Self-Assembly, and Applications. Chem Rev 110:3479
19. Hsieh YC, Yano H, Nogi M, Eichhorn SJ (2008) An estimation of the Young's modulus of bacterial cellulose filaments. Cellulose 15:507
20. Liu HQ, Hsieh YL (2002) Ultrafine fibrous cellulose membranes from electrospinning of cellulose acetate. J Polym Sci B Polym Phys 40:2119
21. Greiner A, Wendorff JH (2007) Electrospinning: A fascinating method for the preparation of ultrathin fibers. Angew Chem Int Ed 46:5670
22. Tang C, Wu M, Wu Y, Liu H (2011) Effects of fiber surface chemistry and size on the structure and properties of poly(vinyl alcohol) composite films reinforced with electrospun fibers. Compos A 42:1100
23. Tang CY, Liu HQ (2008) Cellulose nanofiber reinforced poly(vinyl alcohol) composite film with high visible light transmittance. Compos A 39:1638
24. Wang YX, Cao XD, Zhang LN (2006) Effects of cellulose whiskers on properties of soy protein thermoplastics. Macromol Biosci 6:524
25. Reddy N, Yang YQ (2011) Completely biodegradable soyprotein-jute biocomposites developed using water without any chemicals as plasticizer. Ind Crop Prod 33:35
26. Lu Y, Weng L, Zhang L (2004) Morphology and properties of soy protein isolate thermoplastics reinforced with chitin whiskers. Biomacromolecules 5:1046
27. Chen G, Liu H (2008) Electrospun cellulose nanofiber reinforced soybean protein isolate composite film. J Appl Polym Sci 110:641
28. Huang XS, Netravali A (2009) Biodegradable green composites made using bamboo micro/nano-fibrils and chemically modified soy protein resin. Compos Sci Technol 69:1009
29. Huang XS, Netravali AN (2008) Environmentally friendly green materials from plant-based resources: Modification of soy protein using gellan and micro/nano-fibrillated cellulose. J Macromol Sci A Pure Appl Chem 45:899
30. Huang J, Liu L, Yao J (2011) Electrospinning of Bombyx mori Silk Fibroin Nanofiber Mats Reinforced by Cellulose Nanowhiskers. Fiber Polym 12:1002
31. Jansson PE, Lindberg B, Sandford PA (1983) Structural studies of gellan gum, an extracellular polysaccharide elaborated by Pseudomonas elodea. Carbohydr Res 124:135
32. Petersson L, Kvien I, Oksman K (2007) Structure and thermal properties of poly(lactic acid)/cellulose whiskers nanocomposite materials. Compos Sci Technol 67:2535
33. Mathew AP, Dufresne A (2002) Morphological investigation of nanocomposites from sorbitol plasticized starch and tunicin whiskers. Biomacromolecules 3:609
34. Ifuku S, Morooka S, Morimoto M, Saimoto H (2010) Acetylation of Chitin Nanofibers and their Transparent Nanocomposite Films. Biomacromolecules 11:1326
35. Chen GFS, Liu HQ (2009) Studies of Ultrafine Cellulose Fiber Reinforced Soy Protein Isolate Composite Film with High Light Transmittance. Chem J Chin Univ Chin 30:417

36. Liao H, Wu Y, Wu M, Liu H (2011) Effects of fiber surface chemistry and roughness on interfacial structures of electrospun fiber reinforced epoxy composite films. Polym Compos 32:837
37. Wu M, Wu Y, Liu Z, Liu H (2012) Optically transparent poly(methyl methacrylate) composite films reinforced with electrospun polyacrylonitrile nanofibers. J Compos Mater 46:2731
38. Tian M, Gao Y, Liu Y, Liao YL, Xu RW, Heidi NE, Fong H (2007) Bis-GMA/TEGDMA dental composites reinforced with electrospun nylon 6 nanocomposite nanofibers containing highly aligned fibrillar silicate single crystals. Polymer 48:2720
39. Lodha P, Netravali A (2002) Characterization of interfacial and mechanical properties of "green" composites with soy protein isolate and ramie fiber. J Mater Sci 37:3657
40. Luo L, Wang X, Zhang Y (2008) Physical properties and biocompatibility of cellulose/soy protein isolate membranes coagulated from acetic aqueous solution. J Biomater Sci Polym Ed 19:479

Changes in Wood Properties and Those in Structures of Cellulose Microfibrils in Wood Cell Walls After the Chemical Treatments

24

Yukiko Ishikura

Contents

Abstract

Wood is a natural porous material, obtained from trees, whose cell walls consist of cellulose micrifibrils, lignin and hemicelluloses. Cellulose microfibrils in wood cell walls, whose crystalline regions have high Young's modulus and strength in the direction parallel to the molecular chain axis, play an important rule in mechanical and physical properties of wood. Chemical treatments that cause the transformation of cellulose crystals have been used to improve the mechanical and physical properties of cellulose fibers for a long time. These treatments also cause the changes in cell wall structures of wood and alter the properties of wood.

Keywords

Wood • Chemical treatments • Cellulose microfibrils • Wood properties

Y. Ishikura
Local Independent Administrative Agency, Hokkaido Research Organization, Forest Research Department, Forest Products Research Institute, Asahikawa, Japan
e-mail: ishikura-yukiko@hro.or.jp

J.K. Pandey et al. (eds.), *Handbook of Polymer Nanocomposites. Processing, Performance and Application – Volume C: Polymer Nanocomposites of Cellulose Nanoparticles*,
DOI 10.1007/978-3-642-45232-1_67,

1 Introduction

Cellulose is a polymer which is a linear chain of $\beta(1 \rightarrow 4)$ D-linked glucose units and exists in the cell walls of higher plants. Wood is a renewable natural material, mainly used in buildings (construction), but also widely used as a cellulose resource, upon chemical treatment.

Chemical treatments that cause changes in the structure of cellulose have been used to improve the mechanical and physical properties of ramie, cotton linters, and other plant fibers for a long time, and several treatments are reported to cause the transformation of cellulose crystals. These chemical treatments also alter the properties of wood. However, the changes in cellulose structures in wood that contains matrix substances are reported to be different from those in cellulose fibers. In this chapter, a part of the studies on the changes in structures of cellulose and on the relationship between the changes in wood properties and those in cellulose structures in wood cell wall caused by chemical treatments are introduced.

2 Structure of Wood

Wood is a natural porous material made up of numerous cells that form tubelike structures. There are several types of cells in wood [1–3]. Softwood is mostly composed of tracheid cells and also contains parenchyma and some other types of cells [1, 2]. On the other hand, hardwood consists of fibers, vessels, parenchyma cells, and others [1, 2]. In hardwood, it is reported that the fibers have the function of mechanical support and the vessels have the function of fluid transport, whereas in softwood, the tracheid cells play both of these roles [1–3].

The cell walls of wood consist mainly of cellulose, lignin, and hemicelluloses. Cellulose microfibrils, bundles of cellulose molecular chains, have both crystalline and noncrystalline regions and play an important role as the framework of cell walls. The crystalline parts of cellulose microfibrils have high mechanical properties in the direction parallel to the chain axis [4–7].

In the wood cell walls, cellulose microfibrils are wound helically and embedded in matrix substances such as hemicelluloses and lignin (Fig. 24.1). Many researchers have studied the structures of wood cell walls. There are distinct cell wall layers: the primary wall and the secondary wall (which is composed of S_1, S_2,

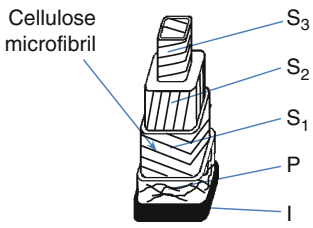

Fig. 24.1 Scheme of cell wall structure of wood *I*, intercellular layer; *P*, primary wall; S_1, outer layer of secondary wall; S_2, middle layer of secondary wall; S_3, inner layer of secondary wall

and S_3 layers), and each layer consists of a lamellae where microfibrils are oriented at different angles in tracheids of softwood and fibers of hardwood [1, 8]. In general, the S_2 layer is the thickest in the cell wall, and its microfibril angle (i.e., the angle between the microfibril and the cell axis) is small compared to that of other layers [8]. Wood generally has higher strength in the longitudinal direction than in transverse directions. It is reported that the longitudinal Young's modulus and strength of wood or pulp fibers decrease, and the strain at yield increases with increasing microfibril angle [9–11].

3 Chemical Treatment of Cellulose

Several agents swell cellulose crystals and cause changes in the structure of cellulose or in the transformation of cellulose crystals. The mechanical and physical properties of fibers such as ramie and cotton are changed by these chemical treatments, which have been used for a long time to improve the properties of cellulose fibers.

Alkali treatment, known as mercerization, is a treatment used to give cotton fabrics a shiny appearance. Natural cellulose, cellulose I, transforms into alkali cellulose when impregnated with alkali aqueous solution at a concentration over a certain threshold and into cellulose II after washing and drying [12–16]. Okano et al. [12, 14] studied the mercerization of ramie cellulose using X-ray diffraction and found that five unique alkali celluloses (Na-cellulose) could be generated, depending on the concentration of the alkali aqueous solution.

Characteristic changes in the morphology of fibers such as twisting, increase in width, and decrease in length are also observed upon impregnation with alkali aqueous solution [17–20]. Nishiyama et al. [20] investigated the morphological changes of ramie fibers treated with alkali solution and observed the twisting and changes in the cross-sectional shape of the fibers.

With alkali treatments that change the cellulose conformation from cellulose I to cellulose II, the cellulose crystallinity index values of fibers such as ramie and cotton linters are reported to decrease [13, 16, 21]. Fengel et al. [16] reported that the transition from cellulose I into II begins with a NaOH concentration of 11–12 % and is complete with a concentration of 16.5 % and that the degree of crystallinity of cellulose in cotton linter decreases at the concentration from 11 % to 13.5 % NaOH.

Cellulose I changes into cellulose III_I or into cellulose I_β after treatments with a series of amines or liquid NH_3. For example, when cotton, ramie, and valonia cellulose are saturated with ethylenediamine (EDA), their cellulose I changes into a cellulose I-EDA complex [22–26]. Moreover, cellulose crystals saturated with EDA can be transformed into cellulose III_I via methanol washing [23, 24, 27–31] and into cellulose I_β through heating or water washing [24].

The tensile properties of fibers are reported to be changed by the treatments for crystalline conversion. With either NaOH treatment or EDA treatment

to convert from cellulose I into II or III_I, the integral crystallinity index decreased, while the Young's modulus of the fiber decreased and the ultimate strain increased [15, 21, 31]. The elastic modulus of the cellulose crystalline regions parallel to the chain axis has been reported to be different for each cellulose polymorph [4–7]. For example, Nishino et al. [7] described elastic moduli of 138 GPa for cellulose I, 88 GPa for cellulose II, and 87 GPa for cellulose III_I, as measured by X-ray diffraction. Ishikawa et al. reported that the estimated Young's modulus values for the cellulose crystalline components were much higher than those for the amorphous components in non-treated, alkali-treated, ethylenediamine-treated, and liquid ammonia-treated ramie fibers [21, 31].

Chemical treatments that cause transformation of cellulose crystals are also used to improve the mechanical properties of fibers or nanofibers in cellulose fiber-based materials or cellulose nanofiber-based materials [32–36] with some treatments reported to increase the fracture strain and improve toughness.

4 Effects of Chemical Treatment on Wood

Chemical treatments that cause the transformation of cellulose crystals also alter the properties of wood. These treatments have been studied as methods to plasticize wood [37–41] to make bentwood.

Wood has been reported to become plastic under water-saturated conditions after being impregnated with aqueous alkali solution, followed by washing with water [40–42]. It was reported that the concentration range where the Young's modulus of wood (*Picea jezoensis* Carr.) in longitudinal direction (by measurement of tensional stress–strain curves at slow strain speed) decreased and the maximum strain increased corresponded to the range where longitudinal contraction of wood was observed [41]. Possible reasons for the changes in mechanical properties of water-saturated wood after treatment are reported to include the increase in microfibril angle [41] or the longitudinal contraction of microfibrils [40]. Nakano et al. [42] investigated the mechanism of longitudinal contraction of wood with the alkali treatment by measuring the stress relaxation and twist angle. Based on the Stöckmann's model [43, 44], he reasoned that contraction occurred by longitudinal contraction of microfibrils via an increase in the entropy-elastic force in less-ordered regions along the microfibril with the treatment.

The properties of wood in the oven-dried condition are also altered after impregnation with alkali aqueous solution followed by washing with distilled water. The Young's modulus values of oven-dried alkali-treated wood samples (*Picea jezoensis* Carr.) increased for NaOH concentrations in the range of 0–10 %, and the Young's moduli and lengths of wood samples decreased for NaOH concentrations in the range of 10–20 %, while the density of oven-dried wood tended to increase over the entire concentration range studied [45]. The decrease in the Young's modulus of wood samples with alkali treatment was supposed to be due to both an increase in microfibril angles with alkali treatment [46] and a decrease in the

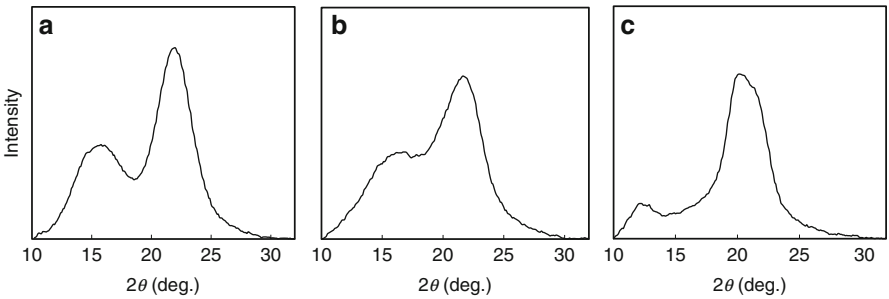

Fig. 24.2 X-ray diffraction patterns of NaOH-treated wood (**a**) NaOH 0 %, (**b**) NaOH 20 %, (**c**) NaOH 20 % after delignification treatment

proportion of crystalline components of cellulose, which have a higher Young's modulus [45]. This explanation was proposed because the concentration range where changes in the mechanical properties of wood occurred [45] agreed with the range in which cellulose structural transformations and decreases in crystallinity are reported to occur in cellulose fibers [13, 16].

Changes in tendencies of the increase in moisture content and of the changes in mechanical properties of wood over the same concentration range in increasing relative humidities can also be explained if the amount of amorphous region in the cellulose microfibrils in the wood cell wall increased with the treatment [45, 47].

X-ray diffraction studies conducted on oven-dried wood samples (*Picea jezoensis* Carr.) treated with various concentrations of aqueous NaOH solution and washed with distilled water followed by freeze-drying (to avoid the effect of collapse during the drying process) showed that the lattice transformation from cellulose I to cellulose II did not occur during alkali treatment and that the relative crystallinity index decreased at NaOH concentrations greater than 10 % [48].

It has been reported that the lattice transformation of cellulose I to cellulose II does not occur in wood cellulose or occurs with difficulty because of the existence of matrix substances such as lignin and hemicelluloses, which prevent swelling of the cellulose crystals by aqueous alkali solution [49–52]. Revol and Goring [49] indicated that only partial conversion occurred in spruce wood treated with 20 % aqueous NaOH solution, whereas complete conversion occurred under the same conditions in a low yield kraft pulp. Shiraishi et al. [50] reported that the ratio of lattice conversion to cellulose II increased with the degree of delignification. Figure 24.2 shows the X-ray diffraction patterns of wood treated with 0 % and 20 % NaOH aqueous solutions and with 20 % NaOH aqueous solution after delignification. After the delignification treatment, transformation into cellulose II was observed as reported by Shiraishi et al. [50]. One can assume that the parallel chains in cellulose I transform into antiparallel chains in cellulose II during the treatment [14]; this transformation has been explained by intermingling of cellulose chains from neighboring microfibrils of opposite polarity [14, 53]. In wood, however, cellulose microfibrils exist in cell walls embedded in matrix substances, and they are thought to prevent cellulose from swelling [49–52].

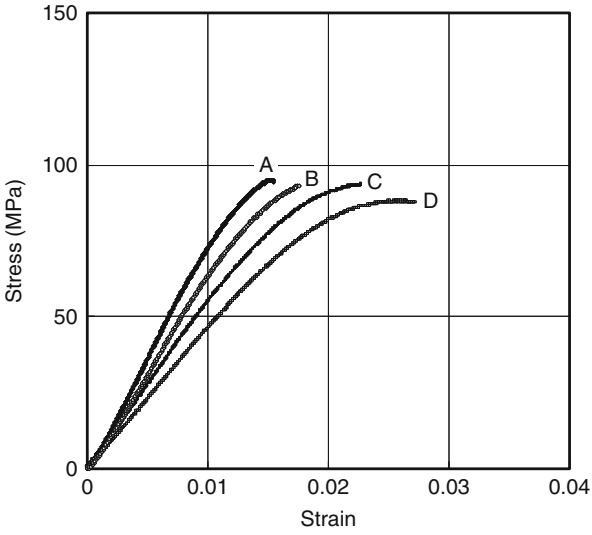

Fig. 24.3 Stress–strain curves of NaOH-treated wood concentration of NaOH aqueous solutions: A, 0 %; B, 10 %; C, 15 %; and D, 20 % (With kind permission from Springer Science+Business Media: Cellulose, Bending properties and cell wall structure of alkali-treated wood, 17, 2009, 47-55, Ishikura Y., Abe K., Yano H., Figure 3, and any original(first) copyright notice displayed with material.) [48]

At NaOH concentrations where the relative crystallinity index of wood decreased, longitudinal contraction and changes in the bending properties of oven-dried wood, such as decreases in the Young's modulus, the specific Young's modulus, and increase in the strain at yield were found [48]. The relative crystallinity index of alkali-treated wood was linearly correlated with these properties, which indicated that the increase in the proportion of amorphous components of the cellulose would contribute to these properties [48]. In addition, it was revealed that the toughness of wood is improved by the alkali treatment (Fig. 24.3) [48].

Changes in the shape, such as contraction and twisting, of wood after impregnation with NaOH aqueous solutions [54, 55] and changes in the swelling anisotropy of wood in the water-saturated condition [56, 57] after impregnation with NaOH aqueous solution followed by washing with distilled water are also reported to occur at almost the same concentration range. These are also explained on the basis of changes in the structure of microfibrils and consequent increases in the longitudinal contractive force of microfibrils [54–57], as reported by Nakano et al. [42].

Series of amines or liquid NH_3 also change the mechanical properties of wood in the swollen state [37–39]. Schuerch reported that wood can be plasticized by liquid ammonia and can then be bent, molded, or compressed [37, 38]. Sadoh et al. [39] reported that the average rigidity, calculated from shear stress–strain curves in torsional tests, decreases, and deformation increases in amine-saturated wood. However, the changes in these mechanical properties in amine-saturated wood were observed even in wood without swelling of cellulose crystals [39]. They indicated that these changes in mechanical properties of amine-saturated wood may possibly be independent of the swelling of cellulose crystals and be due to the swelling of the amorphous region of cellulose, hemicelluloses, and lignin [39].

After impregnation with aqueous EDA followed by a methanol rinse, the bending properties of oven-dried wood samples changed at a certain EDA concentration [58]. In addition, changes in the structures of cellulose crystals, specifically the transformation into cellulose III_I at 70 % EDA, were observed in the X-ray diffraction patterns of treated wood. Transformation into cellulose III has also been observed in wood treated with liquid ammonia [59]. Cellulose III_I has a parallel-chain orientation, as does cellulose I [53, 60, 61], and this can explain how the transformation into cellulose III_I via EDA treatment can occur, even in wood [58]. These indicate the possibility that changes in the structure of the cell wall, accompanied by changes in the structures of cellulose microfibrils, contribute to changes in the mechanical and physical properties of the treated wood samples [58].

5 Concluding Remarks

Wood is a natural porous material, obtained from trees, whose cell walls consist of cellulose microfibrils, lignin, and hemicelluloses. The chemical treatments that swell cellulose crystals cause various changes in wood properties. Observation of changes in the structures of cellulose in wood cell walls such as decrease in crystalline region and changes in the structures of cellulose crystals with these treatments indicate that the changes in cell wall structures accompanied by the changes in the structures of cellulose microfibrils in wood cell walls affect the mechanical and physical properties of wood.

Cellulose microfibrils in wood cell walls, whose crystalline regions have high Young's modulus and strength in the direction parallel to the molecular chain axis, play an important role in the mechanical and physical properties of wood. Trees spend a long time to form their xylem, and their cells or cell walls have complex structures to stand in natural environment for a long time. They may give us important information about the structures of cellulose microfibrils or the materials, and their properties.

Acknowledgments The author would like to thank Prof. Dr. H. Yano and Dr. K. Abe for their cooperation with X-ray diffraction measurements (Fig. 24.2), and also would like to express sincere gratitude to Prof. Dr. H. Yano for his guidance and advice in performing the study of alkali treatment. The author also would like to gratefully acknowledge the tuition and the support of Prof. Dr. T. Nakano in performing the study of alkali-treated wood.

References

1. Bodig J, Jayne BA (1993) I. Characteristics of wood composites. In: Bodig J, Jayne BA (ed) Mechanics of wood and wood composites, (reprint edition) Krieger Publishing Company Krieger Drive, Malabar, p 1
2. Saiki H, Harada H (1994) II. Sinyoujyuzai no saibou. In: Shimaji K, Saiki H, Harada H, Shiokura T, Ishida S, Shigematsu Y, Sudou S (eds) Mokuzai no kouzo, 5th edn. Buneido, Tokyo, p 20

3. Saiki H, Harada H (1994) III. Kouyoujyuzai no saibou. In: Shimaji K, Saiki H, Harada H, Shiokura T, Ishida S, Shigematsu Y, Sudou S (eds) Mokuzai no kouzo, 5th edn. Buneido, Tokyo, p 49
4. Sakurada I, Nukushina Y, Ito T (1962) Experimental determination of the elastic modulus of crystalline regions in oriented polymers. J Polym Sci 57:651
5. Matsuo M, Sawatari C, Iwai Y, Ozaki F (1990) Effect of orientation distribution and crystalliniy on the measurement by x-ray diffraction of the crystal lattice moduli of cellulose I and II. Macromolecules 23:3266
6. Tashiro K, Kobyashi M (1991) Theoretical evaluation of three-dimensional elastic constants of native and regenerated celluloses: role of hydrogen bonds. Polymer 32:1516
7. Nishino T, Takano K, Nakamae K (1995) Elastic modulus of the crystalline regions of cellulose polymorphs. J Polym Sci Part B Polym Phys 33:1647
8. Saiki H, Harada H (1994) V. Saibouheki. In: Shimaji K, Saiki H, Harada H, Shiokura T, Ishida S, Shigematsu Y, Sudou S (eds) Mokuzai no kouzo, 5th edn. Buneido, Tokyo, p 125
9. Page DH, El-Hosseiny F (1983) The mechanical properties of single wood pulp fibres. Part 5. Fibril angle and the shape of the stress–strain curve. J Pulp Pap Sci 9:99
10. Reiterer A, Lichtenegger H, Tschegg S, Fratzl P (1999) Experimental evidence for a mechanical function of the cellulose microfibril angle in wood cell walls. Philos Mag A 79:2173
11. Reiterer A, Lichtenegger H, Fratzl P, Tschegg S (2001) Deformation and energy absorption of wood cell walls with different nanostructure under tensile loading. J Mater Sci 36:4681
12. Okano T, Sarko A (1984) Mercerization of cellulose. I. X-ray diffraction evidence for intermediate structures. J Appl Polym Sci 29:4175
13. Fink HP, Phillip B (1985) Models of cellulose physical structure from the viewpoint of the cellulose I→II transition. J Appl Polym Sci 30:3779
14. Okano T, Sarko A (1985) Mercerization of cellulose. II. Alkali–cellulose intermediates and a possible mercerization mechanism. J Appl Polym Sci 30:325
15. Sao KP, Samantary BK, Bhattacherjee S (1994) X-ray study of crystallinity and disorder in ramie fiber. J Appl Polym Sci 52:1687
16. Fengel D, Jakob H, Strobel C (1995) Influence of the alkali concentration on the formation of cellulose II. Study by X-ray diffraction and FTIR spectroscopy. Holzforschung 49:505
17. Rollins ML (1954) Some Aspects of Microscopy in Cellulose Research. Anal Chem 26:718
18. Warwicker JO, Jefferies R, Colban RL, Robinson RN (1966) A review of the literature on the effect of caustic soda and other swelling agents on the fine structure of cotton. Shirley Institute Pamphlet No. 93, Shirey Institute Disbury, Manchester
19. Okano K, Nishiyama Y (1995) Behavior of alkali-swollen cellulose fibers and the crystal structure. Cell Commun 2:2
20. Nishiyama Y, Okano T (1998) Morphological changes of ramie fiber during mercerization. J Wood Sci 44:310
21. Ishikawa A, Okano T, Sugiyama J (1997) Fine structure and tensile properties of ramie fibres in the crystalline form of cellulose I, II, III_I and IV_I. Polymer 38:463
22. Loeb L, Segal L (1955) Studies of the ethylenediamine-cellulose complex. I. Decomposition of the complex by solvents. J Polym Sci 15:343
23. Numata Y, Kono H, Kawano S, Erata T, Takai M (2003) Cross-polarization/magic-angle spinning ^{13}C nuclear magnetic resonance study of cellulose I-ethylenediamine complex. J Biosci Bioeng 96:461
24. Wada M, Kwon GJ, Nishiyama Y (2008) Structure and thermal behavior of a cellulose I-ethylenediamine complex. Biomacromolecules 9:2898
25. Wada M, Heux L, Nishiyama Y, Langan P (2009) The structure of the complex of cellulose I with ethylenediamine by X-ray crystallography and cross-polarization/magic angle spinning ^{13}C nuclear magnetic resonance. Cellulose 16:943
26. Nishiyama Y, Wada M, Hanson BL, Langan P (2010) Time-resolved X-ray diffraction microprobe studies of the conversion of cellulose I to ethylenediamine-cellulose I. Cellulose 17:735

27. Roche E, Chanzy H (1981) Electron microscopy study of the transformation of cellulose I into cellulose III_I in *Valonia*. Int J Biol Macromol 3:201
28. Chanzy H, Henrissat B, Vuong R, Revol JF (1986) Structural changes of cellulose crystals during the reversible transformation cellulose I↔III_I in *Valonia*. Holzforschung 40(Suppl):25
29. Chanzy H, Henrissat B, Vincendon M, Tanner SF, Belton PS (1987) Solid-state ^{13}C-N.M.R. and electron microscopy study on the reversible cellulose I→cellulose IIII transformation in *Valonia*. Carbohydr Res 160:1
30. Sugiyama J, Harada H, Saiki H (1987) Crystalline morphology of *Valonia macrophysa* cellulose III_I revealed by direct lattice imaging. Int J Biol Macromol 9:122
31. Ishikawa A, Kuga S, Okano T (1998) Determination of parameters in mechanical model for cellulose III fibre. Polymer 39:1875
32. Gomes A, Goda K, Ohgi J (2004) Effects of Alkali Treatment to Reinforcement on Tensile Properties of Curaua Fiber Green Composites. JSME Int J Ser A 47:541
33. Goda K, Sreekala MS, Gomes A, Kaji T, Ohgi J (2006) Improvement of plant based natural fibers for toughening green composites—Effect of load application during mercerization of ramie fibers. Compos A 37:2213
34. Gomes A, Matsuo T, Goda K, Ohgi J (2007) Development and effect of alkali treatment on tensile properties of curaua fiber green composites. Compos A 38:1811
35. Nakagaito AN, Yano H (2008) Toughness enhancement of cellulose nanocomposites by alkali treatment of the reinforcing cellulose nanofibers. Cellulose 15:323
36. Haraguchi K, Suizu N, Uno T, Goda T, Noda J, Ohgi J (2009) Effectt of alkali treatment on the tensile and impact properties of ramie plied yarn-reinforced green composites. J Soc Mater Sci Japan 58:374
37. Schuerch C (1964) Wood plasticization. For Prod J 14:377
38. Schuerch C, Burdick MP, Mahdalik M (1966) Liquid ammonia-solvent combinations in wood plasticization. I&EC Prod Res Dev 5:101
39. Sadoh T, Yamaguchi E (1968) The swelling of wood in amines and the rigidity of wood swollen with amines. Bull Kyoto Univ Forests 40:276
40. Nakano T (1988) Plasticization of wood by alkali treatment. Effects of kind of alkali and concentration of alkaline aqueous solution on stress relaxation. Nihon Reoroji Gakkaishi 16:104
41. Nakano T (1989) Plasticization of wood by alkali treatment: relationship between plasticization and the ultra-structure. Mokuzai Gakkaishi 35:431
42. Nakano T, Sugiyama J, Norimoto M (2000) Contractive force and transformation of microfibril with aqueous sodium hydroxide solution for wood. Holzforschung 54:315
43. Stöckmann VE (1971) Effect of pulping on cellulose structure. Part I. A hypothesis of transformation of fibrils. Tappi 54:2033
44. Stöckmann VE (1971) Effect of pulping on cellulose structure. Part II. Fibrils contract longitudinally. Tappi 54:2038
45. Ishikura Y, Nakano T (2004) Changes of Young's modulus of woods by alkali treatment. Mokuzai Gakkaishi 50:214
46. Fujimoto T, Nakano T (2000) The effect of mercerization on wood structural features. Mokuzai Gakkaishi 46:238
47. Ishikura Y, Nakano T (2005) Adsorption properties and structural features of alkali treated wood. Mokuzai Gakkaishi 51:364
48. Ishikura Y, Abe K, Yano H (2010) Bending properties and cell wall structure of alkali-treated wood. Cellulose 17:47
49. Revol JF, Goring DAI (1981) On the mechanism of the mercerization of cellulose in wood. J Appl Polym Sci 26:1275
50. Shiraishi N, Moriwaki M, Lonikar SV, Yokota T (1984) Lattice conversion of cellulose in wood. J Wood Chem Technol 4:219
51. Murase H, Sugiyama J, Saiki H, Harada H (1988) The effect of lignin on mercerization of cellulose in wood: an electron diffraction study on the transformation from cellulose I to cellulose II. Mokuzai Gakkaishi 34:965

52. Kim NH (2005) An investigation of mercerization in decayed oak wood by a white rot fungus (*Lentinula edodes*). J Wood Sci 51:290
53. Kim NH, Imai T, Wada M, Sugiyama J (2006) Molecular directionality in cellulose polymorphs. Biomacromolecules 7:274
54. Ishikura Y, Nakano T (2005) Shape changes with alkali treatments of woods. Mokuzai Gakkaishi 51:92
55. Ishikura Y, Nakano T (2008) Compressive stress-strain properties of natural materials treated with aqueous NaOH. Holzforschung 62:448
56. Ishikura Y, Nakano T (2007) Contraction of the microfibrils of wood treated with aqueous NaOH: evidence from changes in the anisotropy of the longitudinal and transverse swelling rates of wood. J Wood Sci 53:175
57. Nakano T (2010) Mechanism of microfibril contraction and anisotropic dimensional changes for cells in wood treated with aqueous NaOH solution. Cellulose 17:711
58. Ishikura Y (2011) Changes of wood properties treated with aqueous amine solution, bending tests and X-ray analysis of wood after amine treatment. J Mater Sci 46:3785
59. Isogai A, Usuda M (1992) X-ray diffraction and solid-state ^{13}C-NMR analyses of wood celluloses treated with ammonia. Mokuzai Gakkaishi 38:713
60. Sarko A, Southwick J, Hayashi J (1976) Packing analysis of carbohydrates and polysaccharides. 7. Crystal structure of cellulose IIII and its relationship to other cellulose polymorphs. Macromolecules 9:857
61. Wada M, Chanzy H, Nishiyama Y, Langan P (2004) Cellulose III_I crystal structure and hydrogen bonding by synchrotron X-ray and neutron fiber diffraction. Macromolecules 37:8548

Cellulosic Nanocomposites from Natural Fibers for Medical Applications: A Review

25

H. P. S. Abdul Khalil, A. H. Bhat, A. Abu Bakar, Paridah Md. Tahir, I. S. M. Zaidul, and M. Jawaid

Contents

H.P.S. Abdul Khalil (✉)
School of Industrial Technology, Universiti Sains Malaysia, Penang, Malaysia
e-mail: akhalilhps@gmail.com

A.H. Bhat
Department of Fundamental and Applied Sciences, Universiti Teknologi Petronas, Perak, Malaysia
e-mail: bhataamir@gmail.com

A. Abu Bakar
Materials and Mineral Resources Engineering, Universiti Sains Malaysia, Penang, Malaysia
e-mail: azhar@eng.usm.my

P.M. Tahir
Biocomposite Technology Laboratory, Institute of Tropical Forestry and Forest Products, Universiti Putra Malaysia (UPM), Serdang, Selangor, Malaysia
e-mail: parida.introp@gmail.com

I.S.M. Zaidul
Faculty of Pharmacy, International Islamic University Malaysia, Kuala Lumpur, Malaysia
e-mail: zaidul@iium.edu

M. Jawaid
Department of Biocomposite Technology, Institute of Tropical Forestry and Forest Products, Universiti Putra Malaysia, Serdang, Selangor, Malaysia
e-mail: akhalilhps@gmail.com

J.K. Pandey et al. (eds.), *Handbook of Polymer Nanocomposites. Processing, Performance and Application – Volume C: Polymer Nanocomposites of Cellulose Nanoparticles*,
DOI 10.1007/978-3-642-45232-1_72,

Abstract

The nanocellulose and its composites have been covered in this chapter which is confirmed to be a very versatile material having the wide range of medical applications, including cardiovascular implants, scaffolds for tissue engineering, repair of articular cartilage, vascular grafts, urethral catheters, mammary prostheses, penile prostheses, adhesion barriers, and artificial skin. These implants were produced from bioresorbable and/or biodegradable materials.

Nanocellulose, such as that produced other than microfibrillated cellulose and cellulose nanowhiskers, is also produced by the bacteria (bacterial cellulose, BC) which is also an emerging biomaterial with great potential as a biological implant, wound and burn dressing material, and scaffolds for tissue regeneration. Moreover, the nanostructure and morphological similarities with collagen make cellulose attractive for cell immobilization and cell support. This article describes current and future applications of cellulosic nanofibers in the biomedical field.

Cellulose micro-/nanofibril as a reinforcing material for composites is becoming more and more attractive to researchers in composite science because of its potential lightweight and high strength. In the present article, we have reviewed the nanocellulosic fibers-based nanocomposites for medical applications. Processing methods, properties, and various applications of cellulosic composites are also discussed in this article. However, the separation of cellulose nanofibers along with the manufacture of cellulose nanocomposites is still challengeable. The aim of this chapter is to demonstrate the current state of development in the field of cellulose nanofibril-based nanocomposite research and application through examples.

Keywords
Nanocellulose • Composites • Nanofibers • Cellulose

1 Introduction

The hydrophilic nature of MFC has led most of the studies to be focused on nanocomposites based on hydrophilic matrices. For example, Nakagaito and Yano [1, 2]) impregnated microfibrillated Kraft pulp with a phenol–formaldehyde resin and then compressed the resulting material under high pressure to produce high-strength cellulose nanocomposites.

This study was also designed to clarify how the degree of fibrillation of pulp fibers affects the mechanical properties of cellulose composites. It was found that fibrillation that only influences the fiber surfaces is not effective in improving composite strength but that a complete fibrillation of the bulk of the fibers is required. In the study by Nakagaito and Yano [2], this was achieved by 16–30 passes through a refiner, followed by high-pressure homogenization. The resulting nanocomposites had Young's modulus and bending strength values of 19 GPa and 370 MPa, respectively, as determined by a three-point bending test [1]. More recently, the same authors used aqueous sodium hydroxide-treated MFC and phenolic resin to produce nanocomposites. The tensile properties of MFC–resin nanocomposites were compared with those of wood pulp–resin composites, and it was shown that the tensile strength of the MFC composites was significantly higher than that of the pulp composites, regardless of the treatment or resin content. In contrast, the Young's modulus values were practically the same. These authors thus confirmed the advantage of nanostructured composites over microstructured composites in terms of obtaining high strength and ductility.

Tensile tests showed that strong alkali-treated MFC nanocomposites with resin content around 20 wt% had strain at fracture values twice as high as those of untreated MFC nanocomposites based on the same resin.

In this review we describe various approaches to the synthesis of nanofibers from plant resources. Potential use of nanofibers as reinforcing material for the development of polymer composites specifically for medical applications with enhanced properties of these composites in various biomedical fields is also discussed.

2 Cellulose Fibers

Cellulose fibers are being used as potential reinforcing materials because of so many advantages such as abundantly available, low weight, biodegradable, cheaper, renewable, low abrasive nature, and interesting specific properties, since these are waste biomass and exhibit good mechanical properties [3–5]. Cellulose fibers also have some disadvantages such as moisture absorption, quality variations,

Table 25.1 The family of nanocellulose materials classified in three main subcategories (Table 25.1)

Type of nanocellulose	Selected references and synonyms	Typical sources	Formation and average size
Microfibrillated cellulose (MFC)	Microfibrillated cellulose [85], nanofibrils and microfibrils, nanofibrillated cellulose	Wood, sugar beet, potato tuber, hemp, flax	Delamination of wood pulp by mechanical pressure before and/or after chemical or enzymatic treatment diameter: 5–60 nm length, several micrometers
Nanocrystalline cellulose (NCC)	Cellulose nanocrystals, crystallites [89], whiskers [90], rodlike cellulose microcrystals [151]	Wood, cotton, hemp, flax, wheat straw, mulberry bark, ramie, Avicel, tunicin, cellulose from algae, and bacteria	Acid hydrolysis of cellulose from many sources diameter: 5–70 nm length; 100–250 nm (from plant celluloses); 100 nm to several micrometers (from celluloses of tunicates, algae, bacteria)
Bacterial nanocellulose (BNC)	Bacterial cellulose [38], microbial cellulose [48], biocellulose [48]	Low-molecular-weight sugars and alcohols	Bacterial synthesis diameter: 20–100 nm; different types of nanofiber networks

low thermal stability, and poor compatibility with the hydrophobic polymer matrix [6, 7]. On the basis of their dimensions, functions, and preparation methods, which in turn depend mainly on the cellulosic source and on the processing conditions, nanocellulosics are classified into three main subcategories as shown in Table 25.1.

2.1 Chemistry of Cellulose

Cellulose is the most abundant form of living terrestrial biomass [8] and finds applications in many spheres of modern industry. The existence of cellulose as the common material of plant cell walls was first recognized by Anselme Payen in 1838. Cellulose has been shown to be a long-chain polymer with repeating units of D-glucose, a simple sugar. It occurs in almost pure form in cotton fiber [9].

However, in wood, plant leaves, and stalks, it is found in combination with other materials, such as lignin and hemicelluloses. Although generally considered a plant material, some bacteria are also found to produce cellulose. Cellulose is a natural polymer, a long chain made by the linking of smaller molecules. The links in the cellulose chain consist of sugar, β-D-glucose [10]. The sugar units are linked when water is eliminated by combining the H and –OH group. Linking just two of these sugars produces a disaccharide called cellobiose. In the cellulose chain, the glucose units are in 6-membered rings, called pyranoses. They are joined by single oxygen atoms (acetal linkages) between the C-1 of one pyranose ring and the C-4 of the next ring. Since a molecule of water is lost due to the reaction of an alcohol and a hemiacetal to form an acetal, the glucose units in the cellulose polymer are referred to as anhydroglucose units.

The spatial arrangement or stereochemistries of these acetal linkages are very important. The pyranose rings of the cellulose molecule have all the groups larger than hydrogen sticking out from the periphery of the rings (equatorial positions). The stereochemistry at carbons 2, 3, 4, and 5 of the glucose molecule is fixed, but in pyranose form, the hydroxyl at C-4 can approach the carbonyl at C-1 from either side, resulting in two different stereochemistries at C-1. When the hydroxyl group at C-1 is on the same side of the ring as the C-6 carbon, it is said to be in the configuration. In cellulose, the C-1 oxygen is in the opposite or β-configuration (i.e., cellulose is poly [β-1, 4-D-anhydroglucopyranose]. This β-configuration, with all functional groups in equatorial positions, causes the molecular chain of cellulose to extend in a more or less straight line, making it a good fiber-forming polymer [164].

Because of the equatorial positions of the hydroxyls on the cellulose chain, they protrude laterally along the extended molecule and are readily available for hydrogen bonding. These hydrogen bonds cause the chains to group together in a highly ordered structure. Since the chains are usually longer than the crystalline regions, they are thought to pass through several different crystalline regions, with areas of disorder in between ("fringed-micelle" model) [11]. The interchain hydrogen bonds in the crystalline regions are strong, giving the resultant fiber good strength and insolubility in most solvents. They also prevent cellulose from melting (non-thermoplastic). In the less ordered regions, the chains are further apart and more available for hydrogen bonding with other molecules, such as water. Most cellulose structures can absorb large quantities of water (hygroscopic). Thus, cellulose swells but does not dissolve in water [164].

The cellulose molecule contains three different kinds of anhydroglucose units, the reducing end with a free hemiacetal (or aldehyde) group at C-1, the nonreducing end with a free hydroxyl at C-4, and the internal rings joined at C-1 and C-4. But because of long-chain length, the chemistry of the alcohol groups of the internal units predominates, so long as the chains are not cleaved by the reaction conditions. However, unlike simple alcohols, cellulose reactions are usually controlled by steric factors than would be expected on the basis of the inherent reactivity of the different hydroxyl groups. C-2, C-3, and C-6 hydroxyls and C-H groups are active sites in cellulose for the incorporation of polymeric chains through grafting. In grafting it has been reported that the reactivity of hydroxyl group at C-6 is far less than those at C-2 and C-3 [164].

2.2 Chemical Composition, Structure, and Properties of Cellulose Fibers

Cellulose fibers can be classified according to their origin and grouped into leaf, abaca, cantala, curaua, date palm, henequen, pineapple, sisal, and banana; seed, cotton; bast, flax, hemp, jute, and ramie; fruit, coir, kapok, and oil palm; grass, alfa, bagasse, and bamboo; and stalk, straw (cereal) [12]. The bast and leaf (the hard fibers) types are the most commonly used in composite applications [13–15]. Commonly used plant fibers are cotton, jute, hemp, flax, ramie, sisal, coir, henequen, and kapok. The largest producers of sisal in the world are Tanzania and Brazil.

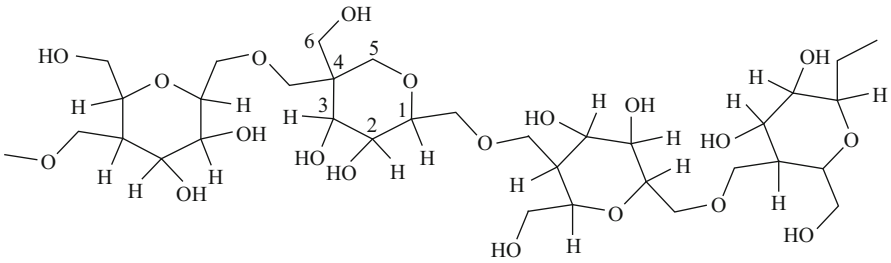

Fig. 25.1 Cellulosic units joined by glycosidic linkages

Henequen is produced in Mexico whereas abaca and hemp in the Philippines. The largest producers of jute are India, China, and Bangladesh [16, 17].

Plant fibers are constitutes of cellulose fibers, consisting of helically wound cellulose microfibrils, bound together by an amorphous lignin matrix. Lignin keeps the water in fibers and acts as a protection against biological attack and as a stiffener to give stem its resistance against gravity forces and wind.

Hemicellulose found in the natural fibers is believed to be a compatibilizer between cellulose and lignin [17]. The cell wall in a fiber is not a homogenous membrane (Fig. 25.1) [18]. Each fiber has a complex, layered structure consisting of a thin primary wall which is the first layer deposited during cell growth encircling a secondary wall [19]. The secondary wall is made up of three layers and the thick middle layer determines the mechanical properties of the fiber. The middle layer consists of a series of helically wound cellular microfibrils formed from long-chain cellulose molecules. The angle between the fiber axis and the microfibrils is called the microfibrillar angle. The characteristic value of microfibrillar angle varies from one fiber to another. These microfibrils have typically a diameter of about 10–30 nm and are made up of 30–100 cellulose molecules in extended chain conformation and provide mechanical strength to the fiber.

The properties of cellulose fibers are affected by many factors such as variety, climate, harvest, maturity, retting degree, decortications, disintegration (mechanical, steam explosion treatment), fiber modification, textile, and technical processes (spinning and carding) [20]. In order to understand the properties of natural fiber-reinforced composite materials, it becomes necessary to know the mechanical, physical, and chemical properties of natural fibers. Flax fibers are relatively strong fibers as compared to other natural fibers. The tensile strength of elementary fibers is in the region of 1,500 MPa, and for technical fibers a value of circa 800 MPa was observed at 3 mm clamp length [21]. Baley [22] and Lamy and Baley [23] investigated the modulus of flax fibers. The modulus of elementary fibers is dependent on the diameter of fiber, and it ranges from 39 GPa for fibers having diameter approximately 35 μm to 78 GPa for fibers having 5 μm diameter. This variation is related to the variation in relative lumen size between fibers having different diameters. An average Young's modulus of 54 GPa was observed after numerous tensile tests on single flax fibers, and the results are within the range of moduli measured on technical fibers. The mechanical, chemical, and physical

properties of plant fibers are strongly harvest dependent, influenced by climate, location, weather conditions, and soil characteristics. These properties are also affected during the processing of fiber such as retting, scotching, bleaching, and spinning [24].

Cellulose fibers have relatively high strength, high stiffness, and low density [25]. The characteristic value for soft-wood-Kraft fibers and flax has been found close to the value for E-glass fibers. Different mechanical properties can be incorporated in natural fibers during processing period. The fiber properties and structure are influenced by several conditions and vary with area of growth, its climate, and age of the plant [26]. Technical digestion of the fiber is another important factor which determines the structure as well as characteristic value of the fiber. The elastic modulus of the bulk natural fibers such as wood is about 10 GPa. Cellulose fibers with moduli up to 40 GPa can be separated from wood by chemical pulping process. Such fibers can be further subdivided into microfibrils within elastic modulus of 70 GPa. Theoretical calculations of elastic moduli of cellulose chain have been given values up to 250 GPa. However, no technology is available to separate these from microfibrils [27]. The tensile strength of natural fibers depends upon the test length of the specimen which is of main importance with respect to reinforcing efficiency. Mieck et al. [28] and Mukherjee and Satyanarayana [29] reported that tensile strength of flax fiber is significantly more dependent on the length of the fiber. In comparison to this, the tensile strength of pineapple fiber is less dependent on the length, while the scatter of the measured values for both is located mainly in the range of the standard deviation. The properties of flax fiber are controlled by the molecular fine structure of the fiber which is affected by growing conditions and the fiber processing techniques used. Flax fibers possess moderately high specific strength and stiffness.

Quality and other properties of fibers depend on factors such as size, maturity, and processing methods adopted for the extraction of fibers. Properties such as density, electrical resistivity, ultimate tensile strength, and initial modulus are related to the internal structure and chemical composition of fibers [25]. Desirable properties for fibers include excellent tensile strength and modulus, high durability, low bulk density, good moldability, and recyclability.

2.3 Cellulose Derivatives

Cellulose derivatives are important commercial products for plastics, textiles, packaging, films, lacquers, and explosives. More recently, cellulose derivatives which are soluble in water or dilute alkali have been developed. Researchers are finding ways to use these derivatives as finishing and sizing agents for textiles; as absorbable surgical gauze, protective colloids, and adhesives; as thickening agents for foods, creams, ointments, and pastes; and in pharmaceutical, printing, paper, and other industries.

Wood cellulose is the principal raw material for cellulose derivative products, and several million tons are produced each year. The second source of cellulose for

Table 25.2 Cellulose derivatives and its properties

Cellulose derivatives	Properties
Cellulose acetate	Can be composted or incinerated
	Can be dyed; however, special dyes and pigments are required since acetate does not accept dyes ordinarily used for cotton and rayon (this also allows cross-dyeing)
Cellulose propionate	Stiffer than cellulose acetate or cellulose acetate butyrate
	Transparent and glossy with better low temperature impact properties than cellulose acetate or cellulose acetate butyrate
Cellulose acetate/ butyrate (CAB)	Better weathering characteristics than cellulose acetate or cellulose propionate
	Tougher than cellulose acetate
Carboxymethyl cellulose (CMC)	Viscosity modifier or thickener and to stabilize emulsions
	More cooling capacity than ice
Hydroxyethyl cellulose (HEC)	Emulsion stabilizer
	Nonionic surfactant stabilizer
Hydroxypropyl cellulose (HPC)	HPC is used as a thickener, as a low level binder, and as an emulsion stabilizer
	As a disintegrant and a binder
Methyl cellulose (MC)	Thickener and emulsifier
	Variable viscosity personal lubricant
	Substitute for tears or saliva
	Bacterial motility inhibitor
Ethyl cellulose (EC)	As a thin-film coating material
	As a food additive and as an emulsifier
Hydroxypropyl methylcellulose (HPMC)	Tile adhesives and renders, rheology modifier, and water retention agent
	Inert, viscoelastic polymer used as an ophthalmic lubricant, as well as an excipient and controlled delivery component in oral medicaments
Cellulose nitrate	Highly flammable compound
	Magician's flash paper leaving no ash
	Nitrocellulose lacquer is also used as an aircraft dope
	Now declining importance due to its unstable nature

cellulose derivatives is cotton linters (chemical cotton). Cotton linters find preferred use in certain products such as in cellulose acetate for plastics or high-tenacity rayon. For other applications cellulose acetate is more often made from wood cellulose as shown in Table 25.2.

3 Cellulose Nanofibers

Cellulose nanofibers have a high potential to be used in many different areas particularly as reinforcement in the development of nanocomposites. Many studies have been done on isolation and characterization of cellulose nanofibers from various sources. Cellulose nanofibers can be extracted from the cell walls by simple mechanical methods or a combination of both chemical and mechanical methods.

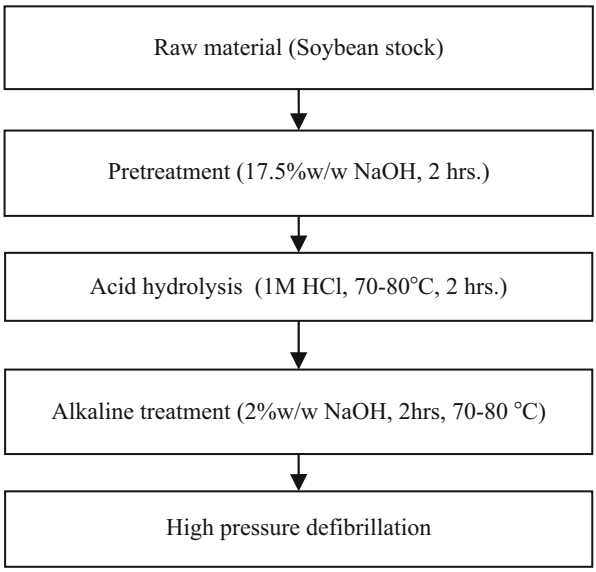

Fig. 25.2 Isolation of nanofibers by chemomechanical treatment [31]

3.1 Synthesis of Cellulose Nanofibers

Alemdar and Sain (2008) have extracted cellulose nanofibers from wheat straw by a chemical treatment, resulting to purified cellulose. To individualize the nanofibers from the cell walls, a mechanical treatment (disintegration and defibrillation steps) was applied to the chemically treated fibers. Cellulose nanofibers were extracted from the agricultural residues, wheat straw, and soy hulls, by a chemomechanical technique (Alemdar and Sain 2008). The wheat straw nanofibers were determined to have diameters in the range of 10–80 nm and lengths of a few thousand nanometers. By comparison, the soy hull nanofibers had a diameter of 20–120 nm and shorter lengths than the wheat straw nanofibers. Zimmermann et al. [30] separated nanofibrillated cellulose (NFC) at the greatest possible lengths and diameters below 100 nm from different starting cellulose materials by mechanical dispersion and high-pressure (up to 1,500 bar) homogenization processes. The treatment resulted in nanoscaled fibril networks.

The cellulose nanofibers were extracted by Wang and Sain [31] from soybean stock by chemomechanical treatments (Fig. 25.2).

The cellulose nanofibrils were extracted from wheat straw using steam explosion, acidic treatment, and high-shear mechanical treatment. Alkaline-treated pulp was soaked in 8 % solution of H_2O_2 (v/v) overnight. Bleached pulp was then rinsed with abundant distilled water. Bleached pulp was then treated with 10 % HCl (1 N) solution and mixed using ultrasonicator at temperature around 60 ± 1 °C for 5 h. Finally, the fibers were taken out and washed several times with distilled water in order to neutralize the final pH and then dried. Fibers were suspended in water and continuously stirred with a high-shear homogenizer for 15 min. High-shearing action breaks down the fiber agglomerates and results in nanofibrils (Fig. 25.3) [32].

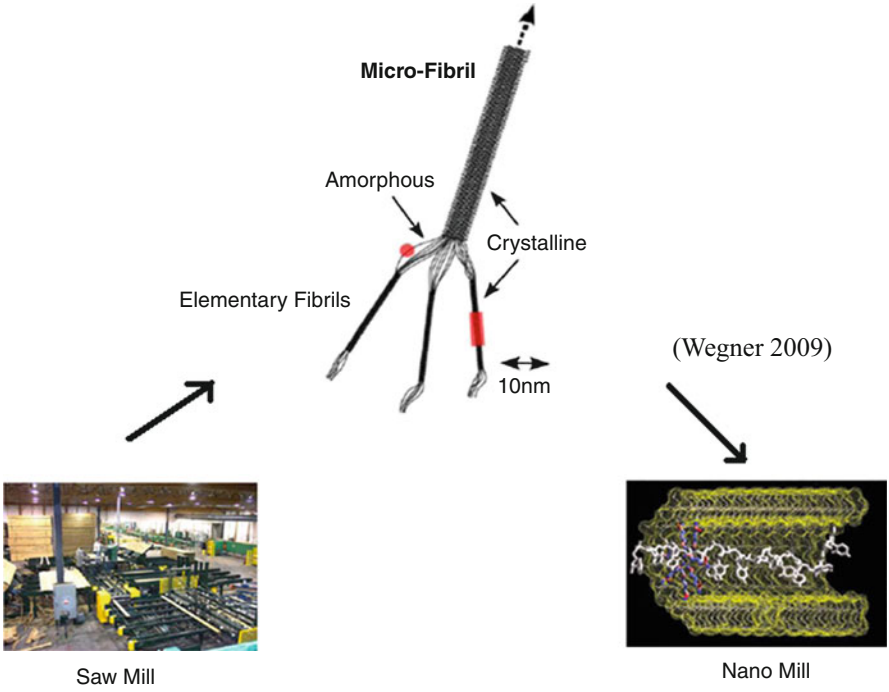

Fig. 25.3 Progress in fiber processing from natural wood to nanofibers

3.2 Structure and Properties of Cellulose Nanofibers

Transmission electron microscopy (TEM), scanning electron microscopy (SEM), field-emission scanning electron microscopy (FE-SEM), atomic force microscopy (AFM), wide-angle X-ray scattering (WAXS), and NMR spectroscopy have been used to study the structure of cellulose nanofibers [165]. A combination of microscopic techniques with image analysis can provide information about widths of cellulose nanofiber, but it is very difficult to find out the lengths of the nanofiber because of entanglements and difficulties in identifying both ends of individual nanofibers. It is often reported that MFC suspensions are not homogeneous and that they consist of cellulose nanofibers and nanofiber bundles (Siro and Plackett 2010).

Teixeira et al. [33] obtained the suspensions of white and colored nanofibers by the acid hydrolysis of white and naturally colored cotton fibers. Possible differences among them in morphology and other characteristics were investigated. Morphological study of cotton nanofibers showed a length of 85–225 nm and diameter of 6–18 nm. It was found that there were no significant morphological differences among the nanostructures from different cotton fibers. The main differences found were the slightly higher yield, sulfonation effectiveness, and thermal stability under dynamic temperature conditions of the white nanofiber. On the other hand, the colored nanofibers showed a better thermal stability than the white in isothermal conditions at 180 °C.

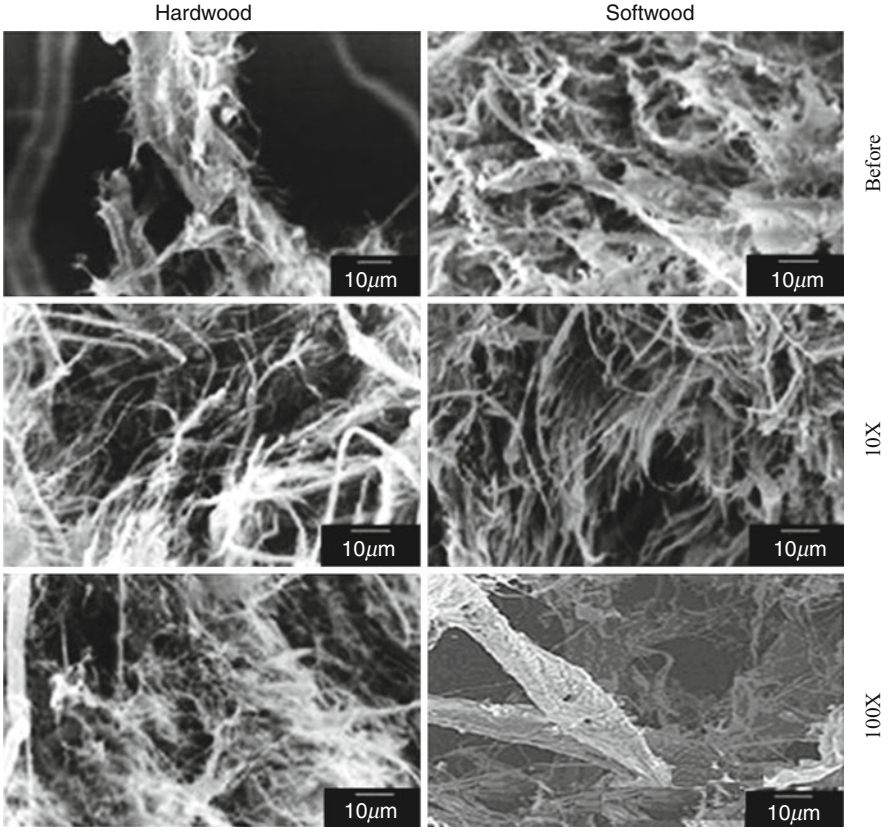

Fig. 25.4 Scanning electron micrographs of hard- and softwood cellulose fibers, before and after 10 passes through the homogenizer [34]

The structure of the cellulose nanofibers from agricultural residues was investigated by Alemdar and Sain (Alemdar and Sain 2008). FTIR spectroscopic analysis demonstrated that chemical treatment also led to partial removal of hemicelluloses and lignin from the structure of the fibers. PXRD results revealed that this resulted in improved crystallinity of the fibers. Thermal properties of the nanofibers were studied by the TGA technique and were found to increase dramatically.

Stelte and Sanadi [34] have studied the mechanical fibrillation process for the preparation of cellulose nanofibers from two commercial hard- and softwood cellulose pulps. The degree of fibrillation was studied using light microscopy (LM), scanning electron microscopy (SEM), and atomic force microscopy (AFM). SEM images (Fig. 25.4) of hard- and softwood fibers showed that the hardwood fibers that were fibrillated only on the surface during the refining step are now disintegrated into a network of small fibers. AFM images of the final products after high-pressure homogenization showed that the size distribution of the hard- and softwood nanofibers is in the range of 10–25 nm in diameter.

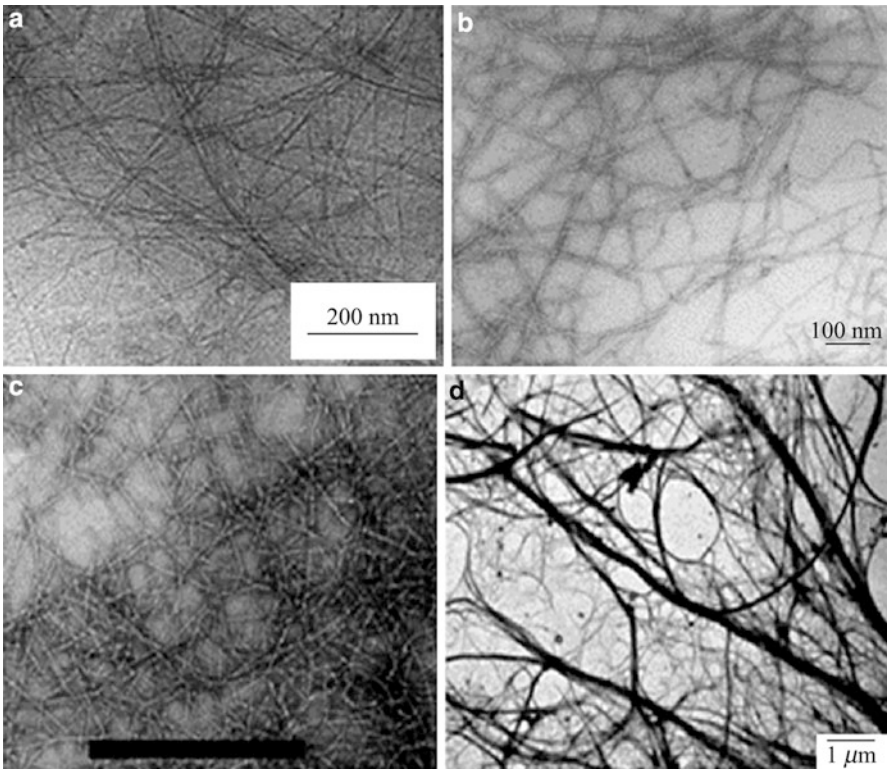

Fig. 25.5 Transmission electron micrographs from dilute suspension of cellulose nanocrystals from (**a**) ramie [35], (**b**) bacterial [36], (**c**) sisal [37], (**d**) microcrystalline cellulose [38], (**e**) sugar beet pulp [151], (**f**) tunicin [39], (**g**) wheat straw [40], and (**h**) cotton [41]

3.3 Cellulose Nanofiber-Reinforced Nanocomposites

The potential of nanocomposites in various sectors of research and application is promising and attracting increasing investments. In the nanocomposite industry, a reinforcing particle is usually considered as a nanoparticle when at least one of its linear dimensions is smaller than 100 nm. Owing to the hierarchical structure and semicrystalline nature of cellulose, nanoparticles can be extracted from this naturally occurring polymer. Native cellulose fibers are built up by smaller and mechanically stronger long thin filaments, the microfibrils consisting of alternating crystalline and noncrystalline domains. Multiple mechanical shearing actions can be used to release more or less individually these microfibrils. This material is usually called microfibrillated cellulose (MFC) as shown in Fig. 25.5.

Longitudinal cutting of these microfibrils can be performed by submitting the biomass to a strong acid hydrolysis treatment, allowing dissolution of amorphous domains. The ensuing nanoparticles occur as rodlike nanocrystals or whiskers with dimensions depending on the source of cellulose and preparation procedure.

Table 25.3 Geometrical characteristics of cellulose nanocrystals from various sources: length (L), cross section (D), and aspect ratio (L/d)

Source	L (nm)	D (nm)	L/D
Acacia pulp	100–250	5–15	–
Alfa	200	10	20
Algal (*Valonia*)	>1,000	10–20	∞
Bacterial	100–several 1,000	5–10 × 30–50	–
Banana rachis	500–1,000	5	–
Bioresidue from wood bioethanol production	>100	10–20	–
Capim dourado	300	4.5	67
Cassava bagasse	360–1,700	2–11	–
Cladophora	–	20 × 20	–
Coconut husk fibers	80–500	6	39
Cotton	100–300	5–15	10
Cottonseed linter	170–490	40–60	–
Curaúa	80–170	6–10	13–17
Date palm tree (rachis/leaflets)	260/180	6.1	43/30
Eucalyptus wood pulp	145	6	24
Flax	100–500	10–30	15
Grass Zoysia	200–700	10–60	–
Hemp	Several 1,000	30–100	–
Luffa cylindrica	242	5.2	47
MCC	150–300	3–7	–
Mulberry	400–500	20–40	–
Pea hull	240–400	7–12	34
Ramie	350–700	70–120	
	(150–250)	6–8	
Recycled pulp	100–1,800	30–80	–
Sisal	100–500	3–5	60/43
	(215)	5	
Sugar beet pulp	210	5	42
Sugarcane bagasse	200–310	2–6	64
Tunicin	100–>1,000	10–20	67
Wheat straw	150–300	5	45
Wood	100–300	3–5	50

The typical geometrical characteristics for nanocrystals derived from different species and reported in the literature are collected in Table 25.3 [42–45].

Impressive mechanical properties and reinforcing capability, abundance, low weight, and biodegradability of cellulose nanocrystals make them ideal candidates for the processing of polymer nanocomposites (Samir et al. 2005; [46–48]. With a Young's modulus around 150 GPa and a surface area of several hundred square meters per gram [49], they have the potential to significantly reinforce polymers at low filler loadings.

A broad range of applications of nanocellulose exists even if a high number of unknown remains at date. Tens of scientific publications and experts show its potential even if most of the studies focus on their mechanical properties as reinforcing phase and their liquid crystal self-ordering properties. However, as for any nanoparticle, the main challenge is related to their homogeneous dispersion within a polymeric matrix.

4 Extraction of Nanofibrils

4.1 Homogenization

The fibrillation of pulp fiber to obtain nano-order-unit weblike network structure, called microfibrillated cellulose, is obtained through a mechanical treatment of pulp fibers, consisting of refining and high-pressure homogenizing processes. The refining process used is common in the paper industry and is accomplished via a piece of equipment called a refiner. In a disk refiner, the dilute fiber suspension to be treated is forced through a gap between the rotor and stator disks, which have surfaces fitted with bars and grooves against which the fibers are subjected to repeated cyclic stresses. This mechanical treatment brings about irreversible changes in the fibers, increasing their bonding potential by modification of their morphology and size. In the homogenization process, dilute slurries of cellulose fibers previously treated by refining are pumped at high pressure and fed through a spring high-pressure-loaded valve assembly.

As this valve opens and closes in rapid succession, the fibers are subjected to a large pressure drop with shearing and impact forces. This combination of forces promotes a high degree of microfibrillation of the cellulose fibers, resulting in microfibrillated cellulose [50]. The refining process is carried out prior to homogenization due to the fact that refining produces external fibrillation of fibers by gradually peeling off the external cell wall layers (*P* and *S*1 layers) and exposing the *S*2 layer and also causes internal fibrillation that loosens the fiber wall, preparing the pulp fibers for subsequent homogenization treatment [51]. Nakagaito and Yano [1] studied how the degree of fibrillation of pulp fibers affects the mechanical properties of high-strength cellulose composites. It was found that fibrillation solely of the surface of the fibers is not effective in improving composite strength, though there is a distinct point in the fibrillation stage at which an abrupt increase in the mechanical properties of composites occurs. In the range between 16 and 30 passes through refiner treatments, pulp fibers underwent a degree of fibrillation that resulted in a stepwise increment of mechanical properties, most strikingly in bending strength. This increase was attributed to the complete fibrillation of the bulk of the fibers. For additional high-pressure homogenization-treated pulps, composite strength increased linearly against water retention values, which characterize the cellulose's exposed surface area, and reached maximum value at 14 passes through the homogenizer (Fig. 25.6).

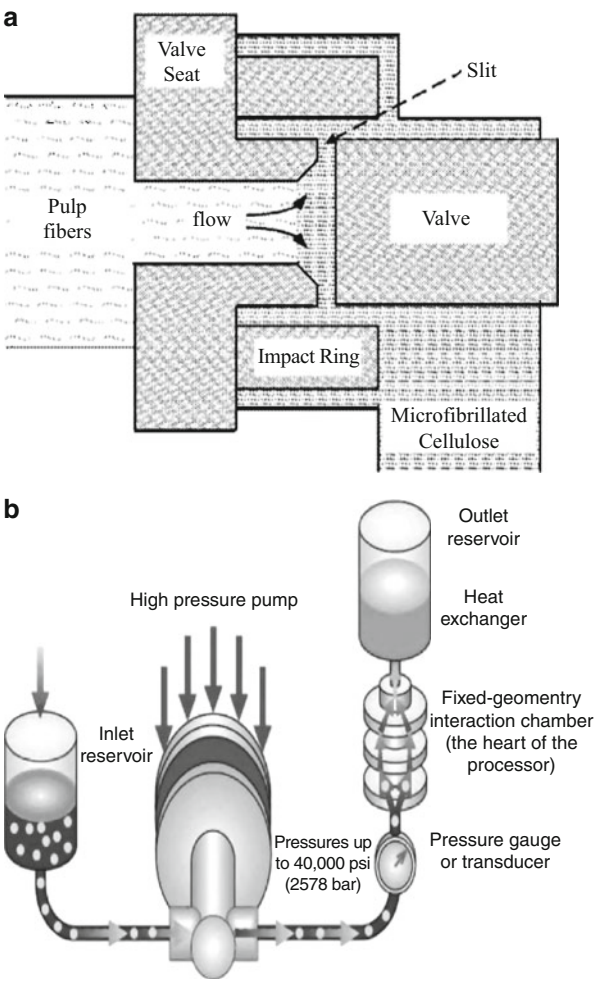

Fig. 25.6 Schematic representation of (**a**) the homogenizer and (**b**) the microfluidizer

4.2 Steam Explosion

Several methods are used to extract highly purified microfibrils from the plant cell wall. They are generally based on successive chemical and mechanical treatments. The steam explosion treatment is currently still being extensively studied as a promising pretreatment method. Lignocellulosic biomass materials can be fractionated into biopolymer constituents by steam explosion technology.

Treating various biomass resources by steam explosion has been studied by many researchers [53–55]. The steam explosion process was first introduced by Mason in 1927 to defibrate wood into fiber for board production [56]. The treatment of lignocellulosic resources with high-pressure steam, for short periods of time, followed by sudden decompression (explosion) represents a simple treatment

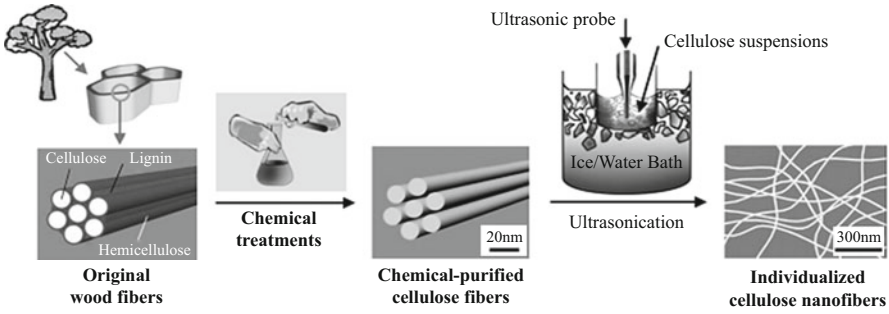

Fig. 25.7 Procedure for individualizing cellulose nanofibers

for biomass that achieves fiberization or "mulching" by a combination of chemical and mechanical action. During the steam explosion process, the raw material is exposed to pressurized steam followed by rapid reduction in pressure resulting in substantial breakdown of the lignocellulosic structure, hydrolysis of the hemicellulose fraction, depolymerization of the lignin components, and defibrillization [57, 58]. Marchessault mentions that the steam explosion is an auto-hydrolysis process [59]. Effects of this process on biomass are:

i. Cleavage of some accessible glycosidic links
ii. Cleavage of b-ether linkages of lignin
iii. Cleavage of lignin–carbohydrate complex bonds
iv. Minor chemical modification of lignin and carbohydrates

Both the aspect ratio and percentage yield of nanocellulose obtained by this technique have been found to be very high as compared to other conventional methods [60].

4.3 High-Intensity Ultrasonication

This process consists of combination of chemical pretreatment and high-intensity ultrasonication (Fig. 25.7). In the chemical pretreatment stage, the wood fibers are being purified to prepare the cellulose fibers according to general methods [61, 62]. First, lignin is removed from the samples using acidified sodium chlorite solution at 75 °C for an hour; this process is then repeated five times until the product became white. Next, the samples are treated in 3 wt% potassium hydroxide at 80 °C for 2 h. and then in 6 wt% potassium hydroxide at 80 °C for 2 h in order to leach hemicellulose, residual starch, and pectin. After a series of chemical treatments, the samples are filtered and rinsed with distilled water until the residues get neutralized. To avoid generating strong hydrogen bonding among nanofibers after matrix removal, the samples are kept in a water-swollen state during the whole chemical process.

After chemical pretreatment, the purified cellulose fibers are soaked in distilled water (concentration: ~0.5 % in mass). About 120 ml of solution containing chemical-purified cellulose fibers are then placed in a common ultrasonic generator

of 20–25 kHz in frequency equipped with a cylindrical titanium alloy probe tip of 1.5 cm in diameter. The subsequent ultrasonication is conducted for 30 min to isolate the nanofibers. To investigate the effect of ultrasonic intensity on the nanofibrillation of the chemical-purified cellulose fibers, the output power of the ultrasonication is conducted at different power, viz., 400, 800, 1,000, and 1,200 W, respectively. The ultrasonic treatment is carried out in an ice/water bath, and the ice is maintained throughout the entire ultrasonication time.

4.4 Electrospining Technique

Electrospinning technique has received a growing attention because polymer fibers prepared by this technique achieve fiber diameters in the range from micrometers down to a few nanometers straightforwardly and cost-effectively. In a typical process, a polymer solution is forced through a capillary, forming a pendent drop at the tip of capillary. Then a high voltage is applied between the capillary and a grounded collection target. When the electric field strength overcomes the surface tension of the droplet, a polymer solution jet is initiated and accelerated toward the collection target. As the jet travels through the air, the solvent evaporates and a nonwoven polymeric fabric is formed on the target. Because the resulting nonwoven fabrics often resemble the superstructure features of natural extracellular matrix, they have gained a great interest in tissue engineering as scaffold materials for tissue regeneration, immobilized enzymes and catalyst systems, and wound dressing articles. In addition, the high specific surface area and highly porous three-dimensional structure enables their use in high density cell and tissue cultures. The diameter and morphology of the resulting fiber has been shown to be effected by all variables in the electrospinning process including the solution composition, applied voltage, collector distance, and collector type [63].

In many respects, the formation of nano- and microscale fibers from cellulose via electrospinning has mirrored the history of conventional cellulose fiber spinning. Just as cellulose was derivatized to form the first manufactured fiber, it is also reported as the first electrospun fiber with patents dating back to Formhals in 1934. Over the last 50 years, several direct solvents for cellulose have been discovered and utilized in wet spinning or dry-jet wet spinning processes. Some of these solvents including *N*-methyl-morpholine *N*-oxide/water (nNMMO/H_2O) [64] and lithium chloride/dimethylacetamide (LiCl/DMAc) have also been investigated for electrospinning cellulose. Additionally, electrospinning cellulose fibers from some more recently developed cellulose solvents such as ionic liquids and ethylene diamine/salt have been reported [65]. The great challenges of spinning cellulose directly from a solvent without derivatization are evident in electrospinning as in wet spinning and dry-jet wet spinning, and many researchers have taken the route of spinning more readily soluble cellulose derivatives and subsequently converting the derivatives back to cellulose.

To date, it has been well established that the ES process allows easy incorporation of particles with different habits, such as 1-dimensional carbon nanotubes, 2-dimensional layered silicates, or 3-dimensional SiO_2 nanoparticles and many others, into the nanofibers.

4.5 Bacterial Synthesis

Cellulose has traditionally been sourced from plants. However, refining of plant cellulose typically involves harsh, aggressive processing to remove noncellulose materials such as lignin and hemicellulose. Fortunately, an alternative source of cellulose where no chemical or mechanical refining is necessary is available. Bacterial cellulose (hereinafter called BC) has been developed as an alternative to plant cellulose. Due to its high water-holding capacity, high crystallinity, high tensile strength, and fine weblike network structure, which means that it can be formed into any size or shape, BC is being used as a promising nanofiber biomaterial for making composites [66, 67–69, 72, 152].

It is well known that cellulose fiber networks – as in the case of paper – provide good mechanical properties because of the degree of hydrogen bonding obtained between the fibers in the network. The greater the hydrogen bonding, the stronger is the paper material. BC synthesized extracellularly by *Acetobacter xylinum* is of nano-size, as a result of which hydrogen bonding between fibrils is greater than with plant cellulose in normal paper. The hydrogen bonds due to the hydroxyl group give rise to properties such as a high degree of crystallinity, high water-holding capacity, and high tensile strength.

Since BC has unique properties, including high hydrophilicity, as well as having a high water-holding capacity and a fine fiber network which can be easily shaped into three-dimensional structures during synthesis, it is an excellent candidate for use as a scaffold for tissue engineering [70, 71]. The porosity of BC, which is necessary to support cell ingrowths and effective mass transport of tissue such as cartilage, makes it a natural medium for growing cells.

Due to its remarkable mechanical properties, an ability to form homogeneous membrane sheets after drying under certain synthesis conditions and an ultrafine network structure, BC is useful for numerous applications [66, 72]. The relative inertness of BC fibers has led to their use as reinforcing agents in composites [73]. Therefore, the methods of producing BC have been developed with the aims of improving yield, structure, and other desired physical properties [74, 75]. Besides using various production methods, the medium used for culture, the pH level, and the source of nitrogen and phosphate as the main foods for *Acetobacter xylinum* have all been varied [76].

Previous research has focused on ensuring that the *Acetobacter xylinum* does not undergo genetic mutation [77, 154]. Efforts to prevent mutation have included adding 20 wt% malt extract to a medium inoculated with *Acetobacter xylinum* as a cryoprotectant [78]. The implications of mutation occurring are the growth of a wild type organism which can reduce *Acetobacter xylinum*'s ability to produce cellulose. Other side effects include affecting the morphological and physiological properties of BC and a fall in the Young's modulus of the BC sheet produced because of the growth of a byproduct known as acetan [79]. Various biosynthesis-related methods of ensuring a high productivity of BC from the *Acetobacter xylinum* have been used, such as expression of sucrose, in which UDP-glucose is efficiently formed from sucrose [80]; the addition of polyacrylamide-co-acrylic acid [166]; and addition of 1 % ethanol in the medium [167]. The most recent was

through cloning of the *Acetobacter xylinum* whereby the resulting yield of BC was far more than that produced by the original bacteria itself [81, 82].

5 Nanocomposite Processing

Cellulose nanoparticles are obtained as stable aqueous suspensions and most investigations focused on hydrosoluble (or at least hydrodispersible) or latex-form polymers. The main advantage is that the dispersion state of the nanoparticles is kept when using an aqueous medium for the processing.

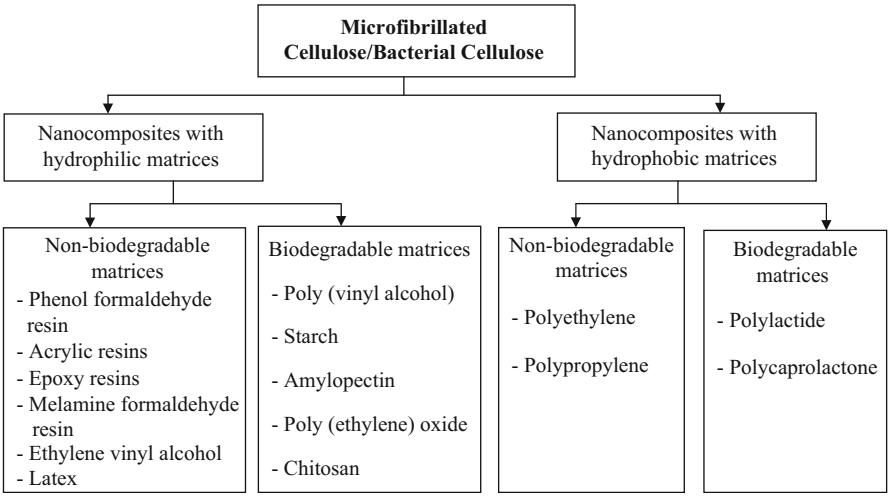

After dissolution of the hydrosoluble or hydrodispersible polymer, the aqueous solution can be mixed with the aqueous suspension of cellulosic nanoparticles. The ensuing mixture is generally cast and evaporated to obtain a solid nanocomposite film. It can also be freeze-dried and hot-pressed. The preparation of cellulose nanofiber-reinforced starch [67, 83–86, 160], silk fibroin [87], poly(oxyethylene) (POE) [88–90]; Samir et al. 2005; [91], polyvinyl alcohol (PVA) [92–96], hydroxypropyl cellulose (HPC) [92, 93], carboxymethyl cellulose (CMC) [97], or soy protein isolate (SPI) [68] has been reported in the literature.

The first publication reporting the preparation of cellulose nanocrystal-reinforced polymer nanocomposites was carried out using a latex obtained by the copolymerization of styrene and butyl acrylate (poly(*S*-co-BuA)) and tunicin (the cellulose extracted from tunicate – a sea animal) whiskers [98]. The same copolymer was used in association with wheat straw [40, 99] or sugar beet (Samir et al. 2004) cellulose nanocrystals. Other latexes such as poly(β-hydroxyoctanoate) (PHO) [100–102], polyvinylchloride (PVC) [103–106], waterborne epoxy [107], natural rubber (NR) [108–110], and polyvinyl acetate (PVAc) [37] were also used as matrix. Recently, stable aqueous nanocomposite dispersion-containing cellulose

whiskers and a poly(styrene-*co*-hexyl-acrylate) matrix were prepared via miniemulsion polymerization [45]. Addition of a reactive silane was used to stabilize the dispersion. Solid nanocomposite films can be obtained by mixing and casting the two aqueous suspensions followed by water evaporation.

The possibility of dispersing cellulosic nanofibers in nonaqueous media has been investigated using surfactants or chemical grafting, and it opens other possibilities for nanocomposites processing. Cellulose nanoparticles possess a reactive surface covered with hydroxyl groups, providing the possibility to extensive chemical modification. Although this strategy decreases the surface energy and polar character of the nanoparticles, improving by the way the adhesion with nonpolar polymeric matrix, a detrimental effect is generally reported for the mechanical performances of the composite. This unusual behavior is ascribed to the originality of the reinforcing phenomenon of polysaccharide nanocrystals resulting from the formation of a percolating network thanks to hydrogen bonding forces. Therefore, grafting of long chains instead of small molecules can be used to preserve the mechanical properties of the material.

Very few studies have been reported concerning the processing of cellulose nanofibers-reinforced nanocomposites by extrusion methods. The hydrophilic nature of cellulose causes irreversible agglomeration during drying and aggregation in nonpolar matrices because of the formation of additional hydrogen bonds between amorphous parts of the nanoparticles. Therefore, the preparation of cellulose whiskers-reinforced PLA nanocomposites by melt extrusion was carried out by pumping the suspension of nanocrystals into the polymer melt during the extrusion process [111]. An attempt to use PVA as a compatibilizer to promote the dispersion of cellulose whiskers within the PLA matrix was reported [112]. Organic acid chlorides-grafted cellulose whiskers were extruded with LDPE [113]. The homogeneity of the ensuing nanocomposite was found to increase with the length of the grafted chains. Polycaprolactone-grafted cellulose nanocrystals obtained by ring-opening polymerization (ROP) of the corresponding lactone were also used as "masterbatches" by melt blending with a PCL matrix [114].

An attempt to use a recently patented concept (dispersed nano-objects protective encapsulation – DOPE process) intended to disperse carbon nanotubes in polymeric matrices was reported. Physically cross-linked alginate capsules were successfully formed in the presence of either cellulose whiskers or microfibrillated cellulose [115]. The ensuing capsules have been extruded with a thermoplastic material.

5.1 Interfacial Interactions

Strong interactions between cellulose nanofibers prepared from cottonseed linters and between the filler and the glycerol-plasticized starch matrix were reported to play a key role in reinforcing properties [116]. In nonpercolating systems, for instance for materials processed from freeze-dried cellulose nanocrystals, strong matrix/filler interactions enhance the reinforcing effect of the filler.

This observation was reported using EVA matrices with different vinyl acetate contents and then different polarities [117]. An improvement of matrix/filler interactions by using cellulose whiskers coated with a surfactant was shown to play a major role on the nonlinear mechanical properties, especially on the elongation at break [168]. Grunert and Winter [36] founded a higher reinforcing effect for unmodified cellulose whiskers than for trimethylsilylated whiskers. Apart from the fact that 18 % of the weight of the silylated crystals was due to the silyl groups, they attributed this difference to restricted filler/filler interactions.

5.2 Nanocomposite Manufacturing Method

Natural fiber composites are prepared using various composites manufacturing methods such as compression molding, injection molding, resin transfer molding (RTM), and vacuum bagging. The preforms are mostly fibers, fabrics, or nonwovens. Prepregs are also widely used to prepare composites [118]. Where V_f is the fiber volume fraction, W_f is the weight of fiber and Wm is the weight of matrix. r_f and r_m are the densities of the fiber and matrix, respectively. The production of the composites is optimized in relation to temperature, pressure, and molding time. It is often necessary to preheat the natural fibers to reduce the moisture before processing the composites. High temperatures degrade the cellulose, thus negatively affecting the mechanical properties of the composites. Inefficient fiber dispersion in the matrix causes fiber agglomeration which decreases the tensile strength [118]. Most of the previous research on natural fiber composites has focused on reinforcements such as flax, hemp, sisal and jute, and thermoplastic and thermoset matrices. Some of these composites have been produced using matrices made of derivatives from cellulose, starch, and lactic acid to develop fully biodegradable composites or biocomposites [119].

The emerging diversity of applications of natural fiber composites has seen the production of sandwich structures based on natural fiber composite skins. In some cases, these sandwich composites have been produced from paper honeycomb and natural fiber-reinforced thermoplastic or thermoset skins, depending on the applications [149].

The main criteria for the selection of the appropriate process technology for natural-fiber composite manufacture include the desired product geometry, the performance needed, the cost, and the ease of manufacture. The fabrication methods for natural fiber composites are similar to those used for glass fibers [150]. The most commonly used manufacturing processes are introduced in the followings. Although many variants on these techniques exist, this overview gives a good indication of the production possibilities.

5.2.1 Hand Laminating

The fibers are placed in a mold and the resin is later applied by rollers. One option is to cure using a vacuum bag, as then excess air is removed and the atmospheric pressure exerts pressure to compact the part. The simplicity, low cost of tooling, and

flexibility of design are the main advantages of the procedure. On the other end, the long production time, intensive labor, and low automation potential consist some of the disadvantages [152].

5.2.2 Resin Transfer Molding (RTM)

The resin transfer molding technique requires the fibers to be placed inside a mold consisting of two solid parts (close mold technique). A tube connects the mold with a supply of liquid resin, which is injected at low pressure through the mold, impregnating the fibers. The resulting part is cured at room temperature or above until the end of the curing reaction, when the mold is opened and the product removed. Parameters such as injection pressure, fiber content, or mold temperature have a great influence on the development of the temperature profiles and the thermal boundary layers, especially for thin cavities. This technique has the advantage of rapid manufacturing of large, complex, and high performance parts. Several types of resins (epoxy, polyester, phenolic, and acrylic) can be used for RTM as long as their viscosity is low enough to ensure a proper wetting of the fibers. Parameters such as injection pressure, fiber content, or mold temperature have a great influence on the development of the temperature profiles and the thermal boundary layers, especially for thin cavities. Good knowledge of all the operating steps is very important to obtain high-quality parts [118].

An alternative variant of this process is the vacuum injection or vacuum assisted resin transfer molding (VARTM), where a single solid mold and a foil (polymeric film) are used. The VARTM process is a very clean and low-cost manufacturing method: resin is processed into a dry reinforcement on a vacuum bagged tool, using only the partial vacuum to drive the resin. As one of the tool faces is flexible, the molded laminate thickness depends partially on the compressibility of the fiber–resin composite before curing and the vacuum negative pressure [153].

5.2.3 Compression Molding

Compression molding is another major technique for the construction of fiber-reinforced polymers, which involves a semifinished composite sheet widely known as sheet molding compound (SMC) that is later molded into the final parts by compression. For the SMC the process consists of a rolling film of resin on which fibers are added. A second film of resin is then added, so as to later be compressed in a composite sheet that may be stored for a few days. To get the final product, the reinforced sheet is then placed into a press to take its desired shape [154].

Advantages of compression molding are the very high volume production ability, the excellent part reproducibility, the short cycle times, and the low crap arising. Processing times of <2 min are reached during the compression molding of three-dimensional components with a high forming degree [155]. It has also been shown that the adhesion of natural fibers and matrix resin is important in order to obtain good mechanical properties of natural fiber composites, and the mechanical properties were improved by the molding condition, molding pressure, and temperature. A big concern with compression molding that needs always to be considered is the maximum pressure before the damage of the fibers and the structure.

5.2.4 Injection Molding

Injection molding process is suitable to form complex shapes and fine details with excellent surface finish and good dimensional accuracy for high production rate and low labor cost. In the injection molding, resin granules and short fibers are mixed into a heated barrel and transported to the mold cavity by a spindle. Injection molding is another process among the most important for the manufacturing of plastics/composites and can produce from very small products such as bottle tops to very large car body parts [156].

5.2.5 Pultrusion

Pultrusion is a continuous process to manufacture composite profiles at any length. The impregnated fibers are pulled through a die, which is shaped according to the desired cross section of the product. The resulting profile is shaped until the resin is dry. Advantages of this process are the ability to build thin wall structures, the large variety of cross-sectional shapes, and the possibility for high degree of automation.

6 Cellulose Fiber-Reinforced Biocomposites

6.1 Polyurethane-Based Composites for Medical Applications

PALF-derived nanocellulose-embedded polyurethane has been utilized as an attractive and readily available range of materials for the fabrication of vascular prostheses. The elastic properties of the material, coupled with low thrombogenicity and exceptional physical and mechanical properties, have led to a considerable research effort aimed at the development of nanocellulose polyurethane vascular grafts (Fig. 25.8). Nanocellulose–PU vascular grafts with a wall thickness of 0.7–1.0 mm showed elongation at break of 800–1,200 % and withstood hydraulic pressures up to 300 kPa.

High tensile strength and high strain-to-failure nanocomposites with strongly improved modulus were synthesized based on nanocellulose and polyurethane. The cellulose nanocomposites were prepared by solvent casting, based on dry crystalline cellulose and hydrophilic polyurethane.

Cellulose dissolution was avoided while still allowing successful dispersion of the cellulose nanofibrils present in dry nanoscale cellulose particles. ESEM proves the presence of dispersed cellulose nanofibrils in the developed nanocomposites. The XRD analysis confirms that cellulose nanofibrils in the prepared nanocomposites preserve the original crystalline structure of cellulose (cellulose I) [157]. The composition with 5 wt% cellulose was optimal and showed the highest strain-to-failure. The produced nanocellulose and its composites confirmed to be a very versatile material having the wide range of medical applications, including cardiovascular implants, scaffolds for tissue engineering, repair of articular cartilage, vascular grafts, urethral catheters, mammary prostheses, penile prostheses, adhesion barriers, and artificial skin [158]. These implants were produced from bioresorbable and/or biodegradable materials. Progressive degradation

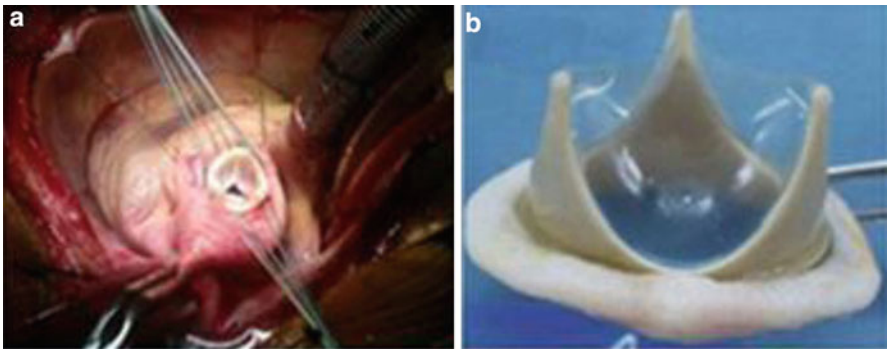

Fig. 25.8 Nanocellulose–polyurethane prosthetic heart valve: (**a**) valve implant, (**b**) heart valve

of the implant material may then be accompanied by the formation of the new tissues. The developed material can also be utilized for construction of non-latex condoms, breathable wound dressing, surgical gloves, surgical gowns or drapes, medical bags, organ retrieval bags, and medical disposables [159].

The development of PALF nanocellulose–polyurethane valve design (Fig. 25.8) with good biological durability, fatigue resistance, and hemodynamics, and a new generation of biostable polyurethanes which have proven themselves of superior biostability in a demanding 6-month, strained, rat implant model. Thus, anticipate early development of a polyurethane valve which has a good hemodynamic function maintained during long-term implant and which neither fails from biological degradation nor from fatigue-induced material failure while maintaining a low thrombogenic surface. In accelerated fatigue tests, five out of five consecutively produced valves exceeded the equivalent of 12 years cycling without failure. The only failure occurred after the equivalent of approximately 13 years cycling, and three valves have reached 608 million cycles (approximately 15 years equivalent) to date.

6.2 Polyvinyl Alcohol-Based Composites for Medical Applications

Polyvinyl alcohol (PVA) is a hydrophilic biocompatible polymer with various characteristics desired for biomedical applications. PVA can be transformed into a solid hydrogel with good mechanical properties by physical cross-linking using freeze-thaw cycles. Hydrophilic nanocellulose fibers of an average diameter of 50 nm are used in combination with PVA to form biocompatible nanocomposites. According to Millon and Wan [120], the resulting nanocomposites possess a broad range of mechanical properties and can be made with mechanical properties similar to that of cardiovascular tissues, such as aorta and heart valve leaflets. On their studies, the stress–strain properties for porcine aorta are matched by at least one type of PVA–nanocellulose nanocomposite in both the circumferential and the axial

tissue directions. A PVA–nanocellulose nanocomposite with similar properties as heart valve tissue is also developed. Relaxation properties of all samples, which are important for cardiovascular applications, were also studied and found to relax at a faster rate and to a lower residual stress than the tissues they might replace. So, finally the new PVA–nanocellulose composite is a promising material for cardiovascular soft tissue replacement applications.

7 Cellulosic Nanocomposite Applications in Biomedical Field

7.1 Pharmaceutical

Cellulose has a long history of use in the pharmaceutical industry. The material has excellent compaction properties when blended with other pharmaceutical excipients so that drug-loaded tablets form dense matrices suitable for the oral administration of drugs. Polysaccharides, natural polymers, fabricated into hydrophilic matrices remain popular biomaterials for controlled-release dosage forms, and use of a hydrophilic polymer matrix is one of the most popular approaches in formulating an extended release dosage forms [121–123]. This is due to the fact that these formulations are relatively flexible, and a well-designed system usually gives reproducible release profiles. Drug release is the process by which a drug leaves a drug product and is subjected to absorption, distribution, metabolism, and excretion (ADME), eventually becoming available for pharmacologic action. Crystalline nanocellulose offers several potential advantages as a drug delivery excipient. Crystalline nanocellulose and other types of cellulose in advanced pelleting systems whereby the rate of tablet disintegration and drug release may be controlled by microparticle inclusion, excipient layering, or tablet coating [124, 125]. The very large surface area and negative charge of crystalline nanocellulose suggests that large amounts of drugs might be bound to the surface of this material with the potential for high payloads and optimal control of dosing.

Other nanocrystalline materials, such as nanocrystalline clays, have been shown to bind and subsequently release drugs in a controlled manner via ion exchange mechanisms and are being investigated for use in pharmaceutical formulations [126]. The established biocompatibility of cellulose supports the use of nanocellulose for a similar purpose. The abundant surface hydroxyl groups on crystalline nanocellulose provide a site for the surface modification of the material with a range of chemical groups by a variety of methods. Surface modification may be used to modulate the loading and release of drugs that would not normally bind to nanocellulose, such as nonionized or hydrophobic drugs. For example, Lonnberg et al. suggested that poly(caprolactone) chains might be conjugated onto nanocrystalline cellulose for such a purpose [127].

Additionally, since crystalline nanocellulose is a low-cost, readily abundant material from a renewable and sustainable resource, its use provides a substantial environmental advantage compared with other nanomaterials.

7.2 Medical

Recently nanocellulose has been called as the eyes of biomaterial highly applicable to biomedical industry which includes skin replacements for burnings and wounds; drug releasing system; blood vessel growth; nerves, gum, and dura mater reconstruction; scaffolds for tissue engineering; stent covering; and bone reconstruction [128–132]. Figure 25.9 shows some applications for nanocellulose within biomedical field.

Tissue engineering looks for new material and devices which could interact positively with biological tissues [133], either working as an in vitro basis for cell growth or rearranging and developing tissue about to be implanted. They also aim new classes of degradable biopolymers that are biocompatible and whose activities are controllable and specific [134], more likely to be used as cell scaffolds [135] or in vitro tissue reconstruction.

As mentioned above, a great variety of biomaterials have been developed recently. They have all sorts of properties (physical/chemical and mechanical) depending mostly in the final application (tissue regeneration, medication holding and releasing, tissue grafting, or scaffolding) [132]. The scaffold's success depends much on the cellular adhesion and growth onto the surface; thus, biopolymer's chemical surface can dictate cellular response by interfering in cellular adhesion, proliferation, migration, and functioning. The surface–cell interaction is extremely important in implant effectiveness, including its rejection. Since the interaction is fully understood in a cell level, new biomaterials and products can be easily developed [136]. The problems still arise due to some methods' inefficiency such as cell seeds and sources, scaffolding, ambient, extracellular matrix producing, analysis, and appropriate models [137].

On the other hand, to regenerate tissues, three specific foundations are taken: cells, support, and growth factors. Cells synthesize the matrix for the new tissues, support holds, and keep the ambient proper for the growth, while the growth factors facilitate and promote the cell regeneration [137]. Material used for implants cannot be either rejected or cause inflammatory response; in others, it should be biocompatible. Furthermore, it should promote regeneration and if necessary, be absorbed after a while or be biodegradable [138]. Studies on support cell interactions are crucial to implants viability. Many cell responses are observed out of different materials, so the cell ability to discriminate and adapt to it whether adhere or not to its surface [139]. This is crucial as it will direct further responses as cell proliferation, migration, and viability.

Due to the clinical importance of skin lesions, many laboratories have been aroused to the search for healing products having benefits including immediate pain relief, close adhesion to the wound bed, and reduced infection rate. The nanocellulose developed having huge superficial area gives great water absorption capacity and elasticity. These are characteristics from an ideal healing bandage. On the other hand, it holds no microbial activity. Nanocellulose mats are very effective in promoting autolytic debridement, reducing pain, and accelerating granulation, all of which are important for proper wound healing. These nanobiocellulose membranes can be created in any shape and size, which is beneficial for the treatment of

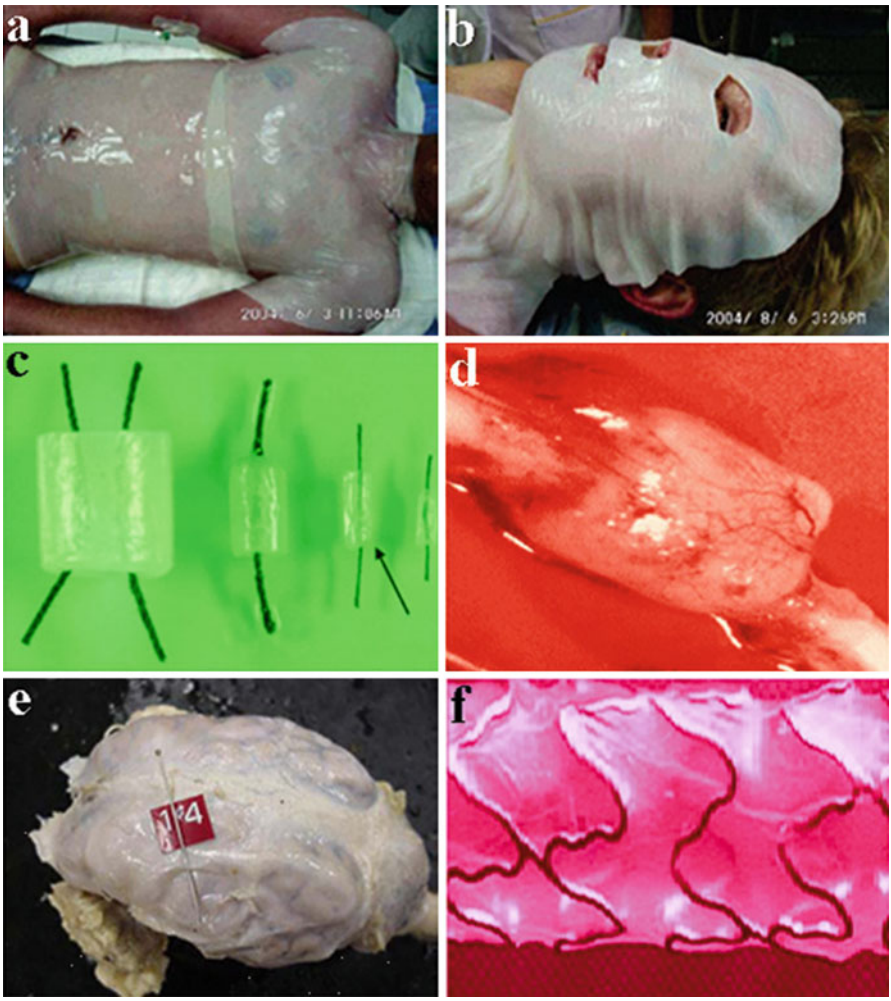

Fig. 25.9 Biomedical applications of nanocellulose (**a**) and (**b**) never-dried nanocellulose membrane [132]; (**c**) and (**d**) artificial blood vessels [130]; (**e**) dura mater reconstruction [129]; and (**f**) covering stents [131]

large and difficult to cover areas of the body. Barud [140] has developed a biological membrane with bacterial cellulose and standardized extract of propolis. Propolis has many biological properties including antimicrobial and anti-inflammatory activities. All the above mentioned characteristics present, which make the membrane (Fig. 25.9) a good treatment for burns and chronic wounds. Odontology is challenged to find ideal materials to replace the bones in several procedures for bone malformation and maxillary and facial deformities. The biggest challenge is the loss of alveolar bone. Nanocellulose having suitable porosity,

which gives the mat an infection barrier, loss of fluids, and painkiller effect, allows medicines to be easily applied, and it also absorbs the purulent fluids during all inflammatory stages, expelling it later on in a controlled and painless manner [141].

7.3 Veterinary

In veterinary medicine, the reports consulted about the use of biocellulose produced by the A. xylinum refer to applications for conduit for isolation in reconstruction of peripheral nerves, healing of experimental wounds of bovine mammary teats, healing of experimental tegument wounds in equine and swine, prophylaxis of the formation of membrane post laminectomy in dogs, and healing of incisional experimental lesions of the cornea in dogs. Clinically, gross (brute) membrane was used in healing of natural wounds of dogs.

Biosynthesized nanocellulose membrane was utilized [142] in experimental trochleoplasty in dogs, and it was found that the use of this biomaterial has advantages instead of the conventional treatment for osteochondral injuries. The cellulose membrane was applied in the tissue formation of fibrocartilage ripe obtaining good integration of the newly formed tissue and the adjacent cartilage, allowing its clinical use in dogs.

The membranes were tested through a lateral parapatellar skin incision 5–7 cm, followed by incision of the retinaculum and articular capsule, until the exposure of the knee joint. With the limb in extension, the patella was displaced by promoting the exposure of the femoral trochlea (Fig. 25.10a) [142].

Iamaguti et al. conducted a bent knee and trochleoplasty through the deepening of the trochlear groove with the aid of gouge forceps (Fig. 25.10b). The nanocellulose membrane, the base of cellulose 5 mm thick, was applied inside the limb of the dogs, after the deepening of the groove, and fixed with 4–5 simple points separated the edge of the normal cartilage, with the use of synthetic absorbable suture thread 6-0 (Fig. 25.10c). The patella was repositioned after the extension of the limb, performing the synthesis of the articular capsule and retinaculum in a type of points of suture, with 3-0 monofilament nylon thread (Fig. 25.10d) [142]. After the inclusion of the membrane, a link was obtained between the subcutaneous tissue in simple continuous pattern and skin, using 3-0 monofilament nylon, with simple stitches apart (Fig. 25.10e).

The cartilage that covers the trochlear groove is composed of chondrocytes embedded in a matrix and has the surface layer formed by flattened chondrocytes. The repaired tissue that covers the region of trochleoplasty consisted of more organized tissue, with higher thickness compared to the previous period.

The nanocellulose membranes were used to repair defects of the abdominal wall in humans or animals. Nanocellulose may be used as treatment of great abdominal wall defects to avoid tension during repair. Falcão et al. [143] investigated the incorporation type by host tissue of membranes of nanocellulose produced by the bacteria and of polytetrafluoroethylene (PTFE) in abdominal wall defects of rats. The cellulose membrane was sutured at the level of the musculoaponeurotic defect

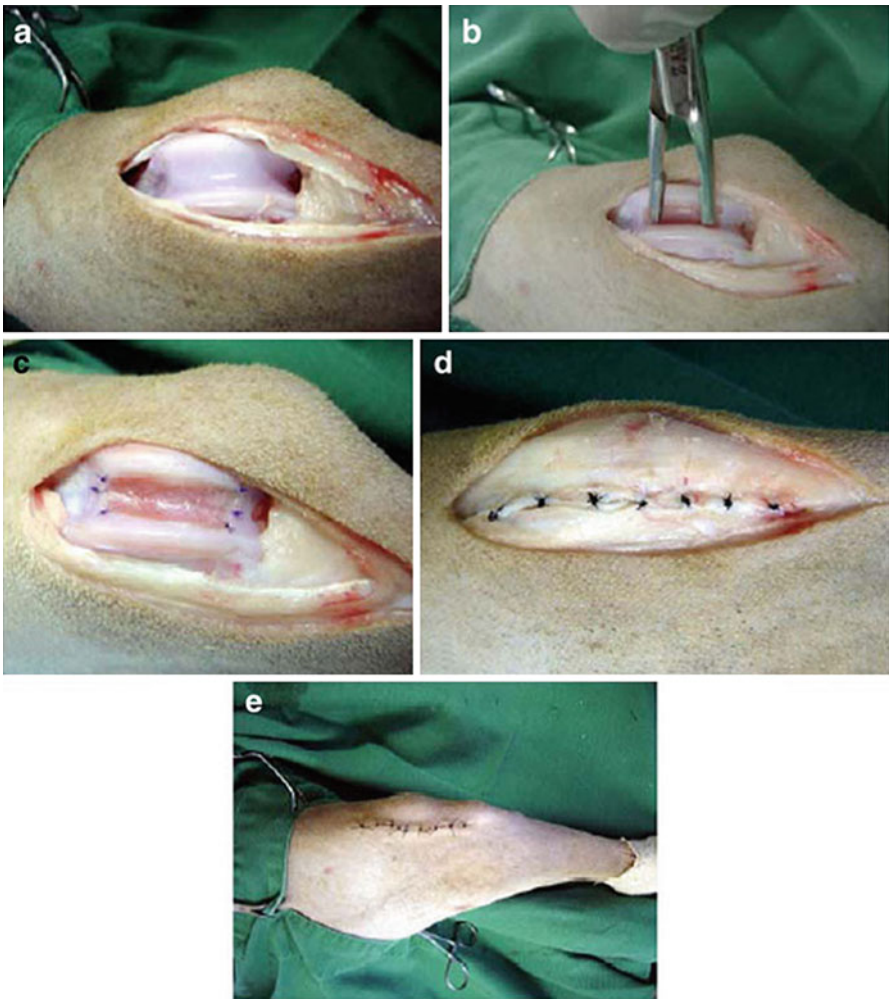

Fig. 25.10 (**a**) Dislocation of the patella to expose the trochlear groove, (**b**) deepening of the groove trochlear with the aid of gouge forceps, (**c**) fixing the biosynthesized cellulose membrane with 6-0 synthetic absorbable sutures, (**d**) suturing the joint capsule and retinaculum in type of points of suture, with 3-0 monofilament nylon thread, and (**e**) suture the skin with simple stitches apart

with Prolene® and continuous suture, anchored at the four angles of the rectangle. Then the skin was closed with thread of Mononylon® through an interrupted suture.

7.4 Dental

Nanocellulose was tested in dental tissue regeneration. Microbial cellulose produced by the Gluconacetobacter xylinus strain can be used to regenerate dental

Fig. 25.11 Nanocellulose used in dental tissue regeneration in a 39-year-old female patient

tissues in humans (Fig. 25.11). Nanocellulose products Gengiflex® and Gore-Tex® have intended applications within the dental industry. It was developed to aid periodontal tissue recovery [144]. A description was given of a complete restoration of an osseous defect around an IMZ implant in association with a Gengiflex® therapy. The benefits included the reestablishment of aesthetics and function of the mouth and that a reduced number of surgical steps were required.

The bandage, called Gengiflex®, consists of two layers: the inner layer is composed of microbial cellulose, which offers rigidity to the membrane, and the outer alkali-cellulose layer is chemically modified [145]. Salata et al. [146] compared the biological performance of Gengiflex® and Gore-Tex® membranes using the in vivo nonhealing bone defect model proposed by Dahlin et al. [147].

The study showed that Gore-Tex® membranes (a composite with polytetrafluoroethylene, urethane, and nylon) were associated with significantly less inflammation, and both membranes promoted the same amount of bone formation during the same period of time. A greater amount of bone formation was present in bone defects protected by either Gore-Tex® or microbial cellulose membrane, when compared to the control sites. Gore-Tex® is better tolerated by the tissues than Gengiflex®. Recently, in a similar vein, Macedo et al. [148] also compared bacterial cellulose and polytetrafluoroethylene (PTFE) as physical barriers used to treat bone defects in guided tissue regeneration.

In this study, two osseous defects (8 mm in diameter) were performed in each hindfoot of four adult rabbits, using surgical burs with constant sterile saline solution irrigation. The effects obtained on the right hindfeet were protected with PTFE barriers, while Gengiflex® membranes were used over wounds created in the left hindfeet. After 3 months, the histological evaluation of the treatments revealed that the defects covered with PTFE barriers were completely repaired with bone tissue, whereas incomplete lamellar bone formation was detected in defects treated with Gengiflex® membranes, resulting in voids and lack of continuity of bone deposition [160].

Nanocellulose with its characteristics, like nanofiber size and distribution, mechanical properties, compatibility, and ability to mold, creates a unique biomaterial indispensable in health area. The nanocellulose composite scaffolds are biocompatible with less rejection with cellular contact and blood contact cells

interaction, to be a promissory biomaterial and may be suitable for cell adhesion/attachment, suggesting that these scaffolds can be used for wound dressing or tissue-engineering scaffolds [161].

8 Conclusions

The potential applicability of cellulose-based biocomposites and nanocomposites are widely extended. Due to a great number of properties, applications of nanocellulose-based materials are mainly considered to be in a wide range of biomaterial applications such as medical products, pharmacy, cosmetics, dental, and veterinary applications are also being considered. The mechanical properties such as high strength and stiffness, the surface reactivity (with numerous hydroxyl groups), and the specific organization as well as the small dimensions of nanocellulose may well impart useful properties to nanocomposite materials reinforced with these fibers.

The aim of this article was to demonstrate the current state of research and development in the field of nanocellulose – a biofabricated sustainable type of polymer material. The extraordinary supramolecular nanofiber network structure and the resulting valuable properties have led to real opportunities and extensive activity in the field of biomedical applications. The intention of this work is to broaden the knowledge in this subject area and to stimulate the practical application of nanocellulose. In the biomedical field, bacterial nanocellulose implants have opened up new uses for bioartificial medical devices.

Acknowledgement The authors would like to express gratitude for extending their support in the form of Research University (RU) grant (1001/PTEKIND/814133)

References

1. Nakagaito AN, Yano H (2005) Novel high-strength biocomposites based on microfibrillated cellulose having nano-order-unit web-like network structure. Appl. Phys. A: Mater. Sci. Process 80:155–159
2. Nakagaito AN, Yano H (2004) The effect of morphological changes from pulp fibre towards nano- scale fibrillated cellulose on the mechanical properties of high-strength plant fibre based composites. Appl Phys A: Mater Sci Process 78:547
3. Bledzki AK, Reihmane S, Gassan J (1996) Properties and modification methods for vegetable fibers for natural fiber composites. J Appl Polym Sci 5:1329
4. Hornsby PR, Hinrichsen E, Tarverdi K (1997) Preparation and properties of polypropylene composites reinforced with wheat and flax straw fibers. J Mater Sci 32:1009
5. Oksman K, Wallstrom L, Berglund LA, Filho RDT (2002) Morphology and mechanical properties of unidirectional sisal-epoxy composites. J Appl Polym Sci 84:2358
6. Nabi Saheb D, Jog JP (1999) Natural fiber polymer composites: a review. Adv Polym Technol 18:351
7. Georgopoulos ST, Tarantili PA, Avgerinos E, Andreopoulos AG, Koukios EG (2005) Thermoplastic polymers reinforced with fibrous agricultural residue. Polym Degrad Stab 90:303

8. Crawford RL (1981) Lignin biodegradation and transformation. Wiley, New York
9. Jawaid M, Abdul Khalil HPS (2011) Cellulosic/synthetic fibre reinforced polymer hybrid composites: A Review. Carbohydr Polym 86:1
10. Dorée C (1947) The methods of cellulose chemistry. Chapman & Hall, London
11. Visakh PM, Thomas S (2010) Preparation of bionanomaterials and their polymer. nanocomposites from waste and biomass. Valorization 1:121
12. Bhat AH, Khalil Abdul HPS (2011) Oil palm biomass: fibre cultivation, production and its varied applications under book publication title: oil palm: cultivation, production and dietary components. Nova Publishers, Hauppauge, New York. ISBN: 978-1-61761-934-2
13. Williams GI, Wool RP (2000) Composites from natural fibers and soy oil resins. Appl Compos Mater 7:421
14. Torres FG, Diaz RM (2004) Morphological characterisation of natural fibre reinforced thermoplastics (NFRTP) processed by extrusion, compression and rotational moulding. Polym Polym Compos 12:705
15. Abdul Khalil HPS, Hanida S, Kang SCW, Nik Fuaad NA (2007) Agro-hybrid composite:the effects on mechanical and physical properties of oil palm fiber (EFB)/glasshybrid reinforced polyester composites. J Reinf Plast Compos 26:203
16. Abdul Khalil HPS, Ismail H, Ahmad MN, Ariffin A, Hassan K (2001) The effect of various anhydride modifications on mechanical and water absorption properties of oil palm empty fruit bunches. Polym Int 50:1
17. Kalia S, Kaith BS, Kaur I (2009) Polym Eng Sci 49:1253
18. Rong MZ, Zhang MQ, Liu Y, Yang GC, Zeng HM (2001) The effect of fiber treatment on the mechanical properties of unidirectional sisal-reinforced epoxy composites. Compos Sci Technol 61:1437
19. Abdul Khalil HPS, Kumar RN, Asri SM, Nik Fuaad NA, Ahmad MN (2007) Hybrid thermoplastic pre-preg oil palm frond fibers (OPF) reinforced in polyester composites. Polym-Plast Technol Eng 46:43
20. Van de Velde K, Kiekens P (2001) Thermoplastic pultrusion of natural fibre reinforced composites. Compos Struct 54:355
21. Boss HL, van den Oever MJA, Peters OCJJ (2002) Tensile and compressive properties of flax fibres for natural fibre reinforced composites. J Mater Sci 37:1683
22. Baley C (2000) Influence of kink bands on the tensile strength of flax fibers. Compos Part A 33:939
23. Lamy B, Baley C (2000) J Mater Sci Lett 19:979
24. Jähn A, Schröder MW, Füting M, Schenzel K, Diepenbrock W (2002) Characterization of alkali-treated flax fibres by means of FT Raman spectroscopy and environmental scanning electron microscopy. Spectrochim Acta A Mol Biomol Spectrosc 58:2271
25. Gassan J, Bledzki AK (1996) Einfluss von haftvermittlern auf das feuchteverhalten naturfaserverstärkter Kunststoffe. Die Angew Makromaol Chem 236:129
26. Michell AJ (1989) Compos Asia Pacific, Adelaid 89:19
27. Moloney TM (1995) In: Lee SM, Rowell RM (eds) International encyclopedia of composites. VCH Publishers, New York, p 656
28. Mieck KP, Nechwatal A, Knobeldorf C (1994) Melliand Texilberichte 11:892
29. Mukherjee PS, Satyanarayana KG (1986) An empirical evaluation of structureproperty relationships in natural fibres and their fracture behaviour. J Mater Sci 21:51
30. Zimmermann T, Bordeanu N, Strub E (2010) Properties of nanofibrillated cellulose from different raw materials and its reinforcement potential. Carbohydr Polym 79:1086
31. Wang B, Sain M (2007) Isolation of nanofibers from soybean source and their reinforcing capability on synthetic polymers. Polym Int 56:538
32. Kaushik A, Singh M, Verma G (2010) Green nanocomposites based on thermoplastic starch and steam exploded cellulose nanofibrils from wheat straw. Carbohydr Polym 82:337
33. Teixeira EM, Corrêa AC, de Oliveira CR (2010) Cellulose nanofibers from white and naturally colored cotton fibers. Cellulose 17:595

34. Stelte W, Sanadi AR (2009) Indust Eng Chem Res 48:11211
35. Habibi Y, Goffin AL, Schiltz N, Duquesne E, Dubois P, Dufresne A (2008) J Mater Chem 18:5002
36. Grunert M, Winter WT (2002) J Polym Environ 10:27
37. Garcia de Rodriguez NL, Thielemans W, Dufresne A (2006) Cellulose 13:261
38. Kvien I, Tanem BS, Oksman K (2005) Biomacromolecules 6:3160
39. Anglés MN, Dufresne A (2000) Macromolecules 33:8344
40. Helbert W, Cavaillé JY, Dufresne A (1996) Polym Compos 17:604
41. Fleming K, Gray D, Prasannan S, Matthews S (2000) J Am Chem Soc 122:5224
42. Revol JF (1982) Carbohydr Polym 2:123
43. Hanley SJ, Giasson J, Revol JF, Gray DG (1992) Polymer 33:4639
44. Pu Y, Zhang J, Elder T, Deng Y, Gatenholm P, Ragauskas AJ (2007) Compos Part B 38:360
45. Elmabrouk AB, Wim T, Dufresne A, Boufi S (2009) J Appl Polym Sci 114:2946
46. Dufresne A (2006) J Nanosci Nanotechnol 6:322
47. Dufresne A (2008) Can J Chem 86:484
48. Hubbe MA, Rojas OJ, Lucia LA, Sain M (2008) BioResources 3:929
49. Sturcova A, Davies GR, Eichhorn SJ (2005) Biomacromolecules 6:1055
50. Herrick FW, Casebier RL, Hamilton JK, Sandberg KR (1982) J Appl Polym Sci 37:797
51. Wagberg L (2005) Wood material science. Finnish-Swedish Research Programme, Stockholm 2007
52. Payen A (1838) Compt Rend 7:1052, 1125
53. Tanahashi M (1990) Wood Res 77:49
54. Kokta BV (1991) Steam explosion pulping. In: Focher B, Marzetti A, Crescenzi V (eds) Steam explosion techniques: fundamentals and industrial applications. Gordon and Breach Science, Philadelphia, pp 163–206
55. Excoffier G, Toussaint B, Vignon MR (1991) Biotechnol Bioeng 38:1308
56. Vignon MR, Garcia-Jaldon C, Dupeyre D (1995) Biomacromolecules 17:395
57. Cristobal C, Encarnacion R, Ignacio B, Maria JN, Eulogio C (2006) Process Biochem 41:423
58. Cristobal C, Encarnacion R, Mercedes B, Paloma M, Jose MN, Eulogio C (2008) Fuel 87:692
59. Marchessault RH (1991) Steam explosion: a refining process for lignocellulosics. In: Focher B, Marzetti V, Crescenci V (eds) Steam explosion techniques: fundamentals and industrial applications. Gordon and Breach Science, Philadelphia, pp 1–19
60. Abdul Khalil HPS, Bhat AH, Ireana Yusra AF (2012) Carbohydr Polym 87:963
61. Abe K, Yano H (2009) Comparison of the characteristics of cellulose microfibril aggregates of wood, rice straw and potato tuber. Cellulose,16 (6), 1017–1023
62. Abe K, Yano H (2010) Cellulose 17:271
63. Lo¨nnberg H, Zhou Q, Brumer H, Teeri TT, Malmstro¨m E, Hult A, Lo¨nnberg H, Zhou Q, Brumer H, Teeri TT, Malmstro¨m E, Hult A (2006) Biomacromolecules 7:2178
64. Bochek A, Petropavlovsky G, Kallistov O (1993) Cellulose Chem Technol 27:137
65. Cui W, Li X, Zhou S, Weng J (2007) J Appl Polym Sci 103:3105
66. Iguchi M, Yamanaka S, Budhiono A (2000) J Mater Sci 35:261
67. Orts WJ, Shey J, Imam SH, Glenn GM, Guttman ME, Revol JF (2005) J Polym Environ 13:301
68. Wang Y, Cao X, Zhang L (2006) Macromol Biosci 6:524
69. Eichhorn SJ, Dufresne A, Aranguren M, Marcovich NE, Capadona JR, Rowan SJ, Weder C, Thielemans W, Roman M, Renneckar S, Gindle W, Veigel S, Keckes J, Yano H, Abe K, Nogi M, Nakagaito AN, Mangalam A, Simonsen J, Benight AS, Bismarck A, Berglund LA, Peijs T (2010) J Mater Sci 45:1–33
70. Svensson A, Nicklasson E, Haraah T, Panilaitis B, Kaplan DL, Brittberg M, Gatenholm P (2005) Bacterial cellulose as a potential scaffold for tissue engineering of cartilage. Biomaterials 26:419–431
71. Helenius G, Backdahl H, Bodin A, Nannmark U, Gatenholm P, Reisberg B (2006) J Biomed Res 76A:431

72. Yamanaka S, Watanabe K, Kitamura N (1989) The structure and mechanical properties of sheets prepared from bacterial cellulose. Journal of Material Science 24:3141–3145
73. Grunet M, Winter T (2002) J Polym Environ 10:27
74. Geyer U, Heinze T, Stein A, Klemm D, Marsch S, Schumann D, Schrnauder HP (1994) Int J Biol Macromol 16:343
75. Yamanaka S, Ishihara M, Sugiyama J (2000) Cellulose 7:213
76. Masaoka S, Ohe T, Sakota N (1993) J Ferment Bioeng 75:18
77. Wulf PD, Joris K, Vandamme EJ (1996) J Technol Biotechnol 62:1290
78. Sokollek SJ, Hertel C, Hammes WP (1998) J Biotechnol 60:195
79. Watanabe K, Tabuchi M, Ishikawa A, Takemura H, Tsuchida T, Morinaga Y, Yoshinaga F (1998) Biosci Biotechnol Biochem 62:1290
80. Nakai T, Tonouchi N, Konishi T, Kojima Y, Tsuchida T, Yoshinaga F, Sakai F, Hayashi T (1999) Appl Biol Sci 96:14
81. Kawano S, Tajima K, Uemori Y, Yamashita H, Erata T, Munekata M, Takai M (2002) DNA Res 9:149
82. Bae SO, Sugano Y, Ohi K, Shoda M (2004) Appl Microbiol Biotechnol 65:315
83. Anglés MN, Dufresne A (2001) Macromolecules 34:2921
84. Mathew AP, Dufresne A (2002) Biomacromolecules 3:609
85. Mathew AP, Thielemans W, Dufresne A (2008) J Appl Polym Sci 109:4065
86. Dagang L, Zhong Tuhua R, Chang P, Kaifu L, Qinglin W (2010) Bioresour Technol 101:2529
87. Noishiki Y, Nishiyama Y, Wada M, Kuga S, Magoshi J (2002) J Appl Polym Sci 86:3425
88. Samir MASA, Alloin F, Paillet M, Dufresne A (2004) Macromolecules 37:4313
89. Samir MASA, Alloin F, Sanchez JY, Dufresne A (2004) Polymer 45:4149
90. Samir MASA, Alloin F, Gorecki WJ, Sanchez Y, Dufresne A (2004) J Phys Chem B 108:10845
91. Samir MASA, Alloin F, Dufresne A (2006) High performance nanocomposite polymer electrolytes. Compos Interfaces 13:545
92. Zimmermann T, P¨ohler E, Geiger T (2004) Cellulose fibrils for polymer reinforcement. Adv Eng Mater 6:754
93. Zimmermann T, P¨ohler E, Schwaller P (2005) Mechanical and morphological properties of cellulose fibril reinforced nanocomposites. Adv Eng Mater 7:1156
94. Lu J, Wang T, Drzal LT (2008) Compos Part A 39:738
95. Paralikar SA, Simonsen J, Lombardi J (2008) J Membr Sci 320:248
96. Roohani M, Habibi Y, Belgacem NM, Ebrahim G, Karimi AN, Dufresne A (2008) Eur Polym J 44:2489
97. Choi Y, Simonsen J (2006) Cellulose nanocrystal-filled carboxymethyl cellulose nanocomposites. J Nanosci Nanotechnol 6:633
98. Favier V, Canova GR, Cavaillé JY, Chanzy H, Dufresne A, Gauthier C (1995) Nanocomposites materials from latex and cellulose whiskers. Polym Adv Technol 6:351
99. Dufresne A, Cavaillé JY, Helbert W (1997) Thermoplastic nanocomposites filled with wheat straw cellulose whiskers. Part II: effect of processing and modeling. Polym Compos 18:198
100. Dufresne A, Kellerhals MB, Witholt B (1999) Transcrystallization in mcl-PHAs/ cellulose whiskers composites. Macromolecules 32:7396
101. Dubief D, Samain E, Dufresne A (1999) Polysaccharide microcrystals reinforced amorphous poly(β-hydroxyoctanoate) nanocomposite materials. Macromolecules 32:5765
102. Dufresne A (2000) Dynamic mechanical analysis of the interphase in bacterial polyester/ cellulose whiskers natural composites. Compos Interfaces 7:53
103. Chazeau L, Paillet M, Cavaillé JY (1999) Plasticized PVC reinforced with cellulose whiskers: 1- linear viscoelastic behavior analyzed through the quasi point defect theory. J Polym Sci Part B 37:2151

104. Chazeau L, Cavaillé JY, Terech P (1999) Mechanical behaviour above Tg of a plasticized PVC reinforced with cellulose whiskers, a SANS structural study. Polymer 40:5333
105. Chazeau L, Cavaillé JY, Canova G, Dendievel R, Boutherin B (1999) Viscoelastic properties of plasticized PVC reinforced with cellulose whiskers. J Appl Polym Sci 71:1797
106. Chazeau L, Cavaillé JY, Perez J (2000) Plasticized PVC reinforced with cellulose whiskers. II. Plastic behavior. J Polym Sci B 38:383
107. Ruiz MM, Cavaillé JY, Dufresne A, Graillat C, Gérard JF (2001) Macromol Symposia 169:211
108. Bendahou A, Habibi Y, Kaddami H, Dufresne A (2009) Physico-chemical characterization of palm from phoenix dactylifera – L, preparation of cellulose whiskers and natural rubber–based nanocomposites. J Biobased Mater Bioenerg 3:81
109. Rosa MF, Medeiros ES, Malmonge JA (2009) Proceedings of the 11th international conference on advanced materials (ICAM'09), Rio de Janeiro, September 2009
110. Bendahou A, Kaddami H, Dufresne A (2010) Investigation on the effect of cellulosic nanoparticles' morphology on the properties of natural rubber based nanocomposites. Eur Polym J 46:609
111. Oksman K, Mathew AP, Bondeson D, Kvien I (2006) Manufacturing process of cellulose whiskers/polylactic acid nanocomposites. Compos Sci Technol 66:2776
112. Bondeson D, Oksman K (2007) Polylactic acid/cellulose whisker nanocomposites modified by polyvinyl alcohol. Compos Part A 38:2486
113. de Menezes AJ, Siqueira G, Curvelo AAS, Dufresne A (2009) Polymer 50:4552
114. Goffin AL, Raquez JM, Duquesne E, Habibi Y, Dufresne A, Dubois P (2011) Polymer 52:1532
115. Lemahieu L, Bras J, Tiquet P, Augier S, Dufresne A (2011) Macromol Mater Eng J 296
116. Lu Y, Weng L, Cao X (2005) Biocomposites of plasticized starch reinforced with cellulose crystallites from cottonseed linter. Macromol Biosci 5:1101
117. Chauve G, Heux L, Arouini R, Mazeau K (2005) Biomacromolecules 6:2025
118. Njuguna J, Wambua P, Pielichowski K, Kayvantash K (2011) Natural fiber-reinforced polymer composites and nanocomposites for automotive applications. In: Kalia S, Kaith BS, Kaur I (eds) Cellulose fibers: bio- and nano-polymer composites. Springer, Heidelberg
119. Mishra S, Mohanty AK, Drzal LT, Misra M, Hinrichsen G (2004) Macromol Mater Eng 289:955
120. Millon LE, Wan WK (2006) The polyvinyl alcohol-bacterial cellulose system as a new nanocomposite for biomedical applications. J Biomed Mater Res Part B 79:245
121. Alderman DAA (1984) Int J Pharm Tech Prod Manuf 5:1
122. Heller J (1987) Use of polymers in controlled release of active agents in controlled drug delivery. In: Robinson JR, Lee VHL (eds) Fundamentals and applications, 2nd edn. Marcel Dekker, New York, pp 210–180
123. Longer MA, Robinson JR (1990) Sustained-release drug delivery systems. In: Remington JP (ed) Remington's pharmaceutical sciences, 18th edn. Mack Publishing, Easton, pp 1676–1693
124. Watanabe Y, Mukai B, Kawamura KI (2002) Yakugaku Zasshi 122:157
125. Baumann MD, Kang CE, Stanwick JC (2009) J Control Release 138:205
126. Shaikh S, Birdi A, Qutubuddin S, Lakatosh E, Baskaran H (2007) Ann Biomed Eng 35:2130
127. Lönnberg H, Fogelstr¨om L, Samir MASA, Berglund L, Malmstr¨om E, Hult A (2008) Eur Polym J 44:2991
128. Fontana JD, de Souza AM, Fontana CK (1990) Appl Biochem Biotech 24–25:253
129. Mello LR, Feltrin Y, Selbach R, Macedo G Jr, Spautz C, Haas LJ (2001) Arq Neuropsiquiatr 59:372
130. Klemm D, Schumann D, Udhardt U, Marsch S (2001) Prog Polym Sci 26:1561
131. Negrão SW, Bueno RRL, Guérios EE (2006) Rev Bras de Cardiologia Invasiva 14:10
132. Czaja WK, Young DJ, Kawecki M, Brown RM Jr (2007) Biomacromolecules 8:1
133. Croce MA, Silvestri C, Guerra D (2004) J Biomater Appl 18:209
134. Madihally SV, Matthew HWT (1999) Biomaterials 20:1133
135. Nehrer S, Breinan HA, Ramappa A (1997) J Biomed Mater Res 38:95

136. Kumari TV, Vasudev U, Kumar A, Menon B (2001) Trends in Biomater Artif Organs 15:37
137. Ikada Y (2006) J R Soc Interface 3:589
138. Chen GQ, Wu Q (2005) Polyhydroxyalkanoates as tissue engineering materials. Biomaterials 26:6565
139. Anselme K (2000) Osteoblast adhesion on biomaterials. Biomaterials 21:667
140. Barud HS (2009) São Paulo Research Foundation – FAPESP, Brazil
141. Czaja W, Krystynowicz A, Bielecki S, Brown RM Jr (2006) Biomaterials 27:145
142. Iamaguti LS, Branda˜o CVS, Minto BW (2008) Vet e Zootec 15:160
143. Falcão SC, Neto JE, Coelho ARB (2008) Acta Cir Bras 23:78
144. Novaes AB Jr, Vidigal GM Jr, Novaes AB, Grisi MFM, Polloni S, Rosa A (1998) Immediate implants placed into infected sites: A histomorphometric study in dogs. Int J oral Maxillofac Implants 13:422–7
145. Novaes AB Jr, Novaes AB (1995) Immediate implants placed into infected sites: a clinical report. Int J oral Maxillofac Implants 10:609–13
146. Salata LA, Craig GT, Brook IM (1995) J Dental Res 74:825
147. Dah Dahlin C, Linde A, Gottlow J, Nyman S (1988) Plast Reconstr Surg 81:672
148. Macedo NL, Matuda FS, Macedo LGS, Monteiro ASF, Valera MC, Carvalho YR (2004) Braz J Oral Sci 3:395
149. Fink H-P, Weigel P, Purz H (2001) Prog Polym Sci 26:1473
150. Mis'kiewicz M, Biele S (2002) J Ind Microbiol Biotechnol 29:189
151. Samir MASA, Mateos AM, Alloin F, Sanchez JY, Dufresne A (2004) Plasticized nanocomposite polymer electrolytes based on poly(oxyethylene) and cellulose whiskers. Electrochim Acta 49:4667
152. Berglund L (2005) Cellulose-based nanocomposites. In: Mohanty A, Misra M, Drzal L (eds) Natural fibers, biopolymers and biocomposites. CRC Press, Boca Raton
153. Samir MASA, Chazeau L, Alloin F, Dufresne A, Sanchez JY (2005) Review of recent research into cellulose whiskers, their properties and their application in nanocomposite field. Biomacromolecules 6:612
154. Saxena IM, Brown RM Jr (2005) Cellulose biosynthesis: Current views and evolving concepts. Ann Bot 96:9–21
155. Ljungberg N, Bonini C, Bortolussi F, Boisson C, Heux L, Cavaillé JY (2005) New nanocomposite materials reinforced with cellulose whiskers in atactic polypropylene: Effect of surface and dispersion characteristics. Biomacromolecules 6:2732
156. Samir MASA, Alloin F, Dufresne A (2005) Review of recent research into cellulosic whiskers, their properties and their application in nanocomposite field. Biomacromolecules 6:612
157. Wan YZ, Hong L, Jia SR, Huang Y, Zhu Y, Wang YL, Jiang HJ (2006) Synthesis and characterization of hydroxyapatite–bacterial cellulose nanocomposites cellulose. Compos Sci Technol 66:1825
158. Alemdar A, Sain M (2008) Biocomposites from wheat straw nanofibres: Morphology, thermal and mechanical properties. Compos Sci Technol 68:557
159. Alemdar A, Sain M (2008) Isolation and characterization of nanofibres from agricultural residues - wheat straw and soy hulls. Bioresour Technol 99:1664
160. Svagan AJ, Hedenqvist MS, Berglund L (2009) Reduced water vapour sorption in cellulose nanocomposites with starch matrix. Compos Sci Tech 69(3–4):500–506
161. Berglund LA, Peijs T (2010) Cellulose biocomposites-from bulk moldings. J Mater Sci 45:1
162. Siro I, Plackett D (2010) Microfibrillated cellulose and new nanocomposite materials: A review. Cellulose 17:459
163. Kalia S, Dufresne A, Cherian BM, Kaith BS, Avérous L, Njuguna J, Nassiopoulos E (2011) Cellulose-Based Bio- and nanocomposites: a review. International Journal of Polymer Science 35:837–875

164. Kalia S, Vashistha S, Kaith BS (2011) Cellulose Nanofibers reinforced bioplastics and their applications. In: Pilla S (ed) Handbook of bioplastics and biocomposites engineering applications. Wiley-Scrivener, New York (Chap 16)
165. Kalia V, Sarkar S, Subramaniam S, Haining WN, Smith KA, Ahmed R (2010) Prolonged interleukin-2Ralpha expression on virus-specific CD8+ T cells favors terminal-effector differentiation in vivo. Immunity 32:91–103
166. Joseph G, Rowe GE, Margaritis A, Wan W (2003) Effects of polyacrylamide-co-acrylic acid on cellulose production by Acetobacter xylinum. J Chem Technol Biotechnol 78:964–970
167. Krystynowicz A, Czaja W, Wiktorowska-Jezierska AM, Turkiewicz M, Gonçalves-Miśkiewicz M, Biele S (2002) Factors affecting the yield and properties of bacterial cellulose. J Indust Microbiol Biotechnol 29:189–195
168. Ljungberg N, Wesslen B (2005) Preparation and Properties of Plasticized Poly(Lactic acid) Films. Biomacromolecules 6:1789–1796